

Copyright is owned by the Author of the thesis. Permission is given for a copy to be downloaded by an individual for the purpose of research and private study only. The thesis may not be reproduced elsewhere without the permission of the Author.

**BREAKDOWN OF RICE AND WHEAT-BASED FOODS DURING
GASTRIC DIGESTION AND ITS IMPLICATIONS ON GLYCEMIC
RESPONSE**

A thesis presented in partial fulfillment of the requirements for the degree of

Doctor of Philosophy

in

Food Technology

at Massey University, Palmerston North,

New Zealand

JOANNA NADIA

2022



*To my mama and papa in Indonesia,
thank you for continuously reminding me
“The fear of the Lord is the beginning of knowledge”.
Here I present my PhD thesis for you.*

ABSTRACT

The composition and structure of starch-based foods determine their breakdown behavior in the digestive tract and consequently their glycemic response. The glycemic response of starch-based foods is known to be influenced by their gastric emptying rate. However, the role of gastric digestion in regulating this process has not been well-understood, especially on how food breakdown behavior in the stomach may be related to the glycemic response. In this project, the link between food structure, food breakdown during gastric digestion, gastric emptying, and glycemic response was investigated *in vivo* using a growing pig model. Durum wheat- and white rice-based foods of varying physical structures (semolina porridge, rice- and wheat couscous, rice grain, rice noodle and wheat noodle/pasta) were studied. It was found that the foods with smaller-sized particles (semolina porridge and couscous products) had faster gastric breakdown rate and gastric emptying rate, resulting in higher glycemic impact (maximum change from the baseline and the overall impact) compared to the foods with larger-sized particles (rice grain and noodle products). The faster gastric breakdown rate of the smaller-sized foods was related to their acidification rate in the stomach, which caused their dilution or dissolution by gastric secretions. For larger-sized foods, their gastric breakdown rate and gastric acidification rate were slower, which extended their contact time with salivary amylase in the proximal stomach.

To elucidate further the role of the proximal and distal phases of gastric digestion in solid food breakdown, a static *in vitro* digestion was conducted with the same food products. In the smaller-sized foods, both the proximal and distal phases led to their dissolution. Meanwhile, for the larger-sized foods, the extended contact time with α -amylase in the proximal phase contributed to the leaching of starch particles from the food, which was important to aid their breakdown during gastric digestion. The distal phase contributed to the softening of the larger-sized foods, but its softening effect was limited. The knowledge on the contributions of the phases of gastric digestion and the identified link between food structure, gastric digestion, and glycemic response in this thesis may be useful for structuring starch-based foods with controlled glycemic properties.

ACKNOWLEDGEMENTS

Before I acknowledge anyone else, I firstly would like to thank God Almighty, for giving me the calling to pursue a PhD and giving me the strength to finish this PhD degree. The PhD journey was indeed very challenging, with many moments where I felt I was not good enough to get a PhD, in addition to challenges arising due to the COVID-19 pandemic. But God in His faithfulness continually strengthened me, with this reminder “My grace is sufficient for you, for My power is made perfect in weakness”. And with that reminder I pushed through the PhD journey and was able to present this thesis report. These past few years have been a life-changing journey for me – I learned so much and I realized more my passion in science, which I believe will have a great impact for my next journey. I am so grateful that God has surrounded me with many great people along the PhD journey, without whose help and contributions I would not be able to complete my PhD.

First, I wish to express my highest appreciation and gratitude to my supervisory panel: Assoc. Prof. Gail Bornhorst, Dist. Prof. Harjinder Singh, Dist. Prof. R. Paul Singh, and Prof. John. Bronlund. It is such an honor to be supervised by world-renowned researchers like them and I never imagined before that I would have the opportunity to work with them. I am grateful for Dr. Bornhorst for being the first person that opened the opportunity to this PhD project, for being available to have weekly meeting with me so that this project could finish within the expected timeframe, and for allowing me to participate in her class and group meetings - I learned so much because of the class and group meetings. I am thankful for Dr. R. Paul Singh and Dr. Harjinder Singh, who despite their busy schedule, still provided their time to give valuable feedback and life advice. Also for Dr. Bronlund, I am grateful to have you in the supervisory panel – thank you for continuously challenging my engineering sense in the PhD, for your feedback, and the life advice in our conversations. I thank all my supervisors for entrusting me to carry this PhD project, for their feedback, for setting examples on how a world-class research should be, and for their humility and kindness that reminded me that these two qualities should also grow as one’s knowledge and influence grows.

This PhD project would not exist without the funding, so next I would like to acknowledge the Riddet Institute for managing the funding for my PhD. This project

was funded by the Tertiary Education Commission with grant number: Center of Research Excellence – Riddet Institute (ref:A914656). I especially thank the Riddet Institute management team: Mr. John Henley-King (Associate Director- Operations), Mrs. Terri Palmer (Office Manager), Mrs. Ansley Te Hiwi (who retired on my final year), Dr. Sarah Golding (used to be the Communications Officer), and Ms. Meg Wedlock (finance administrator). Special mention to Dr. Sarah Golding, for her listening ears and advice during the time when my mental health was highly challenged.

A major part of this thesis would not be present without the successful pig study, which was conducted in collaboration with the Riddet Institute Nutrition Team. For that, I would like to thank the members of the team, especially Dr. Suzanne Hodgkinson as the team leader, Dr. Natascha Stroebling, Paloma Craig, Anneminke Buwalda, and Dr. Carlos Montoya. Thanks to Dr. Eric Neumann who was responsible for the surgical procedures during the pig study. I also thank all casual staff who were involved with animal handling, and staff and students (Anika Hoogeveen, Isuri Jayawardana, Marit van der Zeijden) who were involved on the sampling days. Special thanks to the “Midnight Pig Shepherds” team – Dr. Alexander G. Olenskyj and Talia G. Estevez from UC Davis Food Engineering Lab, who contributed greatly to the pig study during their internship in Semester I/2019. Thanks to Alex for running the rheology measurement, conducting rheology and particle size data analysis, and sharing co-authorship in Chapter 4. Thanks to Talia for doing the image analysis and helping me to set up DNS and OPA assays in the lab. Thanks to both of you for running the GOPOD analysis of the pig plasma samples with me. Also thank you for our random conversations when we worked until midnight for several days in a row during the sampling day, and for the friendship – I enjoyed your companionship. I wish you all the best with pursuing your goals in life.

A special mention goes to Dr. Parthasarathi Subramanian (Riddet Institute), who helped in the GOPOD analysis of the pig plasma samples, conducted scanning electron microscopy work, taught me to perform the confocal microscopy observation, and ran the Mastersizer analyses not only during the pig study period, but also during my static *in vitro* study period – I greatly appreciate your help in the *in vitro* study, that saved 2.5 hours of my day for each of the experiment, so I was able to go home before midnight. Thank you for involving me in the early experiments related to the HGS, and for being a great listener and a friend to talk to about my PhD journey. I also would like to acknowledge: Dr. Carlos Montoya (AgResearch) and Dr. Jonathan Godfrey (Massey

Statistical Consultancy Service) for providing advice in early stage of the statistical analysis and has become my basis to set up the statistical analysis for the rest of the PhD; Prof. Jim Jones (Massey University) for sharing his knowledge on agglomeration, which was very helpful in establishing the rice couscous manufacturing protocol for the study; and the Manawatu Imaging and Microscopy Center for allowing me and Dr. Subramanian to do the microscopy observation.

Being in a PhD project that involved various measurements means I got to work in different labs, and I would like to take the opportunity to thank the technical staff in each lab. Thank you to Ms. Maggie Zou, for assisting with ordering the consumables for my PhD and so many other helps she provided during my PhD – thank you also for your joyful personality that can enlighten students' day when they are filled with anxiety from the PhD journey. Thank you to Ms. Michelle Tamehana for allowing me to work in the Food Characterization Lab during the *in vivo* and *in vitro* study, giving me after-hours access, and ensuring I worked safely in the lab. Thank you to Mr. Steve Glasgow, who let me use the custom-built shaking water bath in his lab and allowing me to use the facility in the Food Chemistry Lab. Thank you to the Microbiology Lab staff: Mrs. Ann Marie-Jackson, Mrs. Kylie Evans, Dr. Haoran Wang (who does not work at Massey anymore, but her help during the beginning of my second year was very helpful to me) and Dr. Baizura Zain, for providing me a bench space in the lab to carry the DNS and OPA assays. Thank you to the PD lab – Pilot Plant duet, Mr. Warwick Johnson and Mr. Garry Radford, for their help during my first year in finding the right sets of equipment to produce more than 100 kg rice couscous; I will not forget how you stayed after hours a few times to ensure I was safe and how you helped me with the clean up after working very long hours each day. Thank you also to Mr. John Edwards and Mr. John Sykes (now retired) from the Chemical Engineering lab, for allowing me to use the facilities in the lab.

My PhD journey was not all about research and studying - the journey was made colorful and much bearable with the presence of friends. I am grateful for Alex and Tiffanie Kanon – my church family and also housemates, for allowing me to stay with them in the last 2.5 years of my PhD, and for treating me like their own sibling. With the recent addition of Kanon Jr., I am even more grateful to partake in your early journey as new parents! I have been enjoying doing life with you and I pray for God's favor and blessing upon you to bless others. I would like to extend my deepest gratitude for my church family, especially Dom and Grace's connect group members who have

been my “family far from home” in the past 3.5 years: dr. Grace G. Lee, Lydia Kim, dr. Ovida Saikam, Ruth Soriano-Ballesfin, Sheila Cagaoan, Martia Julienne, dr. Yan Chuah, Dr. Dominic Lomiwes, Phillip Lee, Al Ballesfin, James Coralde, and dr. Zia Loo. Special mention also to Kudzai Mvere, Briana Bay, Caroline and Abner Chaves with their two boys, and Izzabelle Flores from the church for their supports in prayers and friendship. I am also thankful for the Kids Church Team, where I managed to grow my leadership skills and communications to younger fellows, as well as the Worship Team at church where I could serve others through music.

The days in the office as a PhD student were made fun and enjoyable with the presence of my office mates. I am grateful for my office mates (the Bunkers and the Old Board Room guys) for the ups and downs we shared together: Alex Kanon, Ankita Jena, Anika Hoogeveen, Davide Fraccascia, Giovanna Castillo-Fernandez, Haroon Qazi, Isuri Jayawardana, Laura Payling, Marit van der Zeijden, Patrick Tai, Natasha Nayak, and Xin Wang. Also, I would like to express my gratitude for my close friends outside the office: Chathurika Samarakoon, Hien Truong, Suchima Gonapinuwala, Dr. Syahmeer How, and Dr. Murali Kumar. Not forget to mention, the members of the Riddet Institute Student Society Committee 2020/2021, who embarked with me on the journey to run events and workshops for the students of the Riddet Institute. It is such an honor to have met you guys during my PhD journey and I wish you all the best with completing your studies.

In addition to people I have met in “real-life”, I am also grateful for those I met “virtually” for the past few years – the UC Davis Food Engineering lab members, especially Dr. Yamile Mennah-Govela (for sharing your lab knowledge and positivity), Dr. Clay Swackhamer (for sharing your SAS tips and trick, your valuable image analysis code, and coding tips in general), Berta Lascuevas-Laguna (for the friendship and knowledge exchange), and other lab members for the great (and often funny) conversations in the online lab meetings. I can’t thank you Dr. Bornhorst enough for involving me in her group’s virtual meeting and making me feel welcomed by the group.

Before my two last acknowledgements, I sincerely would like to thank everyone in Indonesia who has been praying for me, particularly my grandma and my aunts. I am also grateful for those from my school days and university days back in Indonesia, who have shaped me to be my current version and have equipped me with all of the attitudes I need to go through the challenges during the PhD. I believe it is not by chance that I

met you during my life journey and I am grateful for each of you. May God bless you and protect you always wherever you are.

Second to last, I would like to thank my husband-to-be, Dr. Steven Shen, who has been staying with me in a long-distance relationship (NZ – USA!) for six years. Thank you for all the encouragement, prayers, and support that you have been giving me. Thank you for continuously reminding me that God is faithful in keeping His promises, to keep my eyes on the finish line, and to keep believing that all the sacrifices would be worth it. I love you and I am so blessed to have you.

Finally, I am very grateful for my mama and papa back home in Indonesia, who have become my main motivation during this PhD. Thank you for always praying for me and supporting my decision to pursue a PhD and to be the first one to do a PhD from both sides of the family – although it means I had to go against the perspective in the family that “a woman does not need that high of education”. I know it must be very hard for you to let your only child to study in a foreign country, which was made worse with not being able to see me for two years due to the COVID-19 pandemic. Thank you for hanging in there, despite your health conditions and many challenges that we have been facing as a family. I love you and miss you so much, and I dedicate this thesis for you.

TABLE OF CONTENTS

ABSTRACT	i
ACKNOWLEDGEMENTS.....	ii
TABLE OF CONTENTS.....	vii
LIST OF TABLES	xiii
LIST OF FIGURES	xvi
LIST OF ABBREVIATIONS	xxii
LIST OF SYMBOLS	xxiii
LIST OF PUBLICATIONS AND PRESENTATIONS	xxv
CHAPTER 1. Introduction and project overview	1
1.1 Background	1
1.2 Research objectives.....	3
1.3 Organization of the thesis.....	4
CHAPTER 2. Literature review	5
2.1 Introduction.....	5
2.2 Structural aspects of starch and starch-based foods.....	6
2.2.1 General overview of starch structure	6
2.2.2 Structural aspects of starch-based foods relevant in digestion processes	8
2.3 Digestive organs that contribute to structural breakdown and glycemic response of solid starch-based foods.....	14
2.3.1 Mouth.....	14
2.3.2 Stomach.....	18
2.3.3 Small intestine.....	24
2.4 Monitoring physical breakdown of solid foods during gastric digestion.....	26
2.4.1 Experimental approaches to investigate food breakdown during gastric digestion.....	27
2.4.2 Methods to quantify physical breakdown of solid foods during gastric digestion.....	29
2.5 Physical changes in the structure of starch-based foods during oral and gastric digestion.....	32
2.5.1 Mastication (oral processing).....	32
2.5.2 Gastric digestion.....	38
2.6 Food structure, gastric digestion, and glycemic response relationship.....	46

2.6.1	The importance of food structure on gastric emptying rate and glycemic response.....	48
2.6.2	Gastric breakdown behavior, gastric emptying rate and glycemic response	56
2.7	<i>In vitro-in vivo</i> correlation (IVIVC) in starch digestion	58
2.7.1	Common <i>in vitro</i> methods for starch digestion and their correlation to <i>in vivo</i> glycemic response	58
2.7.2	Development of IVIVCs in starch digestion studies for future food structure development	61
2.8	Considerations in developing IVIVC of starch-based foods with gastric digestion.....	64
2.8.1	Meal size	65
2.8.2	Effect of mastication	67
2.8.3	Mixed meal effect	69
2.8.4	State of the stomach prior to meal consumption.....	70
2.9	Conclusions and future outlook	71
CHAPTER 3. Selected food systems and experimental approach		74
3.1	Selected food systems	76
3.1.1	Rationale	76
3.1.2	Preparation of selected foods systems	78
3.2	Experimental approach 1: <i>in vivo</i> studies using growing pig model	80
3.2.1	Rationale, related research objectives, and hypotheses	81
3.2.2	Glycemic response measurement in growing pigs.....	83
3.2.3	Gut content collection from growing pigs	88
3.3	Experimental approach 2 – Static <i>in vitro</i> gastric digestion	93
3.3.1	Rationale, related research objectives, and hypotheses	93
3.3.2	Static <i>in vitro</i> digestion procedure	95
CHAPTER 4. Tracking physical breakdown of rice- and wheat-based foods with varying structures during gastric digestion and its influence on gastric emptying in a growing pig model.....		98
4.1	Abstract	98
4.2	Introduction.....	100
4.3	Materials and methods	103
4.3.1	Study diet preparation	103
4.3.2	Animal housing and treatment	103

4.3.3	Digesta collection procedure.....	103
4.3.4	Diet characterization	103
4.3.5	Measurement of physical properties of diets and gastric digesta.....	105
4.3.6	Data and statistical analysis	107
4.4	Results.....	111
4.4.1	Study diet characterization.....	111
4.4.2	Changes in saturation ratio (SR) and moisture addition rate	113
4.4.3	Changes in pH.....	115
4.4.4	Changes in particle size distribution	118
4.4.5	Changes in rheological properties.....	124
4.4.6	Textural changes	128
4.4.7	Gastric emptying.....	132
4.4.8	Relationships between measured variables.....	135
4.5	Discussion	137
4.5.1	Different food structures exhibited different gastric emptying profiles	137
4.5.2	Gastric secretory response was impacted by food buffering capacity	142
4.5.3	Stomach regions affect physical changes of digesta during gastric digestion.....	146
4.5.4	Relationship between physical changes during gastric digestion and gastric emptying.....	151
4.5.5	Methodological considerations in monitoring physical breakdown during gastric digestion <i>in vivo</i>	153
4.6	Conclusions	155
CHAPTER 5. Influence of food macrostructure on the kinetics of acidification in the pig stomach: implications for starch hydrolysis and starch emptying rate		157
5.1	Abstract	157
5.2	Introduction	159
5.3	Materials and methods	161
5.3.1	Study diets preparation and characterization	161
5.3.2	Animal housing and treatment	161
5.3.3	Gastric digesta collection procedure	161
5.3.4	Establishment of intragastric pH colormap.....	162
5.3.5	Particle size analysis	163
5.3.6	Gastric digesta chemical analysis.....	163

5.3.7 Microscopy analysis.....	167
5.3.8 Statistical analysis	168
5.4 Results and discussion	170
5.4.1 Inhomogeneous intragastric pH distribution may extend remaining salivary amylase activity.....	170
5.4.2 Consequences of intragastric pH profile on the chemical composition and microstructure of gastric digesta	176
5.4.3 Link between starch hydrolysis during gastric digestion with physical breakdown of the diets and gastric emptying of starch.....	187
5.5 Conclusions	195
CHAPTER 6. The impact of gastric digestion and emptying of rice- and wheat- based foods on their digestion in the small intestine, glucose absorption, and glycemic response	197
6.1 Abstract	197
6.2 Introduction	199
6.3 Materials and methods	200
6.3.1 Study diets and reference diets preparation	200
6.3.2 Study design and sampling protocol	201
6.3.3 Sample analyses	201
6.3.4 Data and statistical analysis	202
6.4 Results	208
6.4.1 Glycemic response parameters.....	208
6.4.2 Particle size distribution of intestinal digesta.....	214
6.4.3 Intestinal digesta chemical properties and ileal starch digestibility.....	215
6.4.4 Portal vein plasma glucose concentration.....	224
6.5 Discussion	226
6.5.1 Food structure affected glycemic response, with a link to gastric emptying rate.....	226
6.5.2 Possible mechanisms of the effect of gastric digestion on glycemic response.....	229
6.5.3 Limitations of the study	239
6.6 Conclusions	242
CHAPTER 7. Contribution of the proximal and distal gastric phases to the breakdown of starch-rich foods during static <i>in vitro</i> gastric digestion.....	244

7.1	Abstract	244
7.2	Introduction	246
7.3	Materials and methods	249
7.3.1	Materials.....	249
7.3.2	Digestion procedure	249
7.3.3	Cooked food characterization	250
7.3.4	Solid fraction and whole digesta mixture characterization	250
7.3.5	Liquid and suspended solid fraction characterization	251
7.3.6	Data and statistical analysis	252
7.3.7	Statistical analysis	254
7.4	Results	255
7.4.1	Characteristics of the selected food products	255
7.4.2	Whole digesta mixture properties after proximal digestion	256
7.4.3	Properties of solid digesta fraction after proximal-distal digestion	261
7.4.4	Properties of liquid and suspended solid digesta fractions after the proximal and distal phase	274
7.5	Discussion	281
7.5.1	Food breakdown during the proximal phase occurred through leaching of soluble and/or small particles	281
7.5.2	Increased fluid uptake in the distal phase caused softening of solid digesta fraction, but the softening process was not enhanced by proximal phase ..	283
7.5.3	Synergistic effect of proximal and distal phase on the characteristics of liquid and suspended solid fractions of digesta.....	290
7.5.4	Food structure and geometry determine breakdown mechanisms during proximal and distal phase of gastric digestion	292
7.6	Conclusions	297
	CHAPTER 8. Overall discussion, conclusions and future recommendations	299
8.1	Overall discussion and conclusions	299
8.2	Future recommendations	313
	REFERENCES	318
	APPENDIX A	344
	APPENDIX B	346
	APPENDIX C	352
	APPENDIX D	356

APPENDIX E	364
APPENDIX F.....	375
APPENDIX G.....	386

LIST OF TABLES

Table 2.1 Examples of food matrix containing starch granules, showing different continuous and discontinuous phases in the food matrix structure.....	13
Table 2.2 Experimental approaches to monitor physical changes during gastric digestion of solid or semi-solid foods, not limited to starch-based foods. For the definition of length scale of structural breakdown characterized, see Figure 2.1 and Figure 2.3.	34
Table 2.3 Examples of food structure, physical breakdown during mastication, and resulting bolus properties	37
Table 2.4 Previous investigations on the relationship between food structure, gastric emptying rate (GER), and glycemic response (GR) of starch-based foods.	50
Table 2.5 Examples of <i>in vitro</i> starch digestion studies and their comparison with <i>in vivo</i> glycemic responses (GRs).	60
Table 2.6 The food breakdown classification system (FBCS) framework (Bornhorst et al., 2015).	64
 Table 3.1 Manufacturer and cooking method for each of the study diets.	79
 Table 4.1 Composition, chemical properties, and physical properties of the cooked study diets	112
Table 4.2 Statistical significance from mixed model ANOVA of diet type, digestion time, stomach region, and their interactions on the properties of gastric digesta and gastric emptying.	114
Table 4.3 Saturation ratio (SR) and pH values of digesta from proximal and distal stomach regions over 240 min digestion.....	117
Table 4.4 Total moisture added and moisture addition rate to the diets.....	118
Table 4.5 Particle area parameters given by the Rosin-Rammler model (Eqn. 4.5) fit to particle areas measured via image analysis ($R^2 > 0.83$ for all model fits). Particles per gram dry matter was determined based on mass of sample spread on dishes and moisture content during digestion (Table C.1)	122
Table 4.6 Rheological property data from shear rate sweep tests and oscillatory testing. Shear rate sweep data including Herschel-Bulkley model (Eqn. 4.7) fit parameters (average $R^2 = 0.90$ across all samples). Shear stress measured at a shear rate of 0.2 s^{-1} was included to represent a physiologically relevant shear rate in the gastric environment. Oscillatory data were measured at 1 Hz	129
Table 4.7 Weibull kinetic parameters (estimated with Eqn. 4.6) used to calculate the softening half-time of the study diets in the proximal and distal stomach regions presented in Figure 4.7.....	131
Table 4.8 Goodness-of-fit of Weibull and gastric emptying models for the averaged values of the experimental data (normalized hardness data for Weibull model, gastric digesta mass retention for gastric emptying models).....	132
Table 4.9 Gastric emptying parameters (expressed as predicted parameter \pm 95% confidence interval) and predicted emptying half-time of dry matter and whole stomach content.	134
Table 4.10 Spearman's correlation coefficients (r_s) between different physical properties measured in this study. Moderate to very high correlations ($r_s = \pm$ (0.5 to	

1.0)) are shown in bold font. Values presented as r_s followed by the level of statistical significance (see note below the table). 136

Table 5.1 Statistical significance of diet type, digestion time, stomach region, digesta fraction (specific for maltose and NH_2 equivalent analyses), and dry matter remaining in the stomach (specific for intragastric pH) on the pH, chemical content, and particle size parameters of gastric digesta as well as total starch emptying..... 173

Table 5.2 Reducing sugar and free amino groups content in the cooked diets used in the study 180

Table 5.3 Mean diameters and specific surface area (mean \pm SE, $4 \leq n \leq 6$) of the suspended solid fraction of *in vivo* gastric digesta..... 189

Table 5.4 Concentration of maltose in the suspended solid and liquid fractions in the overall digesta (proximal and distal stomach regions combined together) at different digestion time points ($n = 258$ data points)..... 195

Table 6.1 Glycemic response parameters obtained from glycemic response data in catheterized pigs; Gompertz model parameters for iAUC and change in plasma glucose data relative to the baseline (Δ glucose) in catheterized pigs. The goodness of fit of the Gompertz model to the cumulative values of iAUC or change in plasma glucose (Δ plasma) for each diet is indicated by the R^2 . Values are presented as mean \pm SE ($5 < n \leq 7$, except $n = 13$ for bread).....211

Table 6.2 Statistical significance of diet type, digestion time and small intestinal or vein section (where relevant), and batch of pigs on the small intestinal digesta properties.....217

Table 6.3 Mean diameters and specific surface area (mean \pm SE, $4 \leq n \leq 6$) of the intestinal digesta from the proximal jejunum, distal jejunum, and ileum sections.218

Table 6.4 Michaelis-Menten parameters (expressed as predicted parameters \pm 95% confidence interval) for the total intestinal glucose, total intestinal maltose, and portal plasma glucose concentration shown in Figure 6.7225

Table 6.5 Ileal starch digestibility at 120- and 240 min digestion (mean \pm SE ($9 \leq n \leq 12$, pooled across 120 and 240 min digestion time), and glucose flow and maltose flow in the ileum at different digestion time points (mean \pm SE, $3 \leq n \leq 6$), estimated with Eqn. 6.2 and 6.3, respectively225

Table 6.6 Difference between total intestinal maltose measured in the reducing sugar assay with theoretical total intestinal maltose calculated from the glucose data (mean \pm SE, $4 \leq n \leq 6$)234

Table 7.1 Physical properties and chemical content of the selected food products. Values are shown as mean \pm SD ($n = 6$ for each data point)256

Table 7.2 Statistical significance of food type, proximal phase, distal phase, and their interaction effects on the physicochemical properties of digesta from proximal-distal digestion and proximal digestion.258

Table 7.3 Softening kinetics parameter of the food products in the proximal digestion (obtained by fitting the data points to Eqn. 7.2) used to calculate the $t_{1/2, \text{softening}}$ presented in Figure 7.1A.260

Table 7.4 Particle size distribution parameters of whole digesta mixture in the proximal digestion at various proximal phase durations260

Table 7.5 Mitscherlich equation (Eqn. 7.1) parameters of mass retention profile of digesta solid fraction at various proximal phase durations	265
Table 7.6 Softening kinetics parameter of the food products in the proximal-distal digestion at different proximal phase durations, obtained by fitting the data points from each replicate of food × proximal phase combination to Eqn. 7.2.....	269
Table 7.7 Softening kinetics parameter of the food products in the proximal-distal digestion at different proximal phase durations, obtained by fitting all data points for each food × proximal phase combination altogether to Eqn. 7.2 to estimate the overall trends for each treatment.....	270
Table 7.8 Selected particle size parameters of the solid digesta fraction after varying proximal phase followed by 30 or 180 min distal phase in the proximal-distal digestion.....	272
Table 7.9 Additional particle size distribution parameters of digesta solid fraction after varying proximal phase followed by 30 or 180 min distal phase in the proximal-distal digestion... ..	273
Table 7.10 Volume mean diameter (D[4,3]) and surface area mean diameter (D[3,2]) of the liquid and suspended solid digesta fractions measured using Mastersizer	277

LIST OF FIGURES

Figure 1.1 Human digestive organs, their typical working conditions (vary depending on the consistency of the food and amount of food consumed), and their contributions in solid starch-based foods breakdown (the working conditions are adapted from Bornhorst and Singh (2014), Fallingborg (1999), Flynn (2012), Huckabee et al. (2018), and Versantvoort, van de Kamp, and Rompelberg (2004)).	2
Figure 2.1 The wide ranges of structural levels of starch-based foods and analyses used to observe particular structures within its size range (adapted from Conde-Petit (2003) with modifications on the mesoscale definition based on Dona et al. (2010), Dhital et al. (2017), and Mandalari et al. (2018)).	9
Figure 2.2 Roles of the proximal and distal stomach in gastric digestion of solid starch-based foods (adapted from Rodríguez Varón and Zuleta (2010) with modifications).	19
Figure 2.3 Cooked rice grain as an example of the structure of starch-based foods at multiple length scales before and after <i>in vitro</i> or <i>in vivo</i> gastric digestion. Images shown are not necessarily from the same study and they are shown as representatives at each length scale	33
Figure 3.1 Summary of the experimental approach used in this thesis report and how they relate to the research objectives.	75
Figure 3.2 Selected food systems to be used throughout the chapters of this thesis. The ‘Physical structure’ row indicates the structural differences of the food systems as a result of processing. The food systems will be referred to by the notation listed in the ‘Diet name’ row throughout this thesis report. Characteristic dimensions of the food systems are denoted by d for diameter, ℓ for length, w for width, and h for thickness.	76
Figure 3.3 Example of the appearance of 15 mm \times 15 mm bread used as the reference diet for the blood sampling day meal in the glycemic response measurement study.	80
Figure 3.4 Setup of <i>in vivo</i> glycemic response measurement followed by gut content collection studies (A). Setup of <i>in vivo</i> gut content collection study (B)	84
Figure 3.5 Diagram of the glycemic response and gut content collection studies. Stages in the red-dashed box correspond to the glycemic response study, stages in the blue-dashed box correspond to the gut content collection study (A). Timing of sampling for either the gut content collection or glycemic response study (B).	85
Figure 3.6 Photograph of the long-term catheter used in the glycemic response study (A). The appearance of ear catheter that extends to the jugular vein of each pig (B). The application of tape on both ears of the pigs provided balanced weight on the catheterized and non-catheterized ears (C).	87
Figure 3.7 Photographs of gastric digesta of pigs fed with pasta (top row), rice grain (middle row), or rice noodle (bottom row) after 30 (A), 60 (B), 120 (C), or 240 (D) min digestion time.	92
Figure 3.8 Diagram of gastric digesta and small intestinal sampling and types of samples characterized throughout Chapter 4, 5, and 6. The thesis chapters related to the measured properties are indicated by different color codes: blue (Chapter 4), yellow (Chapter 5), and red (Chapter 6).	93

Figure 3.9 Schematic diagram illustrating the rationale behind the experimental design. The filling of proximal stomach results in different locations of food bolus in this region, thus different contact time with α -amylase. Intra-gastric regions of interest simulated by the different proximal duration are highlighted by red dashed lines. Red arrow in each proximal filling scenario indicates the movement of food bolus from the intra-gastric region of interest to the distal phase (A). Block flow diagram of the different steps for proximal or proximal-distal digestion experiments (B). 96

Figure 4.1 Total moisture addition over time during gastric digestion of the six Study diets. Due to the wide span of the y-axis, the error bars of some of the data points are too small to be seen in the figure. (A). Relationship between moisture addition rate at different digestion times and initial buffering capacity of the diets; parallel data points on the x-axis indicate one diet type – for readability, only the 30-min points were labeled with the diet names (B)..... 116

Figure 4.2 Examples of binary images of gastric digesta used for extraction of particle size parameters for the wheat-based diets before digestion and after 30 and 240 min gastric digestion. The scale bar represents 1 cm and is the same for all images. 120

Figure 4.3 Examples of binary images of gastric digesta used for extraction of particle size parameters for the rice-based diets before digestion and after 30 and 240 min gastric digestion. The scale bar represents 1 cm and is the same for all images. 121

Figure 4.4 Bar charts showing the initial (before digestion) particle area distribution and the particle area distribution in proximal and distal stomach digesta during 240 min gastric digestion of (A) rice grain, (B) semolina, (C) rice couscous, (D) couscous, (E) rice noodle, and (F) pasta. 124

Figure 4.5 Example of flow properties of couscous digesta from the proximal (A-B) and distal (C-D) regions of the stomach after 30 (A, C) and 240 (B, D) min gastric digestion. 125

Figure 4.6 Example of viscoelastic properties of couscous digesta from the proximal (A-B) and distal (C-D) regions of the stomach after 30 (A, C) and 240 (B, D) min gastric digestion. 127

Figure 4.7 Normalized hardness values of gastric digesta from (A) proximal and (B) distal stomach regions during 240 min digestion (mean \pm SE, $4 \leq n \leq 6$). The softening half-times of the diets in the proximal and distal stomach regions shown in the table below the figures were predicted from the softening curves. 131

Figure 4.8 Gastric emptying of dry matter (A,C) and whole stomach content (B,D) of pigs fed with wheat-based diets (A,B) or rice-based diets (C,D) during 240 min of digestion. Dry matter half-emptying times from (A) and (C) were plotted against initial median particle area (E) of the cooked diets or gastric softening half-time (F). Gastric softening half-time for each diet was represented by the longest softening half-time between the proximal and distal stomach regions for each diet..... 133

Figure 4.9 Schematic diagram showing the possible relationships between food properties, gastric digestion, and gastric emptying investigated in this study. The heads of the arrows indicate relationships between food and digesta properties and gastric phenomena. Note that the actual relationships are complex and more specific links may be present, but these complex mechanisms are not fully delineated in the illustration for the sake of simplicity. 141

Figure 4.10 Relationships between dry matter emptying half- time with (A) total caloric content, (B) portion size, (C) total protein content, (D) total starch content, (E) total amylose content, and (F) total dietary fiber content of the diets.....	142
Figure 5.1 Example stomach with digesta and approximate pH measurement locations, with description of analyses done for each gastric sample. The dashed line indicates the approximate separation between proximal and distal stomach regions (A). Examples of three fractions obtained after centrifugation of gastric digesta from the proximal (prox) or distal (dist) region when maximum separation was obtained. The approximate separation between fractions is indicated by dashed red lines (B).....	162
Figure 5.2 Example data sets of maltose concentration change over time to estimate apparent salivary amylase in the gastric digesta of pigs fed with couscous after 30 min (A) and 120 min (B) digestion. Dotted lines indicate linear regression lines used to estimate the apparent amylase activity.....	167
Figure 5.3 Illustration of sample sectioned from (A) rice grain and (B) pasta or rice noodle digesta particle used for confocal microscopy observation. The eye with arrow pointing to one side of the section indicates the orientation of the observation under the microscope.	168
Figure 5.4 Color maps of intragastric pH distribution of the six study diets over 240 min gastric digestion (averaged from 4 to 6 pigs for each measurement location). Color maps for one diet type are located within the same column. The stomach shape was approximated from an image of a of full stomach from the study (A). Apparent salivary amylase activity at various digesta pH ranges for each diet. Averaged activity across diets is shown in the inset figure (B).....	172
Figure 5.5 Relationship between apparent salivary amylase activity in gastric digesta with pH >6 (n = 33 data points) and the initial moisture content of each diet (A). Apparent salivary amylase activity at different digestion time points in the proximal and distal stomach, averaged across all diets (B)	176
Figure 5.6 Phase separation of digesta to different fractions (column A), and maltose (column B) and free amino groups (column C) distribution in wet digesta fractions during 240 min digestion in the proximal (Prox) and distal (Dist) stomach regions....	179
Figure 5.7 Concentrations of maltose and free amino groups in different wheat-based (A) or rice-based (B) digesta fractions during 240 min digestion in the proximal (prox) and distal (dist) stomach regions.....	180
Figure 5.8 Comparison between reducing sugar and starch in wheat-based (A) and rice-based (B) digesta expressed as total reducing sugar (summed across the digesta fractions) relative to total available starch in the proximal stomach, distal stomach, and overall stomach (proximal + distal combined) digesta (first row) or concentration of reducing sugar (summed across the digesta fractions) in digesta dry matter as a function of starch emptying profile (second row)	181
Figure 5.9 Confocal scanning laser microscopy images of the six diets before digestion, and after 60- or 240-min digestion in the proximal and distal stomach regions from selected pigs.	184
Figure 5.10 Scanning electron microscope (SEM) images of the six diets before digestion, and after 60- or 240-min digestion in the proximal and distal stomach regions from selected pigs	186

Figure 5.11 Wet mass retention of digesta (Figure 4.8B and D) integrated with the phase separation data (Figure 5.6A) to estimate the total fraction (on a wet basis) of liquid, suspended solids, and solids in digesta of semolina (A), couscous (B), pasta (C), rice grain (D), rice couscous (E), and rice noodle (F).....	188
Figure 5.12 Particle size distribution of the suspended solid fraction of distal (dist) gastric digesta of pigs fed with semolina (A), couscous (B), pasta (C), rice grain (D), rice couscous (E), and rice noodle (F) from 30 – 240 min gastric digestion	190
Figure 5.13 Particle size distribution of the small particle fraction of proximal (prox) gastric digesta of pigs fed with (A) semolina, (B) couscous, (C) pasta, (D) rice grain, (E) rice couscous, and (F) rice noodle after 30, 60, 120, or 240 min digestion	191
Figure 6.1 Plasma glucose concentration of individual pigs following the consumption of bread (A), semolina (B), rice grain (C), couscous (D), rice couscous (E), pasta (F), and rice noodle (G).....	210
Figure 6.2 Averaged glycemic response curves (mean \pm SE, $5 < n \leq 7$, except $n = 13$ for bread) for small-sized (A) and larger-sized diets (B) generated by averaging the values from individual pigs at each digestion time. Relationship between glycemic response parameters with starch emptying half-time (C-D), starch emptying rate parameter, k (E-F), and gastric softening half-time (G-H) of the diets.....	212
Figure 6.3 Example of Gompertz model fit to change in plasma glucose (left column) and iAUC (right column) cumulative values to data set obtained from individual pig (A-B), or averaged glycemic response data for bread (C-D), rice couscous as a representative of smaller-sized diets (E-F), and pasta as a representative of larger-sized diets (G-H).	213
Figure 6.4 Particle size distribution (PSD) of the suspended solid fraction of proximal stomach and distal stomach digesta, as well as small intestinal digesta obtained from the proximal jejunum, distal jejunum, and ileum regions of pigs fed with semolina (A), couscous (B), pasta (C), rice grain (D), rice couscous (E), and rice noodle (F) from 30 (—), 60 (---), 120 (···), and 240 (—) min digestion	220
Figure 6.5 Glucose and maltose concentration in the small intestinal digesta of semolina (A), rice grain (B), couscous (C), rice couscous (D), pasta (E), and rice noodle (F) obtained from the duodenum (“D”), proximal jejunum (“PJ”), distal jejunum (“DJ”), ileum (“I”), and terminal ileum (“TI”) sections at different digestion times.	221
Figure 6.6 Total mass of maltose (column A) and total mass of glucose (column B) in the small intestinal digesta, and portal vein plasma glucose concentration (column C) of semolina (row 1), couscous (row 2), pasta (row 3), rice grain (row 4), rice couscous (row 5), and rice noodle (row 6)	222
Figure 6.7 Michaelis-Menten fit to cumulative intestinal glucose (column A), intestinal maltose (column B), and portal vein plasma glucose concentration (column C).	223
Figure 6.8 Relationship between: total mass of intestinal glucose and intestinal maltose (total 126 data points, 3 data points were not included due to outlier removal) (A); V_{\max} total mass of intestinal glucose and V_{\max} total mass of intestinal maltose (B); K_m total mass of intestinal glucose and K_m total mass of intestinal maltose (C).....	226
Figure 6.9 Summary of glycemic response regulation upon the ingestion of starch-rich food. The actual process involves more complex mechanisms, and the diagram is presented with simplification to aid the explanation in the current study.....	231

Figure 6.10 Relationships between: V_{\max} portal glucose and starch emptying half-time (A); K_m portal glucose and starch emptying half-time (B); V_{\max} portal glucose and V_{\max} total mass of intestinal glucose (C); K_m portal glucose and K_m total mass of intestinal glucose (D); maltose in the 30-min gastric digesta liquid and suspended solid fractions (from Chapter 5, Table 5.4) with starch emptying half-time (E), $\Delta\text{max}_{\text{overall}}$ (F), and $i\text{AUC}_{\text{overall}}$ (G).235

Figure 6.11 Relationships between starch emptying half-time (A-C), $\Delta\text{max}_{\text{overall}}$ (D-F), and $i\text{AUC}_{\text{overall}}$ (G-I) with maltose in the gastric digesta liquid and suspended solid fractions at 60 min (first column), 120 min (second column), or 240 min (third column) digestion.240

Figure 7.1 Textural changes of the foods after being subjected to various proximal phase durations in the proximal digestion and the calculated $t_{1/2, \text{softening}}$ values. Softening kinetic parameters used to calculate $t_{1/2, \text{softening}}$ are given in Table 7.3. The hardness at each time (H_t) was normalized by the hardness of undigested foods (H_0) with lubrication (see section 7.3.4.2) (A). Bar charts showing the particle area distribution of couscous (B), rice couscous (C), pasta (D), rice noodle (E), and rice grain (F) before digestion (Initial), whole digesta mixture after different proximal phase durations (shown as 0 min distal phase), and digesta solid fraction after selected proximal \times distal phase durations in proximal-distal digestion.....259

Figure 7.2 Wet mass retention (W_t/W_0 (dimensionless); left column) and dry matter retention (DM_t/DM_0 (dimensionless); right column) profiles of the solid fraction of digesta during the distal phase after 0 min (■), 2 min (●), 15 min (▲), or 30 min (◇) proximal phase. Figures within the same row correspond to one type of food: couscous (A-B), rice couscous (C-D), pasta (E-F), rice noodle (G-H), and rice grain (I-J). All values were normalized against the wet mass or dry matter of the cooked (undigested) food used in each sample263

Figure 7.3 Mitscherlich equation (Eqn. 7.1) fit to the wet mass retention (A) and dry mass retention (B) data from each experimental replicate of proximal-distal digestion.....264

Figure 7.4 Moisture changes (left column) and normalized hardness (H_t/H_0 ; right column) profiles of the solid fraction of digesta during the distal phase after 0 min (■), 2 min (●), 15 min (▲), or 30 min (◇) proximal phase. Figures within the same row correspond to one type of food: couscous (A-B), rice couscous (C-D), pasta (E-F), rice noodle (G-H), and rice grain (I-J)267

Figure 7.5 Weibull model (Eqn. 7.2) fitting to the H_t/H_0 dataset for each experimental replicate. Data points from the same replicate are indicated with the same symbol and color: black (■), blue (*), and red (×), the model fit has the same color as the symbol for its respective replicate268

Figure 7.6 Particle size distribution (PSD) of liquid and suspended solid fractions in the digesta at different proximal phase durations, over 15 min (—), 60 min (- - -), or 180 min (···) distal phase, established by averaging the PSD data of three replicates.279

Figure 7.7 °Brix profiles during the distal phase, after 0 min (■), 2 min (●), 15 min (▲), or 30 min (◇) proximal phase (left column) and hydrolyzed starch content during the proximal phase after 15 min (○) or 180 min (●) distal phase (right column). Figures

within the same row correspond to one type of food: couscous (A-B), rice couscous (C-D), pasta (E-F), rice noodle (G-H), and rice grain (I-J)	280
Figure 7.8 Examples of the appearance of the solid fraction of rice grain digesta before digestion, and after 0 or 30 min proximal phase followed by 30 or 180 min distal phase, indicating the breakdown of the rice kernels into smaller parts after 180 min distal phase at both proximal phase durations. Pictures for each proximal phase were taken from the same day of experiment.	290
Figure 7.9 Hypothesized breakdown mechanisms of the food structures due to digestive fluids diffusion during proximal and distal phase in the current study, as affected by the geometry and direction of digestive fluid diffusion into the food matrix..	295
Figure 8.1 Summary of the findings from this PhD project. CLSM images of the cooked diets are presented below the diet pictures to indicate the microstructural differences of the diets	301
Figure 8.2 Comparison between <i>in vivo</i> and <i>in vitro</i> particle size distribution of suspended solid gastric digesta fraction. Figures within the same row correspond to one type of diet.....	306
Figure 8.3 <i>In vitro-in vivo</i> correlation between the gastric softening half-time <i>in vivo</i> from Figure 4.7 and <i>in vitro</i> proximal digestion from Figure 7.1A (A) and proximal-distal digestion at 0 min proximal phase from Table 7.6 (B). <i>In vitro-in vivo</i> correlation between the maltose content in the liquid + suspended solid fractions of 30-min <i>in vivo</i> digesta (proximal and distal stomach data combined together) from Table 5.4 with 2-min proximal-15-min distal <i>in vitro</i> digesta from Figure 7.7B (C); <i>in vivo</i> glycemic response $\Delta\text{max}_{\text{overall}}$ from Table 6.1 with 2-min proximal-15-min distal <i>in vitro</i> digesta from Figure 7.7B (D); and <i>in vivo</i> glycemic response $\text{iAUC}_{\text{overall}}$ from Table 6.1 with 30-min proximal-15-min distal <i>in vitro</i> digesta from Figure 7.7B (E).	312

LIST OF ABBREVIATIONS

ANOVA	Analysis of variance
BW	Body weight
CLSM	Confocal laser scanning microscopy
db	Dry basis
DM	Dry matter
GE	Gastric emptying
GI	Glycemic index
GIT	Gastrointestinal tract
GL	Glycemic load
GR	Glycemic response
iAUC	Incremental area under the curve
n	Number of replicates for each treatment
PSD	Particle size distribution
SA/V	Surface area per volume
SD	Standard deviation
SE	Standard error
SEM	Scanning electron microscopy
SGF	Simulated gastric fluid
SR	Saturation ratio
SSF	Simulated salivary fluid
$t_{1/2,DM\ GE}$	Dry matter gastric emptying half-time
$t_{1/2,softening}$	Digesta softening half-time
$t_{1/2,starch\ GE}$	Starch emptying half-time
$t_{1/2,whole\ GE}$	Whole stomach content emptying half-time
v/v	Volume per volume
WHC	Water holding capacity
w/w	Weight per weight
w/v	Weight per volume

LIST OF SYMBOLS

Symbol	Description	Unit
A	The asymptote value of the mass retention curve in <i>in vitro</i> digestion	[-]
A_0	Theoretical initial mass retention without proximal phase (equals to one) in <i>in vitro</i> digestion	[-]
A_G	The plateau value of the growth curve	(mg/dL).min
b	Broadness of the particle size distribution	[-]
d	Particle diameter	mm
DM_t/DM_0	Dry matter retention	[-]
G'	Storage modulus	Pa
G''	Loss modulus	Pa
H_0	The initial hardness of the diet	N
H_t	Hardness of the digesta at time t	N
H_t/H_0	Normalized hardness	[-]
K	Consistency index	Pa·s ⁿ
k	The gastric emptying rate of starch in the dry matter of digesta	min ⁻¹
k_{DM}	The gastric emptying rate coefficient of dry matter	min ⁻¹
k_G	Growth rate coefficient of the growth curve	min ⁻¹
kh	The scale parameter of digesta softening curve	min ⁻¹
k_m	A coefficient describing the rate of mass retention change in <i>in vitro</i> digestion	min ⁻¹
K_m	Half-time to reach the maximum accumulation in the Michaelis-Menten equation	min
k_{whole}	A dimensionless constant representing lag phase in dry matter gastric emptying curve	[-]
M_0	Initial dry mass of the cooked food for each <i>in vitro</i> digestion	[-]
M_t	Dry or wet mass of the digesta at distal time t in <i>in vitro</i> digestion	[-]
n	Flow index	[-]
Q	Cumulative area (%) of particle size distribution generated from image analysis	[-]
t	Time	min
T_i	Time at inflection of the growth curve	min
V_{max}	Maximum accumulation of portal glucose, total intestinal glucose, or total intestinal maltose in the Michaelis-Menten equation	mg/dL, g glucose, g maltose
W_t/W_0	Whole stomach content retention (<i>in vivo</i> data), digesta wet mass retention (<i>in vitro</i> data)	[-]
x	A single area measurement of particle size distribution generated from image analysis	mm ²
x_{10}	The area of a theoretical sieve aperture through which 10% of the particle area can pass	mm ²

Symbol	Description	Unit
x_{50}	The area of a theoretical sieve aperture through which 50% of the particle area can pass	mm ²
x_{90}	The area of a theoretical sieve aperture through which 90% of the particle area can pass	mm ²
β	The theoretical y-intercept in the starch gastric emptying curve	[-]
β_{DM}	The theoretical y-intercept in the dry matter gastric emptying curve	[-]
β_h	The shape factor of digesta softening curve	[-]
β_{whole}	A parameter indicating the concavity of whole stomach content emptying curve	[-]
τ	Shear stress	Pa
τ_0	Yield stress	Pa
$\dot{\gamma}$	Shear rate	s ⁻¹

LIST OF PUBLICATIONS AND PRESENTATIONS

Peer-reviewed papers

- Nadia, J.**, Bronlund, J., Singh, R.P., Singh, H., and Bornhorst, G.M. (2021). Structural breakdown of starch-based foods during gastric digestion and its link to glycemic response: *In vivo* and *in vitro* considerations. *Comprehensive Review in Food Science and Food Safety*, 2021, 20:1–39.
- Nadia, J.**, Olenskyj, A.G., Stroebling, N., Hodgkinson, S.M., Estevez, T.G., Subramanian, P., Singh, H., Singh, R.P., and Bornhorst, G.M. (2021). Tracking physical breakdown of rice- and wheat-based foods with varying structures during gastric digestion and its influence on gastric emptying in a growing pig model. *Food & Function*. 2021, 12: 4349-4372.
- Nadia, J.**, Olenskyj, A.G., Subramanian, P., Hodgkinson, S.M., Stroebling, N., Estevez, T.G., Singh, R.P., Singh, H., and Bornhorst, G.M. Influence of food macrostructure on the kinetics of acidification in the pig stomach: implications for starch hydrolysis and starch emptying rate. *Submitted to Food Chemistry* (Jul 2021).
- Nadia, J.**, Bronlund, J., Singh, H., Singh, R.P., and Bornhorst, G.M. Contribution of the proximal and distal gastric phases to the breakdown of cooked starch-rich solid foods during static *in vitro* gastric digestion. *Submitted to Food Research International* (Mar 2022).

Conference presentations

- Nadia, J.**, Bornhorst, G. M., Bronlund, J., Singh, R. P. and Singh, H. Predicting the breakdown of carbohydrate-based food bolus during gastric digestion. Biomouth Meeting. Christchurch, New Zealand, 29th – 30th October 2018. (Oral presentation)
- Nadia, J.** Modeling food breakdown during gastric digestion. Riddet Institute Visualise Your Thesis Competition 2019. Palmerston North, New Zealand, 22nd July 2019. (Video Presentation)
- Nadia, J.**, Olenskyj, A. G., Subramanian, P., Hodgkinson, S., Stroebling, N., Singh, R. P., Singh, H., Bornhorst, G. M. Softening of carbohydrate-based foods in the proximal and distal stomach during gastric digestion: Case study with rice- and

wheat noodles. Food Structure, Digestion, and Health Conference. Rotorua, New Zealand, 1st – 3rd October 2019. (Poster presentation – received highly commended award)

Nadia, J., Olenskyj, A. G., Subramanian, P., Hodgkinson, S., Stroebinger, N., Singh, R. P., Singh, H., Bornhorst, G. M. Gastric breakdown behavior of carbohydrate-based foods with different structures and their impact on glycemic response in a growing pig model. Institute of Food Technologists' SHIFT20 Virtual Conference. 12th – 15th July 2020. (Poster presentation – awarded third place in the International Division Malcolm Bourne Research Competition)

Nadia, J. The role of the stomach in the digestion of starch-rich foods: not all foods are broken down at the same rate. Massey University Postgraduate Food Science Symposium 2020. Palmerston North, New Zealand. 25th September 2020. (Oral presentation)

Nadia, J. *In vivo* investigation of the stomach as an environment for biochemical digestion of starch-based foods. Riddet Institute Student Colloquium 2021. Wellington, New Zealand, 7th – 9th April 2021. (Oral presentation)

Nadia, J., Olenskyj, A. G., Subramanian, P., Hodgkinson, S., Stroebinger, N., Singh, R. P., Singh, H., Bornhorst, G. M. Effect of food structure on starch hydrolysis during gastric digestion, starch emptying, and glucose absorption *in vivo*. Virtual International Conference on Food Digestion 2021. 6th – 7th May 2021. (Oral presentation – awarded Best Oral PhD Presentation)

Nadia, J., Olenskyj, A. G., Stroebinger, N., Hodgkinson, S. M., Estevez, T. G., Subramanian, P., Singh, H., Singh, R. P., Bornhorst, G. M. Investigating the extent of starch digestion during gastric digestion of starch-rich foods in a growing pig model. Institute of Food Technologists' FIRST Virtual Conference. 18th – 21st July 2021. (Poster presentation and oral presentation – awarded finalist in the Carbohydrate Division Graduate Student Oral Competition)

CHAPTER 1. Introduction and project overview

1.1 Background

Nutrients are extracted from food through a series of digestion processes in the gastrointestinal tract (GIT), making them readily available for absorption, where they ultimately can be used as a source of energy and building materials for growth. An adult typically consumes about 800 g food and up to 2 L of water daily (Feher, 2017b; Smith & Morton, 2010b); most of the energy consumption is derived from carbohydrates (Sadler, 2011). Compared to other sources of carbohydrates, starch provides a readily accessible form of energy to the body via hydrolysis into glucose prior to absorption in the small intestine into the bloodstream (Lentle & Janssen, 2011). These processes occur slowly in the gut, causing a gradual release of glucose to the bloodstream that changes the level of blood glucose after meal (Jenkins et al., 1981), known as postprandial glycemic response. The postprandial glycemic response has been shown to influence health outcomes, such as type 2 diabetes, obesity, and cardiovascular disease (Blaak et al., 2012). Consequently, the impact of consumption of starch-based foods on glycemic response has been studied extensively, but mostly on the microstructure of the starch and their hydrolysis in the small intestine, where the ingested food has already lost most of its macrostructural integrity. Since starch-based foods are commonly consumed in solid or semi-solid form, it is important to understand their breakdown processes during digestion and how this breakdown may impact starch hydrolysis and absorption.

The digestion processes of solid and semi-solid foods begin with mastication in the mouth and ends when digestible and absorbable nutrients have been removed from the food, leaving waste products to be excreted in the form of feces (Feher, 2017c). To

provide suitable conditions for these processes, each organ in the GIT has its own working pH, transit time, and function (Figure 1.1). During transit in each organ, ingested starch-based foods undergo structural changes through physical and biochemical breakdown processes that mainly occur in the mouth, stomach, and small intestine. The mouth and stomach play a major role in the mechanical, and to some extent, biochemical breakdown of starch, whereas the small intestine serves as the major site for starch digestion and nutrient absorption (Dahlqvist & Borgstrom, 1961; Hoebler, Devaux, Karinthi, Belleville, & Barry, 2000; Martens, Flécher, et al., 2019; Meyer, 1980).

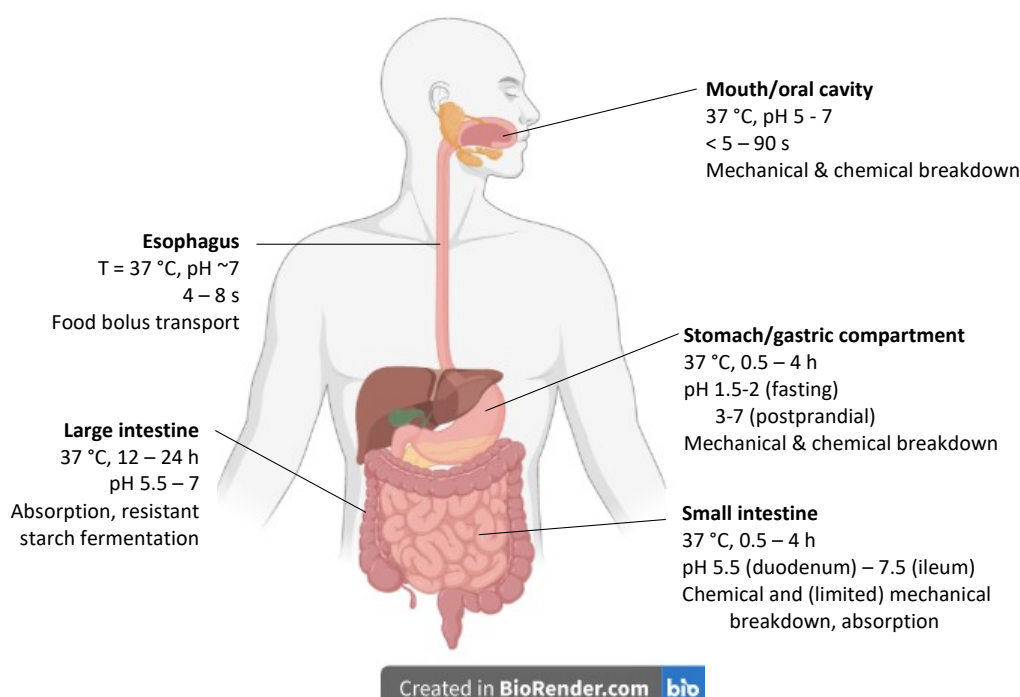


Figure 1.1 Human digestive organs, their typical working conditions (vary depending on the consistency of the food and amount of food consumed), and their contributions in solid starch-based foods breakdown (the working conditions are adapted from Bornhorst and Singh (2014), Fallingborg (1999), Flynn (2012), Huckabee et al. (2018), and Versantvoort, van de Kamp, and Rompelberg (2004)).

Sufficient breakdown of the physical structure of the food is needed to ensure the efficiency of absorption of nutrients from solid or semi-solid food in the small intestine

(Hoebler et al., 1998; Mourot et al., 1988; Read et al., 1986). As such, the macrostructural breakdown of the food matrix will be a determinant in the rate of hydrolysis of macronutrients and their absorption in the small intestine (Bornhorst, Ferrua, & Singh, 2015; Read et al., 1986; Tamura, Okazaki, Kumagai, & Ogawa, 2017). In the context of starch digestion, this implies that the extent of structural breakdown of solid or semi-solid starch-based foods that takes place during mastication and gastric digestion is crucial for the subsequent glucose absorption process. Mastication and gastric digestion are important to consider when studying starch digestion, especially when *in vitro* approaches are used to simulate *in vivo* physiological processes. While more studies on the effect of mastication on glycemic response have been conducted in the recent years (Choy et al., 2021; Ranawana, Henry, & Pratt, 2010; Ranawana, Leow, & Henry, 2014; Sun, Ranawana, Tan, Quek, & Henry, 2015; Tamura et al., 2017; Zhu, Hsu, & Hollis, 2014), gastric digestion is still less studied. There is a gap in understanding the relationship between food structure, the breakdown of starch-based foods during gastric digestion, how both food structure and its breakdown impacts gastric emptying processes and small intestinal digestion, and ultimately glycemic response. Understanding the relationships between these aspects is crucial as part of a food structure-based strategy for glycemic response management.

1.2 Research objectives

This PhD project has an overall goal to understand the contribution of gastric digestion to the glycemic response of starch-based foods with varying macro- and microstructures. Specific research objectives are as follows:

1. To investigate the effect of food composition and structure on the regulation of gastric secretion and food physicochemical breakdown process in an *in vivo* stomach system.
2. To identify how food breakdown processes during gastric digestion affect small intestinal digestion and glycemic response *in vivo*.
3. To establish a link between food structure, gastric digestion, and glycemic response based on *in vivo* findings.
4. To investigate the contribution of the proximal and distal phases of gastric digestion on food breakdown behavior and its consequences on the properties of emptied particles in a static *in vitro* gastric digestion system.

1.3 Organization of the thesis

The research objectives in Section 1.2 were completed through two *in vivo* studies and a static *in vitro* digestion study. An extensive literature review on starch digestion, gastric digestion, and glycemic response (Chapter 2) provides the scientific basis of the execution of the experiments. This report contains four experimental chapters (Chapter 4 to 7), which were derived from the two *in vivo* studies (growing pig model) and a static *in vitro* gastric digestion study. Several rice- and wheat-based food products were used throughout the experimental chapters, and the rationale of the selection of these products is given in Chapter 3. Chapter 3 also contains the rationale of each of the experimental chapter, as well as research objectives and hypotheses related to them. Findings from the experimental chapters are summarized and discussed together in Chapter 8, which also contains general conclusions, *in vitro-in vivo* correlation, and recommendations for future work.

CHAPTER 2. Literature review

2.1 Introduction

The botanical source of starch, degree of starch gelatinization, simultaneous presence of other food components in the meal, and microstructure of food have been identified as the most relevant factors that affect digestibility and glycemic response of starch (Arvidsson-Lenner et al., 2004; Parada & Aguilera, 2011). This highlights that the structure of starch-rich foods is one of the determinants of starch digestibility, and therefore food structuring is a strategy for glycemic response control. Starch digestion and the key factors impacting starch digestion have been previously reviewed (Magallanes-Cruz, Flores-Silva, & Bello-Perez, 2017; Mishra, Monro, & Hardacre, 2011; Parada & Aguilera, 2011; Singh, Dartois, & Kaur, 2010). However, the key factors impacting starch digestibility identified in these reviews are those related to the microstructure of the starch, most of which are derived from *in vitro* studies. Additionally, most previous reviews on starch digestion and glycemic response have been focused on starch hydrolysis and absorption in the small intestine, where the ingested food has already lost most of its macrostructural integrity. The structural breakdown processes of food in the mouth and stomach – the organs prior to the small intestine, have been previously reviewed (Acevedo-Fani & Singh, 2021; Brownlee, Gill, Wilcox, Pearson, & Chater, 2018; Capuano & Pellegrini, 2019; Golding, 2019; Guo, Ye, Singh, & Rousseau, 2020; Singh, Ye, & Ferrua, 2015; Somaratne, Ferrua, et al., 2020; Tamura et al., 2017). However, how breakdown processes in these organs impact

Part of the contents of this chapter has been published as a peer-reviewed paper: Nadia, J., Bronlund, J., Singh, R.P., Singh, H., and Bornhorst, G.M. (2021). Structural breakdown of starch-based foods during gastric digestion and its link to glycemic response: *In vivo* and *in vitro* considerations. *Comprehensive Review in Food Science and Food Safety*, 2021, 20:1–39.

small intestinal digestion and glycemic response of starch-based foods have not been discussed.

Bolus formation and disintegration of carbohydrate-rich foods during digestion, as well as the approaches to understand the processes have been previously reviewed (Bornhorst & Singh, 2012). Since then, significant advancements have been made in understanding starch digestion processes, which provide a body of evidence about the significance of macrostructural breakdown during mastication and gastric digestion on glycemic response of starch-based foods. This literature review focuses on the breakdown of starch-based foods in the mouth and stomach, the quantification of these breakdown processes, the links to physiological outcomes, such as gastric emptying and glycemic response, and considerations in developing *in vitro-in vivo* correlation in starch digestion studies. A general overview of structural aspects of starch-based foods is also given to provide justification on the importance of food structure in the digestion of starch-based foods.

2.2 Structural aspects of starch and starch-based foods

2.2.1 General overview of starch structure

Starch is a biopolymer that naturally consists of two complex carbohydrates, namely amylose (15 to 35%) and amylopectin (65 to 85%), and some other minor components such as lipids, proteins, and minerals (Bates, French, & Rundle, 1943; Ledezma, 2018; Pérez & Bertoft, 2010). However, with genetic modifications, mutants with no amylose (known as waxy starch) or higher amylose content (50 to 80%) have been developed in various crops, as recently reviewed by Seung (2020). Both amylose and amylopectin contain α -D-glucose units linked by α -1,4 and α -1,6 glycosidic chains (Zobel, 1988). These chains can be linear or slightly branched in amylose. In contrast, these chains are

linked with higher branching level in amylopectin. Depending on its botanical source, amylose in starch granules has a number-average degree of polymerization (dp_n) between 900 and 6,400, molecular diameter of around 50 nm, and a molecular weight of about 10^6 Da. Amylopectin is larger than amylose, with a hydrodynamic radius of 21 to 75 nm and a molecular weight between 10^7 to 10^8 Da (Bertoft, 2017; Buléon, Colonna, Planchot, & Ball, 1998; Parker & Ring, 2001). Amylopectin is highly branched has a higher dp_n than that of amylose. The dp_n of amylopectin is between 9600 to 15,900 in various botanical sources, which are present in three molecular species: large (dp_n 13,400 to 26,500), medium (dp_n 4,400 to 8,400), and small (dp_n 700 to 2,100) (Takeda, Shibahara, & Hanashiro, 2003). The chains of amylopectin branches can be classified as short and long chains, with consistently higher molar proportion of short chains compared to long chains in various botanical sources (Bertoft, 2017). The length of amylopectin chains is related to the crystallinity of the starch granules, where A-type and B-type crystallinity are exhibited by short- and long chains, respectively (Biliaderis, 2009).

Starch is synthesized in plants into water-insoluble, semi-crystalline granules that range in size between 1 and 200 μm . The morphologies and molecular structures of starch in plants vary between the botanical sources (Pérez & Bertoft, 2010). The hierarchical structure of starch granules is very complex, but in general, starch granules are considered to be composed of a bulk, amorphous core that is surrounded by concentric, alternating semi-crystalline and amorphous growth rings. The semi-crystalline growth rings (80- to 550-nm thick) consist of lamellae of alternating crystalline and amorphous regions, while the amorphous growth rings (60- to 80-nm thick) contain extended chains of amylopectin that interconnect the crystalline regions and interspersed amylose molecules. The exact location of amylose within these regions

is still a topic of discussion (Wang, Blazek, Gilbert, & Copeland, 2012; Wang, Li, Copeland, Niu, & Wang, 2015). Within these growth rings, blocklet elements with size ranging from 20 to 500 nm are observed. The blocklets contain crystalline and amorphous lamellae that regularly repeat every 9 to 10 nm (Blazek & Gilbert, 2011; Wang, Li, et al., 2015). With the advancement of characterization techniques, understanding has increased about the biosynthesis and molecular and microstructural aspects of starch, which have been described in detail elsewhere (Ai & Jane, 2018; Alcázar-Alay & Meireles, 2015; Bertoft, 2017; Biliaderis, 2009; Blazek & Gilbert, 2011; Dhital, Warren, Butterworth, Ellis, & Gidley, 2017; Dona, Pages, Gilbert, & Kuchel, 2010; Pfister & Zeeman, 2016; Seung, 2020; Wang & Copeland, 2013). These topics are outside the scope of the discussion of this review and readers are referred to those reviews for more details on starch chemistry and microstructure.

2.2.2 Structural aspects of starch-based foods relevant in digestion processes

The chemical and microstructural aspects of starch, which have been studied and discussed by many, are part of the multiple length scales of food structure (Figure 2.1). Starch is commonly present in food products in different forms: (1) isolated starch from its botanical source (e.g., corn starch), which is used in food due to its physical functionality (e.g., as a thickener, gelling agent, and stabilizer); (2) starch raw material (e.g. wheat flour from milled wheat grains), which becomes the main ingredients of starch-rich foods such as bakery products, snacks, and pasta; and (3) starch in plants, where starch is consumed with limited processing or in the original form of its botanical source (e.g., potato, rice grain) (Ai & Jane, 2018; Dhital, Brennan, & Gidley, 2019; Magallanes-Cruz et al., 2017). From a food structure perspective, when starch granules are present as the building block of starch-based foods (i.e., a complex food matrix), they may behave differently than as isolated starch granules (Aguilera, 2019). The

interactions between starch granules and other components in food matrices that consist of starch and other non-starch ingredients determine the properties of foods, such as texture (Conde-Petit, 2003; Delcour et al., 2010; Li, Dhital, & Wei, 2017). Consequently, the behavior of starch granules in real food matrices needs to be examined at different structural levels, together with their interaction with other non-starch components within the respective structural level.

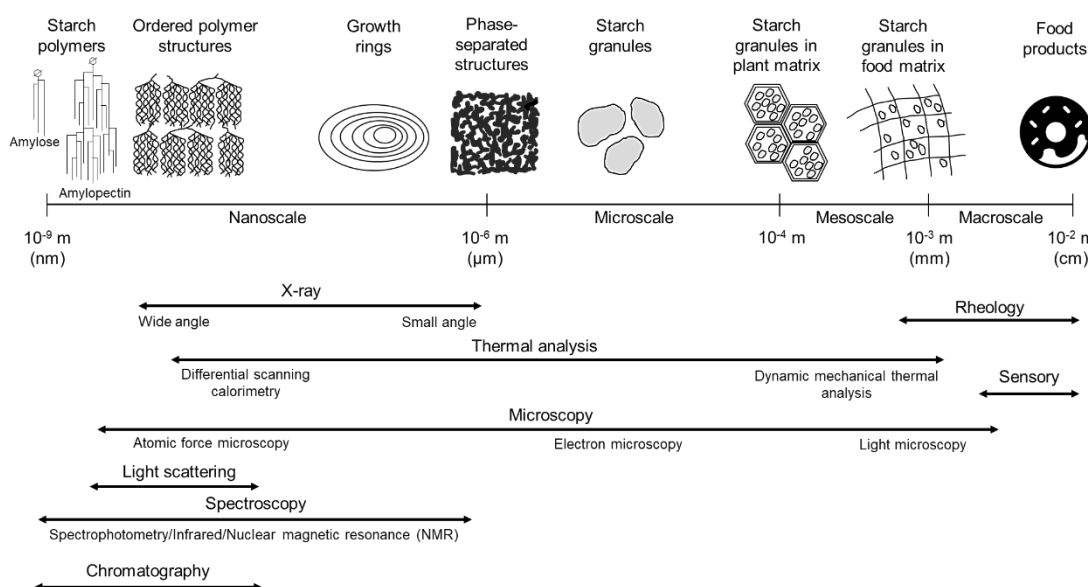


Figure 2.1 The wide ranges of structural levels of starch-based foods and analyses used to observe particular structures within its size range (adapted from Conde-Petit (2003) with modifications on the mesoscale definition based on Dona et al. (2010), Dhital et al. (2017), and Mandalari et al. (2018)).

At the micro- and nano-scale levels, starch granules can be observed as: glucose units of linear amylose and branched amylopectin molecules (0.3 to 0.5 nm); alternating crystalline and amorphous lamellae (9 to 11 nm); growth rings of alternating crystalline and amorphous regions (100 to 500 nm); phase-separated structures of amylopectin units and amylose domains that occur after gelatinization of starch suspension (range widely and variably from 400 nm to 50 μm); and intact granules, which vary from 1 to 200 μm in size depending on the source (Conde-Petit, 2003; Wang & Copeland, 2013).

Within the nano- and microscales, starch interacts with non-starch components (e.g., protein, lipid, and polyphenol) at a granular level (Dhital et al., 2019). To characterize starch at these length scales, various physical techniques can be applied, depending on the structural features of starch to be observed (Figure 2.1). For example, light and electron microscopy can be used to observe starch granule morphological and histological microstructures (Tamura, Singh, Kaur, & Ogawa, 2019), as well as the growth rings (van de Velde, van Riel, & Tromp, 2002) and structural changes of starch in dispersion (Błaszczak & Lewandowicz, 2020); atomic force microscopy (AFM) can be used to observe blocklets within the growth rings (Dang & Copeland, 2003); small angle X-ray scattering (SAXS) provides information on crystalline characteristics of starch lamellar structures (Li, Kong, et al., 2016); high-performance size exclusion chromatography (HPSEC) can be applied to understand chain-length distribution of amylose and amylopectin (Li et al., 2021); and solid state ^{13}C -NMR can be used to provide more precise information on the arrangement of crystalline and amorphous structures of starch (Katoh, Murata, & Fujita, 2020).

At a higher length scale (mesoscale, approximately between 100 μm to 1 mm based on previous reports on endosperm cell size and effect of particle size on starch bioaccessibility (Dhital et al., 2017; Dona et al., 2010; Mandalari et al., 2018)), starch-based foods can be seen as a dispersion of starch granules and other components in a food or plant matrix. This dispersion consists of continuous (dispersed) and discontinuous phases (van der Sman & van der Goot, 2009). Within the mesoscale range, starch granules interact with other components, such as water, lipids, and proteins, which vary in amounts depending on the botanical source or food type. Within this size range, the interaction between starch and non-starch components may affect the physical state, functionality, and digestibility of the starch. For example, protein is an

important structural component in wheat grain; it links the surface of starch granules to a complex matrix of proteins and lipids. The removal of surface protein from wheat starch was reported to increase the crystallinity of the starch granules, the swelling power and starch solubility, as well as the starch digestibility (Li, Wu, et al., 2016; Wang et al., 2014), suggesting that mesoscale level interactions affect the functionality and digestibility of starch granules. At the macroscale (for the purpose of this review, defined as length scale of larger than 1 mm to a few cm, depending on the bite size and mastication behavior), the arrangement of starch granules in its botanical source or processed food matrix (both will be referred to as “food matrix” from this section onwards) forms the visible and tangible attributes of the starch-based foods, such as their texture. Within the meso- and macroscales, interactions between starch and non-starch components occur at the cellular level (Dhital et al., 2019).

The location of starch and its interaction with other components in a food matrix at various structural scales affect the accessibility of starch hydrolyzing enzymes (i.e., α -amylase), thereby affecting starch digestibility (Dhital et al., 2019; Parada & Aguilera, 2011). This also indicates that starch digestion occurs at multiple length scales. Different arrangements of the dispersion of starch granules in continuous food matrices (Table 2.1) may create different barrier levels for α -amylase access, and thereby the starch digestibility of the products. Anything in the food matrix that prevents the access or binding of α -amylase to the starch granules (i.e., physical barriers) and/or the structural features that slow down or prevent α -amylase action can be considered as barriers to starch hydrolysis (Dhital et al., 2017). The presence of physical barriers in a food matrix (e.g., plant cell walls in whole grains (Tamura, Singh, Kaur, & Ogawa, 2016a) and protein matrices in sorghum (Mahasukhonthachat, Sopade, & Gidley, 2010)) is crucial to the digestibility of starch by α -amylase because amylolysis is a

surface phenomenon. The amylolytic process can only be initiated after diffusion of the enzyme to the solid surface, followed by adsorption on the granule surface (Dhital et al., 2017). The enzyme begins the digestion from the surface to create pores that enable it to penetrate further into the center of the granules and only when the center is reached, the hydrolysis occurs from the inside to the outer layers (Hasjim, Lavau, Gidley, & Gilbert, 2010).

Preservation of starch and non-starch component interactions within the cell of its plant source or starch interactions *in planta* (i.e., structural aspects within the meso- and macroscale) is suggested to be an effective way to restrict starch digestion (Dhital et al., 2019; Mandalari et al., 2018). From food processing perspective, this can be achieved by modulating starch structure, preserving the intact structure of plant tissue, and modulating Maillard reaction to limit starch gelatinization in the subsequent processing step (starch gelatinization can enhance starch susceptibility to α -amylase attack), as previously reviewed (Pellegrini, Vittadini, & Fogliano, 2020). Many studies have shown that structural features of starch granules within the micro- and nanoscale, such as the thickness of crystalline lamellae (Wang et al., 2018) and degree of crystallinity (Li et al., 2020) can change the *in vitro* digestibility of starch. However, the *in vitro* digestion procedures are often conducted in samples with highly disrupted macro- and mesoscale structures, which may not always be the case for actual digestion process (will be discussed in Sections 2.5 and 2.6). Moreover, it has been reported that the impact of particle size reduction (i.e., meso- and macrostructural breakdown) on starch digestibility can be similar to or more pronounced than starch structural modulation by gelatinization and retrogradation (Cañas, Perez-Moral, & Edwards, 2020; Dhital, Bhattarai, Gorham, & Gidley, 2016; Tamura et al., 2016a), suggesting that particle size reduction during digestion processes may have considerable impact on starch

digestibility. During the digestion processes, the physical barriers to starch digestion may be eliminated or decreased to certain extent by physical breakdown that occurs mostly in the mouth and stomach. However, there is a lack of knowledge on the physical breakdown of starch-based foods in the digestive system and its effect on starch digestibility.

Table 2.1 Examples of food matrix containing starch granules, showing different continuous and discontinuous phases in the food matrix structure.

Food	Continuous phase	Discontinuous phase	Reference
Cereal seed (e.g., rice, wheat, barley, sorghum kernels)	Matrix of storage proteins	Starch granules or swollen starch granules (when cooked)	(Guerrieri & Cavaletto, 2018)
Wheat bread	Elastic network of cross-linked gluten molecules and leached starch polymers	Gelatinized, swollen, deformed starch granules	(Gray & Bemiller, 2003)
Biscuit	Sugar and fat emulsion	Partially swollen starch granules	
Cake	Sugar and lipid emulsion	Gelatinized and molten starch granules	
Extruded breakfast cereals	Amorphous starch with minor ingredients (e.g., protein)	Air bubbles	(Robin & Palzer, 2015)
Extruded pasta or noodle	Protein network formed during kneading	Partially swollen starch granules	
Mashed potato	Dilute aqueous amylose solution	Concentrated dispersion of swollen and disrupted intracellular starch granules in water	(Alvarez & Canet, 1999)
Starch-thickened white sauce	Milk and solubilized amylose/amylopectin matrix	Swollen starch granules	(Arocas, Sanz, Hernández-Carrión, Hernando, & Fiszman, 2010)
Heated starch solution (e.g., starch-thickened sauce in stir-fry meals)	Solubilized amylose/amylopectin matrix	Swollen starch granules (which disappears at prolonged heating)	
Cooked legumes (whole or coarsely ground)	Protein matrix protected by thick cell wall	Partially swollen starch granules	(Birt et al., 2013)
Starchy fruits (e.g. banana)	Parenchyma cell containing fiber components (cellulose, hemicellulose) protected by cell wall	Starch granules	(Rongkaumpan et al., 2019)

2.3 Digestive organs that contribute to structural breakdown and glycemic response of solid starch-based foods

The breakdown of solid foods occurs in the mouth, stomach, and small intestine through combined physical (i.e., size reduction) and biochemical processes (i.e., hydrolysis by digestive enzymes) that break down the structure of the foods at multiple length scales (macro- to nanoscale) (Bornhorst, Gouseti, Wickham, & Bakalis, 2016). Each of these digestive organs contributes differently to the breakdown process, depending on their physiology and/or anatomy, and the structure of food ingested. These organs have been extensively reviewed from physiological and general food digestion perspective (Bornhorst & Singh, 2012; Chen, 2009; Chen & Rosenthal, 2015; Kong & Singh, 2008; Mackie, 2019). As such, only the main aspects of the organs and their implications to the physical breakdown of solid starch-based foods are summarized here. The information in this section provides the basis for the discussion of more detailed examples of the physical breakdown processes in Section 2.5.

2.3.1 Mouth

The mouth consists of the oral cavity, hard palate, teeth, tongue, and saliva. The oral cavity is the void space where food is manipulated and processed prior to swallowing. The teeth are the main agent for mastication (or chewing), which consist of different geometries allowing them to cut (the incisors), cut and tear (the canines or cuspids), or chew and shear (the molars) solid foods. The tongue consists of striated muscles located on the floor of the mouth (Chen, 2009). Saliva is produced by three major pairs of salivary exocrine glands located around the jaw and oral floor, accumulating to a total of 1 to 1.5 L daily through unstimulated (resting condition, 0.05 to 0.5 mL/min) or stimulated (during eating, 1 to 3 mL/min) saliva production. Saliva is produced by the parotid, submandibular and sublingual glands, resulting in a mixture comprising 99%

water that contains electrolytes (including bicarbonate), phosphate and various proteins (including enzymes, immunoglobulins, and other antimicrobial factors), along with mucins, glucose, urea, ammonia, and salivary α -amylase (de Almeida, Gregio, Machado, de Lima, & Azevedo, 2008; Feher, 2017b).

The breakdown of food in the mouth begins with mastication, which contributes to physical forces generated by the occlusion of the teeth that change over time, of which maximum value can range from 39 to 800 N, depending on the food type (de Las Casas et al., 2007). Mastication drives the breakdown of the macroscopic structure of ingested solid food by the crushing and shearing action of the teeth to form a masticated mass, known as a food bolus (Brownlee et al., 2018). There are four key steps in the process: stage I (moving of food from the front of the mouth to the teeth); processing (crushing/grinding of food particles); stage II (gradual transport of sufficiently disintegrated particles to the back of oral cavity to form a bolus); and stage III or pre-swallowing stage (bolus transport to the back of the tongue as the preparation for swallowing) (Hiimeae & Palmer, 1999). Physical breakdown of solid foods occurs mainly during processing and stage II, where food will be chewed to form a safe-to-swallow bolus (Hutchings & Lillford, 1988; Prinz & Lucas, 1995). In the case of solid food with soft structures, the food can also be broken down by squashing the bolus between the tongue and the hard palate (Hiimeae & Palmer, 1999). During mastication, the food matrix is disintegrated as it is transformed into food boluses. The disintegration of food matrix can lead to increasing (due to formation of small particles) or decreasing surface area (due to increased local density or compactness) of the food bolus, depending on the structure of the food (Flynn, 2012).

As physical breakdown is taking place, saliva is constantly added to lubricate, moisten, and dissolve substances such as sugar in the ingested food. The bicarbonate in

saliva buffers the acidity of the masticated food to maintain the pH inside the oral cavity (de Almeida et al., 2008; Gavião, Engelen, & van der Bilt, 2004). Salivary α -amylase rapidly hydrolyzes starch within disintegrated food particles to lower molecular weight oligosaccharides and simpler sugars; the enzyme attacks starch at its α -1,4 glycosidic bonds in a random fashion, but leaves the α -1,6 link intact. The end products of salivary α -amylase hydrolysis are smaller oligomers, namely maltose, maltotriose, and α -limit dextrins (Roberts & Whelan, 1960; Whelan & Roberts, 1953). However, starch hydrolysis cannot occur extensively to produce these end products in the mouth due to the short mastication duration (typically up to 30 s), and larger intermediates are formed instead. An *in vitro* study using raw and cooked corn starch solutions (representative of a food structure that is most susceptible to starch hydrolysis) reported that after 2 to 30 s of hydrolysis with salivary α -amylase, the hydrolysis products consisted of 7 to 25% smaller oligosaccharides (degree of polymerization of 2 to 8) and up to 75 to 93% larger oligosaccharides for raw and cooked starch samples, respectively. Meanwhile, conversion of the raw and cooked starch solutions to maltose was approximated to be up to 0.2 and 0.5%, respectively (Lapis, Penner, Balto, & Lim, 2017). However, temporary storage of the food bolus in the stomach may extend the hydrolysis duration, allowing for a higher extent of hydrolysis by salivary amylase (to be referred to as ‘salivary amylase’ from here onwards). This will be discussed in detail in Sections 2.3.2 and 2.5.2. During hydrolysis by salivary amylase, there is also a possibility that glucose is produced, although to a very limited extent (Jacobsen, Melvaer, & Hensten-Pettersen, 1972; Martens, Bruininx, Gerrits, & Schols, 2020). The significance of glucose production by salivary amylase in starch digestibility is still not properly understood. However, previous studies have shown that individuals with higher salivary amylase activity exhibited lower glycemic response than those with lower salivary amylase

activity. This counter-intuitive finding was thought to be caused by various possible mechanisms, including: competitive inhibition between maltose and glucose in glucose transport across the small intestinal membranes during absorption process; indirect reduction in the rate of glucose transport from the intestinal lumen to the portal bloodstream; early signaling (by maltose and/or glucose produced by amylase) to the body to prepare for incoming starch and ensuing glucose; and the peripheral release of hormones or incretins by lingual taste cells into the blood stream in response to carbohydrates, which stimulates insulin release from the pancreas (Barling, Shyam, Selvathevan, & Misra, 2016; Mandel & Breslin, 2012)

During the physical and biochemical breakdown processes, the tongue helps to form the bolus through its folding action and food particle manipulation (Hiemae & Palmer, 1999). Heat transfer between saliva, walls of oral cavity, and the food bolus warms/cool the food to physiological temperature and allows food to be tasted during bolus formation (Gray-Stuart, 2016). Through crushing, mixing, particle size reduction, and heat transfer operations in the mouth, ingested solid food is transformed to a bolus that is safe to swallow (Coster & Schwarz, 1987; Gray-Stuart, Jones, & Bronlund, 2017; Pereira, 2012). A food bolus is considered to be safe to swallow when it meets certain threshold levels in the bolus volume, adhesion, consistency, and deformability (Gray-Stuart et al., 2017). Although the threshold levels in these bolus properties may vary between individuals (Gray-Stuart et al., 2017), a general trend is that increasing product hardness leads to longer duration needed to form a food bolus that is safe to swallow from each bite or mouthful of food (Hiemae & Palmer, 1999). However, the duration of mastication is short compared to other digestion processes; for hard foods, the range was found to be between 8 to 30 s, but can last up to 90 s for subjects with impaired mastication performance (Gavião et al., 2004; Hiemae & Palmer, 1999; Huckabee et

al., 2018). The tongue helps the process of swallowing by squeezing the food bolus against the hard palate to push it towards the esophagus (Gray-Stuart, 2016). The swallowing process occurs quickly (within 4 to 8 s) to deliver the food bolus to the stomach (Cordova-Fraga et al., 2008).

2.3.2 Stomach

The stomach, or gastric compartment, is a J-shaped organ that is located between esophagus and the duodenum. The walls of the stomach consist of circular, longitudinal, and inner oblique smooth muscle layers (Feher, 2017c). In accomplishing its function in the digestion process, the stomach is equipped with gastric secretory and motility functions that exhibit different patterns in fasted and fed states. According to the motility and secretory patterns, the stomach can be distinguished further to two functional regions, namely proximal and distal regions (Figure 2.2). Anatomically, the proximal stomach consists of the cardia, fundus, and body with the wall muscle layers thickness of 2 to 3 mm. Meanwhile, the distal stomach comprises the antrum and pylorus, which has thicker longitudinal and circular muscle layers (5 to 7 mm), with greater thickness in the pylorus (Feher, 2017c; Smith & Morton, 2010a).

Gastric secretions, or gastric juice, are a mixture of mainly water, along with hydrochloric acid (HCl), digestive enzymes, and mucus that are produced by different secretory glands in the different stomach regions (Feher, 2017c; Soybel, 2005). The stomach fundus and body are known as the acid-secreting regions; they contain the oxyntic glands that produce gastric acid as the main secretion, along with the chief cells that produce pepsinogen and lipase. The secretory glands in the cardia and pylorus secrete primarily alkaline mucus that lubricates ingested food to enable them to move and be churned by the contractions of the stomach, as well as protecting the stomach wall from digestion by HCl (Feher, 2017c; Smith & Morton, 2010a). Each component

of gastric secretions has a unique function in the biochemical breakdown and dissolution of solid food particles. Water dissolves the components of gastric secretions, allowing the hydrolysis process of different macronutrients (including dietary carbohydrates) to take place in the stomach. HCl initiates protein denaturation, activates pepsinogen to form pepsin, and reduce the pH of stomach content (Waldum, Hauso, & Fossmark, 2014). The amount of HCl produced in the stomach dynamically changes during digestion, and the secretion is reduced when the stomach content becomes more acidic ($\text{pH} \leq 3$).

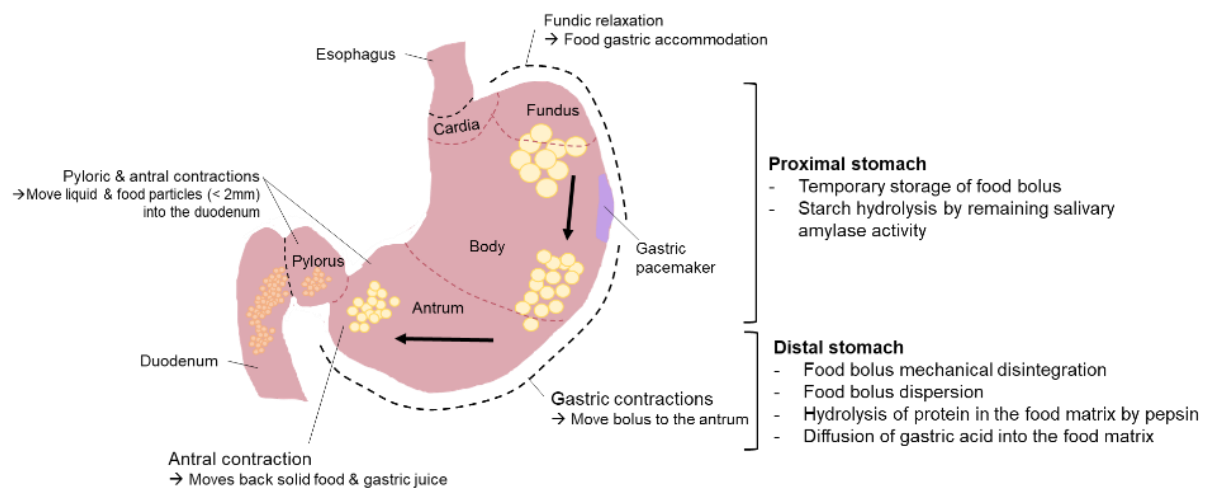


Figure 2.2 Roles of the proximal and distal stomach in gastric digestion of solid starch-based foods (adapted from Rodríguez Varón and Zuleta (2010) with modifications).

The initial pH of the stomach has been reported to vary from 1.4 to 2.1 in fasted state, rise to pH 2.5 to 6.7 in fed state, then lower again to less than 3.1 after eating (Kararli, 1995; McLauchlan, Fullarton, Crean, & McColl, 1989; Simonian, Vo, Doma, Fisher, & Parkman, 2005). The time required for the gastric contents to decrease in pH after a meal depends on the mixing between stomach regions, meal composition, meal buffering capacity, and amount of food eaten. This dynamically changing pH provides a suitable pH for the activity of pepsin (pH 2 to 5) and lipase (pH 4 to 6) (Bornhorst,

2017; Gargouri, Moreau, & Verger, 1989; Minekus et al., 2014; Smith & Morton, 2010a), as well as the remaining activity of salivary amylase (pH 3 to 7) (Freitas, Le Feunteun, Panouille, & Souchon, 2018) that is incorporated in the food bolus (Mackie, 2019) during mastication or from the involuntary swallowing of saliva during and after meal consumption. The remaining salivary amylase activity is important in the digestion of starch-based foods, as it can prolong the contact time between starch granules in food bolus with the amylolytic enzyme (see Section 2.6.2 for further discussion on this topic). Depending on the location of the starch granules in the food matrix, the biochemical digestion by pepsin and lipase may improve the access of starch to hydrolysis in the subsequent small intestinal digestion by weakening the solid matrix where the starch granules are trapped. However, biochemical digestion alone is not sufficient to break down the structure of solid foods. Mechanical action by gastric motility is needed to reduce the particle size of the solid foods as well as to increase the diffusion of digestive enzymes into the food particles.

Gastric motility is the result of contractions of the gastric smooth muscle layers. In the fasted state, the motility pattern follows four-phase movement with different contraction strength and duration, which is known as the migrating motor complex (MMC). Each MMC cycle consists of three phases of contractions with increasing frequency and strength (up to 80 mmHg) to clear undigested particles from the stomach and a transitional phase to the next cycle. After eating, the MMC shifts from fasted-state to fed-state contractile pattern that is composed of contractions of variable intensity (15 to 20 mmHg) and duration (Feher, 2017c; Hasler, 2009; Hellström, Grybäck, & Jacobsson, 2006; Kong & Singh, 2008). The fed-state motility pattern (Figure 2.2) facilitates the dispersion, mechanical disruption, mixing, and emptying of food particles during gastric digestion (Hasler, 2009). The fed-state motility of the proximal stomach

is dominated by sustained tonic contractions with a small proportion of rapid phasic contractions, which contributes to receptive relaxation and gastric accommodation (or adaptive relaxation) reflexes of the proximal stomach as the food bolus enters the stomach (Hasler, 2009). The distension of the fundus due to adaptive relaxation stimulates peristaltic contractions that travel from the proximal stomach to the distal stomach with increasing intensity (Rodríguez Varón & Zuleta, 2010; Smith & Morton, 2010a).

The fed-state motility pattern in the distal stomach is dominated by phasic contractions, or peristaltic waves, at a frequency of three times per minute, known as antral contraction waves (ACWs) (Ehrlein & Schemann, 2005; Hasler, 2009; Smith & Morton, 2010a). The ACWs originate from the pacemaker cells in the body of the stomach and radially travel down the greater and lesser curvatures towards the pylorus with increasing velocity and width due to increasing muscle thickness, propulsively pushing the gastric digesta to the distal region. As the ACW approaches the pylorus, the antral lumen is often nearly occluded by the deepened indentations caused by the contractions (O'Grady et al., 2010; Schulze, 2006). Simultaneously, the contraction pattern changes to systolic, causing the stomach content to be repelled back to the pyloric antrum for further mixing and disintegration due to momentary pyloric sphincter relaxation—an act known as retropulsion (Shafik, Sibai, Shafik, & Shafik, 2007; Spiller & Marciani, 2019).

While a meal is being consumed, gastric emptying is typically minimal. This period of minimal gastric emptying is known as lag phase, of which duration is affected by food-related factors such as meal type and ingested particle size, and physiological factors including fundal tone, stomach volume, and the motility of the antrum (Collins, Horowitz, Cook, Harding, & Shearman, 1983; Nusynowitz & Benedetto, 1994; Siegel

et al., 1988; Urbain et al., 1989). During the lag phase, the rate of gastric secretions also increases significantly due to the presence of food in the stomach (Smith & Morton, 2010a). The rate of gastric secretions can increase from 1 mL/min under fasted conditions to 10 to 50 mL/min immediately after the ingestion of food (Versantvoort et al., 2004). Ingested food is mechanically and chemically broken down to form a multiphase slurry called chyme. As chyme starts to be produced, emptying of solid particles takes place in more rapid linear phase, while the disintegration and mixing of the remaining stomach content continues (Siegel et al., 1988). It is currently accepted that gastric emptying in this linear phase takes place in such a way to achieve an overall emptying rate that varies from 1 to 4 kcal/min during the course of digestion, based on gastric emptying studies in healthy individuals (Brener, Hendrix, & McHugh, 1983; Calbet & MacLean, 1997; Collins, Horowitz, Maddox, Myers, & Chatterton, 1996; Hunt, Smith, & Jiang, 1985).

The wide range of gastric emptying rate was reported to be affected by the caloric density, chemical composition, volume, and the proportion of solid component in the meal (Calbet & MacLean, 1997; Hunt et al., 1985). The presence of glucose or other nutrients in different sections of the small intestine (due to gastric emptying) is also known to trigger the secretion of gut hormones, such as the glucose-dependent insulinotropic polypeptide (GIP; also known as gastric inhibitory polypeptide) and glucagon-like peptide 1 (GLP-1), which leads to delayed gastric emptying as gastric digestion proceeds over time (Brener et al., 1983; Marathe et al., 2015; Mihai et al., 2018). However, as these studies used liquid meals or were focused on the liquid component of the meal, there may be more complexities involved in the gastric emptying of solid food, due to varying rates of solid breakdown and the rate of material delivery to the small intestine due to the gastric sieving effect.

The gastric sieving effect due to contractile activity of the stomach allows liquids and small particles (1 to 2 mm, based on studies in humans and pigs) to exit through the pylorus into the small intestine, while particles that are bigger than the pyloric opening are retained in the stomach for further particle size reduction (Bornhorst, Ferrua, Rutherford, Heldman, & Singh, 2013; Feldman, Smith, & Simon, 1984; Meyer, Elashoff, Porter-Fink, Dressman, & Amidon, 1988). However, another study suggested that 5- × 7-mm non-disintegrating tablets can empty from the stomach during the fed state (Coupe, Davis, Evans, & Wilding, 1991), larger than the commonly accepted 1- to 2-mm threshold. These different reported values on the size of particles that can be emptied during fed state motility suggest a need for further investigation in this area. Considering that studies on the size of particles leaving the stomach are mostly from the 1980s and 1990s, specific size and properties (e.g., deformability, smoothness of surface) of particles leaving the stomach using advanced characterization techniques should be investigated. Remaining particles that cannot be reduced to the required size are emptied during fasted-state motility by the MMC or ‘housekeeper wave’ (Hellström et al., 2006; Itoh, Higuchi, Gardner, & Caldwell, 1986).

This gradual emptying of the stomach content implies that food boluses have various gastric retention times (often expressed as gastric emptying half-time, which reflects the time required to empty 50% of the gastric content). For example, the gastric emptying half-times of various starchy meals were reported to be between 35 to 324 min, depending on the amount consumed, the physical form of the food, and/or the starch source (Cisse et al., 2018; Mourot et al., 1988). Moreover, the extent of structural breakdown of the emptied particles may impact nutrient (i.e., glucose) release in the small intestine, which has been reported to affect gastric emptying rate through feedback mechanisms (such as the ileal brake). For instance, Lin et al. (1992) reported

that perfusion of hydrolyzed starch in canine distal ileum inhibited gastric emptying of solids. Similarly, Cisse et al. (2017) found that pre-loading of starch-entrapped microspheres could slow down the gastric emptying rate of subsequent semi-liquid meal, which was hypothesized to be caused by the ileal brake mechanism.

2.3.3 Small intestine

The small intestine is a 6-m (on average) tubular structure built of circular and longitudinal smooth muscle layers that is coiled in the abdomen of the adult human. The small intestine is divided into several functional regions with decreasing wall (muscle layer) thickness as they move further from the stomach: the duodenum (the first 25 cm), jejunum (around 40% of the small intestine), and ileum (around 60% of the small intestine). The inner wall of the organ (the mucosa) is covered by numerous microscopic finger-like structures called villi with decreasing number and size at further distances from the duodenum (Avvari, 2019; Feher, 2017a; Smith & Morton, 2010c). The duodenum serves as the location of mixing between the chyme emptied from the stomach with secretions from the intestine, pancreas, and liver.

Intestinal secretions consist of alkaline fluid containing electrolytes, mucus, and water that is produced throughout the length of the small intestine. Digestive enzymes are added to the duodenum by the pancreas and liver. Pancreatic secretions (pancreatin) contain enzymes for digesting lipid (lipase), carbohydrates (amylase), and protein (trypsin). The liver produces bile that aids the digestion and absorption of fats (Feher, 2017a). Starch and their derivatives in the chyme are chemically broken down by pancreatic α -amylase to maltose, maltotriose, and α -limit dextrin in the lumen of the small intestine. These oligosaccharides are further hydrolyzed to monosaccharides by the brush border enzymes in the villi to glucose (Holmes, 1971; Nichols et al., 2003). The resulting monosaccharides and water are mostly absorbed in the duodenum and

jejunum by membrane-associated transporters in the brush border and basolateral membranes of the mature enterocytes (Chen, Tuo, & Dong, 2016; Smith & Morton, 2010d). The regulation of the mechanism involves complex roles of ion channels and transporters (Chen et al., 2016), of which details are outside the scope of this project. Briefly, monosaccharides are transported across the intestinal brush-border membrane mediated by a membrane protein, then diffused to the blood capillaries by glucose transporter. In normal condition, this absorption will cause blood glucose to rise to its maximum level within 30 to 60 min after ingestion of the meal, then returns to baseline after 1.5 to 2 h (Smith & Morton, 2010d). Increase in blood glucose stimulates pancreas to secrete insulin into the blood. The insulin promotes glucose uptake into muscle and adipose tissue, lowering glucose level in the blood (Smith & Morton, 2010d). The ileum absorbs vitamin B₁₂ and bile salts, leaving residual materials to be propelled to the large intestine for fermentation (Avvari, 2019; Smith & Morton, 2010c).

There are two motility patterns in the small intestine, namely peristalsis and segmentation. Peristalsis is a wave of circular muscle contraction and relaxation which propagates towards the colon. It has the role of propelling the chyme to transport it slowly from the duodenum to reach the ileum (Feher, 2017a; Smith & Morton, 2010c). In contrast, segmentation occurs due to coordinated constriction or relaxation of the outer longitudinal muscle and inner circular muscle that occurs in local regions in the small intestine. Segmentation occurs more frequently in the duodenum than in other small intestinal regions (Reinke, Rosenbaum, & Bennett, 1967; Rosenbaum, Reinke, & Bennett, 1967). Segmentation is responsible for mixing the secretions with the chyme received from the stomach, homogenizing the intestinal content, aiding in pH regulation in the duodenum, and facilitating contact between food particles and the intestinal mucosa for absorption (Avvari, 2019; Smith & Morton, 2010c).

The small intestine has been the focus of many starch-based foods digestion studies due to its direct contribution to the conversion of starch to glucose and longer retention time (180 to 400 min for standard solid meal or test food) compared to the mouth and the stomach (Mikolajczyk, Watson, Surma, & Rubin, 2015; Versantvoort et al., 2004). Physical breakdown of foods in the small intestine has not been widely studied, possibly due to the complexity of the process, where material delivery from the stomach, secretion of digestive fluid components, biochemical digestion, nutrient absorption, and chyme transport towards the large intestine occur simultaneously. However, considering the lower contraction intensity in the small intestine compared to that of the gastric antrum, as reflected by the difference in their wall thickness (<3 mm in the small intestine (Fernandes et al., 2014) vs. ~5 mm in the antrum (Pickhardt & Asher, 2003)), it is likely that the contribution of small intestinal motility on the physical breakdown of solid food particles is very limited. These factors suggest that the breakdown processes of solid foods that occur in the mouth and stomach are the main contributors to the subsequent digestion and absorption processes in the small intestine.

2.4 Monitoring physical breakdown of solid foods during gastric digestion

Based on the gastric sieving effect explained in Section 2.3.2, the rate and extent of food breakdown in the stomach, which is also affected by the breakdown during mastication, will determine the size and the delivery rate of particles that enter the small intestine. This will impact the available surface area of the starch particles to the enzymes in the small intestine, and hence the rate of release of amylolytic products (Mackie et al., 2017; Pletsch, 2018). With the importance of physical breakdown of food structure on starch digestibility in the small intestine, experimentally monitoring the breakdown processes is necessary to understand the mechanisms and further apply the

understanding for the development of starch-based food structure with controlled glycemic properties. Although food breakdown mechanisms during both mastication and gastric digestion of starch-based foods are still not fully understood, monitoring the breakdown process during mastication is less complex than monitoring the breakdown process during gastric digestion. During mastication, it is relatively easy to procure samples at varying stages of mastication, allowing for a detailed view of the food breakdown process in the mouth. Characterization of solid food breakdown process during mastication has been thoroughly reviewed elsewhere (Bornhorst & Singh, 2012; Chen & Rosenthal, 2015; Deveziaux de Lavergne, van de Velde, & Stieger, 2017). Therefore, only approaches and parameters used to monitor physical breakdown during gastric digestion are discussed here.

2.4.1 Experimental approaches to investigate food breakdown during gastric digestion

Food breakdown during gastric digestion can be investigated through *in vivo* and *in vitro* experiments (Bornhorst & Singh, 2014). *In vivo* gastric digestion can be examined through either human or animal studies. Human studies are carried out with specific objectives to understand certain aspects of the gastric digestion process, such as gastric capacity and accommodation (de Zwart et al., 2007; Goetze et al., 2007), gastric emptying (Simonian et al., 2004), gastric motility (Marciani, Gowland, Fillery-Travis, et al., 2001), and proximal–distal stomach pH distribution (Koziolk et al., 2015; Simonian et al., 2005). Animal studies provide information that sometimes cannot be acquired in human studies. For example, properties such as the pH distribution in specific locations in the stomach (Bornhorst, Rutherford, et al., 2014) and the physical properties of the digesta (Martens, Noorloos, et al., 2019) can be measured in animal studies. Despite being physiologically relevant, *in vivo* studies are limited by

experimental design, inter-individual physiological variations, difficulties in data interpretation, high cost, ethical constraints, and the lack of standard reference methods to compare the results between studies (Alegria, Garcia-Llatas, & Cilla, 2015).

In vitro gastric digestion models have been introduced to overcome the experimental limitations of *in vivo* models, and allow for more replications to be easily conducted for each tested food product (Bornhorst et al., 2016). This type of approach allows the study of digestion of single substrates or simple meals under specific conditions (Alegria et al., 2015). *In vitro* digestion models can be static, dynamic, or semi-dynamic. Static digestion models commonly consist of mixtures of samples and simulated gastric fluid that are incubated at physiological temperature; they rely only on simulated gastric fluid diffusion and leaching of solid particles, resulting in an inability to mimic particle disintegration of food with compact structure (Kong & Singh, 2010).

As static digestion models cannot sufficiently mimic the physical breakdown of food, dynamic gastric digestion models have been developed to simulate the mechanical disintegration of solid food and allow for the dynamics of gastric mixing. Dynamic gastric models typically consist of a synthetic gastric compartment with moving components that simulate mechanical disintegration of food (Thuenemann, 2015). There are many types of *in vitro* dynamic gastric digestion models to simulate the human stomach, such as: the dynamic gastric model (Vardakou et al., 2011), the Human Gastric Simulator (Ferrua & Singh, 2015; Kong & Singh, 2010), and TIM advanced gastric compartment (Bellmann, Lelieveld, Gorissen, Minekus, & Havenaar, 2016). However, these models are customized and are complicated to develop. Therefore, to bridge the limitation of static model while considering the dynamics of pH in the stomach, a semi-dynamic digestion model has been introduced. This model is similar to static digestion model, but equipped with an overhead stirrer to cause mechanical

breakdown, gradual acidification of the system to mimic the dynamics of gastric pH, and sample withdrawal to simulate gastric emptying (Mulet-Cabero et al., 2020).

A detailed description of *in vivo* and *in vitro* methods is outside the scope of this review, and has been previously reviewed in detail (Bornhorst & Singh, 2014; Dupont et al., 2019; Muttakin, Moxon, & Gouseti, 2019; Shani-Levi et al., 2017). In selecting the appropriate method to monitor food breakdown during gastric digestion, it is important to consider the strengths and limitations of each method. The selection of the method and process parameters depends on the specific purpose to be achieved through the experiments. Therefore, *in vitro* and *in vivo* approaches need to complement each other to gain a better understanding of mechanisms of gastric digestion.

2.4.2 Methods to quantify physical breakdown of solid foods during gastric digestion

The process of physical breakdown and deconstruction of food structure during gastric digestion can be attributed to diffusion of gastric secretions into food particles, biochemical breakdown, mechanical breakdown, and gastric mixing (Bornhorst et al., 2015; Somaratne, Ferrua, et al., 2020). Selection of the appropriate quantitative methods, what to measure, and which length scale of structure to characterize are necessary to understand the mechanisms of breakdown during digestion as impacted by food structure. A number of parameters can be measured to quantify and reflect gastric digestion phenomena at various structural levels in an *in vivo* or *in vitro* system (Table 2.2). Characterization of physical breakdown process during gastric digestion may be more relevant if it is conducted at the meso- to macroscale, because samples can be analyzed without further particle size reduction or sample preparation, minimizing the interference of non-digestion related breakdown on the results. However, microstructural observation (Figure 2.3) and nanoscale measurement (e.g., extent of

starch hydrolysis) are often needed to complement the meso- and macrostructural observation.

In previous studies, parameters listed in Table 2.2 have been quantified at varying times during the digestion period to understand the kinetics of the gastric digestion process, rather than at the end of the gastric digestion period in the whole digestion process. Most of these parameters are suitable to be measured *in vivo* through animal models for accurate physiological characterization that is representative of gastric digestion and dynamic *in vitro* models for more specific breakdown observations. In addition, parameters relating to mechanical breakdown such as rheology and particle size may not be suitable to be studied in an *in vitro* static or semi-dynamic model, where the effect of grinding by gastric antrum is absent (Bornhorst & Singh, 2014), or not accurately represented. Although not all the parameters in Table 2.2 have been quantified specifically for starch-based foods, they can be used as a reference and are worth considering for future studies aiming to examine the physical breakdown of solid starch-based foods during gastric digestion.

The overall breakdown effect of gastric digestion on the physical changes of food can be observed through monitoring of rheological and textural changes in the gastric contents (Bornhorst, Ferrua, et al., 2013). Additionally, these parameters can also be used to isolate the effect of biochemical breakdown on the softening of the food matrix, such as in the work of Drechsler and Bornhorst (2018). However, characterizing the rheological characteristics of gastric digesta of solid meals can be a challenging task, because fundamental rheological tests on materials that contain large particles and separate rapidly are difficult to do accurately (Joyner, 2018). Meanwhile, food boluses commonly consist of particles with multi-modal distribution (Foschia, Peressini, Sensidoni, Brennan, & Brennan, 2014; Hoebler et al., 2000; Pallares Pallares,

Loosveldt, Karimi, Hendrickx, & Grauwet, 2019), making them inhomogeneous when they enter the stomach. To isolate the effects of mechanical breakdown, information on the mechanical breakdown behavior of food particles in the stomach and the mechanism of particles disintegration can be acquired through measuring particle size distribution of the digesta (Drechsler & Ferrua, 2016). Particle mechanical breakdown behavior in the stomach will influence the available surface area and the propensity for food particles to be hydrolyzed.

In addition to physical properties of the digesta, the overall breakdown behavior during gastric digestion may be monitored through tracking the uptake of digestive fluids (i.e., gastric secretions and saliva) into the food and gastric mixing. Diffusion of gastric secretions into food particles over time reflects the rate of mass transport between gastric secretion and the food matrix (Somaratne, Ferrua, et al., 2020), reflecting the moisture uptake behavior of the food particles. Moisture uptake behavior is particularly important for starch-based foods with compact or rigid cellular structures, as it enhances the breakdown of the food particles through swelling that weakens the bonds within the food matrix (Mennah-Govela & Bornhorst, 2016a; Somaratne, Ferrua, et al., 2020). When quantified in an *in vitro* system, moisture uptake behavior has been shown to influence the rate and mode of disintegration of the food particles during gastric digestion (Kong & Singh, 2009b). Gastric mixing affects intragastric pH distribution and residence time of the food particles in the stomach, and its quantification provides information on the local biochemical environment for food digestion (Bornhorst, 2017). For starch-based foods, gastric mixing determines whether the chemical degradation within certain location in the stomach is due to remaining salivary amylase activity or acid hydrolysis. Finally, to monitor the extent of starch digestion, starch hydrolysis of the digesta can be quantified (Freitas et al., 2018). The

susceptibility of the food particles in the digesta to hydrolysis can be estimated by standardizing the extent of hydrolysis with particle surface area (Hayes et al., 2020).

2.5 Physical changes in the structure of starch-based foods during oral and gastric digestion

2.5.1 Mastication (oral processing)

The degree of physical breakdown and starch hydrolysis in starch-based foods during mastication is dependent on the chewing time, which reflects the contact time between salivary amylase and starch granules within the food particles in the oral cavity (Bornhorst & Singh, 2012). Although interindividual variations in chewing behavior of the same type of food have been reported in previous mastication studies, the chewing time has been consistently reported to be affected by the initial hardness and moisture content of the food (Iida, Katsumata, & Fujishita, 2011; Maeda et al., 2020; Moongngarm, Bronlund, Grigg, & Sriwai, 2012; Motoi, Morgenstern, Hedderley, Wilson, & Balita, 2013; Ranawana, Monro, Mishra, & Henry, 2010; van Eck et al., 2019). The duration of chewing can be modified by the presence of added lubricating agents, such as in the case of toast consumed with butter (Gavião et al., 2004), cake pre-moistened with water (Motoi et al., 2013), crackers topped with mayonnaise (van Eck et al., 2019), or by drinking immediately after the food enters the mouth. Based on previous studies on mastication of starch-based foods with varying bite size and moisture content, the contact time between salivary amylase and food particles for every bite of food can range from <5 s to 90 s until the food bolus is swallowed (Flynn, 2012; Huckabee et al., 2018).

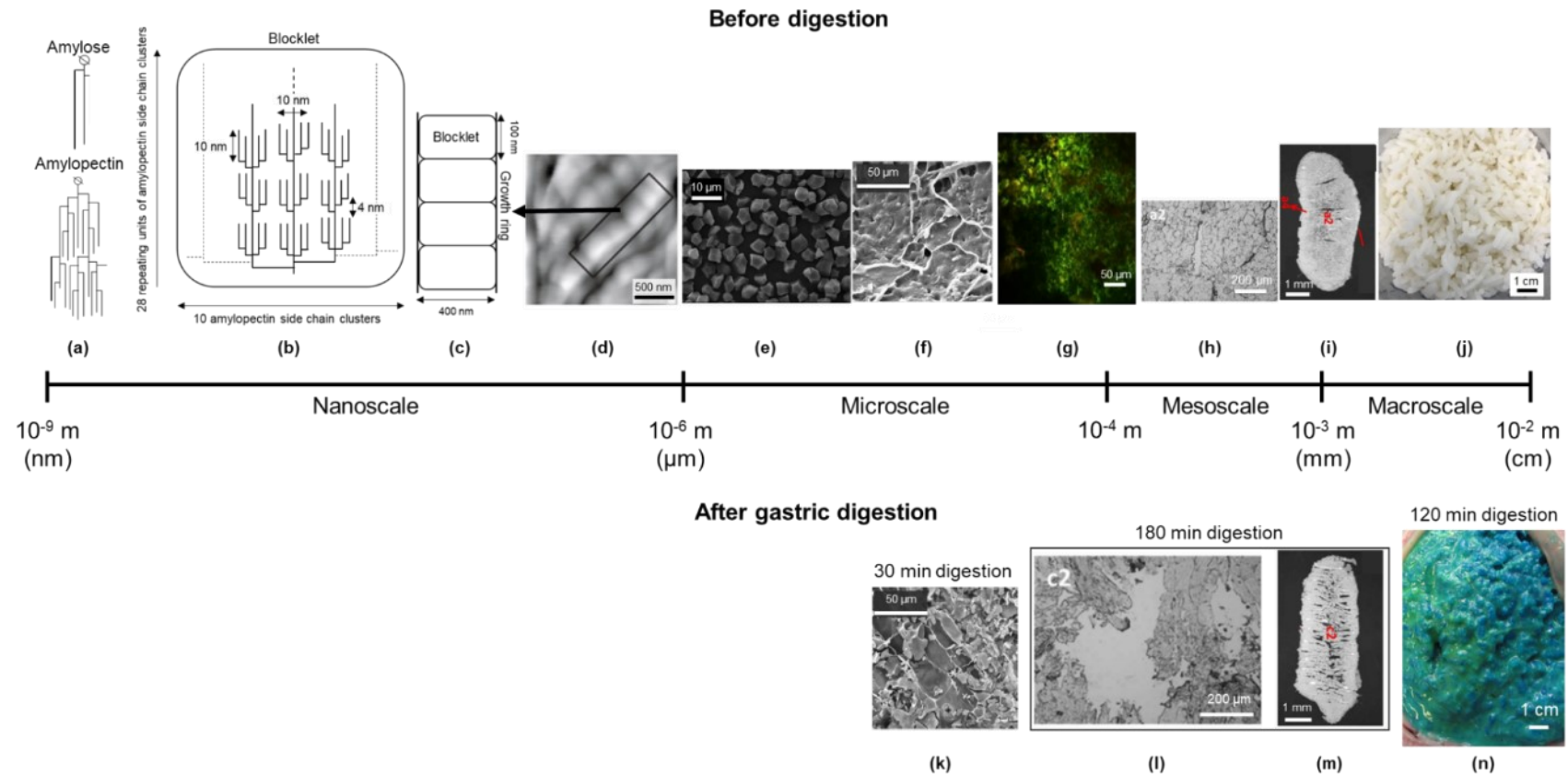


Figure 2.3 Cooked rice grain as an example of the structure of starch-based foods at multiple length scales before and after in vitro or in vivo gastric digestion. Images shown are not necessarily from the same study and they are shown as representatives at each length scale. Amylose and amylopectin structures (a) were adapted from Wang, Li, et al. (2015). Growth ring and blocklet structures (b-d) were adapted from Dang and Copeland (2003). Scanning electron microscopy (SEM) image of isolated rice starch granules (e) was adapted from Li, Kong, et al. (2016). SEM images of the surface of undigested (f) and 30-min in vitro rice digesta (k) were adapted from Tamura, Singh, Kaur, and Ogawa (2016b). Confocal laser scanning microscopy (CLSM) image of undigested rice (g) was adapted from (Nawaz, Gaiani, Fukai, & Bhandari, 2016). SEM images of undigested (h-i) and 180-min rice in vitro digesta (l-m) were adapted from Wu, Deng, et al. (2017). Swine 120-min digesta image (n) was adapted from Bornhorst, Chang, Rutherford, Moughan, and Singh (2013).

Table 2.2 Experimental approaches to monitor physical changes during gastric digestion of solid or semi-solid foods, not limited to starch-based foods. For the definition of length scale of structural breakdown characterized, see Figure 2.1 and Figure 2.3.

Phenomena	Parameter monitored	Method used	Type of study				Length scale of structural breakdown characterized	Examples of work
			<i>In vitro</i> -static/semi-dynamic	<i>In vitro</i> -dynamic	<i>In vivo</i> - animal	<i>In vivo</i> - human		
Gastric secretion incorporation	Moisture content	Gravimetric (oven drying) until constant mass	v	v	v		Micro	(Bornhorst, Ströbinger, Rutherford, Singh, & Moughan, 2013; Kong, Oztop, Singh, & McCarthy, 2011; Kong & Singh, 2009a)
	Bolus acidity (expressed as titratable acidity)	Titration	v				Micro	(Mennah-Govela, Bornhorst, & Singh, 2015)
	Gastric acid addition	Titration of gastric content				v	Macro	(Fordtran & Walsh, 1973)
	Volume of gastric secretions addition	Echo-planar imaging				v	Macro	(Marciani, Gowland, Spiller, et al., 2001)
	Gastric pH kinetics	Measurement with wireless pH capsule			v	v	Macro	(Mikolajczyk et al., 2015; Reynaud et al., 2020)
Gastric mixing	Mixing index (based on marker distribution in the stomach)	Indigestible marker analysis			v		Macro	(Bornhorst, Rutherford, et al., 2014)
	pH values at different locations in the stomach	pH mapping			v		Macro	(Bornhorst, Rutherford, et al., 2014; Nau et al., 2019)
	Meal dilution factor	Echo-planar imaging				v	Macro	(Marciani, Gowland, Spiller, et al., 2001)
Mechanical breakdown only/ combined effect of chemical and mechanical breakdown	Particle size distribution	Image analysis	v	v	v		Macro	(Bornhorst, Kostlan, & Singh, 2013; Swackhamer, Zhang, Taha, & Bornhorst, 2019)
		Laser diffraction	v	v	v	v	Meso	(Bornhorst, Ferrua, et al., 2013; Guo et al., 2015; Hoebler et al., 2002; Tamura et al., 2016a; Wang,

(continued)

Table 2.2 (continued)

Phenomena	Parameter monitored	Method used	Type of study				Length scale of structural breakdown characterized	Examples of work
			<i>In vitro</i> -static/semi-dynamic	<i>In vitro</i> -dynamic	<i>In vivo</i> - animal	<i>In vivo</i> - human		
								Ichikawa, et al., 2015)
		Sieving		v	v		Macro, meso	(Bornhorst, Roman, Dreschler, & Singh, 2014; Kozu et al., 2015)
	Particle half-residence time	Echo-planar imaging				v	Macro	(Marciani, Gowland, Fillery-Travis, et al., 2001)
	Number of intact particles	Sieving		v			Macro, meso	(Wang, Kozu, Uemura, Kobayashi, & Ichikawa, 2021)
Biochemical breakdown only/ combined biochemical and mechanical breakdown	Starch hydrolysis	Reducing sugar assay	v	v	v		Nano	(Freitas et al., 2018; Hayes et al., 2020; Wu, Deng, et al., 2017)
Biochemical breakdown only/ combined effect of biochemical and mechanical breakdown	Textural attributes (hardness, compression work)	Texture analysis	v	v	v		Macro	(Bornhorst, Ferrua, et al., 2013; Drechsler & Bornhorst, 2018; Kong et al., 2011)
Combined effect of biochemical and mechanical breakdown	Rheological properties (storage/loss moduli, viscosity, shear stress)	Rheometer		v	v		Macro	(Bornhorst, Ferrua, et al., 2013; Martens, Noorloos, et al., 2019; Nau et al., 2019; VILLEMEJANE, WAHL, AYMARD, DENIS, & MICHON, 2015; Wu, Deng, et al., 2017)
	Absolute viscosity at certain shear rate	Viscometer			v		Macro	(Guerin et al., 2001; Patarin, Blésès, Magnin, Guérin, & Malbert, 2015)

Bolus properties between different food structures are different, and this leads to varying amounts of breakdown prior to swallowing (Table 2.3). For example, short-dough biscuit, which had a brittle and porous texture with low moisture content, was reported to be masticated until a cohesive mass was formed due to continuous addition of saliva to the food particles. As a result, starch granules were released from the food matrix and suspended in the mixture of saliva with dissolved sugars and fat (Rodrigues, Young, James, & Morgenstern, 2014). On the other hand, spaghetti and rice were masticated to produce a food bolus that consists of both small (also known as the “pasted” fraction) and large particle (also known as the “cut” or “cleaved” fraction) sizes (Foschia et al., 2014; Gray-Stuart, 2016; Hoebler et al., 2000; Ranawana, Henry, et al., 2010). A mastication study on both spaghetti and white rice reported that the dominant particle diameter was >2 mm for the large fraction and <0.5 mm for the small fraction (Ranawana, Henry, et al., 2010). Similarly, other food products such as red kidney beans and white bread also had a bimodal particle size distribution after mastication with a fraction of large particles and a fraction of small particles (Pallares et al., 2019). Based on these studies, limited starch granule release from the food matrix would be expected in those products with a bimodal size distribution (e.g., rice, spaghetti), due to the heterogeneity of the bolus and cell walls that are still surrounding the large fractions. In contrast, for those matrices that are diluted by saliva into a homogeneous bolus of small, suspended particles (e.g., biscuit), the starch granules are more likely to be suspended in the bolus.

The final particle size, release of starch granules from the food matrix, and cut edges of food particles during oral processing are key parameters in starch digestion, as the characteristics of particles in an ingested food bolus can impact the duration of gastric digestion and kinetics of the gastric emptying. For example, a magnetic resonance

imaging (MRI) observation of the layering and emptying of food boluses from wholemeal bread and rice pudding revealed different bolus breakdown behavior in the stomach (Marciani et al., 2013). Rice pudding showed sedimentation of particulates with a fluid layer on the top, while wholemeal bread formed a homogeneous bolus with fluid surrounding it at the edges, close to the stomach walls. The different bolus properties of the foods were hypothesized to cause the slower gastric emptying of wholemeal bread compared to the rice pudding. These different bolus breakdown mechanisms in the stomach may lead to variations in the physical state of the food particles (e.g. particulates or paste-like mass) when they are emptied from the stomach and enter the small intestine.

Table 2.3 Examples of food structure, physical breakdown during mastication, and resulting bolus properties

Food product	Mode of physical breakdown	Resulting bolus properties	Reference
White bread	Separation between smaller particles (starch granules) and larger particles (fragments of bread network)	Cohesive food mass of soft particles with no clearly defined shape and bimodal particle size distribution (smaller fraction: $d = 5$ to $109\ \mu\text{m}$; larger fraction: $d = 757$ to $1647\ \mu\text{m}$)	(Hoebler et al., 2000)
Spaghetti	“Cut and paste”—some noodle strains are cut to short pieces and some are squeezed into small particles	Heterogeneous bolus with bimodal particle size distribution (large particle length: 5 to 30 mm; larger particle area: $>60\ \text{mm}^2$; smaller particle area: 12 to $20\ \text{mm}^2$)	(Foschia et al., 2014; Hoebler et al., 2000)
Cooked white rice	“Cleave and paste”—selected large particles are cleaved into one or a few large particles, the rest are squeezed into fine particles	Heterogeneous bolus with bimodal particle size distribution: large daughter particles (cleaved fraction, $d > 2\ \text{mm}$) and small particles (pasted fraction, $d < 0.5\ \text{mm}$)	(Gray-Stuart, 2016; Ranawana, Henry, et al., 2010)
Shortbread biscuit	Particle fracture, agglomeration of the fractured particles	Individual starch granules suspended in continuous liquid solution of saliva, dissolved sugars and fat	(Rodrigues et al., 2014)
Cooked red kidney beans	Cell rupture and separation	Bolus with multimodal particle size distribution, consisting of two major fractions: small ($d < 125\ \mu\text{m}$, cotyledon-rich) and large ($d > 2\ \text{mm}$, mostly seed coat material)	(Pallares Pallares et al., 2019)

Following the effect of mastication on gastric emptying, the next question is how mastication affects glucose release and absorption in the small intestine, which has been studied widely *in vitro* (Foschia et al., 2014; Gao et al., 2019; Gao et al., 2021; Tamura et al., 2017), but not extensively studied *in vivo*. Previous human studies have shown that higher extent of particle size reduction by mastication decreases the gastric emptying rate and increases the glycemic response of starch-rich foods (Ranawana, Clegg, Shafat, & Henry, 2011; Read et al., 1986; Zhu et al., 2014) although this relationship was later found to be food-dependent. For instance, a higher degree of mechanical disintegration during mastication was found to increase the glycemic response of white rice, but a similar observation was not found in spaghetti (Ranawana, Henry, et al., 2010). Although the authors stated some possible reasons that led to the different trends, a possible link to gastric emptying rate of the food products was not considered. These findings indicate that the relationships between food structure, bolus properties (particularly their particle size and release of starch granules from the food matrix), gastric emptying rate, and small intestinal digestion are not fully understood, thus future studies are required in this area.

2.5.2 Gastric digestion

Studies on gastric digestion of starch-based foods have demonstrated that food breakdown behavior plays a key role in the gastric emptying rate and should be understood in detail for foods of varying structures. The food breakdown behavior can be affected by what occurs during gastric digestion, including: remaining salivary amylase activity, mechanical breakdown by gastric contractions, and hydrolysis by gastric acid and enzymes. *In vitro* studies have shown that different physical breakdown behavior of foods may be related to their gastric emptying rate. For example, Drechsler and Bornhorst (2018) identified that pretzel, couscous, white rice, brown rice, quinoa,

and pasta had different softening rates (fast, intermediate, and slow softening categories) during a static *in vitro* gastric digestion experiment. In other studies using dynamic gastric digestion models, Wang, Ichikawa, et al. (2015) and Kong et al. (2011) reported that brown rice underwent slower diffusion of gastric juice into the rice kernel, which resulted in less acid hydrolysis, textural changes, solid leaching, and granule swelling than white rice.

Although most gastric digestion studies examining breakdown of solid starch-based foods were conducted using *in vitro* systems, *in vivo* studies using animal models have also suggested that the physical changes during gastric digestion influence the gastric emptying rate of solid particles in the stomach. In a study using growing pigs, Guerin et al. (2001) found that diets that resulted in gastric content of higher viscosity (after being diluted with gastric secretions) had slower gastric emptying rate; this higher viscosity did not necessarily depend on the fiber content or initial viscosity of the diets. However, also using a growing pig model, Martens, Noorloos, et al. (2019) found that the rheological properties of the gastric digesta (represented by shear stress measured at 1 Hz, close to the natural frequency of the forces applied by the GIT wall) could only partially explain the variations in the gastric emptying rates of cereal-based diets from different starch sources (barley, maize, and high-amylose maize) with different forms (extruded cereal, ground cereal, isolated starch). Further, it was reported that the variations in gastric emptying rate had better correlation with the moisture uptake of the diets during gastric digestion. While a clear connection between food breakdown behavior and gastric emptying rate is yet to be established, these studies suggest the potential of food breakdown rate in the stomach as a reflection of the gastric emptying rate.

With the use of various *in vitro* and *in vivo* approaches to investigate gastric digestion, it is necessary to assess if they can produce similar output parameters. Wang, Ichikawa, et al. (2015) reported slower dry matter emptying of brown rice compared to white rice in the *in vitro* dynamic model, which agrees with trends in the gastric emptying of brown- and white rice in humans (Pletsch & Hamaker, 2018). However, the dry matter emptying rate of brown and white rice in growing pig model was reported to be not significantly different (Bornhorst, Ferrua, et al., 2013). In another study, Hayes et al. (2020) reported that millet couscous disintegrated faster and thus underwent faster dry matter emptying than wheat couscous in a dynamic gastric digestion model. The observed trend in the emptying rate of the tested products was in contrast with gastric emptying trend from a human study with similar food products (Cisse et al., 2018). These findings imply that the current *in vitro* gastric digestion methods might have not been designed to fully mimic what happens during the actual digestion (i.e., *in vivo* system), due to the absence of physiological-related aspects that can affect the process. Furthermore, this inconsistent agreement between *in vitro* and *in vivo* models suggests the need for additional studies or considerations to correlate *in vitro* and *in vivo* results (for additional information, see Section 2.7).

One of the physiological aspects of the stomach that have not been fully considered in *in vitro* gastric digestion model is the role of functional regions of the stomach in the physical breakdown of solid starch-based foods. A study using a growing pig model by Bornhorst, Ferrua, et al. (2013), in which the pigs were fed with cooked brown- and white rice as intact grains, found distinct breakdown behavior of the study diets in the proximal and distal stomach. It was reported that the extent of physical breakdown of brown- and white rice was greater in the distal stomach, as reflected by lower resistance to flow, greater texture softening of intact food particles, and higher particle size of

gastric content from the distal stomach than from the proximal stomach. In a separate study from the same group, it was reported that the mixing of gastric content (tracked with intragastric indigestible marker and intragastric pH distributions) was lower in the proximal stomach. The extent of mixing correlated well with the rheological properties of the gastric content in the different stomach regions, where lower resistance to flow enhanced gastric mixing. This latter study also reported that the pH in the proximal region was maintained at above pH 3 until 120 min of digestion, which may have further implications on physical changes in the stomach due to biochemical breakdown (Bornhorst, Rutherford, et al., 2014).

While the physical breakdown of solid food in the stomach is known to be the result of mechanical and biochemical breakdown, the biochemical breakdown of starch-based foods in the stomach is less well-understood. The contribution of the stomach to starch digestion is generally considered minimal due to the low pH (Brownlee et al., 2018) and the proteolytic activity of pepsin in gastric secretions; both of which can lead to the loss of salivary amylase activity (Mackie, 2019). However, various *in vivo* and *in vitro* studies have suggested that a considerable amount of starch may be hydrolyzed by remaining salivary amylase activity during gastric digestion, which can be attributed to the slow mixing of gastric secretions with the ingested food bolus (Bergeim, 1926; Freitas & Le Feunteun, 2019; Freitas et al., 2018; Gao et al., 2021; Woolnough, Bird, Monro, & Brennan, 2010; Wu, Deng, et al., 2017).

Although acidic gastric secretions are added continuously to ingested food during gastric digestion, the mixing between gastric secretions and the food bolus in the stomach occurs gradually rather than instantaneously (Spiller & Marciani, 2019). This gradual mixing results in heterogeneous intragastric pH profile between the proximal and distal regions of the stomach when complete mixing has not been achieved, as

demonstrated in studies in growing pigs (Bornhorst, Rutherford, et al., 2014; Nau et al., 2019) and humans (Simonian et al., 2005). Nevertheless, the consequence of the distinct mixing profile in different stomach regions on the biochemical breakdown of starch in the food bolus has not been fully examined and requires future investigation.

The mechanism of gastric mixing causes a slow dilution of food boluses from the periphery towards their interior (Spiller & Marciani, 2019), which means the cohesiveness of food bolus from mastication may determine the rate of its dilution by gastric secretions. As a result, the food bolus softening process due to biochemical breakdown by salivary amylase can still continue during gastric digestion, as long as the pH within the bolus is maintained within the activity range of salivary amylase (Brownlee et al., 2018). This process may be impacted by the buffering capacity of food or food bolus, as it may influence the rate of gastric secretions during digestion, which can subsequently affect the rate of food bolus dilution in the stomach and intragastric pH for enzymatic hydrolysis (Mennah-Govela & Bornhorst, 2021). Additionally, the presence of salivary amylase in the food bolus was found to enhance the diffusion rate of acid into cooked rice boluses *in vitro* (Mennah-Govela et al., 2015). Previous studies have shown that salivary amylase remained active for up to 15 to 30 min during *in vitro* gastric digestion. Despite the short duration, this remaining amylolytic activity was found to hydrolyze 15 to 80% starch in baguette, bread, chickpea, mashed/boiled potato, pasta, and cooked wheat grain (Bergeim, 1926; Freitas & Le Feunteun, 2019; Freitas et al., 2018; Gao et al., 2021; Woolnough et al., 2010).

Another *in vitro* study reported that the inactivation of salivary amylase at pH 3 was slowed down in the presence of polysaccharides and oligosaccharides, which are the product of starch amylolysis (Rosenblum, Irwin, & Alpers, 1988). Since these studies were not conducted in a food matrix rich in dietary fiber (i.e., starch consumed in its

botanical source – see Section 2.2.2), interference of fiber components contained in food matrix on the remaining salivary amylase activity is not known, while fiber components in food have binding potential towards diverse molecules, including digestive enzymes (Gidley & Yakubov, 2019). An *in vitro* study showed that the binding between α -amylase and cellulose (a typical fiber component of plant food) was very rapid compared to the binding between α -amylase and starch granules, and could hinder the hydrolysis of starch granules by α -amylase (Dhital, Gidley, & Warren, 2015). However, this binding is reversible and non-specific, providing a chance for α -amylase to bind with starch granules in the food bolus, depending on the extent of structural breakdown during mastication (Dhital et al., 2015). Therefore, with the weaker gastric contractile activity, higher pH, and slower inactivation of salivary amylase in the proximal stomach, it will most likely be the main site for continuing amylolysis during gastric digestion, which in turn causes further softening of food bolus (Bornhorst, 2017; Bornhorst, Hivert, & Singh, 2014).

Another aspect that may impact starch structural breakdown during gastric digestion that deserves further investigation is the interactions between components in gastric secretions with starch granules in the food bolus. These interactions may impact remaining salivary amylase activity and its accessibility to starch granules in the food bolus. For example, mucin (a major component of mucus) may be secreted at different levels, depending on the meal, which may ultimately affect digesta rheological properties. A previous study using hydrated powder diets found that wheat starch-based powder diets mixed with pectin powder had a greater viscosity than wheat starch-based powder diets mixed with mango powder and the control diet when tested *in vitro*. However, all three diets had a similar gastric digesta viscosity value when tested in a pig model (Wu, Dhital, Williams, Chen, & Gidley, 2016). The authors hypothesized

that mucin contributes to the rheology of *in vivo* gastric digesta, either by increasing (control and mango powder diet) or decreasing (pectin diet) the digesta viscosity to the same mucin level. Although the study was not conducted with typical solid food, the results imply that different amount of mucin may be produced in response to the rheology of gastric content, which is possibly affected by the characteristics of the food ingested. Additionally, considering the alkaline nature of mucus and its role to protect gastric wall from acid (Feher, 2017c), the presence of mucin around food boluses (presumably those located around the gastric wall) may protect the bolus from penetration of gastric acid. A decreased penetration of gastric acid into the food bolus would prolong the duration of contact between starch granules and salivary amylase, potentially modifying the breakdown behavior of food in the stomach.

Additionally, the potential of continuing hydrolysis by gastric acid after the starch is partially digested by salivary amylase has not been explored in the literature. A study on combined acid and enzymatic starch hydrolysis, although not in the context of food digestion, suggested a possibility of further starch hydrolysis by gastric acid after salivary amylase is inactivated in the stomach. Using native waxy rice starch, it was reported that starch that was hydrolyzed by hog pancreatic α -amylase followed by incubation in 2.2 N HCl (for 3 h each) had higher degree of hydrolysis (measured as hydrolysis to soluble sugars) than when the starch was hydrolyzed with the enzyme only at human physiological temperature (Li et al., 2013). Moreover, the enzyme-HCl treatment was reported to increase the rapidly digestible fraction of the starch. These findings indicate that the effect of hydrolysis by salivary amylase that remains active in the stomach followed by hydrolysis by gastric acid needs future investigation using representative digestion conditions and food matrices.

The impact of diffusion of gastric acid on starch digestion, although not clearly understood, may be related to the degradation of the matrix entrapping starch granules followed by acid hydrolysis of the released starch granules from the matrix. *In vitro* studies where cooked sweet potatoes (fried, steamed, or boiled) were incubated with simulated saliva for 30 s, followed by incubation in excess simulated gastric fluid for up to 240 min, reported cell wall rupture and starch degradation under light microscopy after 240 min of digestion (Mennah-Govela & Bornhorst, 2016a, 2016b). Another *in vitro* digestion study using Granny Smith apples, which represent a rigid cellular matrix containing starch granules, reported that the softening and structural changes of the rigid matrix after soaking in simulated gastric fluid may be attributed to solubilization of pectin (a large component of apple tissue) due to acidic gastric conditions (Olenskyj, Donis-González, & Bornhorst, 2020). Although the starch degree of hydrolysis was not measured in these studies, the microstructural changes caused by the diffusion of simulated gastric fluid might have an impact on the susceptibility of starch granules to acid hydrolysis and subsequent small intestinal digestion. However, the impact of gastric acid on starch hydrolysis remains an area for future investigation in controlled *in vitro* conditions to support these hypotheses.

These possible combinations of remaining salivary amylase activity, enhanced acid hydrolysis efficiency, and reduced rate of salivary amylase inactivation may work to enhance the softening process of the food bolus in the stomach. Subsequently, mechanical breakdown processes and gastric mixing in the distal stomach may be accelerated, with potential alterations in gastric emptying. However, the mechanism of accelerated food breakdown due to continuing amylolysis in the stomach requires future investigation. Due to the changes that occur in starch-based foods in the mouth and stomach, the extent of physical breakdown during mastication and gastric digestion will

affect gastric emptying. However, the link between food structure, physical breakdown during oral and gastric digestion, gastric emptying rate, and glycemic response needs to be investigated further.

2.6 Food structure, gastric digestion, and glycemic response relationship

The digestibility of starch in the small intestine has been quantified and classified in multiple ways. Based on the rate and duration of their glycemic response *in vivo*, starch-based foods are classified based on their glycemic index (GI) and glycemic load (GL). Both GI and GL have been widely used as measures to reflect the carbohydrate quality of foods and the quality of carbohydrates in food as affected by the amount of food eaten, respectively (Jenkins et al., 1981; Salmerón et al., 1997; Singh et al., 2010). The GI is officially defined as “the incremental area under the blood glucose response curve of a 50-g carbohydrate portion of a test food expressed as a percent of the response to the same amount of carbohydrate from a standard food taken by the same subject” (FAO, 1998). The response is typically measured between 0 to 120-min after meal in non-diabetic subjects or up to 180 min in diabetic subjects (Brouns et al., 2005). To account for the portion of the food, the GL is calculated by multiplying GI with dietary carbohydrate content in the meal consumed.

Based on their rate of *in vitro* small intestinal digestion, starch fractions in foods are commonly classified as: rapidly digestible starch (RDS), slowly digestible starch (SDS), and resistant starch. This *in vitro*-based classification is further complemented with the classification of glucose in the foods to rapidly available glucose and slowly available glucose, according to the rate at which glucose from sugars and starch in the food products becomes available for absorption in the small intestine (Englyst, Kingman, & Cummings, 1992; Englyst, Englyst, Hudson, Cole, & Cummings, 1999). Although these

classification systems have been widely used for nutritional purpose, they do not necessarily reflect the intrinsic property of the starch because the actual rate of starch digestion is affected by enzyme:substrate ratio, solution conditions, degree of intactness of the food matrix used for the test, and interindividual variations (Dhital et al., 2017).

Using *in vitro* and *in vivo* approaches, together with these starch digestibility classifications, researchers have identified food structure-related factors that affect the digestibility of starch-based foods. These factors include: native starch characteristics (amylose and amylopectin content, granular starch structure, starch granule size, degree of crystallinity); processing methods and conditions (determines degree of starch gelatinization, intactness of the gross matrix and whole grain structure, entrapment of starch granules in the food matrix, and interaction between starch and non-starch components in the food matrix), storage method and conditions (determines retrogradation of the molecular structure), and external factors such as the presence of added fibers, acid, or amylase inhibitor in the food matrix process, which have been previously reviewed (Arvidsson-Lenner et al., 2004; Dhital et al., 2017; Magallanes-Cruz et al., 2017; Parada & Aguilera, 2011; Pellegrini et al., 2020; Singh et al., 2010). The combination of these factors creates food matrices with different complexities at the microstructural level and different accessibility for enzymatic digestion, affecting the glycemic response of the food. In addition to food-related factors, the glycemic response of starch-based foods may also be influenced by the physical breakdown during mastication and gastric digestion, as previously discussed (Section 2.5), as well as gastric emptying rate of the foods.

2.6.1 The importance of food structure on gastric emptying rate and glycemic response

Gastric emptying rate has been reported to account for 35% of the variations in intra-individual glycemic response profile in healthy subjects and those with early type 2 diabetes (Horowitz, Edelbroek, Wishart, & Straathof, 1993; Jones et al., 1996). This variation in gastric emptying rate and glycemic response cannot be separated from the initial structure of the food (Arvidsson-Lenner et al., 2004). There have been previous examinations of the gastric emptying rate and glycemic response of starch-based foods as affected by food structure (Table 2.4). In general, gastric emptying rate and glycemic response have been shown to have a proportional relationship (i.e., foods with slow gastric emptying rate have lower glycemic response) and *vice versa* (Bornhorst & Singh, 2012). As an alternative to gastric emptying rate, the term gastric emptying half-time is also often used. Since the gastric emptying half-time increases when the gastric emptying rate decreases, the gastric emptying half-time has been inversely correlated with glycemic response.

The relationships between gastric emptying rate and glycemic response of starch-based foods can be related to their structural differences at multiple length scales. However, many studies on gastric emptying and glycemic response relationships were conducted using foods that do not require size reduction in the stomach (due to their small particle size). For example, it was found that mixed meals containing of mashed white kidney bean or mashed potato flakes (i.e., similar physical forms) had the same gastric emptying rate, but the potato meal exhibited higher glycemic response than the bean meal (Torsdottir et al., 1989). The glycemic response of the potato meal was found to have a negative correlation with its gastric emptying rate, but no correlation was found for the bean meal. The microstructural nature of legume starch, which has higher

structural integrity of cells that entrap the starch granules, was hypothesized to be the reason for slower hydrolysis and subsequent glycemic response in the kidney bean meal (Torsdottir et al., 1989). Similarly, Cisse et al. (2018) reported that traditional Malian foods (in the form of sorghum- and millet-based thick porridge or couscous) exhibited slower gastric emptying rate when compared to other common carbohydrate sources with larger particle size, such as rice, potatoes, and pasta. They speculated that the slow gastric emptying rate could possibly lead to lower glycemic response. It was also hypothesized that the slower gastric emptying rate was influenced by the intrinsic slow hydrolysis rate of millet and sorghum starches, indicating the microstructure of these botanical sources of starch had a greater effect on gastric emptying rate and glycemic response than the macrostructural differences. These studies suggest that when gastric emptying rate and glycemic response are not affected by macrostructural differences, then assessment at microscale (e.g., network between starch and other food components, morphological characteristics) or nanoscale (e.g., crystallinity of the starch granule) level should be considered to explain potential differences between different food matrices. While it may be true that microstructural differences lead to different starch digestibility, many starch-based foods require further particle size reduction (i.e., macrostructural breakdown) prior to gastric emptying. Therefore, macrostructural differences should also be looked at in examining the digestion of starch-based foods.

Food particle size and viscosity are macrostructural aspects that have been reported to cause differences in the gastric emptying rate and glycemic response of solid and semi-solid starch-based foods. Previous gastric emptying studies using semi-solid test meals of varying viscosity reported a temporary delay or small effect of meal viscosity on gastric emptying (Marciani et al., 2000; Marciani, Gowland, Spiller, et al., 2001; Zhu, Hsu, & Hollis, 2013), as gastric secretions could rapidly dilute the meals due to

their semi-solid consistency. Contradictory to these studies, Wolever et al. (2019) reported a delay in the gastric emptying half-time of breakfast cereals (semi-solid) with higher viscosity, which were consumed with bread (solid), and the delay was consistent until 90 min after consumption of the meals. The study also reported that higher viscosity of the semi-solid phase of the test meals led to lower glycemic response of the meals. However, no significant correlation between the gastric emptying half-time and glycemic response was found because the gastric emptying quantification method used in the study (^{13}C breath test) only reflected the emptying of the semi-solid portion of the meals.

Table 2.4 Previous investigations on the relationship between food structure, gastric emptying rate (GER), and glycemic response (GR) of starch-based foods.

Test foods	GE measurement method	Finding	Reference
Cooked pasta, mashed potatoes, cooked rice, French bread	Scintigraphy	Maximum variation in the GR of the test foods (bread > mashed potato > rice > spaghetti) was negatively correlated with GE half-time of the foods (spaghetti > rice > mashed potato > bread). The different GE emptying half-time and GR of the test meals was hypothesized to be caused by the difference in the initial particle size of the test foods.	(Mourot et al., 1988)
Potato flakes, bean flakes in mixed meal (with fried beef)	Scintigraphy	Although in flaked form, beans still maintain their slow-release properties (GR potato flakes > bean flakes). GER cannot explain the differences between potato and bean flakes because both meals were emptied virtually at the same rate.	(Torsdottir et al., 1989)
Steamed rice, congee, high and low-concentration glucose solution	Scintigraphy	Steamed rice caused higher incremental GR than congee.	(Chang, Passaro, Shain, & Chen, 1991)
Wholemeal pasta served with sides of high fiber content (high fiber meal), white pasta served with sides of low fiber content (low fiber meal)	Real-time ultrasonography	Removal of fiber from the meal caused significant increase in GER and higher postprandial peak GR. Fiber presents naturally in food delayed the return of hunger.	(Benini et al., 1995)

(continued)

Table 2.4 (continued)

Test foods	GE measurement method	Finding	Reference
Fiber-containing cereals (bran flakes, wholemeal oat flakes), corn flakes	Real-time ultrasonography	The intake of fiber-containing cereals on has no significant effect the total postprandial GR, but slowed down GE, when compared to cornflakes.	(Hlebowicz, Wickenberg, et al., 2007)
Rye wholemeal or white wheat bread, consumed with ham, and light fruit drink	Real-time ultrasonography	No difference in postprandial GR or GE between the different treatments, possibly due to different carbohydrate and dietary fiber contents of the bread products.	(Hlebowicz et al., 2009)
Oatmeal- and durum wheat meal-porridge, consumed with mango drink	MRI	Wheat meal porridge, which had lower viscosity than the oatmeal porridge, had slower GER and longer GE half-time, and thus lower GR. The delayed GE was attributed to the higher caloric content and solid particle size in the wheat meal porridge.	(Gopirajah, Raichurkar, Wadhwa, & Anandharamakrishnan, 2016)
Porridge from oat flakes or oat flour	MRI	GR and GER of flour-based porridge were higher than that of flake-based. The smaller size of flour-based porridge caused higher availability of starch for small intestinal digestion, leading to higher GR.	(Mackie et al., 2017)
Traditional Malian foods (decorticated millet/sorghum thick/thin porridges, millet couscous), rice, potato, wheat pasta	¹³ C breath test	Rice, boiled potatoes, pasta, and thin porridge were emptied faster than the thick porridge and couscous. The slower GER of the traditional Malian foods possibly reduced GR too by increasing the feeling of satiety.	(Cisse et al., 2018)
Semolina, cracked wheat, whole wheat flour, refined wheat flour, and reconstituted wheat porridges with matched particle size and viscosity	¹³ C breath test	No significant difference in the GER between test foods. Physical property of wheat grain (particle size in this case) has more impact on GR than the composition and presence of dietary fiber in the test foods.	(Pletsch, 2018)
Breakfast cereals with varying viscosities (cream of rice, oatmeal with low and high added oat-bran, oatmeal with high added oat-bran and β -glucanase), consumed with white bread, butter, jam, and milk	¹³ C breath test	Meal with the highest viscosity had the longest GE half-time and lowest GR, while meal with the lowest viscosity had the shortest GE half-time and highest GR. However, GE half-time and GR were not significantly related.	(Wolever et al., 2019)
White rice and riceberry (deep purple grain) rice consumed with eggs and water	Scintigraphy	Riceberry rice had slower GER, resulted in reduction in postprandial GR, possibly due to its fiber content.	(Muangchan et al., 2021)

The contradictory trends reported in these studies highlight the potential importance of intragastric dilution of meals and its potential link with gastric emptying and glycemic response, and represent a topic of future investigation. Previous studies have reported variations in intragastric dilution of a meal with gastric secretions between high and low viscosity meals (Marciani, Gowland, Spiller, et al., 2001), but these reports did not link the rate and extent of intragastric dilution to gastric emptying or glycemic response of meals. Future studies are recommended to investigate the relationships between meal properties, intragastric dilution and subsequent viscosity changes, gastric emptying, and glycemic response.

Previous studies using growing pig models (Section 2.5.2) suggested that compared to the meal initial viscosity, the rheological properties of gastric content (i.e., meal mixed with gastric secretions) as a result of gastric digestion are more critical to gastric emptying than the initial meal viscosity. In a study where growing pigs were fed with hydrated powdered diets of different rheological properties, Wu et al. (2016) suggested that the pig stomach can maintain a rheological homeostasis of the gastric digesta, regardless of the viscosity of the diet, through the regulation of various factors including gastric secretory response. However, the design of this study was intended to maintain a constant digesta flow, and made it difficult to observe the effect of gastric sieving and emptying on the digesta rheological properties.

In another study on a single meal, it has been reported that the rheological properties of gastric content may be affected by meal initial properties, amount of gastric secretions, extent of intragastric dilution, and gastric sieving (Wolever et al., 2019). A gastric emptying study using MRI by Marciani et al. (2012) revealed that a meal consumed in puréed form had slower gastric emptying rate than the same meal consumed as solids eaten with a liquid (water). While the solid/liquid meal underwent

gastric sieving effect to empty liquid first, the puréed meal remained viscous in the stomach despite intragastric dilution by saliva and gastric secretions. This resulted in delivery of fine particles of nutrients at the early phase of digestion that triggered hormones responsible for slowing gastric emptying rate in the puréed meal. Another study from the same group reported that wholemeal bread meal that entered the stomach as a cohesive bolus experienced minimal gastric sieving. However, creamed rice pudding, that did not form a cohesive bolus, experienced sieving of the liquid fraction of the meal from the stomach (Marciani et al., 2013). These *in vivo* studies in humans and pigs imply that the rheology of gastric digesta may impact the gastric emptying rate, but this may be affected by the gastric sieving effect that is dependent on the heterogeneity of the bolus. However, the inconsistent trends in the link between gastric digesta rheological properties and gastric emptying of solid starch-based meals make the extension of this relationship to glycemic response not well-defined. Furthermore, it may be difficult to apply rheological measurements on meals with solid consistency (i.e., heterogeneous mixture), and alternative measurement methods that can represent the consistency of solid food are needed.

While viscosity or rheological property determination is generally difficult to be done on gastric digesta from solid meals, food particle size is easier to be characterized as representative of macrostructural breakdown (Table 2.2). This results in particle size as a critical factor in determining the gastric emptying rate and glycemic response of a solid meal. The role of particle size in gastric emptying and glycemic response has been studied in starch-based foods over the past several decades. A study in late 1980's reported that durum wheat spaghetti and round rice had longer gastric emptying half-time and lower glycemic response than mashed potato and French bread in humans (Mourot et al., 1988). The relationship between the gastric emptying half-time and

glycemic response of the foods was hypothesized to be caused by the difference in their initial particle size, rather than the meal energy density or composition. Mackie et al. (2017) also found that particle size of oatmeal (flake vs. flour) in porridge affected the gastric emptying rate and glycemic response of the meals. The size of particles in the flour-based porridge, which was small enough to pass through the pylorus, caused the flour-based porridge to be emptied faster than flake-based porridge. This smaller particle size was also attributed to increased availability of starch for hydrolysis in the small intestine and resulted in a higher glycemic response. These studies indicate that particle size of solids in a starch-based meal can impact the gastric emptying rate and glycemic response. Nevertheless, the exact mechanism is not properly understood because in these studies the physical breakdown of the meals during gastric digestion was not quantified.

In addition to impacting both the gastric emptying rate and glycemic response, particle size of food may affect the glycemic response without affecting the gastric emptying rate. A human study where the subjects were fed porridge made of whole- or refined wheat grains with different particle sizes (180- and 425- μm for the grain fractions, and 1700 μm for the bran fractions of whole grain) and similar viscosity found no significant difference in the gastric emptying rate of the test foods due to the initial particle size (<1 to 2 mm) of the grains in the porridge (Pletsch, 2018). However, it was found that porridge made of semolina middlings, which had the second largest size (425 μm) of the grain fraction among the grains studied, had the lowest glycemic response. Interestingly, the glycemic response of the semolina porridge was lower than porridge containing bran layer. Moreover, the highest glycemic response was observed in the whole wheat flour porridge, which had higher fiber content but the smallest size (180 μm) of the grain fraction among the test foods. It was concluded that the particle

size of food is more significant to glycemic response than the presence of fiber in the food when the other physical properties are similar. It was also hypothesized that the breakdown that occurred in the stomach might have occurred in such a way that resulted in equal gastric emptying rate for all test foods used in the study. Although the breakdown mechanisms of the test foods in the study by Pletsch (2018) were not investigated, the finding signifies that the size of particles emptied from the stomach, which may be affected by physical breakdown during gastric digestion, is crucial to the subsequent starch hydrolysis in the small intestine.

From these discussions, it is hypothesized that food structure, gastric emptying rate, and glycemic response can be linked in various ways:

- (1) when ingested food enters the stomach as a non-cohesive mixture and needs further macrostructural breakdown in the stomach, the gastric emptying rate and glycemic response may be governed by the rate of food breakdown in the stomach and gastric sieving;
- (2) when ingested food enters the stomach as a cohesive mixture (as a result of mastication or because of its initial homogeneous physical state), the effect of gastric sieving may be minimal and the rheological properties of the digesta may be a limiting factor for gastric emptying rate and glycemic response; and
- (3) when the initial particle size of the food is small enough to be emptied from the stomach without further mechanical breakdown, the glycemic response may be affected by the starch hydrolysis rate during intestinal digestion (which can be limited by the size and/or microstructure of the solid particle) and their impact on physiological responses that regulate gastric emptying rate.

Food structuring strategy from the microstructural aspects to modulate glycemic response have recently been reviewed (Korompokis, Verbeke, & Delcour, 2021). Future

work is needed to better characterize and explore the relationships between food structure from the macrostructural aspects, gastric emptying rate, and glycemic response, as previous studies have shown different trends for different products and experimental designs.

2.6.2 Gastric breakdown behavior, gastric emptying rate and glycemic response

Studies shown in Table 2.4 have not directly linked the glycemic response and gastric emptying rate or half-time of starch-based foods with their breakdown behavior during gastric digestion, although some of the studies implied the potential contribution of physical breakdown during gastric digestion to gastric emptying. Meanwhile, some gastric digestion studies suggest that gastric breakdown behavior (the physical changes of food during gastric digestion) may play a critical role in understanding the link between food structure, gastric emptying, and glycemic response. For example, Drechsler and Bornhorst (2018) showed that the different softening rates of pretzel, couscous, white rice, brown rice, quinoa, and orzo pasta in a static *in vitro* gastric digestion model were proportional to previously published glycemic indices for similar foods, except for orzo pasta.

Several studies using brown and white rice also suggest the link between gastric breakdown mechanisms and gastric emptying. In both *in vitro* dynamic gastric digestion system (Kong et al., 2011; Wu, Deng, et al., 2017) and *in vivo* growing pig model (Bornhorst, Rutherford, et al., 2014), it was demonstrated that brown rice broke down differently from white rice during gastric digestion. Furthermore, the study using growing pig model also showed that the breakdown mechanism of brown rice occurred in such a way that the bran layer was retained in the distal stomach, resulting in a slower gastric emptying of protein in brown rice (Bornhorst, Chang, et al., 2013). However, the emptying rates of dry matter and starch were similar for brown- and white rice, which

can be linked to the similar glycemic responses between brown- and white rice of the same varieties (Atkinson, Foster-Powell, & Brand-Miller, 2008). On the other hand, in a human study using different varieties of brown- and white rice, Pletsch and Hamaker (2018) found that even with similar amount of SDS and RDS (i.e., minimal microstructural differences), brown rice had slower gastric emptying rate than white rice. It was hypothesized that the slower gastric emptying rate was due to the different physical breakdown between brown- and white rice, which can partially explain lower glycemic response in brown rice of certain varieties.

Despite results from previous studies that show a potential relationship between gastric breakdown behavior and glycemic response of starch-based foods, there have been some conflicting findings between *in vitro* gastric breakdown behavior and *in vivo* glycemic response. For example, Nordlund, Katina, Mykkanen, and Poutanen (2016) compared the extent of disintegration of various types of bread (made of rye or wheat) in a static *in vitro* gastric digestion setup with *in vivo* glycemic response in healthy subjects. Rye sourdough bread (with a dense structure) was chewed less by human participants and thereby disintegrated to a much lower extent during *in vitro* gastric digestion than refined wheat bread (with a very porous structure). However, the *in vivo* glycemic responses of both products were found to be similar, regardless of the differences in their *in vitro* breakdown behavior and initial food structure. The slower disintegration property of rye bread was hypothesized to induce lower insulin response as it disintegrated in the stomach, which lead to lower blood glucose clearance rate.

In another study, Hayes et al. (2020) found that millet couscous broke down and emptied faster than wheat couscous, but underwent slower hydrolysis in a dynamic *in vitro* gastric digestion model. On the other hand, a human study using similar foods showed that millet couscous had very slow gastric emptying half-time (Cisse et al.,

2018). The slow gastric emptying of the millet couscous was hypothesized to induce lower glycemic response due to its slow digestion rate and the presence of the ileal brake, which was only partially captured in the *in vitro* study by Hayes et al. (2020). Based on these conflicting results between *in vitro* breakdown behavior and *in vivo* gastric emptying and glycemic response, there are many factors that need to be considered in understanding the effect of food structure on its behavior during digestion. One of them may be related to gastric sieving, which leads to selective emptying of food particles and may interact with hormonal feedback by the small intestine (see Section 2.3.2). This gastric sieving effect may not be perfectly simulated in *in vitro* models. However, with the right experimental approach to capture the breakdown behavior of particles in the gastric phase, correlation between *in vitro* and *in vivo* data may be drawn.

2.7 *In vitro-in vivo* correlation (IVIVC) in starch digestion

2.7.1 Common *in vitro* methods for starch digestion and their correlation to *in vivo* glycemic response

The GI and GL have been used as a guide to food selection, especially for people with diabetes. Foods with low GI and GL may be beneficial for blood glucose and lipid management (Venn & Green, 2007). Various food products (>750 types) have been tested for their GI and GL in human subjects, resulting in international tables of GI and GL for healthy and diabetics adults in the literature (Foster-Powell, Holt, & Brand-Miller, 2002), indicating that the prediction of GI and GL is an important component in starch digestion studies. However, it is not practical to always conduct human studies to provide GI and GL of new food products due to time- and resource-related constraints. Consequently, *in vitro* methods have become a preferred approach to predict the GI and

GL of starch-based foods (Brand-Miller & Holt, 2004). There have been numerous *in vitro* digestion methods introduced to predict *in vivo* GI and GL such as the widely used *in vitro* Englyst assay to determine nutritionally important fractions in starch (Englyst et al., 1992) and the hydrolysis index method (Goñi, Garcia-Alonso, & Saura-Calixto, 1997). Other available methods (described in detail in a review by Woolnough, Monro, Brennan, and Bird (2008)), and several more recent methods have also been used (Argyri, Athanasatou, Bouga, & Kapsokefalou, 2016; Bellmann, Minekus, Sanders, Bosgra, & Havenaar, 2018; Monro, Mishra, Blandford, Anderson, & Genet, 2009).

Previous studies on the comparison between *in vitro* and *in vivo* glycemic responses of various food products (Table 2.5) reported a high *in vitro-in vivo* correlation based on a generalized comparison between data from many food types. While there are data points from certain food types that deviate from the correlation, their deviations from the correlation were counterbalanced by the data points that exhibit similar *in vitro-in vivo* correlation. Without accounting for certain food types that deviate from the *in vitro-in vivo* correlation, this generalization may cause misprediction of the *in vivo* glycemic response of certain food products (Ferrer-Mairal et al., 2012; Venn et al., 2006). The deviation of certain food products from generalized correlations may suggest that some foods have different breakdown mechanism due to their structure that occur *in vivo* and are not mimicked during *in vitro* studies. The contribution of food breakdown in the *in vitro* system on the predicted glycemic response has not been examined in detail in the previous studies and is an area for future research.

Table 2.5 Examples of *in vitro* starch digestion studies and their comparison with *in vivo* glycemic responses (GRs).

Food	Digestion method	Finding	Reference
Custard, quick-cooking wheat, shortbread biscuits, wholemeal bread, water biscuits, puffed wheat, puffed crispbread	<i>In vivo</i> (human study) <i>In vitro</i> (static model, following Jenkins et al. (1984))	High correlation between <i>in vivo</i> GI and <i>in vitro</i> percent starch digested ($r = 0.86$) when custard was excluded from the relationship. GR of custard was much lower than its <i>in vitro</i> starch digestibility.	(Ross, Brand, Thorburn, & Truswell, 1987)
Corn flakes, white bread, cooked white spaghetti, cooked white barley	<i>In vivo</i> (human study) <i>In vitro</i> (static model, following Englyst et al. (1999))	Rapidly available glucose in the food can explain 68.8% of the GR, after accounting for the effect of subject. However, it was not tested if the correlation will remain if more food is ingested.	(Englyst, Vinoy, Englyst, & Lang, 2003)
Rapidly digested rice starch, moderately rapid-digested rice starch, pea starch, corn starch	<i>In vivo</i> (pig model) <i>In vitro</i> (static model, modified from Englyst et al. (1999))	Better relationship between <i>in vitro</i> cumulative glucose release and <i>in vivo</i> portal vein glucose appearance after correction with gastric emptying ($R^2 = 0.95$ vs. $R^2 = 0.89$ without correction).	(van Kempen, Regmi, Matte, & Zijlstra, 2010)
Bread and muffins (bakery products) with/without resistant starch addition	<i>In vivo</i> (human study) <i>In vitro</i> (static model, following Goñi et al. (1997))	Similar trend of GI reduction between <i>in vitro</i> and <i>in vivo</i> results, but no strong correlation was present between <i>in vitro-in vivo</i> results. <i>In vitro</i> method resulted in higher estimated GI than <i>in vivo</i> GI, but the difference between estimated and actual values was lower in high GI food.	(Ferrer-Mairal et al., 2012)
Foods (16 types) from different categories (sugary beverages, breakfast cereals, cereal grains, fruit, bread, legumes, dairy product, infant formula)	<i>In vitro</i> (static model) Compared with available <i>in vivo</i> data	Better correlation values when <i>in vitro</i> dialyzable glucose data were compared to <i>in vivo</i> GL than GI. Although some data points deviated from the correlation, the correlation level between <i>in vitro-in vivo</i> data was high, especially at longer <i>in vitro</i> incubation period (e.g., Spearman's rho for <i>in vivo</i> GL vs. <i>in vitro</i> dialyzable glucose = 0.656 at 0 min vs 0.953 at 120 min).	(Argyri et al., 2016)
Foxtail millet products (steamed bread, pancake)	<i>In vivo</i> (human study) <i>In vitro</i> (static model, modified from Englyst et al. (1999))	High positive correlation between estimated GI and <i>in vivo</i> GI ($r = 0.988$).	(Ren et al., 2016)
Carob tablet and carob flour	<i>In vivo</i> (human study) <i>In vitro</i> (static model, modified from Goñi et al. (1997))	Linear correlation between <i>in vitro</i> – <i>in vivo</i> glucose concentrations (R^2 of Bland-Altman scatter plot = 0.9563).	(dos Santos, Tulio, Campos, Dorneles, & Krüger, 2015)
Bread from white bean and mung bean	<i>In vivo</i> (human study) <i>In vitro</i> (following van	Predicted GI from <i>in vitro</i> digestion using freeze-dried samples than	(Hefni, Thomsson, &

(continued)

Table 2.5 (continued)

Food	Digestion method	Finding	Reference
	Kempen et al. (2010))	frozen samples complied better with <i>in vivo</i> GI. Predicted GI using fresh samples was lower than <i>in vivo</i> GI.	Witthöft, 2020)

2.7.2 Development of IVIVCs in starch digestion studies for future food structure development

With the increasing use of *in vitro* models to predict *in vivo* nutrient bioavailability and absorption, it is necessary to validate the reliability of the *in vitro* models through *in vivo* studies (Bornhorst & Singh, 2014), which can be done through establishing an *in vitro-in vivo* correlation (IVIVC). The term IVIVC was first introduced in the pharmaceutical field, but researchers in food area are now looking towards the same direction as a tool for food product development (Bornhorst et al., 2015). In the guidance for developing an IVIVC for an extended release oral dosage, United States Food and Drug Administration (FDA) defined that the goal of an IVIVC is to accurately and precisely predict the expected bioavailability characteristics for a product from dissolution profile characteristics (FDA, 1997). The main objective of IVIVC development and evaluation for pharmaceutical products is to establish *in vitro* dissolution tests as a surrogate for human bioequivalence studies. An IVIVC will allow for reduction of the number of human studies performed during the initial approval process of a new formulation of an oral dosage as well as during certain scale-up and post-approval charges (FDA, 1997). The levels of correlation range from a point-to-point relationship between *in vitro* dissolution rate and *in vivo* plasma drug concentration to limited or no meaningful correlation between *in vivo* and *in vitro* data. The highest correlation (point-to-point IVIVC) means that *in vitro* dissolution experiments are sufficient to reflect the drug absorption *in vivo*, despite intra- and inter-individual variations that may affect drug bioavailability, thus reducing the need for

human studies (Emami, 2006). The lowest correlation expects limited or no IVIVC and therefore the use of IVIVC is not recommended in the approval of such new oral dosage formulation (FDA, 1997).

Using the same concept, establishing a robust IVIVC for starch digestion will be a useful tool in deciding whether *in vitro* digestion methods are accurate and sufficient to predict *in vivo* glycemic response of certain food products, based on the correlation level between *in vitro* and *in vivo* data. This is particularly important to ensure that consumers, health professionals, and people with diabetes are provided with accurate information about the glycemic impact of foods when the values are to be tested through *in vitro* experiments (Brand-Miller & Holt, 2004). Moreover, the development of an IVIVC may be important in future food development, for example, if regulatory requirements require *in vitro* or *in vivo* testing as a part of food labelling, as well as to support nutrition and health-related claims.

The inconsistent IVIVC from the commonly used starch digestion methods can be associated with the lack of physiological factors incorporated into the experimental method as well as food-related factors (Brand-Miller & Holt, 2004), in addition to the lack of standardization across the *in vitro* digestion methods (Woolnough et al., 2008). Most of the *in vitro* digestion methods (including those listed in Table 2.5) involve static incubation, are heavily focused on intestinal digestion, and neglect the physical breakdown aspect during digestion by the use of finely ground or homogenized samples – although some methods use chewed food boluses or utilized dynamic digestion models. In a combined *in vitro-in vivo* (pig model) starch digestion study, van Kempen et al. (2010) found that the commonly used classification of nutritional starch fractions to RDS, SDS, and resistant starch had little contribution in the prediction of *in vivo* glycemic responses to different starch sources. Meanwhile, gastric emptying and

intestinal glucose utilization had a greater contribution to the estimation of *in vivo* glycemic response (van Kempen et al., 2010). Similarly, classification of starch-based foods based on their softening rate during *in vitro* gastric digestion (Drechsler & Bornhorst, 2018) was inversely proportional to the reported glycemic indices of the foods, except for orzo pasta that slightly deviated from the trend. These studies suggest the need to incorporate the aspect of food breakdown behavior in the stomach and/or gastric emptying rate to the prediction of *in vivo* glycemic response rather than food structure alone, to take into account the rate of release of material to the small intestine.

To provide justification in establishing an IVIVC, Bornhorst et al. (2015) proposed a food breakdown classification system (FBCS) to classify solid foods according to their initial hardness and rate of softening under physiological gastric conditions, which is expected to allow for prediction of *in vivo* gastric breakdown behavior. The concept was developed based on previous *in vitro* gastric digestion studies that examined changes in food texture along with food particle disintegration, which are affected by several factors, such as initial moisture content and structure (Bornhorst et al., 2015). According to this framework, whether an IVIVC will be possible for certain food products is predicted by the FBCS class. The FBCS class is determined based on the food initial hardness and rate of softening, and can also help predict the rate-limiting mechanism of breakdown during gastric digestion (Table 2.6). Similar to IVIVCs in the pharmaceutical industry, it is worth noting that not all food structures will have a direct IVIVC. The FBCS is a concept that still needs further refinement and validation with more *in vivo* data (Bornhorst et al., 2015). However, the FBCS has been shown to be comparable with *in vivo* data of rheological properties and gastric emptying rate of white and brown rice (Bornhorst, Chang, et al., 2013) or almonds in growing pigs (Bornhorst, Roman, et al., 2014). This framework may potentially be applied in

developing an IVIVC for starch digestion, with an extended application to glycemic response prediction of starch-based food products.

Table 2.6 The food breakdown classification system (FBCS) framework (Bornhorst et al., 2015).

Class	Initial hardness	Rate of softening	Rate limiting mechanism	<i>In vitro-in vivo</i> correlation expectation	Examples of food product
I	High	Fast	Dissolution rate and/or gastric emptying	Yes	Pretzel, candy
II	Medium	Fast	Cellular disruption/breakdown	Yes, if cellular disruption achieved <i>in vitro</i>	Apple, cooked white rice
III	Low	Fast	Dissolution & cellular disruption	Yes, if cellular disruption achieved <i>in vitro</i>	Soft fruits, cooked vegetables
IV	High	Slow	Macro-structural breakdown & acid absorption	No	Seeds/nuts
V	Medium	Slow	Macro-structural breakdown & dissolution	Yes, if dissolution rate is greater than macro-structural breakdown	Cooked pasta, brown rice
VI	Low	Slow	Macro-structural breakdown	No	Cooked meat

2.8 Considerations in developing IVIVC of starch-based foods with gastric digestion

While quantification of food breakdown during gastric digestion may provide a better IVIVC for starch-based foods tested in an *in vitro* digestion system, the digestion process parameters need to be mimicked properly to draw valid conclusions relating to the breakdown behavior of the food. With the function of the stomach as the major site of physical breakdown of food and the gastric digestion mechanism of the stomach, factors related to the physiology of the organs that can impact the gastric breakdown mechanism should be considered. Meal size, particle size after mastication, mixed-meal effects, and the state of the stomach prior to meal consumption are some of the factors to be considered in assessing the effect of gastric digestion on glycemic response. This section provides representative examples of previous studies demonstrating the

importance of these factors on gastric digestion and glycemic response of starchy foods, and provide considerations for future research working to develop realistic digestion models to form the basis of IVIVCs for starch-based foods.

2.8.1 Meal size

The amount of carbohydrate-rich food consumed (meal size) is an important determinant of glycemic response of the food; this is the basis of the GL concept (Arvidsson-Lenner et al., 2004). For example, pasta (low GI food) consumed in a large portion was reported to elicit higher peak glucose and higher overall glycemic impact than a potato meal (high GI food) that was consumed in a small portion (Zurbau et al., 2019). Similarly, meal size also determines the gastric emptying of solid foods, with potential effect on the gastric breakdown rate of the food product. In order to observe the unique functions of the proximal and distal stomach, there is a minimum working volume required to ensure both stomach regions are filled; this is recommended to be equivalent to not less than 300 g of meal (Christian, Datz, & Moore, 1987). Meanwhile, for glycemic response studies it is recommended to use test meal containing 50-g available carbohydrate (Brouns et al., 2005), which may not fulfil the 300-g requirement of stomach working volume (i.e., full stomach scenario) and may impact the gastric breakdown behavior of the meal.

The meal size may also modify the specific biochemical environment in the stomach, further impacting the subsequent gastric emptying and glycemic response. For instance, a study by Freitas et al. (2018) demonstrated that the activity of human salivary amylase during *in vitro* semi-dynamic gastric digestion was preserved for a longer time when bread was digested in different portion sizes (“snack” vs “lunch” portion). In the scenario of a “snack” portion, 50% inhibition of salivary amylase activity was achieved at around 15 min of digestion. Meanwhile, the same level of

inhibition was achieved in the “lunch” portion after 30 min due to longer time required for the acidification of the simulated bolus. This study provides strong evidence that the overall meal size or volume should be considered when developing *in vitro* and *in vivo* studies of starch digestion as they influence the process of gastric secretion mixing with food bolus during gastric digestion. The meal size may also impact the rate and extent of dilution by gastric secretions, which may not be accurately simulated in all *in vitro* models. Nevertheless, the limited availability of the information on the effect of meal size on gastric digestion, residual enzyme activity, meal dilution, and glycemic response suggests that this topic merits future investigation and verification with *in vivo* studies.

In relation to the meal size, the rate of feeding or eating to fill the stomach with a particular meal size has been reported to affect glycemic response. For example, a human study reported that the glycemic response of medium-low amylose white rice eaten using chopsticks (smaller mouthful size and slower feeding rate, therefore longer time to fill the stomach) was ~13% lower than when the rice was eaten using spoon or finger (Sun et al., 2015). The fact that food boluses fill the stomach layer by layer, stacking on top of each other to fill the distal stomach then the proximal stomach (Schulze, 2006), indicates that food boluses may have different retention time in the stomach. Further, this different retention time may affect the extent of breakdown of the food boluses by remaining salivary α -amylase activity prior to gastric emptying, their gastric emptying rates, and ultimately their rate of glucose release to the blood. This also implies the importance of properly simulating the gastric filling mechanism in *in vitro* setup, where the bulk of the test meal is mixed with simulated digestive fluids. Nevertheless, how the retention time of food boluses in the stomach and how their contact time with gastric secretions may subsequently affect their gastric breakdown behavior are not fully understood.

2.8.2 Effect of mastication

It has been previously shown that the particle size of food entering the stomach affected its gastric emptying rate and glycemic response (Table 2.4), which implies that the output of mastication is as important as the gastric digestion process of starch-based foods. Previous human studies have suggested that more chewing cycles caused higher gastric emptying rate, and the change in gastric emptying rate may impact the glycemic response of the food (Pera et al., 2002; Ranawana et al., 2011; Ranawana et al., 2014; Ranawana, Monro, et al., 2010). For example, Pera et al. (2002) found that foods that were chewed with 25 masticatory cycles had longer lag phase and half-emptying time than those chewed with 50 masticatory cycles. Although glycemic response was not measured in this study, extensive particle size reduction due to chewing has been reported to cause an increase in glycemic response (Read et al., 1986). It is worth noting, however, that chewing behavior toward different food structures, which plays an important role in the number of chewing cycles, does not always guarantee an implication on glycemic response. For example, Ranawana, Henry, et al. (2010) reported that cooked spaghetti had lower glycemic response than cooked rice, although the number of chews per mouthful was higher for spaghetti.

In a study conducted to find the best simulated mastication method for spaghetti that can produce similar *in vitro* starch hydrolysis profile with bolus from human mastication, Foschia et al. (2014) reported that cutting the spaghetti strand with a knife and squeezing it with a pestle had the highest resemblance to spaghetti chewed by a human participant. In contrast, homogenization of the spaghetti pieces led to an overestimation of the *in vitro* starch hydrolysis and predicted glycemic response. Similar observation on the effect of degree of particle size reduction on starch hydrolysis during gastrointestinal digestion was also reported in *in vitro* studies using

cooked white rice and bakery products with different physical and structural characteristics (Gao et al., 2019; Gao et al., 2021; Tamura et al., 2017). These studies provide examples that simulating mastication with the appropriate degree of particle size reduction is important in *in vitro* starch digestion studies, as it will affect the gastric digestion step, and may impact the correlation with *in vivo* glycemic response.

Despite the information from human mastication studies which can be adapted to *in vitro* method, a sufficient simulation of the degree of particle breakdown and starch hydrolysis due to mastication poses another challenge, as individuals have different chewing behavior, saliva compositions, and levels of salivary amylase activity (Jeltema, Beckley, & Vahalik, 2015; Lamy et al., 2021; Prodan et al., 2015). For example, individuals with high salivary amylase activity were reported to have lower glycemic response than those with low salivary amylase activity (Mandel & Breslin, 2012). These results suggest that mastication-related factors are important contributors to the extent of starch hydrolysis and physical breakdown of food boluses during gastric digestion, which subsequently can affect glycemic response. Additionally, the properties of the boluses (e.g., cohesiveness) produced through *in vitro* oral processing are worth considering, as they may play a role in the disintegration behavior of the bolus in the stomach. Understanding the disintegration of food boluses in addition to the individual food particle disintegration will lead to a better comprehension of food breakdown in the stomach (Bornhorst & Singh, 2013), and this is an area where future work is needed. There is also an opportunity for food structure design for specific group of individuals based on their individual mastication behavior. This can be achieved by varying the degree of particle size reduction, level of α -amylase activity, and contact time between α -amylase in the simulated saliva with the simulated food bolus to modify bolus properties.

2.8.3 Mixed meal effect

During most meals, starch-based foods are consumed with other types of food as a mixed meal, causing the food system to not always be dominated by starch. Glycemic response of food is also affected by the presence of other components that can affect the gastric emptying rate of the meal or stimulate insulin secretion, consequently modifying the glycemic response. For highly digestible starch (e.g., potato or products of highly disrupted structure after mastication), modification of glycemic response can be achieved through consumption of the starch-based food with protein and/or fat that empty later than carbohydrate. For example, the consumption of protein prior to carbohydrate was reported to stimulate the secretion of insulin and incretin hormones, which slowed down the gastric emptying rate, and resulted in a significantly reduced glycemic response (Ma et al., 2009). Water consumption during a meal has also been reported to increase glycemic response, which was hypothesized to be the result of dilution of gastric content that induced higher gastric emptying rate (Torsdottir & Andersson, 1989).

Additionally, consumption of a carbohydrate-based meal with certain concentrations of bioactive compounds that can stimulate insulin activity was reported to reduce glycemic response without significantly affecting the gastric emptying rate. For instance, Hlebowicz, Darwiche, Bjorgell, and Almer (2007) reported that the presence of 2% (w/w) cinnamon in rice pudding led to reduction in glycemic response without significant reduction of gastric emptying rate. Overall, these studies suggest that interactions between starch and other components in the meal may affect *in vivo* gastric emptying and glycemic response through a mechanism that does not directly affect the physical breakdown of the food in the stomach. This potentially cannot be observed *in vitro* due to the lack of physiological and hormonal regulation in most *in vitro* models.

Care should be taken in the interpretation of *in vitro* data for which hormonal regulation processes may play a large role in the physiological outcome. Additional studies are needed to include more relevant regulation of gastric emptying and glucose release in *in vitro* models, and in comparing the impact of non-starch-based components on the gastric breakdown, emptying, and glycemic response of a meal high in carbohydrate.

2.8.4 State of the stomach prior to meal consumption

In the current standard procedure for *in vivo* GI measurement, it is suggested that food is consumed in the morning after at least 10-h overnight fast (International Standards Organization, 2010). However, the consumption of starch-based foods is not always preceded by overnight fast in most conditions, considering that starch is a major component of the daily diet. Previous studies have reported second-meal effects in GI measurement, i.e., the extension of metabolic effects of the previous meal to the glycemic response of subsequent meal (Wolever, Jenkins, Ocana, Rao, & Collier, 1988). The second-meal effect has been shown to be impacted by prior meal macronutrient composition (Meng, Matthan, Ausman, & Lichtenstein, 2017), the GI/GL of previous meal, and the time between the previous and subsequent meals (Halder et al., 2020; Jenkins et al., 1982; Wolever et al., 1988).

From a gastric digestion perspective, the condition of the stomach (i.e., fasted vs. fed condition) when a food bolus is ingested may affect the pH for biochemical digestion. An early study on gastric function reported pH 2 in the distal stomach region after an overnight fast, which increased after consumption of a solid test meal, followed by a dynamic decrease in intragastric pH, which was affected by the meal buffering capacity (Malagelada, Longstreth, Summerskill, & Go, 1976). Another study showed that the intragastric pH might be different across different times of the meal (Simonian et al., 2005). Initial intragastric pH was reported to be different before breakfast (after

>10 h overnight fast), lunch (4.5 h after breakfast), and dinner (5 h after lunch). The intragastric pH was 1.3 and 1.5 before breakfast, 1.8 and 1.5 before lunch, and 2 and 1.4 before dinner in the proximal and distal regions, respectively. The dynamic changes of intragastric pH after a meal was affected by the food buffering capacity and volume of meal consumed (Simonian et al., 2005). The evidence of different intragastric pH levels throughout different times of meal, as well as second-meal effect in glycemic response studies, suggest that the context and time of the meal should be considered as a factor when establishing an IVIVC for starch-based foods. Furthermore, this concept can also be extended to assessing a suitable “fed-state” or “after-meal” in *vitro* gastric digestion conditions (e.g., pH and digestion mixture viscosity) that simulate food consumption in between normal meal times, such as in the case of food consumed as snacks.

2.9 Conclusions and future outlook

As a major part of daily food intake, starch-based foods have been studied extensively due to their glycemic impact that may lead to metabolic-related health outcomes. *In vivo* and *in vitro* approaches have been used to understand food- and physiological-factors affecting the digestibility of starch in the small intestine. As most starch-based foods are typically consumed in solid or semi-solid form, their breakdown during oral and gastric digestion is crucial in the physical breakdown of food macrostructures prior to further digestion in the small intestine. Compared to mastication, the contribution of gastric digestion on the glycemic impact of starch-based foods has been less studied because it has been assumed that starch chemical breakdown is minimal in the stomach. Meanwhile, recent studies have suggested that the stomach not only serves to mechanically break starch-based food structures, but also provides the environment for biochemical breakdown of starch; this aspect needs further consideration. For these

reasons, understanding the breakdown behavior of starch-based foods in the stomach is essential to understand and predict glucose bioavailability in the small intestine. To achieve this understanding, there is a need to establish links between the structure of starch-based foods, their gastric breakdown behavior, and their glycemic response. However, at present, there are limited studies that investigate the gastric breakdown of solid starch-based foods. More specifically, starch-based foods with high moisture, which did not require much breakdown during mastication, and the role of gastric digestion to break their structure would be critical.

Gastric breakdown of solid and semi-solid meals has been studied using *in vivo* and *in vitro* methods by monitoring the changes in parameters such as textural and rheological properties. These studies suggested the relationship between food structure and physical changes in stomach content (i.e., gastric breakdown behavior), which resulted in different gastric emptying rates. This relationship is important, as *in vivo* glycemic response has been shown to be food-structure specific. However, there are limited studies that focus on linking food structure (especially the macrostructural aspects), gastric digestion, and glycemic response of solid starch-based foods. In addition, the widely used *in vitro* starch digestion methods to predict *in vivo* glycemic response tend to use samples with destroyed physical structure, which can conceal the food-structure specific property of the glycemic response. As such, there is an opportunity to improve the current glycemic response prediction methods by incorporating the gastric breakdown behavior aspect, which can account for the physical structure effect on the glycemic response. Further, knowledge of food breakdown behavior during gastric digestion *in vitro* and *in vivo* can be extended to develop an *in vitro-in vivo* correlation (IVIVC) for starch digestion that can be used as a tool for designing food structures with controlled glycemic impact. Coupled with this IVIVC

development, future studies in specifying the context of the meal, effect of mastication, mixed meal effect, and state of the stomach prior to meal consumption to determine the suitable gastric digestion parameters in the *in vitro* methods need to be undertaken. This approach can be useful to provide *in vitro* glycemic response prediction methods with better accuracy and relevance to *in vivo* conditions.

CHAPTER 3. Selected food systems and experimental approach

This chapter contains information that applies to all experimental chapters in this thesis. Specific analysis methods are described separately in each chapter. Figure 3.1 summarizes the overall objective of this thesis, relevant thesis chapters and the experimental approach, what was measured in each chapter, and related research objectives for each chapter. Results from the *in vivo* studies are presented in Chapter 4, 5, and 6:

- Chapters 4 focuses on the physical changes during gastric digestion in the proximal and distal stomach regions as affected by food structure, and how the different physical processes and food structure resulted in different gastric emptying rate.
- Chapter 5 focuses on the biochemical and microstructural changes during gastric digestion, especially acidification of gastric content, as affected by food structure, and how they relate to starch hydrolysis in the stomach and starch emptying rate.
- Chapter 6 focuses on the small intestinal digestion and glycemc response as a consequence of breakdown processes during gastric digestion.

From the work presented in Chapter 4 and 5, it was proposed that the proximal and distal phases during gastric digestion contributed differently to the breakdown processes. The contribution of proximal and distal phases of gastric digestion to food breakdown was investigated in Chapter 7 using a static *in vitro* digestion study.

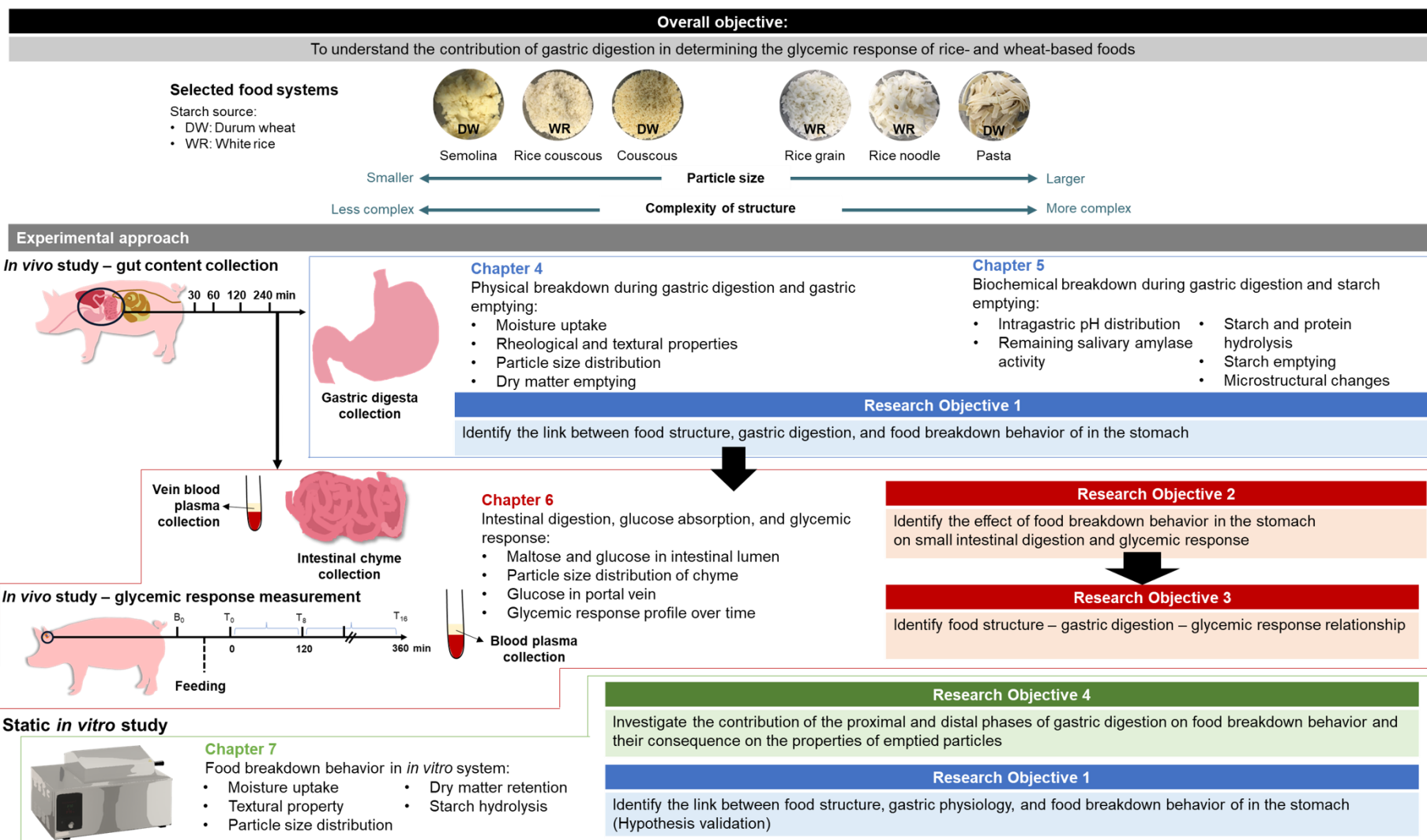


Figure 3.1 Summary of the experimental approach used in this thesis report and how they relate to the research objectives.

3.1 Selected food systems

3.1.1 Rationale

Based on the literature review (Chapter 2), limited studies have been done on solid starch-based food systems with high moisture content, which would have less mechanical breakdown during mastication compared to food with low moisture content. In this thesis, six food systems were selected to represent high-moisture systems with different macro- and microstructures (Figure 3.2). Macrostructural differences were highlighted by the different initial particle size of the food systems (≤ 1 to 2 mm and >2 mm). Microstructural differences were highlighted by the different levels of arrangement of starch granules due to their processing and the difference in the starch source.







Starch source	Durum wheat					
	Diet name	Semolina			Couscous	Pasta
	High amylose white rice					
	Diet name	Rice grain			Rice couscous	Rice noodle
Macrostructure	Physical structure	Native grain	Finely-milled native grain	Agglomerated finely-milled native grain	Starch gel of finely-milled native grain	
	Characteristic dimension	$d \approx 2$ mm $\ell \approx 10$ mm	$d \leq 0.5$ mm	$d = 1 - 2$ mm	$\ell = 10 - 15$ mm (<i>in vitro</i>), 30 – 40 mm (<i>in vivo</i>) $w \approx 7$ mm $h = 1 - 1.5$ mm	

Figure 3.2 Selected food systems to be used throughout the chapters of this thesis. The ‘Physical structure’ row indicates the structural differences of the food systems as a result of processing. The food systems will be referred to by the notation listed in the ‘Diet name’ row throughout this thesis report. Characteristic dimensions of the food systems are denoted by d for diameter, ℓ for length, w for width, and h for thickness.

Durum wheat (to be referred to as only ‘wheat’ from this chapter onwards) and white rice (to be referred to as only ‘rice’ from this chapter onwards) were selected to

represent the starch sources, as these are two globally-important starch sources in human diet (FAO, 2020). Amylose content screening was performed on various wheat and rice-based commercial products prior to selecting the suppliers of the products to minimize the impact of variable amount of amylose content on gastric emptying rate and glycemic response that may interfere with the results. To match the amylose contents of the wheat-based diets, rice-based products with the highest amylose content available were selected. The amylose content of the uncooked rice-based diets selected fell into the USDA classification of high amylose rice (USDA-ARS, 2014), resulting in the selection of high amylose white rice as the other starch source.

Three physical structures (grain, agglomerated/couscous, noodle) for each starch source were selected in this project. These physical structures were associated with their processing method (Figure 3.2). Rice grain represented a structure of intact native grain, semolina represented a structure of finely milled grain, couscous and rice couscous represented a structure resulting from the agglomeration of finely milled grain (Barkouti, Delalonde, Rondet, & Ruiz, 2014), and pasta and rice noodle represented a gel structure that initiated from the paste of finely milled grain (Ahmed, Qazi, Li, & Ullah, 2016; Li, Zhu, Guo, Brijs, & Zhou, 2014). Semolina was purchased from Sherratt Ingredients, Auckland, NZ. Semolina was selected instead of intact durum wheat grain due to unavailability of suppliers because durum wheat is not commonly consumed in the form of intact grain. Wheat couscous, wheat pasta (fettuccine), rice grain, rice noodle, and rice flour were purchased from Davis Trading, Palmerston North, NZ. Rice grain was selected instead of rice flour as it can be consumed as intact grain, as well as to represent the native grain structure for comparison with other food systems. The manufacturers of these commercially available food systems are listed in Table 3.1. As a suitable commercial source was not available, rice couscous was produced at

FoodPilot (Massey University, Palmerston North, NZ) from rice flour. The procedure developed to manufacture rice couscous is provided in APPENDIX A.

3.1.2 Preparation of selected foods systems

3.1.2.1 Study diets for *in vivo* and *in vitro* studies

The term “study diets” refers to the diets that were used on the days of experiments and fed to pigs as their penultimate meals and sampling day meals. The noodle and couscous diets underwent particle size standardization through cutting (noodle) or sieving (couscous). For both *in vivo* and *in vitro* studies, couscous diets were sieved with a vibrating sifter machine (Retsch, Haan, Germany) and only fractions between 1 to 2 mm were used for cooking. For *in vivo* studies, noodle diets (rice noodle and pasta) were manually cut to 30- to 40-mm length to allow the pigs to eat the noodle meals easily. For *in vitro* studies, noodle diets were manually cut to 10- to 15-mm length. The size of noodle and couscous diets used for the *in vivo* studies were within a carefully controlled size range to allow for a more precise examination of particle size changes during gastric digestion. The size of noodle diets used in *in vitro* studies was chosen based on the size of noodle after mastication (Hoebler et al., 2000; Ranawana, Henry, et al., 2010). Rice grain and semolina were used directly from the package for cooking.

All study diets were cooked prior to the experiments following standardized cooking methods (Table 3.1). Rice grain was cooked using a domestic rice cooker (Kambrook, Auckland, NZ), rice couscous and couscous were rehydrated with boiling water, and the rest of the diets were cooked on the larger hotplate of a commercially available double hot plate (Living & Co, Auckland, NZ). After cooking, all the cooked diets were cooled to 40 to 50 °C prior to feeding. The physicochemical properties of these diets will be discussed in Chapter 4.

Table 3.1 Manufacturer and cooking method for each of the study diets.

Diet name	Manufacturer and location	Cooking method
Semolina	Manildra Group, Australia	Mixing with boiling water (1:4.5 w/v) for 5 min, followed by cooking with continuous stirring for 3 min, and boiling without stirring for another 2 min.
Couscous	Warda, Tunisia	Rehydration with boiling water (1:1.5 w/v) for 5 min (covered), followed by fluffing with pasta serving spoon.
Pasta	Colavita, Italy	Cooking in boiling water (1:10 w/v) for 13 min with regular stirring every 2 min, straining to remove the water, and rinsing under running water for 7 s.
Rice grain	C.P. Intertrade, Thailand	Cooking in a standard rice cooker, with rice: water ratio of 1:1.5 w/v, for 26 min.
Rice couscous	Made at the FoodPilot, NZ (details in APPENDIX A) from imported rice flour (C.P. Intertrade, Thailand)	Rehydration with boiling water (1:1.5 w/v) for 5 min (covered), followed by fluffing with slotted spoon.
Rice noodle	Oriental Food, Thailand	Cooking in boiling water (1:10 w/v) for 3 min with regular stirring every 1 min, straining to remove the water, and rinsing under running water for 7 s.

3.1.2.2 Acclimatization diets for *in vivo* studies

The term “acclimatization diets” refers to diets that were fed to pigs during the acclimatization period of the *in vivo* studies (see Section 3.2.2.1 and 3.2.3.1). Preparation of cooked semolina, rice grain, rice noodle, and pasta for the acclimatization period of *in vivo* studies, which were required in large quantity, was done at the FoodPilot (Massey University, Palmerston North, NZ). Larger sizes of noodle and couscous diets (without size standardization as described in Section 3.1.2.1) were used to minimize wasted materials, as the objective of the acclimatization was to familiarize pigs with the study diets. The couscous diets were 0.5 to 2 mm in diameter (separated with vibrating sifter machine, as in Section 3.1.2.1), while the noodle diets were 60 to 70 mm in length (cut manually). The cooking method for scaling up the food volume was adjusted to result in similar moisture content and consistency to the diets cooked with methods in Table 3.1. These cooked diets were frozen (-20 °C) until

needed. The frozen diets were thawed overnight and reheated on the subsequent day with commercially available microwave to 40 to 50 °C prior to feeding to pigs.

3.1.2.3 Reference diet for *in vivo* glycemic response study

For the reference diet in glycemic response measurement study (Section 3.2.2), standard white bread was purchased from a local supermarket (Palmerston North, NZ). The crust of the bread was removed and the crumb was cut to 20 mm × 20 mm (acclimatization period meal) or 15 mm × 15 mm pieces (blood sampling day meal; see Figure 3.3 for the appearance of the cut bread) prior to feeding to enable the pigs to eat the bread easily.



Figure 3.3 Example of the appearance of 15 mm × 15 mm bread used as the reference diet for the blood sampling day meal in the glycemic response measurement study.

3.2 Experimental approach 1: *in vivo* studies using growing pig model

All protocols included in the *in vivo* studies (glycemic response measurement and gut content collection) were approved by the Animal Ethics Committee, Massey University, New Zealand (Protocol 18/128). The protocols took place at Massey University Animal Research Unit, Palmerston North, New Zealand. The studies were conducted in collaboration with the Riddet Institute Nutrition Team and two visiting interns from the University of California, Davis, USA.

3.2.1 Rationale, related research objectives, and hypotheses

3.2.1.1 Rationale

The breakdown of food particles during gastric digestion is the result of biochemical and/or mechanical processes in both the proximal and the distal stomach. While the role of the distal stomach in comminuting food particles has been established in the literature, the function of the proximal stomach in food breakdown is not well-understood. The effect of food composition and structure on the function of the proximal and distal stomach regions also has not been studied in detail in previous studies. Moreover, the consequences of the changes in physicochemical properties during gastric digestion in the proximal and distal stomach regions on the small intestinal digestion and glycemic response of the diets are not well-understood. An *in vivo* study using an animal model was the best approach, as sampling of gastric and small intestinal digesta to quantify their physicochemical properties and blood sampling from different vein locations at certain time intervals were needed. Due to their similar anatomy and physiology of digestive system to that of adult humans, growing pigs were selected (Ziegler, Gonzalez, & Blikslager, 2016). Pigs and humans have also been reported to have similar metabolic responses (Nielsen et al., 2014), making growing pig a suitable model for upper GIT digestion and nutrient absorption. (Herring, 1976; Štembírek, Kyllar, Putnová, Stehlík, & Buchtová, 2012)

The amount of study diet given to the pigs on the day of experiment (final meal) was 250 g starch (dry basis, determined based on the measured total starch and moisture content for that diet), with the following justifications:

- For humans, the suggested amount of carbohydrates for glycemic response measurement is 50 g starch (dry basis), and for pigs it should be 3 to 5 times this amount. This is based on the consideration that the normal stomach capacity of 70-

kg human (approximately 1.5 L) is physiologically equivalent with pig that has 5.5 to 7 L of total stomach capacity (Gandarillas & Bas, 2009).

- This amount is close to the 1/3 of basal dry matter requirement for pigs weighing 23 to 25 kg, assuming that in the case of human, there are three meals per day.

3.2.1.2 Related research objectives

- **Objective 1:** To investigate the effect of food structure and composition on the regulation of gastric secretion and food physicochemical breakdown process in an *in vivo* stomach system.
- **Objective 2:** To identify how breakdown processes during gastric digestion affect small intestinal digestion and glycemic response of the selected food systems *in vivo*.
- **Objective 3:** To establish a link between food structure, gastric digestion, and glycemic response based on *in vivo* findings.

3.2.1.3 Hypotheses

- The distal region of the stomach would contribute more to the overall (biochemical and mechanical) digestion of wheat-based diets, because the lower pH in the distal stomach would provide a suitable biochemical environment for pepsin activity to hydrolyze the protein network that entraps starch granules in the wheat-based diets.
- The digestion of rice-based diets would be due to the combination of the roles of the proximal and distal regions of the stomach. The proximal region would contribute more to the biochemical digestion due to remaining salivary amylase activity; the distal region would be the major site for mechanical breakdown.
- Diets with smaller initial particle size and more porous structure would break faster in the stomach and have faster gastric emptying rate, subsequently caused

higher glycemic response (both the maximum elevation and the overall impact).

For example, rice couscous or couscous was expected to break faster in the stomach than rice noodle or pasta, causing them to induce higher glycemic response.

3.2.2 Glycemic response measurement in growing pigs

3.2.2.1 Animal housing and treatment

On arrival (day zero), 33 Large White × Landrace commercial breed male pigs (21.6 ± 2.7 kg body weight) were distributed in three batches of 9 or 12 pigs each and were housed in $1.5 \text{ m} \times 1.5 \text{ m}$ individual pens that allowed them to see and smell each other. The pens were located in a temperature-controlled room (21 ± 2 °C) with 12-h light/12-h dark cycle. Each pig was randomly assigned to one of the six study diets or bread (reference diet), which became their first diet for glycemic response measurement (D1).

Pigs were fed commercial grower mix on arrival (day zero). Starting the following day (day one), pigs were transitioned to their assigned diets over two days by gradually increasing the proportion of study diets relative to the commercial grower mix (33 and 67% of the study diet on days one and two, respectively; Figure 3.4A). On days three to five, the pigs were fed with 100% of the study diet. The daily food amount was 10% of the metabolic body weight ($\text{body weight (kg)}^{0.75}$), referred to as ‘basal amount’, fed in two equal-sized meals at 0900 and 1600 h. The meals were supplemented with 10% casein, 10% soya oil, and 0.25% vitamin/mineral mix to meet the nutritional requirements of the growing pig according to recommendations by the National Research Council (2012). During this acclimatization period, the pigs were adapted to the presence of humans in their pens and having their ears manipulated (to prepare for blood sampling through an ear vein catheter). Nineteen pigs that adapted well to manipulation on their ears were selected for catheterization. The remaining pigs were

re-acclimatized to randomly assigned study diets for the gut content collection study (Figure 3.5A).

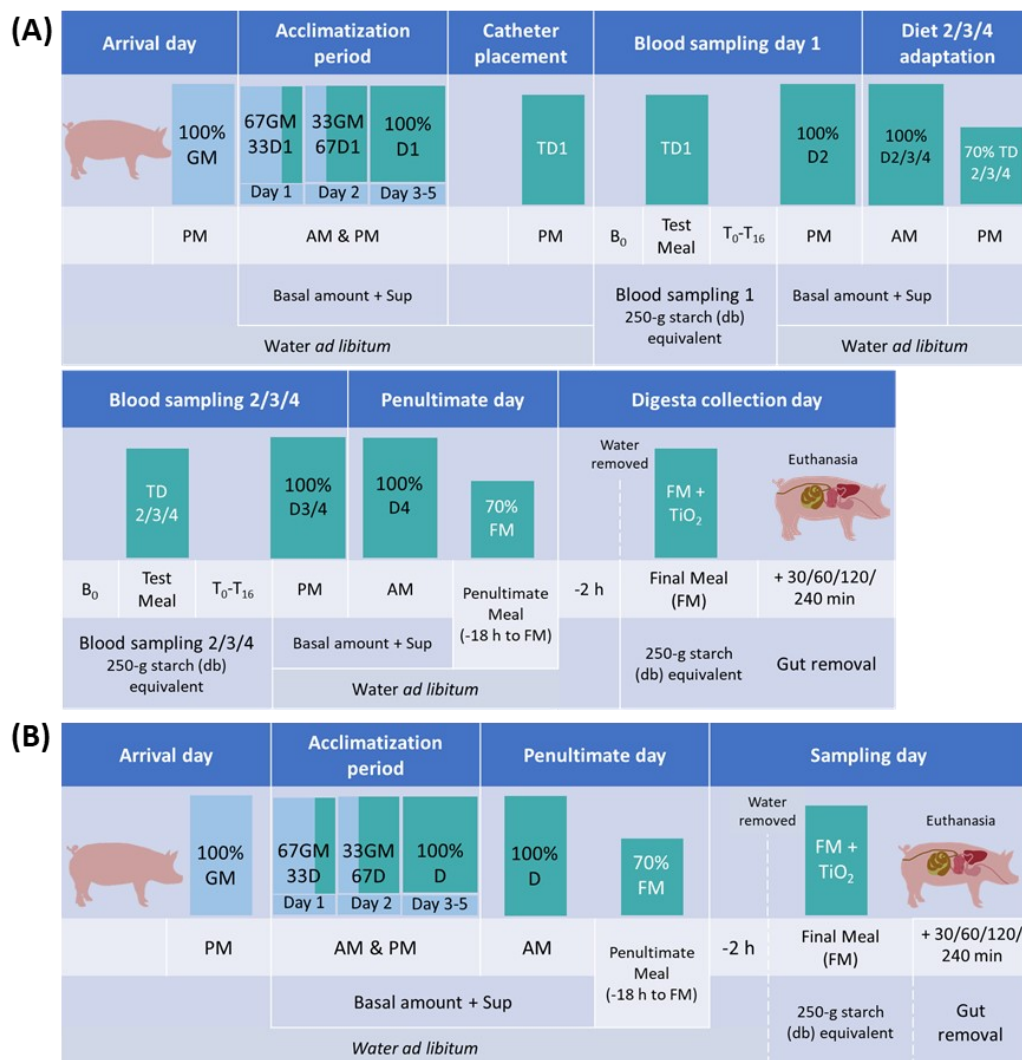


Figure 3.4 Setup of *in vivo* glycemic response measurement followed by gut content collection studies (A). Setup of *in vivo* gut content collection study (B). GM: commercial grower mix; D1/2/3/4: diet 1/2/3/4 for adaptation in the glycemic response study, given as microwave-reheated diets; TD1/2/3/4: diet 1/2/3/4 for blood sampling day, 250-g starch (dry basis) equivalent, given as freshly cooked diets; D: diet for gut content collection study, given as microwave-reheated diets; FM: final meal, 250-g starch (dry basis) equivalent in the gut content collection study; Sup: supplemental ingredients added to the daily meal.

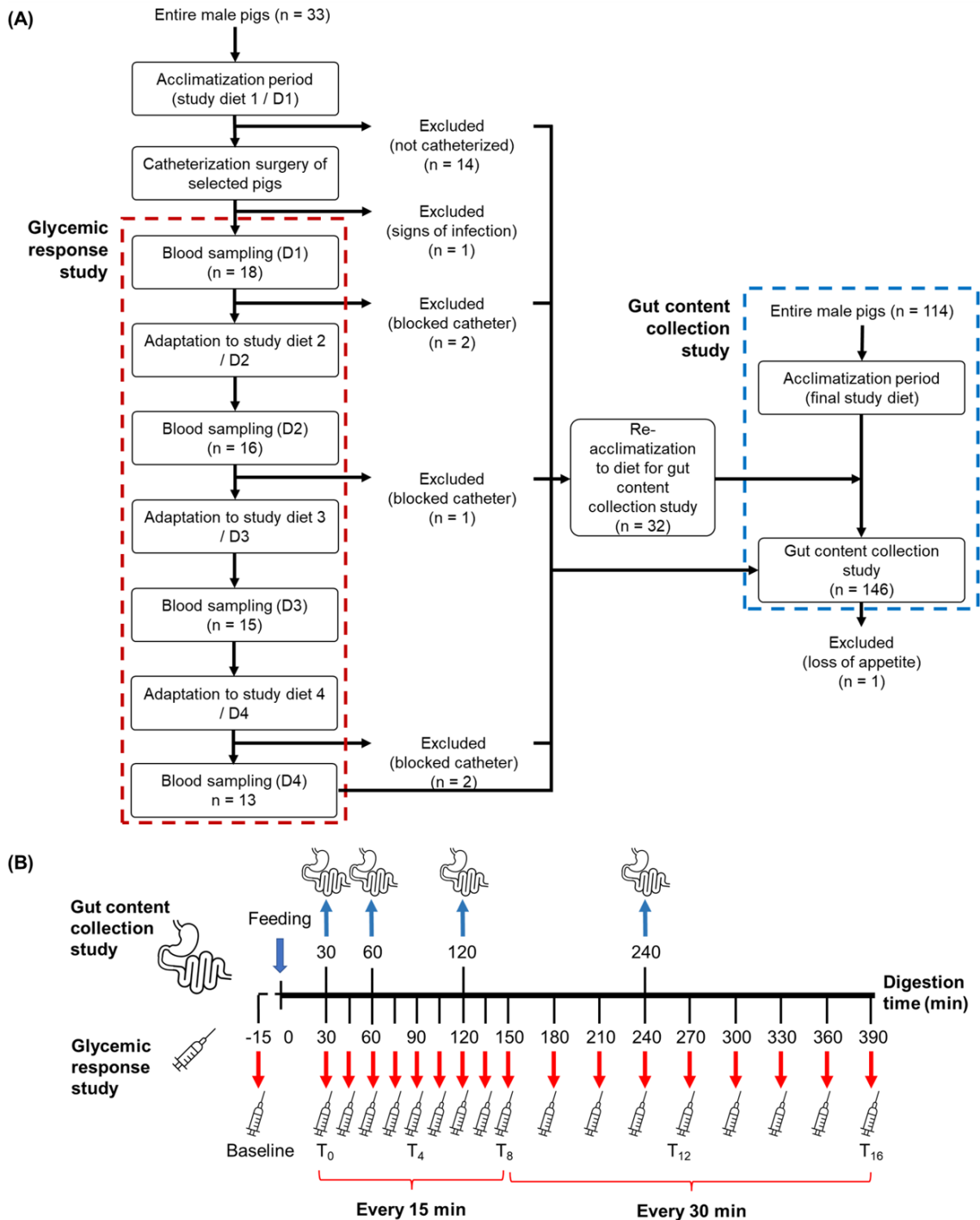


Figure 3.5 Diagram of the glycemic response and gut content collection studies. Stages in the red-dashed box correspond to the glycemic response study, stages in the blue-dashed box correspond to the gut content collection study (A). Timing of sampling for either the gut content collection or glycemic response study (B).

On day 5, an in-dwelling catheter was inserted into the ear of each of the 19 pigs. Each pig was anesthetized with a mix of Zoletil 100 (zolazepam and tiletamine, both 50 mg/mL; Virbac NZ) reconstituted with 2.5 mL Ketamine and 2.5 mL Xylazine, both

100 mg/mL (both PhoenixPharm NZ) after a 16-h fasting period. The final solution contained 50 mg/mL of each drug and was administered at a dose rate of 0.03 to 0.04 mL of the mixed solution/kg BW by intramuscular injection in the neck. While under anesthesia, a Long Term MILACATHTM catheter was inserted into one ear of the pig according to the manufacturer's instructions, using a guiding wire that allowed the catheter to reach as far as the jugular vein (Figure 3.6A-B). The catheter was flushed with heparinized saline and subsequently taped into position. Tape was also applied to the other ear of the pig, which had the effect of tranquilizing the pigs (balanced weight on each ear; Figure 3.6C). Each catheter was flushed with sterile heparinized saline at least twice daily. One pig was excluded from the study due to signs of bacterial infection after the catheterization. Catheterized pigs had *ad libitum* access to water except during the sampling period.

3.2.2.2 Sampling day procedure

To minimize interference from their previous meal, pigs were fed with 70% of the standardized meal amount (freshly cooked, see Section 3.1.2.1) without supplemental ingredients in the penultimate meal (≥ 16 h prior to the beginning of blood sampling). On each blood sampling day, pigs were fed their assigned study diet as their morning meal without supplemental ingredients (freshly cooked, see Section 3.1.2.1). Pigs were given 20 to 30 min to consume their meals. Access to water was removed 2 hours prior to and until the second hour of blood sampling period. Blood samples were then collected through the in-dwelling catheters at different time points (Figure 3.5B): baseline (B_0 , 15 min prior to meal), immediately following the meal (T_0), then every 15 min until 2 h after meal (T_1 to T_8), then every 30 min until 6 h after meal (T_9 to T_{16}). The catheter was flushed with 2 mL sterile heparinized saline before sampling at B_0 . Each sampling (from B_0 to T_{16}) was preceded by the withdrawal of 2 mL of sample that

was not considered due to potential dilution in the catheter with heparinized saline. Subsequently, the blood sample (2 mL) was collected, and immediately transferred to a 2-mL BD Vacutainer® fluoride tube containing NaF and Na₂EDTA; all samples were stored on ice until centrifugation. After sampling at T₀ to T₁₆, the catheter was flushed with 4 mL sterile heparinized saline to prevent blood clotting. Each blood sample was centrifuged for 10 min at 1,200× g (Tabletop Centrifuge DSC-200A-2, Digisystem Laboratory Inc., Taipei, Taiwan). The plasma was separated and stored on ice until free glucose analysis, which was carried out within 3 hours of sampling.

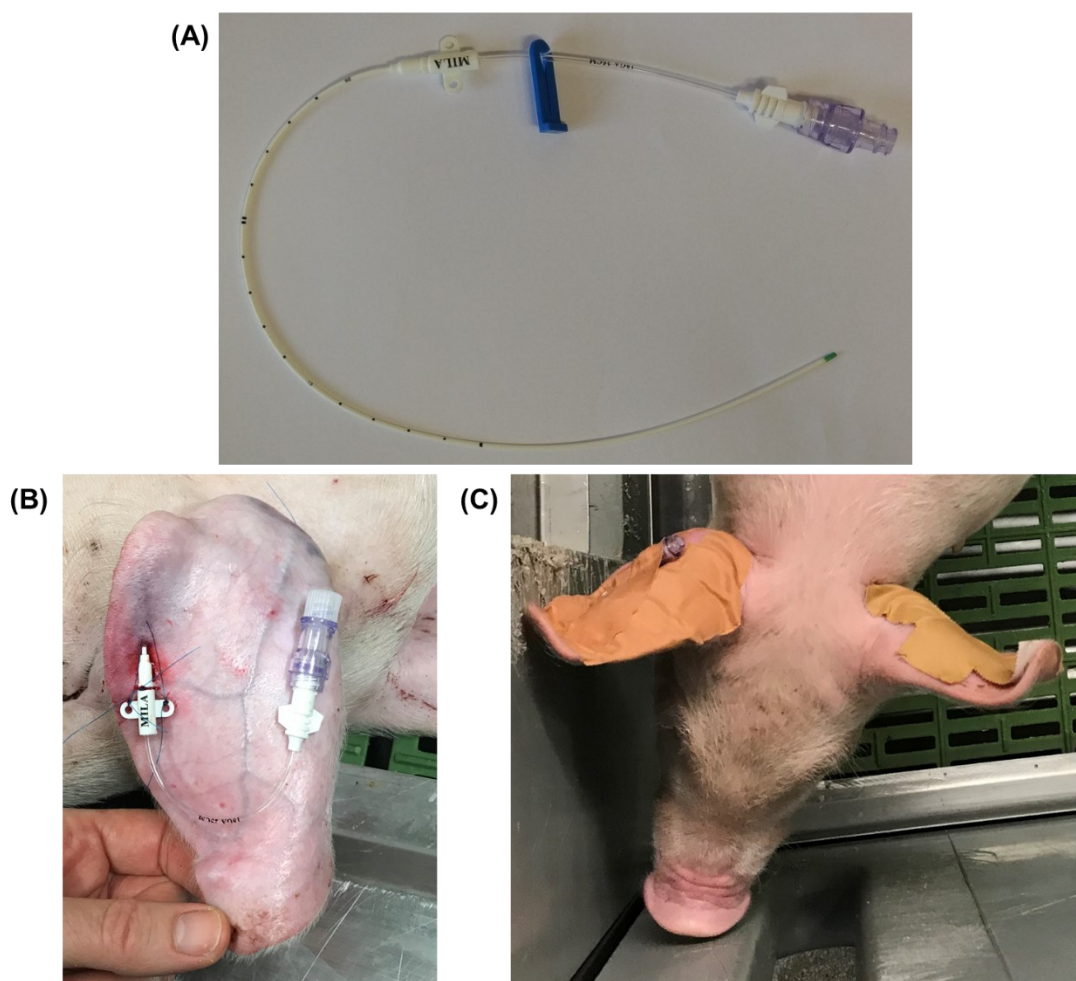


Figure 3.6 Photograph of the long-term catheter used in the glycemic response study (A). The appearance of ear catheter that extends to the jugular vein of each pig (B). The application of tape on both ears of the pigs provided balanced weight on the catheterized and non-catheterized ears (C).

After the first blood sampling period, pigs began to receive their next assigned diets (D2/D3/D4) during the afternoon meal and were given one day to adjust to the new assigned diet before the next blood sampling day. Diets selected as D2/D3/D4 and the sequences of D2/D3/D4 were randomly determined using a random number generator in Microsoft Excel, with the initial plan that each pig would receive the reference diet (white bread) and three study diets. Over the study period for D2 to D4, however, five pigs were excluded from the glycemic response study due to blocked catheters and their catheters were removed. Two of these pigs had blocked catheters before receiving the reference diet. These pigs were re-acclimatized to study diets for the gut content collection study (Figure 3.5A). Due to blocked catheters, the randomization of the diets in the last batch of study was modified in such a way to obtain at least five replicates for each study diet. At the end of glycemic response study (day 14), catheters were removed from all remaining pigs. The pigs proceeded to the gut content collection study with their D4 diet being their assigned study diet for the gut collection study.

3.2.3 Gut content collection from growing pigs

3.2.3.1 Animal housing and treatment

A total of 146 male pigs (21.7 ± 1.8 kg body weight) were involved in experimental approach 2; 32 of them were involved in the glycemic response measurement study (both the catheterized and non-catheterized). The remaining 114 (21.3 ± 1.6 kg body weight) were directly used in the gut content collection study (Figure 3.5A). The 114 pigs were distributed in four batches of 24 or 30 pigs each and housed individually in metabolism crates that allowed them to see and smell each other. These batch sizes were determined based on the availability of pig housing and sampling feasibility within each batch. The crates were located in a temperature-controlled room (21 ± 2 °C) with 12-h light/12-h dark cycle. Each pig was assigned randomly to one of 24 treatment groups

(six study diets \times four digestion time points), so that there were at least six pigs per treatment.

All pigs were fed commercial grower mix on day zero, then were transitioned gradually to their assigned diets on day one and two (Figure 3.4B). The transition to study diets, daily meal amount, and supplements added to the daily meals were the same as described in Section 3.2.2.1. The pigs were fed 100% study diets from day three until sampling day (day five to seven). Pigs were given 20 to 30 min to eat their meals to prepare them for the final day of the study. From day zero until sampling day, the pigs had access to water *ad libitum* until two hours before the final meal. On the two last meals (penultimate and final meals), the pigs were fed their study diets without supplemental ingredients. The penultimate meal (70% of the final meal amount; freshly cooked as described in Section 3.1.2.1) was given at least 18 h before the final meal to minimize the amount of food left in the gastrointestinal tract.

On the sampling day, all freshly prepared study diets (Section 3.1.2.1) were mixed with titanium dioxide (0.5% of the dry matter of the Study diet) as an indigestible marker prior to feeding. For cooked pasta, 15 g soybean oil was added to improve palatability. Pigs were given 30 min to consume their meals, and any uneaten food was removed and weighed. After their final meal (30, 60, 120, or 240 min from feeding time), the pigs were anesthetized through intramuscular injection in the neck with a mixture of Zoletil 100 (zolazepam and tiletamine, both 50 mg/mL; Virbac, NZ) reconstituted with 2.5 mL Ketamine and 2.5 mL Xylazine, both 100 mg/mL (Phoenix Pharm, NZ). The final solution contained 50 mg/mL of each drug and was administered at a dose rate of 0.03 to 0.04 mL/kg body weight via intramuscular injection in the neck.

3.2.3.2 Sampling day procedure

a. Venous blood sampling

While anesthetized, blood sample (~2 mL) was collected from the jugular vein, vena cava, portal vein, hepatic vein, and left ventricle vein of each pig. Each blood sample was collected into a 2-mL BD Vacutainer® fluoride tubes containing NaF and Na₂EDTA. Blood samples were stored on ice until centrifugation for plasma separation as described in Section 3.2.2.2, then the plasma was immediately frozen on dry ice. Plasma samples were stored at -20 °C until analysis, which was done within 2 weeks of sample collection. Pigs were euthanized 20 min after anesthesia and blood sample collection by an intracardial injection of a lethal dose of pentobarbitone (0.3 mL Pentobarb 300/kg body weight) by a registered veterinarian.

b. Gastrointestinal digesta collection

After euthanasia, clamps were placed at each end of the stomach and small intestine, and the entire gastrointestinal tract was removed. The stomach was removed, clamped at the esophageal and duodenal ends. The small intestine was removed and divided with clamps into different sections: duodenum (~25 cm from the pyloric sphincter), terminal ileum (~10 cm from the ileal-cecal junction), and proximal jejunum, distal jejunum, and ileum (three equally long sections of the remaining small intestine portion). The stomach and each small intestinal section were cleaned under running water and patted dry with absorbent paper prior to sample collection.

The stomach was laid down horizontally on a sampling tray. It was dissected laterally with a single cut from middle of the proximal region towards the middle of the distal stomach region, then the cut outer muscles were clamped and moved to the side. Example pictures of pasta, rice grain, and rice noodle digesta in the stomach are presented in Figure 3.7. After measuring intragastric pH at several locations (details on

the method are given in Chapter 5), gastric contents were carefully removed from the proximal and distal stomach regions to separate containers and weighed. The content of each container was carefully mixed to achieve uniform pH, then the mixture pH was measured. From each stomach region, a subsample (10 to 15 g) was taken and immediately frozen in dry ice for enzyme activity analysis. After pH measurement, samples from each region were brought to pH 8 to 10 with <1 mL 50%-w/w NaOH solution to inactivate digestive enzymes and gently mixed to reach uniform pH distribution. Subsamples of pH-adjusted digesta from each region were taken distributed to containers and stored on ice for physical property analysis that was completed no longer than 9 h after sampling (fresh sample). The remaining digesta was frozen for chemical and microstructural analysis (frozen or freeze-dried sample).

Small intestinal digesta from each small intestinal segment was carefully removed by gradual flushing with 50 to 300 mL distilled water. Subsamples (~10 to 15 mL) of the diluted small intestinal content were taken and kept on ice until analysis for same-day particle size measurement. A subsample (~2 mL) was taken for reducing sugar and glucose analysis. This subsample and the rest of the diluted small intestinal content were immediately frozen at -20 °C for future analysis (followed by freeze drying or directly analyzed as frozen samples). Details on samples collected from the stomach and small intestine, along with analyses conducted on them are summarized in Figure 3.8.

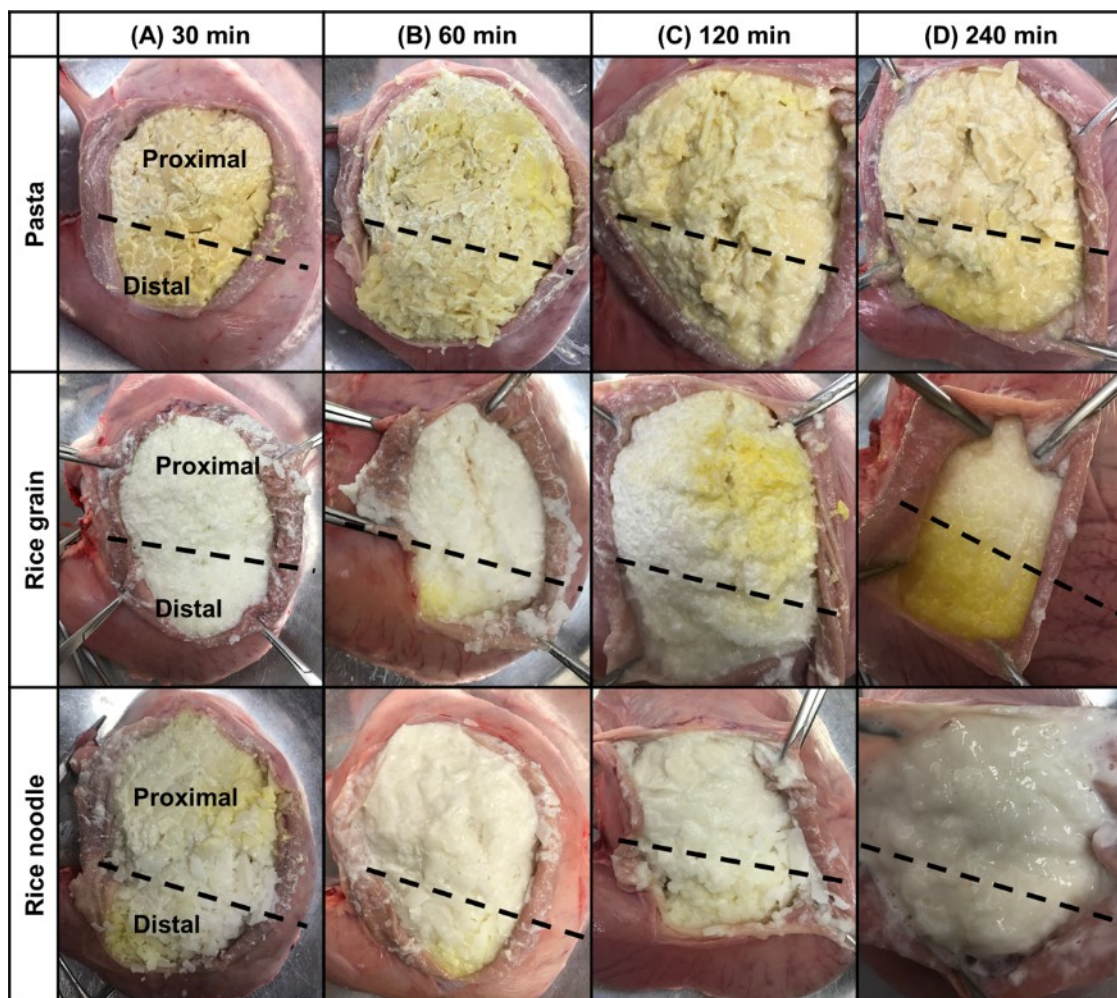


Figure 3.7 Photographs of gastric digesta of pigs fed with pasta (top row), rice grain (middle row), or rice noodle (bottom row) after 30 (A), 60 (B), 120 (C), or 240 (D) min digestion time. The black dash lines indicate approximate separation between the proximal and distal region, with the proximal region is the region above the lines, and the distal region is the region below the lines. The photographs of the other three diets (couscous, rice couscous, and semolina) in the stomach are not presented due to difficulties in handling their digesta that had liquid-like consistency and prevent clear images of digesta to be taken prior to sampling. For the appearance of the digesta after sampling, readers are referred to APPENDIX B.

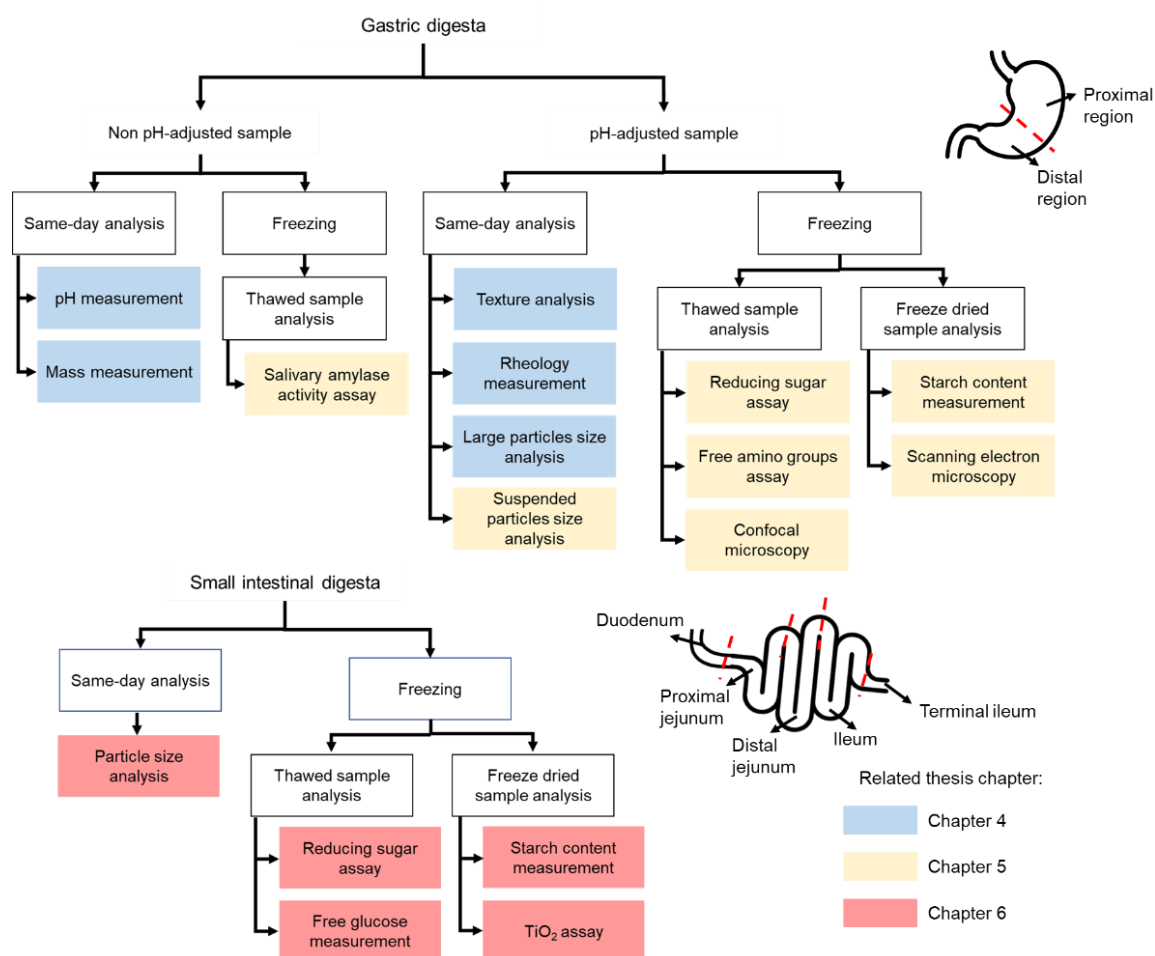


Figure 3.8 Diagram of gastric digesta and small intestinal sampling and types of samples characterized throughout Chapter 4, 5, and 6. The thesis chapters related to the measured properties are indicated by different color codes: blue (Chapter 4), yellow (Chapter 5), and red (Chapter 6).

3.3 Experimental approach 2 – Static *in vitro* gastric digestion

3.3.1 Rationale, related research objectives, and hypotheses

3.3.1.1 Rationale

Results from *in vivo* studies in Chapter 4 and 5 suggested that the proximal and distal stomach may contribute differently to the breakdown of solid food particles during gastric digestion. Extended contact time between the ingested food with salivary amylase occurred in the proximal stomach, while more gastric mixing between ingested food with acidic gastric secretions occurred in the distal stomach. The consequences of biochemical changes in the proximal stomach digestion on the breakdown behavior of

food particles in the distal stomach have not been investigated in detail in the literature. However, the dynamic nature of gastric digestion that involves a range of complex processes (gastric secretory response, different gastric emptying rate, and physiological regulation to maintain glucose homeostasis) limits the understanding of the precise contributions of the proximal and distal phases of gastric digestion from *in vivo* studies. As such, *in vitro* static digestion is an appropriate approach to isolate the biochemical changes that occur during the proximal and distal phases of gastric digestion. All food systems used in the *in vivo* study, except semolina (due to its porridge structure that did not require additional breakdown during gastric digestion), were tested in the *in vitro* digestion study.

3.3.1.2 Related research objectives

- **Objective 4:** To investigate the contribution of the proximal and distal phases of gastric digestion on food gastric breakdown behavior and its consequences on the properties of emptied particles.
- **Objective 1:** To investigate the effect of food structure and composition on the regulation of gastric secretion and food physicochemical breakdown process in an *in vivo* stomach system (hypothesis validation).

3.3.1.3 Hypotheses

- Extended contact time with α -amylase would result in more starch hydrolysis in the food matrix, causing the leaching of small particles.
- Changes due to starch hydrolysis in the proximal phase would change the breakdown behavior of food particles during the distal stomach phase.
- Food with smaller particle size and porous microstructures (couscous and rice couscous) would be more prone to breakdown during the proximal phase, causing more profound physical and chemical changes during the distal phase.

3.3.2 Static *in vitro* digestion procedure

Simulated salivary fluid (SSF) and simulated gastric fluid (SGF) were prepared by dissolving salts formulated following INFOGEST standardized method (Brodkorb et al., 2019) in ultrapure water (Milli-Q Water Purification System, Merck Millipore, USA). Additionally, mucin type II (Sigma-Aldrich, MO, USA; MyBiosource, CA, USA) was added to the simulated digestive fluids at a concentration of 1 g/L SSF and 1.5 g/L SGF, respectively (Swackhamer et al., 2019). The SSF was prepared at pH 7 and was mixed with porcine pancreatic α -amylase (109 U/mg, Megazyme, Ireland) to reach an activity level of 75 U/mL SSF. The SGF was prepared at pH 1.8 and was mixed with pepsin from porcine gastric mucosa (622 U/mg, Sigma-Aldrich, USA) to achieve an activity level of 2000 U/mL SGF. No lipase was added to the SGF formulation because the foods tested had low fat content (Minekus et al., 2014). The pH of the SSF and SGF were adjusted to 7 and 1.8, respectively, after mixing with enzymes. Both SSF and SGF were pre-warmed to 37 °C prior to digestion experiments.

The digestion procedure was designed based on the movement of food bolus from different locations of the proximal stomach to the acidic distal stomach (Figure 3.9A). It consisted of an oral phase followed by two stages of gastric phase (Figure 3.9B), namely the proximal phase (prolonged incubation in SSF after the oral phase) and distal phase (sequential incubation in SGF). For each food, experiments were conducted in batches; one experimental batch consisted of one proximal phase duration followed by immediate sampling (proximal digestion) or addition of SGF to simulate the distal phase (proximal-distal digestion). Each digestion was conducted in a container with lid, where each container represented one replicate for one food and one proximal-distal condition, such that there were 6 containers for each proximal phase duration (1 for proximal digestion and 5 for proximal-distal digestion) in one experimental batch.

Digestion experiments were conducted in triplicate for each food and proximal-distal condition.

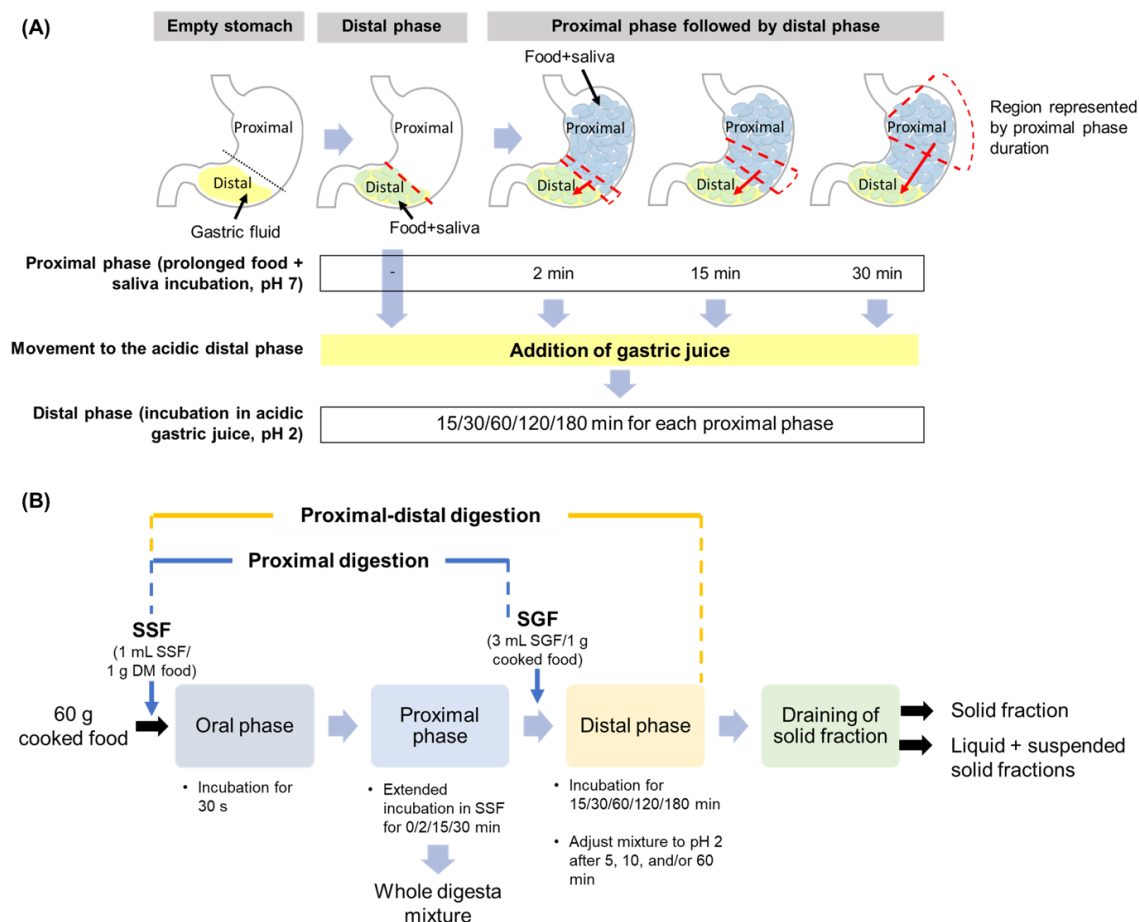


Figure 3.9 Schematic diagram illustrating the rationale behind the experimental design. The filling of proximal stomach results in different locations of food bolus in this region, thus different contact time with α -amylase. Intra-gastric regions of interest simulated by the different proximal duration are highlighted by red dashed lines. Red arrow in each proximal filling scenario indicates the movement of food bolus from the intra-gastric region of interest to the distal phase (A). Block flow diagram of the different steps for proximal or proximal-distal digestion experiments (B).

The oral phase was simulated by mixing cooked food (60 g) with SSF at a ratio of 1:1 mL SSF/g dry matter of food (Brodkorb et al., 2019). The food-SSF mixture was incubated in a shaking water bath (37 °C, 35 rpm) for 30 s (Hoebler et al., 2000). Following the oral phase, the proximal phase was simulated by extending the oral phase incubation time for 2, 15, or 30 min, or without extension (0 min). For proximal digestion not followed by the distal phase (proximal digestion), the sample container

was removed from the water bath after the proximal phase (0/2/15/30 min proximal digestion). The entire digestion mixture from the proximal digestion were carefully mixed with 0.4 mL of 6 M NaOH immediately after incubation to reach uniform pH (pH ~10) to terminate enzymatic reactions without changing the physical properties of the bolus. The proximal phase samples were treated as a whole digesta mixture in the subsequent analyses, as the free liquid was not easily removable in a majority of samples.

For proximal-distal digestion, after a selected proximal phase, 180 mL SGF was added (3 mL SGF/g cooked food) to the food-SSF mixture, gently mixed, and incubated in a shaking water bath (37 °C, 35 rpm) for an additional 15, 30, 60, 120, or 180 min to simulate the distal phase. After 5 and 10 min of SGF addition, the pH of the mixture was measured and adjusted to $\text{pH } 2 \pm 0.1$ with 6 M HCl. When necessary, the pH was readjusted 60 min after SGF addition. The volume of HCl used for pH adjustment was between 0.14 and 0.30% of the volume of SGF added. The sample container was removed from the water bath after a selected distal phase time point (15/30/60/120/180 min), then the remaining solid (solid fraction) was drained from the liquid and suspended solid fractions of the mixture using a flexible mesh (1 mm \times 2 mm aperture). The solid fraction was weighed and 0.8 mL of 6 M NaOH was added and mixed gently to reach uniform pH (pH ~10). On the same day of experiments, the solid fraction was analyzed for texture, moisture content, and particle size, while the mixture of liquid and suspended fractions was analyzed for total soluble solids and particle size. Subsamples of liquid and suspended solid fractions (0.95 mL aliquot mixed with 0.05 mL of 2 M NaOH) were frozen (-20 °C) for chemical analysis.

CHAPTER 4. Tracking physical breakdown of rice- and wheat-based foods with varying structures during gastric digestion and its influence on gastric emptying in a growing pig model

4.1 Abstract

There is currently a limited understanding of the effect of food structure on physical breakdown and gastric emptying of solid starch-based foods during gastric digestion. Moisture uptake, pH, particle size, rheological, and textural properties of six solid starch-based diets from different sources (Durum wheat and high amylose white rice) and of different macrostructures (porridge, native grain, agglomerate/couscous, and noodle) were monitored during 240 min of gastric digestion in a growing pig model. Changes in the physical properties of the gastric digesta were attributed to the influence of gastric secretions and gastric emptying, which were both dependent on the buffering capacity and initial macrostructure of the diets. Differences between the proximal and distal stomach regions were found in the intragastric pH and texture of the gastric digesta. For example, rice couscous, which had the smallest particle size and highest buffering capacity among the rice-based diets, had the shortest gastric emptying half-time and no significant differences between proximal and distal stomach digesta physical properties. Additionally, a relationship between gastric breakdown rate, expressed as gastric softening half-time from texture analysis, and gastric emptying half-time of dry matter was also observed. These findings provide new insights into the breakdown processes of starch-based solid foods in the stomach, which can be beneficial for the development of food structures with controlled rates of breakdown and gastric emptying during digestion.

Keywords: carbohydrate, food structure, gastric digestion, gastric emptying, physical breakdown, starch digestion

Part of the contents of this chapter has been published as a peer-reviewed paper: Nadia, J., Olenskyj, A.G., Stroebinger, N., Hodgkinson, S.M., Estevez, T.G., Subramanian, P., Singh, H., Singh, R.P., and Bornhorst, G.M. (2021). Tracking physical breakdown of rice- and wheat-based foods with varying structures during gastric digestion and its influence on gastric emptying in a growing pig model. *Food Funct.* 2021, 12: 4349-4372.

Main authorship of the peer-reviewed paper was shared with A.G. Olenskyj (UC Davis).

Chapter 4 Overview

Physical breakdown during gastric digestion and gastric emptying:

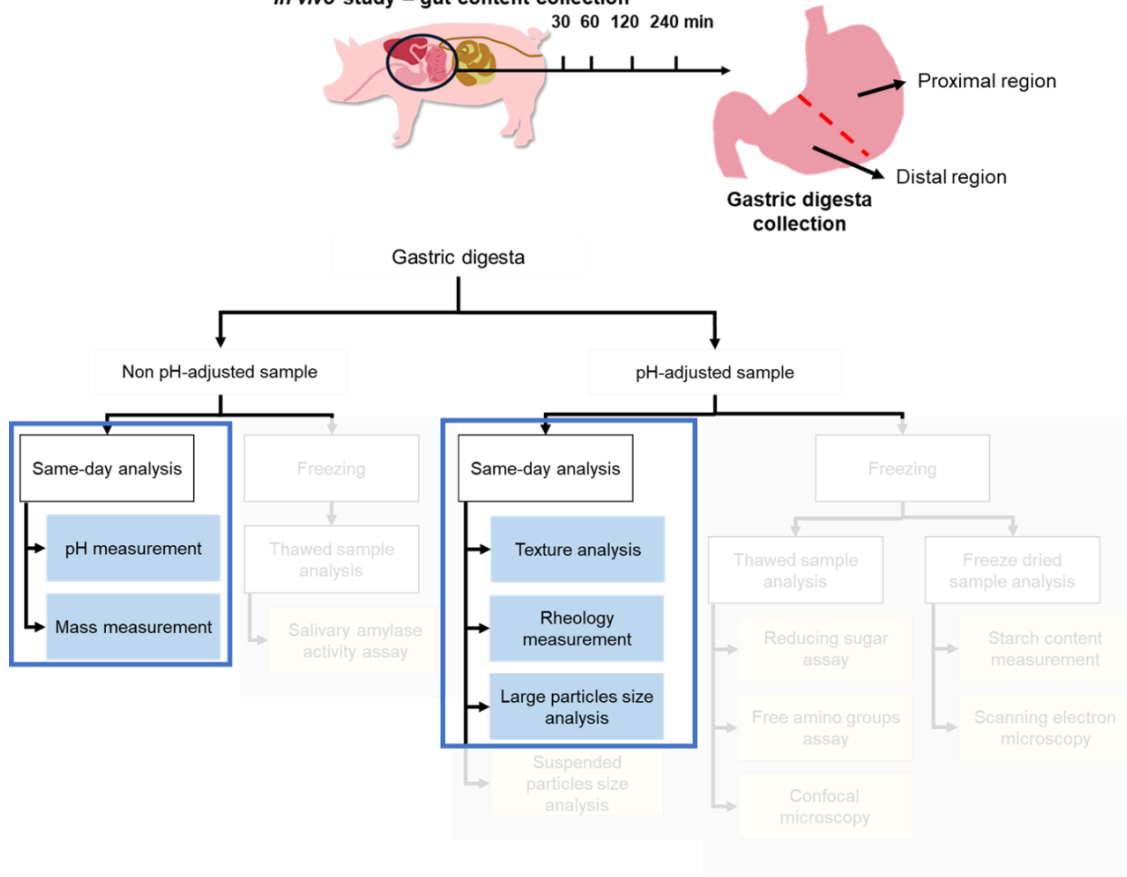
- Moisture uptake
- Rheological and textural properties
- Particle size distribution
- Dry matter emptying

Research Objective 1

Identify the link between food structure, gastric physiology, and food breakdown behavior of in the stomach

Experimental approach

In vivo study – gut content collection



Sample analyses in this chapter were conducted in collaboration with other people:

- Rheology measurement, image processing for particle size analysis, and analysis and interpretation of rheological and particle size data (Section 4.3.5.3, 4.3.5.4, 4.3.6.3, 4.3.6.5, 4.4.5, and 4.4.4) were conducted by Dr. Alexander G. Olenskyj (UC Davis).
- Pictures for image analysis (Section 4.3.5.4) were taken by Talia G. Estevez (UC Davis).

4.2 Introduction

As consumers become more conscious of the impact of diet on health, the relationship between food and the body has become the subject of considerable interest (Norton, Wallis, Spyropoulos, Lillford, & Norton, 2014; Sensoy, 2014). Among nutrients needed by the human body, carbohydrates are the most crucial after water due to their large proportion (45 to 55%) of daily calorie intake (Blaak et al., 2012). This required proportion is mainly fulfilled by consuming starch-based foods, which during digestion processes are converted to glucose. Glucose absorption from the small intestine to the blood leads to changes in blood glucose level or glycemia (Sadler, 2011). However, uncontrolled changes in blood glucose are not desired, as they lead to chronic metabolic diseases such as type 2 diabetes mellitus and cardiovascular disease (Blaak et al., 2012). These health-related issues have motivated the investigations of the digestion processes of starch-based foods and the resulting glycemic impact. While the relationship between the structure of starch-based foods (as affected by starch source, processing method, and composition) and their glycemic response has been studied widely, blood glucose control mechanisms by the digestive system are still not fully understood (Brownlee et al., 2018; Parada & Aguilera, 2011; Singh et al., 2010)

Based on what is understood about the influence of the digestive system on blood glucose, gastric emptying is thought to be one of the key factors that regulate glycemic response by affecting the transport rate of foods to the small intestine from the stomach (Ballance et al., 2013). To ensure efficient absorption of nutrients from solid or semi-solid food in the small intestine, sufficient breakdown of their physical structure is needed prior to gastric emptying (Kong & Singh, 2008; Mourot et al., 1988). This breakdown begins in the mouth through chewing and limited starch hydrolysis by salivary amylase, but the main physical breakdown process occurs during gastric

digestion through combined biochemical (i.e., remaining salivary amylase activity, acid hydrolysis) and mechanical breakdown processes (i.e., gastric peristaltic contractions) (Kong & Singh, 2008; Parada & Aguilera, 2011; Somaratne, Ferrua, et al., 2020). As a result of these breakdown processes, ingested foods undergo changes in their physical properties during gastric digestion. The pattern of the changes, or the gastric breakdown behavior, may differ between foods of varying structures. Previous *in vitro* (Drechsler & Bornhorst, 2018; Hayes et al., 2020) and *in vivo* (growing pig model) (Bornhorst, Chang, et al., 2013) gastric digestion studies showed that starch-based foods of different structures exhibited different patterns in their textural changes, gastric secretions addition, and degree of starch hydrolysis per unit area of digested particles, leading to different gastric emptying rates (Bornhorst, Chang, et al., 2013; Hayes et al., 2020). While these studies suggest a relationship between food structure, gastric breakdown behavior, and gastric emptying rate, there is limited evidence to confirm this relationship. Further, variations in gastric breakdown behavior and gastric emptying rate of different food structures may affect the delivery rate and extent of structural breakdown (biochemical and physical) of the materials emptied, which may modify the conversion rate of starch to glucose in the small intestine, and ultimately impact the glycemic response of the food (Bornhorst et al., 2015; Brener et al., 1983; Read et al., 1986; Tamura et al., 2017).

In understanding gastric digestion of starch, the physiology of the stomach should be considered. As solid food enters the stomach, a mid-gastric transverse band divides the stomach into two physiological regions without physical boundaries, namely the proximal and distal regions (Hellström et al., 2006). In the context of food breakdown, the proximal stomach acts as a reservoir that retains large solid food particles until they are slowly moved to the distal stomach. The distal stomach is the active site for grinding

and trituration of solid food, as well as gastric emptying (Hasler, 2009). Nevertheless, the roles of these physiological regions in starch digestion are still not properly understood. Limited available information in the literature suggests that the food physical and biochemical breakdown processes in different stomach regions are affected by the type and composition of the food. Specifically, it was reported that the physical properties of the gastric digesta of pigs fed with rice were different in the proximal and distal stomach (Bornhorst, Ströbinger, et al., 2013). In contrast, raw or roasted almonds and egg white gels fed to growing pigs did not behave differently in these two stomach regions (Bornhorst, Roman, et al., 2013; Nau et al., 2019). This highlights that the potential role of functional regions of the stomach in starch digestion merits further investigation.

Considering that there is still limited understanding of the role of the stomach and its functional regions in starch digestion, the aim of this study was to understand the physical breakdown processes of starch-based foods in the stomach as affected by food structure, and how the breakdown processes affect the gastric emptying rate *in vivo*. The scope of this chapter was on physical breakdown during gastric digestion, while biochemical aspects of digestion and their impact on glycemic response will be presented in Chapter 5 and 6. The growing pig model was selected due to the similar anatomy and physiology of their digestive system to that of humans (Ziegler et al., 2016). The starch sources used were rice and wheat, as these two starch sources make up the majority of carbohydrates consumed globally (Kearney, 2010) and represent contrasting starch granule compositions. Four different food structures (porridge, native grain, agglomerate, and noodle) were selected to represent different macrostructures and levels of starch granule arrangements in food matrix. In this study, the gastric breakdown was monitored through quantification of moisture uptake from gastric

secretions, intragastric pH, particle size, and rheological and textural properties. These changes were monitored to understand their impact on gastric emptying process.

4.3 Materials and methods

4.3.1 Study diet preparation

Study diet preparation is described in Chapter 3, Section 3.1.2.

4.3.2 Animal housing and treatment

Animal housing and treatment is described in Chapter 3, Section 3.2.3.1.

4.3.3 Digesta collection procedure

Digesta collection procedure is described in Chapter 3, Section 3.2.3.2.

4.3.4 Diet characterization

Prior to analysis, cooked diets were freeze-dried and diet samples (uncooked and freeze-dried, cooked) were ground ($d < 1$ mm). Total starch and amylose content were measured for both uncooked and cooked diets using the Megazyme Total Starch Kit and the Megazyme Amylose/Amylopectin Kit (Megazyme, Wicklow, Ireland), respectively. Gross energy, protein, ash, fat, and dietary fiber content were measured for cooked diets only. Total dietary fiber (TDF) content was determined using Megazyme Total Dietary Fiber Assay Kit (Megazyme, Wicklow, Ireland). Gross energy was measured using an adiabatic bomb calorimeter (Kienzle, Schrag, Butterwick, & Opitz, 2002). Crude protein, ash content, and fat content of the diets were measured according to AOAC official methods 968.06, 923.3, and 922.06, respectively (AOAC International, 2012). The analyses were done at least in duplicate.

Buffering capacity, pH, volume of cooked diet, and water holding capacity (WHC) were measured on at least two batches of freshly cooked diets in duplicate. The pH of

freshly cooked diets was measured using a bench-top pH meter (PL-700 PV Bench Top Meter, GonDo, Taiwan). Buffering capacity (the resistance to pH change after addition of HCl) was measured as the total acid added ($\mu\text{mol H}^+/\text{g sample}$) to decrease the pH of the mixture to 1.5. It was done by addition of 0.5 mL aliquots of 0.16 M HCl to 20 g sample until a total of 7 mL, followed by addition of 1 mL of the solution until the pH of the sample reached 1.5 under constant and gentle stirring using a glass rod. The pH of the HCl-diet mixture was recorded after each HCl addition, then the acid titration curve (pH vs H^+ added) was plotted. The buffering capacity was calculated as $\mu\text{mol H}^+$ per ($\text{g sample} \times \text{total pH change}$) following Mennah-Govela, Singh, and Bornhorst (2019).

The volume of the cooked diets was determined using a modified water displacement method with at least eight measurements for each sample batch, using at least two batches of samples. A flat-bottom container was filled with 10 mL water and the water level was marked on the side. The volume of the diet was defined as the volume of water displaced from the marked level after addition of 5 g sample, which was determined by transferring the displaced volume to a 10-mL measuring cylinder. The bulk density of the diets was calculated by dividing the mass of the diet by the volume of the diet.

WHC of the cooked diets was measured using a centrifugation method and was defined as the maximum amount of moisture that could be held by the diets in its undigested form (Elhardallou & Walker, 1993). Each cooked diet sample (2.5 g) was weighed in a pre-weighed centrifuge tube and mixed with 30 mL distilled water. The tubes were kept in a shaking water bath (50 rpm, 37 °C) for 4 h, then centrifuged for 20 min at 4,200 rpm, 25 °C. Each diet was removed from its tube, weighed (weight of wet

sample), dried for 16 h at 105 °C, and the dry weight was recorded (weight of dried sample). The WHC of the cooked diets was defined as:

$$WHC_{diet} \left(\frac{g H_2O}{g DM} \right) = \frac{\text{weight of wet sample}}{\text{weight of dried sample}} - 1 \quad (4.1)$$

4.3.5 Measurement of physical properties of diets and gastric digesta

4.3.5.1 Moisture content

Moisture content of fresh digesta samples and cooked diets was determined gravimetrically by drying at 105 °C in a convection oven for 16 to 20 h until constant mass (Bornhorst, Ströbinger, et al., 2013). Each sample was analyzed in duplicate.

4.3.5.2 Texture

Textural changes in the cooked diet and digesta samples were measured with a texture analyzer (TA.XT plus, Stable Micro Systems, Surrey, UK) using previously reported bulk compression method with minor modifications (Drechsler & Bornhorst, 2018). A back extrusion cell (42-mm inner diameter) was filled with sample to ~15-mm height. The sample was compressed with a 37-mm diameter plunger at 1 mm/s to 50% strain. The hardness of the sample was quantified as the peak force during compression. At least two replicate measurements were done for each sample.

4.3.5.3 Rheological properties

Rheological properties of digesta were measured using a stress-controlled rheometer (Anton Paar MCR 302, Graz, Austria) with a 40-mm parallel plate geometry (Bornhorst, Ferrua, et al., 2013). The gap size was 5 mm for pasta, rice grain, and rice noodle digesta, 1.5 to 3 mm for couscous and rice couscous digesta, and 1.5 to 5 mm for semolina digesta. Samples were equilibrated to 37 °C for 30 to 120 s. A sample cover with a solvent trap was used to minimize sample drying.

Flow properties of the digesta were measured using a shear rate sweep, with shear rates increasing logarithmically from 0.001 to 10 s⁻¹. A hundred shear stress measurements (measured in Pa) were acquired over 4 min. Analysis was performed using data from 0.001 to approximately 1 s⁻¹ (77 data points per test), as samples would frequently flow out from the bottom of the plate at higher shear rates, similar to previous study (Bornhorst, Ferrua, et al., 2013).

Viscoelastic properties of digesta samples were measured using oscillatory testing. An amplitude sweep was performed from strain values of 0.01 to 0.1 % at a frequency of 1 Hz to determine the linear viscoelastic region. Based on the results of the amplitude sweep, most samples were tested at 0.05% strain, with a small number of samples tested at 0.03% strain. A frequency sweep was performed from 0.1 to 10 Hz.

4.3.5.4 Particle size

The cooked diets and gastric digesta were analyzed using a previously reported image analysis procedure with minor modifications (Gebauer, Novotny, Bornhorst, & Baer, 2016; Swackhamer et al., 2019). At least two sub-samples (0.5 to 1 g per sub-sample) were taken from each cooked diet or gastric digesta sample, spread over two to four 140-mm petri dishes, and dispersed in 15 mL of water per dish. Approximately 100 µL of 0.5% iodine solution was added to each petri dish to enhance contrast. After manually separating the particles, each dish was placed on an LED lightbox (AGPtek HL0163, Brooklyn, NY, USA) under a digital camera (Canon PowerShot G9 X Mark II, Tokyo, Japan) pointed vertically downwards. A photomacrographic scale (ABFO No. 2) was placed on the light box within the image frame and an image was recorded. Image analysis was conducted in MATLAB R2018b (The MathWorks Inc., Natick, MA, USA) according to Swackhamer et al. (2019) with the following modifications: (i) RGB input images were processed to remove the red and green channels, as the blue

channel provided the highest contrast between particles and the background; (ii) the Kittler method was used for binarization of particles (Kittler & Illingworth, 1986).

4.3.6 Data and statistical analysis

4.3.6.1 Determination of saturation ratio (SR)

Saturation ratio (SR) of each cooked diet and the digesta from each pig was calculated as (Martens, Noorloos, et al., 2019):

$$SR = \frac{\text{Diet or digesta moisture content (g H}_2\text{O/g DM)}}{WHC_{\text{diet}} \text{ (g H}_2\text{O/g DM)}} \quad (4.2)$$

4.3.6.2 Gastric emptying of dry matter (DM) and whole stomach content

The total DM consumed by each pig (DM_0 (g)) was determined using the moisture content of the cooked diet along with the mass of food consumed by the given pig. The DM remaining in the stomach at each digestion time (DM_t (g)) was determined using the total mass and the moisture content of the digesta. The values obtained from pigs fed the same type of diet were fit to a modified power-exponential model (Bornhorst, Chang, et al., 2013):

$$\frac{DM_t}{DM_0} = 1 - (1 - e^{-k_{DM} \cdot t})^{\beta_{DM}} \quad (4.3)$$

where k_{DM} : the gastric emptying rate of dry matter (min^{-1}), and β_{DM} : the theoretical y-intercept.

Gastric emptying of whole stomach content (consisting of dry matter of the diet, moisture from the cooked diet, and added digestive secretions) was analyzed by fitting the mass of the stomach content at digestion time t (W_t (g)) relative to the mass of the cooked diet consumed (W_0 (g)) to a linear-exponential model, which can describe the initial increase in the mass retention (W_t/W_0) of stomach content due to the continuous addition of gastric secretions (Goetze et al., 2007; Kong & Singh, 2009b):

$$\frac{W_t}{W_0} = (1 + k_{whole}\beta_{whole}t)e^{-\beta_{whole}t} \quad (4.4)$$

where k_{whole} : a dimensionless constant that represents lag phase, β_{whole} : a parameter that measures the concavity of the curve (min^{-1}).

Fitting of the DM and whole stomach content emptying data to Eqn. 4.3 and Eqn. 4.4 was done using non-linear least squares fitting in MATLAB R2018a (The MathWorks Inc., Natick, MA, USA). For both DM and whole stomach content emptying of each diet, emptying half-time (i.e., the time required to reach mass retention of 0.5) was calculated using the obtained gastric emptying parameters.

4.3.6.3 Determination of particle size distribution from image analysis data

The areas of all particles for each sample were fit to the Rosin-Rammler equation using non-linear least squares fitting in MATLAB R2018a (Hutchings et al., 2011):

$$Q = 1 - e^{-\left(\frac{x}{x_{50}}\right)^b \cdot \ln(2)} \quad (4.5)$$

where Q : the cumulative area (%), x : a single area measurement (mm^2), x_{50} : the area of a theoretical sieve aperture through which 50% of the particle area can pass (mm^2), and b : the broadness of the distribution (dimensionless). After model fitting, the area of a theoretical sieve aperture through which 10% and 90% of the particle area can pass (x_{10} and x_{90}), and number of particles per gram sample were extracted. The sample moisture content (Table C.1) was used to convert the number of particles per gram to particles per gram dry matter.

4.3.6.4 Softening kinetics of gastric digesta

Hardness values of gastric digesta at time t (H_t) relative to the initial hardness of the diet (H_0) were fit to the Weibull model using non-linear least squares fitting in MATLAB R2018a (Drechsler & Bornhorst, 2018):

$$\frac{H_t}{H_0} = e^{-(k_h * t)^{\beta_h}} \quad (4.6)$$

where H_t : the hardness of the digesta (N) at time t (min), H_0 : the initial hardness of the diet (N), k_h : the scale parameter (min^{-1}) and β_h : the shape factor (dimensionless).

In the present study, the measured hardness values of digesta samples were higher than the initial hardness of their respective diets, except for semolina, because the initial diet property measurement was done without additional lubrication. A previous study with similar carbohydrate-based foods and compression method found that cooked, undigested food particles stuck together and formed large void spaces when they were prepared for bulk compression, resulting in a lower initial hardness due to compression of air spaces (Drechsler & Bornhorst, 2018). To correct for void spaces in the non-lubricated particles, the initial hardness of each diet was multiplied with a correction factor of 2.14 calculated from that study (Table C.2). This corrected initial hardness value was used as the H_0 in the fitting of H_t/H_0 in Eqn. 4.6.

4.3.6.5 Rheological properties data analysis

Flow property data from the shear rate sweep were fit to the Herschel-Bulkley model (Steffe, 1996):

$$\tau = \tau_0 + K \cdot \dot{\gamma}^n \quad (4.7)$$

where τ : shear stress (Pa), τ_0 : yield stress (Pa), $\dot{\gamma}$: shear rate (s^{-1}), K : the consistency index ($\text{Pa} \cdot \text{s}^n$), and n : the flow index (dimensionless). Data were fit using non-linear least squares with the *SciPy* package in Python 3.7 (Virtanen et al., 2020). The trust region reflective least squares algorithm was selected due to its robustness and ability to be bounded by physical constraints. τ_0 and K were restricted to positive values, and the consistency index was constrained between 0 and 1.

4.3.6.6 Statistical analysis

Statistical analysis was conducted using SAS®Studio 3.8 (SAS Institute, Cary, NC, USA). For each initial (undigested diet) property, the difference between diets was

identified using a one-way ANOVA. Initial property data that were not normally distributed (x_{10} , x_{50} , x_{90} , b , and particles per gram dry matter) were transformed with a Box-Cox transformation prior to the one-way ANOVA. For digesta properties, data from 16 pigs were excluded from data presentation and statistical analysis because the pigs did not meet the minimum required feed intake (50% for semolina or 70% for the other five diets) to ensure that the stomach achieved its minimum working volume to demonstrate normal gastric emptying processes (Christian et al., 1987); this resulted in five to six replicates for each treatment.

The effect of diet, digestion time, and stomach region on digesta properties was analyzed using a multi-factor, mixed model ANOVA. The individual pig was the experimental unit, the between-subject factors were the diet (semolina, couscous, pasta, rice grain, rice couscous, or rice noodle) and digestion time (30, 60, 120, or 240 min). The repeated factor was the stomach region (proximal or distal). The batch of pigs was included in the model as a main effect to account for interindividual variability. Preliminary statistical analysis was completed to detect outliers. Data points with internally studentized residuals outside the range of (-3, 3) were considered outliers, with up to seven data points that were excluded from the subsequent statistical analysis for each property. Data sets that were not normally distributed (x_{10} , x_{50} , x_{90} , particles per gram dry matter) were transformed with a Box-Cox transformation. Where main effects were significant, the Tukey-Kramer procedure was used to identify differences between means. A correlation matrix between physical properties and gastric emptying was established using Spearman's correlation procedure. All values are reported as mean \pm standard error of the mean (SE). Statistical significance was considered at $p < 0.05$.

4.4 Results

4.4.1 Study diet characterization

The composition and all initial properties of the diets except pH (Table 4.1) were significantly influenced ($p < 0.05$) by diet type. The amylose content of pasta ($32.33 \pm 1.89\%$ total starch) was significantly higher ($p < 0.05$) than rice noodle and rice couscous (19.70 ± 0.71 and $24.40 \pm 1.32\%$ total starch, respectively), while the rest of the diets did not have significantly different amylose content from pasta. Variations in amylose content between the diets were controlled to be as small as possible, but due to the different commercial sources and cooking methods used (Table 3.1), slight variations could not be avoided. All cooked rice-based diets had significantly higher total starch but lower fat, protein, TDF, and ash contents than wheat-based diets ($p < 0.05$). When averaged across diets from the same starch source, wheat-based diets contained 14.85 ± 0.18 g protein and 5.92 ± 0.38 g TDF/100 g DM, whereas rice-based diets contained 8.01 ± 0.04 g protein and 2.14 ± 0.18 g TDF/100 g DM, respectively, similar to values reported in the literature for rice- and wheat-based products (Delcour et al., 2010). Semolina had a significantly ($p < 0.05$) higher buffering capacity ($74.48 \pm 3.23 \mu\text{mol H}^+ / (\text{g sample} \times \Delta\text{pH})$) than all other diets, and couscous had the second highest buffering capacity, which was significantly lower than semolina, but greater than the rest of the diets ($p < 0.05$). The buffering capacity values between pasta, rice noodle, rice couscous, and rice grain were not significantly different from each other.

Table 4.1 Composition, chemical properties, and physical properties of the cooked Study diets. Values shown are mean \pm SE ($n \geq 3$ for each property, except for buffering capacity, bulk density, total dietary fiber, and WHC, $n \geq 2$). Diets with different superscripts within the same property are significantly different ($p < 0.05$).

	Wheat-based			Rice-based		
	Semolina	Couscous	Pasta	Rice grain	Rice couscous	Rice noodle
Composition and chemical properties						
Total starch, uncooked (g/100 g DM)	68.93 \pm 0.58 ^d	69.09 \pm 0.42 ^d	75.00 \pm 0.10 ^{cd}	79.30 \pm 0.71 ^{bc}	85.53 \pm 0.82 ^{ab}	91.58 \pm 1.32 ^a
Total starch, cooked (g/100 g DM)	65.58 \pm 1.63 ^c	65.92 \pm 1.29 ^c	72.73 \pm 1.65 ^b	82.31 \pm 1.49 ^a	83.58 \pm 0.93 ^a	80.64 \pm 1.12 ^a
Amylose, cooked (% of total starch)	27.70 \pm 1.47 ^{ab}	25.28 \pm 2.12 ^{abc}	32.33 \pm 1.89 ^a	28.81 \pm 1.68 ^{ab}	24.40 \pm 1.32 ^{bc}	19.70 \pm 0.71 ^c
Resistant starch (g/100 g DM)	2.18 \pm 0.08 ^{bc}	1.82 \pm 0.05 ^c	2.08 \pm 0.11 ^{bc}	3.08 \pm 0.08 ^a	2.46 \pm 0.05 ^b	1.99 \pm 0.08 ^c
Total dietary fiber (g/100 g DM)	6.34 \pm 0.57 ^a	6.45 \pm 0.24 ^a	4.97 \pm 0.68 ^a	2.60 \pm 0.06 ^b	2.17 \pm 0.18 ^b	1.64 \pm 0.05 ^b
Crude protein (g/100 g DM)	15.76 \pm 0.10 ^a	14.38 \pm 0.09 ^b	14.12 \pm 0.06 ^b	7.91 \pm 0.08 ^c	8.13 \pm 0.02 ^c	7.94 \pm 0.06 ^c
Fat (g/100 g DM) [§]	2.83 \pm 0.09 ^b	2.05 \pm 0.08 ^c	6.22 \pm 0.16 ^a	1.17 \pm 0.02 ^d	1.17 \pm 0.04 ^d	1.18 \pm 0.08 ^d
Ash (g/100 g DM)	1.50 \pm 0.01 ^a	1.40 \pm 0.05 ^a	1.11 \pm 0.04 ^b	0.72 \pm 0.01 ^c	0.69 \pm 0.01 ^c	0.77 \pm 0.01 ^c
Gross energy (kJ/g DM)	17.49 \pm 0.11 ^b	17.51 \pm 0.03 ^b	18.49 \pm 0.04 ^a	16.97 \pm 0.05 ^c	16.98 \pm 0.03 ^c	16.97 \pm 0.06 ^c
Buffering capacity ($\mu\text{mol H}^+$ /(g sample $\times\Delta\text{pH}$))	74.48 \pm 3.23 ^a	55.26 \pm 3.47 ^b	31.29 \pm 0.20 ^c	26.67 \pm 1.99 ^c	31.02 \pm 1.48 ^c	24.41 \pm 0.18 ^c
Initial pH	6.58 \pm 0.01	6.27 \pm 0.05	6.39 \pm 0.06	6.34 \pm 0.08	6.46 \pm 0.15	6.49 \pm 0.11
Physical properties						
Dry basis moisture content (g H ₂ O/g DM)	4.80 \pm 0.05 ^a	1.73 \pm 0.01 ^{de}	1.98 \pm 0.08 ^b	1.54 \pm 0.02 ^c	1.76 \pm 0.05 ^{cd}	1.94 \pm 0.03 ^{bc}
Hardness (N)	5.51 \pm 0.85 ^d	24.31 \pm 2.23 ^{ab}	13.72 \pm 2.18 ^{cd}	31.12 \pm 1.99 ^a	31.38 \pm 2.21 ^a	18.11 \pm 0.49 ^{bc}
Particle area, x_{10} (mm ²) [†]	0.016 \pm 0.003 ^b	0.60 \pm 0.27 ^{ab}	238.50 \pm 106.57 ^a	3.76 \pm 2.15 ^{ab}	0.02 \pm 0.002 ^b	174.42 \pm 95.18 ^a
Particle area, x_{50} (mm ²) [†]	0.35 \pm 0.02 ^c	6.72 \pm 0.85 ^c	504.15 \pm 148.86 ^a	28.12 \pm 6.28 ^b	0.86 \pm 0.09 ^d	304.04 \pm 130.73 ^a
Particle area, x_{90} (mm ²) [†]	1.09 \pm 0.02 ^c	25.73 \pm 9.66 ^c	1680.4 \pm 790.89 ^a	225.12 \pm 52.15 ^b	3.55 \pm 0.50 ^d	958.65 \pm 306.73 ^{ab}
Broadness of particle area distribution, b^{\dagger}	1.06 \pm 0.04	1.26 \pm 0.26	7.53 \pm 3.09	1.47 \pm 0.68	0.87 \pm 0.02	5.38 \pm 2.02
Particles per gram dry matter (1/g DM)	160403 \pm 26265 ^a	13648 \pm 4324 ^c	1833 \pm 1512 ^d	6558 \pm 1246 ^{cd}	46422 \pm 8414 ^b	2468 \pm 895 ^{cd}
Bulk density (g/mL)	0.97 \pm 0.007 ^a	0.84 \pm 0.005 ^b	0.72 \pm 0.013 ^d	0.84 \pm 0.004 ^b	0.87 \pm 0.003 ^b	0.79 \pm 0.009 ^c
Water holding capacity (g H ₂ O/g DM)	5.50 \pm 0.11 ^a	4.18 \pm 0.07 ^c	3.64 \pm 0.09 ^d	3.37 \pm 0.06 ^d	4.10 \pm 0.05 ^c	4.87 \pm 0.10 ^b
Saturation ratio	0.87 \pm 0.01 ^a	0.41 \pm 0.003 ^{cd}	0.55 \pm 0.02 ^b	0.46 \pm 0.01 ^c	0.36 \pm 0.01 ^e	0.40 \pm 0.01 ^{de}

[§]Pasta had higher fat content than other diets due to addition of 15 g oil prior to feeding to enhance palatability.

[†]Particle area-related parameters are parameters given by the Rosin-Rammler model (Eqn. 4.5) fit to particle areas measured via image analysis.

Initial hardness values of the diets ranged from 5.51 ± 0.85 N (semolina) to 31.12 ± 1.99 N (rice grain). Pasta and rice noodle had significantly larger particle area (x_{50} and x_{90}) than the other diets ($p < 0.05$). In general, diets with a smaller median particle area (x_{50}) had larger number of particles per gram dry matter. For instance, the number of particles per gram dry matter (160403 ± 26265) was the highest in semolina, which had the lowest x_{50} (0.35 ± 0.02 mm²), whereas pasta with the highest x_{50} (504.15 ± 148.86 mm²) had the lowest particles per gram dry matter (1833 ± 1512). The WHC of the cooked diets was significantly different ($p < 0.05$) between the diets and decreased as the x_{50} of the diet increased for wheat-based diets. As a result, the WHC of the diets ranged from 5.50 ± 0.11 g H₂O/g DM (semolina) to 3.64 ± 0.09 g H₂O/g DM (pasta). Unlike wheat-based diets, the WHC of rice-based diets did not increase with decreasing x_{50} . The SR of the cooked diets, which reflects the amount of water held by the diet relative to its maximum capacity for holding water in the diet matrix, was the highest in semolina (0.87 ± 0.01) and the lowest in rice couscous (0.36 ± 0.01).

4.4.2 Changes in saturation ratio (SR) and moisture addition rate

To compare the water absorption behavior of the diets, the SR of the digesta (Table 4.3) was calculated. An SR >1 indicates that more water than what can be held by the food was present in the stomach (Martens, Noorloos, et al., 2019) or that the particles were possibly more swollen due to changes in the matrix during digestion. The SR of the diets was significantly influenced by diet, digestion time, and stomach region ($p < 0.0001$), the interaction between diet \times stomach region ($p < 0.0001$), and the batch of pigs ($p < 0.01$; Table 4.2). Similar to the trend in moisture content, a significant increase in SR (averaged across stomach regions) from 30 to 240 min was observed in couscous, rice couscous, and semolina ($p < 0.01$; Table 4.3). For example, semolina SR significantly increased from 1.02 ± 0.02 after 30 min gastric digestion to 1.64 ± 0.15

after 240 min digestion, averaged across both stomach regions. Of the six diets, rice noodle was the only diet that did not reach $SR > 1$ even after 240 min digestion in the distal stomach. Higher SR (averaged across all digestion times) in the distal stomach digesta compared to the proximal stomach digesta was observed in couscous, pasta, rice grain, and rice noodle (e.g. 0.58 ± 0.02 vs. 0.71 ± 0.03 for proximal and distal stomach, respectively in rice noodle).

Table 4.2 Statistical significance from mixed model ANOVA of diet type, digestion time, stomach region, and their interactions on the properties of gastric digesta and gastric emptying.

Parameter	<i>p</i> -value							
	Diet	Time	Region	Diet × Time	Diet × Region	Region × Time	Diet × Region × Time	Batch of pigs
Digesta properties								
MC,db	****	****	****	*	*	NS	NS	**
SR	****	****	****	NS	****	NS	NS	**
pH	NS	****	****	***	****	****	**	****
x ₁₀	****	*	NS	NS	NS	NS	NS	****
x ₅₀	****	*	***	NS	**	NS	NS	***
x ₉₀	****	NS	**	NS	****	NS	NS	*
<i>b</i>	****	***	NS	NS	**	NS	NS	****
Particles/g DM	****	NS	NS	NS	NS	NS	*	****
Stress at 0.2 s ⁻¹	****	****	****	****	***	NS	NS	NS
Yield stress	****	****	NS	****	NS	*	NS	***
<i>K</i>	****	****	****	****	**	*	NS	NS
<i>n</i>	****	**	NS	NS	NS	***	**	NS
<i>G'</i> 1 Hz	****	****	****	****	**	***	*	NS
<i>G''</i> 1 Hz	****	****	****	****	****	****	**	NS
tan(δ)	****	NS	NS	****	****	NS	*	NS
Hardness	****	****	NS	***	****	NS	**	NS
Gastric emptying								
Dry matter	****	****	-	NS	-	-	-	NS
Whole stomach content	****	****	-	*	-	-	-	NS

MC, db: moisture content (dry basis); SR: saturation ratio; x₁₀, x₅₀, x₉₀: 10th, 50th, 90th percentile of the particle areas; *b*: broadness of particle area distribution; Particles/g DM: particles per gram dry matter; *K*: consistency index; *n*: flow index; *G'* 1 Hz: storage modulus measured at 1 Hz; *G''* 1 Hz: loss modulus measured at 1 Hz; %DM: percentage of dry matter left in the stomach.

Asterisk (*) symbols indicate different levels of statistical significance. *: $p < 0.05$; **: $p < 0.01$, *** : $p < 0.001$, ****: $p < 0.0001$. NS: not significant.

Gastric secretory response to each diet was estimated by calculating the moisture addition during the 240-min period using a mass balance of stomach content, assuming that the moisture content of emptied gastric digesta was the same as the moisture content of distal stomach digesta. Based on this calculation, it was found that the total moisture added to the diets increased over time (Figure 4.1A). Moisture addition rate to the diets, calculated based on the difference of moisture added between digestion times, ranged from 0.21 (rice grain, 60 min) to 15.18 g/min (couscous, 30 min), with an average value of 4.14 g/min (Table 4.4). In the first 30 min of digestion, the average moisture addition rate was 9.07 g/min across all diets and decreased to an average of 2.49 g/min in the subsequent time points (60 to 240 min). Visualization of the moisture addition rate to each diet at each digestion time as a function of diet initial buffering capacity (Figure 4.1B) indicated a potential relationship between moisture addition rate at early digestion times and food buffering capacity for all diets except semolina.

4.4.3 Changes in pH

The pH values of the gastric digesta (Table 4.3) were significantly influenced by digestion time, stomach region, and all interactions between diet, time, and stomach region ($p < 0.05$; Table 4.2). Across stomach regions and for all diets, the pH of the digesta decreased over time such that the pH at 30 min was always significantly higher than the pH at 240 min ($p < 0.05$). The pH values of proximal and distal stomach contents of semolina and rice couscous were not significantly different at any digestion time ($p > 0.05$), whereas the distal stomach content had significantly lower pH until at least 120 min of digestion for couscous, rice grain, and rice noodle ($p < 0.05$), or for the entire 240-min digestion for pasta ($p \leq 0.0019$). For example, in semolina, the pH after 30 min was 5.96 ± 0.30 in the proximal stomach compared to 4.84 ± 0.23 in the distal stomach. The pH decreased to 1.93 ± 0.45 in the proximal stomach and 1.84 ± 0.42 in

the distal stomach after 240 min. However, in pasta, the pH was significantly higher ($p < 0.05$) in the proximal stomach compared to the distal stomach at all digestion times, with values of 6.42 ± 0.25 in the proximal and 3.30 ± 0.58 in the distal stomach after 30 min, decreasing to 3.58 ± 0.60 in the proximal and 1.53 ± 0.16 in the distal stomach after 240 min.

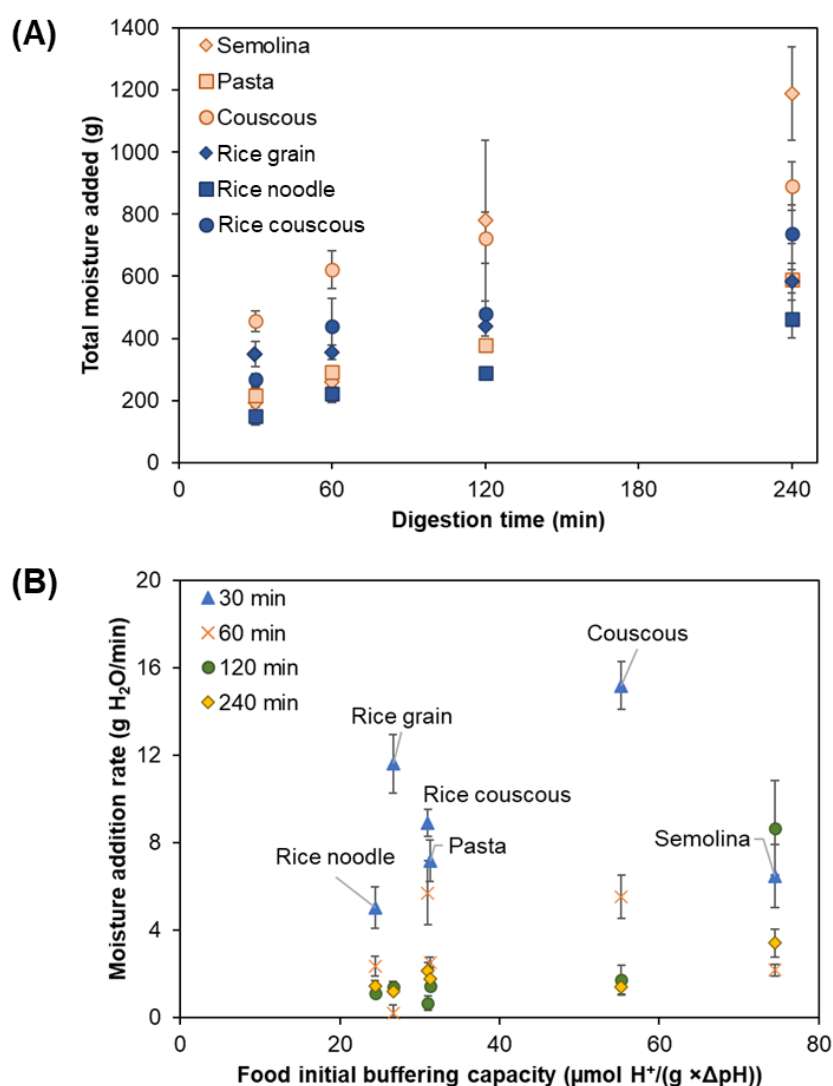


Figure 4.1 Total moisture addition over time during gastric digestion of the six Study diets. Due to the wide span of the y-axis, the error bars of some of the data points are too small to be seen in the figure. (A). Relationship between moisture addition rate at different digestion times and initial buffering capacity of the diets; parallel data points on the x-axis indicate one diet type – for readability, only the 30-min points were labeled with the diet names (B). All values are presented as mean \pm SE ($3 \leq n \leq 6$). The exact mean value and SE of each data point can be found in Table 4.4.

Table 4.3 Saturation ratio (SR) and pH values of digesta from proximal and distal stomach regions over 240 min digestion. All values are presented as mean \pm SE ($3 \leq n \leq 6$). Significantly different values within the same row (differences across diet \times stomach regions within the same digestion time) are represented by different letters (abcd; $p < 0.05$); significantly different values of each physical property within the same column (differences across digestion times within the same diet \times stomach region) are represented with different letters (zyx; $p < 0.05$).

Diet	Semolina		Couscous		Pasta		Rice Grain		Rice Couscous		Rice Noodle	
Time (min)	Proximal	Distal	Proximal	Distal	Proximal	Distal	Proximal	Distal	Proximal	Distal	Proximal	Distal
Saturation ratio (SR)												
30	0.98 \pm 0.02 ^{abc,y}	1.06 \pm 0.02 ^{ab,y}	0.73 \pm 0.04 ^{abcd,y}	0.80 \pm 0.04 ^{abcd,y}	0.70 \pm 0.02 ^{abcd}	0.76 \pm 0.02 ^{abcd}	0.74 \pm 0.03 ^{bcd}	0.88 \pm 0.05 ^{acd}	0.71 \pm 0.04 ^{cd,y}	0.71 \pm 0.03 ^{cd}	0.49 \pm 0.02 ^d	0.57 \pm 0.04 ^d
60	1.05 \pm 0.03 ^{ab,y}	1.11 \pm 0.03 ^{a,y}	0.85 \pm 0.07 ^{abc,zy}	0.92 \pm 0.04 ^{abc,zy}	0.75 \pm 0.02 ^{bc}	0.86 \pm 0.02 ^{abc}	0.75 \pm 0.02 ^{bc}	0.89 \pm 0.03 ^{ac}	0.83 \pm 0.08 ^{abc,zy}	0.81 \pm 0.08 ^{abc}	0.55 \pm 0.02 ^c	0.66 \pm 0.03 ^c
120	1.49 \pm 0.27 ^{a,zy}	1.32 \pm 0.20 ^{ab,zy}	0.90 \pm 0.07 ^{cde,zy}	0.99 \pm 0.06 ^{bcd,zy}	0.84 \pm 0.03 ^{cde}	0.95 \pm 0.04 ^{bcd}	0.84 \pm 0.05 ^{de}	1.01 \pm 0.04 ^{bc}	0.86 \pm 0.02 ^{cde,zy}	0.93 \pm 0.04 ^{bcd}	0.57 \pm 0.01 ^e	0.75 \pm 0.02 ^{cd}
240	1.58 \pm 0.20 ^{ab,z}	1.75 \pm 0.28 ^{a,z}	1.14 \pm 0.12 ^{cd,z}	1.19 \pm 0.10 ^{bcd,z}	0.97 \pm 0.08 ^{cde}	1.05 \pm 0.10 ^{cde}	0.96 \pm 0.09 ^{de}	1.13 \pm 0.06 ^c	1.02 \pm 0.08 ^{cd,z}	1.03 \pm 0.06 ^{cde}	0.67 \pm 0.05 ^e	0.82 \pm 0.05 ^{cd}
pH												
30	5.96 \pm 0.30 ^{a,z}	4.84 \pm 0.23 ^{ab,z}	6.15 \pm 0.37 ^{a,z}	3.3 \pm 0.46 ^b	6.42 \pm 0.25 ^{a,z}	3.30 \pm 0.58 ^b	6.38 \pm 0.34 ^{a,z}	3.23 \pm 0.52 ^b	5.36 \pm 0.32 ^{a,z}	5.20 \pm 0.19 ^{a,z}	6.64 \pm 0.15 ^{a,z}	2.97 \pm 0.91 ^b
60	5.31 \pm 0.16 ^{ab,zy}	4.07 \pm 0.10 ^{bcd,zy}	5.46 \pm 0.20 ^{ab,zy}	2.52 \pm 0.39 ^{cd}	5.86 \pm 0.47 ^{a,z}	1.87 \pm 0.32 ^{de}	5.69 \pm 0.37 ^{a,z}	2.02 \pm 0.29 ^{de}	4.42 \pm 0.53 ^{ab,z}	4.01 \pm 0.36 ^{abc,z}	5.96 \pm 0.19 ^{a,z}	1.47 \pm 0.10 ^e
120	3.17 \pm 0.86 ^{bcd,yx}	2.82 \pm 0.67 ^{bcd,zy}	3.86 \pm 0.58 ^{abc,yx}	2.01 \pm 0.16 ^{de}	4.33 \pm 0.42 ^{ab,zy}	1.52 \pm 0.11 ^{de}	5.19 \pm 0.36 ^{a,z}	1.60 \pm 0.11 ^{de}	2.27 \pm 0.14 ^{cde,y}	2.23 \pm 0.15 ^{cde,y}	2.90 \pm 0.30 ^{bc,y}	1.14 \pm 0.08 ^e
240	1.93 \pm 0.45 ^{ab,x}	1.84 \pm 0.42 ^{ab,y}	1.95 \pm 0.46 ^{ab,x}	1.82 \pm 0.42 ^{ab}	3.58 \pm 0.60 ^{a,y}	1.53 \pm 0.16 ^b	2.89 \pm 0.41 ^{ab,y}	1.68 \pm 0.17 ^b	1.35 \pm 0.10 ^{b,y}	1.37 \pm 0.11 ^{b,y}	2.96 \pm 0.35 ^{ab,y}	1.53 \pm 0.12 ^b

Table 4.4 Total moisture added and moisture addition rate to the diets (mean values \pm SE, $3 \leq n \leq 5$ for each diet \times time). Significantly different values of moisture added over time for each diet are represented with superscripts abcd ($p < 0.05$)

Diet	Time (min)	Total moisture added (g)	Moisture addition rate [§] (g /min)
Semolina	30	194.34 \pm 43.09 ^a	6.48 \pm 1.44
	60	259.61 \pm 15.38 ^a	2.18 \pm 0.26
	120	779.65 \pm 259.01 ^b	8.67 \pm 2.16
	240	1188.67 \pm 150.67 ^b	3.41 \pm 0.63
Pasta	30	215.25 \pm 28.06	7.17 \pm 0.94
	60	291.34 \pm 14.05	2.54 \pm 0.23
	120	379.13 \pm 12.36	1.46 \pm 0.10
	240	590.37 \pm 114.50	1.76 \pm 0.48
Couscous	30	455.45 \pm 32.71 ^a	15.18 \pm 1.09
	60	621.00 \pm 60.05 ^{ab}	5.52 \pm 1.00
	120	723.93 \pm 82.62 ^{ab}	1.72 \pm 0.69
	240	891.85 \pm 78.02 ^b	1.40 \pm 0.33
Rice grain	30	348.35 \pm 40.61	11.61 \pm 1.35
	60	354.75 \pm 22.77	0.21 \pm 0.38
	120	438.69 \pm 31.89	1.40 \pm 0.27
	240	583.83 \pm 36.61	1.21 \pm 0.15
Rice noodle	30	150.69 \pm 28.56	5.02 \pm 0.95
	60	221.40 \pm 28.17	2.36 \pm 0.47
	120	288.81 \pm 12.78	1.12 \pm 0.11
	240	461.51 \pm 60.77	1.44 \pm 0.25
Rice couscous	30	267.74 \pm 18.50 ^a	8.92 \pm 0.62
	60	439.04 \pm 88.51 ^{ab}	5.71 \pm 1.48
	120	479.61 \pm 40.00 ^{ab}	0.68 \pm 0.33
	240	735.85 \pm 92.91 ^b	2.14 \pm 0.39

[§]Moisture addition rate, $t_2 = \frac{\text{Moisture added}, t_2 - \text{Moisture added}, t_1}{t_2 - t_1}$; t_2 = current time point (30/60/120/240 min), t_1 = previous time point (0/30/60/120 min). Moisture added at $t = 0$ min was assumed to be zero.

4.4.4 Changes in particle size distribution

Examples of binary images used to obtain the particle size distribution parameters are presented in Figure 4.2 and 4.3. The particle size distribution data from the cooked diets and gastric digesta fit well to the Rosin-Rammler model, with $R^2 > 0.83$ for all samples. All parameters used to represent particle size (x_{10} , x_{50} , x_{90} , b , and particles per gram dry matter; Table 4.5) were significantly influenced by diet ($p < 0.0001$). x_{10} , x_{50} , and b

were significantly influenced by time ($p < 0.05$), and x_{50} and x_{90} were significantly influenced by stomach region ($p < 0.003$). b was significantly influenced by the diet \times time interaction ($p < 0.0001$). x_{50} , x_{90} , and b were significantly influenced by the diet \times stomach region interaction ($p < 0.004$). Particles per gram dry matter was significantly influenced by the diet \times stomach region \times time interaction ($p < 0.05$; Table 4.2).

When compared between stomach regions across all time points, both the x_{50} and x_{90} values in rice grain were significantly larger in the distal stomach digesta as compared to the proximal stomach digesta, with average x_{50} values across all time points of 1.23 ± 0.10 and $2.50 \pm 0.32 \text{ mm}^2$ for proximal and distal stomach, respectively ($p < 0.0014$). Other diets and percentiles did not show significant differences across stomach regions. Significant differences in particle size parameters over time were observed only in the rice noodle distal stomach for x_{10} , b , and particles per gram dry matter; and in the couscous distal stomach for b .

Figure 4.4 exemplifies the overall changes in particle area of the diets and their proportion in the digesta during the 240-min digestion. With this visualization, the changes in the particle area distribution in rice grain, pasta, and rice noodle during the first 30 min of digestion can be seen. However, as the digestion progressed from 30 to 240 min, the particle area distribution did not show visual differences, mirroring results seen in the x_{10} , x_{50} , and x_{90} data. Large particles ($>200 \text{ mm}^2$ for noodle diets and rice grain, or between 10 to 100 mm^2 for agglomerate diets and semolina), which in the first 60 or 120 min of digestion became less or even disappeared from the distribution, reappeared in the distribution at 240 min for all diets, although only as a small percentage in the gastric digesta.

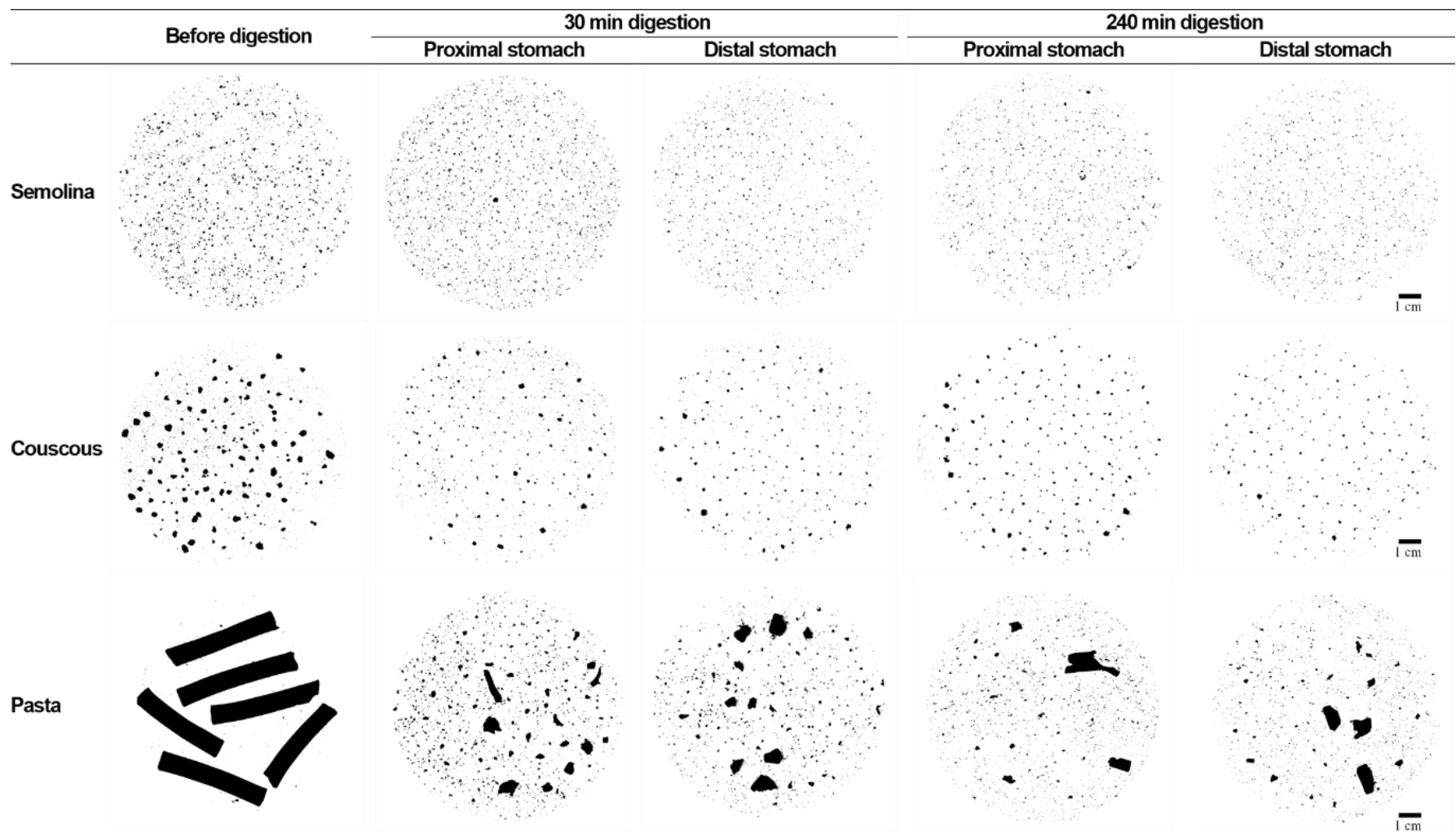


Figure 4.2 Examples of binary images of gastric digesta used for extraction of particle size parameters for the wheat-based diets before digestion and after 30 and 240 min gastric digestion. The scale bar represents 1 cm and is the same for all images.

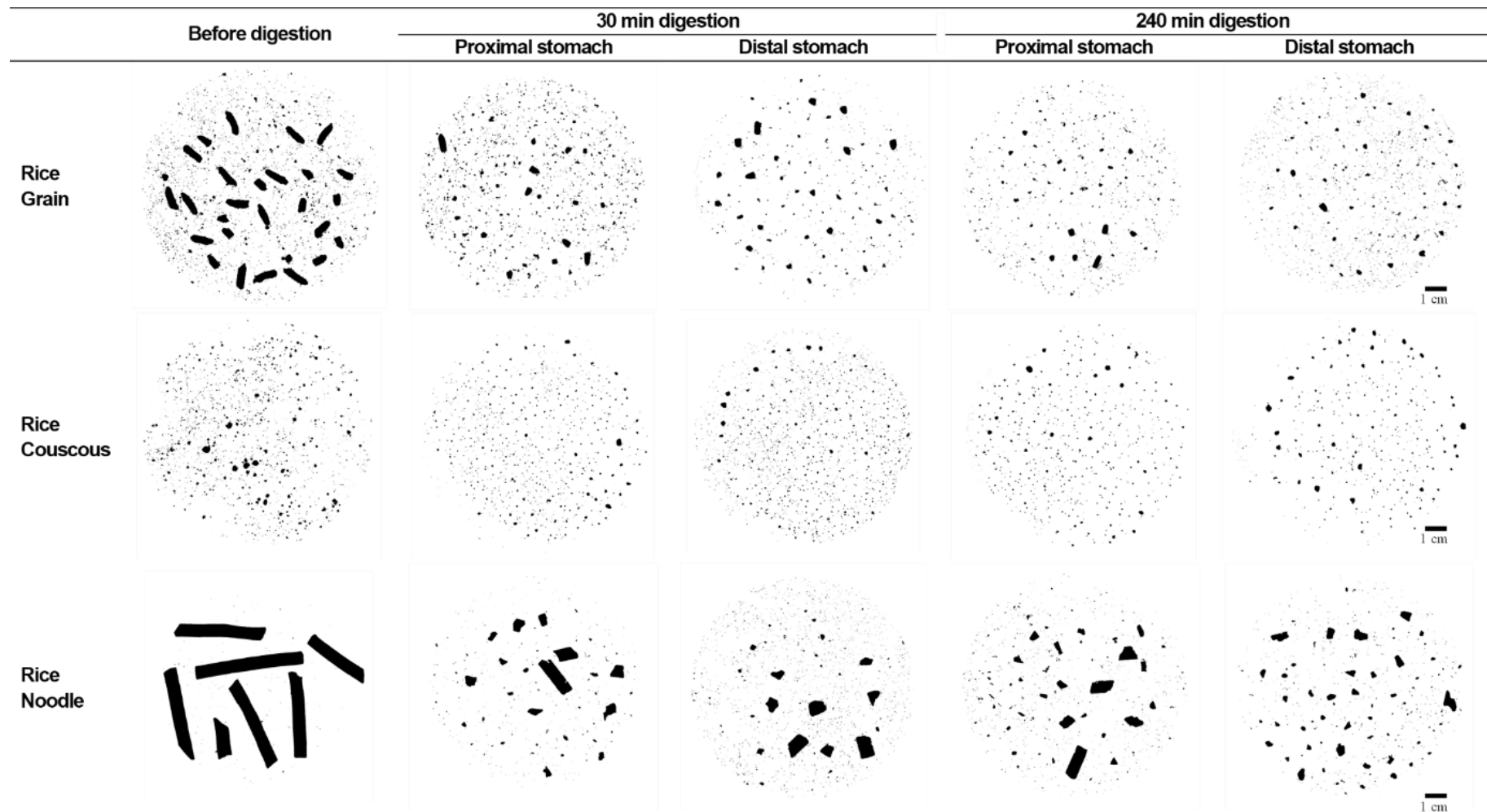


Figure 4.3 Examples of binary images of gastric digesta used for extraction of particle size parameters for the rice-based diets before digestion and after 30 and 240 min gastric digestion. The scale bar represents 1 cm and is the same for all images.

Table 4.5 Particle area parameters given by the Rosin-Rammler model (Eqn. 4.5) fit to particle areas measured via image analysis ($R^2 > 0.83$ for all model fits). Particles per gram dry matter was determined based on mass of sample spread on dishes and moisture content during digestion (Table C.1). All values represent mean \pm SE ($3 \leq n \leq 6$). Significantly different values within the same row (differences across diet \times stomach regions within the same digestion time) are represented by different letters (abcd; $p < 0.05$); significantly different values of each physical property within the same column (differences across digestion times within the same diet \times stomach region) are represented with different letters (zyx; $p < 0.05$).

	Semolina		Couscous		Pasta		Rice grain		Rice couscous		Rice noodle	
Time (min)	Proximal	Distal	Proximal	Distal	Proximal	Distal	Proximal	Distal	Proximal	Distal	Proximal	Distal
x₁₀ (mm²)												
30	0.04 \pm 0.01	0.04 \pm 0.01	0.03 \pm 0.01	0.03 \pm 0.01	0.02 \pm 0.00	0.02 \pm 0.00	0.02 \pm 0.00	0.04 \pm 0.02	0.01 \pm 0.00	0.02 \pm 0.01	0.10 \pm 0.04	0.05 \pm 0.02 ^y
60	0.04 \pm 0.01 ^{abc}	0.04 \pm 0.01 ^{abc}	0.03 \pm 0.01 ^{ab}	0.04 \pm 0.01 ^{ab}	0.01 \pm 0.00 ^{abc}	0.01 \pm 0.00 ^c	0.02 \pm 0.00 ^{abc}	0.02 \pm 0.01 ^{abc}	0.02 \pm 0.01 ^{bc}	0.02 \pm 0.01 ^{abc}	0.14 \pm 0.09 ^{ab}	0.11 \pm 0.02 ^{a,zy}
120	0.03 \pm 0.01 ^{ab}	0.03 \pm 0.01 ^{ab}	0.04 \pm 0.01 ^{ab}	0.06 \pm 0.02 ^a	0.01 \pm 0.00 ^b	0.03 \pm 0.01 ^{ab}	0.02 \pm 0.00 ^{ab}	0.01 \pm 0.00 ^b	0.03 \pm 0.01 ^{ab}	0.02 \pm 0.01 ^{ab}	0.25 \pm 0.18 ^a	0.13 \pm 0.10 ^{ab,zy}
240	0.03 \pm 0.01 ^{bcd}	0.03 \pm 0.01 ^{bcd}	0.11 \pm 0.04 ^{abcd}	0.13 \pm 0.02 ^{ab}	0.02 \pm 0.00 ^{cd}	0.01 \pm 0.00 ^d	0.02 \pm 0.00 ^{cd}	0.02 \pm 0.01 ^{bcd}	0.03 \pm 0.01 ^{bcd}	0.03 \pm 0.01 ^{bcd}	0.12 \pm 0.06 ^{abc}	0.63 \pm 0.22 ^{a,z}
x₅₀ (mm²)												
30	0.39 \pm 0.06 ^f	0.49 \pm 0.11 ^{ef}	1.34 \pm 0.22 ^{cde}	1.30 \pm 0.11 ^{cde}	4.86 \pm 1.04 ^{abc}	9.76 \pm 5.57 ^{abc}	1.24 \pm 0.17 ^{cde}	2.46 \pm 0.2 ^{bcd}	0.59 \pm 0.16 ^{ef}	0.90 \pm 0.26 ^{def}	33.1 \pm 5.17 ^a	23.5 \pm 5.71 ^{ab}
60	0.42 \pm 0.10 ^{de}	0.35 \pm 0.05 ^e	1.10 \pm 0.14 ^{bc}	0.99 \pm 0.04 ^{bcd}	4.38 \pm 0.84 ^{ab}	4.14 \pm 1.13 ^{ab}	1.00 \pm 0.07 ^{bcd}	1.61 \pm 0.53 ^{bc}	0.53 \pm 0.15 ^{cde}	0.88 \pm 0.25 ^{cde}	24.08 \pm 5.52 ^a	24.08 \pm 5.00 ^a
120	0.41 \pm 0.05 ^f	0.42 \pm 0.05 ^f	1.26 \pm 0.25 ^{def}	1.13 \pm 0.11 ^{def}	5.58 \pm 2.98 ^{bcd}	21.72 \pm 9.90 ^{abc}	1.21 \pm 0.18 ^{de}	2.27 \pm 0.51 ^{cde}	0.9 \pm 0.14 ^{ef}	0.69 \pm 0.08 ^{ef}	29.75 \pm 4.45 ^a	27.74 \pm 5.99 ^{ab}
240	0.33 \pm 0.04 ^e	0.33 \pm 0.06 ^e	1.27 \pm 0.20 ^{cd}	1.28 \pm 0.12 ^{cd}	9.63 \pm 4.56 ^{abc}	27.38 \pm 19.13 ^{ab}	1.48 \pm 0.32 ^{cd}	3.71 \pm 1.03 ^{bcd}	1.22 \pm 0.39 ^{de}	1.35 \pm 0.30 ^{cd}	19.47 \pm 4.33 ^{ab}	20.81 \pm 4.97 ^a
x₉₀ (mm²)												
30	0.93 \pm 0.13 ^e	1.28 \pm 0.39 ^{de}	5.99 \pm 0.60 ^{bc}	5.41 \pm 0.64 ^{bc}	42.83 \pm 11.37 ^{ab}	133.74 \pm 94.72 ^{ab}	6.35 \pm 1.02 ^{bc}	15.65 \pm 2.87 ^b	2.47 \pm 0.67 ^{cde}	3.72 \pm 1.23 ^{cd}	318.04 \pm 48.59 ^a	258.21 \pm 69.11 ^a
60	1.09 \pm 0.24 ^e	0.81 \pm 0.08 ^e	4.16 \pm 0.50 ^{cd}	3.46 \pm 0.23 ^{cd}	40.17 \pm 9.78 ^{ab}	48.46 \pm 14.86 ^{ab}	4.61 \pm 0.28 ^{cd}	8.85 \pm 2.62 ^{bc}	1.97 \pm 0.54 ^{de}	4.04 \pm 1.39 ^{cd}	211.16 \pm 25.9 ^a	212.96 \pm 51.37 ^a
120	1.10 \pm 0.13 ^f	1.13 \pm 0.17 ^f	4.77 \pm 0.78 ^{de}	3.49 \pm 0.21 ^{de}	73.3 \pm 47.33 ^{abc}	321.98 \pm 174.3 ^{ab}	6.02 \pm 0.97 ^{cde}	17.64 \pm 3.17 ^{bcd}	3.55 \pm 0.48 ^e	2.95 \pm 0.55 ^{ef}	290.71 \pm 61.03 ^a	286.82 \pm 114.36 ^{ab}
240	0.87 \pm 0.12 ^e	0.83 \pm 0.14 ^e	3.50 \pm 0.21 ^d	3.03 \pm 0.40 ^d	119.61 \pm 63.6 ^{ab}	314.58 \pm 204.16 ^a	7.98 \pm 1.83 ^{bcd}	26.28 \pm 8.29 ^{abc}	4.73 \pm 1.31 ^d	5.81 \pm 1.10 ^{cd}	152.30 \pm 25.55 ^a	91.80 \pm 25.61 ^a

(continued)

Table 4.5 (continued)

	Semolina		Couscous		Pasta		Rice grain		Rice couscous		Rice noodle	
Time (min)	Proximal	Distal	Proximal	Distal	Proximal	Distal	Proximal	Distal	Proximal	Distal	Proximal	Distal
Broadness of distribution, <i>b</i> (dimensionless)*												
30	1.38 ± 0.05 ^a	1.32 ± 0.09 ^a	0.80 ± 0.05 ^{bcd}	0.86 ± 0.04 ^{bc,y}	0.60 ± 0.05 ^{cd}	0.60 ± 0.07 ^{cd}	0.75 ± 0.02 ^{bcd}	0.64 ± 0.02 ^{bcd}	0.86 ± 0.04 ^{bc}	0.90 ± 0.06 ^b	0.54 ± 0.02 ^d	0.53 ± 0.03 ^{d,y}
60	1.39 ± 0.03 ^a	1.42 ± 0.07 ^a	0.91 ± 0.06 ^{bc}	0.99 ± 0.07 ^{b,y}	0.56 ± 0.01 ^{de}	0.57 ± 0.06 ^{de}	0.79 ± 0.02 ^{bcd}	0.71 ± 0.04 ^{cde}	0.91 ± 0.04 ^{bc}	0.86 ± 0.05 ^{bcd}	0.55 ± 0.04 ^e	0.60 ± 0.02 ^{de,zy}
120	1.24 ± 0.06 ^a	1.25 ± 0.08 ^a	0.89 ± 0.05 ^{bc}	1.08 ± 0.09 ^{ab,y}	0.56 ± 0.03 ^d	0.52 ± 0.02 ^d	0.76 ± 0.03 ^{cd}	0.59 ± 0.03 ^{cd}	0.90 ± 0.07 ^{bc}	0.83 ± 0.06 ^{bcd}	0.58 ± 0.08 ^d	0.69 ± 0.1 ^{cd,zy}
240	1.26 ± 0.10 ^a	1.29 ± 0.05 ^a	1.24 ± 0.14 ^a	1.45 ± 0.08 ^{a,z}	0.58 ± 0.05 ^b	0.59 ± 0.07 ^b	0.72 ± 0.05 ^b	0.65 ± 0.03 ^b	0.85 ± 0.05 ^b	0.83 ± 0.05 ^b	0.59 ± 0.04 ^b	0.84 ± 0.06 ^{b,z}
Particles per gram dry matter (1/g DM)												
30	89263 ± 16259 ^{ab}	109462 ± 33404 ^a	38948 ± 7093 ^{abc}	34025 ± 3061 ^{abcd}	16220 ± 1736 ^{cde}	17409 ± 3113 ^{cde}	28529 ± 3622 ^{abcd}	17074 ± 2030 ^{cde}	30829 ± 5811 ^{abcd}	21774 ± 2423 ^{bcd}	5823 ± 709 ^e	11420 ± 2381 ^{de,zy}
60	106757 ± 32240 ^a	77072 ± 6578 ^a	37618 ± 11186 ^{abc}	30625 ± 2971 ^{abc}	16459 ± 1934 ^{bcd}	34721 ± 12289 ^{abc}	27447 ± 2150 ^{abc}	29870 ± 7596 ^{abc}	49788 ± 12371 ^{ab}	38452 ± 12487 ^{abc}	8107 ± 2132 ^d	16239 ± 7417 ^{cd,z}
120	81665 ± 19093 ^{ab}	94260 ± 29417 ^a	38073 ± 13179 ^{abc}	28033 ± 5436 ^{abc}	23220 ± 2911 ^{cd}	25876 ± 6203 ^{cd}	31072 ± 2723 ^{abc}	30447 ± 4585 ^{abc}	20713 ± 5188 ^{cd}	22641 ± 2963 ^{bc}	7674 ± 1651 ^d	15201 ± 4807 ^{cd,z}
240	65956 ± 18403 ^a	51971 ± 14927 ^a	39604 ± 13117 ^a	21064 ± 1978 ^{ab}	21314 ± 6595 ^{ab}	30022 ± 13599 ^{ab}	34999 ± 8323 ^a	28019 ± 8482 ^{ab}	41073 ± 13686 ^{ab}	33210 ± 6649 ^{ab}	10252 ± 1831 ^{bc}	4450 ± 950 ^{c,y}

* A higher value of *b* corresponds to a narrower distribution.

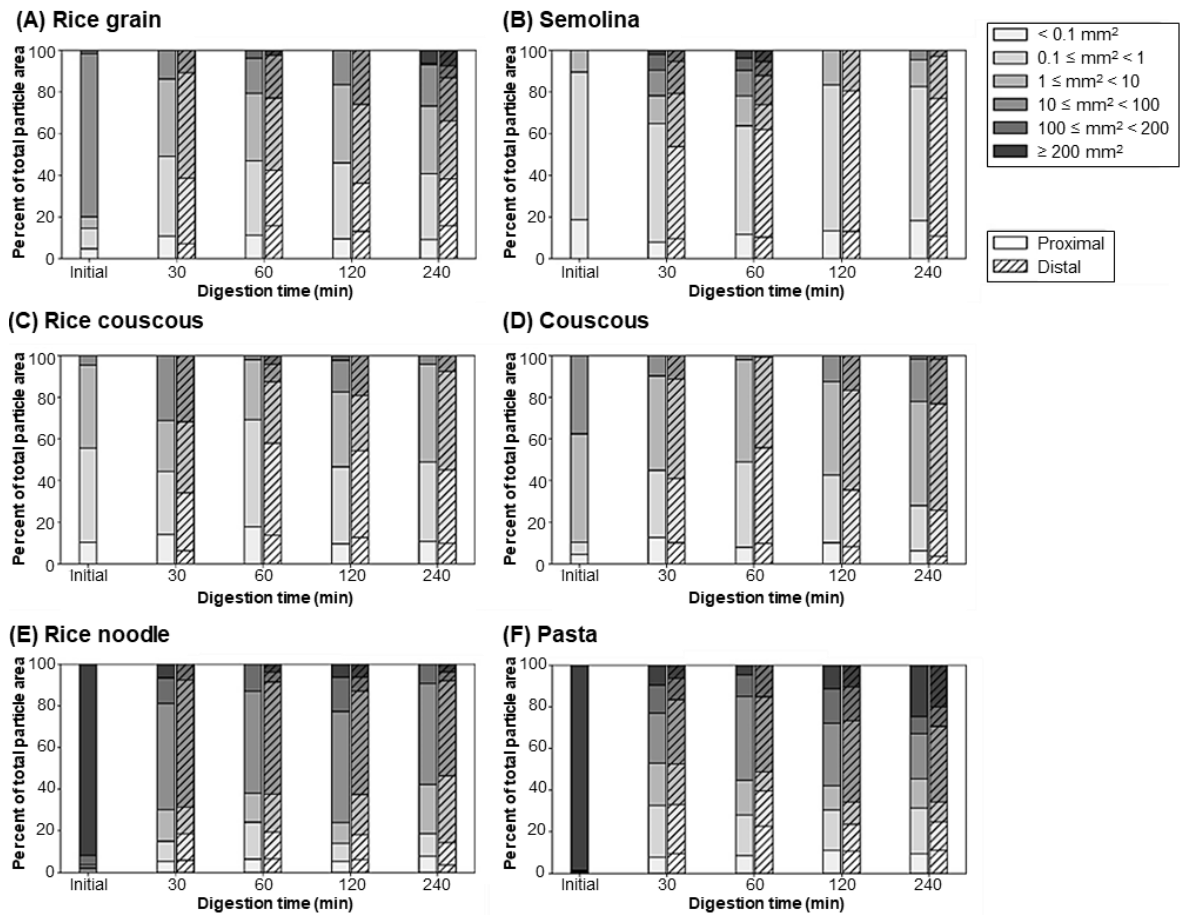


Figure 4.4 Bar charts showing the initial (before digestion) particle area distribution and the particle area distribution in proximal and distal stomach digesta during 240 min gastric digestion of (A) rice grain, (B) semolina, (C) rice couscous, (D) couscous, (E) rice noodle, and (F) pasta.

4.4.5 Changes in rheological properties

4.4.5.1 Shear measurements

The Herschel-Bulkley model (Eqn. 4.7) fit well to the measured shear sweep data (Table 4.6), with an overall average $R^2 = 0.90$ across all samples (see Figure 4.5 for example plots). Since the digesta was non-Newtonian, shear stress values at a shear rate of 0.2 s^{-1} (hereafter referred to as shear stress at 0.2 s^{-1}) were determined as an indication of the shear stress at a shear rate that may occur in gastric environment (0.0093 to 0.45 s^{-1} in the proximal and distal stomach, respectively) (Ferrua, Xue, & Singh, 2014). Shear stress at 0.2 s^{-1} , yield stress, K , and n were significantly influenced by the main effects of diet and time ($p < 0.005$). Shear stress at 0.2 s^{-1} and K were

significantly influenced by stomach region ($p < 0.0001$), as well as diet \times time ($p \leq 0.0035$) and diet \times stomach region ($p \leq 0.0035$). Yield stress was significantly influenced by diet \times time ($p < 0.0001$). Yield stress, K , and n were significantly influenced by stomach region \times time ($p \leq 0.0281$). n was influenced by diet \times stomach region \times time ($p < 0.0052$; Table 4.2).

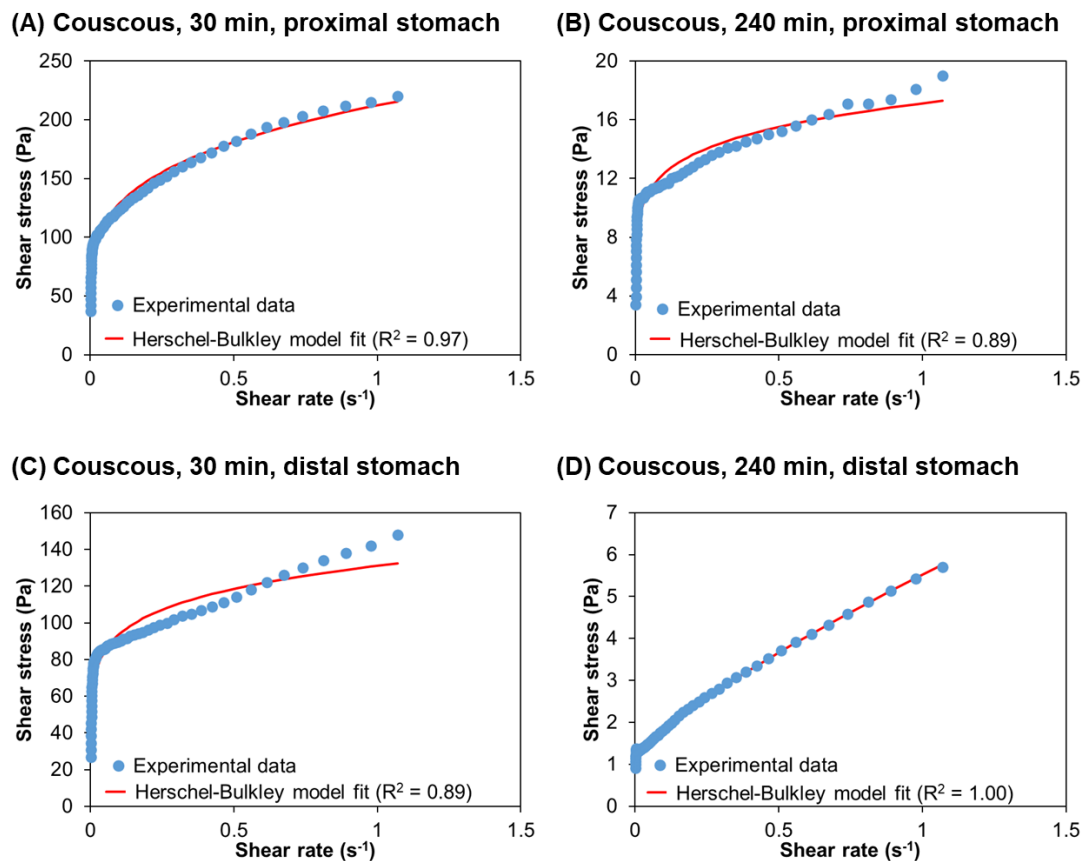


Figure 4.5 Example of flow properties of couscous digesta from the proximal (A-B) and distal (C-D) regions of the stomach after 30 (A, C) and 240 (B, D) min gastric digestion.

All shear measurements were significantly impacted by diet ($p < 0.0001$) as well as all two-way interactions including diet. Shear stress at 0.2 s⁻¹ averaged over the two stomach regions significantly decreased from 30 to 240 min in couscous (169.80 ± 33.24 to 14.90 ± 3.21 Pa, $p = 0.0237$), rice grain (230 ± 38.29 to 94.87 ± 13.91 Pa, $p = 0.0305$), and rice noodle (252.67 ± 35.96 to 73.24 ± 11.24 Pa, $p < 0.0001$). In addition

to showing the largest changes over digestion time, couscous samples were also significantly different between proximal (255.20 ± 133.20 Pa) and distal (84.40 ± 14.96 Pa) regions at 30 min ($p = 0.0239$). These differences indicated the impact of diet on the changes in rheological properties over time as well as the regional differences in these properties.

The K parameter of the Herschel-Buckley model demonstrated similar trends to the shear stress at 0.2 s^{-1} , with couscous, rice grain, and rice noodle showing significant decreases over time and couscous samples at 30 min showing significant differences between stomach regions. Likewise, couscous demonstrated the largest change in K during digestion, decreasing from $219.68 \pm 43.92 \text{ Pa}\cdot\text{s}^n$ at 30 min to $18.31 \pm 3.57 \text{ Pa}\cdot\text{s}^n$ at 240 min, averaged over both regions. It is noteworthy that all diets showed yield stress values greater than zero (except couscous, for which only one measurement >0 was obtained for each treatment). Average yield stress after 240 min digestion was lower than at 30 min for all diets, although this difference was only significant in the distal stomach for pasta (105.77 ± 21.41 to 20.37 ± 11.96 Pa, $p = 0.0005$) and rice grain (60.34 ± 17.71 to 2.43 ± 2.43 , $p = 0.0126$).

4.4.5.2 Oscillatory measurements

Storage (G') and loss moduli (G'') at 1 Hz were significantly influenced by the main effects of diet, time, and stomach region as well as all interactions ($p < 0.01$). The ratio of G' and G'' , $\tan(\delta)$, was only influenced by diet and the interactions of diet \times time, diet \times region, and diet \times region \times time ($p < 0.05$; Table 4.2). Based on the magnitude of $\tan(\delta)$, the samples could be classified as gels, demonstrating viscoelastic behavior (Steffe, 1996). The $\tan(\delta)$ magnitude was similar at all tested frequencies (see Figure 4.6 for example plots). Both pasta and rice grain showed significant decreases in G' and G'' over time in both regions, while G' and G'' for rice noodle decreased significantly

over time in the proximal region only. Rice grain in the proximal stomach showed the largest change in G' , decreasing from 20173 ± 2373 to 5974 ± 968 Pa between 30 and 240 min of digestion (Table 4.6). Similarly, couscous in the proximal stomach showed the greatest change in G'' , decreasing from 871 ± 97 to 127 ± 39 Pa between 30 and 240 min of digestion.

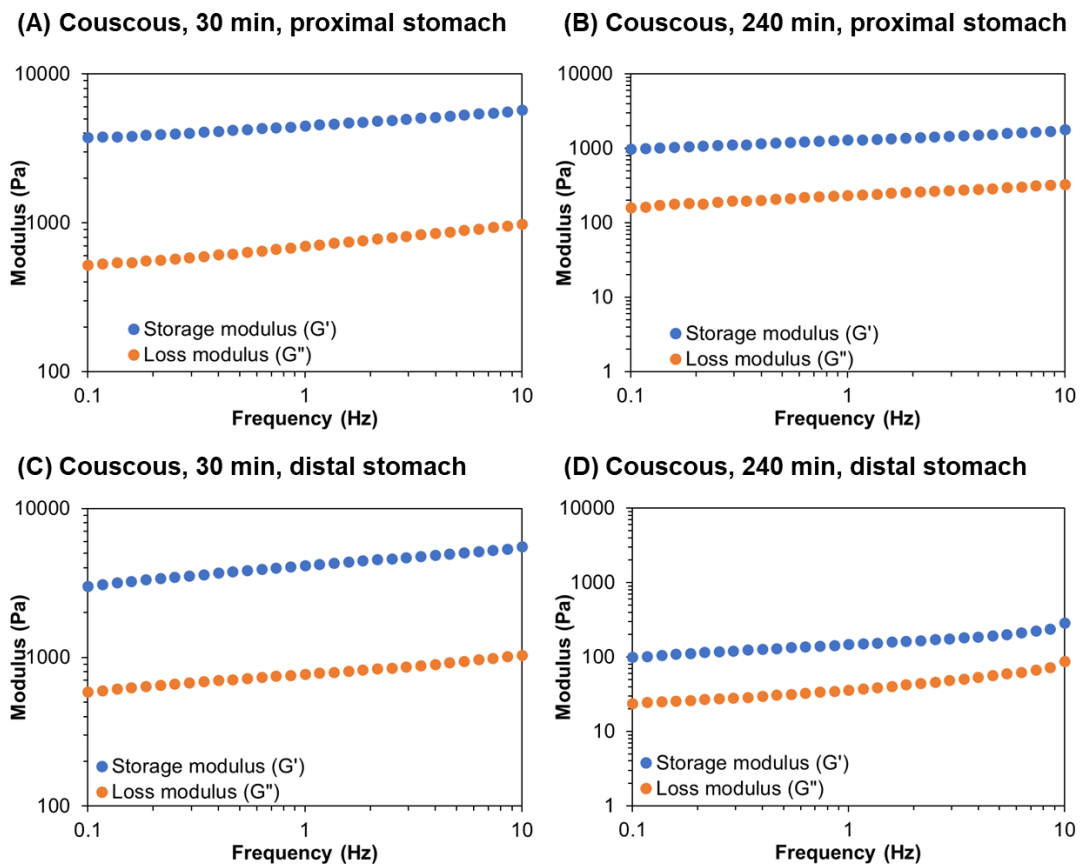


Figure 4.6 Example of viscoelastic properties of couscous digesta from the proximal (A-B) and distal (C-D) regions of the stomach after 30 (A, C) and 240 (B, D) min gastric digestion.

G' and G'' were lower in the distal stomach compared with the proximal stomach during digestion ($p < 0.0001$), with the largest regional difference presenting in couscous after 60 min, where the average G'' value in the proximal stomach, 647 ± 159 Pa, was more than double that of the distal stomach at 283 ± 43 Pa ($p < 0.0001$). Within individual diets and across all digestion times, significant differences between stomach

regions were observed in couscous and rice grain for both G' and G'' , and in pasta for G'' ($p < 0.05$).

4.4.6 Textural changes

The hardness of gastric digesta (Table C.3) was significantly influenced by diet, digestion time, and the interactions of diet \times time, diet \times stomach region ($p < 0.001$), and diet \times time \times stomach region ($p < 0.01$; Table 4.2). At each digestion time, in either stomach region, the hardness of rice grain was the highest, followed by pasta, rice noodle, couscous, rice couscous, and semolina. To enable the comparison of the softening behavior between diets, each hardness value of the gastric digesta from each stomach region and digestion time point was normalized against the initial hardness of its respective diet (Drechsler & Bornhorst, 2018). Softening half-time (i.e., the time needed to reduce the hardness by 50%, $H_t/H_0 = 0.5$), was calculated using the obtained Weibull parameters for each diet in each stomach region (Table 4.7). Although some diets had $R^2 < 0.80$ due to variability of the data across pigs (Figure C.1), Eqn. 4.6 fit well to the data when averaged over each diet \times time combination (Figure 4.7), with $R^2 > 0.95$ for all diets (Table 4.8). The softening half-time ($t_{1/2, \text{softening}}$) from the Weibull model parameters ranged from 0.3 min (rice couscous in proximal stomach) to 151.9 min (pasta in proximal stomach). Comparing the slowest $t_{1/2, \text{softening}}$ between stomach regions for each diet as the limiting rate, the order of softening rate of the diets was (from fastest to slowest): rice couscous $>$ semolina $>$ couscous $>$ rice noodle $>$ rice grain $>$ pasta.

Table 4.6 Rheological property data from shear rate sweep tests and oscillatory testing. Shear rate sweep data including Herschel-Bulkley model (Eqn. 4.7) fit parameters (average $R^2 = 0.90$ across all samples). Shear stress measured at a shear rate of 0.2 s^{-1} was included to represent a physiologically relevant shear rate in the gastric environment. Oscillatory data were measured at 1 Hz. All values represent mean \pm SE ($3 \leq n \leq 6$). Significantly different values within the same row are represented by different letters (abcd; $p < 0.05$); significantly different values of each physical property within the same column are represented with different letters (zyx; $p < 0.05$).

	Semolina		Couscous		Pasta		Rice grain		Rice couscous		Rice noodle	
Time (min)	Proximal	Distal	Proximal	Distal	Proximal	Distal	Proximal	Distal	Proximal	Distal	Proximal	Distal
Shear stress at 0.2 s^{-1} (Pa)												
30	18.28 \pm 5.78 ^c	17.95 \pm 3.83 ^c	255.20 \pm 33.20 ^{a,z}	84.40 \pm 14.96 ^{bc}	222.6 \pm 61.30 ^{ab}	244.0 \pm 15.99 ^{ab}	309.0 \pm 71.36 ^{a,z}	182.6 \pm 32.87 ^{abc}	10.76 \pm 1.23 ^c	16.72 \pm 3.36 ^c	266.55 \pm 56.77 ^{ab,z}	238.78 \pm 50.00 ^{ab}
60	13.21 \pm 2.77 ^c	8.29 \pm 1.03 ^c	137.16 \pm 43.17 ^{abc,zy}	34.47 \pm 6.34 ^c	150.40 \pm 12.03 ^{abc}	224.8 \pm 28.53 ^{ab}	315.6 \pm 67.1 ^{a,z}	155.06 \pm 19.18 ^{abc}	43.44 \pm 13.76 ^{bc}	22.80 \pm 4.18 ^c	157.98 \pm 27.4 ^{abc,zy}	143.80 \pm 31.33 ^{abc}
120	3.60 \pm 1.61 ^c	3.22 \pm 1.35 ^c	150.53 \pm 33.02 ^{abc,zy}	42.82 \pm 13.58 ^{bc}	197.77 \pm 57.62 ^{ab}	115.27 \pm 8.39 ^{abc}	266.33 \pm 69.43 ^{a,zy}	174.17 \pm 18.36 ^{abc}	81.76 \pm 39.21 ^{abc}	78.85 \pm 30.98 ^{bc}	93.20 \pm 5.72 ^{abc,zy}	89.40 \pm 8.19 ^{bc}
240	3.33 \pm 1.79 ^b	2.10 \pm 1.33 ^b	16.13 \pm 4.48 ^{ab,y}	13.67 \pm 5.06 ^{ab}	186.96 \pm 53.13 ^a	199.48 \pm 54.28 ^a	89.54 \pm 15.1 ^{ab,y}	100.2 \pm 25.07 ^{ab}	81.37 \pm 39.48 ^{ab}	76.53 \pm 26.54 ^{ab}	71.40 \pm 22.09 ^{ab,y}	75.08 \pm 8.16 ^{ab}
Yield Stress (Pa)												
30	6.96 \pm 1.14 ^{cd}	5.27 \pm 2.01 ^{cd}	*9.23 \pm 9.23 ^{cd}	*4.88 \pm 4.88 ^d	87.03 \pm 28.75 ^{ab}	105.77 \pm 21.4 ^{a,z}	47.33 \pm 29.25 ^{abcd}	60.34 \pm 17.71 ^{abc,zy}	3.89 \pm 0.62 ^d	4.19 \pm 0.50 ^d	24.73 \pm 12.64 ^{cd}	29.55 \pm 11.63 ^{bcd}
60	2.82 \pm 0.77 ^{bc}	1.26 \pm 0.58 ^c	*9.58 \pm 9.58 ^{bc}	*3.04 \pm 2.44 ^c	65.60 \pm 10.22 ^{ab}	89.99 \pm 6.08 ^{a,zy}	37.01 \pm 22.87 ^{abc}	78.24 \pm 14.36 ^{a,z}	5.45 \pm 3.66 ^{bc}	3.88 \pm 2.22 ^c	27.85 \pm 7.58 ^{abc}	48.44 \pm 6.95 ^{abc}
120	1.40 \pm 1.08 ^b	1.49 \pm 0.9 ^b	*3.10 \pm 3.10 ^b	*2.29 \pm 2.29 ^b	51.03 \pm 15.41 ^{ab}	62.92 \pm 4.33 ^{a,zy}	0.36 \pm 0.36 ^b	8.94 \pm 8.94 ^{ab,yx}	1.08 \pm 1.08 ^b	21.03 \pm 12.92 ^{ab}	22.80 \pm 2.05 ^{ab}	28.70 \pm 5.21 ^{ab}
240	0.21 \pm 0.19 ^b	0.20 \pm 0.17 ^b	*0.24 \pm 0.24 ^{ab}	*0.24 \pm 0.24 ^{ab}	61.79 \pm 22.47 ^a	20.37 \pm 11.96 ^{ab,y}	31.73 \pm 10.86 ^{ab}	2.43 \pm 2.43 ^{ab,x}	3.88 \pm 3.88 ^{ab}	2.47 \pm 1.68 ^{ab}	18.58 \pm 14.09 ^{ab}	10.38 \pm 3.91 ^{ab}
K (Pa·sⁿ)												
30	35.71 \pm 12.32 ^c	30.52 \pm 7.89 ^c	330.83 \pm 44.69 ^{a,z}	108.52 \pm 22.46 ^{bc}	306.92 \pm 64.31 ^{ab}	258.09 \pm 21.86 ^{abc}	312.98 \pm 64.9 ^{ab,zy}	262.94 \pm 67.17 ^{abc}	22.92 \pm 3.38 ^c	28.82 \pm 3.65 ^c	412.36 \pm 95.47 ^{a,z}	371.01 \pm 80.28 ^{a,z}
60	19.67 \pm 3.38 ^{bc}	11.87 \pm 1.10 ^c	171.58 \pm 53.71 ^{abc,zy}	41.54 \pm 7.34 ^{bc}	238.73 \pm 7.42 ^{abc}	265.86 \pm 36.96 ^{ab}	379.99 \pm 94.94 ^{a,z}	148.6 \pm 15.75 ^{bc}	61.08 \pm 14.55 ^{bc}	34.95 \pm 5.15 ^{bc}	231.27 \pm 46.97 ^{abc,zy}	203.11 \pm 53.41 ^{abc,zy}
120	5.82 \pm 2.48 ^b	5.55 \pm 2.36 ^b	174.7 \pm 40.03 ^{ab,zy}	51.62 \pm 15.32 ^b	224.50 \pm 50.95 ^{ab}	115.9 \pm 10.16 ^{ab}	313.27 \pm 72.65 ^{a,zy}	211.18 \pm 21.39 ^{ab}	88.27 \pm 34.52 ^{ab}	93.03 \pm 37.34 ^{ab}	150.34 \pm 16.79 ^{ab,y}	119.77 \pm 7.42 ^{ab,y}
240	4.50 \pm 2.45	2.95 \pm 1.99	19.66 \pm 4.78 ^y	16.96 \pm 5.79	208.35 \pm 67.39	212.79 \pm 59.53	97.47 \pm 13.87 ^y	129.51 \pm 33.69	102.43 \pm 53.01	101.82 \pm 36.32	87.80 \pm 24.20 ^y	108.01 \pm 9.23 ^y
n (dimensionless)												
30	0.81 \pm 0.09 ^{a,z}	0.53 \pm 0.11 ^{abc}	0.30 \pm 0.1 ^{bc}	0.16 \pm 0.01 ^c	0.55 \pm 0.06 ^{abc}	0.40 \pm 0.06 ^{abc}	0.32 \pm 0.06 ^{bc}	0.26 \pm 0.04 ^c	0.73 \pm 0.04 ^{ab,z}	0.56 \pm 0.10 ^{abc}	0.38 \pm 0.05 ^{abc}	0.40 \pm 0.05 ^{abc}
60	0.47 \pm 0.14 ^{ab,zy}	0.36 \pm 0.08 ^{ab}	0.19 \pm 0.07 ^b	0.16 \pm 0.05 ^b	0.68 \pm 0.02 ^a	0.47 \pm 0.07 ^{ab}	0.25 \pm 0.06 ^{ab}	0.39 \pm 0.03 ^{ab}	0.44 \pm 0.13 ^{ab,zy}	0.44 \pm 0.12 ^{ab}	0.42 \pm 0.02 ^{ab}	0.50 \pm 0.04 ^{ab}

(continued)

Table 4.6 (continued)

	Semolina		Couscous		Pasta		Rice grain		Rice couscous		Rice noodle	
Time (min)	Proximal	Distal	Proximal	Distal	Proximal	Distal	Proximal	Distal	Proximal	Distal	Proximal	Distal
120	0.35 ± 0.13 ^{ab,zy}	0.65 ± 0.09 ^a	0.11 ± 0.03 ^b	0.23 ± 0.13 ^{ab}	0.47 ± 0.10 ^{ab}	0.52 ± 0.03 ^{ab}	0.16 ± 0.03 ^b	0.14 ± 0.02 ^b	0.27 ± 0.06 ^{ab,zy}	0.32 ± 0.10 ^{ab}	0.52 ± 0.02 ^{ab}	0.44 ± 0.03 ^{ab}
240	[†] 0.30 ± 0.14 ^y	0.58 ± 0.17	0.13 ± 0.03	0.09 ± 0.01	0.50 ± 0.17	0.51 ± 0.13	0.31 ± 0.05	0.20 ± 0.04	0.25 ± 0.06 ^y	0.25 ± 0.04	0.35 ± 0.04	0.37 ± 0.09
G' 1 Hz (Pa)												
30	651 ± 115 ^f	510 ± 109 ^f	5374 ± 869 ^{def}	2895 ± 411 ^c	12275 ± 1319 ^{bc,z}	10665 ± 1275 ^{bcd,z}	20173 ± 2373 ^{a,z}	12948 ± 2456 ^{bc,z}	1116 ± 184 ^f	1100 ± 137 ^f	14549 ± 1734 ^{ab,z}	8352 ± 1981 ^{cde}
60	399 ± 53 ^f	227 ± 36 ^f	3819 ± 1044 ^{def}	1496 ± 38 ^f	10911 ± 399 ^{abc,z}	9753 ± 535 ^{abc,zy}	15295 ± 2517 ^{a,zy}	12351 ± 1154 ^{ab,z}	1476 ± 461 ^{ef}	1753 ± 489 ^{def}	7257 ± 832 ^{bcd,y}	6826 ± 1132 ^{cde}
120	166 ± 94 ^e	133 ± 69 ^e	3927 ± 1004 ^{cde}	1672 ± 37 ^{de}	7500 ± 1210 ^{abc,zy}	6403 ± 262 ^{abcd,zy}	10279 ± 1154 ^{a,yx}	9912 ± 1012 ^{ab,zy}	4314 ± 1668 ^{bcd,e}	2631 ± 997 ^{cde}	4892 ± 739 ^{bcd,e,y}	4573 ± 416 ^{bcd,e}
240	74 ± 29 ^b	63 ± 54 ^b	670 ± 222 ^{ab}	610 ± 53 ^{ab}	4283 ± 780 ^{ab,y}	4585 ± 622 ^{ab,y}	5974 ± 968 ^{a,x}	5152 ± 933 ^{ab,y}	2532 ± 1176 ^{ab}	1633 ± 435 ^{ab}	2313 ± 452 ^{ab,y}	3249 ± 258 ^{ab}
G'' 1 Hz (Pa)												
30	109 ± 16 ^g	86 ± 17 ^g	871 ± 97 ^{cde,z}	540 ± 77 ^{defg}	1418 ± 148 ^{bc,z}	1106 ± 119 ^{bcd,z}	2541 ± 300 ^{a,z}	1540 ± 231 ^{b,z}	187 ± 32 ^{fig,z}	187 ± 25 ^{fig,z}	759 ± 149 ^{def,z}	505 ± 92 ^{efg,z}
60	72 ± 9 ^f	42 ± 6 ^f	647 ± 159 ^{cde,zy}	283 ± 43 ^f	1196 ± 63 ^{bc,zy}	972 ± 63 ^{bcd,zy}	2475 ± 236 ^{a,z}	1520 ± 133 ^{b,z}	181 ± 59 ^{ef,z}	217 ± 60 ^{ef,z}	530 ± 60 ^{def,zy}	460 ± 59 ^{def,z}
120	30 ± 16 ^e	24 ± 11 ^e	619 ± 142 ^{cde,zy}	291 ± 48 ^{de}	848 ± 122 ^{bc,yx}	618 ± 30 ^{cd,zy}	1472 ± 136 ^{a,y}	1155 ± 86 ^{ab,zy}	398 ± 147 ^{cde,z}	237 ± 76 ^{de,z}	392 ± 45 ^{cde,zy}	327 ± 22 ^{cde,z}
240	12 ± 4 ^c	10 ± 7	127 ± 39 ^{bc,y}	117 ± 43 ^{bc}	509 ± 93 ^{abc,x}	497 ± 75 ^{abc,y}	876 ± 144 ^{a,x}	672 ± 104 ^{ab,y}	185 ± 76 ^{bc,z}	132 ± 34 ^{bc,z}	205 ± 33 ^{bc,y}	235 ± 18 ^{bc,z}
tan(δ) 1 Hz (dimensionless)												
30	0.171 ± 0.005 ^a	0.171 ± 0.004 ^{a,y}	0.167 ± 0.010 ^{abc}	0.186 ± 0.004 ^a	0.116 ± 0.006 ^d	0.104 ± 0.004 ^{de}	0.123 ± 0.005 ^{bcd}	0.123 ± 0.005 ^c	0.166 ± 0.002 ^{ab,z}	0.169 ± 0.004 ^{a,z}	0.070 ± 0.007 ^c	0.068 ± 0.008 ^c
60	0.182 ± 0.004 ^a	0.186 ± 0.003 ^{a,zy}	0.177 ± 0.009 ^a	0.191 ± 0.005 ^a	0.110 ± 0.004 ^b	0.104 ± 0.004 ^{bc}	0.132 ± 0.009 ^b	0.124 ± 0.007 ^b	0.124 ± 0.011 ^{b,zy}	0.129 ± 0.015 ^{b,zy}	0.073 ± 0.001 ^c	0.069 ± 0.003 ^c
120	0.195 ± 0.013 ^{ab}	0.216 ± 0.021 ^{a,z}	0.163 ± 0.009 ^{bc}	0.179 ± 0.013 ^{abc}	0.115 ± 0.004 ^{de}	0.096 ± 0.001 ^{ef}	0.141 ± 0.006 ^{cd}	0.118 ± 0.004 ^{de}	0.100 ± 0.007 ^{def,y}	0.100 ± 0.008 ^{def,yx}	0.083 ± 0.005 ^{ef}	0.073 ± 0.003 ^f
240	0.181 ± 0.009 ^{bc}	0.235 ± 0.029 ^{a,z}	0.200 ± 0.008 ^{ab}	0.204 ± 0.012 ^{ab}	0.119 ± 0.004 ^{def}	0.108 ± 0.005 ^{defg}	0.146 ± 0.002 ^{cd}	0.134 ± 0.006 ^{cde}	0.086 ± 0.008 ^{fg,y}	0.082 ± 0.008 ^{fg,x}	0.092 ± 0.004 ^{efg}	0.07 ± 0.004 ^g

* For all couscous time points, only one greater-than-zero value of yield stress was obtained, causing the SE values to be the same as the mean values.

(A) Gastric digesta softening kinetics, proximal region

(B) Gastric digesta softening kinetics, distal region

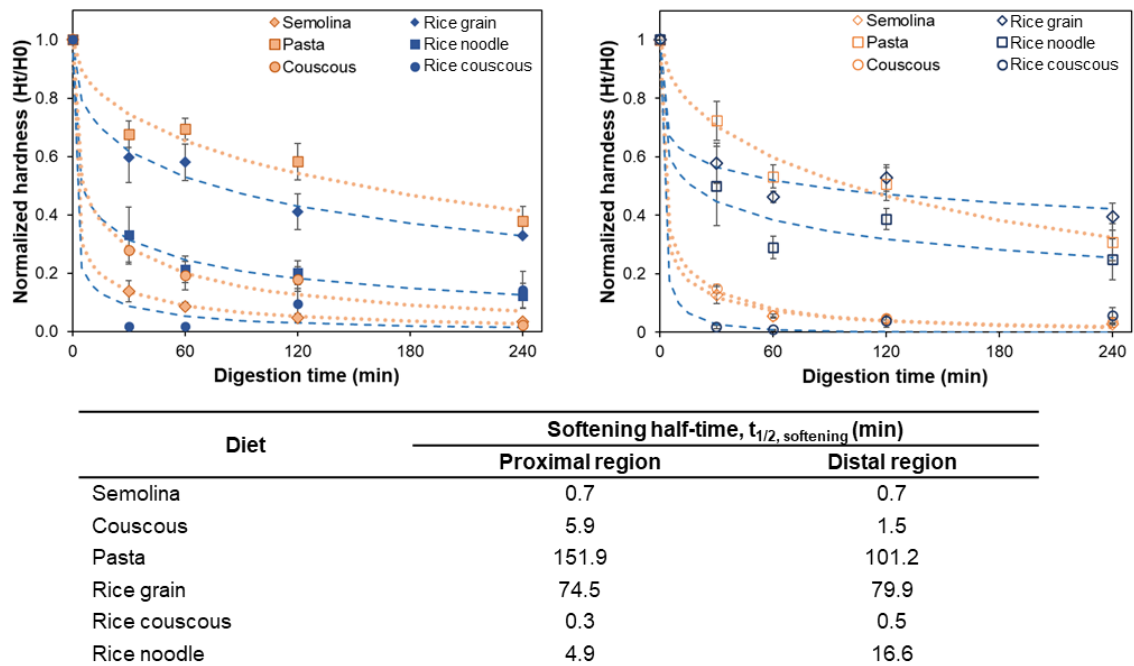


Figure 4.7 Normalized hardness values of gastric digesta from (A) proximal and (B) distal stomach regions during 240 min digestion (mean \pm SE, $4 \leq n \leq 6$). The predicted softening curves from Weibull model parameters are represented as dashed-lines (rice-based diets) or dotted-lines (wheat-based diets). Rice- and wheat-based diets are represented as dark blue- and orange-colored data points and lines, respectively. The softening half-times of the diets in the proximal and distal stomach regions shown in the table below the figures were predicted from the softening curves.

Table 4.7 Weibull kinetic parameters (estimated with Eqn. 4.6) used to calculate the softening half-time of the study diets in the proximal and distal stomach regions presented in Figure 4.7. Each parameter is presented as predicted parameter \pm 95% confidence interval. The goodness-of-fit of the model is indicated by the R^2 .

Diet	Stomach region	Weibull model parameter		R^2
		$k_h (\times 10^2 \text{ min}^{-1})$	β_h (dimensionless)	
Semolina	Proximal	37.50 ± 97.10	0.28 ± 0.28	0.96
	Distal	41.64 ± 110.65	0.30 ± 0.30	0.97
Couscous	Proximal	6.18 ± 6.01	0.36 ± 0.25	0.82
	Distal	22.98 ± 28.76	0.35 ± 0.20	0.98
Pasta	Proximal	0.33 ± 0.19	0.53 ± 0.26	0.66
	Distal	0.51 ± 0.22	0.56 ± 0.25	0.67
Rice grain	Proximal	0.55 ± 0.35	0.41 ± 0.26	0.53
	Distal	0.20 ± 0.38	0.20 ± 0.21	0.51
Rice couscous	Proximal	98.82 ± 2331.58	0.26 ± 1.95	0.67
	Distal	75.70 ± 5698.60	0.41 ± 12.15	0.93
Rice noodle	Proximal	5.55 ± 7.62	0.28 ± 0.25	0.67
	Distal	1.42 ± 1.30	0.25 ± 0.29	0.43

Table 4.8 Goodness-of-fit of Weibull and gastric emptying models for the averaged values of the experimental data (normalized hardness data for Weibull model, gastric digesta mass retention for gastric emptying models).

Diet	R ² Weibull model		R ² DM emptying model	R ² whole stomach content emptying model
	Proximal region	Distal region		
Semolina	1.00	1.00	0.97	0.96
Couscous	0.99	1.00	0.98	0.91
Pasta	0.99	1.00	0.97	0.94
Rice grain	0.99	0.97	0.99	0.76
Rice couscous	0.96	0.96	0.99	0.93
Rice noodle	1.00	0.96	0.97	1.00

4.4.7 Gastric emptying

Gastric emptying of both DM and whole stomach content was significantly influenced by diet type and digestion time ($p < 0.0001$). Whole stomach content emptying was significantly affected by the diet \times time interaction ($p < 0.05$; Table 4.2). The predicted gastric emptying curves (using Eqn. 4.3 and 4.4) fit well to the averaged data points (Figure 4.8A to D), although the predicted curves had $0.75 \leq R^2 \leq 0.89$ when compared to all data due to the spread of the individual data points (Figure C.2). With the good fit of the model to the averaged data points ($0.97 \leq R^2 \leq 0.99$, Table 4.8), the predicted curves can provide information about gastric emptying parameters and the emptying half-times (Table 4.5) to enable comparisons with previous studies.

The DM retention of the diets (Figure 4.8A and C) decreased significantly from 30 to 240 min ($p < 0.05$), except for pasta. No lag phase ($\beta_{DM} < 1$) was observed in the DM emptying profile for all diets except rice grain and rice noodle ($\beta_{DM} > 1$). Pasta had the lowest DM emptying rate parameter ($k_{DM} = 0.81 \times 10^{-3} \text{ min}^{-1}$) – almost one order of magnitude lower than the other five diets, while couscous had the highest k_{DM} ($4.16 \times 10^{-3} \text{ min}^{-1}$). Of the six diets, the DM emptying half-time ($t_{1/2,DM \text{ GE}}$) was the longest in pasta (360 min), followed by rice grain (223 min), rice noodle (213 min), couscous (160 min) and rice couscous (150 min), and semolina (88 min).

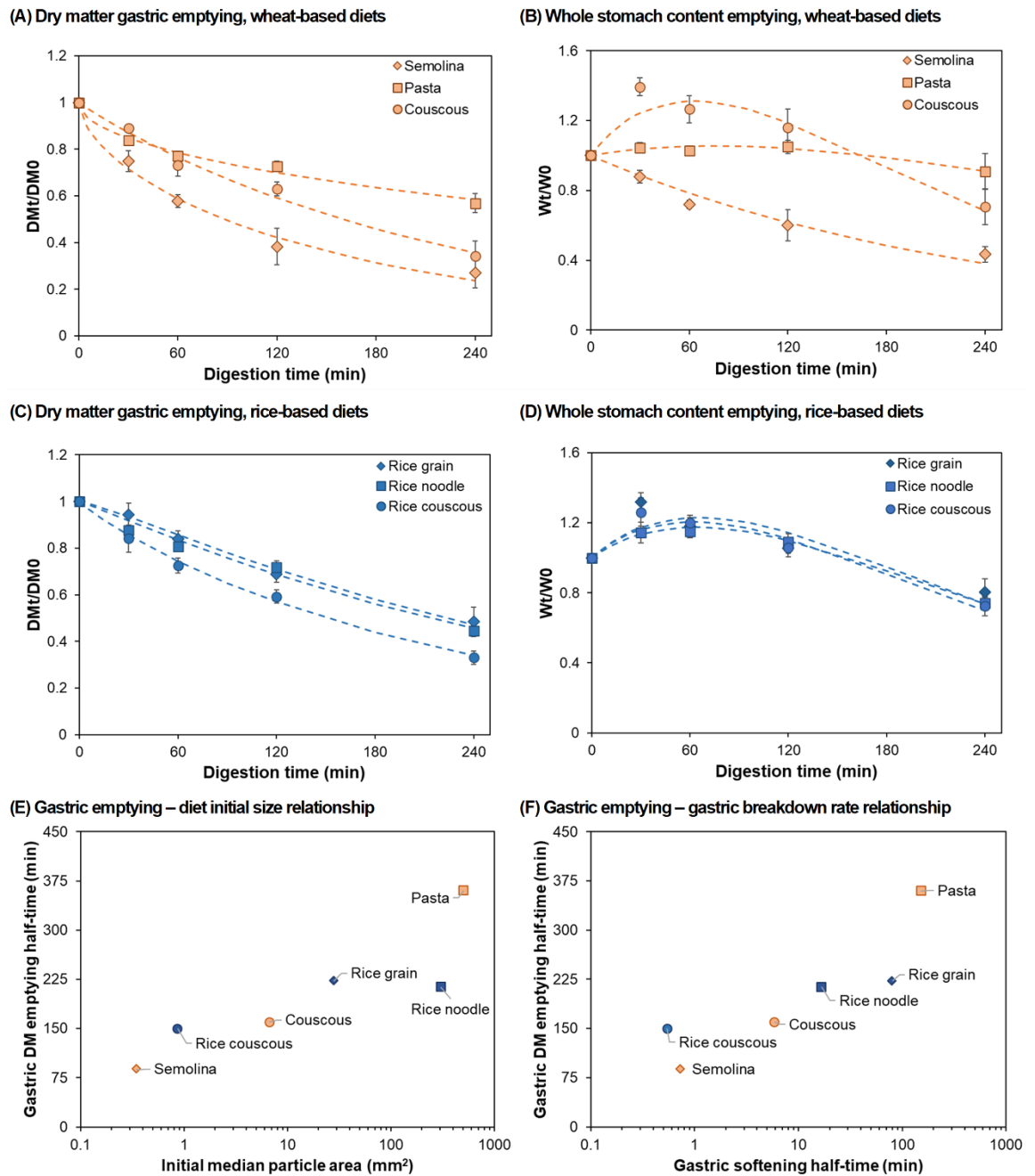


Figure 4.8 Gastric emptying of dry matter (A,C) and whole stomach content (B,D) of pigs fed with wheat-based diets (A,B) or rice-based diets (C,D) during 240 min of digestion. Points represent measured values (mean \pm SE $n \geq 5$ for each diet \times time, except rice grain \times 60 min ($n = 4$)). Dashed lines represent the predicted dry matter gastric emptying profile based on modified exponential model (Eqn. 4.3)) or predicted total meal gastric emptying profile based on linear-exponential model (Eqn. 4.4). Dry matter half-emptying times from (A) and (C) were plotted against initial median particle area (E) of the cooked diets or gastric softening half-time (F). Gastric softening half-time for each diet was represented by the longest softening half-time between the proximal and distal stomach regions for each diet. Note that the x-axis for (E) and (F) is shown on a log-scale due to the wide range of the values across the six diets.

Unlike the DM emptying profiles, the emptying profiles of whole stomach content (Figure 4.8B and D) were preceded by a lag phase (reflected by $k_{whole} > 1$, Table 4.9), except in pigs fed with semolina ($k_{whole} \approx 0$, Table 4.9). This lag phase represented the increasing whole stomach content retention in the first 60 min of digestion. As digestion progressed from 30 to 240 min, all diets except pasta underwent significant changes in whole stomach content retention ($p < 0.05$). The emptying half-time of whole stomach content ($t_{1/2, \text{whole GE}}$) was the highest in pasta (536 min), followed by rice noodle (329 min), rice grain (319 min), rice couscous (302 min), couscous (288 min), and semolina (173 min). Although the order of $t_{1/2, \text{DM GE}}$ was slightly different from $t_{1/2, \text{whole GE}}$, the $t_{1/2, \text{DM GE}}$ and $t_{1/2, \text{whole GE}}$ were linearly correlated ($R^2 = 0.95$, Figure C.3).

Table 4.9 Gastric emptying parameters (expressed as predicted parameter \pm 95% confidence interval) and predicted emptying half-time of dry matter and whole stomach content.

Dry matter gastric emptying (predicted with modified-exponential model, Eqn. 4.3)				
Diet	Gastric emptying parameter		R²	Emptying half-time, $t_{1/2, \text{DM GE}}$ (min)
	$k_{DM} \times 10^3 \text{ (min}^{-1}\text{)}$	$\beta_{DM} \text{ (dimensionless)}$		
Semolina	4.14 \pm 3.12	0.59 \pm 0.32	0.75	88
Couscous	4.16 \pm 2.18	0.96 \pm 0.42	0.82	160
Pasta	0.81 \pm 0.73	0.50 \pm 0.18	0.79	360
Rice grain	3.72 \pm 2.20	1.21 \pm 0.62	0.80	223
Rice couscous	4.13 \pm 1.75	0.90 \pm 0.32	0.87	150
Rice noodle	3.51 \pm 1.34	1.09 \pm 0.35	0.89	213
Whole stomach content gastric emptying (predicted with linear-exponential model, Eqn. 4.4)				
Diet	Gastric emptying parameter		R²	Emptying half-time, $t_{1/2, \text{whole GE}}$ (min)
	$k_{whole} \text{ (dimensionless)}$	$\beta_{whole} (\times 10^3 \text{ min}^{-1})$		
Semolina	0.009 \pm 204.09	4.04 \pm 832.98	0.65	173
Couscous	2.38 \pm 0.39	9.38 \pm 2.04	0.61	288
Pasta	1.40 \pm 0.35	3.81 \pm 2.10	0.18	536
Rice grain	2.06 \pm 0.33	7.88 \pm 1.72	0.54	319
Rice couscous	2.01 \pm 0.29	8.21 \pm 1.49	0.70	302
Rice noodle	1.84 \pm 0.21	7.21 \pm 1.08	0.78	329

4.4.8 Relationships between measured variables

Measured physical properties of the digesta were interrelated, and their relationships with dry matter gastric emptying (represented by %DM remaining) were assessed using Spearman's correlation coefficient (r_s) (Table 4.10). Hardness had a high positive correlation ($0.7 < r_s \leq 0.9$, $p < 0.0001$) with rheological parameters K , G' , and G'' . Moisture content was negatively correlated with almost all physical properties shown in Table 4.10, except SR, particles per gram dry matter, and x_{10} . Hardness and rheological parameters were negatively correlated with x_{10} and particles per gram dry matter, but positively correlated with x_{50} and x_{90} . In contrast to the digesta physical properties, digesta pH was only significantly correlated to moisture content, rheological parameters (K , G' , G''), and SR at weaker level of correlation ($r_s = \pm(0.138 - 0.464)$, $p < 0.05$). Of the comparisons tested, all physical properties were significantly correlated ($p < 0.05$) to %DM. Hardness, G' , and K were positively correlated with %DM, but at lower correlation levels ($0.3 < r_s < 0.5$, $p < 0.0001$). A moderate negative correlation was present between %DM with digesta moisture content and SR ($0.6 < r_s < 0.7$, $p < 0.0001$).

Table 4.10 Spearman's correlation coefficients (r_s) between different physical properties measured in this study. Moderate to very high correlations ($r_s = \pm (0.5 \text{ to } 1.0)$) are shown in bold font. Values presented as r_s followed by the level of statistical significance (see note below the table).

	Hardness	pH	MC,db	Yield stress	K	G' 1 Hz	G'' 1 Hz	Particles/g DM	X10	X50	X90	SR
pH	NS											
MC,db	-0.62****	-0.46****										
Yield stress	0.39****	NS	-0.40****									
K	0.79****	0.18**	-0.65****	0.36****								
G' 1 Hz	0.89****	0.14*	-0.74****	0.48****	0.91****							
G'' 1 Hz	0.90****	0.21***	-0.72****	0.41****	0.86****	0.96****						
Particles/g DM	-0.32****	NS	0.47****	-0.29****	-0.38****	-0.42****	-0.31****					
X10	-0.25****	NS	0.14*	-0.13*	-0.20**	-0.25****	-0.30****	-0.45****				
X50	0.52****	NS	-0.48****	0.39****	0.54****	0.58****	0.48****	-0.84****	0.32****			
X90	0.61****	NS	-0.55****	0.43****	0.63****	0.68****	0.57****	-0.77****	NS	0.97****		
SR	-0.38****	-0.42****	0.86****	-0.34****	-0.52****	-0.52****	-0.45****	0.55****	NS	-0.52****	-0.55****	
%DM	0.37****	0.69****	-0.69****	0.29****	0.49****	0.49****	0.51****	-0.19**	-0.12*	0.19**	0.24***	-0.63****

MC,db: moisture content (dry basis); K: consistency index; G' 1 Hz: storage modulus measured at 1 Hz; G'' 1 Hz: loss modulus measured at 1 Hz; Particles/g DM: particles per gram dry matter; SR: saturation ratio; %DM: percentage of dry matter left in the stomach.

Asterisk (*) symbols indicate significant correlation at different levels of statistical significance. *: $p < 0.05$; **: $p < 0.01$, *** : $p < 0.001$, ****: $p < 0.0001$. NS: no significant correlation.

4.5 Discussion

4.5.1 Different food structures exhibited different gastric emptying profiles

In the present study, six diets were used to represent common starch-based foods of different macrostructures (as observed by physical properties) and starch sources (as observed by chemical properties and composition). Based on the physical properties of the cooked diets, particularly their x_{50} , particles per gram dry matter, and moisture content, the six study diets can be classified into four different structures from the smallest to the largest size: porridge (semolina), agglomerate (couscous and rice couscous; average $x_{50} = 3.56 \pm 1.92 \text{ mm}^2$), grain (rice grain), and noodle (pasta and rice noodle; average $x_{50} = 404.10 \pm 161.99 \text{ mm}^2$). Major differences between the starch source of the diets were highlighted by higher protein content, buffering capacity, and TDF in wheat-based diets compared to rice-based diets.

The trends observed in buffering capacity of the diets in this study can be attributed to the protein content and particle size of the diets, where higher protein content or smaller particle area leads to higher buffering capacity, in agreement with previous studies (Mennah-Govela et al., 2020; Mennah-Govela et al., 2019). As a result, the buffering capacity of the wheat-based diets increased with decreasing x_{50} and increasing number of particles per gram dry matter. Similarly, in the rice-based diets, although their protein content was not significantly different between each other, diets with smaller particle size (e.g., rice couscous) had higher buffering capacity compared to those diets with larger particle size (e.g., rice noodle). Protein content and particle size have been reported to significantly affect food buffering capacity (Mennah-Govela et al., 2020; Mennah-Govela et al., 2019). Since the different physicochemical properties and structures of the diets in the current study were highlighted by different protein content and particle size, buffering capacity was selected as a parameter to capture the

overall structural differences in the study diets. The buffering capacity of the diets was hypothesized to cause distinctions in gastric emptying profiles due to variations in breakdown behavior in the gastric environment (Figure 4.9), as suggested by the correlation between buffering capacity and gastric secretion rate during digestion (Fordtran & Walsh, 1973). This hypothesis also aligns with a recent review paper highlighting the importance of buffering capacity in the context of digestion (Mennah-Govela & Bornhorst, 2021).

Both the gastric emptying of whole stomach content and dry matter (DM) were quantified in the current study. Measurement of gastric emptying of solid meals in humans is commonly conducted using a test meal consisting of wet solid and liquid components, which together with gastric secretions added during digestion, constitute the whole stomach content (Donohoe et al., 2009; Goetze et al., 2009). For comparison with previous human studies, the emptying of whole stomach content was compared, as emptying of meal dry matter cannot be easily quantified in a human study. The range of $t_{1/2, \text{whole GE}}$ (Table 4.9) of the diets in the current study ranged from 173 min (semolina) to 536 min (pasta). The $t_{1/2, \text{whole GE}}$ of the diets obtained in this study, except for pasta, are within the range of the values reported from studies with human subjects for similar food types (30 to 324 min) (Cisse et al., 2018; Mourot et al., 1988; Pletsch, 2018). Although the specific values varied between studies, the trend in gastric emptying was the same as these human studies, with semolina (porridge structure) having the most rapid gastric emptying, followed by rice grain, and pasta having the slowest gastric emptying. The similar order of magnitude obtained in the present study suggests similar gastric physiological response between pigs and humans. However, it is difficult to compare specific values obtained in the present study with the previous human studies because of the difference in the mastication behavior between human and pigs, larger

portion sizes fed to the pigs, different cooking methods, and different methods used to quantify gastric emptying.

The $t_{1/2,DM\ GE}$ of the diets ranged from 88 min (semolina) to 360 min (pasta). For all diets, $t_{1/2,whole\ GE}$ were longer than $t_{1/2,DM\ GE}$, which might be attributed to different amounts of gastric secretions added to the diet, as well as different amounts and solid:liquid ratios of the gastric content emptied at each time. As a liquid-phase indigestible marker was not used in the diets, the gastric emptying of whole stomach content cannot be compared with the dry matter gastric emptying to draw conclusions on the differences between solid and liquid emptying in the study diets. Future studies using an indigestible marker in the liquid phase of the diets are needed to further elucidate on both the solid and liquid gastric emptying of the test meals. Assessment of DM gastric emptying is commonly done in animal studies to minimize the interference of liquid addition due to gastric secretory response and to understand the retention of the solid phase of the meal (Bornhorst, Chang, et al., 2013; Johansen, Knudsen, Sandström, & Skjøth, 1996; Wu et al., 2016). To the author's knowledge, the present study is the first to investigate gastric emptying of diets with porridge, noodle, and agglomerated structures in growing pigs.

A previous study using growing pigs fed with brown and white rice reported $t_{1/2,DM\ GE}$ of 227 to 229 min (Bornhorst, Chang, et al., 2013), which was similar to the value obtained in the current study for rice grain ($t_{1/2,DM\ GE}$ of 223 min). Another study involving growing pigs used an interval feeding setup, where the reported gastric mean retention times of barley, maize, and high-amylose maize in isolated starch, ground cereal, and extruded cereal forms were between 129 to 225 min (Martens, Noorloos, et al., 2019). This range is comparable to the values obtained for couscous, rice couscous, rice grain, and rice noodle (150 to 223 min) in the current study. Compared with these

studies, the $t_{1/2,DM\ GE}$ values found in the present study were either lower (semolina) or higher (pasta). This might have been due to the small particle size and high moisture content in semolina, or the larger particle size and more compact structure in pasta, which highlights the potential role of food structure in determining gastric emptying rate of solid starch-based foods, similar to previous studies (Bornhorst, Chang, et al., 2013; Cisse et al., 2018; Mackie et al., 2017; Mourot et al., 1988; Pletsch & Hamaker, 2018).

Based on the differences in initial particle size (macrostructure) and protein content (composition) in the cooked diets, it was hypothesized in this study that the gastric emptying half-times would follow the trend of: wheat noodle > rice noodle > rice grain > wheat couscous > rice couscous > wheat porridge. This expected trend was observed in the wheat-based diets, where the $t_{1/2,DM\ GE}$ and $t_{1/2,whole\ GE}$ of pasta > couscous > semolina, aligning with the order of initial particle size (represented as x_{50}). In contrast, for rice-based diets, the $t_{1/2,whole\ GE}$ of rice-based diets was the longest rice noodle, followed by rice grain and rice couscous, but the $t_{1/2,DM\ GE}$ was the longest in rice grain, followed by rice noodle and rice couscous, although the initial particle size of rice noodle was larger than rice grain (Figure 4.8E). To identify the cause of this discrepancy, the relationship between $t_{1/2,DM\ GE}$ and factors that have been reported to influence gastric emptying process were investigated, including: volume/weight and caloric content of the meal (Maegdenbergh, Urbain, Siegel, Mortelmans, & Roo, 1990; Velchik, Reynolds, & Alavi, 1989), type and amount of the solid (Siegel et al., 1988), food buffering capacity (Simonian et al., 2005); consistency and composition of the meal (Wolever et al., 2019); and the presence of bioactive compounds (Montoya et al., 2014) or dietary fiber (Benini et al., 1995) in the meal.

Limited relationships were observed between $t_{1/2,DM\ GE}$ and portion size, caloric content of the meal, diet initial protein content, or total dietary fiber of the diet (Figure 4.10). Therefore, it was proposed that the difference in $t_{1/2,DM\ GE}$ of the diets in this study, particularly the rice-based diets, might have been linked to their breakdown rates, as a link between solid food disintegration kinetics and gastric emptying was previously reported in an *in vitro* study of food disintegration using a model stomach system (Kong & Singh, 2009b). It was hypothesized that the longer $t_{1/2,DM\ GE}$ in rice grain compared to rice noodle was a result of slower breakdown of rice grain compared to rice noodle. Rice grain also had lower initial moisture content, which might have influenced the breakdown. Diets with slower breakdown and gastric emptying rate, such as pasta and rice grain, are likely to have lower glycemic response due to a slower rate of material delivery to the small intestine for further hydrolysis and glucose absorption.

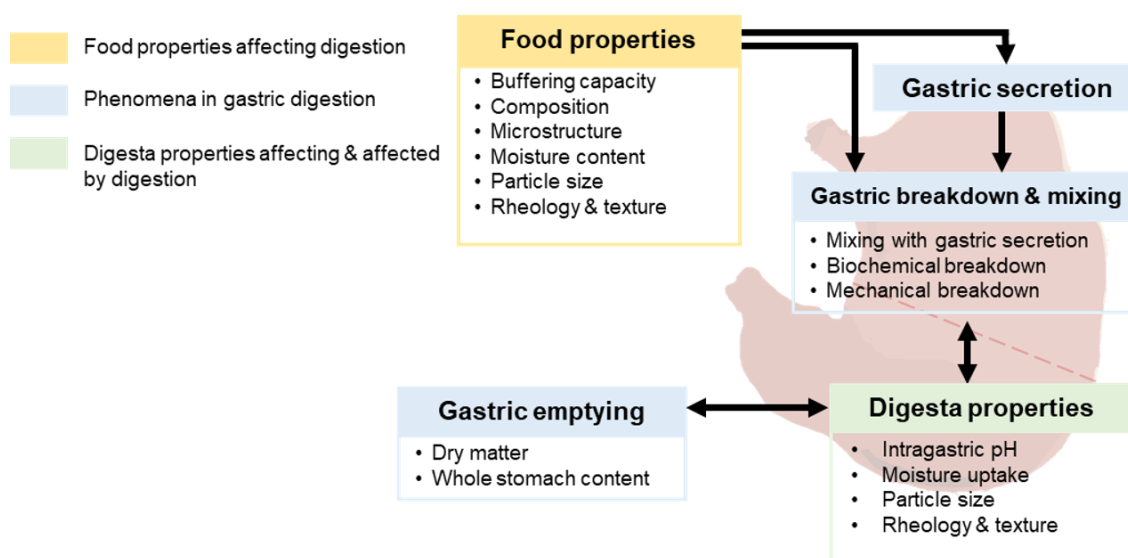


Figure 4.9 Schematic diagram showing the possible relationships between food properties, gastric digestion, and gastric emptying investigated in this study. The heads of the arrows indicate relationships between food and digesta properties and gastric phenomena. Note that the actual relationships are complex and more specific links may be present, but these complex mechanisms are not fully delineated in the illustration for the sake of simplicity.

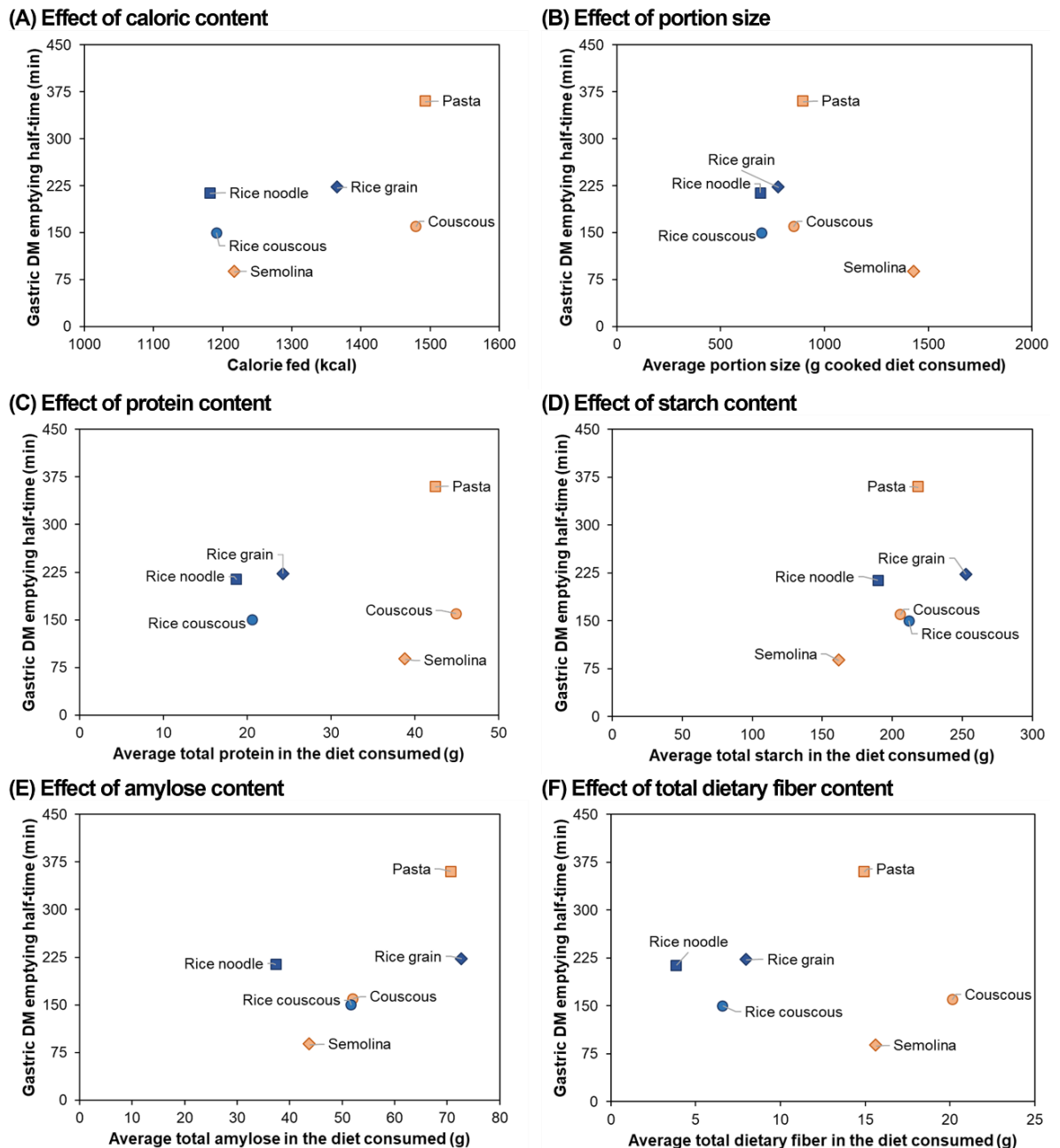


Figure 4.10 Relationships between dry matter emptying half- time with (A) total caloric content, (B) portion size, (C) total protein content, (D) total starch content, (E) total amylose content, and (F) total dietary fiber content of the diets.

4.5.2 Gastric secretory response was impacted by food buffering capacity

Gastric digestion of solid foods consists of several key phenomena: (1) mixing of gastric secretions with ingested food, (2) biochemical breakdown by either gastric acid and/or digestive enzymes, and (3) mechanical disintegration of food particles by gastric motility. These phenomena are known to impact digesta properties, while their

regulation is also impacted by digesta properties (Figure 4.9). Gastric secretions play an important role in the occurrence of these phenomena by facilitating biochemical breakdown and dissolution of food particles in the stomach (Feher, 2017c; Kong & Singh, 2008; Soybel, 2005), as suggested by the significant correlation between digesta moisture content and each of the measured physical parameters (Table 4.10). The gastric secretion rate may affect the pH changes of the gastric digesta. A higher gastric pH may prolong the duration of contact with salivary amylase, which would result in greater gastric starch hydrolysis and enhanced softening of the food matrix (Bornhorst, Hivert, et al., 2014; Freitas et al., 2018). These alterations in breakdown during gastric digestion may impact the gastric emptying and glycemic response.

Estimated gastric secretory response to each diet obtained from the moisture addition rate (Table 4.4) ranged from 9.07 g/min at 30 min to 1.89 g/min at 240 min (averaged across all diets), with an overall average (across all diets and time points) of 4.14 g/min. Although potential variations in liquid emptying between the meals and addition of saliva from involuntary swallowing were not considered in the calculation of moisture addition rate, the values indicate that there was a clear increase in gastric secretions at the beginning of digestion. For comparison, previous study suggested that the basal gastric secretion rate in pigs is ~1.05 mL/min (Kararli, 1995). The high initial moisture addition rate seen in this study can explain the initial increase in whole stomach content of the diets other than semolina (Figure 4.8B and D). The decreasing moisture addition rate over time may be attributed to the significant reduction in the intragastric pH over time for all diets (Figure 4.9).

Gastric secretory response to different meals has been studied in humans, but to the author's knowledge, the current study is the first to report such observation in a pig model. Interestingly, the trend in the secretory response found in the current study

agrees with findings in human studies. Gardner, Sloan, Miner, and Robinson (2003) reported that meal-stimulated gastric acid secretion in humans has a direct correlation with integrated gastric acidity in the first 3.5 h after a meal, which may be influenced by the buffering capacity of gastric content. A study on gastric acid secretion rate after consumption of sirloin steak in normal and duodenal ulcer subjects showed that secretion of acid increased rapidly from basal rate to reach a peak within 1 to 1.5 h, then diminished gradually until the fourth hour of digestion, but not to the initial rate of secretion (Fordtran & Walsh, 1973). Similarly, Hoad et al. (2015) reported rapid gastric secretion after consumption of nutrient liquid meal, observed with MRI. Gastric secretions continued as gastric emptying took place, such that half of the volume of the gastric contents consisted of secretions after 75 min.

Gastric secretory response to food has been shown to be influenced by gastric distention due to meal portion (Richardson, Walsh, Hicks, & Fordtran, 1976), meal viscosity (Marciani, Gowland, Spiller, et al., 2001), food acidity (Walsh, Richardson, & Fordtran, 1975), and buffering capacity of the food (Fordtran & Walsh, 1973). It should be noted that buffering capacity is not an independent food property, but represents the combined effects of physicochemical and structural differences between food matrices. As such, it may be a suitable parameter to provide links between food structure and composition to digestion processes. It was hypothesized that the different buffering capacity of the diets resulted in differences in the pH and overall buffering capacity of gastric content, leading to variations in gastric secretions, resulting in different rates of moisture addition during gastric digestion.

The rate of moisture addition at each time point for all diets besides semolina, increased with increasing buffering capacity (Figure 4.1B), especially at earlier digestion times (30 and 60 min). While semolina had the highest buffering capacity

among the six diets, it had the lowest moisture addition rate at 30 min of gastric digestion (6.48 ± 1.44 g/min, compared to the 9.58 g/min averaged across the other five diets). This may be attributed to its high initial moisture content and semisolid nature, which may have caused it to behave like a viscous liquid rather than a solid meal that requires mechanical breakdown in the stomach (Malagelada, Go, & Summerskill, 1979). The inconsistent trend in moisture addition rate in semolina might have also been due to the larger volume of semolina consumed compared to the other diets that affected gastric emptying rate, which might interfere with gastric secretory response (Jolliffe, 2009). However, these factors were outside the scope of this study.

Pasta, which had similar buffering capacity to rice couscous, had a lower moisture addition rate after 30 min of digestion (7.17 ± 0.94 g/min) compared to rice couscous (8.92 ± 0.62 g/min). This discrepancy might have been caused by mastication of the diets, which generated smaller particles size than those used for buffering capacity analysis, although the particle size after mastication was not measured in the current study. It has been demonstrated in model food that buffering capacity has an inverse relationship with particle size (Mennah-Govela et al., 2019). As shown in Figure 4.4, smaller particles were more prevalent in the digesta after 30 min digestion, compared to the initial particle area distribution of the diets, although the significance of this difference on the buffering capacity was not assessed. Additionally, the presence of bicarbonate in saliva (Helm et al., 1982) that was added to the diets and starch hydrolysis by salivary amylase during mastication might also have caused chemical changes in the diets, leading to changes in buffering capacity when the diets entered the stomach. The potential contribution of mastication to the buffering capacity of ingested meals and the subsequent gastric secretory response during gastric digestion merits future investigation.

Despite the deviation in semolina, results from the current study (Figure 4.1B) indicate that the buffering capacity, which takes into account both composition and structural factors, may be utilized in future studies to link food composition and structure to gastric secretions at early stages of the gastric digestion process. Additionally, mechanisms of how food buffering capacity may govern gastric secretory response are worth exploring.

4.5.3 Stomach regions affect physical changes of digesta during gastric digestion

Physiological differences between the proximal and distal regions of the stomach may also influence the gastric digestion process, further impacting digesta properties. Previous research has suggested that the proximal stomach acts as a reservoir for ingested food, while the majority of mechanical breakdown takes place in the distal stomach (Hasler, 2009). Furthermore, pH differences across the regions have been observed (Bornhorst, Roman, et al., 2013; Bornhorst, Ströbinger, et al., 2013; Nau et al., 2019). Distinctions between the proximal and distal stomach regions were identified in the physical properties of the digesta in the current study.

The distal stomach digesta had significantly higher ($p < 0.05$) dry basis moisture content (3.67 vs. 4.02 g H₂O/g DM on average in the proximal and distal stomach, respectively) and SR (0.86 vs. 0.94 on average in the proximal and distal stomach, respectively) for the six diets across all digestion times, which agrees with previous studies using growing pigs (Bornhorst, Chang, et al., 2013; Bornhorst, Rutherford, et al., 2014; Bornhorst, Ströbinger, et al., 2013). Although most gastric secretions are produced in the proximal stomach (Lærke & Hedemann, 2012), the higher moisture uptake of the diets in the distal stomach may be attributed to: (1) limited mixing in the proximal stomach that limited the diffusion of gastric secretions to food particles (Bornhorst, 2017; Mennah-Govela et al., 2015); or (2) emptying of liquid (from the diet

and gastric secretions) from the proximal stomach to the distal stomach (Kelly, 1980), which caused liquid to accumulate in the distal stomach prior to emptying. This variation in moisture uptake across the two stomach regions was food-structure-specific, as the SR of proximal and distal stomach digesta were not significantly different for rice couscous and semolina. These diets had smaller initial particle area than the other four diets, and it is likely that they could be more easily mixed with gastric secretions in both stomach regions.

Mixing of gastric secretions with the diets in the stomach also influenced the intragastric pH of the digesta, as supported by the negative correlation between digesta pH and moisture content. As a result, both rice couscous and semolina, that likely mixed faster with gastric secretions, did not exhibit significantly higher pH in the distal stomach compared to the proximal stomach at any digestion time. Meanwhile, higher pH in the proximal stomach was observed until 120 min of digestion in couscous, rice grain, and rice noodle, and for the entire 240 min in pasta, which matches with the higher SR in the distal stomach across digestion times and suggests slower gastric mixing. While the interregional difference in SR and pH in pasta, rice grain, and rice noodle could be explained by their larger initial particle size, this difference was not expected in couscous. The significantly higher buffering capacity of couscous compared to rice grain and noodle diets may have caused the slow intragastric pH change in couscous, which underlines the influence of food buffering capacity not only to gastric secretory function, but also to the gastric mixing process. This finding agrees with a previous study using growing pigs, where the mixing efficiency of gastric secretions with ingested meals was attributed to the rate of diffusion of secretion into the diets, total amount of gastric secretions present, and the buffering capacity of the diets (Bornhorst, Rutherford, et al., 2014).

With higher motility and gastric mixing in the distal stomach, it was expected that distal stomach digesta would have smaller particles than that of the proximal stomach, and that the particle area would be smaller over time. In the first 30 min, the particle area distribution showed a size reduction compared to undigested diets, which may be attributed to mastication. However, the changes in the particle area distribution between 30 to 240 min of gastric digestion were less notable (Figure 4.4). Rice grain had significantly larger x_{50} and x_{90} values averaged over the entire digestion time in the distal stomach, which contradicted the expected trend, but may indicate the presence of gastric sieving, which causes smaller particles to be emptied and leaves larger particles to be broken down for a longer time (Bornhorst, Kostlan, et al., 2013). The indication of gastric sieving was also supported by qualitative particle area distribution given by Figure 4.4, which shows the re-occurrence of particles of large areas at 240 min digestion for all diets, which were not observed in the first 60 or 120 min. Another possible explanation for this larger particle size in the distal region at 240 min is agglomeration of individual particles, where smaller particles interacted to form agglomerates due to gastric mixing, although this phenomenon has not been previously reported in the literature as per the authors' knowledge.

Distinction between the stomach regions was more apparent in the hardness measurement. Due to the bulk compression method used in this study, both the softening of the bulk digesta (that reflects biochemical breakdown) and mechanical breakdown of individual food particles during gastric digestion contributed to the changes in hardness values. The hardness values of the rice-based diets, averaged across diets and across all digestion times, were significantly lower ($p < 0.05$) in the proximal stomach (average of 14.27 N) than in the distal stomach (average of 16.64 N). This observed regional difference in the textural properties was contradictory to a previous *in*

vivo study with brown- and white-rice, where the hardness of the digesta was found to be lower in the distal stomach (Bornhorst, Ferrua, et al., 2013). However, the hardness of rice grain reported in that study (31.7 and 26.4 N in the proximal and distal stomach regions, respectively) was similar to the values obtained in the current study (averaged across digestion time, 30.66 and 33.90 N in the proximal and distal stomach regions, respectively). The difference in the trend might be due to different compression methods used, as the previous study applied uniaxial compression on individual rice grains and was done to quantify only the effect of gastric secretions on the softening of intact food particles (Bornhorst, Ferrua, et al., 2013). In contrast to rice-based diets, the hardness of wheat-based diets, averaged across diets and all digestion times was significantly lower ($p < 0.05$) in the distal stomach (6.77 N) compared to the proximal stomach (8.94 N).

In terms of the softening behavior of the diets, the hardness values in the rice- and wheat-based diets in the two stomach regions were consistent with their $t_{1/2, \text{softening}}$, where all rice-based diets had lower $t_{1/2, \text{softening}}$ in the proximal stomach and wheat-based diets had lower $t_{1/2, \text{softening}}$ in the distal stomach (Figure 4.7). This difference can be related to different gastric mixing in the proximal and the distal stomach, which influenced the digesta pH in each stomach region. The proximal stomach could provide suitable conditions for remaining salivary amylase activity (optimum pH ≥ 3) (Brownlee et al., 2018), which was supported by pH > 3 in this stomach region during the first 60 min of digestion (Table 4.3). Meanwhile, the presence of a protein network in wheat-based diets, which has been reported to hinder the accessibility of α -amylase to digest the starch granules (Zou, Sissons, Warren, Gidley, & Gilbert, 2016), is hypothesized to have suppressed the softening process in the proximal stomach by remaining salivary amylase activity. In the distal stomach, the breakdown of the protein network in the

diets by pepsin in gastric secretion (maximum activity at pH 1.8 to 2.5) may have allowed the gastric acid to hydrolyze the starch, resulting in greater softening in the distal stomach (Mennah-Govela & Bornhorst, 2021). Biochemical changes of the diets due to prolonged salivary amylase activity (e.g. in rice grain or rice noodle) or peptic hydrolysis of the protein network that entraps starch granules in the wheat-based diets (e.g., pasta) may increase starch hydrolysis in the stomach and small intestine (Zou et al., 2016). The correlation between intragastric pH and textural changes was not significant, likely due to the interactions between food macrostructure and buffering capacity, as well as the gastric emptying process that occurred simultaneously with food breakdown (Table 4.10). Future studies are required to investigate the contribution of enzymatic breakdown as affected by gastric pH on the softening of diets with varying macrostructure, and its impact on starch hydrolysis and glycemic response.

Distinction between the proximal and distal stomach digesta rheological parameters, measured using both shear and oscillatory testing, was only found in couscous, pasta, rice grain, and rice noodle. Semolina and rice couscous exhibited no significant rheological differences between stomach regions, with G' , G'' , K , and shear stress at 0.2 s^{-1} that were lower than the other four diets. This observation generally agreed with the texture results, as exemplified by the strong and significant correlations observed between measurements of hardness and rheological parameters K , G' , and G'' ($r_s = 0.787$, 0.890 , and 0.902 , respectively, $p < 0.0001$). The rheological measurements quantified the overall breakdown of the diets, encompassing the addition of gastric secretions and disintegration of food particles. It is likely that addition of gastric secretions impacted the rheological properties due to dilution and the presence of mucin, which may modify viscosity and adhesiveness (Minekus et al., 2014). A

previous *in vitro* study demonstrated that addition of mucin to digesta significantly increased the digesta consistency coefficient (K) (Wu, Bhattarai, et al., 2017).

The trend in measured rheological parameters further supports that gastric digestion phenomena may be influenced by not only gastric physiological regions, but also the structure of the ingested food. Some of the regional distinctions observed in the rheological properties may be explained by increased gastric mixing in digesta with lower consistency (e.g., lower shear stress at 0.2 s^{-1} or lower K value). None of the rheological properties were significantly different across regions in semolina or rice couscous. One potential explanation for this result is that the reduced gel-like characteristic (G' for semolina and rice couscous digesta together at 30 min was $844 \pm 89 \text{ Pa}$ compared with $10564 \pm 968 \text{ Pa}$ for the other diets) and lower consistency of digesta (K for semolina and rice couscous together at 30 min was $29.49 \pm 3.70 \text{ Pa}\cdot\text{s}^n$, compared with $294.20 \pm 24.45 \text{ Pa}\cdot\text{s}^n$ for the other diets) from rice couscous and semolina may have increased the amount of gastric mixing. Consequently, the contribution of gastric regions may be less apparent in diets with lower consistency due to increased gastric mixing. This increased mixing was also supported by a recent study involving particle tracking inside a dynamic stomach model with solutions of different viscosity (Keppler, O'Meara, Bakalis, Fryer, & Bornhorst, 2020). In that study, the velocity of a particle in the gastric environment was shown to be inversely related to the K of the digesta.

4.5.4 Relationship between physical changes during gastric digestion and gastric emptying

A relationship between $t_{1/2, \text{softening}}$ in the gastric environment with its $t_{1/2, \text{DM GE}}$ was identified (Figure 4.8F). Correlation with DM emptying was selected because it reflects the actual solid portion of the ingested meals without the impact of varying amounts of

gastric secretion addition during digestion. For example, a longer $t_{1/2, \text{softening}}$ of rice grain (79.9 min) compared to rice noodle (16.6 min) correlated to a lower $t_{1/2, \text{DM GE}}$ of rice noodle (213 min) compared to rice grain (223 min), despite the significantly smaller x_{50} of rice grain compared to rice noodle. In general, the relationship ($R^2 = 0.7614$) suggests that gastric emptying of solid starch-based foods in the present study is controlled by their breakdown rate, which agrees with food breakdown classification system (FBCS) (Bornhorst et al., 2015). In the FBCS, it was hypothesized that the rate of food softening during gastric digestion determines the gastric emptying rate of food products. However, pasta does not follow as clear of a trend, as the $t_{1/2, \text{DM GE}}$ should be lower if it followed the trend of $t_{1/2, \text{softening}}$. This might indicate that the gastric emptying of pasta is possibly limited by other factors in addition to its breakdown rate, including physiological response-related factors that were outside the scope of this study.

Regardless of the slight deviation in the trend, this finding still demonstrates the relationship between food structure and food breakdown rate during gastric digestion with its gastric emptying rate, which may have further implication on the glycemic response of the food. For those diets with increased breakdown and emptying rate, such as semolina and rice couscous, this will affect the rate of delivery and state of particles when they arrive in the small intestine. As a result, there may be more rapid conversion to glucose and subsequent absorption, which may result in a more rapid glycemic response in semolina and couscous. On the other hand, diets with slower breakdown and emptying rate, such as rice grain and pasta might have enhanced gastric starch hydrolysis due remaining salivary amylase or pepsin activity, but the rate of delivery of particles to the small intestine would not be as high as semolina and couscous. As previous studies using human subjects have suggested an inverse relationship between gastric emptying half-time and glycemic response of starch-rich meals (Cisse et al.,

2018; Mourot et al., 1988; Torsdottir et al., 1989), it is hypothesized that for the diets with slower breakdown and emptying rate, there will be less material available for small intestinal digestion and glucose absorption, resulting in a lower glycemic response. These relationships are investigated in Chapter 6

In linking the food breakdown rate with gastric emptying, gastric secretory response should not be neglected (Figure 4.9). For example, rice couscous had the lowest $t_{1/2, \text{softening}}$, despite its agglomerated structure, compared with semolina porridge. This could be due to the higher initial moisture addition to rice couscous than to semolina (Figure 4.1A and B). The added gastric secretions might have rapidly dissolved some of the ingested rice couscous. This proposed mechanism is supported by the lower stress of rice couscous compared to semolina in the first 30 min of digestion (13.74 Pa for rice couscous vs. 18.11 Pa for semolina, averaged across stomach regions). This observation also suggests that changes of physical properties during gastric digestion have a greater contribution to gastric emptying rate than the initial diet physical properties, as has been shown in previous studies (Guerin et al., 2001; Martens, Noorloos, et al., 2019).

4.5.5 Methodological considerations in monitoring physical breakdown during gastric digestion *in vivo*

The present study brings insights into methodological considerations to characterize the breakdown of solid foods during gastric digestion. To measure particle size distribution as a result of mechanical breakdown, image analysis was utilized. Image analysis measures 2D projections of particles and generally does not characterize their 3D shape. It is possible that changes in particle size that impacted particle height, such as swelling due to absorption of gastric secretions, were not visualized by image analysis. Gastric digestion of solid food consists of physical breakdown (i.e., biochemical and mechanical) and gastric emptying processes that occur simultaneously. It may be

difficult to isolate the effect of each of these processes, but their combined effect can be captured through rheological and textural analyses.

In this study, three methods of characterizing digesta physical properties were utilized: shear rate sweep, oscillatory measurement, and texture analysis using a bulk compression method. The rheological analyses, specifically the Herschel-Bulkley parameters K and G' (shear rate vs. oscillatory testing), showed a high level of correlation when the measured properties were compared across all treatments ($r_s = 0.907$, $p < 0.0001$). However, digesta samples in this study contained particles mixed with gastric secretions (in which the particles may change in size and shape during digestion) (Bornhorst, Ströbinger, et al., 2013). The particulate nature of the digesta resulted in some samples demonstrating slight deviations from the Herschel-Bulkley fits (Figure 4.5), despite the high R^2 . Specifically, overprediction by the model at low values of shear rate may have been due to sample slip, and underprediction at higher values may have been due to a transition of the material to a turbulent regime during the test, as was also found in a previous study on the rheology of pulp fiber suspensions (Derakhshandeh, Hatzikiriakos, & Bennington, 2010). Consequently, characterization of the rheology of digesta using fundamental methods is challenging (Joyner, 2018) and alternative analysis methods, such as texture analysis, may be needed.

From a logistical point of view, the shear rate sweeps and oscillatory tests conducted in this study required approximately 4 and 8 min to perform per sample, respectively. Texture testing required approximately 2 min per sample. Although the time required for rheological testing is longer, it provides properties that may be more easily compared across studies or with the literature. However, a recent study suggested that fundamental rheological properties may vary due to the use of different geometries or instruments if not tested within specific ranges (Tan et al., 2019). Likewise, it may be

difficult to compare textural properties across studies if the same sample geometry and loading conditions are not used. Nevertheless, texture analysis is commonly used in food analysis (Bourne, 2002; Lu, 2013; Szczesniak, 1963) and the existence of more standardized methods to quantify textural changes during digestion may help facilitate comparison across studies.

Based on these considerations, texture analysis may be a suitable alternative to rheological properties based on challenges with inhomogeneity of the digesta and time required for analysis of large volumes of samples. This is also supported by strong and significant ($p < 0.0001$) correlative relationships between digesta hardness and rheological parameters K , G' , and G'' ($r_s = 0.787$, 0.890 , and 0.902 , respectively). Unlike rheological properties that are more commonly characterized in *in vivo* gastric digestion studies (Bornhorst, Ferrua, et al., 2013; Nau et al., 2019; Schop, Jansman, de Vries, & Gerrits, 2020; Shelat et al., 2015; Wu et al., 2016), textural changes of *in vivo* gastric digesta are less studied (Bornhorst, Ferrua, et al., 2013; Bornhorst, Roman, et al., 2014). However, future investigation over a wider array of food products is required to compare between these techniques, and to determine the most suitable method for physical property measurement in the gastric digesta of varying food types.

4.6 Conclusions

The physical breakdown processes of six solid starch-based foods were monitored and their relationships with gastric emptying rate were investigated. Gastric emptying of dry matter and whole stomach content was influenced by the initial macrostructure of the diets, which in turn influenced other biological processes in the stomach, such as the quantity and distribution of gastric secretions, gastric mixing, and gastric sieving. For example, rice couscous and semolina had the smallest initial particle size (represented

by median particle area, x_{50}) and the shortest dry matter- and whole stomach content gastric emptying half-times ($t_{1/2,DM\ GE}$ and $t_{1/2,whole\ GE}$, respectively) within the rice-and wheat-based diets. Those two diets also demonstrated no significant differences in their gastric digesta properties (e.g., pH and hardness) between the proximal and distal stomach. In contrast, significant differences in pH and hardness between proximal and distal gastric regions during digestion were found in gastric digesta with higher K and G' values (couscous, pasta, rice grain, and rice noodle). It was hypothesized that diets with higher K and G' decreased gastric mixing, which led to regional differences in the moisture content and pH of the gastric digesta. Additionally, although cooked diets with larger initial x_{50} generally had longer $t_{1/2,DM\ GE}$ and $t_{1/2,whole\ GE}$, their initial x_{50} could not fully explain the trend observed in their $t_{1/2,DM\ GE}$. The trend in the $t_{1/2,DM\ GE}$ was likely governed by the breakdown rate of the diets, which occurred differently in different stomach regions, depending on the digesta properties. This breakdown was quantified as softening half-time ($t_{1/2,softening}$), which was obtained by monitoring textural changes in the digesta over time.

This study is the first to explore the relationship between gastric emptying and gastric breakdown rates for starch-based foods of varying botanical sources and structures *in vivo*. Additional analysis of food physical properties during gastric digestion is required using a wider array of diets to better quantify this relationship. Future work is needed to link the findings in the present study to glycemic response, to allow for development of food structures with controlled breakdown rate in the stomach for glycemic response management.

CHAPTER 5. Influence of food macrostructure on the kinetics of acidification in the pig stomach: implications for starch hydrolysis and starch emptying rate

5.1 Abstract

The role of the stomach as a biochemical environment for digestion of starch in food matrices was investigated using a growing pig model. Study diets from wheat and rice with different food structures were assessed. Diets with larger and smaller initial particle size were found to undergo different acidification kinetics during gastric digestion, affecting starch hydrolysis process in the stomach. Larger-sized diets exhibited clear distinctions between the proximal and distal regions of the stomach, with higher pH maintained in the proximal stomach digesta up to 240 min digestion, resulting in extended remaining salivary amylase activity and accumulation of maltose in the stomach. This study indicates the importance of food macrostructure in providing a suitable biochemical environment for starch hydrolysis in the stomach, which may affect physical breakdown of the food, gastric emptying of starch, and may influence the small intestinal digestion and glycemic response of the food.

Keywords: food structure; gastric digestion; salivary amylase activity; starch hydrolysis

Part of the contents of this chapter has been submitted for peer review in *Food Chemistry*: Nadia, J., Olenskyj, A.G., Subramanian, P., Hodgkinson, S.M., Stroebling, N., Estevez, T.G., Singh, R.P., Singh, H., and Bornhorst, G.M. Influence of food macrostructure on the kinetics of acidification in the pig stomach: implications for starch hydrolysis and starch emptying rate.

Chapter 5 Overview

Biochemical breakdown during gastric digestion and starch emptying:

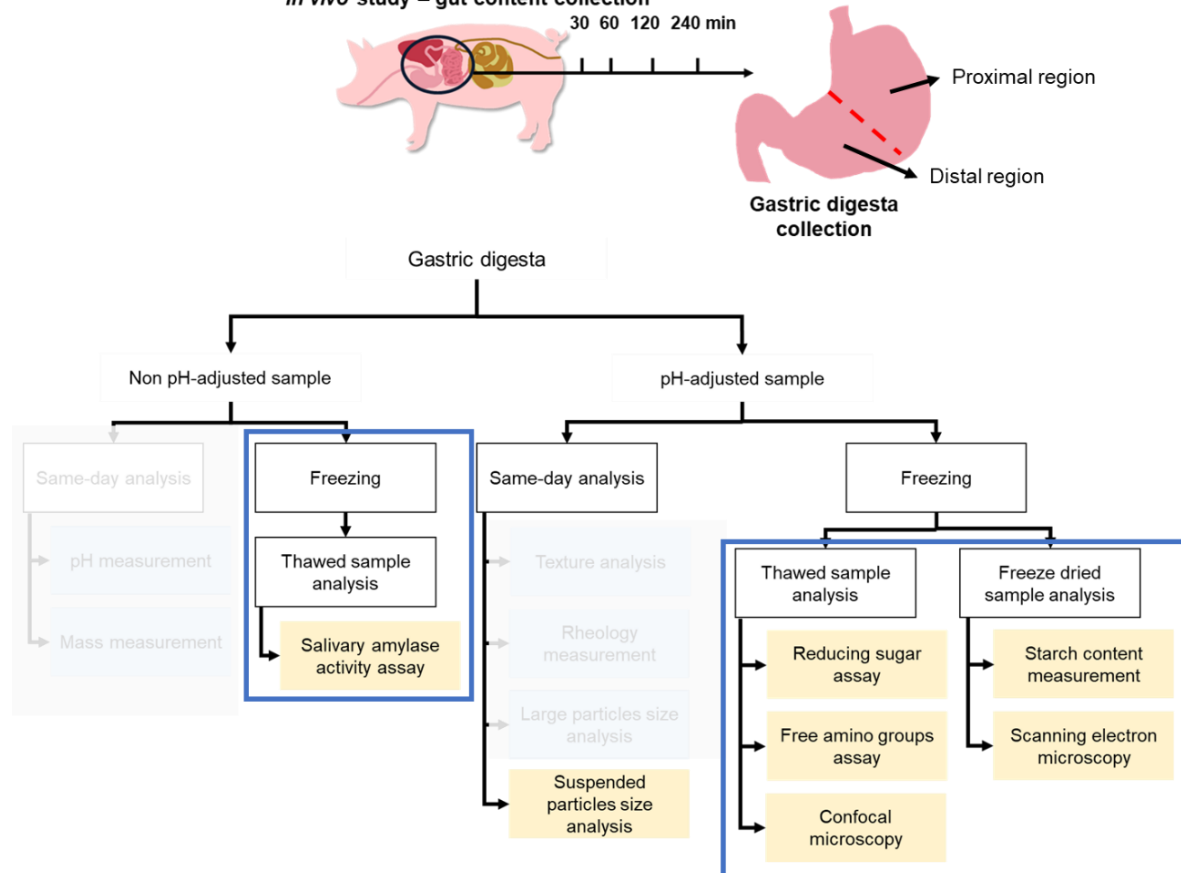
- Intragastric pH distribution
- Remaining salivary amylase activity
- Starch and protein hydrolysis
- Starch emptying
- Microstructural changes

Research Objective 1

Identify the link between food structure, gastric physiology, and food breakdown behavior of in the stomach

Experimental approach

In vivo study – gut content collection



Sample analyses in this chapter were conducted in collaboration with other people:

- Particle size measurement using Mastersizer and SEM analysis (Sections 5.3.5 and 5.3.7.2) were conducted by Dr. Parthasarathi Subramanian (Riddet Institute).
- Preliminary analyses of reducing sugar and free amino groups assay (Section 5.3.6.1) were conducted by Talia G. Estevez (UC Davis).

5.2 Introduction

During gastrointestinal digestion, starch in food is converted to oligosaccharides by salivary amylase and pancreatic amylase, producing maltose, maltotriose, and dextrins as the end products. These oligosaccharides are hydrolyzed further by the brush border enzymes in the small intestine to produce glucose, which is absorbed into the bloodstream (Holmes, 1971). Hydrolysis of starch has been associated mainly with the action of pancreatic amylase during small intestinal digestion. In contrast, the contribution of salivary amylase during mastication on starch hydrolysis is less well-understood, as mastication only lasts for <5 to 90 s. As highlighted in the literature review (Chapter 2), gastric digestion occurs between mastication and intestinal digestion (typically from 0 to 4 h) and has not been commonly considered as a location for starch hydrolysis due to the low pH of gastric secretions. However, recent *in vitro* studies using a gastric digestion system with dynamic pH profile reported hydrolysis of 30 to 80% starch in food matrices during gastric digestion (Freitas & Le Feunteun, 2018, 2019; Martens et al., 2020), suggesting that salivary amylase can remain active during gastric digestion. Extended salivary amylase activity during gastric digestion may impact the subsequent small intestinal digestion, further affecting glucose production and absorption. A recent study reported that lowering the pH of starch-rich foods by consuming an acidic beverage could lower glycemic response in humans, which could be attributed by an early inhibition of salivary amylase during gastric digestion (Freitas et al., 2021).

Although the contribution of salivary amylase activity in the stomach to the digestion of starch has been suggested in previous studies, the underlying mechanisms and contributing factors have not been fully elucidated. Slow mixing between acidic gastric secretions with ingested food bolus (i.e., gastric mixing) has been suggested as a

possible mechanism describing how the stomach could be a suitable location for remaining salivary amylase activity as long as the pH within the bolus is maintained at $\text{pH} > 3$ (Bornhorst, 2017; Brownlee et al., 2018). Gastric mixing process was reported to be affected by the buffering capacity and viscosity of the meal (Bornhorst, Rutherford, et al., 2014; Freitas & Le Feunteun, 2019; Freitas et al., 2018), indicating the potential contribution of food structure to remaining salivary amylase action in a starch-based meal. Nevertheless, there has not been a clear link established between food structure, remaining salivary amylase activity in the stomach, and resulting starch hydrolysis. Understanding this link in an *in vivo* system is essential to demonstrate the impact of food structure and food breakdown during gastric digestion on starch digestibility.

The present study determined *in vivo* biochemical changes during gastric digestion in starch from various rice and wheat-based foods, which are dominant global cereal grain sources (Shewry, 2008). Small intestinal digestion-related aspects of the study will be presented in Chapter 6. It was demonstrated in Chapter 4 that physical breakdown during gastric digestion of rice- and wheat-based diets of varying macrostructures impacted the dry matter gastric emptying. Different breakdown rates in the proximal and distal stomach regions for different diets were considered to be affected by initial macrostructures of the diets, leading to different extent of mixing between gastric secretions with the ingested diets. However, it is important to understand how these different physical breakdown rates and gastric mixing processes are related to biochemical modification of the digesta. Therefore, apparent salivary amylase activity, reducing sugar and free amino group concentrations (as the measures of starch and protein hydrolysis, respectively), and the particle size of the suspended solid fraction in gastric digesta were quantified. Gastric mixing was qualitatively observed through intragastric pH measurement. It was hypothesized that slower gastric

mixing would lead to a longer period of high pH in the proximal stomach and allowed salivary amylase to continue hydrolyzing starch until the proximal stomach content was acidified by gastric secretions. This may contribute to the structural breakdown during gastric digestion and gastric emptying mechanisms of solid particles.

5.3 Materials and methods

5.3.1 Study diets preparation and characterization

Study diets preparation and characterization were described in Chapter 3 (Section 3.1.2.1) and Chapter 4 (Section 4.3.4).

5.3.2 Animal housing and treatment

Animal housing and treatment were described in Chapter 3 (Section 3.2.3.1).

5.3.3 Gastric digesta collection procedure

Procedure of stomach removal and dissection for gastric digesta collection was described in Chapter 3 (Section 3.2.3.2). Intragastric pH was immediately measured at 10 locations around the stomach (Figure 5.1A) with a pH meter (PL-700 PV Bench Top Meter, GonDo, Taiwan), following Bornhorst, Rutherford, et al. (2014). At each location, pH was measured under the gastric tissue at approximately the center height of the digesta. Afterwards, gastric digesta from proximal and distal regions were taken out separately, weighed and mixed carefully to achieve uniform pH (as described in Section 3.2.3.2). From each stomach region, a 10- to 15-g subsample was taken and immediately frozen in dry ice for remaining salivary amylase activity analysis. After this sampling, the rest of the gastric digesta from each region was adjusted to pH 8 to 10 by careful mixing with <1 mL 50%-w/w NaOH solution to inactivate digestive enzymes. The pH-adjusted digesta was distributed to containers for same-day analysis of fresh sample, and the remaining was frozen or frozen then freeze-dried for chemical

and microstructural analysis (Figure 5.1A). A major portion of same-day analysis results (physical properties of gastric digesta) were discussed in Chapter 4. The only same-day analysis results discussed in this chapter are particle size measurement using the Mastersizer.

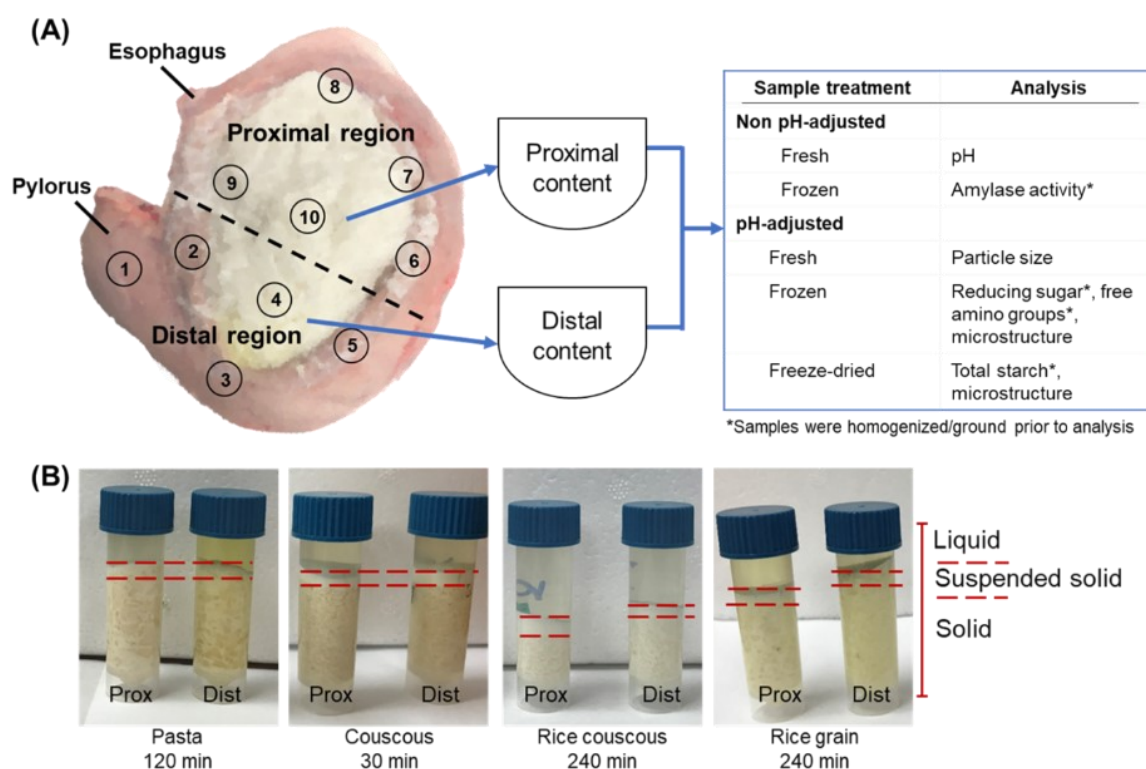


Figure 5.1 Example stomach with digesta and approximate pH measurement locations, with description of analyses done for each gastric sample. The dashed line indicates the approximate separation between proximal and distal stomach regions (A). Examples of three fractions obtained after centrifugation of gastric digesta from the proximal (prox) or distal (dist) region when maximum separation was obtained. The approximate separation between fractions is indicated by dashed red lines (B).

5.3.4 Establishment of intragastric pH colormap

Average pH values from each diet \times time \times measurement location were used to generate intragastric pH maps using the “jet” color map in MATLAB 2018A. pH between measurement locations was interpolated with linear interpolation method using a surface plot function.

5.3.5 Particle size analysis

Particle size distribution (PSD) of the suspended solid fraction in pH-adjusted fresh digesta was determined using the Mastersizer-2000 (Malvern Instruments Ltd., Worcestershire, UK) following Bornhorst, Ferrua, et al. (2013), with a refractive index of 1.530 for starch-based samples (Angelidis, Protonotariou, Mandala, & Rosell, 2016). Couscous, semolina and rice couscous digesta were tested directly due to their liquid-like consistency. Pasta, rice grain, and rice noodle digesta contained many large particles, hence ~500 mg of sample was added to ~3 mL distilled water to allow small particles to disperse, then the particle dispersion was analyzed. Samples were analyzed in triplicate. Averaged PSD data from each diet \times time \times stomach region was fit to a lognormal function on DistFit software (DistFit™, Chimera Technologies Inc., USA) to analyze the multimodality of the distribution.

5.3.6 Gastric digesta chemical analysis

5.3.6.1 Reducing sugar and free amino groups

The pH-adjusted frozen samples (~7 g) were thawed at 37°C for 1 h, transferred to pre-weighed tubes, and centrifuged ($4,122 \times g$, 20 min) to separate the digesta into three fractions: solid, suspended solid, and liquid (Figure 5.1B). Each fraction was transferred to a different container and weighed. The solid fraction (containing particles larger than 5 mm) was homogenized without any liquid addition using a handheld homogenizer (Scilogex D160 Homogenizer, Scilogex, USA) at 8,000 rpm for 0.5 to 1 min to reach a slurry-like consistency. When solids, suspended solids, and liquids did not effectively separate after centrifugation (in 16 out of 90 rice noodle or rice grain digesta samples), the entire sample was treated as solid fraction. For comparison to initial (undigested) condition, three batches of freeze-dried cooked diets were analyzed for reducing sugar and free amino groups. The undigested diets were treated as solid fraction.

Reducing sugar content in the fractions of pH-adjusted digesta was quantified using the dinitrosalicylic acid (DNS) method (Miller, 1959) with modifications. The liquid fraction of the digesta was used directly for analysis. Reducing sugars from solid and suspended solid fractions were recovered by mixing 0.1 g solid (homogenized) or suspended solid sample with 1.5 mL water (equivalent to 1:15 solid/liquid ratio, w/v) on a vortex for 15 s. The mixtures were left undisturbed for 1 h at room temperature, then centrifuged ($6,800 \times g$, 10 min) to separate the supernatant, which was used for analysis.

DNS reagent (0.4 mL) was mixed with 0.4 mL sample (maltose standard solution, liquid fraction, or supernatant from solid/suspended solid fractions), incubated in boiling water for 20 min, then cooled on ice for 10 min. Aliquots of sample (225 μ L) were transferred to three wells in a 96-well microplate, and the absorbance was read on a microplate reader (SPECTROstar Nano, BMG Labtech, Germany) at 540 nm. Reducing sugar content in the digesta was expressed as maltose equivalent, based on a maltose standard curve (0 to 2 mg maltose/mL), per gram digesta (referred to as mg maltose/g).

Free amino groups in digesta fractions were quantified using the o-phthalaldehyde (OPA) method (Church, Porter, Catignani, & Swaisgood, 1985). The liquid fraction of the digesta was used directly for analysis. The solid and suspended solid fractions were prepared in the same way as the reducing sugar analysis, except that the addition of water was replaced with sodium tetraborate buffer (0.0125 M, with 2% SDS, pH 9). After 1 h of contact time with the buffer and centrifugation ($6,800 \times g$, 10 min), the supernatant of the solid and suspended solid fractions were used for analysis. Aliquots of each sample (20 μ L, liquid fraction or supernatant from solid or suspended solid fraction) or glycine standard solutions were added to three wells. OPA reagent or

reagent blank (200 μL) was added and allowed to react for 3 to 4 min under minimum lighting. The absorbance was read on a microplate reader at 340 nm. Free amino groups content in the samples was expressed as NH_2 equivalent, calculated from a glycine standard curve (0 to 0.5 mg glycine/mL sodium tetraborate buffer), per gram digesta (referred to as $\mu\text{g NH}_2/\text{g}$).

5.3.6.2 Apparent salivary amylase activity

Apparent salivary amylase activity in gastric digesta was measured by modifying the original method for purified amylase (Bernfeld, 1955), where the non pH-adjusted digesta was treated as the starch substrate. With this method, amylolytic activity could be observed in the digesta without having to undergo an additional step of liquid separation from the digesta, thus minimizing additional time that may cause further starch hydrolysis during sample preparation. Moreover, the method enabled the measurement of samples with minimum amount of liquid in the digesta (e.g., 30-min rice grain and rice noodle digesta). Measurements were initially performed on digesta from all time points for pasta, rice grain, rice noodle, and semolina. Results from these measurements indicated minimal activity at $\text{pH} \leq 2$, therefore measurements on the remaining two diets were only performed on samples that had $\text{pH} > 2$ (30-, 60-, and 120-min digesta for couscous; 30- and 60-min digesta for rice couscous).

Non pH-adjusted frozen digesta samples were thawed in a water bath at 37 $^{\circ}\text{C}$ for 3 min, then the tubes were immediately placed in an ice bath. Samples were kept on ice at all times during the assay, unless otherwise stated, to minimize enzymatic activity that may occur after thawing frozen samples. Thawed samples (2 to 2.5 g) were transferred to another container, followed by addition of 20 mM sodium phosphate buffer containing 6.7 mM NaCl (1:2 w/v, digesta:buffer ratio). The pH of the buffer solution was adjusted to a pH similar to that of the specific digesta sample to be analyzed. In the

ice bath, the mixture was homogenized at 8,000 rpm (Scilogex D160 Homogenizer, Scilogex, USA) for 0.5 to 1 min to form a slurry. The resulting slurry was aliquoted (0.25 mL) to five microtubes, then diluted with 0.25 mL of the same buffer solution used for homogenization. The dilution was done to lower the starch concentration in the sample to enable the observation of amylase activity.

Diluted sample aliquot was immediately incubated for 1, 2, 3, or 5 min in a water bath (37 °C) after 2 min equilibration. One aliquot was immediately removed after equilibration to represent the initial maltose concentration ($t = 0$ min). After incubation, each sample was immediately placed on ice for 10 min, then centrifuged at $6,800 \times g$ for 10 min. The supernatant (0.1 mL) was diluted to 0.4 mL with water and mixed with 0.4 mL DNS reagent. Maltose content in the sample was determined as described in Section 5.3.6.1. When present, apparent salivary amylase activity in the sample was calculated from the slope of the linear portion of maltose vs. incubation time curve for each sample (example curves are given in **Error! Reference source not found.**). The apparent activity was expressed as the amount of maltose released per minute per gram digesta dry matter ((mg maltose//min)/g DM) during 3 min incubation, as data points from 0 to 3 min exhibited a linear trend for most samples, in agreement with the original method (Bernfeld, 1955).

5.3.6.3 Total starch content

Starch content of freeze-dried digesta samples (ground and sieved with a 1-mm sieve prior to analysis) was measured using Megazyme Total Starch Kit (Megazyme, Wicklow, Ireland), following the procedure for samples not containing free glucose or maltodextrins. Gastric emptying of starch (i.e., starch content in digesta \times dry matter of digesta from Chapter 4) was determined using a modified power-exponential model for gastric emptying (Siegel et al., 1988):

$$\frac{X_t}{X_0} = 1 - (1 - e^{-k \cdot t})^\beta \quad (5.1)$$

where X_t/X_0 : starch remaining in the stomach at digestion time t (min) relative to the initial starch in the diet consumed (g DM starch in digesta/g DM starch in diet), k : the gastric emptying rate of starch in the dry matter of digesta (min^{-1}), and β : the theoretical y-intercept (unitless).

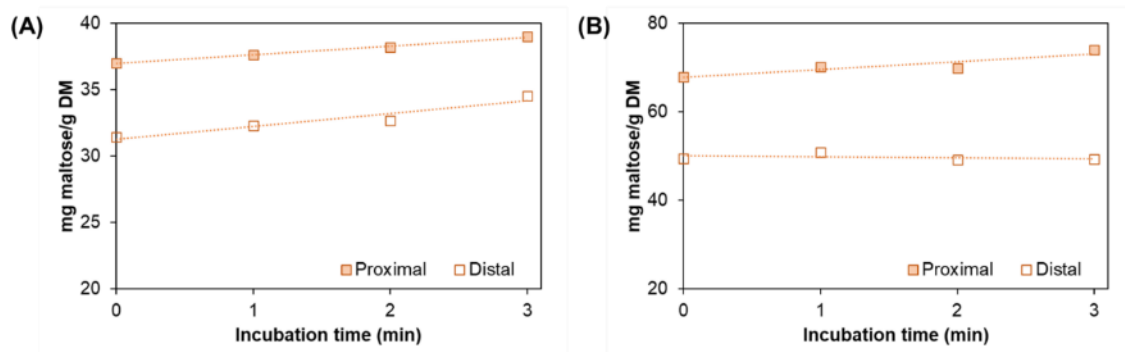


Figure 5.2 Example data sets of maltose concentration change over time to estimate apparent salivary amylase in the gastric digesta of pigs fed with couscous after 30 min (A) and 120 min (B) digestion. Dotted lines indicate linear regression lines used to estimate the apparent amylase activity.

5.3.7 Microscopy analysis

5.3.7.1 Confocal microscopy

Microstructure of the diet and digesta were observed using a confocal laser scanning microscope (CLSM; Leica SP5 DM600B, Heidelberg, Germany) at the Manawatu Microscopy and Imaging Center, Massey University Turitea Campus. Frozen, cooked diets and representative samples from 60 and 240 min proximal and distal stomach digesta for each diet were selected and thawed at 37°C. Semolina and couscous samples were sampled directly, noodle samples were cut to 2.5 mm × 2.5 mm slices, and rice grain samples were cross-sectioned to 1 mm × 2 mm slices with a scalpel blade (Figure 5.3). Protein and starch in the samples were double-stained using FITC (20 µL, 1%-w/v in ethanol) and Rhodamine B (20 µL, 0.1% in ethanol) solutions (Zheng, Stanley,

Gidley, & Dhital, 2016). Samples were stained at least 90 min prior to observation. Prior to transferring to microscope slides, samples were washed 4 times with 1 mL distilled water to remove excess stains. During CLSM observation, a He-Ne laser was used with excitation wavelengths of 488 nm and 561 nm for FITC and rhodamine B, respectively.

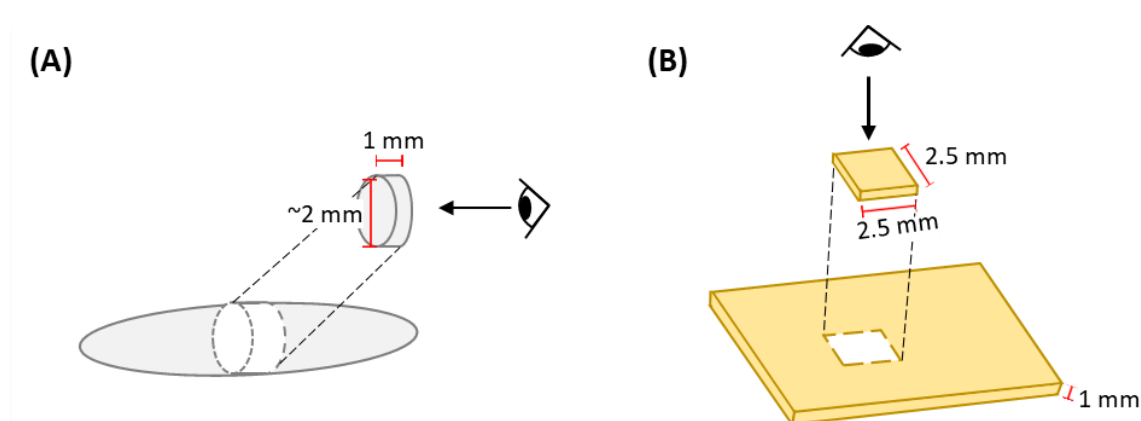


Figure 5.3 Illustration of sample sectioned from (A) rice grain and (B) pasta or rice noodle digesta particle used for confocal microscopy observation. The eye with arrow pointing to one side of the section indicates the orientation of the observation under the microscope.

5.3.7.2 Scanning electron microscopy (SEM)

Digesta samples (60 and 240 min) and cooked diets were freeze-dried, and a small portion of freeze-dried samples were affixed with double-faced adhesive tape on a metal stub. The samples were sputtered (SCD 050, Balzers, Liechtenstein) with gold for 200 s. Images were recorded with a scanning electron microscope (FEI ESEM Quanta 200, FEI Electron Optics, Eindhoven, The Netherlands) at the Manawatu Microscopy and Imaging Center, Massey University Turitea Campus, and observed at 20 kV accelerating voltage.

5.3.8 Statistical analysis

Only data points from pigs that consumed more than 50% of semolina or 70% of the other diets were used for data analysis (as described in Chapter 4). Statistical analysis

was conducted using SAS®Studio 3.8. ANOVA on reducing sugar and amino groups content, total starch, gastric pH, and PSD parameters (D[4,3], d[3,2], d₁₀, d₅₀, d₉₀) was conducted using a multi-factor, mixed model ANOVA (PROC MIXED). Each pig was an experimental unit, the diet type and digestion time were the between-subject factors, and the stomach region was the repeated factor within each pig. The batch of pigs (corresponds to different experimental periods) was included as a main effect in the model to account for interindividual variability. For pH data, the fraction of dry matter remaining in the stomach taken from Chapter 4 (Section 4.4.7) was included as an additional predictor due to better model fit with the inclusion of the parameter, based on Akaike's information criteria (Bornhorst, Rutherford, et al., 2014). For reducing sugar and amino group concentration in digesta and digesta fractions, a square root transformation was performed to achieve normality of residuals. Sample fraction (liquid, suspended solid, or solid fraction) was used as an additional factor in the statistical model for reducing sugar and amino group content; it was nested within each stomach region (proximal or distal).

Preliminary statistical analysis with the mixed model was run to remove independent data points that were outside ± 3 internally studentized residuals, followed by the final statistical analysis on data sets with outliers removed. Differences between means where the main effects were significant were determined with the Tukey-Kramer test at a significance level of $p < 0.05$. Averaged apparent amylase activity data at various pH ranges were analyzed with the Kruskal-Wallis test; the differences between means at different pH ranges were determined with the Dwass, Steel, Critchlow-Fligner test at $p < 0.05$. All values are reported as mean \pm SE.

5.4 Results and discussion

5.4.1 Inhomogeneous intragastric pH distribution may extend remaining salivary amylase activity

The acidification process of each diet during gastric digestion was estimated through visualization of the average intragastric pH from each of the 10 measurement locations (Figure 5.4A; Table D.1). The intragastric pH was significantly influenced by digestion time, measurement location, diet \times measurement location, time \times measurement location, diet \times time \times measurement location, and the batch of pigs ($p < 0.01$). Dry matter remaining was significant to the pH only when it interacted with measurement location, diet \times measurement location, time \times measurement location, and diet \times time \times measurement location ($p < 0.05$; Table 5.1). For all diets at all digestion times, lower pH was observed near the pylorus (location 1), which might be attributed to higher contractile activity in the pylorus that enhanced mixing of the digesta with gastric secretions (Bornhorst, 2017). Locations 3 and 5 also had lower pH compared to the rest of the stomach, most likely due to the flow of gastric acid toward the pylorus and accumulation of gastric acid (produced in the proximal stomach) in these locations, similar to previous studies (Lærke & Hedemann, 2012; Nau et al., 2019). Based on the overall pH profile of the six diets by the end of 240 min digestion (Figure 5.4A), the diets can be classified into those that reached uniform pH (semolina, couscous, and rice couscous) and those that had distinct pH separations (pasta, rice grain, and rice noodle). The first group consisted of diets with smaller initial particle surface area (to be referred to as ‘smaller-sized diets’ from here onwards) than the latter group (to be referred to as ‘larger-sized diets’ from here onwards; Table 4.1), highlighting the influence of food initial macrostructure and particle size on its acidification kinetics and mixing during gastric digestion, as reported in Chapter 4.

Between the smaller-sized diets, semolina and rice couscous had less variations in their pH profiles compared to couscous. Couscous exhibited significantly higher pH in the proximal stomach compared to the distal stomach in the first 120 min digestion (5.17 ± 0.32 vs. 2.61 ± 0.24 in the proximal and distal stomach, respectively, averaged from 30 to 120 min, $p < 0.0001$), but reached a homogeneous intragastric pH at 240 min (1.95 ± 0.46 vs. 1.82 ± 0.42 in the proximal and distal stomach, respectively, $p = 1$). Among these three diets, the final pH of the digesta (averaged across measurement locations) was lower in rice couscous (1.29 ± 0.03), compared to couscous (1.84 ± 0.13) and semolina (1.85 ± 0.13). This difference was possibly due to the higher buffering capacity of couscous and semolina (55.26 and $74.48 \mu\text{mol H}^+ / (\text{g sample} \times \Delta\text{pH})$, respectively) compared to rice couscous ($31.02 \mu\text{mol H}^+ / (\text{g sample} \times \Delta\text{pH})$), as a result of higher protein content in the wheat-based diets. The effect of food buffering capacity on intragastric pH has been reported in previous gastric digestion studies using egg white gels (Nau et al., 2019), brown and white rice (Bornhorst, Rutherford, et al., 2014), and liquid nutrient meals (Weinstein et al., 2013).

The larger-sized diets (pasta, rice grain, and rice noodle) had an inhomogeneous pH profile, with a distinct intragastric pH gradient up to 240 min digestion. At 240 min, the pH of proximal stomach digesta (3.13 ± 0.26 , averaged across the three diets) was still significantly higher ($p = 0.0022$) than the distal stomach digesta (1.58 ± 0.08). Variations between the larger-sized diets in their intragastric pH profiles even after 240 min of gastric digestion may reflect different extent of mixing and breakdown, in addition to different rates of gastric secretion addition to the diets during digestion due to their different buffering capacity values (as discussed in Chapter 4). Similar pH gradients during digestion of egg white gels, rice, and almond have been previously observed using a pig model (Bornhorst, Rutherford, et al., 2014; Nau et al., 2019).

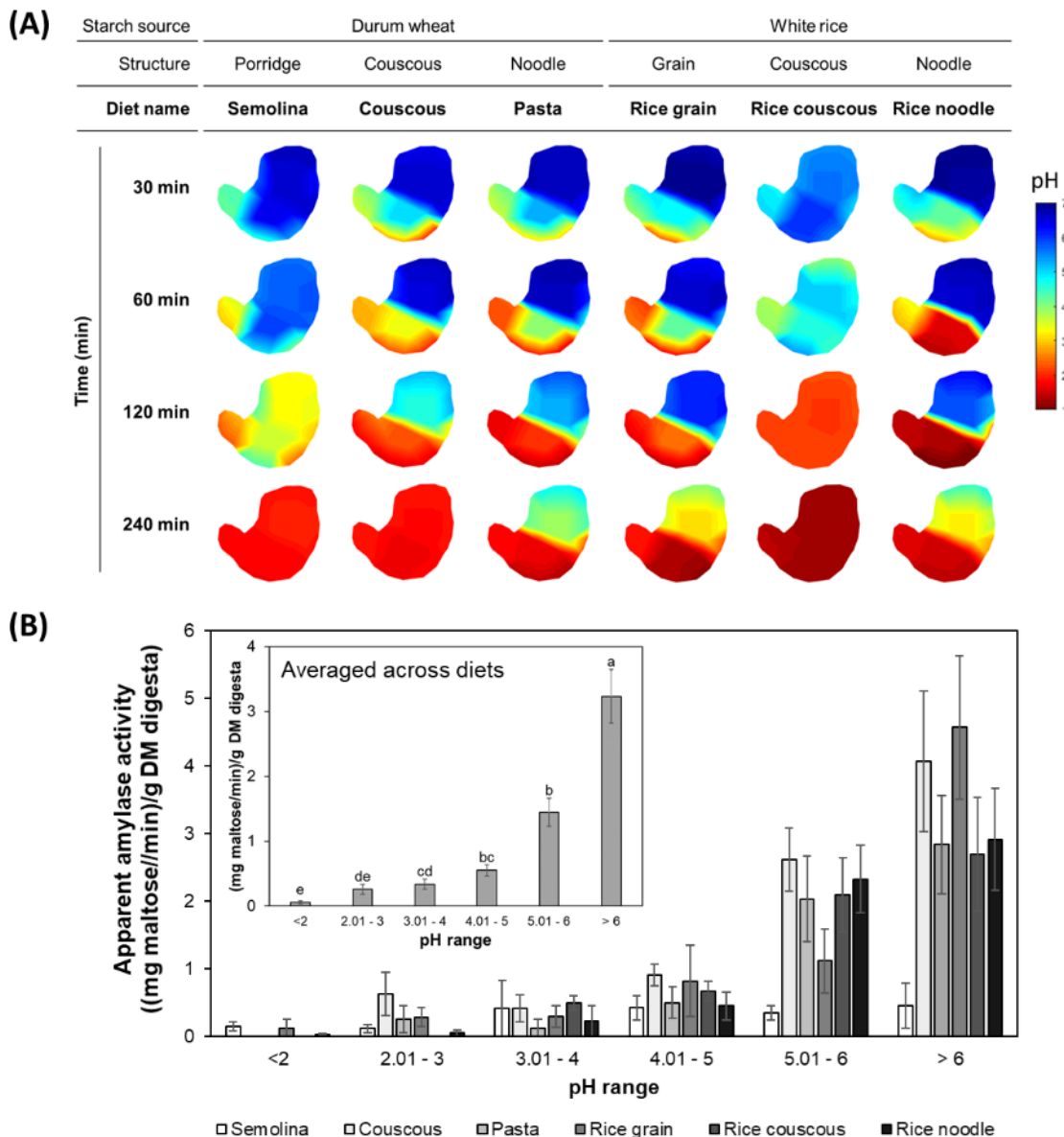


Figure 5.4 Color maps of intragastric pH distribution of the six study diets over 240 min gastric digestion (averaged from 4 to 6 pigs for each measurement location). Color maps for one diet type are located within the same column. The stomach shape was approximated from an image of a of full stomach from the study (A). Apparent salivary amylase activity at various digesta pH ranges for each diet. Averaged activity across diets is shown in the inset figure (B). Values in the inset figure that share the same letters are not significantly different ($p < 0.05$). Values are presented as mean \pm SE ($n = 215$ total data points).

Table 5.1 Statistical significance of diet type, digestion time, stomach region, digesta fraction (specific for maltose and NH₂ equivalent analyses), and dry matter remaining in the stomach (specific for intragastric pH) on the pH, chemical content, and particle size parameters of gastric digesta as well as total starch emptying.

Effect	pH [§]	mg maltose/g digesta	µg NH ₂ /g digesta	mg maltose/g digesta fraction	µg NH ₂ /g digesta fraction	D[4,3]	D[3,2]	SSA	d ₁₀	d ₅₀	d ₉₀	Starch gastric emptying
Group	**	*	*	NS	NS	****	**	*	*	*	****	NS
Diet	NS	****	****	****	**	****	****	****	****	****	****	**
Time	**	***	****	****	****	NS	*	*	NS	**	NS	****
Stomach region	****	****	*	****	**	*	*	**	NS	****	NS	
Digesta fraction		****	****	****	NS							
Diet × Time	NS	*	*	**	*	**	*	NS	NS	***	**	**
Diet × Stomach region	**	****	NS	****	*	***	**	**	****	*	****	
Diet × Digesta fraction		****	****	****	****							
Time × Stomach region	**	NS	NS	NS	NS	NS	NS	NS	NS	**	*	
Time × Digesta fraction		****	****	****	NS							
Diet × Time × Stomach region	***	NS	*	NS	*	NS	NS	NS	NS	NS	NS	
Diet × Time × Digesta fraction		****	****	****	*							
Diet × Stomach region × Digesta fraction		**	****	***	*							
Time × Stomach region × Digesta fraction		NS	NS	NS	NS							
Diet × Stomach region × Time × Digesta fraction		NS	NS	NS	NS							
DM left[†]	NS											
Diet × DM left	NS											
Time × DM left	NS											
Stomach region × DM left	****											
Diet × Time × DM left	NS											
Diet × Stomach region × DM left	*											
Stomach region × Time × DM left	*											
Diet × Stomach region × Time × DM left	***											

[§]For pH measurement, “stomach region” effect refers to the measurement location (Locations 1 – 10). [†]Dry matter remainig (DM left) data were taken from Chapter 4. Asterisk (*) symbols indicate different levels of statistical significance. *: $p < 0.05$; **: $p < 0.01$, ***: $p < 0.001$, ****: $p < 0.0001$. NS: not significant.

The observed variations in gastric acidification kinetics among the six diets may affect the remaining salivary amylase activity in the stomach. Although salivary amylase was not separated from the digesta, the relative apparent salivary amylase activity was able to be quantified in the gastric digesta (Figure 5.4B and D.1). The apparent activity ranged from 0 to 10.45 (mg maltose/min)/g DM digesta. This value is lower than salivary amylase activity reported in studies using specifically collected porcine or human saliva, with pre-gelatinized potato starch as the substrate (Freitas et al., 2018; Martens et al., 2020). Porcine salivary amylase was found to have optimal activity at between pH 3 and 8.5, with a maximum activity equivalent to 154.0 (mg maltose/min)/mg DM saliva at pH 7.8 (Martens et al., 2020). Meanwhile, human salivary amylase was reported to have optimal activity at between pH 3 and pH 7, with a maximum activity of 117.3 (mg maltose/min)/mL saliva at pH 6.2 (Freitas et al., 2018). The different procedure and unit used to measure the enzyme activity (i.e., per saliva amount in previous studies vs. per digesta amount in this study), in addition to the difference in substrate (i.e., potato starch in previous studies vs. starch present in the digesta in this study) makes the specific values in this study difficult to compare with previous studies. However, the trend of decreasing salivary amylase activity at lower pH in the present study was similar to those studies, despite variability in the results that might have occurred from the lack of standardization of starch content in the digesta sample (Table D.4) and variations in salivation level between pigs. This suggests that the method utilized in the current study may be useful to determine the relative amylase activity in gastric digesta as a consequence of different biochemical environment in the stomach.

Classification of the average apparent salivary amylase activity across all diets based on pH range (Figure 5.4B) showed that the apparent activity was the highest (3.23

± 0.42 (mg maltose/min)/g DM digesta) at pH >6. As the pH dropped to pH 5.01 - 6, the activity decreased to more than 50% of the highest activity (1.45 ± 0.22 (mg maltose/min)/g DM digesta), followed by gradual reduction as the pH became more acidic to an average of 0.06 ± 0.02 (mg maltose/min)/g DM digesta at pH <2. Although it is generally considered that salivary amylase becomes inactive at pH <3 (Brownlee et al., 2018; Freitas et al., 2018; Rosenblum et al., 1988), low amylase activity was still observed at pH between 2 and 4 in the present study. It is possible that oligosaccharides produced by amylolysis during early digestion times protected salivary amylase from inactivation by low pH and/or proteolysis by pepsin, likely due to specific binding of amylolysis products on the enzyme's active site (Rosenblum et al., 1988). Variations between diets in the reduction of the apparent activity at lower pH might be attributed to different specificity of salivary amylase on the starch sources, the enzyme affinity to the surface of the diets as affected by the diet and digesta structure (Dhital et al., 2017), the amount of available starch substrate (Table D.4), as well as different rate of gastric secretions (as discussed in Chapter 4) and extent of mixing between diets and gastric secretions that may lead to different rates of enzyme inactivation.

Among the six diets, semolina exhibited the lowest apparent salivary amylase activity even at pH >6 (0.45 ± 0.33 (mg maltose/min)/g DM digesta), possibly due to its porridge form and higher initial moisture content, which led to minimal mastication and lower saliva incorporation into the meal (Figure 5.5A). Meanwhile, higher apparent activity was found in the other diets at pH >6 (3.57 ± 0.43 (mg maltose/min)/g DM digesta, averaged across five diets at pH >6), which required longer time for mastication due to their larger initial particle size. This observation agrees with a mastication study that reported that food with softer texture and higher moisture content required less time

for mastication, and that the amount of saliva added to food bolus decreased with increasing food initial moisture content (Motoi et al., 2013).

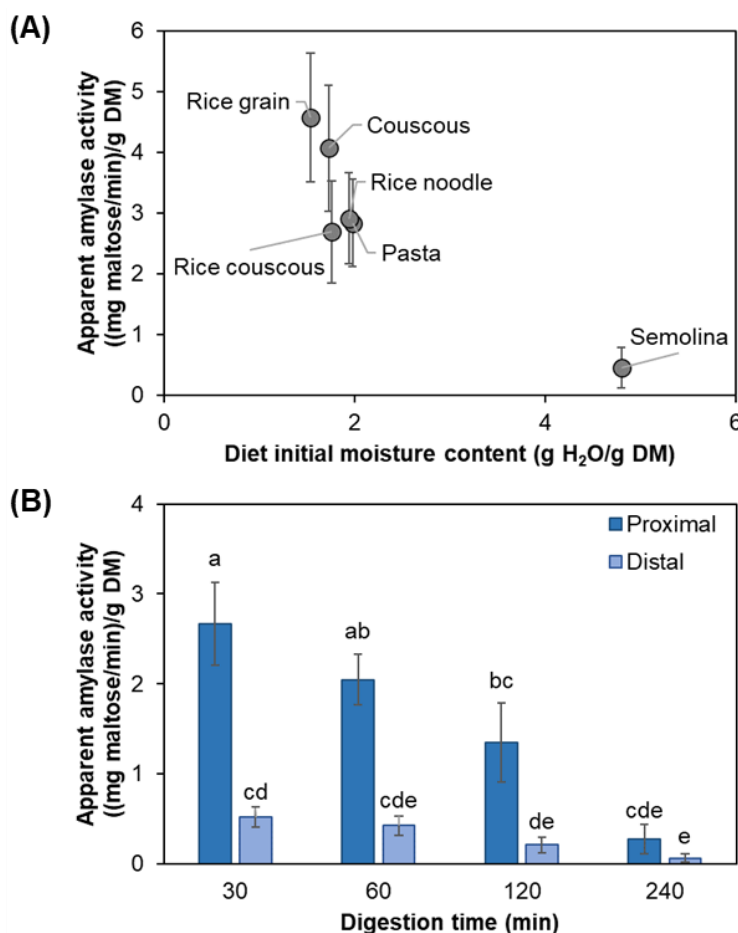


Figure 5.5 Relationship between apparent salivary amylase activity in gastric digesta with pH >6 (n = 33 data points) and the initial moisture content of each diet (A). Apparent salivary amylase activity at different digestion time points in the proximal and distal stomach, averaged across all diets (B). Values that shared the same letters are not significantly different ($p < 0.05$). All values are shown as means \pm SE ($20 \leq n \leq 31$).

5.4.2 Consequences of intragastric pH profile on the chemical composition and microstructure of gastric digesta

The digesta was separated into three fractions (liquid, solid, and suspended solid) and each fraction was analyzed separately for maltose and NH₂ content as indicators of starch and protein hydrolysis, respectively (Figure 5.6). It was hypothesized that the suspended solid fraction in the digesta was mainly a result of starch hydrolysis by

salivary amylase that remained active in the stomach and digested the surface of the diets (Dhital et al., 2017); this caused leaching of smaller particles from the diet matrices, or erosion of the matrix surface which removed small particles. This was supported by higher maltose in the suspended solid fraction compared to the liquid and solid fractions (i.e., 36.26 ± 1.55 mg/g suspended solid vs. 26.78 ± 1.06 mg/g liquid and 26.67 ± 1.20 mg/g solid, averaged across diet \times digestion time \times stomach region, $p < 0.0001$ for each comparison), and the absence of differences in NH_2 content across the fractions (Figure 5.7).

Maltose concentration in the wet digesta, which was distributed across liquid, solid, and suspended solid fractions, was significantly influenced by all factors and their interactions ($p < 0.05$), except any effects that included the stomach region \times time interaction (Table 5.1). Total maltose concentration in the digesta (summed across digesta fractions) ranged from 12.60 to 54.56 mg maltose/g digesta (Figure 5.6B), higher than the initial maltose concentration in the diets (1.68 ± 0.31 to 11.98 ± 0.93 mg maltose/g digesta; Table 5.2). As an indirect indicator for starch hydrolysis, total maltose concentration was compared to the total starch content in digesta. The values that range from 0.14 ± 0.01 to 0.32 ± 0.03 g maltose/g starch (calculated across proximal and distal stomach; Figure 5.8) were within the range of percent starch hydrolysis reported in previous *in vitro* digestion studies of various starch-rich foods (Freitas & Le Feunteun, 2019; Freitas et al., 2018; Woolnough et al., 2010). These observations are the combination of hydrolysis that occurred during mastication and gastric digestion. Maximum value of starch hydrolysis was achieved at 30 min gastric digestion for all smaller-sized diets (i.e., not long after mastication), at 120 min for rice grain, and 240 min for pasta and rice noodle. Since the starch hydrolysis increased during gastric digestion for larger-sized diets, these diets likely underwent additional

starch hydrolysis during gastric digestion. For the smaller-sized diets, the starch hydrolysis after 30 min gastric digestion may have occurred during either mastication or gastric digestion. However, the starch hydrolysis after mastication was not measured in the present study and represents a limitation in this analysis; this should be considered in future studies.

The starch hydrolysis during gastric digestion in larger-sized diets can be attributed to their longer gastric residence time/slower gastric emptying rate (see Section 5.4.3) and higher pH in the proximal stomach, which led to higher apparent salivary amylase activity in the proximal stomach up to 120 min digestion (averaged across digestion times and diets, Figure 5.5B; $p < 0.05$). Consequently, the proximal stomach digesta of pasta, rice noodle, and rice grain had significantly higher ($p < 0.001$) total maltose concentration (44.7 ± 1.7 vs. 25.6 ± 1.4 mg/g in the proximal and distal stomach, respectively, summed across digesta fractions and averaged across diet \times time; Figure 5.6B). In contrast, total maltose concentration in smaller-sized diets was not significantly different between stomach regions ($p = 0.8238$; Figure 5.6B), as a result of their easier mixing with gastric secretions that led to more rapid inactivation of salivary amylase. This can be seen in a higher proportion of liquid fraction in the digesta of smaller-sized diets (0.18 ± 0.01 vs. 0.44 ± 0.02 , for smaller- vs. larger-sized diets, averaged across diet \times stomach region \times time; Figure 5.6A) that indicates more presence of acidic gastric secretions.

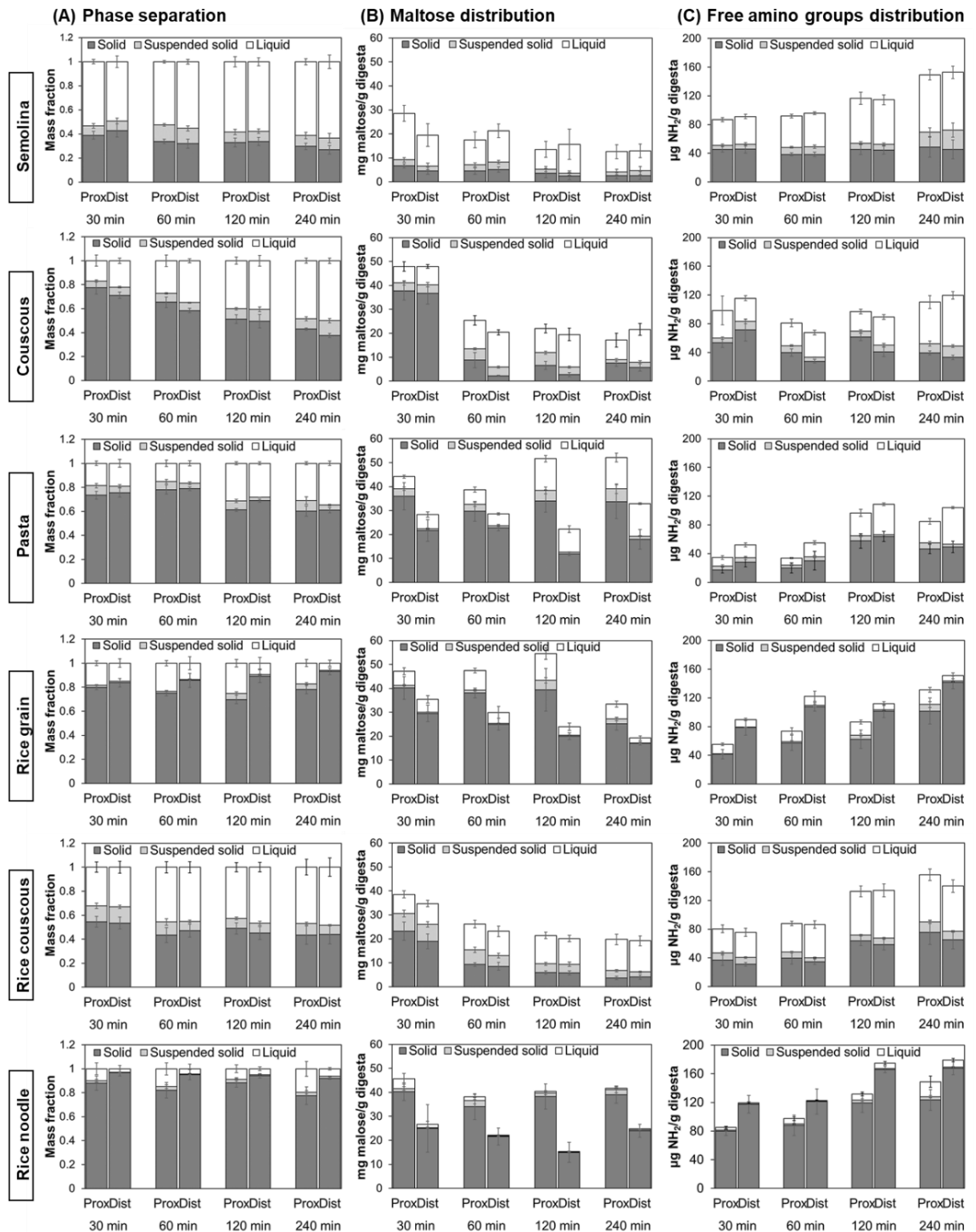


Figure 5.6 Phase separation of digesta to different fractions (column A), and maltose (column B) and free amino groups (column C) distribution in wet digesta fractions during 240 min digestion in the proximal (Prox) and distal (Dist) stomach regions. Figure within the same row represent digesta for one diet. Bars for solid (dark grey), suspended solid (light grey), and liquid (white) fractions are shown within each digesta sample. Values are presented as mean ± SE (5 ≤ n ≤ 6 for each diet × time × stomach region × digesta fraction). Results are presented in digesta wet basis to enable the comparison across different digesta fractions.

Table 5.2 Reducing sugar and free amino groups content in the cooked diets used in the study. Values are presented as mean \pm SEM ($n \geq 3$ for each property listed in one column). Diets with different superscripts within the same property are significantly different ($p < 0.05$).

Diet	Reducing sugar (mg maltose/g cooked diet)	Free amino groups ($\mu\text{g NH}_2/\text{g}$ cooked diet)
Semolina	2.58 ± 0.31^b	0.70 ± 0.07
Couscous	11.91 ± 2.03^a	0.83 ± 0.11
Pasta	11.98 ± 0.93^a	0.62 ± 0.43
Rice grain	2.07 ± 0.48^b	0.23 ± 0.04
Rice couscous	4.47 ± 1.50^b	0.28 ± 0.02
Rice noodle	1.68 ± 0.31^b	0.12 ± 0.01

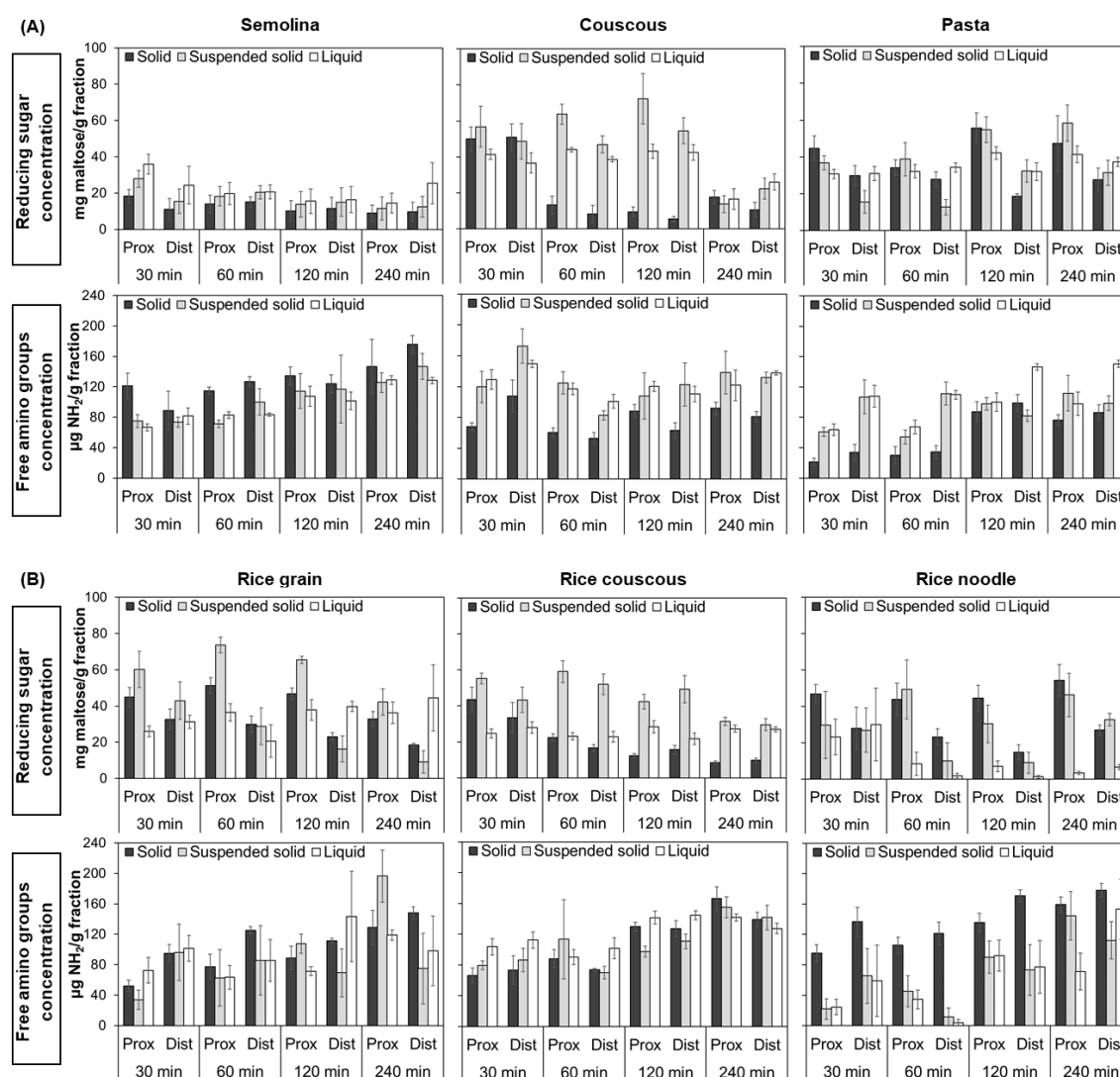


Figure 5.7 Concentrations of maltose and free amino groups in different wheat-based (A) or rice-based (B) digesta fractions during 240 min digestion in the proximal (prox) and distal (dist) stomach regions. Figures within the same column of either wheat-based (A) or rice-based (B) diets represent the digesta composition for one diet type. Values are presented as mean \pm SE ($5 \leq n \leq 6$ for each diet \times time \times stomach region \times digesta fraction).

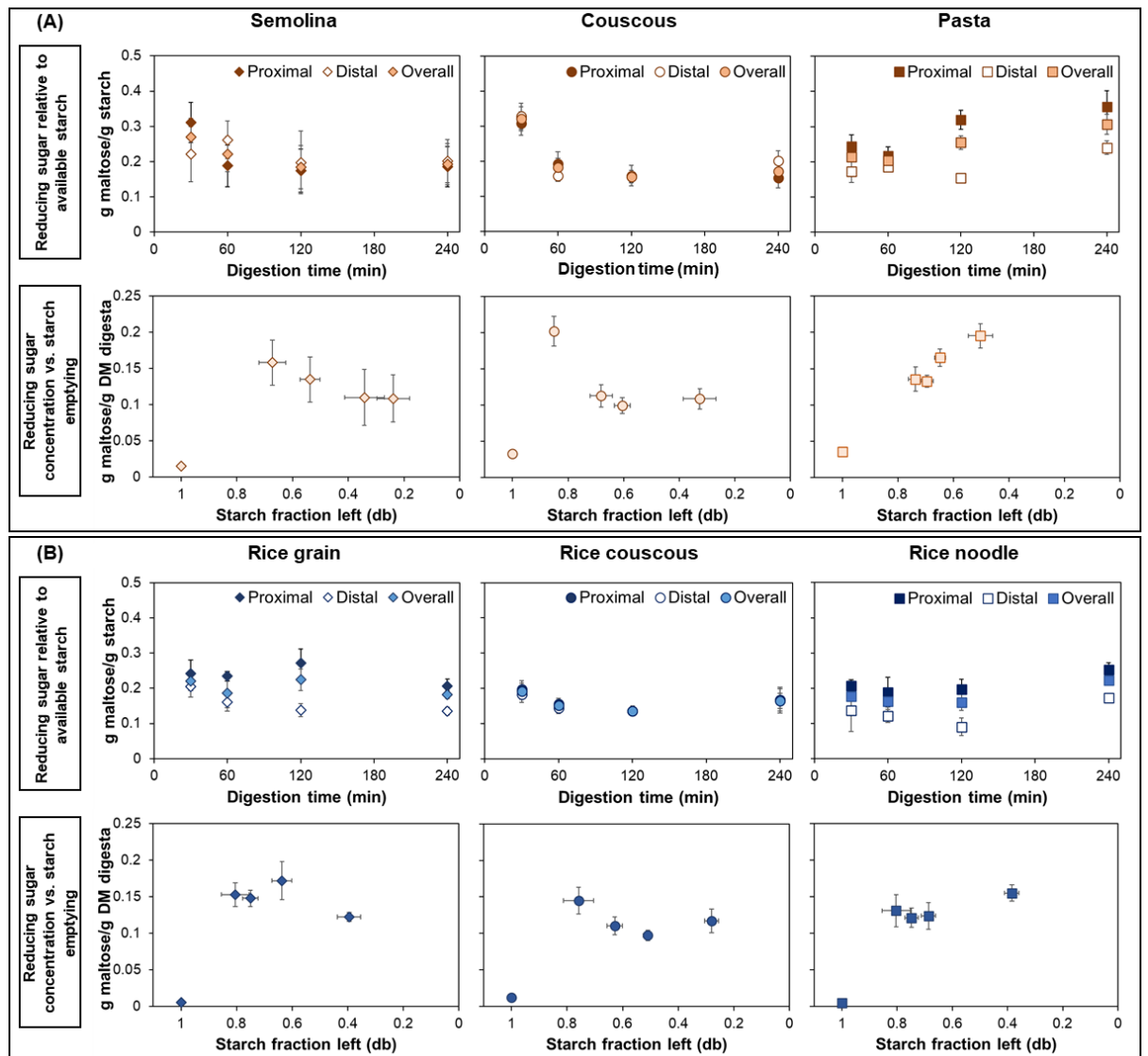


Figure 5.8 Comparison between reducing sugar and starch in wheat-based (A) and rice-based (B) digesta expressed as total reducing sugar (summed across the digesta fractions) relative to total available starch in the proximal stomach, distal stomach, and overall stomach (proximal + distal combined) digesta (first row) or concentration of reducing sugar (summed across the digesta fractions) in digesta dry matter as a function of starch emptying profile (second row). The x-axis of starch fraction left is presented in a reversed order for easier tracking of gastric emptying effect and changes in maltose concentration with increasing digestion time. Figures within the same column represent data for one diet type. Values are presented as mean \pm SE ($5 \leq n \leq 6$ for each data point presented in each graph).

NH₂ concentration in wet digesta was significantly influenced by all effects tested ($p < 0.05$), except diet \times stomach region, stomach region \times time \times digesta fraction, and diet \times stomach region \times time \times digesta fraction (Table 5.1). Although the percentage of protein hydrolysis was not calculated, protein hydrolysis in the diets was suggested by higher NH₂ concentration in the solid and suspended solid fractions (ranging from 22.62 ± 4.82 to 169.20 ± 9.45 $\mu\text{g/g}$, summed across the two fractions; Figure 5.6C) compared to initial NH₂ concentration in the diets (0.12 ± 0.01 to 0.83 ± 0.11 $\mu\text{g/g}$, Table 5.2). Increasing NH₂ concentration in the liquid fraction over time might also indicate protein hydrolysis. However, there might be interference from NH₂ in gastric secretions and saliva added during digestion to the values, which was not considered in this analysis. This interference, together with simultaneous gastric emptying, was a limitation in the estimation of total NH₂ available for protein hydrolysis calculation in this chapter. For future study with similar design, a control treatment (protein-free diet or empty stomach condition) should be considered to estimate total NH₂ present in digestive secretions in the stomach to correct for the values measured in gastric digesta. *In vitro* study should also be conducted to investigate the maximum NH₂ released, so that the extent of protein hydrolysis for each diet can be calculated.

Total NH₂ concentration was higher in the distal stomach digesta compared to the proximal stomach in pigs fed with pasta, rice grain, and rice noodle (89.6 ± 5.4 vs. 117.3 ± 5.4 $\mu\text{g/g}$ in the proximal and distal stomach, respectively, averaged across diet \times time \times digesta fraction, $p < 0.001$). In contrast, total NH₂ concentration in couscous, rice couscous, and semolina digesta were not significantly different between stomach regions (107.0 ± 4.1 vs. 107.0 ± 4.0 $\mu\text{g/g}$ in the proximal and distal stomach, respectively, averaged across diet \times time, $p = 0.9998$). Consistent trends between the smaller- and larger-sized diets in their maltose and NH₂ concentration indicate the

impact of variations in gastric mixing in the proximal and distal regions (Figure 5.4A) on nutrient hydrolysis (starch and protein in this case), due to changes in intragastric pH for digestive enzyme activity. Variations in protein hydrolysis may be due to the influence of gastric mixing on pepsin activity, which was not measured in the current study (as the focus of this project was on starch digestion), but merits future investigation.

Protein hydrolysis is particularly important for couscous, pasta, and rice grain that contained starch granules surrounded by a protein matrix (Figure 5.9), as it may affect the availability of starch granules for the subsequent small intestinal digestion and weaken the matrix structure, leading to increased breakdown. The other diets (semolina, rice couscous, rice noodle) did not have encapsulation of starch granules in protein matrix because the grinding processes (to produce the fine particles in the raw materials) disrupted the matrix, resulting in protein scattered between gelatinized starch network (Figure 5.9).

Microstructural changes in the diets and the digesta were also observed (Figure 5.9 and 5.10). Different arrangements of starch granules in the matrices of the diets were observed that may have impacted their susceptibility to enzymatic hydrolysis and breakdown during digestion: a mixture of solubilized and swollen starch with protein network interspersed between the matrix in semolina (Figure 5.9A); swollen starch granules arranged between a protein-starch matrix and/or pores in couscous (Figure 5.9F); swollen starch granules arranged tightly between starch-protein matrix in pasta (Figure 5.9K); swollen starch granules in a constricted matrix, with scattered starch-protein interactions in rice grain (Figure 5.9P); clusters of swollen starch granules within a porous matrix in rice couscous (Figure 5.9U); and a gel matrix comprised of

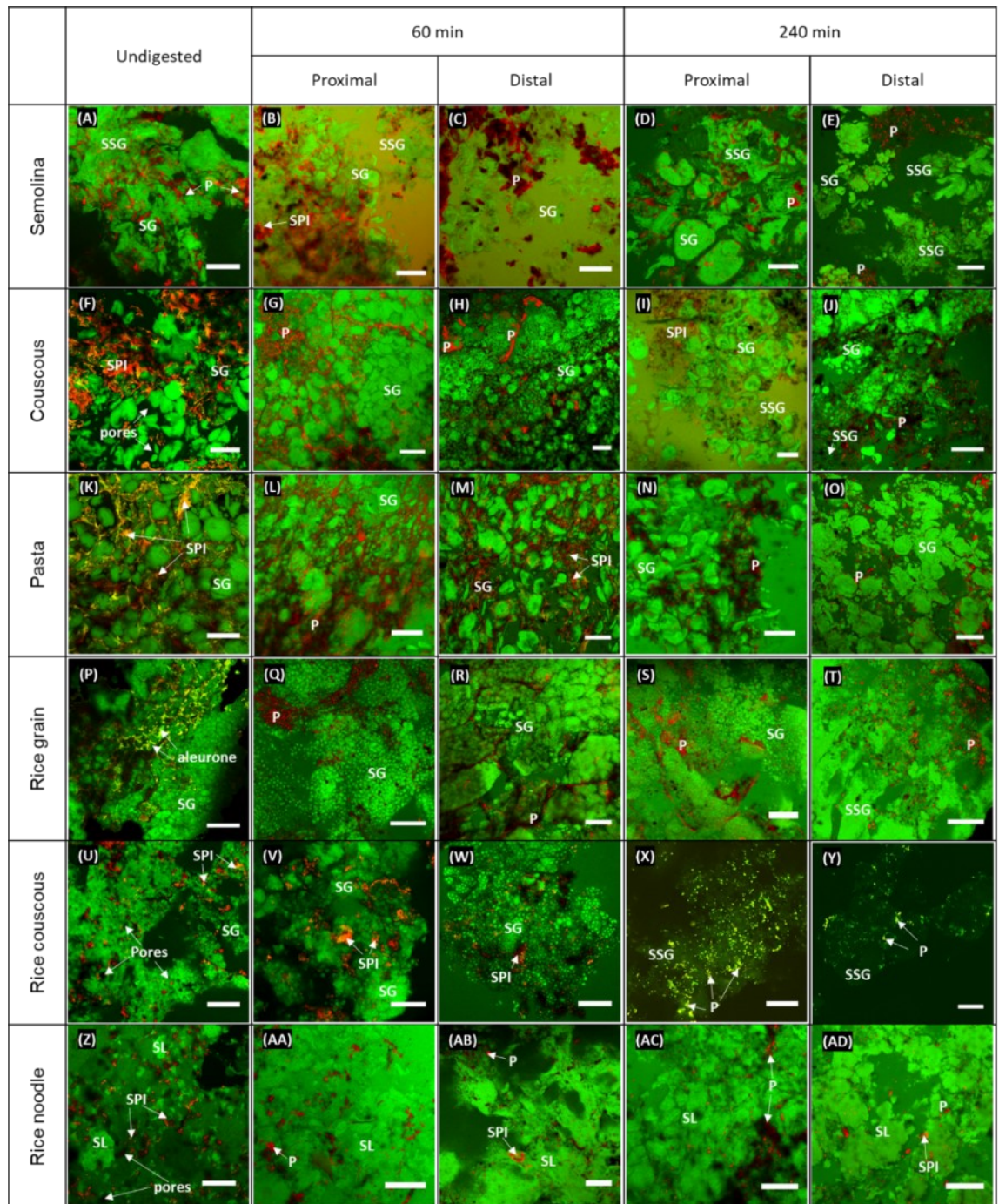


Figure 5.9 Confocal scanning laser microscopy images of the six diets before digestion, and after 60- or 240-min digestion in the proximal and distal stomach regions from selected pigs. Starch component (in the form of starch granules (SG), starch lumps (SL), or solubilized starch granules (SSG)), protein (P), and starch-protein interaction (SPI), and are indicated by green, red, and yellow/orange color in the figure, respectively. Scale bars represent 50 μ m.

lumps of solubilized starch granules in rice noodle (Figure 5.9Z) (Sangpring, Fukuoka, & Ratanasumawong, 2015; Tamura et al., 2016a; Zou, Sissons, Gidley, Gilbert, & Warren, 2015). Each diet had different surface morphology (Figure 5.10A, 5.10F, 5.10K, 5.10P, 5.10U, 5.10Z) and pores (except semolina). The surface morphology and presence of pores might have facilitated diffusion of saliva and gastric secretions to increase enzymatic and acidic hydrolysis in the stomach (Wu, Deng, et al., 2017).

The starch-protein interactions that were initially present in wheat-based diets became less prevalent at longer digestion times (Figure 5.9B-E, 5.9G-J, 5.9L-O), especially in the distal stomach. This might be due to hydrolysis of protein by pepsin, as evidenced by a general increase in NH_2 content in the digesta over time (Figure 5.6C). For example, solubilization of starch granules was observed in couscous, rice couscous, and semolina at longer digestion times (Figure 5.9D-E, 5.9I-J, 5.9X-Y) as a result of dilution of the digesta by gastric secretions over time (Figure 5.6A and 5.11**Error! Reference source not found.**). Semolina was the only diet that had a limited number of pores in the undigested structure. However, pores were observed in semolina digesta (Figure 5.10A-E), which might be due to digestion by salivary amylase and acid hydrolysis. Changes on the surface of couscous and rice couscous digesta were also observed, with the presence of smaller fragments at longer digestion times (Figure 5.10G-J and 5.10U-Y).

In pasta, rice grain, and rice noodle, the presence of more pores in the digesta (compared to the undigested structure; Figure 5.10K-O, 5.10P-T, 5.10Z-AD) indicated that amylolysis (more pores and rough-surfaced layered structures) and acid hydrolysis (more pores and fragmented structures) occurred at least on the surface of the diets (Li et al., 2013). In some digesta samples, it was observed that starch granules or starch

lumps were more swollen, possibly due to an increased uptake of digestive secretions

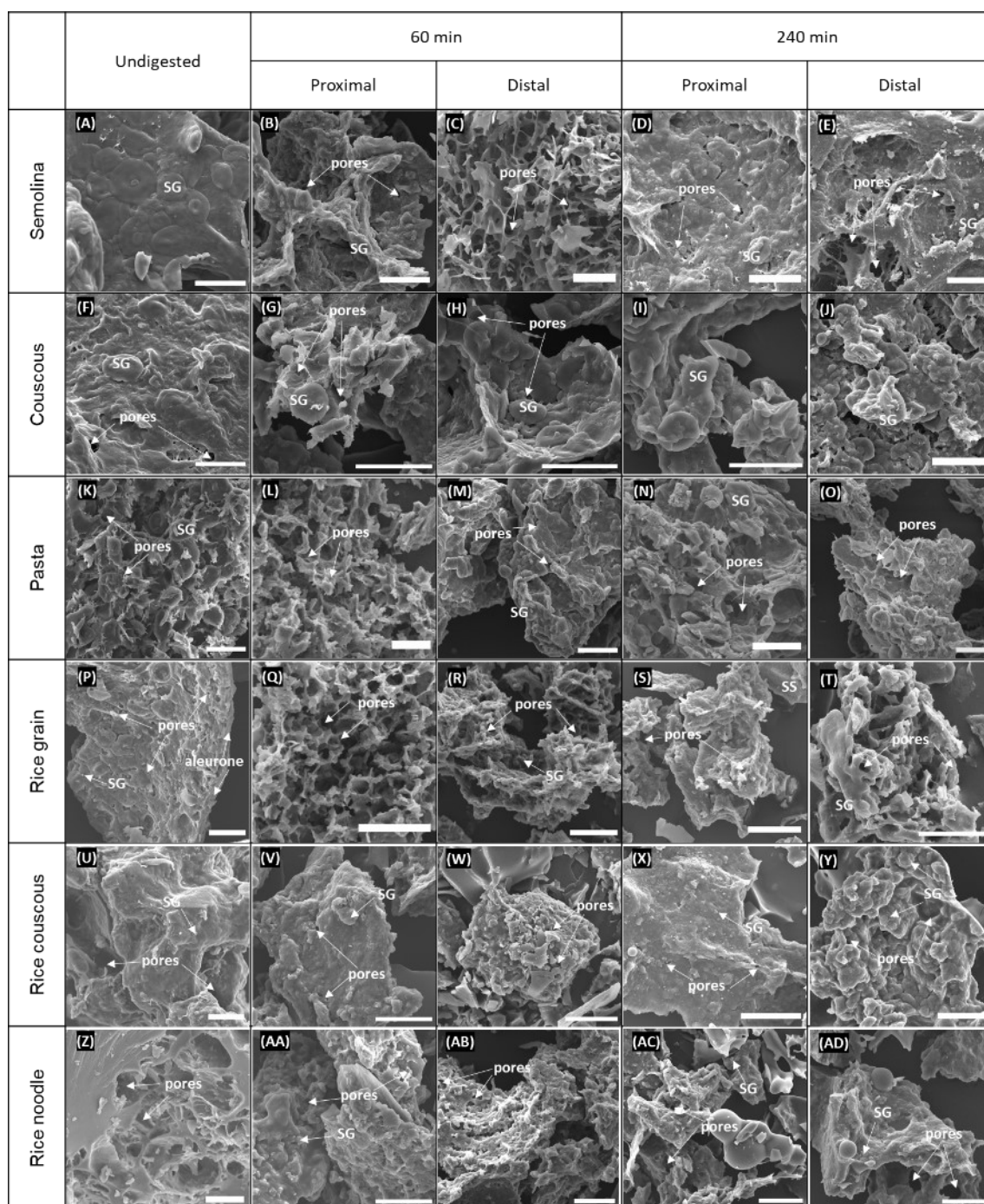


Figure 5.10 Scanning electron microscope (SEM) images of the six diets before digestion, and after 60- or 240-min digestion in the proximal and distal stomach regions from selected pigs. Starch granules embedded in the matrix or leached into the surface of the diet or digesta are indicated with SG in the pictures, and examples of visible pores on the surface of the structures are shown. Scale bars represent 50 μ m.

into the digesta (as reported in Chapter 4; Figure 4.1 and Table 4.4). Nevertheless, these trends may not be fully representative of the whole digesta, as they were only observed on small samples that may have had varying pH and biochemical conditions, depending on their specific location in the stomach. Moreover, there might be artifacts due to sample preparation that can affect the interpretation of the observations. Further investigation using an *in vitro* system with controlled amounts of enzymes and digestive fluids is needed to test the hypotheses arising from the microstructural changes observed in this thesis.

5.4.3 Link between starch hydrolysis during gastric digestion with physical breakdown of the diets and gastric emptying of starch

PSD of large particles of digesta from this study was presented in Chapter 4 to investigate physical breakdown during gastric digestion. In the current study, PSD of suspended solid fraction of digesta was investigated to reflect the impact of biochemical changes during digestion on the physical breakdown of diets that occurred as a surface phenomenon. The volume-mean diameter ($D[4,3]$), surface mean diameter ($D[3,2]$), and specific surface area (SSA) of the digesta were significantly influenced by diet type ($p < 0.0001$), stomach region and diet \times stomach region interaction ($p < 0.05$), and batch of pigs ($p < 0.05$). Time was a significant variable for $D[3,2]$ and SSA ($p < 0.05$). Diet \times time was significant for $D[4,3]$ and $D[3,2]$ ($p < 0.05$). Limited trends can be observed in these PSD parameters (Table 5.3), although SSA was expected to indicate differences, considering that starch hydrolysis is a surface phenomenon (Dhital et al., 2017). The 10th, 50th, and 90th percentile diameters (d_{10} , d_{50} , and d_{90}) were also quantified (Table D.2). Nevertheless, these parameters may not sufficiently describe the changes in PSD during digestion due to the multimodality of the PSD (Figure 5.12A-F

and 5.13). As such, additional particle size parameters were analyzed: location, spread, and volume of each peak of the multimodal distribution (Table D.3).

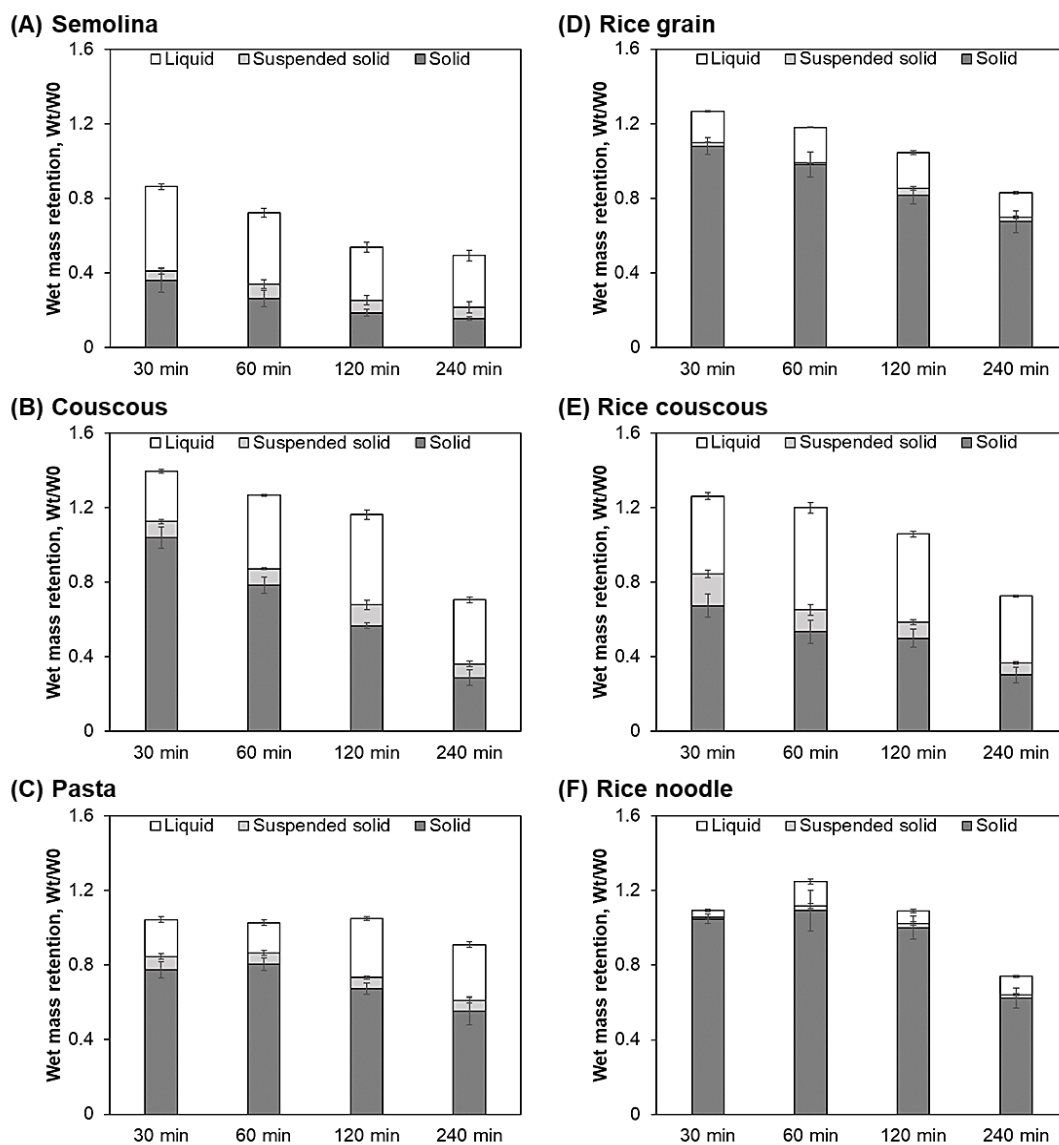


Figure 5.11 Wet mass retention of digesta (Figure 4.8B and D) integrated with the phase separation data (Figure 5.6A) to estimate the total fraction (on a wet basis) of liquid, suspended solids, and solids in digesta of semolina (A), couscous (B), pasta (C), rice grain (D), rice couscous (E), and rice noodle (F). Wet mass retention data was obtained from Chapter 4. Values are shown as mean \pm SE ($4 \leq n \leq 6$ for each individual component of each bar graph).

Table 5.3 Mean diameters and specific surface area (mean \pm SE, $4 \leq n \leq 6$) of the suspended solid fraction of *in vivo* gastric digesta. Within the same row, significantly different values are noted by superscripts abcd ($p < 0.05$). For each particle size parameter, no significant difference was found between values across digestion times (i.e., data within the same column (diet \times stomach region)).

	Semolina		Couscous		Pasta		Rice grain		Rice couscous		Rice noodle	
Time (min)	Proximal	Distal	Proximal	Distal	Proximal	Distal	Proximal	Distal	Proximal	Distal	Proximal	Distal
Volume weighted mean, D[4,3] (μm)												
30	306.59 \pm 35.65 ^a	267.77 \pm 28.36 ^a	210.01 \pm 41.48 ^{ab}	142.18 \pm 42.56 ^{abc}	254.39 \pm 34.57 ^{ab}	131.58 \pm 26.45 ^{abc}	265.18 \pm 28.60 ^a	270.41 \pm 5.08 ^a	95.71 \pm 8.79 ^{abc}	51.79 \pm 6.41 ^c	81.47 \pm 30.71 ^c	107.26 \pm 37.08 ^{bc}
60	181.07 \pm 24.51 ^{abc}	149.92 \pm 31.91 ^{abc}	140.47 \pm 14.20 ^{abc}	196.70 \pm 57.89 ^{ab}	162.64 \pm 30.03 ^{abc}	90.04 \pm 9.91 ^{abc}	270.85 \pm 46.91 ^a	250.85 \pm 19.34 ^a	99.54 \pm 14.41 ^{abc}	74.33 \pm 11.20 ^{bc}	57.42 \pm 6.81 ^c	94.41 \pm 24.25 ^{bc}
120	204.94 \pm 26.26 ^{ab}	202.64 \pm 23.97 ^{ab}	162.16 \pm 44.06 ^{abc}	174.44 \pm 43.52 ^{abc}	119.43 \pm 23.81 ^{abc}	78.94 \pm 6.42 ^{bc}	259.73 \pm 34.09 ^a	261.60 \pm 8.71 ^a	154.85 \pm 31.01 ^{abc}	180.61 \pm 43.54 ^{abc}	69.97 \pm 11.41 ^c	90.48 \pm 12.97 ^{bc}
240	208.82 \pm 12.13 ^{abcd}	205.69 \pm 17.53 ^{abcd}	320.36 \pm 56.88 ^a	294.45 \pm 64.01 ^{ac}	122.30 \pm 31.07 ^{bcde}	90.11 \pm 10.98 ^{bde}	250.21 \pm 30.81 ^{abcd}	254.39 \pm 16.51 ^{abcd}	130.49 \pm 44.63 ^{bde}	98.93 \pm 26.65 ^{bde}	78.76 \pm 18.94 ^c	83.02 \pm 28.45 ^c
Surface weighted mean, D[3,2] (μm)												
30	45.95 \pm 2.27 ^a	39.22 \pm 2.88 ^{ab}	24.50 \pm 2.09 ^{abce}	19.88 \pm 1.13 ^{bcd}	34.44 \pm 3.20 ^{ab}	23.42 \pm 1.47 ^{abcd}	24.97 \pm 1.78 ^{abce}	34.71 \pm 11.23 ^{abc}	15.97 \pm 0.77 ^{def}	12.80 \pm 1.04 ^f	16.23 \pm 1.72 ^{df}	17.42 \pm 1.30 ^{cdf}
60	31.96 \pm 1.17 ^a	29.51 \pm 1.99 ^a	20.72 \pm 0.97 ^{abc}	21.90 \pm 1.94 ^{abc}	28.22 \pm 2.94 ^a	23.92 \pm 1.46 ^{ab}	23.19 \pm 2.71 ^{abc}	22.42 \pm 1.71 ^{abc}	16.72 \pm 1.41 ^{bc}	15.57 \pm 1.33 ^c	15.85 \pm 0.43 ^{bc}	17.15 \pm 1.37 ^{bc}
120	34.82 \pm 1.93 ^a	34.20 \pm 2.05 ^a	20.97 \pm 1.29 ^{abc}	19.51 \pm 1.23 ^{abcd}	24.70 \pm 2.32 ^{ab}	22.16 \pm 0.92 ^{ab}	23.14 \pm 2.18 ^{abc}	21.93 \pm 0.76 ^{abc}	16.58 \pm 1.08 ^{bcd}	15.52 \pm 0.95 ^{cd}	15.04 \pm 0.77 ^d	20.03 \pm 2.63 ^{bcd}
240	32.57 \pm 1.80 ^a	31.44 \pm 1.51 ^{ab}	32.70 \pm 9.15 ^{ab}	24.77 \pm 3.02 ^{ab}	24.35 \pm 3.30 ^{ab}	21.79 \pm 0.77 ^{ab}	19.63 \pm 1.55 ^{bcd}	21.04 \pm 0.60 ^{abc}	13.75 \pm 1.00 ^{de}	12.52 \pm 0.60 ^c	14.61 \pm 0.51 ^{cde}	14.39 \pm 1.11 ^{de}
Specific surface area (m^2/kg)												
30	0.121 \pm 0.015 ^f	0.133 \pm 0.019 ^{ef}	0.246 \pm 0.017 ^{bcd}	0.295 \pm 0.018 ^{abcd}	0.155 \pm 0.027 ^{def}	0.251 \pm 0.014 ^{bcd}	0.245 \pm 0.017 ^{bcd}	0.228 \pm 0.033 ^{cdef}	0.368 \pm 0.022 ^{abc}	0.476 \pm 0.037 ^a	0.384 \pm 0.031 ^{ab}	0.336 \pm 0.02 ^{abc}
60	0.186 \pm 0.006 ^b	0.201 \pm 0.014 ^b	0.256 \pm 0.04 ^{ab}	0.273 \pm 0.02 ^{ab}	0.215 \pm 0.017 ^{ab}	0.249 \pm 0.016 ^{ab}	0.276 \pm 0.048 ^{ab}	0.270 \pm 0.019 ^{ab}	0.356 \pm 0.041 ^{ab}	0.381 \pm 0.032 ^a	0.366 \pm 0.012 ^{ab}	0.350 \pm 0.025 ^a
120	0.167 \pm 0.007 ^c	0.168 \pm 0.012 ^{bc}	0.242 \pm 0.047 ^{abc}	0.305 \pm 0.016 ^{ac}	0.243 \pm 0.023 ^{abc}	0.265 \pm 0.013 ^{abc}	0.257 \pm 0.035 ^{abc}	0.276 \pm 0.011 ^{abc}	0.344 \pm 0.025 ^a	0.383 \pm 0.028 ^a	0.391 \pm 0.024 ^a	0.320 \pm 0.044 ^{ac}
240	0.204 \pm 0.028 ^c	0.183 \pm 0.009 ^c	0.221 \pm 0.043 ^c	0.248 \pm 0.026 ^{de}	0.248 \pm 0.027 ^{de}	0.267 \pm 0.008 ^{cde}	0.299 \pm 0.024 ^{abcde}	0.284 \pm 0.011 ^{bde}	0.437 \pm 0.026 ^{abc}	0.474 \pm 0.023 ^a	0.400 \pm 0.014 ^{abcd}	0.419 \pm 0.03 ^{ab}

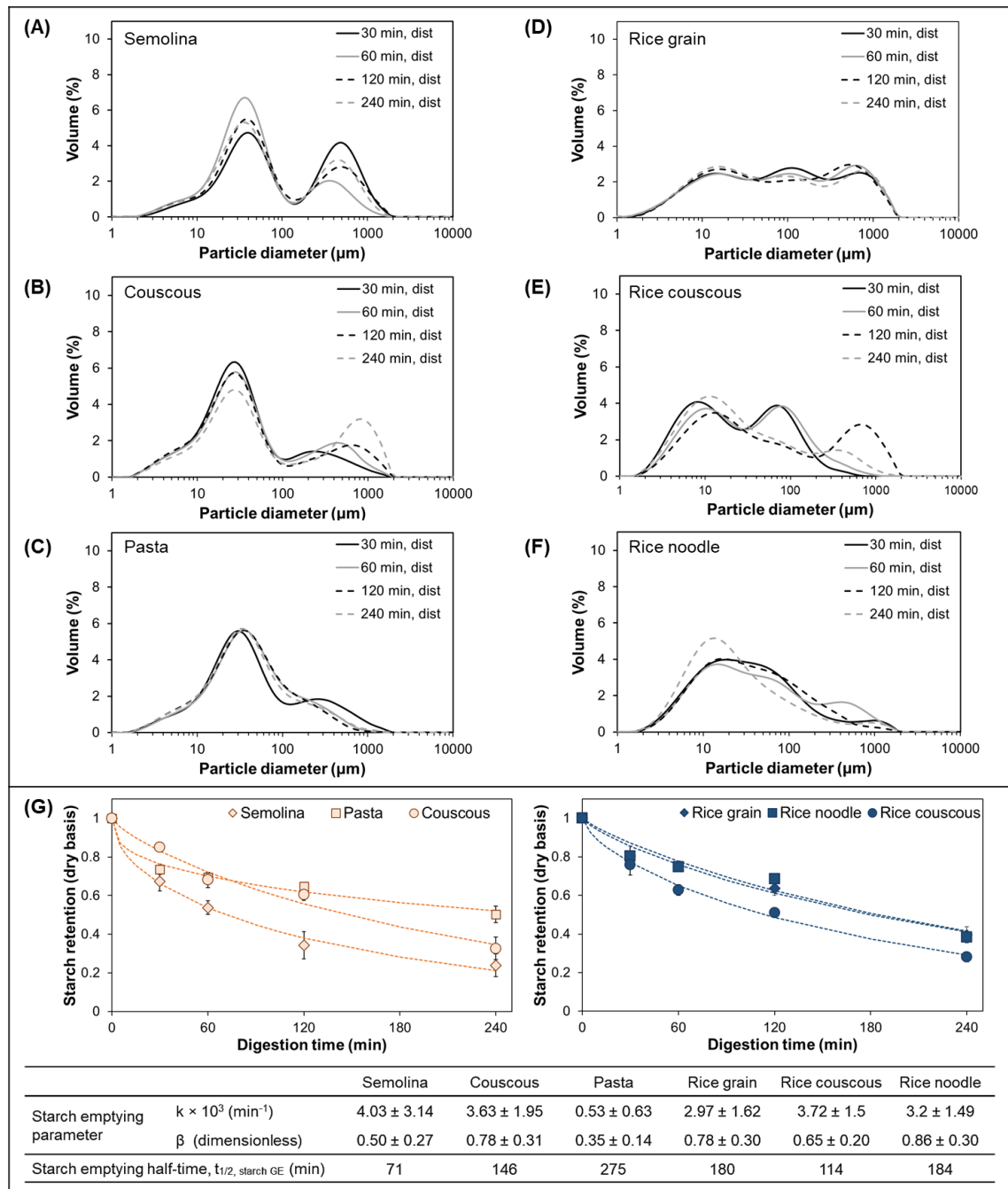


Figure 5.12 Particle size distribution of the suspended solid fraction of distal (dist) gastric digesta of pigs fed with semolina (A), couscous (B), pasta (C), rice grain (D), rice couscous (E), and rice noodle (F) from 30 – 240 min gastric digestion. Curves represent the average from 4 to 6 pigs. Individual PSD plots with error shades to indicate the range of the distribution are given in Figure D.2 to D.7. Starch gastric emptying profiles of wheat-based (left) and rice-based (right) diets during 240 min gastric digestion (G). Each data point represents mean \pm SE ($5 \leq n \leq 6$ for each point). Dashed lines indicate the predicted starch emptying profile based on obtained gastric emptying parameters (listed in the table below the graphs; predicted parameter \pm 95% confidence interval) from fitting of data from each diet to Eqn. 5.1. Starch emptying half-time was calculated by fitting the gastric emptying parameters to Eqn. 5.1 to obtain $X_t/X_0 = 0.5$.

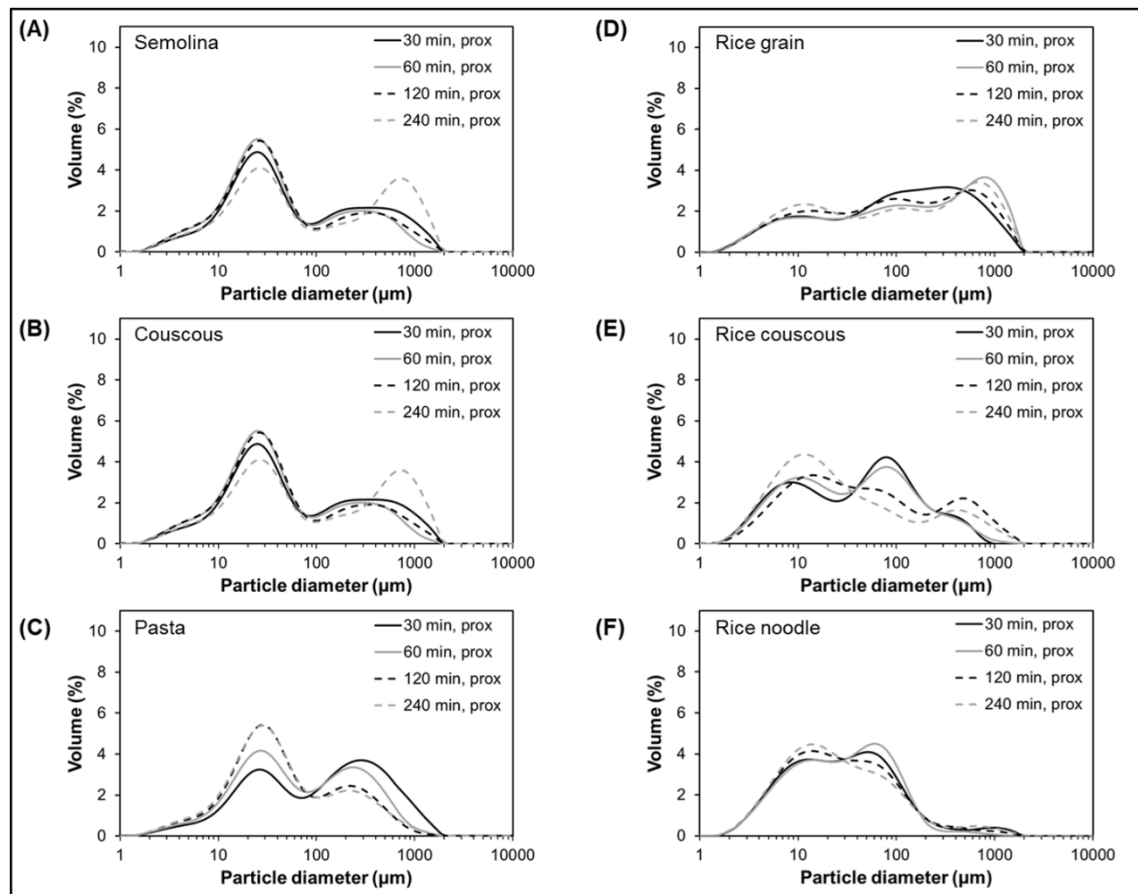


Figure 5.13 Particle size distribution of the small particle fraction of proximal (prox) gastric digesta of pigs fed with (A) semolina, (B) couscous, (C) pasta, (D) rice grain, (E) rice couscous, and (F) rice noodle after 30, 60, 120, or 240 min digestion. Each curve (diet \times time \times stomach region) was plotted using averaged data from 4 to 6 pigs. Individual PSD plots with error shades to indicate the range of the distribution are given in Figure D.2 to D.7.

Visualization of the PSD of the suspended solid fraction showed that semolina, pasta, and rice noodle had three peaks, whereas couscous, rice couscous, and rice grain had up to four peaks in their distribution (Figure 5.12A-F and 5.13). For wheat-based diets, the first peak occurred at between 4.6 and 9.4 μm ; the second peak occurred at between 26.2 and 35.6 μm . The second peak is close to the diameter of Durum wheat granules (20 to 25 μm) (Abecassis, Cuq, Boggini, & Namoune, 2012), thus particles occurring within the first peak range might be digested or dissolved starch granules. For rice-based diets, the first peak occurred at between 4.4 and 14.6 μm , which is within the range of rice starch granule diameter (3 to 15 μm) (Ramadoss et al., 2019); the second peak appeared at between 11.3 and 152.8 μm . Across all six diets, the third peak

occurred between 85.3 to 959.6 μm ; and the fourth peak (when present) occurred between 425.5 to 918.6 μm . It was hypothesized that the occurrence of peaks not attributed to starch granules might be attributed to surface erosion (due to starch hydrolysis), and chipping and fragmentation of digesta particles (Drechsler & Ferrua, 2016) due to mechanical breakdown (either by gastric contractions or friction between particles in the stomach). Different PSD profiles between the diets and their changes over time were thought to be correlated with the extent of biochemical breakdown in the stomach, gastric emptying, and subsequent intestinal digestion. However, simultaneous mechanical breakdown, gastric secretion addition, and material emptying that occur in addition to biochemical breakdown (as shown in Chapter 4), as well as dissolution of the particles into the dispersing agent during measurement, may interfere with the PSD results from the suspended solid fraction, thus limiting the interpretation of the observations.

Gastric emptying of starch was significantly influenced by diet type, time, and diet \times time interaction ($p < 0.01$). Starch emptying half-time ($t_{1/2, \text{starch GE}}$) of the diets ranged from 71 min (semolina) to 275 min (pasta), where smaller-sized diets had shorter $t_{1/2, \text{starch GE}}$ (71 to 146 min) than the larger-sized diets (180 to 275 min). The $t_{1/2, \text{starch GE}}$ had the same order to a previously reported trend in dry matter emptying half-time for the same diets (Chapter 4, Section 4.4.7). Distinction in the $t_{1/2, \text{starch GE}}$ between smaller- and larger-sized diets signifies the impact of food initial macrostructure not only on gastric mixing, but also starch emptying rate, by affecting the physical breakdown mechanisms.

Semolina, couscous and rice couscous had small initial particle size ($d < 2 \text{ mm}$); they did not require extensive mechanical breakdown prior to gastric emptying and were able to be emptied more easily. It was hypothesized that the gastric emptying of the smaller-

sized diets was primarily controlled by meal dilution or dissolution by gastric secretions. This can be seen in consistently increasing liquid proportion in phase separation of their digesta (Figure 5.11**Error! Reference source not found.**) as a result of solid emptying and more addition of gastric secretions. In contrast, pasta, rice grain, and rice noodle had larger initial particle size, and they were reported to have physical breakdown rates (quantified as softening half-times) that were at least a magnitude higher than those of smaller-size diets (Chapter 4, Section 4.4.6). Consequently, their starch emptying process may be limited by the rate of physical breakdown rather than the rate of dilution or dissolution by gastric secretions. In the digesta of larger-sized diets, there was more solid fraction (a mixture of dry matter, moisture in the cooked diet, and absorbed gastric secretions) compared to the liquid and suspended solid fractions at all digestion times (Figure 5.11**Error! Reference source not found.**). Biochemical breakdown during gastric digestion was assumed to aid their physical breakdown by weakening the food matrix (through diffusion of gastric secretions and enzymatic processes) and eroding the surface of the diets (through enzymatic processes) to generate the suspended solid fraction. The suspended solid fraction, together with liquid fraction, might contribute to ensuring constant material emptying from the stomach (as observed in their starch emptying profile; Figure 5.12G) – since gastric emptying process prioritizes liquid and particles <2 mm, or occasionally up to 7 mm (Coupe et al., 1991).

Interestingly, while starch was emptied over time for all diets, the concentration of maltose in digesta (which was expected to decrease as a result of secretion addition and gastric emptying) did not decrease until 120 min digestion for rice grain, or did not decrease at any digestion time for pasta and rice noodle (Figure 5.8). This suggests an accumulation of starch hydrolysis products in the stomach for larger-sized diets, which

can be attributed to extended salivary amylase activity in the proximal stomach due to their slower gastric mixing and breakdown rate. The accumulation might also be enhanced by slower delivery of materials (a mixture of mostly starch and hydrolysis products, together with other non-starch components) to the small intestine, which might also impact physiological responses related to gastric emptying that were not measured in this study. For example, a negative feedback mechanism by the presence of hydrolyzed starch or glucose in the small intestine was reported to reduce gastric emptying rate (Brener et al., 1983; Lin et al., 1992).

Finally, the different $t_{1/2, \text{starch GE}}$ of the six diets, and the maltose content of emptied fractions were expected to affect the subsequent small intestinal digestion and glucose absorption, which were outside the scope of this chapter and will be discussed in Chapter 6. The liquid and suspended solid fractions of digesta from smaller-sized diets contained higher maltose concentration than those of larger-sized diets (14.58 ± 0.74 vs. 7.15 ± 0.64 mg/g digesta, respectively, averaged across diet \times time for each diet classification, $p < 0.0001$; Table 5.4). Combined with the shorter $t_{1/2, \text{starch GE}}$ of smaller-sized diets, this might imply there was a high rate of delivery of starch and its hydrolysis products to the small intestine for couscous, rice couscous, and semolina, which might impact the rate of small intestinal digestion and glucose absorption. Findings from clinical and *in vitro* dynamic digestion studies on various couscous products showed that millet couscous had a slow gastric emptying rate and slower starch hydrolysis during gastric digestion compared to wheat couscous, resulting in lower glycemic response in humans (Cisse et al., 2018; Hayes et al., 2020). Therefore, it was expected in this study that diets with smaller particle size and easier mixing with gastric secretions would result not only in faster emptying of starch and its hydrolysis products, but also more rapid conversion to glucose in the small intestine, and

subsequently higher glycemic response. The relationship between food structure, physical and biochemical changes during gastric digestion, and small intestinal digestion will be discussed in Chapter 6.

Table 5.4 Concentration of maltose in the suspended solid and liquid fractions in the overall digesta (proximal and distal stomach regions combined together) at different digestion time points (n = 258 data points). The values were significantly affected by diet type ($p < 0.0001$) and diet \times time ($p = 0.0154$).

Diet	Time (min)	Maltose in liquid + suspended solid fraction of digesta (mg/g digesta)
Semolina	30	18.52 \pm 4.08
	60	14.65 \pm 6.36
	120	11.61 \pm 0.60
	240	10.16 \pm 5.33
Couscous	30	10.95 \pm 1.91
	60	17.36 \pm 1.39
	120	15.93 \pm 1.97
	240	12.2 \pm 2.53
Pasta	30	7.60 \pm 1.10
	60	7.66 \pm 0.82
	120	14.65 \pm 0.98
	240	16.88 \pm 1.90
Rice grain	30	6.48 \pm 1.43
	60	7.18 \pm 1.09
	120	10.89 \pm 2.01
	240	5.93 \pm 0.98
Rice couscous	30	15.65 \pm 1.88
	60	15.91 \pm 1.83
	120	14.92 \pm 1.48
	240	16.12 \pm 2.14
Rice noodle	30	3.79 \pm 2.12
	60	2.57 \pm 1.02
	120	1.34 \pm 0.57
	240	1.89 \pm 0.72

5.5 Conclusions

Results obtained in the present chapter indicate the effect of initial macrostructure of food on the mixing between acidic gastric secretions with the ingested food bolus, which influenced the biochemical environment for starch hydrolysis in the proximal and

distal stomach regions. Pasta, rice grain, and rice noodle, which had larger initial particle size, showed higher intragastric pH in the proximal stomach digesta compared to that of the distal stomach until 240 min gastric digestion. Meanwhile, couscous, rice couscous, and semolina, which had smaller initial particle size, formed digesta with uniform pH by the end of 240 min digestion. Consequently, the digesta of the larger-sized diets had an extended period of salivary amylase activity in the proximal stomach, which increased starch hydrolysis in the digesta. Smaller-sized diets, which had more rapid gastric content acidification, had faster inactivation of salivary amylase. However, they were rapidly hydrolyzed by salivary amylase in the early digestion times or during mastication, as suggested by similarly high maltose concentration in both proximal and distal stomach digesta over time.

The different starch hydrolysis between the larger- and smaller-sized diets during gastric digestion might be related to the breakdown mechanisms, subsequently affecting the starch emptying rate. Smaller-sized diets could easily be broken down by dilution or dissolution by gastric secretions, hence could be emptied rapidly. Larger-sized diets were hypothesized to be broken down by simultaneous biochemical and mechanical breakdown in the stomach, where biochemical breakdown aids the physical breakdown of the diets. The findings suggest the importance of remaining salivary amylase activity in aiding the physical breakdown of larger-size diets. The suspended solid fraction generated during gastric digestion was rich in maltose, and it might affect the subsequent small intestinal digestion. Further implication of these findings on small intestinal digestion and glucose absorption is investigated in Chapter 6.

CHAPTER 6. The impact of gastric digestion and emptying of rice- and wheat-based foods on their digestion in the small intestine, glucose absorption, and glycemic response

6.1 Abstract

The impact of gastric processing on starch digestion in the small intestine and glycemic response was studied using a growing pig model. Cooked white rice- and Durum wheat-based diets of varying initial structures (rice grain, semolina porridge, wheat and rice couscous, and wheat- and rice noodle) were investigated. Growing pigs were fed with 250-g starch equivalent of one of the diets, then their glycemic response, small intestinal content particle size, small intestinal glucose and reducing sugar content, and portal vein plasma glucose were measured. Glycemic response of each pig was measured as plasma glucose collected from an in-dwelling jugular vein catheter for up to 360 min postprandial, while portal vein blood samples and small intestinal content were measured after sedation and euthanasia of the pigs at 30, 60, 120, or 240 min postprandial. It was found that food macrostructure affected the glycemic response; diets with smaller initial particle size (couscous and porridge diets) had a higher $\Delta\text{max}_{\text{overall}}$ and $\text{iAUC}_{\text{overall}}$ than diets with larger initial particle size (rice grain and noodle diets); 29.0 ± 3.2 vs. 21.7 ± 2.6 mg/dL and 5659.2 ± 727.1 vs. 2704 ± 521.3 , for the smaller- and larger-sized diets, respectively, $p < 0.05$). The difference in the glycemic response was associated with the lower starch emptying rate of the smaller-sized diets than the larger-sized diets. Different starch emptying rates of the diets was considered to cause different rate of small intestinal glucose loadings and glucose absorption to the portal vein, subsequently affecting the observed glycemic response.

Keywords: food structure; gastric emptying rate; glycemic response; small intestinal digestion, starch-based foods.

Chapter 6 Overview

Intestinal digestion, glucose absorption, and glycemic response:

- Maltose and glucose in intestinal lumen
- Particle size distribution of chyme
- Glucose in portal vein
- Glycemic response profile over time

Research Objective 2

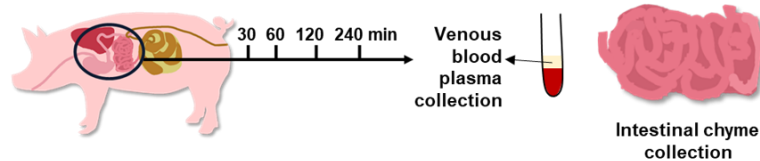
Identify the effect of food breakdown behavior in the stomach on small intestinal digestion and glycemic response

Research Objective 3

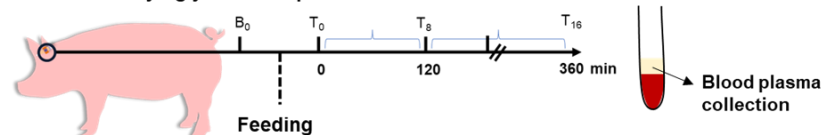
Identify food structure – gastric digestion – glycemic response relationship

Experimental approach

In vivo study – gut content collection

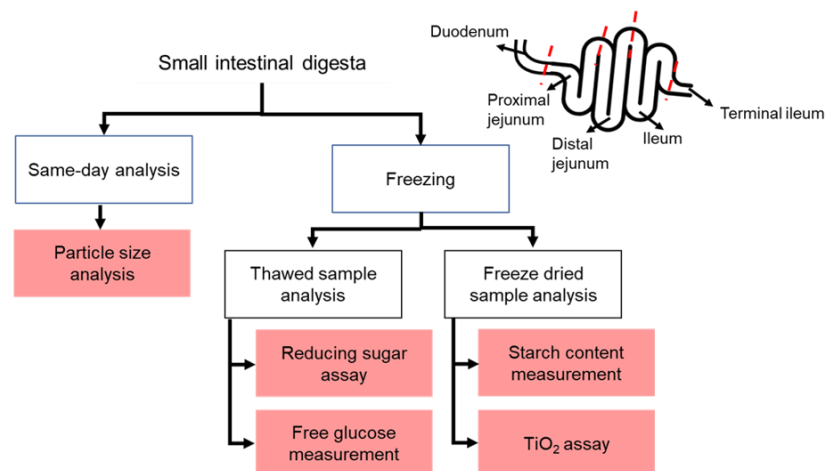


In vivo study– glycemic response measurement



Data retrieved from previous chapters:

- Gastric breakdown rate (softening half-time) from [Chapter 4](#)
- Starch emptying half-time, maltose content of liquid and suspended solid digesta fraction from [Chapter 5](#)



Sample analyses in this chapter were conducted in collaboration with other people:

- Plasma glucose analysis (Section 6.3.3.1) was conducted together with Dr. Parthasarathi Subramanian (Riddet Institute), Dr. Alexander G. Olenskyj (UC Davis), and Talia G. Estevez (UC Davis).
- Particle size measurement (Section 6.3.3.2) was conducted by Dr. Parthasarathi Subramanian (Riddet Institute).
- Most (85%) of TiO₂ assay was performed by the Riddet Institute Nutrition Team and Massey University Nutrition Lab.

6.2 Introduction

Consumption of starch-based foods has a large impact on glucose metabolism, which if not well managed, may increase the risk of type 2 diabetes and obesity (Cai, Dou, Pugh, Lett, & Frost, 2021). The conversion of starch to glucose during digestion in the small intestine has been studied in an attempt to understand how food structure can be used to modulate glycemic response. It has been shown that food microstructure is important in regulating the rate and extent of starch digestion in the small intestine. A meta-analysis review showed that glucose and insulin responses in human subjects were significantly lowered upon consumption of starch-based foods with higher amylose-amylopectin ratio, less gelatinized starch, and more retrograded starch (Cai et al., 2021). Additionally, many factors have been studied in linking food structure to glycemic response management, such as resistant starch type and content (Haub, Hubach, Al-Tamimi, Ornelas, & Seib, 2010; Tuaño, Barcellano, & Rodriguez, 2021), initial viscosity (Wolever et al., 2019), initial particle size (Mackie et al., 2017), fiber content (Anjana et al., 2019), starch interactions with other components in the food matrix (Jin, Bai, Chen, & Bai, 2019), and processing methods (Ramdath et al., 2018).

Despite the prevalence of studies on digestibility of starch-based foods, the mechanisms on how food structure affect the rate and extent of digestion in the small intestine have not been investigated in detail. More specifically, there is a knowledge gap in how small intestinal digestion is affected by the food breakdown during gastric digestion. In several studies where the macrostructural differences in the foods were clear (e.g. contrasting particle size, viscosity, or the presence of bran), foods with lower gastric emptying rate were reported to have lower glycemic response (Gopirajah et al., 2016; Mourot et al., 1988; Pletsch & Hamaker, 2018). However, in other studies using porridge or a hydrated flaked meal, glycemic response was not found to be dependent

on gastric emptying rate (Mackie et al., 2017; Torsdottir et al., 1989; Wolever et al., 2019), which was attributed to different starch microstructures and/or size of particles in the porridge. These contradictory findings may be related to the gastric emptying mechanism that typically only allows particles with $d \leq 1$ to 2 mm to enter the small intestine after a meal, as well as how the food structure breaks down in the stomach. However, gastric digestion has not been considered in detail in these studies.

It has been shown in Chapter 4 that macro- and microstructural differences of rice and wheat-based foods led to different breakdown rates in the stomach, and subsequently different gastric emptying rates were observed. Foods with initial size <1 to 2 mm emptied faster than foods with initial size >2 mm. The differences in the gastric emptying and gastric breakdown rates were expected to affect the glycemic response of the foods. It also has been demonstrated in Chapter 5 that the food products examined here have different gastric acidification rates. The focus of this chapter was to investigate the small intestinal digestion and glucose absorption of varying structures of rice- and wheat-based foods as affected by gastric digestion. Understanding the link between gastric digestion, small intestinal digestion, and glycemic response through the selected food structures in this study will be beneficial for better food structuring strategies, with a broader application of food structure development for glycemic response management.

6.3 Materials and methods

6.3.1 Study diets and reference diets preparation

Preparation of the study diets (couscous, pasta, rice couscous, rice grain, rice noodle, semolina) and reference diets (white bread) is described in Chapter 3 (Section 3.1.2).

6.3.2 Study design and sampling protocol

Study design and sampling protocol for this chapter are described in Chapter 3 (Sections 3.2.2 and 3.2.3).

6.3.3 Sample analyses

6.3.3.1 Blood plasma glucose analysis

Glucose in plasma samples was analyzed using a glucose oxidase/peroxidase assay kit (GOPOD, Megazyme, Wicklow, Ireland). Sample (0.1 mL, previously diluted up to 4 times with Milli-QTM water) was mixed with 3 mL of GOPOD reagent. The mixture was immediately incubated at 50 °C for 20 min. Absorbances of the incubated mixtures were read at 510 nm against the reagent blank on a UV-Vis spectrophotometer and were compared to the absorbance of 0.1 mg glucose standard within the same incubation batch. Analysis was done in duplicate for each sample.

6.3.3.2 Intestinal content particle size analysis

Particle size distribution (PSD) of diluted intestinal digesta was used directly for analysis. Analysis was conducted using the Mastersizer as in Chapter 5 (Section 5.3.5). Data with obscuration <2% were considered unreliable (Sotomayor & Schalkwijk, 2020) and not used for statistical analysis. PSD parameters extracted from the analysis were D[4,3], D[3,2], d₁₀, d₅₀, d₉₀, and specific surface area (SSA).

6.3.3.3 Intestinal content chemical analysis

Frozen intestinal content (the 2-mL subsample) was analyzed for reducing sugar and free glucose content. Frozen samples were warmed in a 37 °C temperature-controlled room for 15 min and maintained at 4 °C until analysis. Subsequently, samples were heated at ≥90 °C for 20 min to denature digestive enzymes, cooled on ice for 10 min, and centrifuged (4,300 × g, 10 min). The mass of each tube containing sample was

measured before centrifugation (tube + diluted intestinal digesta) to estimate the mass of diluted small intestinal digesta for analysis and after centrifugation (tube + pellet) to estimate the mass of supernatant in the sample. The supernatant from each sample was analyzed for reducing sugar and free glucose content. Reducing sugar content was quantified as maltose equivalent using the dinitrosalicylic acid (DNS) method (Miller, 1959) with modifications, as described in Chapter 5 (Section 5.3.6.1). Free glucose was determined using a glucose oxidase/oxidase assay kit as described in Section 6.3.3.1.

Freeze-dried intestinal contents were ground and sieved with a 1-mm sieve, then analyzed for TiO_2 , total starch content, and moisture content. TiO_2 content was analyzed following Short, Gorton, Wiseman, and Boorman (1996). Briefly, 0.1 to 0.5 g samples were ashed overnight (550 °C, 16 h), then dissolved in 7.4 M H_2SO_4 solution on a heating block (210 °C, 1.5 h). The dissolved samples were cooled, transferred to 10-mL volumetric flasks, then diluted to 10 mL with distilled water. Aliquots (1 to 4 mL) of samples were transferred to test tubes containing 1 mL of 30% v/v H_2O_2 solution, then the total volume of the mixture was adjusted to 5 mL. The absorbance of each sample was read at 410 nm on a UV-Vis spectrophotometer. TiO_2 concentration in the samples was determined based on a TiO_2 standard curve (0 to 0.834 mg/mL). Total starch content was quantified using Megazyme Total Starch Kit (Megazyme, Wicklow, Ireland), following the procedure for samples not containing free glucose or maltodextrins to enable starch digestibility calculation. Moisture content was determined gravimetrically as described in Chapter 4 (Section 4.3.5.1).

6.3.4 Data and statistical analysis

6.3.4.1 Glycemic response

The incremental area under the curve (iAUC) and maximum change in plasma glucose relative to the baseline (Δ_{max}) was determined for each pig and study diet from the

glycemic response data. The iAUC was quantified using the trapezoid rule using the plasma glucose concentration at B_0 as the baseline (FAO, 1998). Negative areas (due to lower plasma glucose concentration than the baseline) were not included in the calculation (Freitas et al., 2021). The Δ_{max} was expressed as the maximum difference between the plasma glucose concentration at time t with the baseline concentration.

To identify the overall impact of the diets on the progression of glycemic response, cumulative change of plasma glucose ($\Delta_{glucose}$) and iAUC values of the diets over time from $t = 0$ min to $t = 360$ min were fit to the Gompertz model (Tj rve & Tj rve, 2017):

$$\text{Cumulative } \Delta_{glucose} \text{ or } iAUC(t) = A_G \exp(-\exp(-k_G(t - T_i))) \quad (6.1)$$

where: A_G : the plateau value of the growth curve ((mg/dL).min), k_G : growth rate coefficient (min^{-1}), T_i : time at inflection (min).

6.3.4.2 Ileal starch digestibility and glucose or maltose flow

Ileal starch digestibility was calculated using pooled 120- and 240-min data for each diet to ensure constant digesta passage with the following formula (Weurding, Veldman, Veen, van der Aar, & Verstegen, 2001):

$$\text{Ileal starch digestibility (\%)} = \left[1 - \frac{(\text{starch}_{ileum}/Ti_{ileum})}{(\text{starch}_{diet}/Ti_{diet})} \right] \times 100\% \quad (6.2)$$

where: starch_{ileum} or starch_{diet} : starch content in ileum content or the diet, respectively (g/kg DM sample); Ti_{ileum} or Ti_{diet} : TiO_2 content in ileum content or the diet, respectively (g/kg DM sample).

The flow of glucose or maltose in the ileum for each diet was calculated with the following formula (Nyachoti, de Lange, & Schulze, 1997):

$$\text{Component}_{flow} = \text{Component}_{ileum} \times \left(\frac{Ti_{diet}}{Ti_{ileum}} \right) 100\% \quad (6.3)$$

where: $\text{Component}_{\text{flow}}$: the flow (g/kg DM eaten) of maltose or glucose at the ileum; $\text{Component}_{\text{ileum}}$: the concentration of maltose or glucose in the ileal digesta (g/kg DM digesta); T_{ileum} or T_{diet} : TiO_2 content in ileum content or the diet, respectively (g/kg DM sample).

6.3.4.3 Mass balance of intestinal glucose and maltose

Total glucose and maltose present in intestinal digesta were estimated from the 2-mL subsample that was not freeze-dried (Section 6.3.3.3) using a mass balance approach with the following assumptions: (1) glucose/maltose in intestinal content is concentrated in the supernatant only; (2) density of the supernatant can be estimated as 1 g/mL; (3) the subsample had a similar homogeneity to the whole intestinal content and can represent the overall intestinal digesta. Calculations for maltose are shown in the following steps, and similar steps applied for glucose, but using the glucose content measured in the supernatant of the intestinal digesta instead of the total maltose measured in the supernatant of the intestinal digesta in Eqn. 6.4.

a. Calculate total maltose in the analyzed supernatant of diluted intestinal digesta:

Total maltose in analyzed supernatant of diluted intestinal digesta (mg) =

$$\text{maltose in supernatant} \left(\frac{\text{mg}}{\text{mL}} \right) \times (\text{supernatant mass (g)} / (1 \frac{\text{g}}{\text{mL}})) \quad (6.4)$$

where: maltose in supernatant = concentration of maltose in the supernatant of diluted intestinal digesta measured in Section 6.3.3.3; supernatant mass = the mass of supernatant recorded after sample centrifugation measured in Section 6.3.3.3.

b. Calculate maltose concentration in the whole diluted intestinal digesta sample (supernatant + pellet):

$$\text{Maltose in diluted intestinal digesta (mg/g)} \quad (6.5)$$

$$= \text{Total maltose from Eqn. 6.4} / \text{mass of uncentrifuged sample}$$

where: mass of uncentrifuged sample (g) = the mass of tube + diluted intestinal digesta recorded before centrifugation measured in Section 6.3.3.3.

c. Conversion to dry basis maltose concentration:

$$\begin{aligned} &\text{Maltose in intestinal digesta dry matter (mg/g DM)} \\ &= \frac{\text{maltose in diluted intestinal digesta } \left(\frac{\text{mg}}{\text{g}}\right) \text{ from Eqn. 6.4}}{\left(1 - H_{2O_{\text{loss, diluted digesta}}} \left(\frac{\text{g } H_2O}{\text{g wet sample}}\right)\right)} \\ &\quad \frac{1 - MC_{FD \text{ digesta}} \left(\frac{\text{g } H_2O}{\text{g FD sample}}\right)}{\quad} \end{aligned} \quad (6.6)$$

where: $H_{2O_{\text{loss, diluted digesta}}}$ = moisture loss of diluted digesta, determined after freeze drying in section 6.3.3.2 ; $MC_{FD \text{ digesta}}$ = moisture content of freeze-dried (FD) digesta, measured in Section 6.3.3.3.

d. Use the dry basis maltose or glucose concentration obtained from Eqn. 6.6 to calculate total maltose or glucose present in a section of the small intestine (to be referred to as ‘intestinal maltose’ and ‘intestinal glucose’, respectively, from this section onwards):

$$\begin{aligned} &\text{Total intestinal maltose in section } i \text{ (g)} \\ &= \text{Eqn. 6.6 result } \left(\frac{\text{mg}}{\text{g DM}}\right) \times \text{digesta DM (g DM)} / 1000 \end{aligned} \quad (6.7)$$

where: i = identifier for a small intestinal section ($i = 1$ for duodenum, 2 for proximal jejunum, 3 for distal jejunum, 4 for ileum, and 5 for terminal ileum); digesta DM = the mass of dry matter in the small intestinal section i , obtained from the mass of FD digesta (measured in Section 6.3.3.3) multiplied by $(1 - MC_{FD \text{ digesta}})$.

Total maltose in the small intestinal lumen was calculated by summing up the results of Eqn. 6.7 across the five small intestinal sections.

6.3.4.4 Accumulation of portal glucose, intestinal glucose, or intestinal maltose

It was difficult to compare the glycemic response profile obtained from catheterized pigs with portal glucose and small intestinal starch hydrolysis data in the gut content collection study due to different number of data points in the two studies (18 in glycemic response study vs. 4 in gut content collection study). Thus, to compare and estimate the overall impact of diet consumption on starch digestion in the small intestine and subsequent glucose absorption into the portal vein, a cumulative approach was adapted.

Three variables were examined separately: averaged portal glucose concentration (from measurement in Section 6.3.3.1), as well as averaged total mass of intestinal glucose and averaged total mass of intestinal maltose (from measurement in Section 6.3.3.3 and calculation in Section 6.3.4.3). Because each pig from the gut content collection study represented only one data point for one diet × digestion time, the averaged value for each diet × digestion time (from 4 to 6 pigs) of the variable of interest was summed over time. This resulted in a cumulative curve consisting of only one data point for each digestion time. The cumulative value over time was fitted to the Michaelis-Menten non-linear model, which has been used to model the kinetics of glucose uptake and utilization (Bizzotto et al., 2016; Goyal, Aydas, Ghazaleh, & Rajasekharan, 2019):

$$Accumulation (mg/dL or g) = \frac{V_{max} \times time}{K_m + time} \quad (6.8)$$

where V_{max} : maximum accumulation (mg/dL for portal glucose, g glucose for total intestinal glucose accumulation, or g maltose for total intestinal maltose accumulation); K_m : half-time to reach the maximum accumulation (min).

Note that the Michaelis-Menten model use in this chapter is not as a mechanistic model to explain starch hydrolysis or glucose absorption mechanism of the diets. The model was used as an empirical model that describes the overall accumulation behavior during digestion in the small intestine and absorption into the portal vein, such that the interpretation of the V_{\max} and K_m here was different from when they are used to describe starch hydrolysis or glucose utilization kinetics.

6.3.4.5 Statistical analysis

Data from pigs that consumed <50% (for semolina) or <70% (the other five diets) of the study meal were excluded from analysis in both Stage 1 and Stage 2 to ensure normal gastric emptying processes, as described in Chapter 4. Exclusion of pigs by this criterion and blocked catheters resulted in an incomplete block design for the glycemic response study, with $5 < n \leq 7$ for each study diet and $n = 13$ for bread. Exclusion of pigs with the meal consumption criterion for the gut content collection study resulted in $5 < n \leq 6$ for each Study diet. Statistical analysis was performed using SAS®Studio 3.8.

One-way ANOVA was performed on glycemic response parameters (Δ_{\max} and iAUC) and ileal starch digestibility with the study diet as the main effect. Glycemic response parameters (Δ_{\max} , iAUC, and Gompertz model parameters) obtained for each diet were screened for outliers using ± 3 interquartile range prior to statistical analysis. Square-root transformation was applied to the iAUC data to achieve normality and homoscedasticity of residuals. Multi-factor, repeated measures mixed model ANOVA (PROC MIXED) was performed on Δ_{glucose} at each measurement point (B_0 to T_{16}) to analyze the effects of diet type, time, and their interactions, where pig was the experimental unit, diet type and sampling time were the main effects, sampling time was a repeated factor within the pig.

Multi-factor, repeated measures ANOVA (PROC MIXED) was performed on intestinal content properties (mg glucose/DM digesta, mg maltose/DM digesta, particle size parameters). Pig was the experimental unit, diet type and digestion time (30, 60, 120, or 240 min) were the between-subject factors, and intestinal section (duodenum, proximal jejunum, distal jejunum, ileum, terminal ileum) was the repeated factor within each pig. To achieve normality and homoscedasticity of residuals, square-root transformation was applied to glucose and maltose concentration in digesta, and logarithmic transformation was applied to all particle size parameters except d_{90} . Multi-factor ANOVA was performed on portal vein plasma glucose, total intestinal glucose, total intestinal maltose, ileal glucose flow, and ileal maltose flow data, where diet type and digestion time were the main effects.

For all statistical analyses (both glycemic response and intestinal content data), batch of pigs was included in the model to consider variability between study periods. The Tukey-Kramer procedure was used to identify differences between averages of the measurements. All values are reported as mean \pm SE and statistical significance was determined at $p < 0.05$.

6.4 Results

6.4.1 Glycemic response parameters

The catheterized pigs from the glycemic response study had no significant difference in their baseline plasma glucose concentration across different diets and sampling days (averaged value of 83.9 ± 1.2 mg/dL, or 4.7 ± 0.07 mmol/L, $p = 0.1689$). The glycemic response after consumption of the experimental and reference diets was variable between pigs (Figure 6.1). The average glycemic response curve for each study diet (established from the averaged plasma glucose concentration at each time; Figure 6.2A-

B) generally indicated biphasic behavior. The first peak appeared at 30 to 90 min digestion time, and the second peak appeared at between 90 to 210 min digestion time. Due to the variation between pigs, only the maximum change in plasma glucose throughout the 390 min digestion time ($\Delta\text{max}_{\text{overall}}$) was considered for comparison. The iAUC was examined at 90 (iAUC_{90min}), 150 (iAUC_{150min}), 270 (iAUC_{270min}), and 390 min (iAUC_{overall}) digestion time. Diet did not significantly affect $\Delta\text{max}_{\text{overall}}$, iAUC_{90min}, and iAUC_{150min} ($p > 0.05$), but it significantly affected iAUC_{270min} and iAUC_{overall} ($p < 0.05$; Table 6.1).

Small-sized (couscous, rice couscous, and semolina) and larger-sized (pasta, rice grain, rice noodle) diets exhibited different trends relative to the reference diet (bread), as indicated in the averaged glycemic response curve (Figure 6.2A-B), as well as the averaged glycemic response parameters. The $\Delta\text{max}_{\text{overall}}$ of reference, small-sized, and larger-sized diets were 27.8 ± 4.0 , 29.0 ± 3.2 , and 21.7 ± 2.6 mg/dL, respectively (small- and larger-sized diets were averaged together within the category). The iAUC_{overall} of reference, small-sized, and larger-sized diets were 3647.2 ± 762.2 , 5659.2 ± 727.1 , and 2704 ± 521.3 , respectively.

The Gompertz model (Eqn. 6.1) fit well to the cumulative change in plasma glucose relative to the baseline ($\Delta\text{glucose}$) and cumulative iAUC, with $R^2 \geq 0.95$ (Table 6.1; example plots can be found in Figure 6.3). The asymptote of the $\Delta\text{glucose}$ curve ($\Delta\text{glucose } A_G$) was not influenced by diet ($p = 0.1027$). The growth rate coefficient of the $\Delta\text{glucose}$ curve ($\Delta\text{glucose } k_G$) was significantly influenced by diet ($p = 0.0153$). Diet was also significant to iAUC A_G ($p = 0.0096$), iAUC k_G ($p = 0.0704$), and the inflection time of iAUC curve (iAUC T_i ; $p = 0.0392$). Smaller-sized and larger-sized diets indicated similar trend to the conventional glycemic response parameters, where the impact A_G and k_G for the $\Delta\text{glucose}$ and iAUC curves was in the following order:

smaller-sized diets > reference diet > larger-sized diets. For example, the A_G of the Δ glucose curve for the smaller-sized diets, reference diet, and larger-size diets were 202.8 ± 22.1 , 163.6 ± 34.1 , and 113.3 ± 19.4 mg/dL, respectively; the k_G were 1.19 ± 0.09 , 1.15 ± 0.07 , and 0.95 ± 0.10 min⁻¹, respectively.

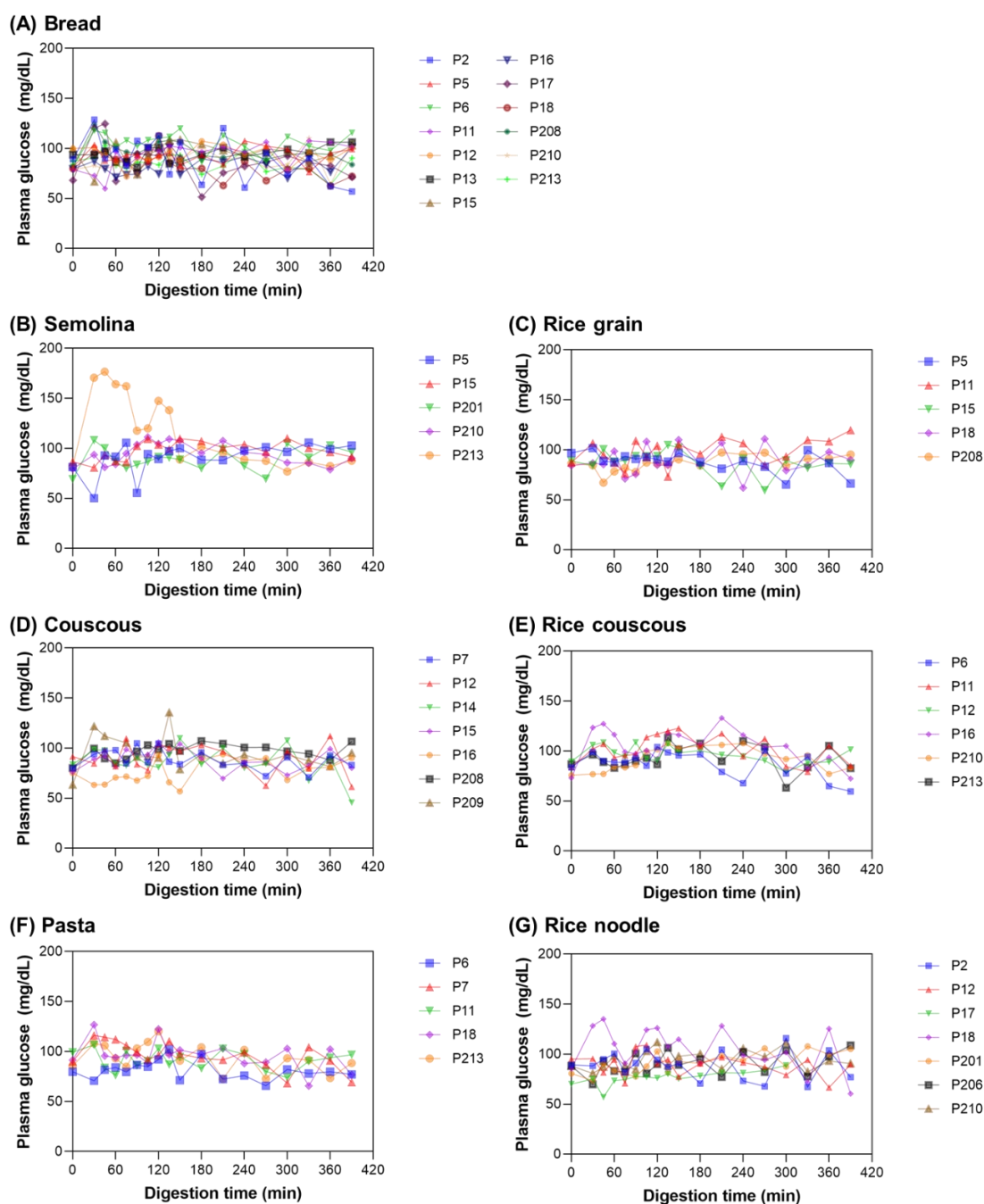


Figure 6.1 Plasma glucose concentration of individual pigs following the consumption of bread (A), semolina (B), rice grain (C), couscous (D), rice couscous (E), pasta (F), and rice noodle (G). Data set over time for each pig for one type of diet is indicated with the same symbol. The legend for each diet shows the ID of the pigs involved in the glycemic response measurement of the respective diet.

Table 6.1 Glycemic response parameters obtained from glycemic response data in catheterized pigs; Gompertz model parameters for iAUC and change in plasma glucose data relative to the baseline (Δ glucose) in catheterized pigs. The goodness of fit of the Gompertz model to the cumulative values of iAUC or change in plasma glucose (Δ plasma) for each diet is indicated by the R^2 . Values are presented as mean \pm SE ($5 < n \leq 7$, except $n = 13$ for bread). Significantly different values between diets for each parameter (data within the same row) are denoted with abcd superscripts ($p < 0.05$).

	Study Diet							<i>p</i> -value diet [§]
	Bread	Semolina	Couscous	Pasta	Rice grain	Rice couscous	Rice noodle	
Glycemic response parameters								
Δmax _{overall} (mg/dL)	27.8 ± 4.0	29.7 ± 6.6	24.6 ± 3.8	25.1 ± 5.2	18.1 ± 5.0	32.9 ± 6.2	21.8 ± 3.9	0.4198
iAUC _{90min} (mg/dL.min)	775.9 ± 212.6	839.9 ± 305.8	625.4 ± 164.7	705.1 ± 251.2	239.8 ± 105.1	633.3 ± 165.2	188.9 ± 26.6	0.1640
iAUC _{150min} (mg/dL.min)	1657.6 ± 370.5	2001.2 ± 389.5	1353.4 ± 337.9	1338.8 ± 375.2	593.7 ± 231.8	2202.9 ± 598.1	635.5 ± 60.7	0.0880
iAUC _{270min} (mg/dL.min)	2632.3 ± 529.1	3984.5 ± 517.3	3396.4 ± 866.9	1928.7 ± 518.7	1835.1 ± 541.1	4731.9 ± 1248.7	1521.8 ± 307.3	0.0254
iAUC _{overall} (mg/dL.min)	3647.2 ± 761.2 ^{ab}	6785.2 ± 988 ^a	4713.2 ± 1174 ^{ab}	2256.5 ± 621.7 ^{ab}	2193 ± 878.4 ^b	5824.6 ± 1545.1 ^{ab}	3505.2 ± 1093.8 ^{ab}	0.0181
Gompertz model (Eqn. 6.1) parameters								
iAUC <i>A</i> _{<i>G</i>} (mg/dL.min)	4736.6 ± 929.8 ^{ab}	9197.3 ± 1422.9 ^a	4138.7 ± 886.5 ^{ab}	3126.5 ± 1140.3 ^b	1733.8 ± 724.0 ^b	4930.8 ± 1108.6 ^{ab}	5445.0 ± 1266.2 ^{ab}	0.0096
iAUC <i>k</i> _{<i>G</i>} (min ⁻¹)	0.71 ± 0.06	1.02 ± 0.29	0.96 ± 0.11	1.19 ± 0.09	1.23 ± 0.35	1.05 ± 0.07	0.65 ± 0.09	0.0704
iAUC <i>T</i> _{<i>i</i>} (min)	161 ± 76 ^{ab}	194 ± 101 ^{ab}	162 ± 42 ^{ab}	88 ± 49 ^b	207 ± 114 ^{ab}	148 ± 36 ^{ab}	244 ± 120 ^a	0.0392
iAUC R ²	0.98 ± 0.003	0.99 ± 0.002	0.99 ± 0.003	0.98 ± 0.013	0.99 ± 0.004	0.99 ± 0.001	0.99 ± 0.002	-
Δglucose <i>A</i> _{<i>G</i>} (mg/dL)	163.6 ± 34.1	259.1 ± 19.2	160.4 ± 33.5	101.0 ± 31.2	96.7 ± 37.5	208.6 ± 45.5	137.5 ± 35.0	0.1027
Δglucose <i>k</i> _{<i>G</i>} (min ⁻¹)	1.15 ± 0.07 ^{ab}	1.12 ± 0.19 ^{ab}	1.27 ± 0.2 ^a	1.31 ± 0.25 ^a	0.94 ± 0.1 ^{ab}	1.17 ± 0.09 ^{ab}	0.74 ± 0.08 ^a	0.0153
Δglucose <i>T</i> _{<i>i</i>} (min)	98 ± 40 ^{ab}	104 ± 40 ^{ab}	103 ± 42 ^{ab}	71 ± 37 ^b	88 ± 67 ^{ab}	101 ± 35 ^{ab}	147 ± 63 ^a	0.1191
Δglucose R ²	0.95 ± 0.022	0.98 ± 0.005	0.99 ± 0.003	0.96 ± 0.019	0.98 ± 0.014	0.99 ± 0.002	0.98 ± 0.009	-

Δ max_{overall} : maximum change in plasma glucose relative to the baseline (mg/dL) within 390 min digestion.

iAUC_{*t*}: incremental area under the curve calculated within *t* min digestion

iAUC_{overall}: incremental area under the curve calculated throughout the examined digestion time (390 min).

A_G : the plateau value of the growth curve within 390 min digestion.

k_G : growth rate coefficient of the growth curve within 390 min digestion.

T_i : time at inflection of the growth curve within 390 min digestion.

[§]Only the effect of diet is presented, as batch of pigs was not significant to the glycemic response parameters ($p > 0.05$).

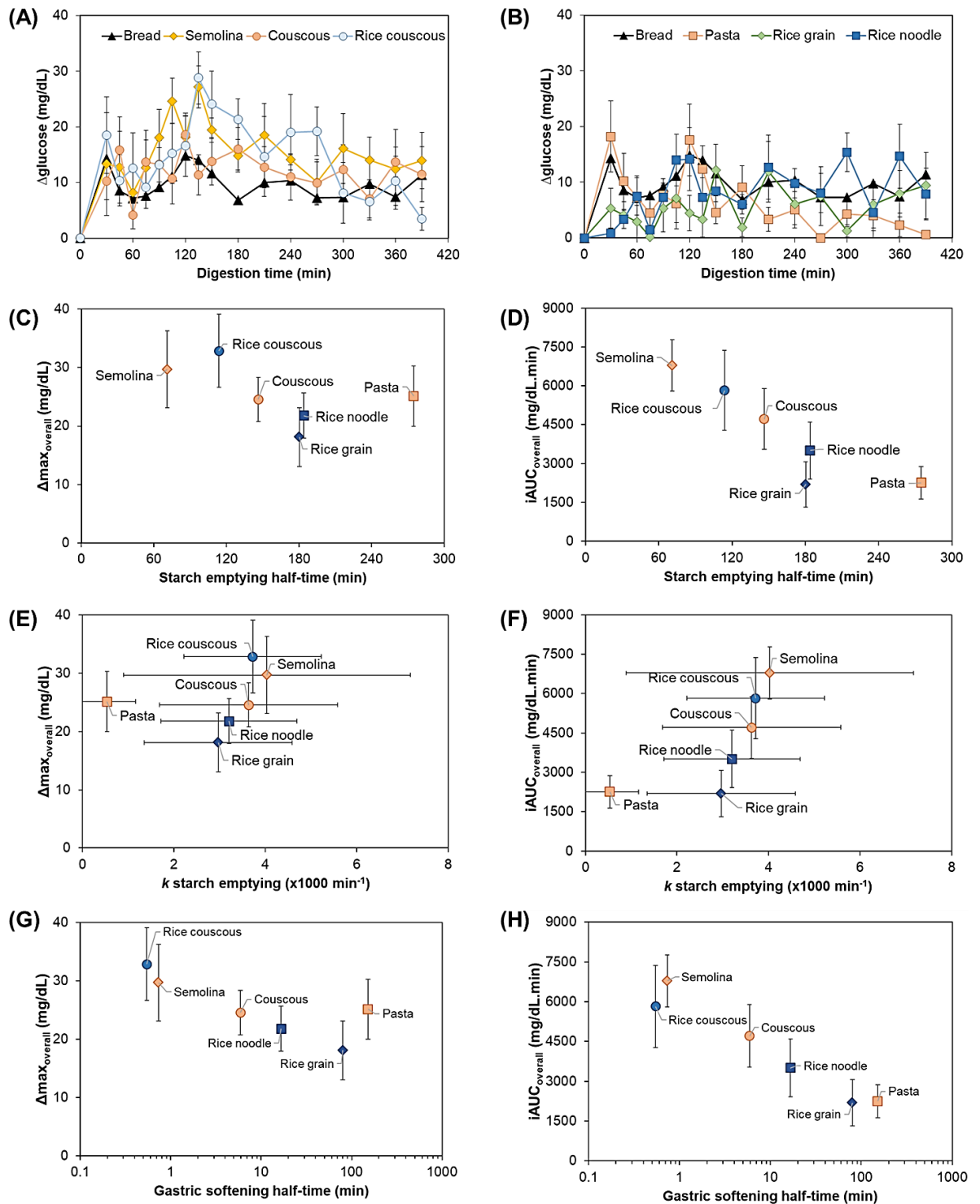


Figure 6.2 Averaged glycemic response curves (mean \pm SE, $5 < n \leq 7$, except $n = 13$ for bread) for small-sized (A) and larger-sized diets (B) generated by averaging the values from individual pigs at each digestion time. Relationship between glycemic response parameters with starch emptying half-time (C-D), starch emptying rate parameter, k (E-F), and gastric softening half-time (G-H) of the diets. Note that the gastric softening half-time is in logarithmic scale due to the wide range of the values across the six diets. Starch emptying half-time, k starch emptying, and gastric softening half-time were obtained from Figure 5.12G and Figure 4.7, respectively. Error bars for $\Delta\text{glucose}$ in averaged glycemic response curves, $\Delta\text{max}_{\text{overall}}$, and $\text{iAUC}_{\text{overall}}$ were obtained from experimental data (mean \pm SE). Error bars for k starch emptying were obtained from model fitting (fitted parameter \pm 95% confidence interval).

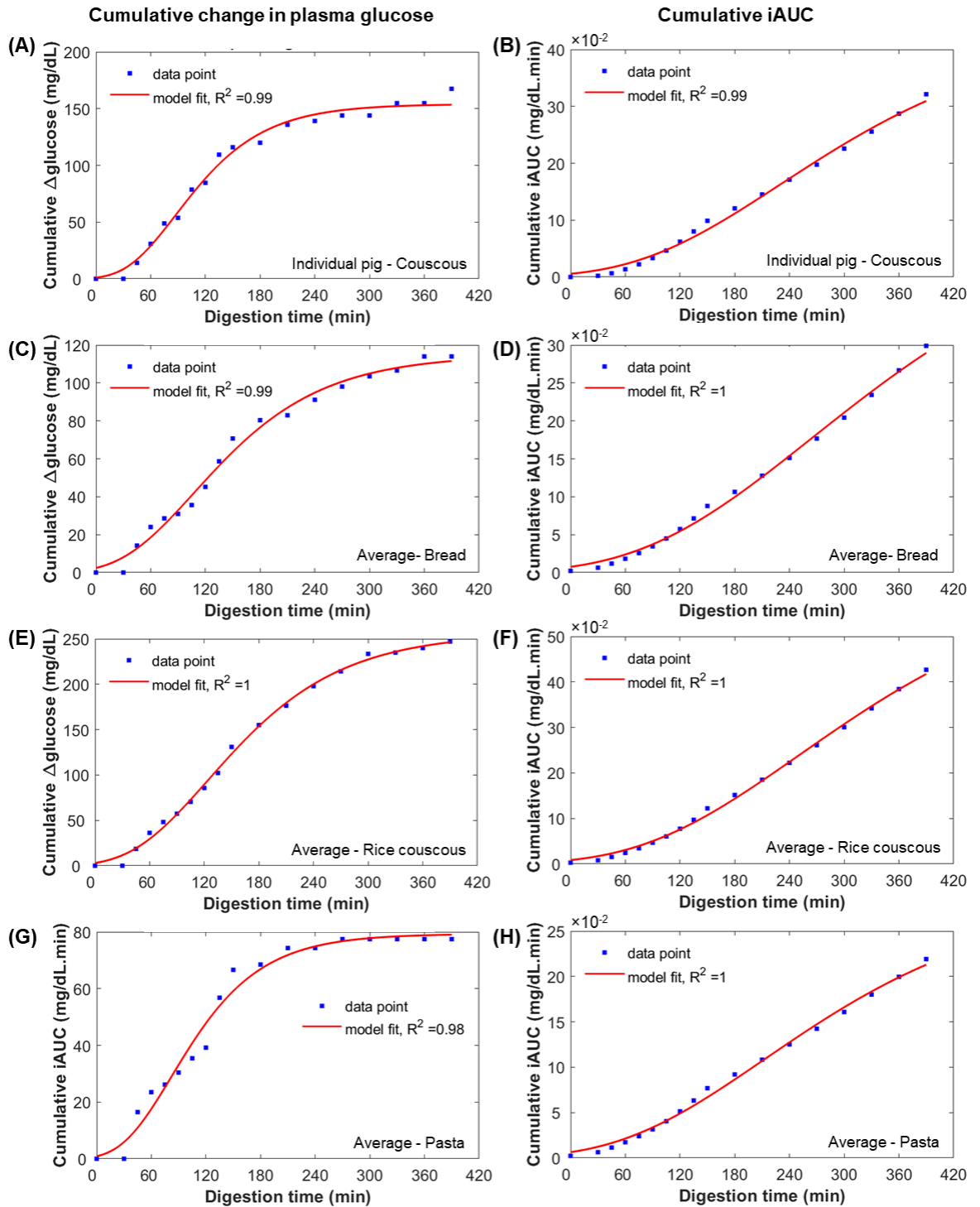


Figure 6.3 Example of Gompertz model fit to change in plasma glucose (left column) and iAUC (right column) cumulative values to data set obtained from individual pig (A-B), or averaged glycemic response data for bread (C-D), rice couscous as a representative of smaller-sized diets (E-F), and pasta as a representative of larger-sized diets (G-H).

6.4.2 Particle size distribution of intestinal digesta

A considerable proportion of samples from duodenum (58%) and terminal ileum (30%) had obscuration <2%, therefore data from these intestinal regions (Table E.1) were excluded from statistical analysis. All particle size parameters ($D[4,3]$, $D[3,2]$, d_{10} , d_{50} , d_{90} , and specific surface area (SSA)) of digesta from proximal jejunum, distal jejunum, and ileum (Tables 6.3 and E.2) were influenced by diet ($p < 0.0001$), and intestinal region ($p < 0.01$), and diet \times intestinal region ($p < 0.0001$; Table 6.2). Digestion time was significant to all particle size parameters ($p < 0.05$) except $D[4,3]$ and SSA; time \times intestinal region was significant for $D[4,3]$, $D[3,2]$, and SSA ($p < 0.05$); diet \times time \times intestinal region was significant only to $D[4,3]$ and d_{50} ($p < 0.01$).

Overall, rice couscous and rice noodle always had the smallest $D[4,3]$ and $D[3,2]$, followed by pasta and rice grain, then couscous and semolina in any small intestinal section. The trend was reversed in the SSA, where the SSA of rice couscous and rice noodle $>$ pasta and rice grain $>$ couscous and semolina ($p < 0.05$). For example, the SSA of rice couscous and rice noodle in the ileum was 0.654 ± 0.027 and 0.685 ± 0.028 (averaged across digestion times), respectively, while the other four diets had SSA of 0.134 ± 0.031 (averaged across digestion times and diets). A significant reduction of $D[4,3]$ and $D[3,2]$, coupled with an increase in SSA, with more distal small intestinal section (i.e., towards the ileum) was also observed in rice couscous and rice noodle at any digestion time (Table 6.3).

The particle size distributions were visualized to monitor changes in the profile along the small intestine (Figure 6.4, E.1-E.6) that could not be observed through the derived particle size parameters. Particle size distributions of the gastric digesta from the same diets (data retrieved from Chapter 5; Figure 5.12A-F and 5.13) are also presented for comparison. It can be seen that all diets initially had at least two large

peaks in the proximal and distal stomach, but the percent volume of the peaks changed during small intestinal digestion. In the more distal small intestinal sections, peaks for particles smaller than 100 μm diminished in semolina, couscous, and rice grain; peaks for particles larger than 100 μm diminished in rice couscous and rice noodle; while pasta did not show notable changes across the small intestinal sections.

6.4.3 Intestinal digesta chemical properties and ileal starch digestibility

Glucose and reducing sugar in the intestinal lumen were quantified as their concentration in small intestinal digesta dry matter (mg glucose/g DM digesta or mg maltose/g DM digesta; Figure 6.5 and Table E.3) and their total mass in the small intestine (g glucose or g maltose; Figure 6.6 column A-B) to identify differences due to starch digestion in the different small intestine sections and due to different delivery rate of the starch to the small intestine, respectively. Diet, small intestinal region, and their interaction effect was significant to maltose and glucose concentration ($p < 0.05$). Digestion time was significant only to maltose concentration ($p = 0.0003$); time \times region and diet \times time \times region interactions were significant to glucose concentration ($p < 0.05$; Table 6.2).

The highest concentration of maltose and glucose was found in the proximal and distal jejunum for all diets and times (492.8 ± 16.3 and 448.6 ± 14.9 mg maltose/g DM digesta, and 256.3 ± 7.3 and 219.2 ± 6.8 mg glucose/g DM digesta in the proximal and distal jejunum sections, respectively, averaged across all diets), while the lowest concentration of maltose and glucose was in the terminal ileum (111.8 ± 13.4 mg maltose/g DM digesta and 12.5 ± 1.5 mg glucose/g DM digesta, averaged across all diets). No significant difference between diets was found in the concentration of glucose or maltose in the proximal jejunum ($p > 0.05$). Meanwhile, maltose concentration in the ileum was the highest for rice couscous (344.3 ± 41.9 mg maltose/g

DM digesta, averaged across digestion times) and the lowest for pasta (172.8 ± 22.6 mg maltose/g DM digesta, averaged across digestion times).

Total mass of glucose and maltose in the small intestinal lumen at each digestion time (Figure 6.6 column A-B) were significantly affected by diet and digestion time ($p < 0.0001$). Diet \times time interaction was significant only to the total intestinal maltose ($p < 0.0001$). Total intestinal glucose ranged from 1.31 ± 0.40 g (pasta, 240 min) to 5.06 ± 0.24 g (rice couscous, 60 min), while the total intestinal maltose ranged from 2.99 ± 0.15 g (rice noodle, 30 min) to 19.42 ± 2.00 g (rice couscous, 60 min). For all diets, the highest glucose and maltose amount was achieved after 60 min (3.27 ± 0.23 g glucose and 8.36 ± 1.00 g maltose, respectively averaged across diets). The Michaelis-Menten model (Eqn. 6.8) fit well to the cumulative values of total intestinal maltose and glucose over time (Table 6.4, $R^2 \geq 0.95$, except total intestinal maltose for rice couscous, $R^2 = 0.87$; Figure 6.7). Both V_{\max} and K_m of total maltose and total glucose were correlated between each other (Figure 6.8B-C). For both total intestinal maltose and glucose, the order of V_{\max} of the diets was: rice couscous $>$ rice grain \approx couscous $>$ semolina $>$ rice noodle $>$ pasta, while the order of K_m of the diets was: rice noodle $>$ couscous $>$ pasta $>$ rice grain \approx rice couscous $>$ semolina.

Table 6.2 Statistical significance of diet type, digestion time and small intestinal or vein section (where relevant), and batch of pigs on the small intestinal digesta properties.

Parameter	Effect							Pig Batch
	Diet	Time	Region	Diet × Time	Diet × Region	Time × Region	Diet × Time × Region	
Ileum digesta, 120- and 240-min data pooled together								
Ileal starch digestibility	NS	-	-	-	-	-	-	NS
Small intestinal digesta, analysis by section								
D[4,3]	****	NS	****	***	****	**	**	*
D[3,2]	****	*	****	**	****	*	NS	NS
d ₁₀	****	**	***	NS	****	NS	NS	NS
d ₅₀	****	**	****	**	****	NS	**	*
d ₉₀	****	*	****	*	****	NS	NS	**
Specific surface area (SSA)	****	NS	****	NS	****	*	NS	NS
Glucose concentration (mg/g DM digesta)	***	NS	****	NS	*	****	*	NS
Maltose concentration (mg/g DM digesta)	***	***	****	NS	***	NS	NS	NS
Small intestinal digesta, all sections combined together								
Overall glucose concentration (mg/g DM digesta)	**	****	-	NS	-	-	-	**
Overall maltose concentration (mg/g DM digesta)	****	****	-	**	-	-	-	*
Total intestinal glucose (g glucose)	****	****	-	NS	-	-	-	*
Total intestinal maltose (g maltose)	****	****	-	****	-	-	-	**
Pre-euthanasia venous plasma glucose concentration								
Portal vein	*	***	-	NS	-	-	-	-
Hepatic vein	NS	NS	-	NS	-	-	-	-
Vena cava	NS	NS	-	NS	-	-	-	-
Left ventricle vein	NS	*	-	NS	-	-	-	-
Jugular vein	NS	*	-	NS	-	-	-	-

Asterisk (*) symbols indicate different levels of statistical significance. *: $p < 0.05$; **: $p < 0.01$, ***: $p < 0.001$, ****: $p < 0.0001$. NS: not significant. Main or interaction effects not included in the statistical models for certain parameters are indicated by “-”.

Table 6.3 Mean diameters and specific surface area (mean \pm SE, $4 \leq n \leq 6$) of the intestinal digesta from the proximal jejunum, distal jejunum, and ileum sections. Significantly different values within one column for each parameter (one type of diet across times \times small intestinal regions) are indicated with superscript abcd ($p < 0.05$). Significantly different values between diets within one row for each parameter (one digestion time \times small intestinal region) are indicated by superscript zyxw ($p < 0.05$).

Region	Time (min)	Diet					
		Semolina	Couscous	Pasta	Rice grain	Rice couscous	Rice noodle
D[4,3] (μm)							
Proximal jejunum	30	384.65 ± 15.79 ^z	528.61 ± 65.89 ^z	150.99 ± 3.52 ^{yx}	380.63 ± 41.01 ^z	141.83 ± 26.20 ^{ab,x}	223.19 ± 28.88 ^{ab,y}
	60	397.98 ± 14.16 ^z	514.33 ± 50.10 ^z	137.41 ± 8.35 ^y	416.26 ± 61.41 ^z	80.74 ± 19.27 ^{bc,x}	203.99 ± 43.11 ^{a,y}
	120	342.80 ± 26.18 ^z	574.26 ± 51.32 ^z	151.18 ± 24.10 ^y	454.83 ± 30.46 ^z	135.46 ± 28.99 ^{ab,y}	192.92 ± 31.38 ^{a,y}
	240	353.87 ± 17.13 ^{yx}	629.95 ± 50.92 ^z	178.08 ± 13.93 ^w	422.38 ± 24.04 ^{zy}	202.69 ± 15.21 ^{a,xw}	179.36 ± 35.03 ^{ab,w}
Distal jejunum	30	378.11 ± 21.46 ^z	611.13 ± 44.90 ^z	139.27 ± 13.9 ^y	444.71 ± 32.63 ^z	108.85 ± 19.93 ^{b,y}	104.33 ± 19.83 ^{bcd,y}
	60	379.01 ± 4.53 ^z	580.63 ± 35.16 ^z	124.67 ± 11.66 ^y	378.06 ± 19.66 ^z	50.02 ± 6.51 ^{cd,x}	103.21 ± 15.01 ^{bc,y}
	120	371.84 ± 14.35 ^y	645.64 ± 17.89 ^z	158.93 ± 24.39 ^x	463.18 ± 38.65 ^{zy}	113.58 ± 10.78 ^{b,xw}	83.33 ± 15.73 ^{cde,w}
	240	342.45 ± 46.2 ^y	645.58 ± 31.15 ^z	161.64 ± 26.81 ^x	539.66 ± 20.11 ^z	86.16 ± 20.66 ^{bc,w}	48.73 ± 1.86 ^{ef,w}
Ileum	30	397.08 ± 15.03 ^z	696.33 ± 20.84 ^z	136.52 ± 4.5 ^y	574.28 ± 47.51 ^z	48.11 ± 5.97 ^{cd,x}	61.58 ± 8.46 ^{def,x}
	60	401.91 ± 8.58 ^z	700.45 ± 18.76 ^y	127.35 ± 7.94 ^x	640.18 ± 18.06 ^{zy}	62.83 ± 12.07 ^{cd,w}	48.00 ± 3.01 ^{ef,w}
	120	398.50 ± 4.17 ^y	700.01 ± 14.91 ^z	128.33 ± 3.11 ^x	516.86 ± 12.39 ^{zy}	39.62 ± 4.25 ^{d,w}	51.44 ± 11.57 ^{f,w}
	240	399.57 ± 11.21 ^y	694.96 ± 13.60 ^z	195.61 ± 45.91 ^x	547.23 ± 18.60 ^{zy}	35.87 ± 0.96 ^{d,w}	40.00 ± 2.26 ^{f,w}
D[3,2] (μm)							
Proximal jejunum	30	99.33 ± 11.51 ^{abc,z}	78.49 ± 14.78 ^{ab,z}	30.59 ± 2.14 ^{a,yx}	40.31 ± 3.62 ^y	16.92 ± 2.16 ^{a,w}	25.45 ± 3.47 ^{a,x}
	60	95.82 ± 11.00 ^{abc,z}	62.19 ± 8.38 ^{b,y}	25.88 ± 1.46 ^{abc,w}	38.16 ± 4.72 ^x	10.89 ± 0.35 ^{abcd,v}	20.20 ± 4.48 ^{ab,w}
	120	93.92 ± 5.51 ^{abc,z}	91.39 ± 18.56 ^{ab,z}	28.18 ± 1.77 ^{abc,y}	34.19 ± 2.95 ^y	13.68 ± 0.80 ^{ab,x}	13.50 ± 1.32 ^{bcd,x}
	240	72.60 ± 3.51 ^{c,z}	92.9 ± 17.52 ^{ab,z}	29.19 ± 1.14 ^{ab,y}	30.81 ± 5.62 ^y	12.24 ± 0.87 ^{abc,x}	17.18 ± 1.46 ^{abc,x}
Distal jejunum	30	117.42 ± 12.12 ^{abc,z}	89.9 ± 10.81 ^{ab,z}	29.13 ± 3.23 ^{abc,y}	33.00 ± 2.38 ^y	11.17 ± 1.03 ^{bcd,x}	9.85 ± 0.85 ^{def,x}
	60	114.65 ± 5.33 ^{ab,z}	84.43 ± 7.71 ^{ab,z}	25.34 ± 2.75 ^{abc,y}	28.09 ± 2.39 ^y	9.63 ± 0.22 ^{bcd,x}	11.11 ± 1.08 ^{cde,x}
	120	103.15 ± 4.83 ^{abc,z}	97.16 ± 11.71 ^{a,z}	27.78 ± 0.56 ^{abc,y}	28.12 ± 2.08 ^y	9.84 ± 0.44 ^{bcd,x}	10.11 ± 0.75 ^{cdef,x}
	240	95.23 ± 7.80 ^{abc,z}	87.75 ± 9.71 ^{ab,z}	26.60 ± 0.91 ^{abc,y}	28.90 ± 1.67 ^y	9.38 ± 0.49 ^{bcd,x}	9.12 ± 0.86 ^{defg,x}

(continued)

Table 6.3 (continued)

Region	Time (min)	Diet					
		Semolina	Couscous	Pasta	Rice grain	Rice couscous	Rice noodle
Ileum	30	98.41 ± 9.40 ^{abc,z}	104.28 ± 9.15 ^{a,z}	19.86 ± 1.10 ^{bc,x}	37.98 ± 4.68 ^y	8.59 ± 0.36 ^{cd,w}	8.68 ± 0.25 ^{efg,w}
	60	131.75 ± 4.63 ^{a,z}	108.93 ± 7.49 ^{a,z}	19.13 ± 0.77 ^{c,x}	37.65 ± 2.35 ^y	8.65 ± 0.60 ^{cd,w}	7.40 ± 0.71 ^{fg,w}
	120	113.71 ± 4.65 ^{ab,z}	104.10 ± 4.75 ^{a,z}	23.97 ± 1.04 ^{abc,y}	29.86 ± 0.55 ^y	8.00 ± 0.47 ^{d,x}	6.62 ± 0.72 ^{g,x}
	240	91.44 ± 5.57 ^{abc,z}	100.64 ± 4.61 ^{a,z}	26.90 ± 1.12 ^{abc,y}	31.76 ± 1.42 ^y	7.74 ± 0.15 ^{d,x}	8.20 ± 0.46 ^{efg,x}
Specific surface area, SSA (×10² m²/kg)							
Proximal jejunum	30	5.83 ± 0.95 ^x	6.69 ± 0.94 ^x	12.9 ± 1.13 ^{d,y}	12.1 ± 0.78 ^y	29.0 ± 5.11 ^{f,z}	16.2 ± 3.16 ^{d,y}
	60	6.26 ± 0.98 ^x	8.71 ± 1.21 ^x	17.2 ± 1.85 ^{abcd,y}	15.4 ± 1.33 ^y	39.1 ± 6.18 ^{cdef,z}	17.5 ± 2.6 ^{d,y}
	120	4.99 ± 0.77 ^x	5.81 ± 0.58 ^x	15.7 ± 2.28 ^{abc,y}	15.3 ± 2.11 ^y	27.0 ± 3.98 ^{ef,z}	22.0 ± 4.16 ^{d,zy}
	240	6.41 ± 0.56 ^x	5.49 ± 1.30 ^x	13.3 ± 1.02 ^{cd,y}	15.8 ± 4.07 ^{zy}	27.2 ± 9.70 ^{def,z}	24.0 ± 8.25 ^{cd,zy}
Distal jejunum	30	4.90 ± 0.61 ^x	6.00 ± 0.93 ^x	15.3 ± 3.18 ^{bcd,y}	17.7 ± 1.72 ^y	48.1 ± 5.50 ^{abc,z}	40.6 ± 5.82 ^{bc,z}
	60	5.00 ± 0.28 ^x	6.84 ± 0.52 ^x	20.7 ± 3.4 ^{abcd,y}	19.0 ± 3.48 ^y	56.3 ± 2.36 ^{abc,z}	42.5 ± 4.50 ^{bc,z}
	120	5.40 ± 0.47 ^x	6.08 ± 0.75 ^x	16.5 ± 0.9 ^{abcd,y}	16.8 ± 1.47 ^y	45.3 ± 4.94 ^{bcd,z}	46.7 ± 7.42 ^{bc,z}
	240	5.47 ± 0.56 ^x	6.38 ± 0.64 ^x	18.6 ± 1.04 ^{abcd,y}	19.7 ± 1.62 ^y	50.3 ± 4.77 ^{abc,z}	53.0 ± 6.65 ^{ab,z}
Ileum	30	6.29 ± 0.6 ^w	5.57 ± 0.39 ^w	25.7 ± 1.30 ^{a,y}	15.3 ± 1.41 ^x	63.5 ± 4.48 ^{abc,z}	56.3 ± 1.86 ^{ab,z}
	60	4.39 ± 0.15 ^w	5.41 ± 0.20 ^w	25.7 ± 0.77 ^{a,y}	15.7 ± 1.03 ^x	56.0 ± 8.29 ^{abc,z}	71.6 ± 3.65 ^{a,z}
	120	5.19 ± 0.29 ^x	5.74 ± 0.24 ^x	22.9 ± 1.78 ^{abd,y}	19.1 ± 0.72 ^y	67.8 ± 4.39 ^{ab,z}	78.9 ± 6.78 ^{a,z}
	240	6.72 ± 0.41 ^x	5.84 ± 0.42 ^x	22.2 ± 0.40 ^{ab,y}	18.1 ± 0.70 ^y	72.5 ± 1.87 ^{a,z}	65.4 ± 4.61 ^{ab,z}

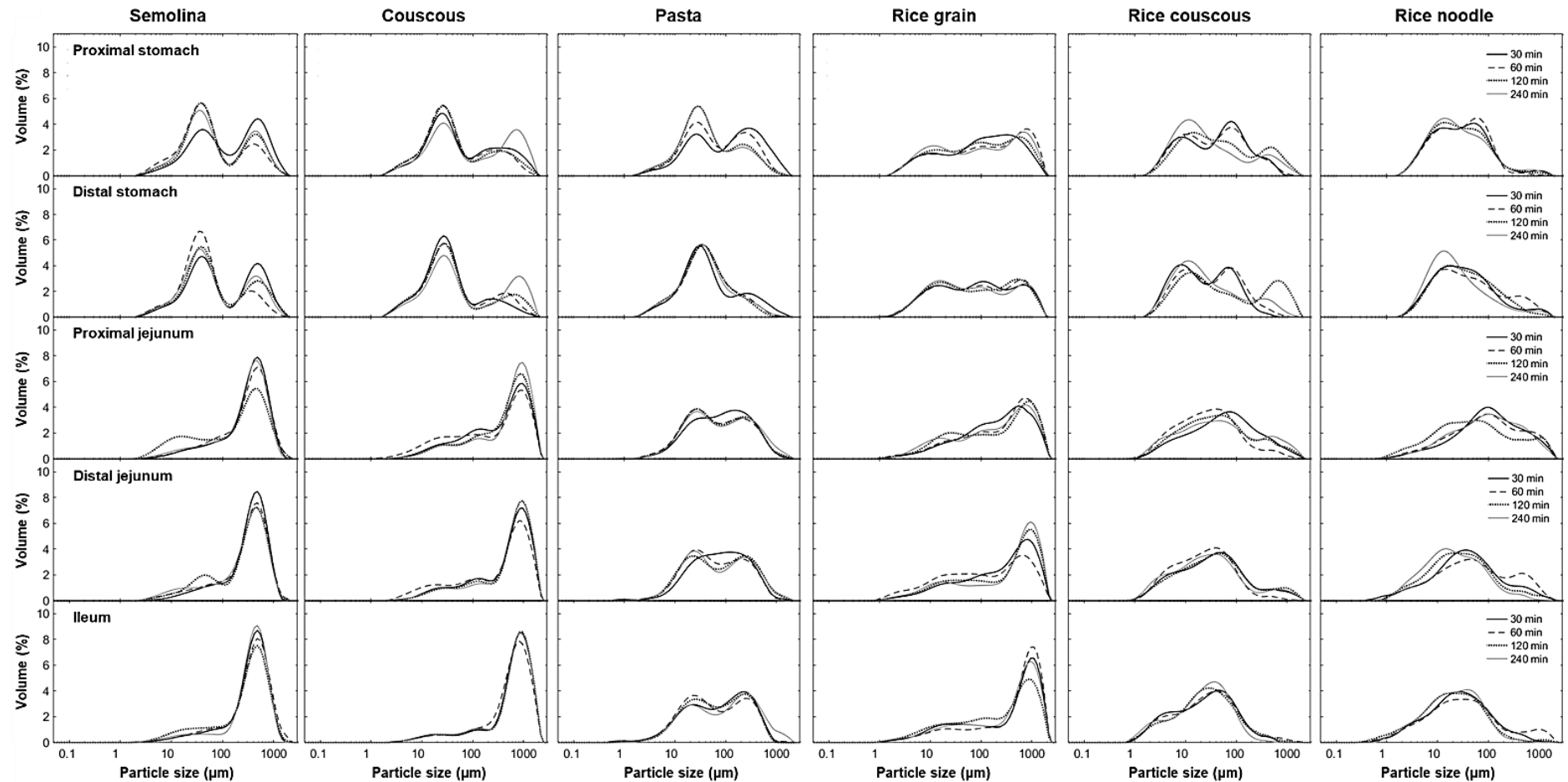


Figure 6.4 Particle size distribution (PSD) of the suspended solid fraction of proximal stomach and distal stomach digesta, as well as small intestinal digesta obtained from the proximal jejunum, distal jejunum, and ileum regions of pigs fed with semolina (A), couscous (B), pasta (C), rice grain (D), rice couscous (E), and rice noodle (F) from 30 (—), 60 (---), 120 (···), and 240 (— · —) min digestion. Each curve represents the average from 2 to 6 pigs. Individual PSD plots with error shades to indicate the range of the distribution are given in Figure E.1-E.6.

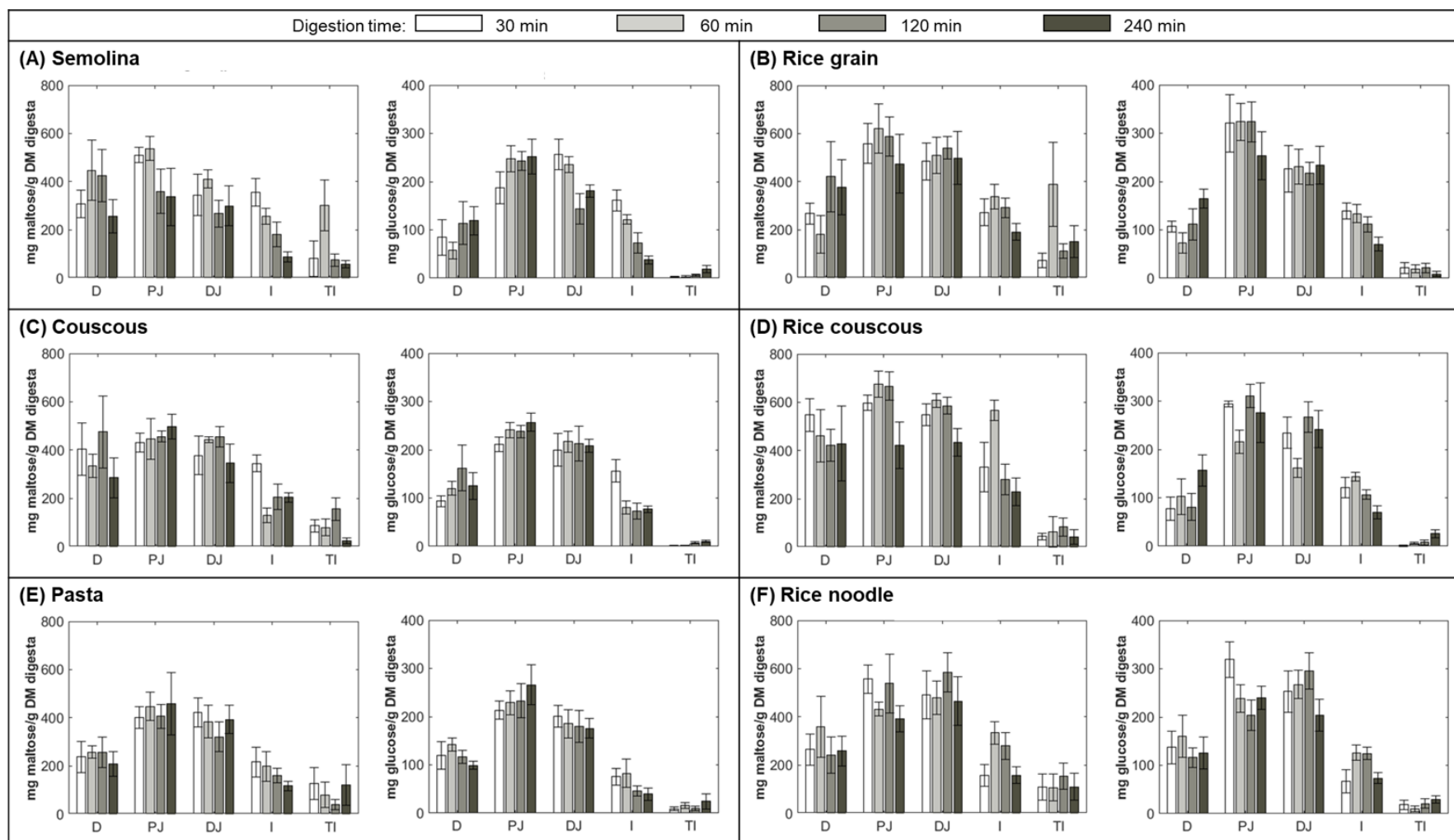


Figure 6.5 Glucose and maltose concentration in the small intestinal digesta of semolina (A), rice grain (B), couscous (C), rice couscous (D), pasta (E), and rice noodle (F) obtained from the duodenum (“D”), proximal jejunum (“PJ”), distal jejunum (“DJ”), ileum (“I”), and terminal ileum (“TI”) sections at different digestion times. Values are mean \pm SE ($4 \leq n \leq 6$). Note that the y-axis scales vary for glucose and maltose, but are the same across the diets. Increasing shades of the bars correspond to longer digestion times: 30 min (□), 60 min (▒), 120 min (▓), and 240 min (■). Statistical comparison of the treatments can be found in Table E.3.

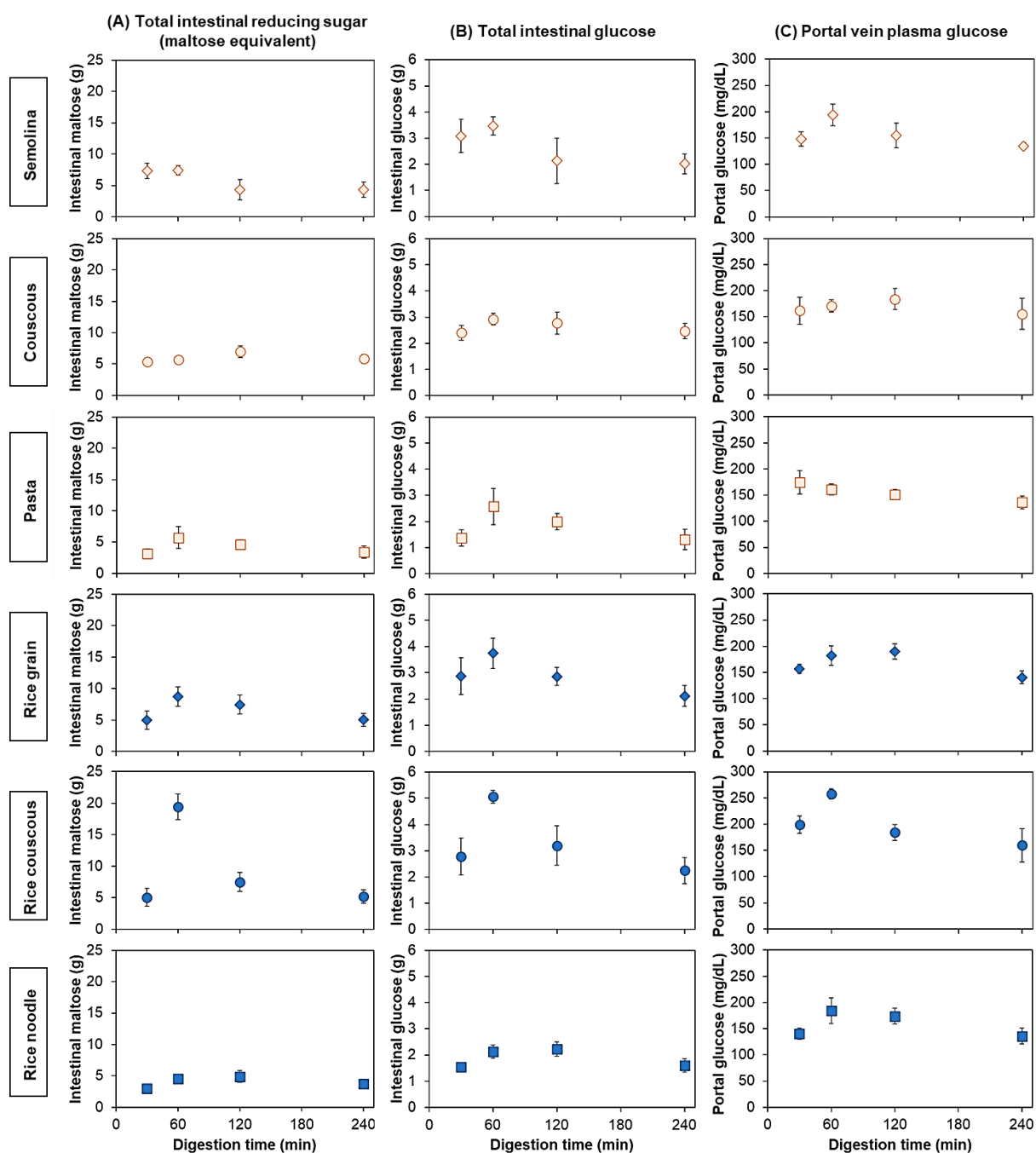


Figure 6.6 Total mass of maltose (column A) and total mass of glucose (column B) in the small intestinal digesta, and portal vein plasma glucose concentration (column C) of semolina (row 1), couscous (row 2), pasta (row 3), rice grain (row 4), rice couscous (row 5), and rice noodle (row 6). Values are mean \pm SE ($4 \leq n \leq 6$). Standard error is not always visible due to the small error bar. Total intestinal maltose and glucose were calculated by summing the results from Eqn. 6.7 for the five small intestinal sections.

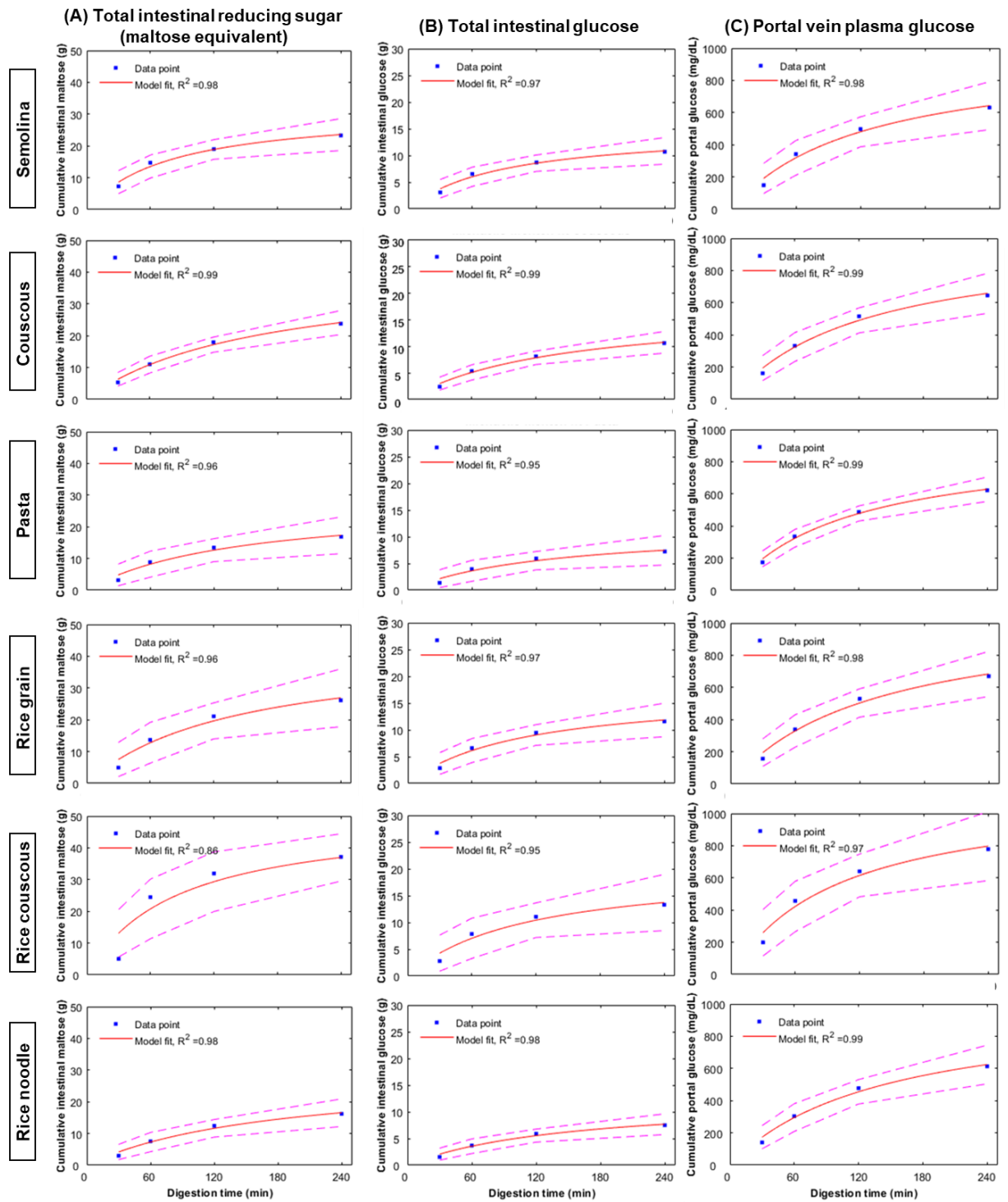


Figure 6.7 Michaelis-Menten fit to cumulative intestinal glucose (column A), intestinal maltose (column B), and portal vein plasma glucose concentration (column C). Confidence bounds of the fit at 95% confidence level are indicated by dashed lines surrounding the model fit. Averaged value for each digestion time point from Figure 6.6 was used to establish the cumulative plot for each diet.

Maltose and glucose flow in the ileum (calculated with Eqn. 6.3) were significantly influenced by diet, digestion time, and diet \times time ($p < 0.0001$). Both glucose flow and maltose flow at 30 min digestion were the highest in semolina and couscous, followed

by rice grain, rice couscous, and the noodle diets (Table 6.5). Couscous, semolina, and rice grain underwent a decrease in glucose flow over time ($p < 0.05$), especially between 30 and 120 min digestion. Ileal starch digestibility determined after 120 and 240 min digestion ranged from 96.68 ± 0.51 (semolina) to $98.08 \pm 0.27\%$ (pasta), but the values were not significantly different between diets ($p = 0.0978$; Table 6.2).

6.4.4 Portal vein plasma glucose concentration

In plasma samples collected from anesthetized pigs (in the gut content collection study), statistical analysis was conducted only on portal vein glucose data as it was the only vein location that indicated statistical significance of diet ($p = 0.0104$) and the most appropriate data to estimate absorption from the small intestinal lumen. The values of plasma glucose concentration in other vein locations are given in Table E.4 for comparison with the portal plasma glucose. Portal glucose concentration was significantly influenced by digestion time ($p < 0.05$), with values ranging from 134.7 ± 6.5 mg/dL (semolina, 240 min) to 257.7 ± 9.9 mg/dL (rice couscous, 60 min). Similar patterns in portal plasma glucose were observed between semolina and rice couscous, and between rice grain and rice noodle. Couscous exhibited a sharp increase until 120 min then a sudden decrease, while pasta had declining trend (Figure 6.6 column C). However, no significant differences were observed between time points for all diets, except in rice couscous.

The cumulative values of the portal plasma glucose concentration over time fit well to the Michaelis-Menten model ($R^2 \geq 0.97$; Table 6.4, Figure 6.7). The V_{\max} for portal plasma glucose was the lowest in semolina, followed by pasta, rice grain, rice noodle, couscous, and rice couscous. The K_m was the lowest in rice couscous and semolina, followed by pasta, rice grain and rice noodle, and couscous as the highest.

Table 6.4 Michaelis-Menten parameters (expressed as predicted parameters \pm 95% confidence interval) for the total intestinal glucose, total intestinal maltose, and portal plasma glucose concentration shown in Figure 6.7. The parameters have large confidence intervals because only one data point was present for each digestion time (due to the use of averaged value). The goodness-of-fit of the model to the data for each variable is indicated with the R^2 .

Parameter	Diet					
	Semolina	Couscous	Pasta	Rice grain	Rice couscous	Rice noodle
Total intestinal glucose (g)						
V_{\max} (g glucose)	14.86 \pm 7.49	17.01 \pm 9.18	11.57 \pm 11.7	17.17 \pm 11.04	20.09 \pm 19.01	12.52 \pm 9.43
K_m (min)	88 \pm 106	141 \pm 153	132 \pm 274	108 \pm 153	111 \pm 231	151 \pm 223
R^2	0.98	0.99	0.95	0.97	0.95	0.98
Total intestinal maltose (g)						
V_{\max} (g maltose)	31.35 \pm 13.87	40.48 \pm 19.77	27.59 \pm 26.49	42.69 \pm 41.04	56.83 \pm 90.33	28.68 \pm 24.9
K_m (min)	79 \pm 87	162 \pm 152	142 \pm 273	141 \pm 272	110 \pm 385	176 \pm 283
R^2	0.98	0.99	0.96	0.96	0.87	0.98
Portal plasma glucose concentration (mg/dL)						
V_{\max} (mg/dL)	918.1 \pm 272.7	1077.4 \pm 470.7	972.4 \pm 592.2	1018 \pm 661.9	1184.2 \pm 716.9	1066.3 \pm 607.2
K_m (min)	110 \pm 72	140 \pm 123	123 \pm 158	137 \pm 181	109 \pm 145	134 \pm 156
R^2	0.98	0.99	0.98	0.98	0.97	0.98

Table 6.5 Ileal starch digestibility at 120- and 240 min digestion (mean \pm SE (9 \leq n \leq 12, pooled across 120 and 240 min digestion time), and glucose flow and maltose flow in the ileum at different digestion time points (mean \pm SE, 3 \leq n \leq 6), estimated with Eqn. 6.2 and 6.3, respectively. For each parameter, significantly different values between diets for each digestion time (data within the same row) are denoted with abcd superscripts ($p < 0.05$); significantly different values between digestion time for each diet (data within the same column) are denoted with zyx superscripts ($p < 0.05$).

Time (min)	Diet					
	Semolina	Couscous	Pasta	Rice grain	Rice couscous	Rice noodle
Starch digestibility (%)						
-	96.68 \pm 0.51	97.38 \pm 0.33	98.08 \pm 0.27	96.83 \pm 0.49	97.80 \pm 0.24	97.69 \pm 0.24
Glucose flow (g/kg DM eaten)						
30	101.29 \pm 8.88 ^{a,z}	84.75 \pm 13.89 ^{ab,z}	14.17 \pm 3.85 ^d	69.43 \pm 11.42 ^{bc,z}	47.36 \pm 8.04 ^{c,z}	9.06 \pm 3.48 ^d
60	35.66 \pm 5.05 ^{ab,y}	20.00 \pm 6.70 ^{bc,y}	9.30 \pm 3.34 ^c	30.81 \pm 2.24 ^{abc,y}	41.17 \pm 2.86 ^{a,z}	20.23 \pm 6.56 ^{bc}
120	17.41 \pm 5.46 ^{yx}	13.08 \pm 3.38 ^y	6.33 \pm 2.01	16.81 \pm 2.70 ^{yx}	16.96 \pm 3.64 ^y	12.98 \pm 2.22
240	7.89 \pm 1.86 ^x	12.85 \pm 2.17 ^y	6.17 \pm 2.31	10.66 \pm 4.52 ^x	7.49 \pm 1.46 ^y	9.17 \pm 1.52
Maltose flow (g/kg DM eaten)						
30	226.49 \pm 27.12 ^{a,z}	205.91 \pm 17.68 ^{ab,z}	39.63 \pm 11.21 ^{cd}	160.79 \pm 25.72 ^{b,z}	92.88 \pm 23.28 ^{c,y}	19.63 \pm 5.11 ^d
60	76.48 \pm 14.07 ^{b,y}	26.11 \pm 4.67 ^{c,y}	23.07 \pm 6.88 ^c	79.58 \pm 8.41 ^{bc,y}	166.72 \pm 21.74 ^{a,z}	52.41 \pm 16.52 ^{bc}
120	43.84 \pm 14.47 ^{yx}	36.54 \pm 9.62 ^y	21.75 \pm 6.10	44.50 \pm 7.81 ^{yx}	38.99 \pm 8.23 ^x	29.90 \pm 7.04
240	18.02 \pm 3.99 ^x	34.48 \pm 6.55 ^y	16.89 \pm 4.00	28.50 \pm 11.30 ^x	24.67 \pm 5.90 ^x	20.60 \pm 5.24

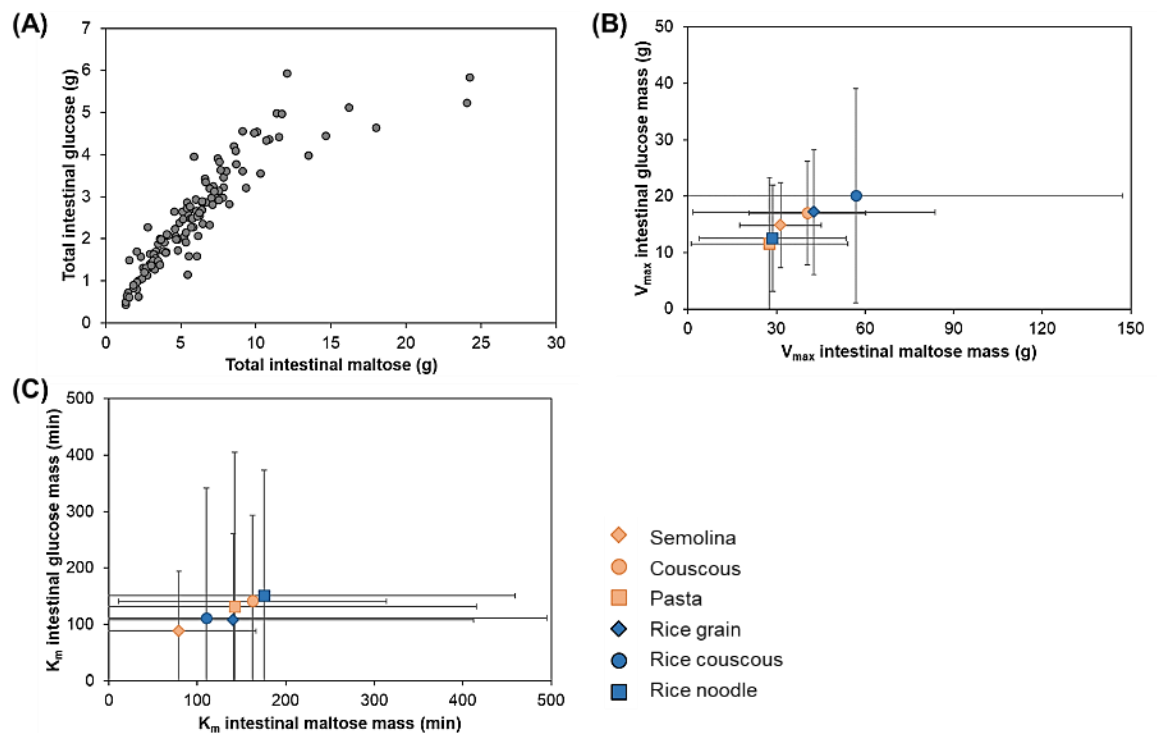


Figure 6.8 Relationship between: total mass of intestinal glucose and intestinal maltose (total 126 data points, 3 data points were not included due to outlier removal) (A); V_{\max} total mass of intestinal glucose and V_{\max} total mass of intestinal maltose (B); K_m total mass of intestinal glucose and K_m total mass of intestinal maltose (C). V_{\max} and K_m values are presented as predicted parameter \pm 95% confidence interval, obtained from fitting the data points to the Michaelis-Menten model (Eqn. 6.8).

6.5 Discussion

6.5.1 Food structure affected glycemic response, with a link to gastric emptying rate

The glycemic responses of growing pigs after consumption of various starch-based diets were measured. Despite the intra- and interindividual variances of the pigs (Figure 6.1), differences in the glycemic response still could be observed. The generally biphasic profile of the averaged glycemic response curve (Figure 6.2A-B), with the second peak appeared at ≥ 90 min, was previously reported in studies using jugular-catheterized pigs (Barone et al., 2019; Manell, Hedenqvist, Svensson, & Jensen-Waern, 2016; Pluschke et al., 2018) and in humans (Bervoets, Mewis, & Massa, 2015; Tschritter et al., 2003). In these studies, biphasic glycemic response profile was associated with good glucose tolerance.

Based on their Δ_{\max} and iAUC values, as well as the overall glycemic impact modeled with the Gompertz model (Table 6.1), the glycemic impact of the smaller-sized diets (couscous, rice couscous, and semolina) was higher than bread. Meanwhile, the larger-sized diets (pasta, rice grain, rice noodle) had a lower glycemic impact than bread. This difference was also reflected in the averaged glycemic response curves established for the two groups of diets (Figure 6.2A-B). The separation in the trend between smaller- and larger-sized diets was also observed in previous chapters (Chapter 4 and 5), where the smaller-sized diets had shorter gastric emptying half-time and faster acidification of gastric content, while the larger-sized diets had longer gastric emptying half-time and slower acidification of gastric content. The reference diet (white bread) behaved between the two groups of diets, which might be related to the properties of the food bolus. A bread-based meal was reported to form a homogeneous food bolus that underwent slow mixing with gastric secretions (Marciani et al., 2013). The slower gastric mixing but homogeneous consistency of the bread digesta might cause its glycemic response profile to be between the smaller- and larger-sized diets, implying the role of breakdown during gastric digestion on glycemic response.

To identify the relationship of the glycemic response observed in the current study with gastric digestion processes, the glycemic response parameters were plotted as a function of gastric emptying parameters of starch: rate parameter (k_{starch}), indicator of lag phase (β_{starch}), and emptying half-time ($t_{1/2, \text{starch GE}}$) from Chapter 5. It was found that the $\Delta_{\max \text{ overall}}$ and $\text{iAUC}_{\text{overall}}$ were inversely related to the $t_{1/2, \text{starch GE}}$ and gastric emptying β parameter of the diets, but proportionally related to the k_{starch} (Figure 6.2C-F and E.7), indicating that diets with slower gastric emptying or more lag phase in the gastric emptying process generally had lower $\Delta_{\max \text{ overall}}$ and $\text{iAUC}_{\text{overall}}$. Similar trends were also expected for the general gastric emptying (gastric emptying of dry matter), as

it was shown that dry matter and starch emptying were proportional (Chapter 5). Additionally, the asymptote (A_G) of both $\Delta\text{glucose}$ and $i\text{AUC}$ growth curve showed a similar trend to the $\Delta\text{max}_{\text{overall}}$ and $i\text{AUC}_{\text{overall}}$ in their relationships with the gastric emptying parameters (Figure E.7), suggesting that growth rate curve approach can also be applied to interpret glycemic response data. The correlations between the glycemic response and starch gastric emptying data agreed with the study of Mourot et al. (1988), which reported an inverse relationship between the maximum variation in blood glucose levels and gastric emptying half-time of bread, mashed potato, rice, and spaghetti in healthy humans. Similarly, it was reported that the initial and the maximum rise in plasma glucose after a 75-g oral glucose load in healthy humans were proportionally related to the gastric emptying rate (Horowitz et al., 1993; Marathe et al., 2015).

Diets with slower gastric emptying and lower glycemic impact ($\Delta\text{max}_{\text{overall}}$ and $i\text{AUC}_{\text{overall}}$) were the larger-sized diets (rice grain, rice noodle, pasta). This emphasizes the importance of food macrostructure, either solely due to its larger initial size or size when entering the stomach due to mastication, on the gastric emptying and glycemic impact of the food, as also highlighted in previous studies (Mourot et al., 1988; Ranawana et al., 2014; Ranawana, Monro, et al., 2010). The impact of particle size was also observed in the smaller-sized diets (couscous, rice couscous, semolina), as differences in their glycemic impact and gastric emptying was proportional to their initial particle size ($\text{semolina} < \text{rice couscous} \leq \text{couscous}$). Previous human studies using porridge with different suspended particle size ($d < 2$ mm) or contrasting particle size ($d = 2$ mm vs. $d < 0.2$ mm) also reported lower gastric emptying rate and glycemic impact with increasing size of the suspended particles (Edwards et al., 2015; Mackie et al., 2017; Pletsch, 2018). Additionally, the effect of initial particle size may also be enhanced by the microstructural differences of the foods. The larger-sized diets had

tighter starch arrangements in their microstructure (“more compact structure”) than the smaller-sized diets (Chapter 5). These microstructural differences could lead to a lower breakdown rate in the stomach due to reduced diffusion of digestive fluids into the food matrix (Bornhorst et al., 2015), contributing to the slower gastric emptying rate and lower glycemic impact of the larger-sized diets compared to the smaller-sized diets.

In Chapter 4, it was observed that the gastric emptying rate of the diets was limited by their breakdown rate during gastric digestion (quantified as gastric softening half-time, $t_{1/2, \text{softening}}$), especially for larger-sized diets. Figure 6.2G-H shows an inverse relationship between $t_{1/2, \text{softening}}$ and $\Delta \text{max}_{\text{overall}}$ and $\text{iAUC}_{\text{overall}}$, indicating that food with slower breakdown during gastric digestion resulted in lower glycemic impact. The finding aligns with a previous *in vitro* gastric digestion study using various carbohydrate-rich foods that identified a negative correlation between $t_{1/2, \text{softening}}$ and the glycemic indices of the foods (Drechsler & Bornhorst, 2018). The link between $t_{1/2, \text{softening}}$, $t_{1/2, \text{DM GE}}$, and the glycemic response parameters suggests that the gastric breakdown rate of the diets in the current study limited their gastric emptying rate, and subsequently limited their glycemic response. The negative-exponential relationship between the $t_{1/2, \text{softening}}$ and the glycemic response parameters (Figure 6.2G-H) may indicate a certain maximum limit of gastric breakdown rate to cause low glycemic response, which merits further investigation.

6.5.2 Possible mechanisms of the effect of gastric digestion on glycemic response

The glycemic response after a meal (as measured in the glycemic response measurement study) is a consequence of complex physiological processes, as summarized in Figure 6.9. Upon mastication and gastric digestion of starch-rich foods, liquid and food particles (typically ≤ 2 mm, or up to 7 mm (Coupe et al., 1991; Meyer et al., 1988)) containing starch and hydrolyzed starch are released to the small intestine for

amylolysis and hydrolysis to glucose by the brush border enzymes (Warren, Zhang, Waltzer, Gidley, & Dhital, 2015). Glucose produced in the small intestinal lumen is absorbed to the portal vein, followed by glucose circulation in the blood through a series of glucose metabolism processes involving the brain, liver, pancreas, muscle, and adipose tissue to maintain the blood glucose within a normal range (homeostasis) (Kim et al., 2020; Woerle et al., 2003). The small intestine also contributes to the glucose homeostasis by releasing hormones from the gut epithelium that amplify insulin secretion in response to the presence of nutrients in the small intestine (Holst, Gribble, Horowitz, & Rayner, 2016), which is also known as the incretin effect.

The gut content collection study was expected to provide the understanding on the possible mechanisms of how gastric digestion affects glycemic response. Based on Figure 6.9, several parameters can be measured to investigate the mechanisms of glycemic response regulation: (1) hormonal responses; (2) plasma glucose level in the systemic circulation; and (3) nutrient level in the small intestine. Hormonal responses were outside the scope of the current study, plasma glucose in the systemic circulation and nutrient level in the small intestine were measured in the gut content collection study. Plasma glucose was measured in the portal vein, hepatic vein, vena cava, left ventricle vein, and jugular vein (Table E.4), with the expectations that a glucose metabolism could be observed. However, no clear trends were observed between the diets in the plasma glucose measured under anesthesia from all veins of interest (including the jugular vein, which was also the location of blood sampling in the glycemic response measurement study), except the portal vein. The lack of trends might be attributed to the anesthesia that might have interfered with the glucose metabolism process. Anesthesia using Ketamine and Xylazine has been reported to cause hyperglycemia 30 min after administration of the anesthetics in goats (Okwudili,

Chinedu, & Anayo, 2014), rats (Saha, Xia, Grondin, Engle, & Jakubowski, 2005), rabbits (Sharif, Abouazra, & Toxicology, 2009), and pigs (Manell, Jensen-Waern, & Hedenqvist, 2017), especially after an oral glucose tolerance test.

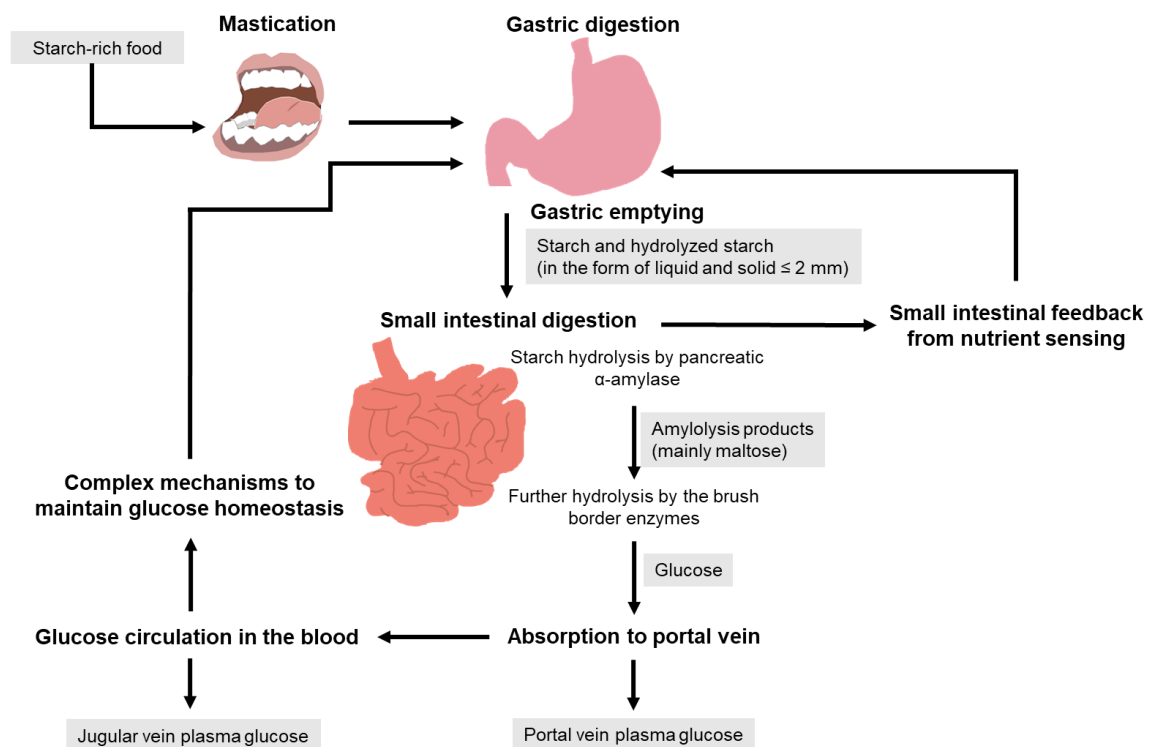


Figure 6.9 Summary of glycemic response regulation upon the ingestion of starch-rich food. The actual process involves more complex mechanisms, and the diagram is presented with simplification to aid the explanation in the current study. Major steps in the process are indicated by bold font. Input (food properties) and parameters of processes colored in grey were quantified in this study and the previous studies (Chapter 4 and 5). Major changes to starch in the small intestine are indicated by normal font.

The portal plasma glucose concentration over time was dynamic, but all diets showed a declining trend after 120 min digestion (Figure 6.6 column C), suggesting the presence of mechanisms to maintain glucose homeostasis. The observed portal plasma glucose profiles were due to the different delivery of starch over time into the portal vein, which depended on the diet type; each diet indicated a relationship between portal vein plasma glucose with $t_{1/2, \text{starch GE}}$ (data obtained from Chapter 5, Section 5.4.3; Figure 6.10A-B). The V_{max} for the portal plasma glucose, which represented the maximum accumulation effect in the portal vein, had an inverse relationship with

$t_{1/2, \text{starch GE}}$ for all diets except semolina. The deviation in semolina might be because it had the shortest $t_{1/2, \text{starch GE}}$ among the smaller-sized and fast-emptying diets. The K_m parameter, which represented the time at which the accumulation is half maximal (thus reflecting the half-time of portal glucose accumulation), had an inverse relationship with $t_{1/2, \text{starch GE}}$ for all diets except semolina and rice couscous. These correlations suggest there was a minimum $t_{1/2, \text{starch GE}}$ (or maximum starch delivery rate) that affected the accumulation of glucose in the portal vein. Above this minimum value, accumulation of glucose in the portal vein due to absorption was hypothesized to be dependent on $t_{1/2, \text{starch GE}}$. If starch delivery rate was fast enough (as observed in semolina and rice couscous), the rate of glucose accumulation in the portal vein was fast, possibly due to the fast disappearance of glucose from the portal vein to the circulatory system (Figure 6.9) – as reflected in their highest $\Delta\text{max}_{\text{overall}}$ and $\text{iAUC}_{\text{overall}}$ in the glycemic response measurement study (Table 6.1) measured from samples taken from the jugular vein.

Previous clinical studies reported that the glycemic response of healthy and type 2 diabetes human subjects after intraduodenal infusion of glucose at 1 kcal/min was lower than at 2 and 4 kcal/min, but little difference was found between the glycemic response at 2 and 4 kcal/min (Ma et al., 2012; Pilichiewicz et al., 2007). This finding suggests the effect of certain gastric emptying rate on glucose loading into the small intestine, which in turn affects glycemic response. The effect is also reflected in the similar pattern of the change over time between portal glucose, intestinal glucose, and intestinal maltose (Figure 6.6), indicating that the small intestinal digestion and portal glucose absorption are interrelated.

In the current study, both the K_m and V_{max} of glucose absorption into the portal vein are proportional to the K_m and V_{max} of glucose in the small intestinal lumen (Figure

6.10C-D), suggesting that the faster accumulation and higher amount of glucose in the small intestinal lumen, the higher glucose absorbed into the portal vein. Combined with the relationship found between $t_{1/2, \text{starch GE}}$ and the rate of portal glucose accumulation, this implies that $t_{1/2, \text{starch GE}}$ affected the glycemic response by affecting the rate of glucose loading in the small intestine, which influenced the rate of portal glucose accumulation and disappearance to the circulatory system. However, a certain minimum $t_{1/2, \text{starch GE}}$ is required before these correlations can be observed, and this merits future investigation.

Since glucose absorption into the portal vein is related to the presence of maltose and glucose in the small intestine, changes in the glucose and maltose content in the small intestine were investigated further. In the small intestine, two major processes occur to the materials delivered from the stomach: (1) amylolysis of starch to smaller sugars (mainly maltose); and (2) further hydrolysis of the smaller sugars to produce glucose (Figure 6.9). Results of the current study indicate that total intestinal glucose was proportional to total intestinal maltose (Figure 6.8), where both measurements were obtained by combining the mass of glucose or maltose in the duodenum, proximal jejunum, distal jejunum, ileum, and terminal ileum. It is noteworthy that maltose in this study was selected as a reference to express the reducing sugar content in the small intestinal digesta quantified using the DNS assay, thus the quantified “intestinal maltose” comprised of any reducing sugars produced by the starch hydrolysis processes. In contrast, the GOPOD analysis used to quantify glucose was specific to glucose only and reflected the amount of free glucose in the digesta. To identify if the results from the DNS assay and GOPOD analysis overlap, the glucose mass was converted to theoretical maltose mass using the ratio of the molar mass of maltose to glucose (equals to 1.90). With this calculation, it was found that the measured maltose equivalent was

generally larger than the theoretical maltose mass (Table 6.6), indicating that the digesta comprised of a mixture of glucose, maltose, and other starch hydrolysis products with reducing ends. This aligns with a previous study that reported that starch digestion in the small intestine of pigs produced debranched starch with different degree of polymerization, and the digestion process occurred differently in the different small intestinal sections (Hasjim et al., 2010).

Table 6.6 Difference between total intestinal maltose measured in the reducing sugar assay with theoretical total intestinal maltose calculated from the glucose data (mean \pm SE, $4 \leq n \leq 6$). Theoretical total intestinal maltose was calculated by multiplying the total glucose mass with 1.90 (molar ratio between the molar mass of maltose:glucose). Values with SE larger than the mean were due to negative values for some of the replicates, possibly due to variations between pigs.

Time (min)	Measured maltose equivalent – theoretical maltose from glucose measurement (g)					
	Semolina	Couscous	Pasta	Rice grain	Rice couscous	Rice noodle
30	1.43 \pm 0.46	0.77 \pm 0.27	0.55 \pm 0.23	1.12 \pm 0.78	0.88 \pm 0.48	0.05 \pm 0.09
60	0.84 \pm 0.25	0.14 \pm 0.51	0.82 \pm 0.45	1.59 \pm 0.51	9.80 \pm 1.65	0.50 \pm 0.26
120	0.87 \pm 0.65	1.70 \pm 0.61	0.81 \pm 0.31	2.02 \pm 0.92	1.39 \pm 0.35	0.67 \pm 0.45
240	0.47 \pm 0.60	1.12 \pm 0.23	0.93 \pm 0.26	1.00 \pm 0.27	0.93 \pm 0.38	0.21 \pm 0.49

To identify the difference between the small intestinal sections in starch digestion, the concentration of maltose and glucose in the five sections was examined. At any digestion time, maltose and glucose concentration in the duodenal and terminal ileal digesta was the lowest among the five small intestinal sections (Figure 6.5), most likely due to rapid digestion and absorption in the duodenum, as well as digestion and glucose absorption that mostly takes place in the jejunum (Smith & Morton, 2010b; Weurding et al., 2001) – in agreement with >95% starch digestibility in the ileum for all diets (Table 6.5). The trend also agreed with the low obscuration of many duodenal and terminal ileal samples during particle size measurement, indicating minimum amount of particles were retained in the small intestinal sections. This can be attributed to the shorter length of the duodenum and terminal ileum (~25 and ~10 cm, respectively) compared to the

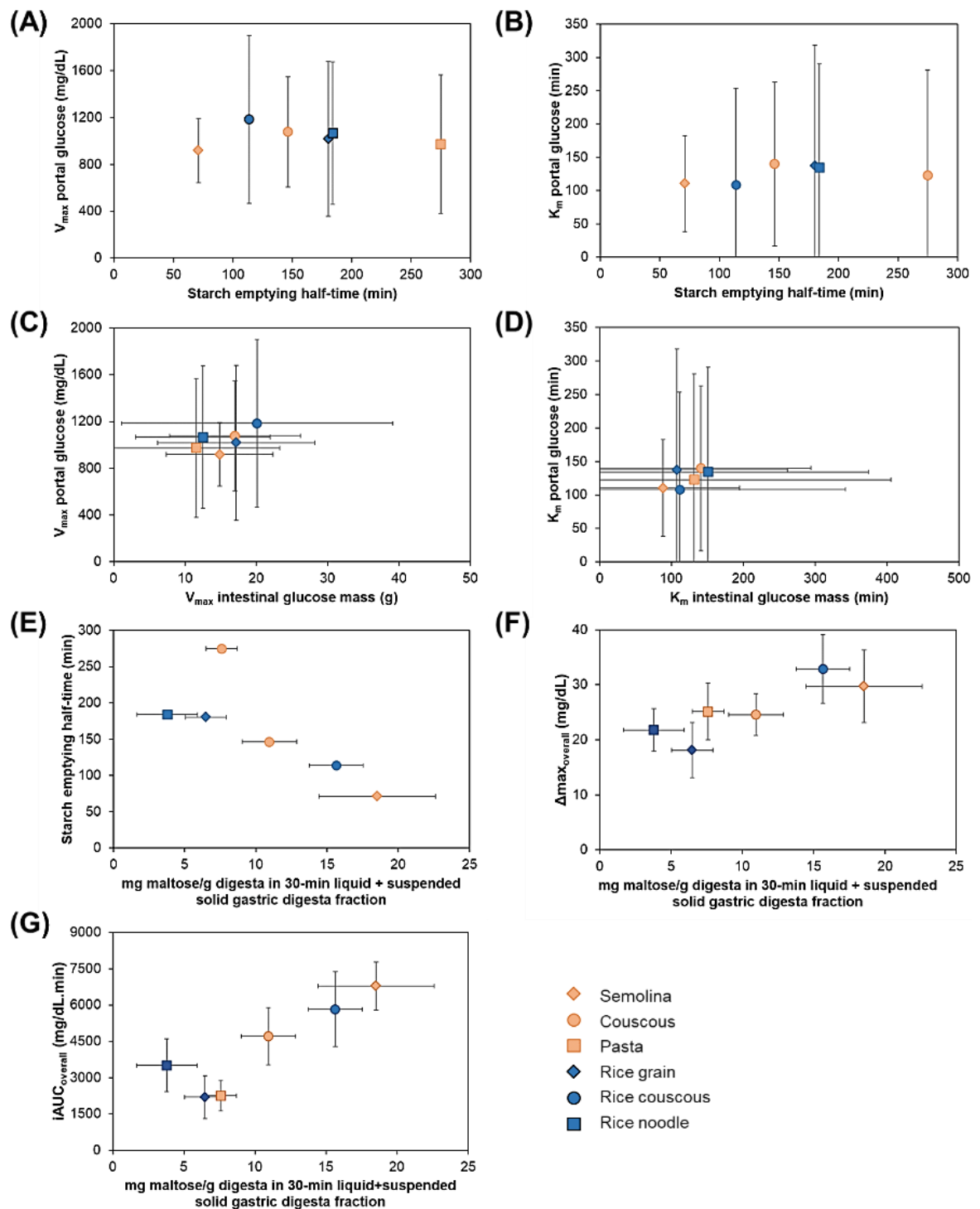


Figure 6.10 Relationships between: V_{\max} portal glucose and starch emptying half-time (A); K_m portal glucose and starch emptying half-time (B); V_{\max} portal glucose and V_{\max} total mass of intestinal glucose (C); K_m portal glucose and K_m total mass of intestinal glucose (D); maltose in the 30-min gastric digesta liquid and suspended solid fractions (from Chapter 5, Table 5.4) with starch emptying half-time (E), $\Delta\text{max}_{\text{overall}}$ (F), and $\text{iAUC}_{\text{overall}}$ (G). Error bars for mg maltose/g digesta, $\Delta\text{max}_{\text{overall}}$, and $\text{iAUC}_{\text{overall}}$ were obtained from experimental data (mean \pm SE). Error bars for K_m and V_{\max} were obtained from model fitting (fitted parameter \pm 95% confidence interval). Starch half-emptying time was calculated using fitted starch emptying parameters in Chapter 5. Each symbol in the figure corresponds to one diet, as indicated by the legend at the bottom right of the figure: semolina (♦), couscous (●), pasta (■), rice grain (◆), rice couscous (●), rice noodle (■).

three other intestinal sections (>2 m each) that leads to shorter retention time of digesta in these sections.

It was shown in Chapter 5 that the liquid and suspended solid fractions of gastric digesta were the main materials emptied during gastric emptying. Therefore, the particle size distribution of these gastric digesta fractions from Chapter 5 with the small intestinal digesta was compared to investigate changes in particle size during small intestinal digestion. With this comparison, consistent trends across all diets were observed: peaks located between 1 to 30 μm diminished over time and as the digesta travelled further from the proximal small intestine (proximal jejunum) towards the distal small intestine (ileum) (Figure 6.5). This observation might reflect the digestion of starch granules (ranging from 3 to 15 μm for rice, or 20 to 25 μm for Durum wheat (Abecassis et al., 2012; Ramadoss et al., 2019)) by digestive enzymes in the small intestine and their disappearance due to absorption. Different profiles of the particle size distribution curves and particle size parameters ($D[4,3]$, $D[3,2]$, SSA) between diets suggest different mechanisms of starch digestion along the small intestine, which merits future investigation. However, the trends observed generally suggested more starch digestion towards the ileum due to the disappearance of peaks that occurred within the size range of starch granules.

The ileal starch digestibility of the diets after 120 and 240 min digestion (pooled together due to the insignificant effect of digestion time in a preliminary statistical analysis) ranged between 96 and 98% and was not significantly different between diets (Table 6.5). This range of starch digestibility is similar to the values reported in the literature (92.9 to 99.4%) for white-rice and wheat-based milled diets in pigs (Cervantes-Pahm, Liu, & Stein, 2014; McGhee & Stein, 2018; Vicente, Valencia, Serrano, Lázaro, & Mateos, 2009). However, the diets in those previous studies were

fed in milled form and did not require further breakdown during gastric digestion prior to gastric emptying. The similar ileal digestibility of the diets in the current study, although they were in different physical forms, suggests that the kinetics of starch digestion in the small intestine was crucial in determining the observed differences in the glycemic response, portal glucose absorption, intestinal glucose and maltose, and the particle size distribution between diets.

The kinetics of starch digestion in the small intestine, as previously discussed, was affected by $t_{1/2, \text{starch GE}}$. This implication of the influence of gastric emptying on small intestinal digestion is important, particularly when starch digestibility is used as a measure to predict glycemic response using *in vitro* approach. Previously, van Kempen et al. (2010) also reported that portal glucose appearance in a growing pig model upon the consumption of various starch sources can be accurately predicted with the *in vitro* Englyst assay (Englyst et al., 1992) if the *in vitro* results are corrected for *in vivo* gastric emptying data. Additionally, an association between the kinetics of *in vitro* starch digestibility with *in vivo* portal glucose absorption in growing pigs of breads with varying dietary fiber content and composition has been reported (Rojas-Bonzi et al., 2020), indicating the importance of starch digestion kinetics (which is influenced by gastric emptying) on glucose absorption and subsequently glycemic response.

The gastric emptying rate of the diets in the current study was limited by their breakdown rate during gastric digestion. The different breakdown rate was hypothesized to affect the flow of material along the small intestine, especially at early digestion times, which might impact the small intestinal feedback due to the presence of nutrients (Figure 6.9) (Jain et al., 1989; Lin et al., 1992; Zhang et al., 2019). The flow of maltose and glucose to the ileum at 30 min digestion was examined to elucidate further the potential mechanisms in the small intestine that affected the observed $t_{1/2, \text{starch GE}}$ and

glycemic response of the diets, especially for the larger-sized, slow-emptying diets. While it was expected that the glucose and maltose flow to the ileum at 30 min would align with the trend in the glycemic response, some discrepancies were observed. Glucose and maltose flow was the lowest in pasta and rice noodle among the six diets, but rice grain had a greater maltose and glucose flow compared to the noodle diets (69.43 ± 11.42 g glucose/kg DM eaten and 160.79 ± 25.72 g maltose/kg DM eaten in rice grain vs. 11.61 ± 2.59 g glucose/kg DM eaten and 29.63 ± 6.70 g maltose/kg DM eaten in pasta and rice noodle, averaged together). Despite its higher glucose and maltose flow than pasta and rice noodle, rice grain had the lowest $iAUC_{\text{overall}}$ among the three diets. Similarly, in the smaller-sized, fast-emptying diets, the order of their glucose and maltose flow (semolina \geq couscous $>$ rice couscous) did not follow the order of their glycemic response parameters (semolina \geq rice couscous $>$ couscous).

The disagreement between the trend of glucose and maltose flow with the trend in glycemic response might indicate indirect effects of the presence of nutrients (starch and/or its hydrolysis product, such as glucose and reducing sugars) on the physiological response, which might have occurred at a hormonal level but was not measured in the current study (Jain et al., 1989; Lin et al., 1992; Zhang et al., 2019). Alternatively, it might also indicate that the presence of nutrients in the ileum is not the only factor determining the physiological response to regulate plasma glucose level. Although the feedback mechanisms were not directly observed, the current study still demonstrates that the trends in the gastric emptying and glycemic response can be associated with the output of gastric digestion at early digestion time. The maltose content of the suspended solid and liquid fraction of 30-min gastric digesta (proximal and distal regions combined together; data obtained from Chapter 5, Table 5.4) had an inverse relationship with $t_{1/2, \text{starch GE}}$ and a proportional relationship with the glycemic response parameters

($\Delta\text{max}_{\text{overall}}$ and $\text{iAUC}_{\text{overall}}$) of the diets (Figure 6.10E-G). In contrast, such relationship with $t_{1/2, \text{starch GE}}$ or $\text{iAUC}_{\text{overall}}$ was not observed at other digestion times (Figure 6.11). These identified relationships were in agreement with previous oral glucose tolerance and gastric emptying studies in human subjects, which reported a high correlation between gastric emptying rate of glucose with only up to 60-min glycemic response (Horowitz et al., 1993; Marathe et al., 2015). Regardless of interindividual variations and other factors regulating gastric emptying, the identified relationships between gastric digestion and glycemic response strongly suggest the importance of food structure in determining gastric digestion output and glycemic response. Future studies should include the measurement of hormonal responses to elucidate the mechanisms of small intestinal feedback as affected by gastric digestion.

6.5.3 Limitations of the study

The glycemic response profiles of the pigs were found to be variable between pigs and diets, although a trend still could be observed in the $\Delta\text{max}_{\text{overall}}$ and $\text{iAUC}_{\text{overall}}$, as well as the Gompertz model parameters for $\Delta\text{glucose}$ and iAUC . It is noteworthy that the biphasic profile of the average glycemic response curve (Figure 6.2A-B) was similar to previous studies using growing pigs, where the pigs were fed with different types of cereal soluble dietary fiber (Pluschke et al., 2018), glucose solution (Manell et al., 2016), or different types of breads (Barone et al., 2019). The similarity of the averaged glycemic response profiles with previous studies suggests that the majority of the pigs in this study had similar response after feeding with a diet. However, noises in the data could not be avoided, likely due to the low number of replicates.

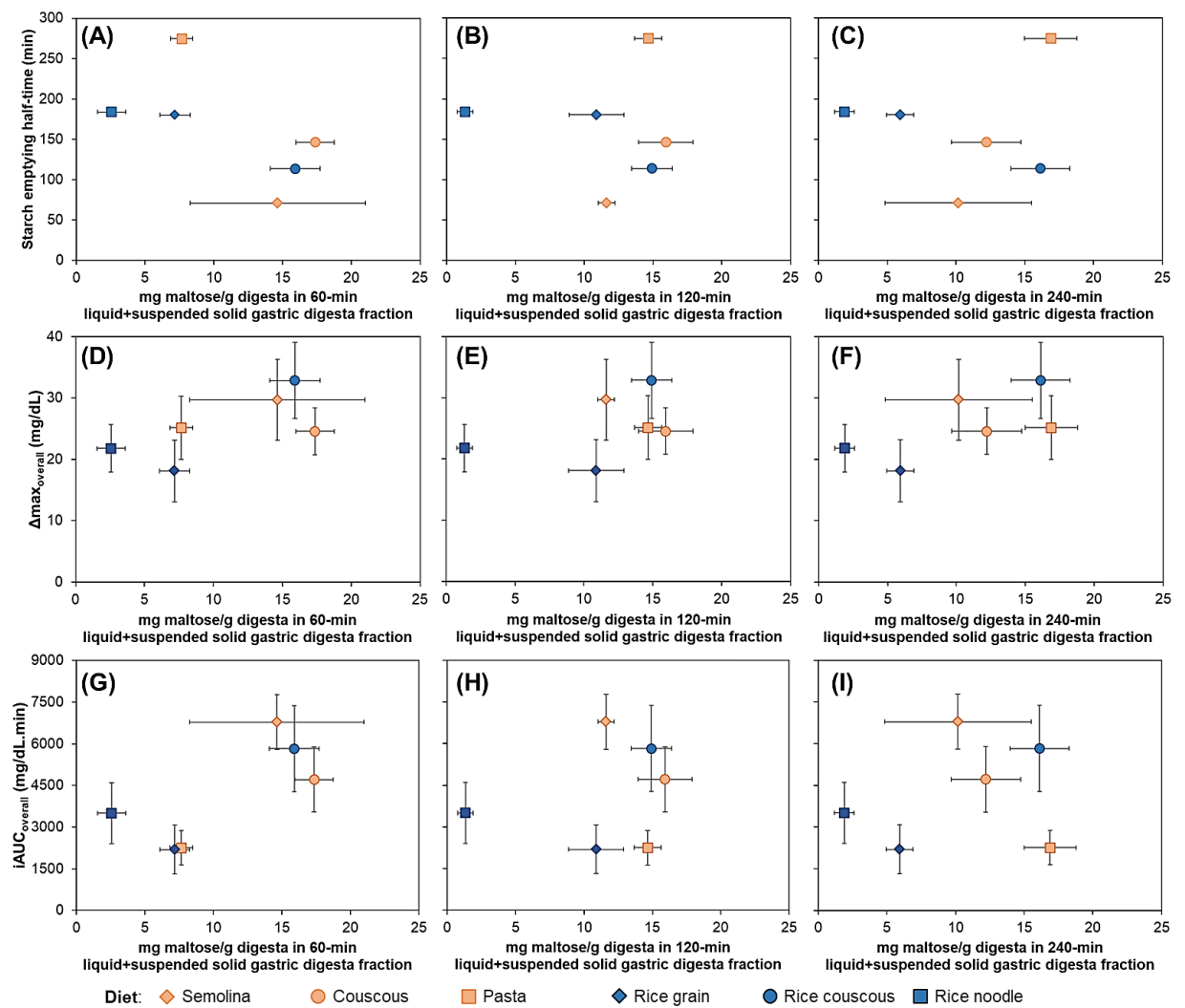


Figure 6.11 Relationships between starch emptying half-time (A-C), $\Delta\text{max}_{\text{overall}}$ (D-F), and $\text{iAUC}_{\text{overall}}$ (G-I) with maltose in the gastric digesta liquid and suspended solid fractions at 60 min (first column), 120 min (second column), or 240 min (third column) digestion. Values are presented as mean \pm SE. Each symbol in the figure corresponds to one diet, as indicated by the legend at the bottom of the figure: semolina (\diamond), couscous (\circ), pasta (\square), rice grain (\diamond), rice couscous (\bullet), rice noodle (\blacksquare).

The current glycemic response study was limited by the number of replicates that varied between diets, which might have caused the lack of statistical significance between diets. In human studies, it is recommended that a glycemic response study involves at least ten subjects to provide a reasonable degree of power (80%) and precision at a significance level of $p < 0.05$ (Brouns et al., 2005). For pigs, the minimum number of subjects is expected to be less, as the environment is carefully

controlled and external factors that might affect glycemic response can be minimized. It was initially expected that all 18 pigs in the glycemic response study could be fed with four types of diets (reference diet and three study diets) until the end of study period, resulting in 9 replicates for each study diet and 18 replicates for the reference diet, which would provide sufficient power to observe significant differences. While ideally sufficient number of replicates should still be achieved after excluding ineligible subjects, this was not achieved in the current study due to the difficulties in maintaining the catheter from being blocked in several pigs and ensuring the pigs ate the minimum amount required for each diet.

The glycemic response study reported here was coupled with a gut content collection study, with the overall goal to understand the link between changes to food structure during gastrointestinal digestion (mainly the gastric phase) and the resulting glycemic response. To match the minimum amount of food consumed to ensure that the stomach was filled to its working volume (see Chapter 4), pigs in the glycemic response study were required to consume the same amount as in the gut content collection study. Some pigs could not consume the minimum required amount, possibly due to the bulkiness of the diets (due to their intact food form and high moisture) compared to conventional pig diets (powder form). Moreover, there was an indication of the delivery of glucose and maltose to the ileum at as early as 30-min digestion for all the diets (Table 6.5), which might have triggered the ileal brake and led to reduced food intake (Cisse et al., 2017; Hasek et al., 2020). Although hormonal responses were outside the scope of the current study, future studies should consider meal portion size and time given for meal consumption to avoid potential effects of physiological feedback mechanisms on food consumption, such as the ileal brake.

There are limited studies using pigs catheterized in their jugular vein for comparison, but available information from the literature implies that the size of pigs and the structure of the diets might have contributed to the limitations of the current study. A study using 48-kg growing pigs catheterized in their jugular vein reported a consistent biphasic response for all pigs (Pluschke et al., 2018), which was not observed in the current study. Pigs in that study were fed with powder diet (~90% dry matter) or 50 mL glucose solution, which were easier to consume than diets with high moisture and intact food structure in the current study (it was reported that the pigs finished the study diets in <15 min). Another study involving 60-kg pigs with catheterization on their mesenteric artery and portal vein reported that the pigs could finish 200-g starch equivalent of bread in 15 min (Christensen et al., 2013). The larger size of the pigs in these studies might have contributed to the ability of the pigs to consume a larger meal portion. Giuberti, Gallo, and Masoero (2012) used 35-kg growing pigs with a jugular catheter – a similar size of pigs used in the current study, but they used ground bread, hence the pigs could finish the study diets within 15 min. This comparison with other studies suggests that for future studies with similar design to the present study, the size of the pigs and the meal portion should be considered. Despite these limitations, the current study still was able to identify the relationship between food structure, gastrointestinal digestion, and glycemic response, which would be of useful for food structuring strategy to modify nutrients release and absorption rate.

6.6 Conclusions

This study was the first to comprehensively identify the link between food structure, gastric breakdown rate, and glycemic response *in vivo*. It was found that food macrostructure affected the maximum change in plasma glucose ($\Delta\text{max}_{\text{overall}}$), as well as

the overall glycemic impact ($iAUC_{\text{overall}}$) of starch-rich diets by affecting the gastric emptying rate of the diets, which further influenced the kinetics of intestinal digestion of the diets and glucose absorption to the portal vein. Diets with smaller initial size (semolina, couscous, and rice couscous) had a higher $\Delta\text{max}_{\text{overall}}$ and $iAUC_{\text{overall}}$ than diets with larger initial size (29.0 ± 3.2 vs. 21.7 ± 2.6 mg/dL and 5659.2 ± 727.1 vs. 2704 ± 521.3 , for the smaller- and larger-sized diets, respectively). With the variations between diets in their glycemic response, it was noteworthy that the ileal starch digestibility was not significantly different between the diets, which indicated the importance of starch digestion kinetics on glycemic response.

The starch digestion kinetics, which resulted in different glycemic responses, was attributed to the different starch emptying of the diets from the stomach, where smaller-sized diets had a shorter starch emptying half-time compared to the larger-sized diets. The different emptying half-times between the diets were associated with their breakdown rates during gastric digestion. These identified relationships will be useful for food structuring strategy to modulate glycemic response. Additionally, the application of the Michaelis-Menten model to empirically estimate the overall effect of starch digestion, absorption, and physiological regulations on the maltose and glucose present in the intestinal lumen, as well as glucose absorption into the portal vein, was successful to elucidate the potential relationships between food structure, food breakdown rate in the stomach, small intestinal digestion, and glucose absorption.

CHAPTER 7. Contribution of the proximal and distal gastric phases to the breakdown of starch-rich foods during static *in vitro* gastric digestion

7.1 Abstract

In vitro gastric digestion studies commonly focus on the acidic environment of the stomach (the distal phase), neglecting that the contact time between food and salivary amylase can be extended during the proximal phase due to minimal gastric mixing. Consequently, the role of the proximal phase of gastric digestion on the breakdown of solid starch-based foods is not well understood. This study aimed to address this question using a static *in vitro* digestion approach. Cooked starch-rich foods of different physical structures (couscous, pasta, rice couscous, rice noodle, and rice grain) were subjected 30 s oral phase digestion, followed by prolonged incubation of the oral phase mixture (pH 7) for up to 30 min representing different proximal phase digestion times. Each proximal phase sample was sequentially incubated in excess simulated gastric fluid (distal phase, pH 2) for up to an additional 180 min. Results suggested that the proximal phase aided solid food breakdown through starch hydrolysis that caused leaching of particles <2 mm. The distal phase led to softening of food particles, but the softening process was not enhanced with longer proximal phase. In foods with smaller initial size (couscous and rice couscous), a proximal phase of 15 min or longer followed by 180-min distal phase also increased starch hydrolysis in the liquid and suspended solid fractions of the digesta, indicating the influence of food structure on acid hydrolysis during *in vitro* gastric digestion.

Keywords: amylolysis, acid hydrolysis, biochemical breakdown, gastric digestion, physical breakdown, starch

Chapter 7 Overview

Food breakdown behavior in *in vitro* system:

- Moisture uptake
- Textural property
- Particle size distribution
- Dry matter retention
- Starch hydrolysis

Research Objective 4

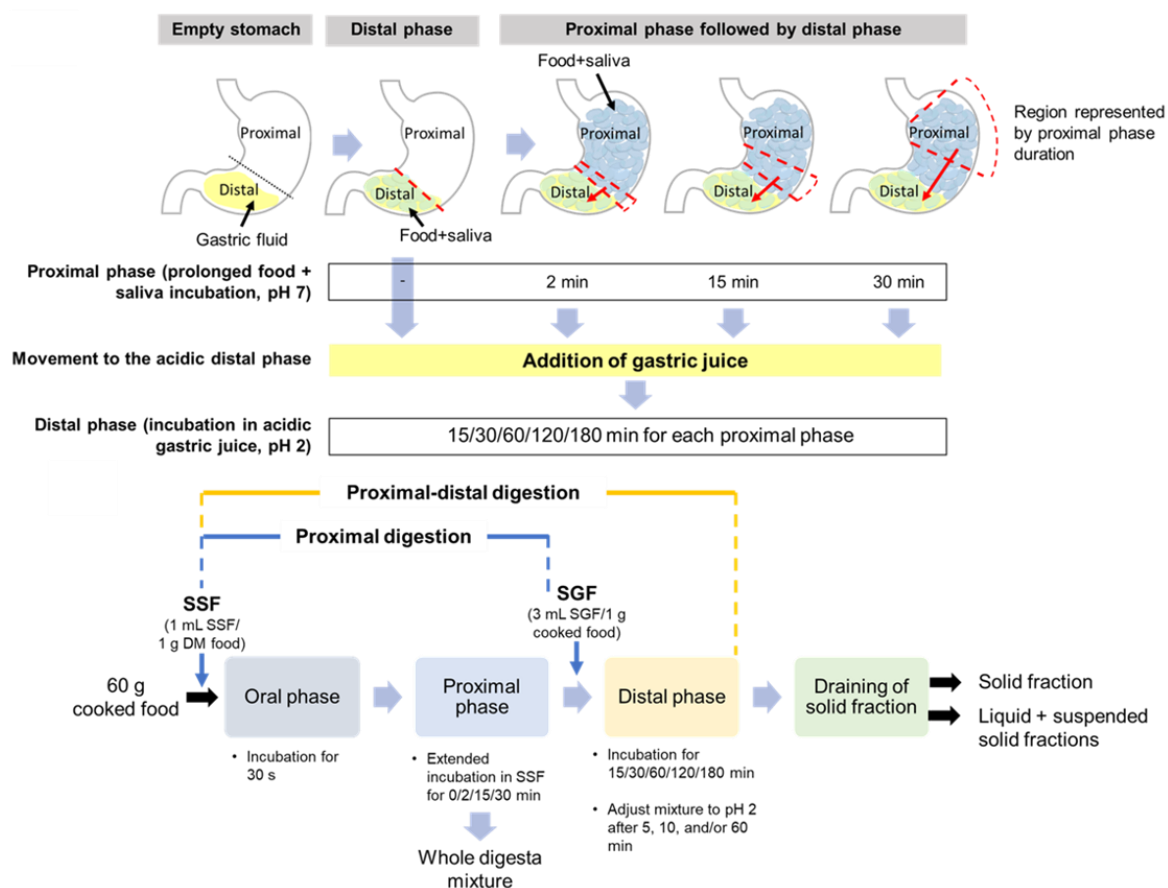
Investigate the contribution of the proximal and distal phases of gastric digestion on food gastric breakdown behavior and their consequence on the properties of emptied particles

Research Objective 1

Identify the link between food structure, gastric physiology, and food breakdown behavior of in the stomach (Hypothesis validation)

Experimental approach

Static *in vitro* study



Analysis of particle size using the Mastersizer in this chapter (Section 7.3.5.2) was conducted with the assistance of Dr. Parthasarathi Subramanian (Riddet Institute).

7.2 Introduction

Gastric digestion (together with mastication) is an important process for the physical breakdown of food prior to further digestion and nutrient absorption in the small intestine. Particularly for starch-rich foods, gastric emptying rate is crucial to their glycemic response profile, which may be modified through food structuring to alter food breakdown rate in the stomach. Physical changes to solid foods during gastric digestion have been partially associated with diffusion of gastric fluid and hydrolysis by gastric enzymes, which aid to soften food texture, enhancing the rate of mechanical breakdown in the stomach by gastric wall contractions (Somaratne, Ye, et al., 2020). The commonly accepted view that the stomach has an acidic environment ($\text{pH} \leq 3$) and inconducive for salivary amylase activity in the food bolus to continue starch hydrolysis in solid starch-rich foods (Brownlee et al., 2018) makes its contribution on the breakdown of starch-based foods less understood. Consequently, *in vitro* starch digestion procedures commonly simulate the gastric digestion step at $\text{pH} < 3$ with excess gastric fluid (Englyst et al., 1999; Goñi et al., 1997; Monro, Mishra, & Venn, 2010) and heavily focus on the small intestinal stage. Other non-starch specific *in vitro* methods that focus on biochemical changes during digestion, such as the INFOGEST static digestion protocol (Brodkorb et al., 2019; Minekus et al., 2014), define gastric digestion to be conducted at $\text{pH} 3$ with limited amount of gastric fluid. These procedures are also generally conducted using ground samples, thus eliminating the physical structure of the foods.

However, the stomach does not always have an acidic environment; it consists of two physiological regions: proximal and distal. After meal consumption, the proximal region acts as temporary bolus storage with minimal contractions, while the distal region serves as the location for initial gastric fluid accumulation as well as a grinder for

mechanical breakdown of solid foods (Hasler, 2009; Rodríguez Varón & Zuleta, 2010; Soybel, 2005). With the different features of the proximal and distal regions of the stomach, their biochemical environment is expected to be different after meal consumption. Previous *in vivo* studies, where growing pigs were fed with food of varying composition and structures, reported higher intragastric pH in the proximal region compared to the distal region as a result of gradual addition of gastric fluid, different rates of acidification of gastric content, and variations in meal mixing with gastric secretions (Bornhorst, Rutherford, et al., 2014; Nau et al., 2019); this was also observed in Chapter 5. These studies indicated that in the gastric environment, the intragastric pH may remain within the working pH range of salivary amylase ($\text{pH} \geq 3$) for up to 1 hour.

As a result of prolonged contact between the ingested food and active salivary amylase, starch hydrolysis may continue to a certain extent during gastric digestion, as demonstrated in the *in vivo* study in Chapter 5, as well as in *in vitro* studies using various solid starch-based products (Freitas & Le Feunteun, 2019; Freitas et al., 2018; Gao et al., 2021; Wu, Deng, et al., 2017). It was proposed in Chapter 5 that continuing starch hydrolysis in the proximal stomach generated small food particles through surface erosion of the food matrix, subsequently affecting the gastric breakdown and emptying mechanisms, as well as the properties of food particles that are released to the small intestine. However, there is limited information available on the effect of starch digestion in the proximal stomach on solid food breakdown. Hence, the contribution of continuing starch hydrolysis in aiding the physical breakdown of starch-based foods is not properly understood.

As food is temporarily stored in the proximal stomach during gastric digestion, gastric fluid is secreted and gradually fills the stomach, causing acidification of stomach

contents. The acidification begins from the periphery of stomach and occurs faster in the distal stomach (Bornhorst, Rutherford, et al., 2014; Spiller & Marciani, 2019). Physical changes of starch-rich foods during gastric digestion without the proximal phase (i.e., only considering the distal phase with instantaneous acidification) have been previously studied (Drechsler & Bornhorst, 2018; Kong et al., 2011; Mennah-Govela & Bornhorst, 2016a; Somaratne, Ye, et al., 2020). Meanwhile, the consequences of proximal stomach phase on the physical and chemical changes of food particles during the distal stomach phase have not been investigated in detail. It is also not understood if changes that occur during proximal phase may affect the properties of particles that are emptied from the distal stomach (Chapter 2). Understanding how the proximal and distal stomach phases of gastric digestion contributes to food breakdown, including how they affect the properties of the emptied food particles, will be beneficial to improving food structuring strategies intended for controlled release of nutrients.

It has been reported in Chapter 4 that the study diets exhibited distinct breakdown rates in the proximal and distal stomach of growing pigs, which impacted their gastric emptying rate. The different breakdown rates were thought to be influenced by distinct digesta pH between the stomach regions (proximal pH > distal pH). However, the simultaneous processes of gastric secretion, gastric emptying, and mechanical breakdown by gastric wall contractions *in vivo* limited the specific examination of the contribution of the proximal and distal gastric phases on food breakdown. This study sought to investigate the roles of proximal and distal gastric digestion phases on the physicochemical properties of food particles and emptied particles for varying starch-based foods studied. A static digestion approach was used to isolate the roles of α -amylase during the proximal stomach phase and gastric fluid during the distal stomach phase on the breakdown behavior of food particles during gastric digestion, while

minimizing any mechanical breakdown. It was hypothesized that longer contact with α -amylase during the proximal phase would hydrolyze more starch in the food matrix, leading to leaching of small particles. Changes due to starch hydrolysis in the proximal phase were thought to change the breakdown behavior of food particles during the distal stomach phase. To examine how food structure may affect the process, durum wheat- and white rice-based foods of different micro- and macrostructure were investigated. It was hypothesized that foods with less compact microstructure and smaller initial size (macrostructure) would be more prone to breakdown during the proximal phase, causing more profound physical and chemical changes during the distal phase.

7.3 Materials and methods

7.3.1 Materials

Couscous, pasta, rice couscous, rice grain, and rice noodle used in the study were the same as in Chapter 4 to 6. The couscous and rice couscous used for cooking had initial diameter of 1 to 2 mm. The pasta and rice noodles used had initial length of 10 to 15 mm. Rice grain was used directly for cooking. The food products were cooked as described in Chapter 3. Water used for cooking rice-based products was mixed with 1.5% (v/v) yellow coloring to provide similar color contrast to the wheat-based products in the image analysis (Section 7.3.4.3). Cooked foods were cooled to $\sim 40^\circ\text{C}$ prior to *in vitro* digestion. Formulation of simulated digestive fluids (SSF and SGF) was described in Chapter 3 (Section 3.3.2).

7.3.2 Digestion procedure

The static *in vitro* digestion procedure used was described in Chapter 3 (Section 3.3.2). Experiments were conducted in batches; one experimental batch consisted of the proximal digestion and the proximal-distal digestion of one food at one proximal phase

duration. Proximal digestion samples were analyzed as whole digesta mixtures, whereas proximal-distal digestion samples were analyzed separately as solid and liquid – suspended solid fractions (separation method was described in Section 3.3.2).

7.3.3 Cooked food characterization

The properties (moisture content, particle size, texture, starch content, and reducing sugar content) of cooked food samples were measured as described in Chapter 4 (Sections 4.3.4, 4.3.5.1, 4.3.5.2, and 4.3.5.4) and Chapter 5 (Section 5.3.6.1). Starch content was determined from freeze-dried samples. Other analyses were performed on fresh samples in the intact form, except reducing sugar content analysis that used homogenized samples.

7.3.4 Solid fraction and whole digesta mixture characterization

7.3.4.1 Moisture content

Moisture content of each cooked food and digesta sample was determined gravimetrically as described in Chapter 4 (Section 4.3.5.1).

7.3.4.2 Texture analysis

Texture analysis of digesta samples was conducted with a bulk compression method as described in Chapter 4 (Section 4.3.5.2) to obtain the hardness values. Each measurement was done on 18 to 21 g sample, depending on the food type. The individual food particles of undigested food tended to stick to each other, causing void spaces that affected the measured hardness values. Hence, measurement for undigested food was conducted on samples mixed with water at 1:1 (mL water:g dry matter of food) ratio, similar to the food:SSF ratio in the oral phase. This addition of water was done to minimize the interference of void spaces on the textural measurement, as

previously reported (Drechsler & Bornhorst, 2018). Analyses were conducted on at least duplicate aliquots of each sample.

7.3.4.3 Particle size

The particle size of the solid fraction was determined using the image analysis procedure described in Chapter 4 (Section 4.3.5.4), but without staining using potassium iodide solution; this was to minimize the overlap with characterization of suspended solids using the Mastersizer and to minimize artefacts during image processing. Duplicate samples were analyzed after the proximal phase, and after 30- and 180-min distal phase (for each proximal phase duration). Two images were taken per sample from each replicate, and results from image processing from the two images were averaged to represent that particular sample. After image processing, particles $<0.05 \text{ mm}^2$ (equivalent to 0.25 mm diameter) were not considered to minimize noise (shadow) in the results.

7.3.5 Liquid and suspended solid fraction characterization

7.3.5.1 Total soluble solids

Total soluble solids in the liquid – suspended solid mixture were measured using a digital refractometer (PAL-1 Pocket Refractometer, Atago, Japan). Each sample was measured in triplicate. The °Brix of SGF and SSF were subtracted (calculated as the weighted average based on the volume ratio of SGF and SSF) to determine the actual °Brix values of the samples.

7.3.5.2 Particle size

The size distribution of the suspended solid particles (two aliquots per sample) in the liquid - suspended solid mixture was measured using Mastersizer-2000, as described in Chapter 5 (Section 5.3.5).

7.3.5.3 Hydrolyzed starch analysis

Frozen samples (a mixture of liquid and suspended solid fraction) were thawed prior to analysis. The mixture was centrifuged ($6,800 \times g$, 10 min) to separate leached small particles (suspended solid fraction) from the liquid fraction. The liquid fraction was used directly for analysis. The suspended solid fraction from each sample was mixed with 1.5 mL water, mixed on a vortex for 15 s, then incubated for 1 h at room temperature. Afterwards, the supernatants (0.1 to 0.4 mL) of the mixtures were separated by centrifugation ($6,800 \times g$, 10 min) for analysis. Reducing sugar content (measured as maltose equivalent) in the liquid and supernatant of suspended solid samples was quantified using the dinitrosalicylic acid (DNS) method adapted to 96-well microplates, as described in Chapter 5 (Section 5.3.6.1). Hydrolyzed starch content in each sample was expressed as g maltose/g starch, considering the starch content of each cooked food.

7.3.6 Data and statistical analysis

7.3.6.1 Solid retention calculation

For each proximal phase followed by distal phase digestion, the dry and wet mass retention data of the digesta solid fraction exhibited asymptotic behavior. To empirically describe this asymptotic behavior, the Mitscherlich equation (Eqn 7.1) on the “law of diminishing increments” was selected. The equation had been used in the past to describe the effect of fertilization on crop yields (Harmsen, 2000):

$$\frac{M_t}{M_0} = A - (A - A_0)e^{-k_m t} \quad (7.1)$$

where M_t : dry or wet mass of the digesta at distal time t ; M_0 : initial dry mass of the cooked food for each digestion; A : the asymptote value of the curve; A_0 : theoretical initial mass retention without proximal phase (equals to one); k_m : a coefficient

describing the rate of mass retention change (min^{-1}). Model fitting to obtain the A and k_m parameters was conducted using MATLAB R2018a (non-linear least squares method).

7.3.6.2 Softening kinetics of solid fraction and whole digesta mixture

For each food, the hardness values of the digesta at time t (H_t) were normalized relative to the initial hardness of undigested food with lubrication (H_0), and fitted to the Weibull model (Drechsler & Bornhorst, 2018):

$$\frac{H_t}{H_0} = e^{-(k_h * t)^\beta} \quad (7.2)$$

where H_t : the hardness of the digesta (N) at time t (min), H_0 : the initial hardness of the food (N), k_h : the scale parameter (min^{-1}) and β : the shape factor (dimensionless).

Model fitting was conducted using MATLAB R2018a (non-linear least squares method). Textural changes of the whole digesta during proximal digestion were modelled to identify the softening kinetics of the foods due to contact with α -amylase; one model fitting was conducted on the data points from all three replicates altogether because experiments were conducted on different days. Textural changes of the solid fraction after proximal-distal digestion were modelled to identify the further impact of proximal phase on softening kinetics by gastric fluid diffusion during distal phase; model fitting was conducted on each set of replicates. The half-softening time ($t_{1/2}$, softening) was calculated using the obtained softening kinetic parameters, by defining $H_t/H_0 = 0.5$.

7.3.6.3 Particle size distribution of solid fraction

Particle size data from the solid fraction were fit to the Rosin-Rammler model using MATLAB R2018a using non-linear least squares method (Hutchings et al., 2011):

$$Q = 1 - e^{-\left(\frac{x}{x_{50}}\right)^b \cdot \ln(2)} \quad (7.3)$$

where Q : the cumulative particle area (% of total area), x : n^{th} area measurement (mm^2), x_{50} : the area of a theoretical sieve aperture through which 50% of the particle area can pass (mm^2), and b : the broadness of the distribution (dimensionless) – a higher value of b indicates a narrower distribution.

The x_{10} and x_{90} of the sample were also calculated with Eqn. 7.3 as the area of a theoretical sieve aperture (mm^2) through which 10 or 90% of the particle area can pass, respectively. The total particle area and the number of particles in each sample were utilized to calculate the particle area per gram digesta, number of particles per gram dry matter (particles/g DM), and average area per particle. The moisture content of the sample was used to calculate number of particles per gram dry matter.

7.3.7 Statistical analysis

Statistical analysis was conducted in SAS®Studio 3.8. The normality and heteroscedasticity of the properties data of undigested diets were assessed with Shapiro-Wilk's test and Levene's test, respectively. The properties of undigested foods (moisture content, hardness, starch content, hydrolyzed starch content) were analyzed with one-way ANOVA. The particle size parameters of undigested diets were analyzed with the Kruskal-Wallis test due to non-normal distribution.

For statistical analysis of digestion data, a mixed-model ANOVA (PROC GLIMMIX) was employed. The batch of experiments was assigned as the experimental unit. The effect of food type was analyzed on the softening kinetics parameters of digesta from proximal digestion. The effect of food type, proximal phase duration, and their interaction was analyzed on particle size parameters and hardness data from proximal digestion, as well as model parameters of solid retention (Eqn. 7.1) and softening kinetics (Eqn. 7.2) from proximal-distal digestion. The effect of food type, proximal and distal phase duration, and their two- and three-way interactions were

analyzed on both solid (moisture content, wet mass and dry matter retention, hardness, particle size parameters) and liquid + suspended solid fractions (°Brix, particle size parameters, and total gram maltose/gram starch in the mixture) of digesta from proximal-distal digestion. Logarithmic transformation was applied to particle size parameters (both on the solid and suspended fractions), $t_{1/2, \text{softening}}$, and k_h parameter data to achieve normality of residuals.

Preliminary statistical analyses were conducted on all data sets to remove outliers (data points with internally studentized residuals outside $(-3, 3)$), then the data sets were re-analyzed. When main effects were significant, the Tukey-Kramer procedure was used to identify differences between individual means at a significance level of $p < 0.05$. All values are presented as mean \pm standard deviation (SD).

7.4 Results

7.4.1 Characteristics of the selected food products

The average area per particle, x_{10} , x_{50} , and x_{90} of the cooked foods were significantly different between the five foods ($p < 0.01$; Table 7.1). Overall, these particle size parameters of the foods were: agglomerated products (couscous, rice couscous) $<$ rice grain $<$ noodles (pasta, rice noodle). The hardness values (measured with lubrication) were: noodle products (51.46 ± 9.67 N) $<$ agglomerated products (66.39 ± 11.87 N) $<$ rice grain (112.59 ± 8.72 N; $p < 0.01$ for each pair of comparison). The moisture content of the food was similar, except rice couscous and rice grain that were lower than the other three foods ($p < 0.05$). Reducing sugar content in the wheat-based foods (0.02 to 0.03 g maltose/g starch) was significantly higher than rice-based foods (0.003 to 0.004 g maltose/g starch; $p < 0.0001$).

Table 7.1 Physical properties and chemical content of the selected food products. Values are shown as mean \pm SD ($n = 6$ for each data point). Significantly different values between food products within the same measured parameter are indicated with abcd superscript ($p < 0.05$).

Parameter	Couscous	Rice couscous	Pasta	Rice noodle	Rice grain
x_{10} (mm ²)	0.77 ± 0.42^c	0.20 ± 0.10^d	119.77 ± 27.35^a	89.67 ± 26.51^a	10.68 ± 2.12^b
x_{50} (mm ²)	5.41 ± 1.92^c	4.03 ± 1.99^c	228.8 ± 50.64^a	195.94 ± 15.44^a	35.5 ± 6.91^b
x_{90} (mm ²)	11.22 ± 3.48^c	12.43 ± 6.09^c	296.54 ± 77.97^a	266.83 ± 20.11^a	56.08 ± 13.28^b
b	1.64 ± 0.17^c	1.07 ± 0.06^d	5.70 ± 1.91^a	4.43 ± 1.45^{ab}	2.77 ± 0.41^b
Specific surface area (mm ² /gram)	1886.0 ± 507.5^a	2419.9 ± 294.0^a	788.9 ± 141.8^c	1274.7 ± 48.8^b	912.3 ± 177.1^c
Average area (mm ²)/particle	3.17 ± 1.18^c	1.55 ± 0.57^c	69.86 ± 19.87^a	62.89 ± 39.39^a	10.4 ± 2.18^b
Particles/g DM	1728 ± 296^b	4432 ± 1170^a	35 ± 12^d	95 ± 79^d	230 ± 23^c
Moisture content (g H ₂ O/g DM)	1.79 ± 0.06^a	1.60 ± 0.08^b	1.87 ± 0.07^a	1.78 ± 0.11^a	1.61 ± 0.09^b
Initial hardness (N)*	74.21 ± 9.73^b	58.58 ± 8.29^{bc}	56.07 ± 9.56^c	46.86 ± 7.97^c	112.59 ± 8.72^a
Starch content (g/ 100 g DM) [§]	67.16 ± 2.30^b	82.36 ± 1.76^a	71.43 ± 4.86^b	81.9 ± 3.55^a	82.38 ± 2.87^a
Reducing sugar content (g maltose/g starch)	0.020 ± 0.003^a	0.004 ± 0.001^b	0.018 ± 0.004^a	0.004 ± 0.002^b	0.003 ± 0.001^b

x_{10} , x_{50} , x_{90} : the area of a theoretical sieve aperture through which 10, 50, and 90% particle area can pass, respectively; b : the broadness of particle area distribution – higher value of b corresponds to a narrower distribution.

*Initial hardness was measured with addition of water at the same food:SSF (w/v) ratio for the respective diet.

[§]Measured using Megazyme Total Starch kit, following the procedure for samples not containing free sugars or resistant starch.

7.4.2 Whole digesta mixture properties after proximal digestion

Hardness and normalized hardness (H_t/H_0) during proximal digestion were significantly influenced by food type and proximal phase duration (Table 7.2 and F.1; Figure 7.1A; $p < 0.0001$). A significant decrease in H_t/H_0 between 0- or 2- and 30-min proximal phase was observed only in couscous, pasta, and rice noodle (Figure 7.1A; $p < 0.05$). The $t_{1/2}$, softening of the foods, as estimated with Eqn. 7.2, was significantly influenced by food type ($p < 0.0001$). Among the five foods, agglomerated products had the shortest $t_{1/2}$, softening (<1 min), followed by rice noodle (123.5 min), rice grain (355.9 min), and pasta (541.8 min). The softening kinetics parameters of the foods to calculate $t_{1/2}$, softening are given in Table 7.3.

Food type significantly impacted all PSD parameters (x_{10} , x_{50} , x_{90} , particles/g DM, area/particle, particle area/g, and broadness of distribution (b)) of the whole digesta mixture (Table 7.2; $p < 0.01$), proximal phase significantly impacted x_{10} , x_{50} , and x_{90} , while the food \times proximal interaction significantly impacted only x_{10} ($p < 0.05$), indicating that particles with smaller area were associated with both food type and the length of proximal phase digestion. Among the foods, only rice grain exhibited a significant decrease in its x_{10} and x_{50} between 0- and 30-min proximal phase (Table 7.4; $p < 0.05$). To include a greater number of particles in the distribution for each treatment, data from three experimental replicates were pooled to establish overall PSD for each proximal and selected proximal-distal digestion condition (Figure 7.1B-F and F.2-F.6; Table F.3). Compared to the cooked (undigested) food, an increasing proportion of particles $\leq 4 \text{ mm}^2$ was observed in rice grain and noodles with a longer proximal phase duration (from 1.42% to 3.52% at 0 and 30 min proximal phase, averaged between rice grain and both noodles, respectively). Similarly, an increasing proportion of particles $\leq 4 \text{ mm}^2$ was observed in agglomerated products with increasing proximal phase duration (from 37.88% to 44.02% at 0 and 30 min proximal phase, averaged between agglomerated products, respectively).

Table 7.2 Statistical significance of food type, proximal phase, distal phase, and their interaction effects on the physicochemical properties of digesta from proximal-distal digestion and proximal digestion.

Measured variable	Food	Proximal	Distal	Food × Proximal	Food × Distal	Proximal × Distal	Food × Proximal × Distal
Proximal-distal digestion data							
Mass retention, solid fraction							
W _t /W ₀	****	****	****	****	****	****	NS
W _t /W ₀ profile asymptote (A)	****	****	-	****	-	-	-
W _t /W ₀ profile k _m	****	NS	NS	****	-	-	-
DM _t /DM ₀	****	****	****	****	****	NS	NS
DM _t /DM ₀ profile asymptote (A)	****	****	-	NS	-	-	-
DM _t /DM ₀ profile k _m	NS	NS	NS	NS	NS	NS	NS
Moisture content, solid fraction							
Moisture content (dry basis)	****	****	****	****	****	NS	NS
Moisture change	****	****	****	***	****	NS	NS
Textural changes, solid fraction							
Hardness	****	****	****	***	****	NS	***
Normalized hardness (H _t /H ₀)	****	****	****	**	****	NS	*
Softening kinetics k _h	****	*	-	NS	-	-	-
Softening kinetics β	*	NS	-	*	-	-	-
Softening kinetics t _{1/2,softening}	***	*	-	NS	-	-	-
Particle size parameters, solid fraction							
X ₁₀	****	NS	****	**	****	NS	NS
X ₅₀	****	****	****	*	****	NS	NS
X ₉₀	****	****	***	NS	**	NS	NS
Particles/g DM	****	NS	****	NS	***	NS	NS
Average area/particle	****	NS	****	NS	****	*	NS
Area/gram	****	*	*	**	NS	NS	NS
Broadness of distribution (b)	****	NS	NS	NS	**	NS	NS
Liquid and suspended solid fraction							
°Brix	****	****	****	****	***	*	NS
Hydrolyzed starch content	****	****	****	****	****	****	****
d ₁₀	**	****	****	****	****	NS	NS
d ₅₀	****	****	****	****	**	*	**
d ₉₀	****	****	****	****	****	NS	NS
D[4,3]	****	****	****	***	****	NS	NS
D[3,2]	****	****	****	****	****	NS	NS
Proximal digestion data							
X ₁₀	****	*	-	*	-	-	-
X ₅₀	****	**	-	NS	-	-	-
X ₉₀	****	*	-	NS	-	-	-
Particles/g DM	****	NS	-	NS	-	-	-
Average area/particle	****	NS	-	NS	-	-	-
Area/gram	**	NS	-	NS	-	-	-
Broadness of distribution (b)	****	NS	-	*	-	-	-
Hardness	****	****	-	****	-	-	-
Normalized hardness (H _t /H ₀)	****	****	-	NS	-	-	-

Asterisk (*) symbols indicate different levels of statistical significance. *: $p < 0.05$; **: $p < 0.01$, ***: $p < 0.001$, ****: $p < 0.0001$. NS: not significant

Effects with “-“ sign for a single variable were not included in the statistical model for that variable.

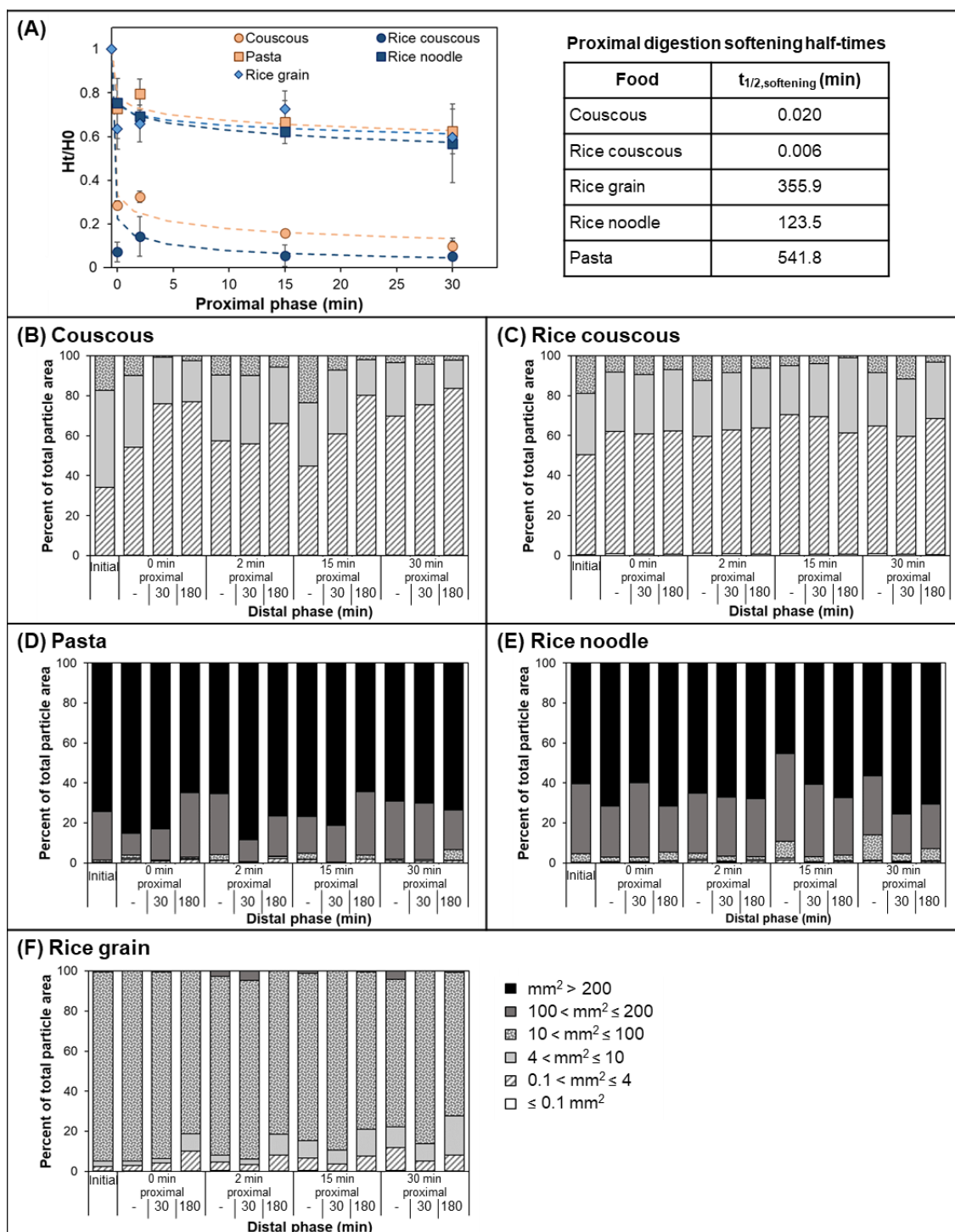


Figure 7.1 Textural changes of the foods after being subjected to various proximal phase durations in the proximal digestion and the calculated $t_{1/2, \text{softening}}$ values. Softening kinetic parameters used to calculate $t_{1/2, \text{softening}}$ are given in Table 7.3. The hardness at each time (H_t) was normalized by the hardness of undigested foods (H_0) with lubrication (see section 7.3.4.2) (A). Bar charts showing the particle area distribution of couscous (B), rice couscous (C), pasta (D), rice noodle (E), and rice grain (F) before digestion (Initial), whole digesta mixture after different proximal phase durations (shown as “–” min distal phase), and digesta solid fraction after selected proximal \times distal phase durations in proximal-distal digestion. The exact value for each area bin can be found in Table F.3.

Table 7.3 Softening kinetics parameter of the food products in the proximal digestion (obtained by fitting the data points to Eqn. 7.2) used to calculate the $t_{1/2, \text{softening}}$ presented in Figure 7.1A. The model fit of the softening curves is indicated by R^2 . Softening kinetics parameters (k_h and β_h) for each food are expressed as predicted parameter \pm 95% confidence interval.

Food	Softening kinetics parameter		R^2
	$k_h (\times 100 \text{ min}^{-1})$	β_h	
Couscous	406.10 ± 522.20	0.14 ± 0.06	0.98
Rice couscous	1930.62 ± 8558.14	0.18 ± 0.20	0.92
Pasta	0.016 ± 0.35	0.15 ± 0.17	0.69
Rice noodle	0.087 ± 0.47	0.16 ± 0.12	0.82
Rice grain	0.014 ± 0.38	0.12 ± 0.15	0.70

Table 7.4 Particle size distribution parameters of whole digesta mixture in the proximal digestion at various proximal phase durations. Values are shown as mean \pm SD ($n = 3$ for each individual value). Significantly different values between proximal phase for one type of food are indicated with abcd superscript. Significantly different values between food types within the same proximal phase are indicated with zyxw superscript ($p < 0.05$).

Food	Proximal phase (min)			
	0	2	15	30
$x_{10} (\text{mm}^2)$				
Couscous	0.25 ± 0.21^x	0.27 ± 0.20^x	0.30 ± 0.14^x	0.20 ± 0.05^x
Rice couscous	0.11 ± 0.03^x	0.10 ± 0.03^x	0.14 ± 0.01^x	0.14 ± 0.11^x
Pasta	126.26 ± 52.8^z	133.43 ± 66.3^z	123.22 ± 24.4^z	140.42 ± 45.3^z
Rice noodle	151.95 ± 62.13^z	107.16 ± 57.94^z	82.48 ± 38.39^z	73.64 ± 29.51^z
Rice grain	$14.00 \pm 7.99^{a,y}$	$7.03 \pm 3.18^{ab,y}$	$3.36 \pm 2.84^{bc,y}$	$1.66 \pm 1.32^{c,y}$
$x_{50} (\text{mm}^2)$				
Couscous	$3.01 \pm 1.86^{ab,x}$	$2.90 \pm 1.93^{ab,x}$	$3.99 \pm 2.07^{a,x}$	$2.31 \pm 0.69^{b,x}$
Rice couscous	2.60 ± 0.64^x	2.82 ± 1.13^x	2.46 ± 0.22^x	2.64 ± 1.27^x
Pasta	264.11 ± 18.01^z	235.95 ± 111.35^z	233.73 ± 37.12^z	225.95 ± 80.98^z
Rice noodle	236.38 ± 90.42^z	205.98 ± 55.37^z	169.01 ± 54.22^z	179.31 ± 52.46^z
Rice grain	$35.69 \pm 6.75^{a,y}$	$34.2 \pm 10.9^{ab,y}$	$23.8 \pm 11.06^{ab,y}$	$20.86 \pm 10.74^{b,y}$
$x_{90} (\text{mm}^2)$				
Couscous	$7.61 \pm 4.07^{ab,x}$	$7.03 \pm 4.49^{ab,x}$	$10.36 \pm 5.52^{a,x}$	$5.79 \pm 1.88^{b,x}$
Rice couscous	8.53 ± 3.23^x	9.93 ± 4.68^x	7.19 ± 0.76^x	7.94 ± 3.16^x
Pasta	358.95 ± 59.42^z	291.64 ± 134.94^z	303.30 ± 49.20^z	270.36 ± 102.31^z
Rice noodle	281.60 ± 111.11^z	274.9 ± 79.26^z	225.29 ± 62.06^z	250.83 ± 69.49^z
Rice grain	52.43 ± 6.31^y	63.95 ± 21.60^y	53.17 ± 12.16^y	59.48 ± 19.89^y
Broadness of distribution, b (dimensionless)[#]				
Couscous	1.27 ± 0.11	1.35 ± 0.08	1.27 ± 0.03	1.32 ± 0.06
Rice couscous	1.05 ± 0.12	0.99 ± 0.14	1.13 ± 0.03	1.09 ± 0.11
Pasta	5.44 ± 3.68	5.66 ± 0.49	6.68 ± 2.09	7.52 ± 2.85
Rice noodle	8.10 ± 2.13^a	5.90 ± 3.05^{ab}	4.83 ± 1.66^{ab}	3.65 ± 0.72^b
Rice grain	3.62 ± 1.43^a	2.08 ± 0.32^{ab}	1.54 ± 0.48^b	1.16 ± 0.36^b
Particle area (mm^2)/gram				
Couscous	1139.44 ± 367.96	1150.58 ± 355.64	1828.93 ± 646.37^z	1290.68 ± 299.66
Rice couscous	1174.83 ± 65.9	1117.32 ± 57.7	1186.34 ± 474.79^{zy}	838.46 ± 255.81
Pasta	730.16 ± 91.97	689.42 ± 324.44	616.3 ± 142.31^x	696.29 ± 303.58
Rice noodle	1205.13 ± 418.35	1059.93 ± 327.87	947.12 ± 144.47^{zyx}	1097.94 ± 333.35

(continued)

Table 7.4 (continued)

Food	Proximal phase (min)			
	0	2	15	30
Rice grain	721.05 ± 75.02	719.38 ± 205.5	776.55 ± 197.96 ^{yx}	754.19 ± 141.53
Average area (mm²)/particle				
Couscous	1.61 ± 0.99 ^x	1.59 ± 0.99 ^x	2.01 ± 0.87 ^x	1.29 ± 0.35 ^x
Rice couscous	1.00 ± 0.10 ^x	0.98 ± 0.16 ^x	1.07 ± 0.04 ^x	1.03 ± 0.35 ^x
Pasta	22.43 ± 7.55 ^z	35.86 ± 23.63 ^z	21.39 ± 12.78 ^z	34.12 ± 17.11 ^z
Rice noodle	74.76 ± 57.19 ^z	37.9 ± 9.27 ^z	30.35 ± 13.23 ^z	39.77 ± 13.07 ^z
Rice grain	7.94 ± 1.45 ^y	6.36 ± 2.84 ^y	5.72 ± 3.29 ^y	4.32 ± 2.42 ^y
Particles/g DM				
Couscous	2906 ± 854 ^z	3018 ± 824 ^z	3499 ± 697 ^z	3797 ± 547 ^z
Rice couscous	4208 ± 639 ^z	4377 ± 1021 ^z	4071 ± 1635 ^z	3324 ± 1490 ^z
Pasta	137 ± 62 ^{yx}	95 ± 60 ^x	154 ± 112 ^x	118 ± 117 ^x
Rice noodle	81 ± 59 ^x	114 ± 61 ^{yx}	135 ± 65 ^x	104 ± 20 ^x
Rice grain	330 ± 27 ^y	341 ± 222 ^y	685 ± 523 ^y	844 ± 626 ^y

[#] A higher value of *b* corresponds to a narrower distribution.

7.4.3 Properties of solid digesta fraction after proximal-distal digestion

7.4.3.1 Solid retention profile

The wet mass retention (W_t/W_0) was measured to provide information on the simultaneous effect of SGF uptake into the food particles and leaching of solids that occurred during digestion. The dry mass retention (DM_t/DM_0) was measured to investigate true solid retention of the food particles as impacted by leaching of solids due to biochemical digestion and/or acid hydrolysis during digestion. Both W_t/W_0 and DM_t/DM_0 of the foods were influenced by food type, proximal and distal phase, and food × distal interaction ($p < 0.0001$). Proximal × distal interaction was significant only to W_t/W_0 ($p < 0.0001$; Table 7.2). When averaged across proximal phase (food × distal effect), the W_t/W_0 of rice grain and noodles increased asymptotically during the distal phase, rice couscous decreased asymptotically (Figure 7.2), while couscous did not show significant change. The DM_t/DM_0 of agglomerated products and pasta decreased asymptotically with longer distal phase times, while no significant change in DM_t/DM_0 was observed in rice noodle and rice grain across distal phase time. When averaged across the distal phase (food × proximal effect), all foods underwent a significant

decrease in both their W_t/W_0 and DM_t/DM_0 with increasing proximal phase time ($p < 0.05$).

The asymptotes of W_t/W_0 and DM_t/DM_0 (A in Eqn. 7.1) after 180-min distal phase after different proximal phase times were generally predicted well by the Mitscherlich equation (Table 7.5; see Figure 7.3 for model fit to individual dataset from each proximal-distal digestion replicate), with average $R^2 > 0.80$, except the DM_t/DM_0 of foods with larger initial size at proximal phase ≤ 2 min and the W_t/W_0 of several food \times proximal phases combination with relatively flat mass retention profile (15-min proximal phase rice couscous and 30-min proximal phase pasta). The asymptotes for W_t/W_0 were significantly affected by food type, proximal phase duration, and food \times proximal effect ($p < 0.0001$; Table 7.2). The asymptote of both W_t/W_0 and DM_t/DM_0 decreased significantly with increasing proximal phase for all foods, especially between 0 and 15-min proximal phase ($p < 0.05$; Table 7.5). Among the foods, agglomerated products underwent a greater reduction in their W_t/W_0 and DM_t/DM_0 asymptote due to proximal phase compared to the other three foods. For instance, even at 0 min proximal phase, the DM_t/DM_0 of agglomerated products and the three other foods were 0.78 ± 0.10 and 0.95 ± 0.04 , respectively (averaged within agglomerated products and the three other foods).

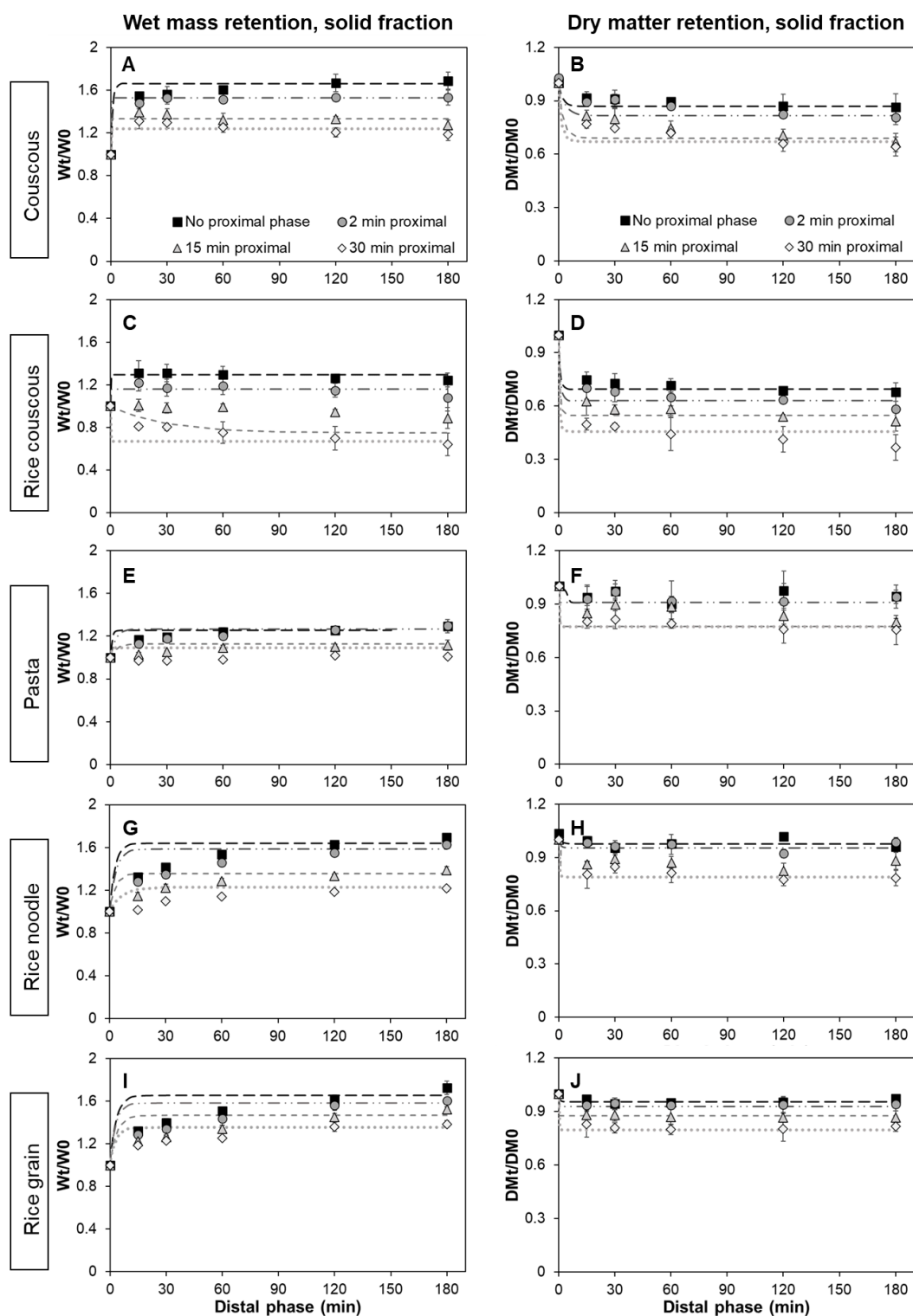


Figure 7.2 Wet mass retention (W_t/W_0 (dimensionless); left column) and dry matter retention (DM_t/DM_0 (dimensionless); right column) profiles of the solid fraction of digesta during the distal phase after 0 min (■), 2 min (●), 15 min (▲), or 30 min (◇) proximal phase. Figures within the same row correspond to one type of food: couscous (A-B), rice couscous (C-D), pasta (E-F), rice noodle (G-H), and rice grain (I-J). All values were normalized against the wet mass or dry matter of the cooked (undigested) food used in each sample. Values are shown as mean \pm SD ($n = 3$ for each time point, except rice couscous 15 min proximal-180 min distal, $n = 2$ due to outlier removal). Lines indicate Mitscherlich equation (Eqn. 7.1) fit with average parameters (Table 7.5) at 0 min (— — —), 2 min (— · —), 15 min (— - -), or 30 min (·· ·) proximal phase.

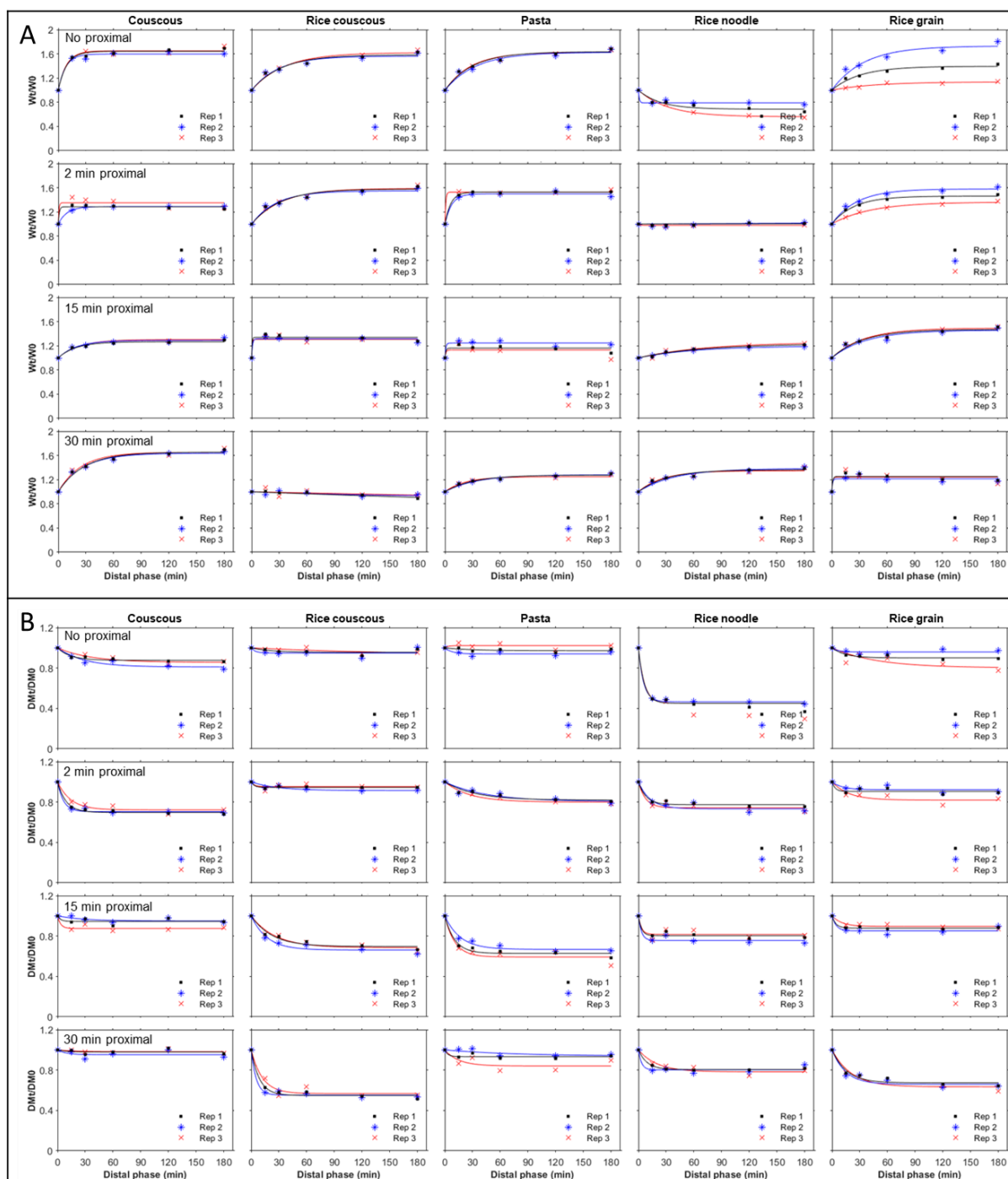


Figure 7.3 Mitscherlich equation (Eqn. 7.1) fit to the wet mass retention (A) and dry mass retention (B) data from each experimental replicate of proximal-distal digestion. Data points from the same replicate are indicated with the same symbol and color: Replicate 1: black (■), Replicate 2: blue (*), and Replicate 3: red (×); the model fit has the same color as the symbol for its respective replicate. Plots within the same row correspond to the same proximal phase duration, as noted in the leftmost column. Plots within the same column represent particle size distribution data for one type of food, as noted in the uppermost figure for each column.

Table 7.5 Mitscherlich equation (Eqn. 7.1) parameters of mass retention profile of digesta solid fraction at various proximal phase durations. k_m : a coefficient describing the rate of mass retention change (min^{-1}), A : asymptote values of the mass retention curve. The goodness of fit of the model to the data points is indicated by R^2 . Values are shown as mean \pm SD ($n = 3$ for each food \times proximal phase duration, except values indicated with asterisk (*), $n = 2$ due to outlier removal). For a single parameter, significantly different values between proximal phase for one type of food are indicated with abcd superscript. Significantly different values between food types within the same proximal phase are indicated with zyxw superscript ($p < 0.05$).

Food	Proximal phase (min)	Wet mass retention			Dry mass retention		
		$k_m (\times 10 \text{ min}^{-1})$	A	R^2	$k_m (\times 10 \text{ min}^{-1})$	A	R^2
Couscous	0	$1.13 \pm 0.13^{\text{b,zy}}$	$1.66 \pm 0.07^{\text{a,z}}$	0.97 ± 0.01	0.47 ± 0.33	$0.87 \pm 0.06^{\text{a,y}}$	0.85 ± 0.13
	2	$4.95 \pm 6.23^{\text{b,z}}$	$1.53 \pm 0.03^{\text{b,z}}$	0.99 ± 0.004	0.30 ± 0.07	$0.82 \pm 0.02^{\text{a,y}}$	0.87 ± 0.06
	15	$18.95 \pm 4.29^{\text{a,z}}$	$1.33 \pm 0.04^{\text{c,zy}}$	0.92 ± 0.05	0.41 ± 0.16	$0.69 \pm 0.03^{\text{b,x}}$	0.96 ± 0.02
	30	$11.93 \pm 1.12^{\text{ab,z}}$	$1.24 \pm 0.05^{\text{c,z}}$	0.79 ± 0.10	0.68 ± 0.19	$0.67 \pm 0.05^{\text{b,y}}$	0.95 ± 0.02
Rice couscous	0	$11.40 \pm 9.55^{\text{ab,z}}$	$1.29 \pm 0.06^{\text{a,y}}$	0.92 ± 0.10	1.16 ± 0.4	$0.70 \pm 0.03^{\text{a,x}}$	0.97 ± 0.03
	2	$10.49 \pm 0.53^{\text{a,z}}$	$1.16 \pm 0.07^{\text{b,y}}$	0.54 ± 0.30	1.04 ± 0.54	$0.63 \pm 0.02^{\text{b,x}}$	0.98 ± 0.01
	15	$0.03 \pm 0.03^{\text{c,x}}$	$0.75 \pm 0.26^{\text{c,w}}$	0.52 ± 0.31	1.30 ± 0.54	$0.55 \pm 0.01^{\text{c,w}}$	0.98 ± 0.01
	30	$8.49 \pm 14.29^{\text{b,y}}$	$0.67 \pm 0.12^{\text{d,y}}$	0.91 ± 0.12	1.73 ± 0.13	$0.46 \pm 0.01^{\text{d,x}}$	0.93 ± 0.07
Pasta	0	$0.52 \pm 0.16^{\text{b,y}}$	$1.26 \pm 0.04^{\text{a,y}}$	0.98 ± 0.003	0.27 ± 0.23	$*0.91 \pm 0.06^{\text{a,zy}}$	0.50 ± 0.42
	2	$0.38 \pm 0.18^{\text{b,y}}$	$1.27 \pm 0.04^{\text{a,y}}$	0.97 ± 0.01	10.29 ± 17.06	$0.91 \pm 0.10^{\text{a,zy}}$	0.59 ± 0.25
	15	$0.32 \pm 0.29^{\text{b,y}}$	$1.13 \pm 0.05^{\text{b,x}}$	0.97 ± 0.03	3.75 ± 6.24	$0.77 \pm 0.08^{\text{b,yx}}$	0.81 ± 0.06
	30	$2.33 \pm 4.02^{\text{a,x}}$	$1.09 \pm 0.11^{\text{b,x}}$	0.19 ± 0.20	4.12 ± 5.33	$0.77 \pm 0.06^{\text{b,z}}$	0.91 ± 0.01
Rice noodle	0	$0.37 \pm 0.05^{\text{y}}$	$1.64 \pm 0.03^{\text{a,z}}$	0.98 ± 0.002	0.50 ± 0.52	$0.97 \pm 0.03^{\text{a,z}}$	0.33 ± 0.33
	2	$0.31 \pm 0.03^{\text{y}}$	$1.58 \pm 0.03^{\text{a,z}}$	0.96 ± 0.01	1.05 ± 1.31	$0.95 \pm 0.003^{\text{a,z}}$	0.62 ± 0.25
	15	$0.33 \pm 0.14^{\text{y}}$	$1.36 \pm 0.04^{\text{b,zy}}$	0.99 ± 0.02	3.37 ± 5.13	$0.85 \pm 0.03^{\text{b,zy}}$	0.80 ± 0.07
	30	$0.16 \pm 0.02^{\text{y}}$	$1.23 \pm 0.03^{\text{c,z}}$	0.99 ± 0.01	3.38 ± 5.18	$0.79 \pm 0.03^{\text{c,z}}$	0.93 ± 0.06
Rice grain	0	$0.31 \pm 0.03^{\text{y}}$	$1.66 \pm 0.07^{\text{a,z}}$	0.96 ± 0.02	1.43 ± 1.09	$0.95 \pm 0.01^{\text{a,zy}}$	0.69 ± 0.24
	2	$0.34 \pm 0.06^{\text{y}}$	$1.58 \pm 0.03^{\text{ab,z}}$	0.97 ± 0.02	3.03 ± 4.18	$0.93 \pm 0.02^{\text{ab,z}}$	0.71 ± 0.14
	15	$0.30 \pm 0.03^{\text{y}}$	$1.47 \pm 0.02^{\text{b,z}}$	0.94 ± 0.03	9.92 ± 14.41	$0.88 \pm 0.02^{\text{b,z}}$	0.89 ± 0.08
	30	$0.36 \pm 0.01^{\text{y}}$	$1.35 \pm 0.01^{\text{c,zy}}$	0.93 ± 0.04	3.82 ± 5.58	$0.80 \pm 0.01^{\text{c,z}}$	0.91 ± 0.02

7.4.3.2 Texture and moisture content

Hardness (Table F.2) and H_t/H_0 (Figure 7.4) values were influenced by food, proximal phase, distal phase, and their two- and three-way interactions ($p < 0.05$), except the proximal \times distal interaction ($p \geq 0.582$; Table 7.2). When averaged across the distal phase (food \times proximal effect), no significant difference in H_t/H_0 was present between proximal phase in the foods ($p > 0.05$), except in rice couscous that underwent increasing H_t/H_0 with increasing proximal phase duration. When averaged across proximal phase (food \times distal effect) and compared with 15-min distal phase as the earliest distal phase sample, a significant reduction in H_t/H_0 was observed ($p < 0.05$) after 30 min for couscous, 60 min for pasta and rice grain, and 120 min distal phase for rice couscous and rice noodle (Figure 7.4).

The $t_{1/2, \text{softening}}$ of the solid digesta fraction was affected by food type ($p < 0.001$) and proximal phase ($p < 0.05$; Table 7.2). No significant changes in the $t_{1/2, \text{softening}}$ were present between proximal phase durations ($p > 0.05$). When averaged across the proximal phase, the $t_{1/2, \text{softening}}$ of agglomerate products were lower than that of rice grain and noodle products (53.9 ± 81.8 vs. 1029.9 ± 1295.9 min, averaged between agglomerate products and the three other foods, respectively; $p < 0.05$). Since large variations in the softening curves were observed between replicates (Figure 7.5) and resulted in variable $t_{1/2, \text{softening}}$, the data points for each food \times proximal phase were fit to the Weibull model (Eqn. 7.2) altogether to estimate the overall trends between the treatments (indicated by the green dashed lines in Figure 7.5). The model parameters from this approach and the calculated $t_{1/2, \text{softening}}$ are presented in Table 7.7. The $t_{1/2, \text{softening}}$ of the solid fraction with no proximal phase was the smallest in agglomerate products (<13 min), followed by rice grain, pasta, and rice noodle (>100 min). The $t_{1/2, \text{softening}}$ of the agglomerate products were lower than rice grain, pasta, and rice noodle

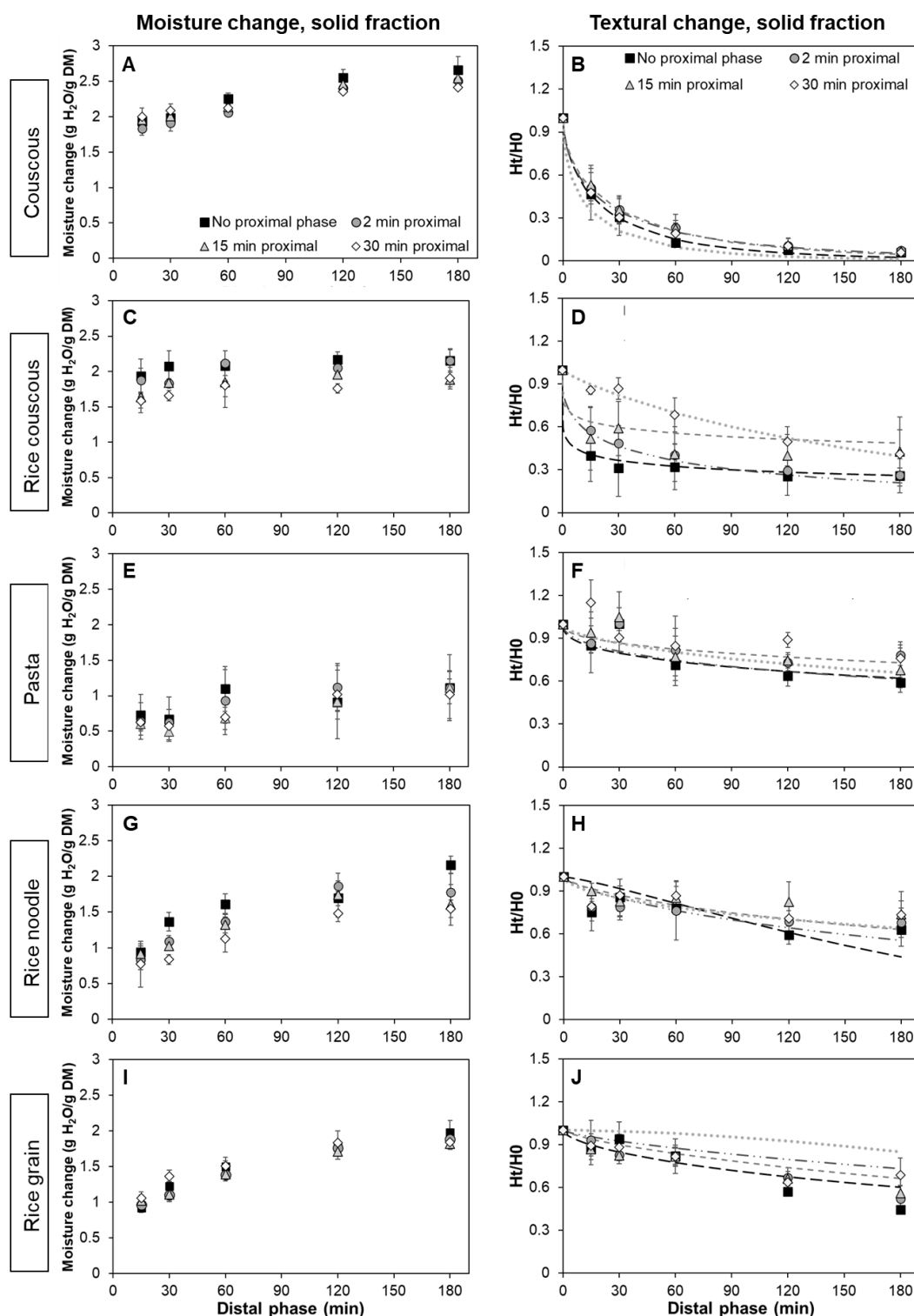


Figure 7.4 Moisture changes (left column) and normalized hardness (H_t/H_0 ; right column) profiles of the solid fraction of digesta during the distal phase after 0 min (■), 2 min (●), 15 min (▲), or 30 min (◇) proximal phase. Figures within the same row correspond to one type of food: couscous (A-B), rice couscous (C-D), pasta (E-F), rice noodle (G-H), and rice grain (I-J). For each food, moisture change at each distal phase duration was calculated as the change from the moisture content of cooked (undigested) food. Hardness value was normalized against the hardness of cooked (undigested) food, and normalized hardness at 0 min distal phase was set to 1 for all proximal phase durations. Values are shown as mean \pm SD ($n = 3$ for each time point). Lines in the H_t/H_0 graphs indicate the Weibull model (Eqn. 7.2) fit with average parameters (Table 7.6) at 0 min (—), 2 min (— · —), 15 min (— — —), or 30 min (····) proximal phase.

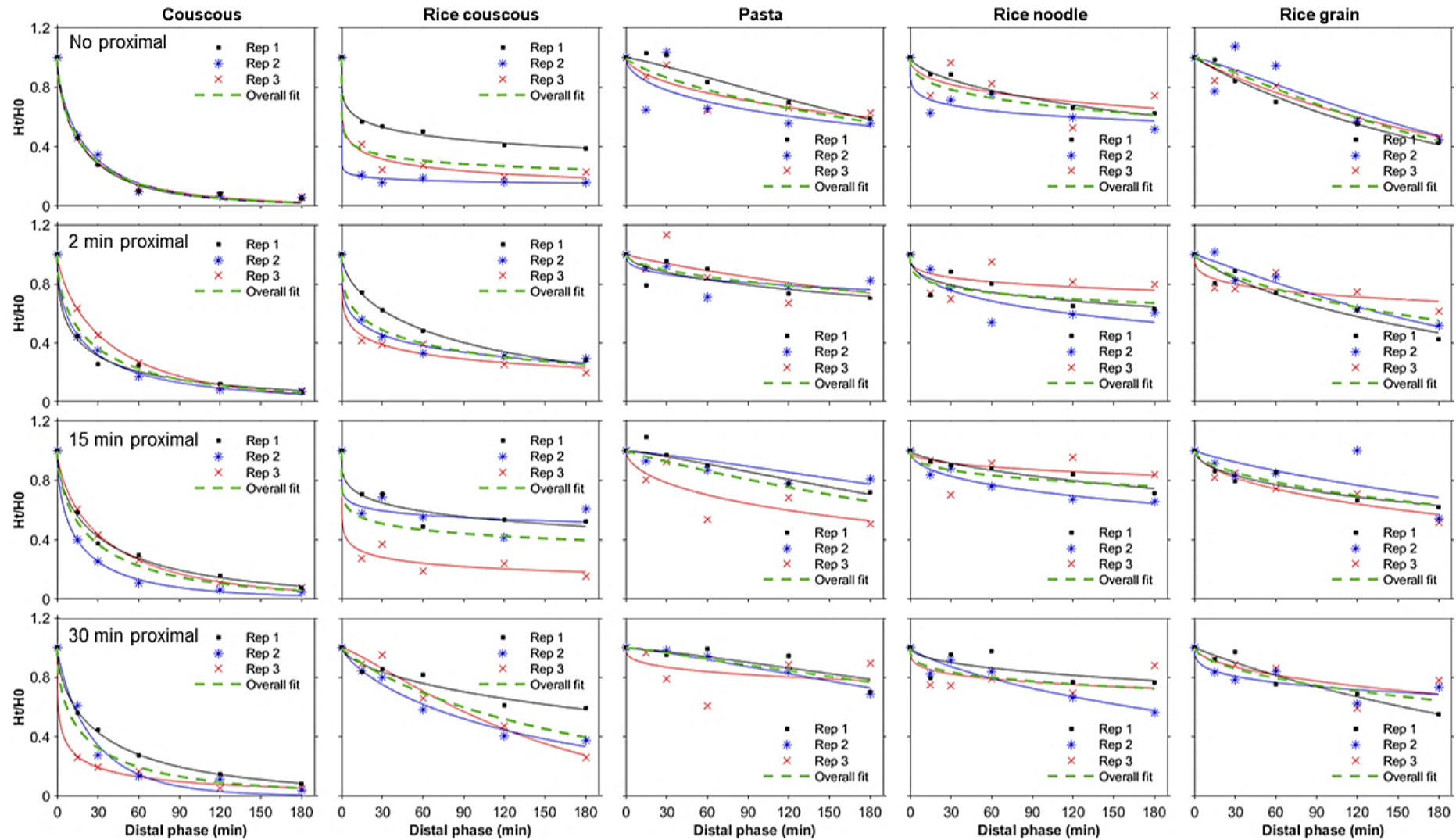


Figure 7.5 Weibull model (Eqn. 7.2) fit to the H_t/H_0 dataset for each experimental replicate. Data points from the same replicate are indicated with the same symbol and color: black (■), blue (*), and red (×), the model fit has the same color as the symbol for its respective replicate. Model fit for when data points from all three replicates were fitted altogether ('Overall fit') is indicated with the green dashed line (— — —). Plots within the same row correspond to the same proximal phase duration, as noted in the leftmost column. Plots within the same column represent data for one type of food, as noted in the uppermost figure for each column.

Table 7.6 Softening kinetics parameter of the food products in the proximal-distal digestion at different proximal phase durations, obtained by fitting the data points from each replicate of food \times proximal phase combination to Eqn. 7.2. The model fit of the softening curves is indicated by R^2 . Values are mean \pm SD ($n = 3$ for each food \times proximal phase duration, except values indicated with asterisk (*), $n = 2$ due to outlier removal). Significantly different values between proximal phase durations for one type of food are indicated with abcd superscript. Significantly different values between food types within the same proximal phase duration are indicated with zyxw superscript ($p < 0.05$).

Food	Proximal phase (min)	Softening kinetics parameter		R^2	$t_{1/2, \text{softening}}$ (min)
		$k_h (\times 100 \text{ min}^{-1})$	β_h (dimensionless)		
Couscous	0	4.54 ± 0.33^z	0.64 ± 0.04^{zy}	0.99 ± 0.003	12.5 ± 1.33^y
	2	3.77 ± 1.21^z	0.57 ± 0.16	1.00 ± 0.005	15.5 ± 8.83^y
	15	3.58 ± 1.98^z	0.61 ± 0.07	1.00 ± 0.001	18.4 ± 8.21
	30	7.40 ± 7.45^z	0.58 ± 0.27^{zy}	0.99 ± 0.01	13.5 ± 10.0^y
Rice couscous	0	$*3.51 \pm 4.38^{zy}$	0.16 ± 0.08^y	0.99 ± 0.01	$*24.0 \pm 30.3^y$
	2	1.70 ± 0.81^z	0.40 ± 0.23	0.99 ± 0.01	27.5 ± 24.1^y
	15	$*0.09 \pm 0.10^{zy}$	0.18 ± 0.08	0.91 ± 0.08	151.1 ± 145.2
	30	0.51 ± 0.27^{zy}	0.87 ± 0.33^{zy}	0.96 ± 0.02	158.7 ± 97.7^{zy}
Pasta	0	0.19 ± 0.10^{zy}	$0.63 \pm 0.35^{b,zy}$	0.86 ± 0.10	280.4 ± 39.0^z
	2	0.13 ± 0.11^y	0.78 ± 0.41^b	0.63 ± 0.21	1276.5 ± 1536.4^z
	15	0.17 ± 0.13^{zy}	0.75 ± 0.44^b	0.78 ± 0.08	857.8 ± 1043.1
	30	0.21 ± 0.17^y	$*1.83 \pm 0.25^{a,z}$	0.70 ± 0.13	1719.1 ± 2514.1^z
Rice noodle	0	0.09 ± 0.08^y	0.41 ± 0.21^{zy}	0.76 ± 0.25	491.4 ± 165.7^z
	2	0.12 ± 0.09^y	0.47 ± 0.15	0.60 ± 0.45	1115.5 ± 1430.5^z
	15	0.04 ± 0.05^y	0.44 ± 0.04	0.83 ± 0.21	2910.9 ± 2116.4
	30	0.12 ± 0.18^y	0.58 ± 0.43^y	0.63 ± 0.28	1329.3 ± 978.0^z
Rice grain	0	0.48 ± 0.04^{zy}	1.27 ± 0.47^z	0.92 ± 0.12	153.9 ± 10.3^z
	2	0.26 ± 0.21^{zy}	0.71 ± 0.38	0.86 ± 0.13	572.8 ± 691.3^z
	15	0.18 ± 0.05^{zy}	0.67 ± 0.25	0.76 ± 0.31	329.0 ± 68.4
	30	0.13 ± 0.19^y	0.56 ± 0.35^y	0.80 ± 0.12	1322.1 ± 1310.3^z

(non-parametric Kruskal-Wallis $p = 0.0020$ between the agglomerate products and three other foods, averaged across proximal phase durations). In general, the $t_{1/2, \text{softening}}$ increased with longer proximal phase for all foods, except couscous.

Both moisture content and moisture change (dry basis) of the solid fraction during digestion was affected by the main effects of food, proximal phase, and distal phase, together with the food \times proximal and food \times distal interactions ($p < 0.01$; Table 7.2). Moisture change in the solid fraction relative to the undigested, cooked food was calculated to compare the difference in the moisture uptake between food during gastric digestion for foods with varying initial moisture content after cooking (Figure 7.4). When averaged across proximal

phase times (food \times distal effect), all foods had increasing moisture change with increasing distal phase time. At any distal phase time, moisture change in agglomerated products > rice grain > noodles ($p < 0.05$). Overall, the moisture change between these three categories was 2.06 ± 0.29 vs. 1.46 ± 0.35 and 1.10 ± 0.45 g H₂O/g DM for agglomerated products, rice grain, and noodles, respectively (averaged across all proximal and distal phase times; $p < 0.01$). When averaged across distal phase time (food \times proximal effect), moisture change decreased significantly between 2- and 15-min proximal phase in rice couscous, pasta, and rice noodle ($p < 0.05$).

Table 7.7 Softening kinetics parameter of the food products in the proximal-distal digestion at different proximal phase durations, obtained by fitting all data points for each food \times proximal phase combination altogether to Eqn. 7.2 to estimate the overall trends for each treatment. The model fit of the softening curves is indicated by R^2 . Softening kinetics parameters (k_h and β_h) for each treatment are expressed as predicted parameters \pm 95% confidence interval.

Food	Proximal phase (min)	Softening kinetics parameter		R^2	$t_{1/2, \text{softening}}$ (min)
		k_h ($\times 100 \text{ min}^{-1}$)	β_h (dimensionless)		
Couscous	0	4.53 ± 0.005	0.64 ± 0.09	0.99	12.4
	2	3.4 ± 0.007	0.56 ± 0.13	0.97	15.2
	15	3.29 ± 0.007	0.59 ± 0.15	0.96	16.3
	30	4.16 ± 0.015	0.54 ± 0.21	0.94	12.2
Rice couscous	0	5.19 ± 0.105	0.15 ± 0.22	0.82	1.70
	2	1.33 ± 0.005	0.36 ± 0.14	0.92	27.5
	15	0.35 ± 0.012	0.17 ± 0.29	0.63	34.7
	30	0.51 ± 0.002	0.85 ± 0.30	0.85	127.9
Pasta	0	0.26 ± 0.003	0.76 ± 0.48	0.66	233.8
	2	0.06 ± 0.002	0.54 ± 0.52	0.49	869.5
	15	0.22 ± 0.003	0.95 ± 0.97	0.47	306.8
	30	0.16 ± 0.004	1.08 ± 1.71	0.33	440.2
Rice noodle	0	0.09 ± 0.003	0.39 ± 0.31	0.64	440.4
	2	0.02 ± 0.003	0.28 ± 0.34	0.53	1242.5
	15	0.02 ± 0.002	0.37 ± 0.44	0.48	2145.9
	30	0.01 ± 0.002	0.30 ± 0.41	0.48	2389.3
Rice grain	0	0.47 ± 0.001	1.14 ± 0.42	0.86	154.6
	2	0.27 ± 0.002	0.72 ± 0.31	0.80	224.0
	15	0.15 ± 0.002	0.59 ± 0.38	0.65	368.1
	30	0.09 ± 0.003	0.54 ± 0.46	0.54	390.5

7.4.3.3 Particle size

Food was a significant effect ($p < 0.0001$) to all particle size parameters of the solid digesta fraction (x_{10} , x_{50} , x_{90} , particles/g DM, area/particle, particle area/gram, and broadness of distribution (b); Table 7.2). The distal phase duration significantly influenced ($p < 0.05$) all particle size parameters except the broadness of distribution. The proximal phase duration significantly impacted x_{50} , x_{90} , and particle area/gram ($p < 0.05$). Food \times proximal interaction was significant to only x_{10} , x_{50} , and particle area/gram ($p < 0.05$). Food \times distal interaction was significant to all particle size parameters except particle area/g ($p < 0.01$). Proximal \times distal effect was significant only to average area/particle ($p = 0.0101$).

When averaged across proximal phase time (food \times distal effect) and compared between 30- and 180-min distal phase, x_{10} and b decreased significantly in rice grain, x_{50} and x_{90} decreased significantly in couscous and rice grain, particle area/gram increased significantly in rice grain, area per particle decreased significantly in all foods except rice couscous, and particles/g DM increased significantly in non-agglomerated products with longer distal phase time (Table 7.8 and 7.9; $p < 0.05$). When averaged across the distal phase (food \times proximal effect) and observed within longer proximal phase, x_{10} decreased significantly in rice grain, x_{50} and x_{90} decreased significantly in couscous and rice grain, and area per gram increased significantly in couscous and rice noodle ($p < 0.05$).

The overall PSD of each diet \times proximal \times distal combination (Figure 7.1B-F and F.2-F.6; Table F.3) provides additional information on particle size changes during the proximal-distal digestion. Couscous and rice couscous digesta had less particles between 10 and 100 μm^2 at 30 or 180 min distal phase compared to their undigested condition (6.89, 3.69, and 18.04%, respectively; averaged across the agglomerated products and proximal phase). Particles $>100 \mu\text{m}^2$ in pasta and rice noodle digesta slightly decreased between 30 and 180 min distal phase (97.69 and 95.42%, respectively; averaged across the noodles and proximal

phase). The proportion of particles between 10 and 100 mm² in rice grain digesta decreased between 30 or 180 min distal phase (89.45 and 78.24%, respectively; averaged across proximal phase). Although most particles ≤ 4 mm² should have been removed in the digesta separation step, the proportion of particles ≤ 4 mm² in couscous, rice grain, and noodle products decreased after 30 min distal phase when compared to the proximal digestion with no distal phase, then increased after 180 min distal phase at any proximal phase (Table F.3). Meanwhile, rice couscous did not exhibit changes in the proportion of particles ≤ 4 mm² during the distal phase (remained ~63-64% throughout different distal phase durations).

Table 7.8 Selected particle size parameters of the solid digesta fraction after varying proximal phase followed by 30 or 180 min distal phase in the proximal-distal digestion. Values are shown as mean \pm SD (n = 3 for each food \times proximal \times distal phase duration). Significantly different values between distal phase durations for one type of food are indicated with ab superscript. Significantly different values between proximal phase durations for one type of food are indicated with zyxw superscript ($p < 0.05$).

Food	Distal phase (min)	Proximal phase (min)			
		0	2	15	30
x ₅₀ (mm ²)					
Couscous	30	2.20 ± 0.29	3.39 ± 2.05 ^a	2.94 ± 1.22 ^a	2.03 ± 0.60
	180	1.94 ± 0.1 ^z	2.33 ± 1.22 ^{b,z}	1.8 ± 0.73 ^{b,y}	1.76 ± 0.59 ^{zy}
Rice couscous	30	2.81 ± 1.26	2.71 ± 1.1	2.50 ± 1.09	2.84 ± 1.25
	180	2.84 ± 0.33	2.61 ± 0.79	3.10 ± 0.64	2.47 ± 0.55
Pasta	30	269.69 ± 46.17	291.7 ± 35.52	255.75 ± 55.39	231.84 ± 92.96
	180	211.81 ± 54.06	283.73 ± 77.96	202.52 ± 68.75	232.35 ± 26.04
Rice noodle	30	203.71 ± 55.76	207.94 ± 46.49	204.26 ± 42.47	233.42 ± 15.22
	180	224.47 ± 51.25	215.77 ± 31.84	208.49 ± 71.17	217.59 ± 34.17
Rice grain	30	40.97 ± 6.65 ^{a,z}	45.75 ± 18.66 ^{a,z}	24.7 ± 3.86 ^{a,y}	23.22 ± 7.03 ^{a,y}
	180	19.75 ± 6.19 ^{b,z}	21.63 ± 7.54 ^{b,z}	20.47 ± 2.91 ^{b,z}	16.51 ± 4.89 ^{b,y}
Particles/g DM					
Couscous	30	4227 ± 1641	3762 ± 1373	5311 ± 1621	7614 ± 1265
	180	4478 ± 800	4649 ± 673	7315 ± 1784	8662 ± 2104
Rice couscous	30	5467 ± 1618	5737 ± 1751	4984 ± 1797	4885 ± 2314
	180	6169 ± 1967	5998 ± 3190	4214 ± 2441	4342 ± 1338
Pasta	30	69 ± 42 ^b	35 ± 11 ^b	39 ± 9 ^b	70 ± 44
	180	120 ± 42 ^a	148 ± 95 ^a	133 ± 35 ^a	111 ± 79
Rice noodle	30	49 ± 14 ^b	59 ± 18 ^b	60 ± 5	91 ± 14
	180	100 ± 53 ^a	114 ± 50 ^a	102 ± 51	130 ± 76
Rice grain	30	282 ± 120	385 ± 311	472 ± 264	633 ± 197
	180	484 ± 309	621 ± 493	580 ± 86	490 ± 73

(continued)

Table 7.8 (continued)

Food	Distal phase (min)	Proximal phase (min)			
		0	2	15	30
Average area (mm ²)/particle					
Couscous	30	1.3 ± 0.13	1.78 ± 0.88	1.72 ± 0.64 ^a	1.26 ± 0.33
	180	1.13 ± 0.11	1.34 ± 0.59	1.17 ± 0.38 ^b	1.15 ± 0.31
Rice couscous	30	1.2 ± 0.33	1.12 ± 0.28	1.13 ± 0.36	1.19 ± 0.45
	180	1.27 ± 0.07	1.20 ± 0.28	1.42 ± 0.23	1.19 ± 0.29
Pasta	30	56.69 ± 34.52 ^{a,zy}	88.79 ± 30.77 ^{a,zy}	71.92 ± 4.78 ^{a,z}	51.22 ± 26.25 ^{a,y}
	180	23.19 ± 6.36 ^b	29.8 ± 22.6 ^b	22.91 ± 6.73 ^b	36.22 ± 15.32 ^b
Rice noodle	30	87.05 ± 24.84 ^a	72.6 ± 5.14 ^a	78.4 ± 13.39 ^a	68.31 ± 6.51
	180	58.66 ± 30.29 ^b	46.79 ± 8.51 ^b	57.49 ± 9.13 ^b	59.20 ± 25.95
Rice grain	30	8.23 ± 0.70 ^a	8.95 ± 2.99 ^a	8.01 ± 4.06 ^a	6.25 ± 2.90
	180	4.82 ± 2.21 ^b	5.08 ± 2.16 ^b	6.66 ± 1.12 ^b	6.63 ± 1.55

Table 7.9 Additional particle size distribution parameters of digesta solid fraction after varying proximal phase followed by 30 or 180 min distal phase in the proximal-distal digestion. Values are shown as mean ± SD (n = 3 for each food × proximal × distal phase duration, except values indicated with asterisk (*), n = 2 due to outlier removal). For each food, significantly different values between distal phase durations within the same proximal phase duration are indicated with ab superscript; significantly different values between proximal phase durations within the same distal phase duration are indicated with zyxw superscript ($p < 0.05$).

Food	Distal phase (min)	Proximal phase (min)			
		0	2	15	30
x ₁₀ (mm ²)					
Couscous	30	0.24 ± 0.04	0.27 ± 0.12	0.29 ± 0.12	0.25 ± 0.09
	180	0.17 ± 0.04	0.2 ± 0.10	0.24 ± 0.08	0.26 ± 0.05
Rice couscous	30	0.15 ± 0.04	0.14 ± 0.05	0.16 ± 0.07	0.14 ± 0.08
	180	0.18 ± 0.04	0.17 ± 0.08	0.25 ± 0.08	0.2 ± 0.12
Pasta	30	113.73 ± 27.22	146.01 ± 47.62	141.19 ± 23.91	156.51 ± 80.61
	180	123.89 ± 20.13	118.47 ± 52.99	118.69 ± 63.58	125.89 ± 33.43
Rice noodle	30	88.56 ± 18.82	108.16 ± 38.09	98.78 ± 19.85	105.19 ± 20.96
	180	91.3 ± 35.08	91.59 ± 28.39	82.41 ± 46.37	100.9 ± 13.29
Rice grain	30	9.99 ± 1.27 ^{a,z}	12.36 ± 7.44 ^{a,z}	4.95 ± 1.47 ^{a,y}	3.60 ± 1.14 ^{a,y}
	180	2.69 ± 1.75 ^b	2.48 ± 0.99 ^b	2.46 ± 0.51 ^b	2.61 ± 1.37 ^b
x ₉₀ (mm ²)					
Couscous	30	5.07 ± 0.82	8.71 ± 5.71 ^a	6.97 ± 2.94 ^a	4.46 ± 1.24
	180	4.87 ± 0.48 ^z	5.85 ± 3.01 ^{b,z}	3.88 ± 1.86 ^{b,y}	3.58 ± 1.44 ^{zy}
Rice couscous	30	8.4 ± 4.35	8.37 ± 4.08	6.94 ± 2.92	8.78 ± 3.57
	180	7.93 ± 1.18	7.19 ± 1.69	7.93 ± 1.32	6.51 ± 1.00
Pasta	30	373.55 ± 56.48 ^a	387.83 ± 64.31	321.64 ± 78.93	268.8 ± 96.34
	180	259.77 ± 77.13 ^{b,zy}	409.79 ± 148.42 ^z	251.04 ± 67.29 ^y	295.92 ± 14.45 ^{zy}
Rice noodle	30	281.15 ± 88.27	266.04 ± 49.6	267.99 ± 57.51	315.02 ± 15.22
	180	318.73 ± 49.26	301.74 ± 37.41	303.92 ± 101.2	292.46 ± 69.69
Rice grain	30	69.82 ± 13.33 ^{a,z}	75.58 ± 24.67 ^{a,zy}	45.19 ± 5.68 ^{zy}	46.46 ± 13.95 ^{a,y}
	180	44.24 ± 7.38 ^{b,z}	49.24 ± 18.83 ^{b,z}	45.32 ± 5.52 ^z	33.39 ± 7.13 ^{b,y}

(continued)

Table 7.9 (continued)

Food	Distal phase (min)	Proximal phase (min)			
		0	2	15	30
Broadness of distribution, <i>b</i> (dimensionless) [#]					
Couscous	30	1.46 ± 0.11	1.31 ± 0.09	1.39 ± 0.08	1.53 ± 0.14
	180	1.32 ± 0.13	1.31 ± 0.03	1.64 ± 0.21	1.76 ± 0.21
Rice couscous	30	1.12 ± 0.07	1.1 ± 0.12	1.19 ± 0.03	1.06 ± 0.05
	180	1.18 ± 0.09	1.18 ± 0.09	1.28 ± 0.06	1.26 ± 0.20
Pasta	30	3.86 ± 0.40 ^{b,zy}	5.62 ± 2.39 ^{zy}	6.94 ± 3.16 ^z	8.05 ± 2.28 ^z
	180	6.78 ± 1.59 ^a	*5.48 ± 0.94	7.92 ± 0.59	5.78 ± 1.30
Rice noodle	30	4.13 ± 0.63	5.01 ± 1.12	4.50 ± 0.21	4.11 ± 0.73
	180	3.71 ± 0.54	4.08 ± 1.01	3.48 ± 1.15	4.54 ± 1.38
Rice grain	30	2.36 ± 0.23 ^a	2.41 ± 0.48 ^a	2.02 ± 0.24 ^a	1.74 ± 0.04
	180	1.57 ± 0.27 ^b	1.52 ± 0.21 ^b	1.55 ± 0.06 ^b	1.73 ± 0.30
Area (mm ²)/ gram					
Couscous	30	1144.26 ± 392.26	1300.19 ± 379.00	1825.08 ± 564.31	1934.04 ± 511.73
	180	938.26 ± 228.03 ^y	1132.68 ± 346.84 ^{zy}	1573.48 ± 501.95 ^{zy}	1868.43 ± 577.05 ^z
Rice couscous	30	1340.51 ± 234.93	1397.23 ± 176.93	1185.09 ± 264.14	1335.13 ± 600.17
	180	1614.27 ± 452.90	1408.85 ± 474.80	1247.84 ± 463.30	1106.64 ± 216.80
Pasta	30	823.76 ± 110.65	821.98 ± 43.29	838.87 ± 132.21	850.51 ± 310.75
	180	650.52 ± 95.82	755.36 ± 150.88	748.46 ± 193.53	824.12 ± 107.82
Rice noodle	30	986.41 ± 213.21 ^y	1113.68 ± 329.94 ^{zy}	1237.57 ± 195.34 ^{zy}	1707.96 ± 196.5 ^z
	180	1008.71 ± 191.81	1109.86 ± 283.80	1263.79 ± 295.79	1470.47 ± 317.60
Rice grain	30	897.31 ± 159.08 ^a	989.82 ± 334.62	832.16 ± 80.99	896.88 ± 274.70 ^a
	180	680.40 ± 170.77 ^b	772.42 ± 116.24	866.39 ± 90.83	711.30 ± 129.39 ^b

[#] A higher value of b corresponds to a narrower distribution.

7.4.4 Properties of liquid and suspended solid digesta fractions after the proximal and distal phase

Food, proximal phase, distal phase and the interactions of food × proximal and food × distal significantly influenced ($p < 0.05$) all particle size parameters (d_{10} , d_{50} , d_{90} , $D[4,3]$, and $D[3,2]$), °Brix, and hydrolyzed starch content of the liquid and suspended solid digesta fractions. °Brix, d_{50} , and hydrolyzed starch content were influenced by proximal × distal interaction ($p < 0.05$). Food × proximal × distal interaction significantly influenced d_{50} ($p = 0.0012$; Table 7.2). When averaged across the proximal phase (food × distal effect), longer distal phase duration led to increasing $D[4,3]$ and $D[3,2]$ in wheat-based foods (i.e., couscous and pasta; $p < 0.05$), but no significant trends were observed in rice-based foods (Table 7.10).

For example, the $D[4,3]$ of wheat-based foods (couscous and pasta averaged together) changed from 65.38 ± 34.95 to 108.70 ± 39.91 μm after 15 and 180 min distal phase, respectively. When averaged across distal phase (food \times proximal effect), longer proximal phase duration resulted in decreasing $D[4,3]$ and $D[3,2]$ in all rice-based diets and decreasing $D[3,2]$ in pasta ($p < 0.05$).

The particle size distribution profile of all foods was multimodal (Figure 7.6), thus d_{10} , d_{50} , and d_{90} (Table F.4) were not assessed further as they provided limited information with respect to the overall changes in particle size distribution during *in vitro* digestion. Figure 7.6 indicates that for wheat-based foods, the location of largest peak, which initially appeared between 20 to 40 μm after 15 min distal phase, shifted to a larger size with increasing distal phase time; the shape of the curve and %volume of the largest peak was maintained throughout different proximal phase. For all rice-based foods, with increasing proximal phase time, the maximum %volume of the peak occurring between 5 to 15 μm increased and the peak between 100 and 1000 μm disappeared. However, longer distal phase duration did not appear to change the shape of the curve, except in rice grain.

$^{\circ}\text{Brix}$, which represents the amount of soluble solids in the liquid digesta fraction, increased with longer proximal and distal phase duration for all foods (Figure 7.7; $p < 0.05$). However, the increase in $^{\circ}\text{Brix}$ was larger with longer proximal rather than distal phase times. When averaged across all foods (proximal \times distal effect), for instance, the $^{\circ}\text{Brix}$ values for samples with no proximal phase were 0.60 ± 0.42 and 0.99 ± 0.47 after 15 and 180 min distal phase, respectively. However, for samples with 30-min proximal phase, the $^{\circ}\text{Brix}$ were 2.35 ± 0.96 and 2.91 ± 0.95 , after 15 and 180 min distal phase, respectively. When averaged across all proximal and distal durations, the $^{\circ}\text{Brix}$ value of agglomerate products (2.45 ± 1.05) was higher than that of grain and noodle products (1.12 ± 0.64).

Hydrolyzed starch content in the liquid and suspended solid fractions for each diet was defined as the summation of the maltose content measured in the liquid and suspended solid fractions, divided by the initial starch content of the respective diet. The value increased with increasing proximal phase duration for all foods, regardless of the distal phase duration (Figure 7.7). At any proximal and distal phase, agglomerated products had higher hydrolyzed starch compared to the three other foods. For example, after 30 min proximal phase followed by 180 min distal phase (maximum digestion duration), the hydrolyzed starch content in agglomerated products and non-agglomerated products was 0.54 ± 0.24 and 0.39 ± 0.13 g maltose/g starch, respectively. In agglomerated products, the hydrolyzed starch content after 180 min distal phase was significantly higher than 15 min distal phase, when preceded by 15 or 30 min of proximal phase ($p \leq 0.0025$). For instance, 30 min of proximal phase digestion in rice couscous followed by 15 or 180 min of distal phase digestion increased starch hydrolysis from 0.51 ± 0.03 to 0.74 ± 0.14 g maltose/g starch, respectively ($p < 0.0001$).

Table 7.10 Volume mean diameter (D[4,3]) and surface area mean diameter (D[3,2]) of the liquid and suspended solid digesta fractions measured using Mastersizer. Values are mean \pm SD (n = 3 for each food \times proximal \times distal combination). Significantly different values between distal phase duration for one type of food are indicated with abcd superscript. Significantly different values between proximal phase for one food type within the same distal phase duration are indicated with zyxw superscript ($p < 0.05$).

Food	Proximal phase (min)	Distal phase (min)				
		15	30	60	120	180
D[4,3] (μm)						
Couscous	0	42.63 ± 11.31 ^{c,y}	57.52 ± 13.09 ^{bc}	72.98 ± 25.25 ^{ab}	92.94 ± 35.18 ^a	103.57 ± 33.43 ^a
	2	90.31 ± 65.50 ^z	65.63 ± 4.20	93.85 ± 16.53	105.51 ± 36.37	132.33 ± 69.06
	15	94.69 ± 54.68 ^{ab,z}	94.34 ± 41.51 ^{ab}	85.23 ± 41.47 ^a	130.81 ± 63.49 ^{ab}	155.55 ± 51.17 ^a
	30	74.78 ± 22.86 ^{zy}	85.59 ± 36.10	105.24 ± 68.01	121.69 ± 46.98	129.45 ± 27.95
Rice couscous	0	198.61 ± 71.40	212.26 ± 66.71	203.27 ± 37.45	208.23 ± 34.42 ^{zy}	286.34 ± 36.63 ^z
	2	199.53 ± 43.29	210.76 ± 47.41	214.73 ± 43.19	235.79 ± 71.96 ^z	237.26 ± 100.25 ^{zy}
	15	153.41 ± 20.75	181.83 ± 71.28	141.27 ± 33.19	150.44 ± 33.29 ^{zy}	165.07 ± 61.62 ^{zy}
	30	126.56 ± 60.43	131.5 ± 64.02	114.95 ± 21.60	113.28 ± 24.07 ^y	125.67 ± 30.83 ^y
Pasta	0	58.2 ± 8.10 ^{ab}	55.69 ± 10.24 ^b	71.73 ± 16.48 ^{ab}	82.53 ± 15.15 ^{ab}	97.87 ± 20.61 ^a
	2	46.68 ± 2.69 ^b	60.22 ± 6.81 ^{ab}	74.91 ± 14.07 ^{ab}	87.67 ± 15.82 ^a	95.24 ± 8.74 ^a
	15	60.82 ± 21.83	51.02 ± 8.68	58.42 ± 9.23	77.92 ± 4.77	83.00 ± 8.53
	30	54.96 ± 14.19	58.71 ± 18.53	66.39 ± 13.92	69.02 ± 13.67	72.56 ± 15.67
Rice noodle	0	113.62 ± 29.17 ^z	99.64 ± 42.06 ^z	104.08 ± 36.88 ^z	116.45 ± 34.56 ^z	111.31 ± 58.69 ^z
	2	84.17 ± 13.05 ^z	70.34 ± 28.80 ^z	76.99 ± 43.14 ^{zy}	77.72 ± 35.04 ^z	60.08 ± 15.11 ^y
	15	35.90 ± 9.91 ^y	25.69 ± 6.49 ^y	37.71 ± 13.73 ^{yx}	32.65 ± 11.45 ^y	32.52 ± 7.12 ^y
	30	29.69 ± 6.90 ^y	27.04 ± 8.82 ^y	33.47 ± 12.78 ^x	30.59 ± 12.76 ^y	33.46 ± 8.76 ^y
Rice grain	0	302.86 ± 77.71 ^z	277.04 ± 24.07 ^z	223.01 ± 10.33	211.86 ± 31.48 ^z	209.58 ± 69.85 ^z
	2	138.20 ± 27.30 ^y	178.91 ± 56.91 ^{zy}	158.89 ± 30.94	162.44 ± 28.99 ^z	158.73 ± 35.87 ^{zy}
	15	96.89 ± 49.36 ^y	91.93 ± 36.46 ^x	129.96 ± 58.20	128.28 ± 50.49 ^{zy}	106.34 ± 34.18 ^y
	30	115.05 ± 34.65 ^{ab,y}	124.77 ± 40.52 ^{ab,yx}	149.26 ± 35.19 ^a	78.07 ± 1.24 ^{b,y}	100.85 ± 20.87 ^{ab,y}
D[3,2] (μm)						
Couscous	0	16.01 ± 3.70	16.55 ± 3.39	19.35 ± 3.41	19.66 ± 1.41	18.39 ± 3.05
	2	16.00 ± 3.37	15.79 ± 3.19	17.76 ± 2.36	19.00 ± 2.07	19.27 ± 3.07

(continued)

Table 7.10 (continued)

Food	Proximal phase (min)	Distal phase (min)				
		15	30	60	120	180
	15	16.88 ± 3.34	17.40 ± 3.07	17.99 ± 2.10	20.02 ± 2.94	19.23 ± 2.38
	30	16.41 ± 2.60	17.61 ± 3.61	18.72 ± 2.25	18.74 ± 2.70	19.2 ± 2.27
Rice couscous	0	24.27 ± 3.51 ^{zy}	24.28 ± 2.22 ^z	25.05 ± 3.29 ^z	24.49 ± 3.94 ^z	27.35 ± 3.18 ^z
	2	25.16 ± 2.72 ^z	24.13 ± 1.49 ^z	23.81 ± 4.25 ^z	26.81 ± 4.57 ^z	25.92 ± 7.17 ^z
	15	18.60 ± 2.74 ^y	18.15 ± 3.97 ^y	17.15 ± 3.05 ^y	17.48 ± 3.85 ^y	16.36 ± 4.67 ^y
	30	15.10 ± 2.85 ^{b,x}	17.16 ± 5.24 ^{ab,y}	17.38 ± 5.05 ^{ab,y}	16.58 ± 3.17 ^{ab,y}	17.45 ± 5.05 ^{a,y}
Pasta	0	16.45 ± 2.87 ^{d,z}	19.38 ± 2.19 ^{cd,z}	23.53 ± 1.38 ^{bc,z}	27.07 ± 2.95 ^{ab,z}	30.69 ± 0.84 ^{a,z}
	2	13.60 ± 2.22 ^{c,zy}	17.9 ± 0.63 ^{b,zy}	20.98 ± 2.86 ^{ab,z}	24.61 ± 1.52 ^{a,z}	25.35 ± 1.31 ^{a,z}
	15	12.64 ± 1.97 ^{c,y}	13.70 ± 1.70 ^{bc,y}	15.12 ± 1.45 ^{abc,y}	17.18 ± 1.50 ^{ab,y}	18.77 ± 0.86 ^{a,y}
	30	13.89 ± 1.56 ^{zy}	14.65 ± 1.71 ^y	15.86 ± 1.87 ^y	16.87 ± 1.97 ^y	17.16 ± 1.96 ^y
Rice noodle	0	11.34 ± 5.09 ^z	12.83 ± 7.72 ^z	13.52 ± 6.64 ^z	13.52 ± 5.97 ^y	12.72 ± 7.78 ^z
	2	8.31 ± 5.51 ^y	8.27 ± 5.16 ^y	10.06 ± 7.77 ^y	8.41 ± 5.41 ^y	9.17 ± 3.46 ^y
	15	12.24 ± 6.77 ^z	10.31 ± 4.47 ^z	12.5 ± 7.46 ^z	12.34 ± 7.47 ^z	11.38 ± 5.91 ^z
	30	11.71 ± 5.27 ^z	12.15 ± 5.18 ^z	13.77 ± 8.13 ^z	13.45 ± 7.83 ^z	14.15 ± 6.47 ^z
Rice grain	0	34.01 ± 8.47 ^z	32.05 ± 6.79 ^z	27.94 ± 4.27 ^z	29.33 ± 5.39 ^z	33.28 ± 9.70 ^z
	2	17.03 ± 4.29 ^y	18.22 ± 2.73 ^y	20.81 ± 3.83 ^z	22.15 ± 1.54 ^z	21.81 ± 4.49 ^{zy}
	15	15.64 ± 2.67 ^y	15.14 ± 1.52 ^x	16.52 ± 3.66 ^y	17.18 ± 2.77 ^y	19.09 ± 1.05 ^{yx}
	30	15.10 ± 2.14 ^y	15.72 ± 3.13 ^x	15.46 ± 2.38 ^y	13.63 ± 1.16 ^y	16.66 ± 1.12 ^x

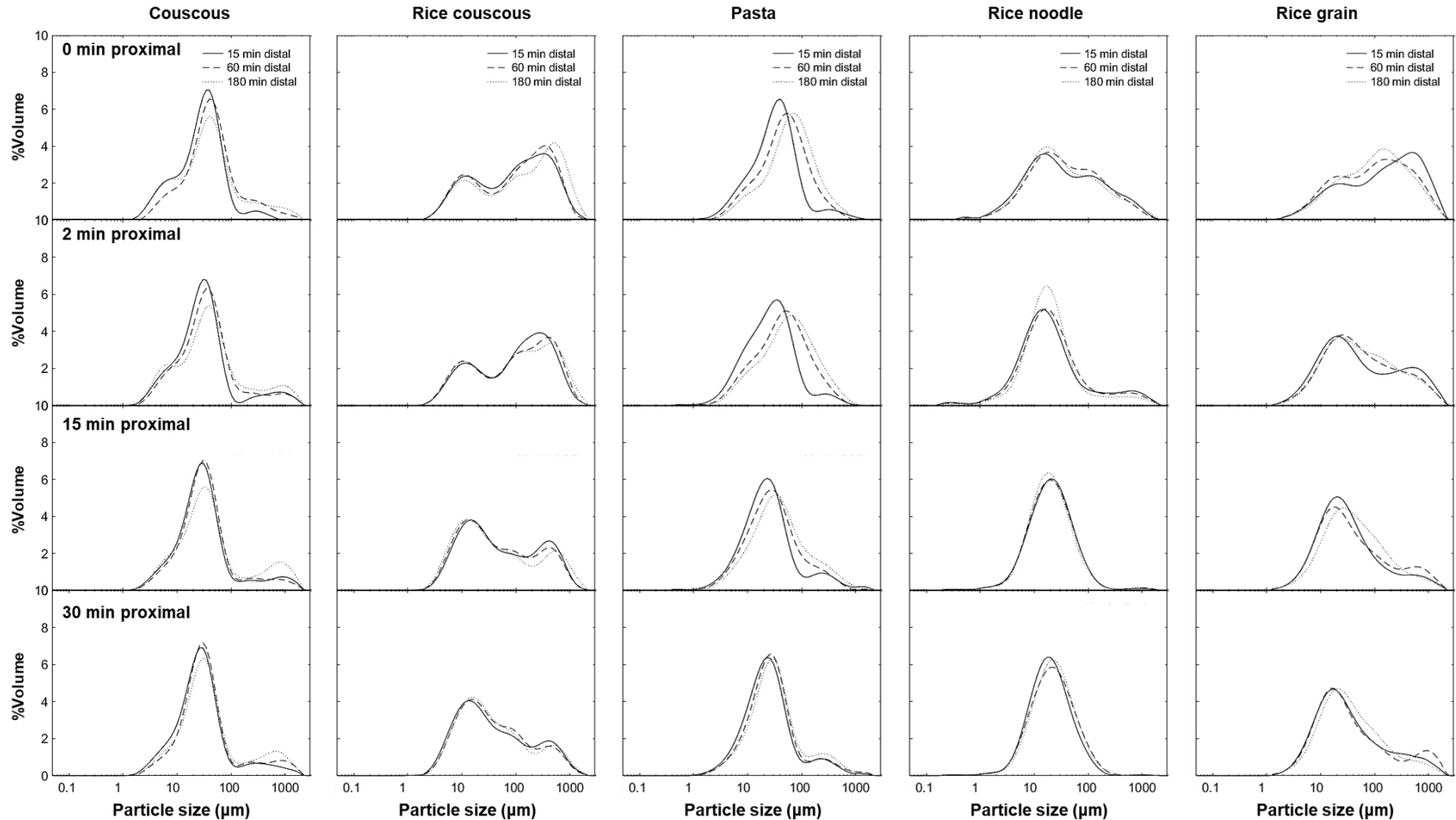


Figure 7.6 Particle size distribution (PSD) of liquid and suspended solid fractions in the digesta at different proximal phase durations, over 15 min (—), 60 min (---), or 180 min (···) distal phase, established by averaging the PSD data of three replicates. One figure corresponds to one food type and proximal phase duration. Plots within the same row correspond to the same proximal phase duration, as noted in the leftmost column. Plots within the same column represent particle size distribution data for one type of food, as noted in the uppermost figure for each column. Individual PSD plots with error shades to indicate the range of the distribution are given in Figure F.7 to F.11.

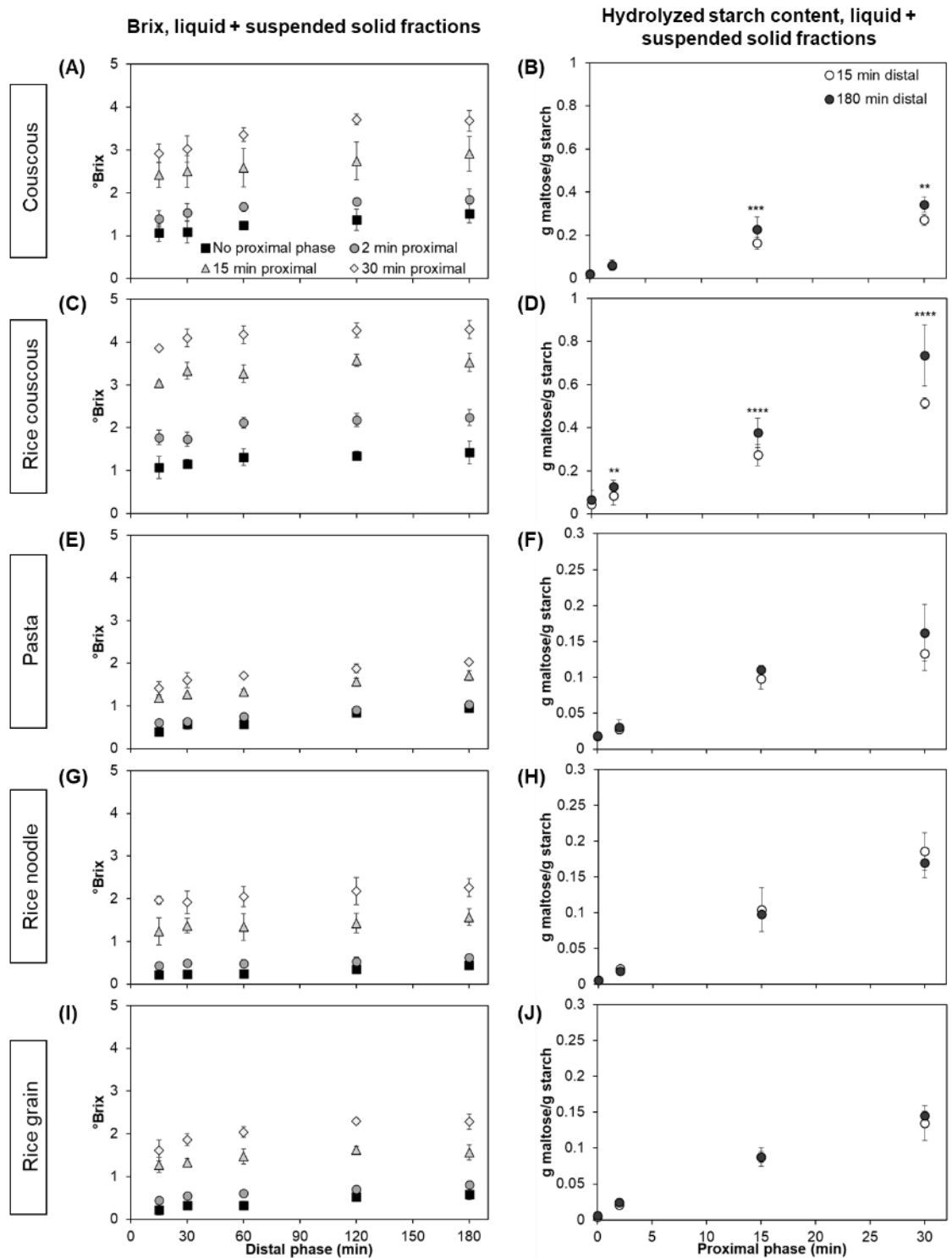


Figure 7.7 °Brix profiles during the distal phase, after 0 min (■), 2 min (●), 15 min (▲), or 30 min (◇) proximal phase (left column) and hydrolyzed starch content during the proximal phase after 15 min (○) or 180 min (●) distal phase (right column). Figures within the same row correspond to one type of food: couscous (A-B), rice couscous (C-D), pasta (E-F), rice noodle (G-H), and rice grain (I-J). Values are shown as mean ± SD (n = 3 for each data point); error bars are too small to be seen for some samples. For the hydrolyzed starch content data, significant differences between distal phase at one proximal phase duration are indicated by asterisks (*: $p < 0.05$, **: $p < 0.01$, ***: $p < 0.001$, ****: $p < 0.0001$).

7.5 Discussion

7.5.1 Food breakdown during the proximal phase occurred through leaching of soluble and/or small particles

In those samples that only underwent proximal phase digestion, a longer proximal phase duration caused a reduction in hardness (i.e., softening) of the whole digesta, but this softening occurred at different rates for different foods. Based on their $t_{1/2, \text{softening}}$ during the proximal phase, couscous and rice couscous (agglomerated products, $t_{1/2, \text{softening}} < 1$ min) were classified as fast softening, while rice grain ($t_{1/2, \text{softening}} = 356$ min) and noodle products (pasta and rice noodle, $t_{1/2, \text{softening}} = 124$ and 542 min) were classified as slow softening (Drechsler & Bornhorst, 2018). It was hypothesized that longer proximal phase durations would lead to longer contact time with α -amylase, which gave more time for starch hydrolysis to reduce the H_t/H_0 of the whole digesta mixture (Figure 7.1A).

In this study, the agglomerated products had more loose starch granules in the food matrix, compared to the rice grain and noodle products (Chapter 5), which caused faster softening in the agglomerated products. The $t_{1/2, \text{softening}}$ of rice grain and noodle products that were beyond the selected proximal phase durations suggests that the macro- and microstructural aspects of these foods limited starch hydrolysis by α -amylase during the 30-min proximal phase (Dhital et al., 2017; Hasjim et al., 2010). Bornhorst, Hivert, et al. (2014) reported that a prolonged incubation of brown rice boluses with increasing amount of saliva did not cause further softening of the boluses, which was attributed to the presence of the outer bran layer in brown rice that slowed the diffusion of α -amylase into the bolus. Meanwhile, the softening of white rice boluses was generally enhanced with higher amount of saliva, except the long grain variety due to its higher amylose

content. Similarly, Gao et al. (2021) reported that smaller initial particle size of bread subjected to *in vitro* oral processing significantly decreased the hardness of the bolus.

Starch hydrolysis by α -amylase that occurred during the proximal phase was hypothesized to generate soluble and/or small particles. This was supported by the increased proportion of particles $\leq 4 \text{ mm}^2$ (measured via image analysis) with longer proximal phase in the whole digesta mixture (0-min distal bar graphs in Figure 7.1B-F), which was observed in all foods. These particles likely leached into the SGF during the distal phase as soon as SGF was added, which were identified as the suspended solid fraction after separation of the large solids from the digestion mixture. Moreover, significant reduction in the asymptotes of both W_t/W_0 and DM_t/DM_0 with longer proximal phase in the proximal-distal digestion (Figure 7.2, Table 7.5) implied more leaching of particles $\leq 4 \text{ mm}^2$ from the food matrices due to prolonged proximal phase, even in the absence of mechanical forces. The 4-mm^2 limit for definition of the small particle fraction was selected based on the aperture of the mesh used to separate the solid fraction of digesta ($1\text{-mm} \times 2\text{-mm}$; assuming circular-shaped area, the theoretical projected area was rounded up to 4 mm^2 for practicality).

The hypothesis that starch hydrolysis during the proximal phase generated soluble and/or small particles was also supported by the increasing °Brix and hydrolyzed starch content in the liquid-suspended solid mixture with longer proximal phase at 15 min distal phase (Figure 7.7), where the contribution of the distal phase was limited. Meanwhile, preliminary tests using water with the similar durations of proximal-distal digestion did not result in such increase. At any proximal phase duration, both °Brix and hydrolyzed starch content in the liquid and suspended solid phases were higher in the agglomerate products compared to the three other foods (Figure 7.7), implying food structure affected the kinetics of starch hydrolysis. Previous *in vitro* gastrointestinal

studies using solid and semi-solid starch-based products also reported that the rate and extent of starch digestion by α -amylase increased significantly with smaller initial particle size (Abhilasha, Kaur, Monro, Hardacre, & Singh, 2021; Mandalari et al., 2018; Tamura et al., 2017). Moreover, the first peak of liquid and suspended solid fractions PSD at 15 min distal phase (Figure 7.6) appeared between 20 to 40 μm for wheat-based foods and between 5 to 15 μm for rice-based foods, which matches with the diameter of Durum wheat starch granules (20 to 25 μm) and rice starch granules (3 to 15 μm) reported in the literature (Abecassis et al., 2012; Ramadoss et al., 2019). The proportion of particles in this first peak generally increased with increasing proximal phase, indicating more starch granules were released to the SGF. These observations strongly suggest that the suspended starch (and soluble, hydrolyzed starch) particles with $d < 2$ mm that leached into the liquid fraction in the beginning of the distal phase can be attributed to starch hydrolysis during the proximal phase. Therefore, in a broader context, starch hydrolysis that may continue during the proximal phase plays an important role in aiding the overall breakdown of solid foods during gastric digestion.

7.5.2 Increased fluid uptake in the distal phase caused softening of solid digesta fraction, but the softening process was not enhanced by proximal phase

Previous *in vitro* static gastric digestion studies without proximal phase have reported that macro- and microstructural changes to food particles during gastric digestion were associated with the diffusion of gastric fluid components (acid, moisture, and enzymes) into the food matrix (Kong et al., 2011; Mennah-Govela & Bornhorst, 2016a; Somaratne et al., 2019). In the current study, the increased diffusion of SGF into the food matrices during the distal phase was indicated by the increasing W_t/W_0 in rice grain and noodle products (Figure 7.2, left column) and increasing moisture uptake of digesta solid fraction of all foods (Figure 7.4, left column). Consequently, the solid

fraction of digesta exhibited decreasing H_t/H_0 (softening) during the distal phase digestion, regardless of the duration of the preceding proximal phase (Figure 7.4, right column).

Large variations in the softening kinetics of the solid fraction during distal phase were observed (Figure 7.5, Table 7.6). Previously, Drechsler and Bornhorst (2018) also reported large variations in the softening kinetics of carbohydrate-based foods when measurement was conducted using bulk compression method. The additional approach of fitting the data points altogether provided a better estimate (Table 7.7). However, the results from this approach did not change the conclusions obtained if the data were fitted per replicate (Figure 7.5, Table 7.6). Distal phase digestion preceded with 0 to 2 min proximal phase resulted in the classification of agglomerated products ($t_{1/2, \text{softening}} < 30$ min) as fast softening, and the three other foods ($t_{1/2, \text{softening}} > 150$ min) as slow softening (Drechsler & Bornhorst, 2018). At 15 and 30 min proximal phase, this softening rate classification remains despite the increased $t_{1/2, \text{softening}}$ in all foods, except for rice couscous that transitioned into slow softening.

The fast-softening behavior of couscous at any proximal phase and rice couscous at 0- and 2-min proximal phase can be associated with their small initial particle size ($1 < d \leq 2$ mm), porous microstructure (based on microstructural observation in Chapter 5), and spherical geometry of the agglomerated products, which altogether contributed to their dissociation and dissolution (Bornhorst et al., 2015). The effect of dissociation and dissolution was also reflected by their decreasing W_t/W_0 during the distal phase at ≥ 15 min proximal phase for couscous, or at any proximal phase for rice couscous (Figure 7.2). Rice couscous in the current study was a mixture of brittle, porous and hard, compact particles due to the manufacturing procedure (APPENDIX A). Hence, the change in the softening rate of rice couscous at 15 and 30 min proximal phase can be

associated with the dissolution of brittle particles during the proximal phase, leaving behind the hard particles that softened slowly. Food particles with high hardness and compact structure, such as almonds, have been reported to undergo slow softening during gastric digestion *in vitro* and *in vivo* (Bornhorst, Roman, et al., 2014). The inhomogeneity of the rice couscous therefore explained the high variability in the softening kinetics between replicates; the overall softening behavior was able to be described by the results from fitting of all data points altogether (Table 7.7).

For the slow-softening foods, the softening rate in the current proximal-distal digestion experiments was selected as a parameter to reflect the limiting factor in the physical breakdown of the foods during gastric digestion. This softening rate is a combined consequence of food structure and the amount of gastric fluid that penetrated the food matrix (Bornhorst et al., 2015). As such, the estimated $t_{1/2, \text{softening}}$ for rice grain and noodles that were mostly >180 min (longer than the distal phase tested) indicated that gastric fluid diffusion was not a limiting factor in the breakdown of the foods during gastric digestion. Moreover, incubation in distal phase of longer than 180 min is unlikely to cause further change in the softening parameters, as reported in an *in vitro* gastric digestion study using carbohydrate-based foods that compared the effect of 60, 120, 180, and 240 min digestion on the softening parameters of the foods (Drechsler & Bornhorst, 2018).

Apart from rice couscous, the unchanged classification of softening rate of the foods suggested that the proximal phase did not enhance the softening during the distal phase. With the increased softening of digesta during proximal phase (Figure 7.1A), it was initially expected that longer proximal phase times would enhance softening during distal phase, resulting in a faster food breakdown rate. Moreover, a previous study using rice of various types suggested that contact with α -amylase increased the effective

diffusivity of acid into rice boluses (Mennah-Govela et al., 2015). However, it was found that longer proximal phase durations led to increased H_t/H_0 of solid fraction of digesta at any distal phase time (Figure 7.4) instead of decreasing H_t/H_0 . When averaged across food \times distal phase, H_t/H_0 values increased significantly from 0.54 ± 0.29 after no proximal phase to 0.68 ± 0.29 ($p < 0.0001$) after 30 min proximal phase. As a result, longer proximal phase trended to increase the $t_{1/2, \text{softening}}$ of the digesta solid fraction (Figure 7.4).

Although Mennah-Govela et al. (2015) reported that acid and moisture uptake increased with longer incubation with SGF, their study utilized an isolated system to study diffusion in one-dimension, and did not account for possible variations in bolus properties in an excess of gastric fluid. In the current study, the hydrolyzed starch particles generated during the proximal phase settled at the bottom of the SGF-food mixture, together with the food particles. These leached starch particles were thought to hinder the diffusion of SGF into the intact food particles. Increasing concentration of suspended starch particles in the liquid-suspended solid mixture (as reflected by the decreasing DM_t/DM_0 ; Figure 7.2) due to the proximal phase may have increased the viscosity of the SGF-suspended particle mixture (Nguyen et al., 2021), subsequently slowing the diffusion of SGF into food particles (Kong & Singh, 2011). The reduced diffusion of SGF into food particles was also supported by the reduction in moisture change that occurred during the distal phase following longer proximal phase times (Figure 7.4). The reduced moisture change resulted in less softening effect, and might contribute to the variations observed in the slow-softening foods. This trend would be expected, as previous studies have reported that increased moisture content (or uptake) resulted in decreasing rheological and textural attributes of digesta (Bornhorst, Ferrua,

et al., 2013; Martens, Noorloos, et al., 2019; Swackhamer, Doan, & Bornhorst, 2022), which was also reported in Chapter 4.

With the trend of reduced softening effect in the distal phase following longer proximal phases in the larger-sized foods, the textural change in the whole digesta mixture of larger-sized foods during the proximal phase appeared to be due to the generation of particles $\leq 4 \text{ mm}^2$ that together with SSF, constituted the bulk textural properties of the mixture. SSF used in the current study also contained mucin, which is a lubricating agent and might contribute to the bulk textural properties (Minekus et al., 2014). Longer proximal phase leached more hydrolyzed starch particles into the limited volume of SSF and increased the concentration of hydrolyzed starch in the mixture, which might decrease the storage modulus and complex viscosity of the mixtures (Khatoon, Sreerama, Raghavendra, Bhattacharya, & Bhat, 2009). Since rheological and textural properties of digesta are correlated (as discussed in Chapter 4, Table 4.10), reduced hardness in the whole digesta mixture were expected with increasing starch hydrolysis.

It was previously reported in Chapter 4 and 5 that gastric digesta of pigs fed with the same foods used in this chapter consisted of 40% or more particles $\leq 10 \text{ mm}^2$ and a certain proportion of liquid, indicating that the bulk of *in vivo* gastric digesta was comprised of a mixture of large and small particles with digestive secretions. However, in this *in vitro* study, the separation of solid fraction from the excess fluid in the digesta mixture at the end of each distal digestion removed free fluid and particles $\leq 4 \text{ mm}^2$ in the mixture. The separation process removed the liquid needed to fill the void space between the food particles when bulk compression method is used (Drechsler & Bornhorst, 2018); this is particularly important for the larger-sized foods, which remained as individual particles throughout the digestion experiments. Similar

experiments using a limited amount of SGF and with no liquid separation are suggested for future studies to examine the actual synergistic effect of proximal and distal phase on the bulk rheological and textural properties of digesta during gastric digestion.

To investigate the effect of the distal phase on solid particle breakdown, the DM_t/DM_0 profiles (Figure 7.2) and particle size parameters of the solid digesta fraction (Table 7.8 and 7.9) were examined. A significant decrease in DM_t/DM_0 during the distal phase was observed in rice couscous even with no proximal phase, as well as in couscous and pasta at proximal phase ≥ 2 min. The proportion of particles $\leq 4 \text{ mm}^2$ between 30- and 180-min distal phase also increased in these foods (Figure 7.1B-D). In rice grain and rice noodle at any proximal phase duration, no significant change DM_t/DM_0 during the distal phase was observed, but the proportion of particles $\leq 4 \text{ mm}^2$ between 30 and 180 min distal phase increased (Figure 7.1E-F). The increasing proportion of particles $\leq 4 \text{ mm}^2$ suggested the formation of smaller particles under minimum mechanical force (except the gentle shaking and stirring during pH adjustment) during the distal phase.

While the trends in DM_t/DM_0 and particles $\leq 4 \text{ mm}^2$ during the distal phase of couscous and rice couscous can be explained with the erosion of the particles and dissolution of these foods (observed as decreasing W_t/W_0 , increasing °Brix in the distal phase, and decreasing particles between 10 and 100 mm^2 with longer distal phase), the trends observed in the noodle products might be associated with erosion on the surface of the food particles by acid and pepsin in the SGF. In noodle products, the majority (>85%) of the particles remained $>100 \text{ mm}^2$ throughout the distal phase, indicating no notable breakdown, although the slightly decreasing proportion of particles $>100 \text{ mm}^2$ might reflect surface damages of the noodle. Moreover, the area of 4 mm^2 was less than 7% of the initial average area per particle for the noodles, which can be categorized as

fine debris resulting from surface damages of the food particles during gastric digestion (Drechsler & Ferrua, 2016). Particularly in pasta, the changes might be attributed to hydrolysis of its gluten network during the distal phase (Zou et al., 2016), which might allow more starch granules to leach from the food matrix. It was previously reported that 30 min *in vitro* gastric digestion of intact pasta piece allowed pepsin in the SGF to penetrate only into the surface of the pasta matrix (Zou et al., 2015). However, with the distal phase that lasted >30 min in the current study, it was possible that pepsin in the SGF might have penetrated further into the matrix and released starch granules from the pasta matrix, especially when preceded by proximal phase. Future studies should include the microstructural observation to characterize the penetration of digestive enzymes into various types of food matrix as affected by proximal and distal phase.

It is noteworthy that in rice grain, most of its particle size parameters underwent significant decrease with longer distal phase time, except the particles/g DM that increased between 30- and 180-min distal phase (Table 7.8 and 7.9). These trends were due to fragmentation of the rice kernels into several parts (Figure 7.8), possibly due to the increased acid diffusion into the rice kernels that took place radially (the shortest dimension of the rice kernels) at longer distal phase time. The fragmentation that was only observed in rice grain, but not the noodle products, might be related to their different microstructure and geometry, which will be discussed in Section 7.5.4.

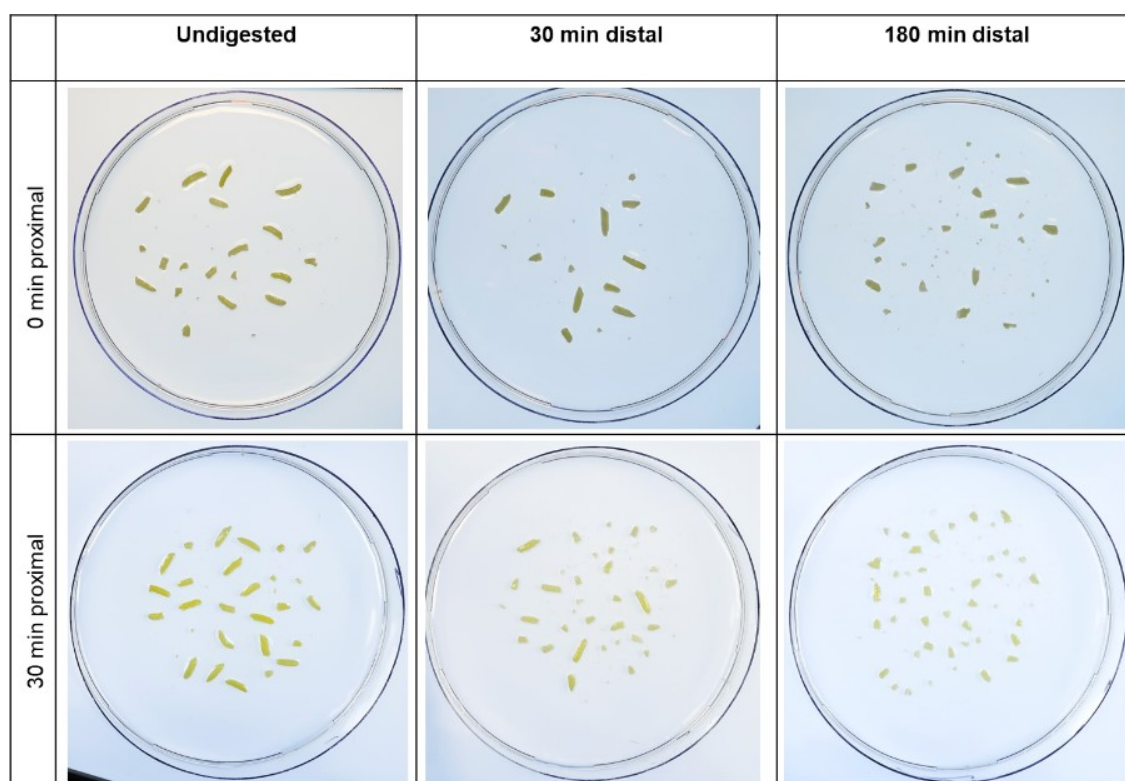


Figure 7.8 Examples of the appearance of the solid fraction of rice grain digesta before digestion, and after 0 or 30 min proximal phase followed by 30 or 180 min distal phase, indicating the breakdown of the rice kernels into smaller parts after 180 min distal phase at both proximal phase durations. Pictures for each proximal phase were taken from the same day of experiment.

7.5.3 Synergistic effect of proximal and distal phase on the characteristics of liquid and suspended solid fractions of digesta

It was hypothesized that generation of particles $\leq 4 \text{ mm}^2$ was due to surface erosion during the proximal and distal phase; these particles were observed as the suspended solid fraction that mixed together with the liquid fraction. Compared to the particles $>4 \text{ mm}^2$ that had more physical barriers to the digestive enzymes, these small particles were considered to have more propensity to be digested by α -amylase during the proximal phase, or acid and pepsin during the distal phase at a longer digestion time. Changes to the liquid and suspended solid fractions of the digesta were examined through particle size, °Brix, and hydrolyzed starch content measurement in the mixture.

While no significant differences between rice- and wheat-based foods were observed in the particle size parameters of solid digesta fraction, possibly due to the more significant contribution of the food macrostructure in the bulk of the solids, the effect of starch source was observed in the liquid and suspended solid fractions of digesta. Changes in the D[4,3] and D[3,2] of rice-based foods were more sensitive to the proximal phase, while wheat-based foods were more sensitive to the distal phase (Table 7.10), which can also be seen in their PSD profiles (Figure 7.6). This might indicate that the size characteristics of leached particles depend on changes that occur during the proximal phase for rice-based foods or during the distal phase for wheat-based foods. This is possibly linked to their hydrolysis characteristics; an *in vitro* study using native starches reported that hydrolysis by α -amylase was higher in rice starch, whereas hydrolysis by HCl was higher in wheat starch (Singh & Ali, 2006). Additionally, the pattern observed in the wheat-based foods during the distal phase was similar to the weight distributions of branched starch molecules during *in vitro* digestion of Durum-wheat based products that occurred in the nanoscale (Zou et al., 2016), suggesting that changes in the particle size in the liquid and suspended solid digesta fractions occur in a similar pattern to their chemical changes. The effect of starch source that was observed in liquid and suspended solid fraction possibly suggests that starch properties govern the characteristic of digestion when food macrostructural/physical barrier is absent. The D[4,3] and D[3,2] at any food \times proximal or food \times distal combinations that were always in the order of: rice grain \geq rice couscous \geq couscous \geq pasta $>$ rice noodle might also have implications on their digestion in the small intestinal phase.

Hydrolyzed starch content and °Brix for all foods increased with longer proximal phase time at any distal phase time, which was expected. Contrasting starch hydrolysis

profiles were observed between the agglomerated and non-agglomerated products, where the increase in °Brix and hydrolyzed starch during the distal phase digestion for the agglomerated products was faster than the non-agglomerated products (Figure 7.7). Increasing distal phase time from 15 to 180 min did not increase the starch hydrolysis in non-agglomerated products, but interestingly, there was a significant increase ($p < 0.01$) in starch hydrolysis observed in the agglomerated products at proximal phase ≥ 2 min for rice couscous or ≥ 15 -min for couscous. This aligns with a study using native waxy rice starch dispersion that reported increased hydrolysis due to amylolysis followed by acid hydrolysis at human physiological temperature (Li et al., 2013). The significantly increasing hydrolysis that was only observed in the agglomerated products implies that acid hydrolysis during gastric digestion might enhance starch hydrolysis, but only if amylolysis and acid diffusion are not limited by the microstructural or macrostructural barrier. Together with the difference in the particle size, the trends observed in the hydrolyzed starch content of the foods due to proximal-distal gastric digestion is expected to impact the starch digestibility of these food products during small intestinal digestion and merits future investigation.

7.5.4 Food structure and geometry determine breakdown mechanisms during proximal and distal phase of gastric digestion

In all parameters measured, food was always a significant effect, signifying that changes that occur during the proximal and distal phase are dependent on the food matrix. In addition to their different particle size that contributes to different macrostructures (Table 7.1), these foods also differed in their microstructural arrangement of starch granules in the food matrix (as reported in Chapter 5; Figure 5.9 and 5.10) and protein content (as reported in Chapter 4). Based on the changes during

the proximal and distal phases of gastric digestion, the breakdown mechanisms of these different food structures were proposed (Figure 7.9).

In agglomerated products, due to their porous microstructure (Figure 5.9), α -amylase can diffuse into their internal structure and hydrolyze the starch in the matrix (Dhital et al., 2017), weakening the bonding between particles constituting the agglomerates. With weakened structure of the agglomerated products during proximal phase, longer distal phase time led to an increase in gastric fluid uptake from all directions due to the spherical shape of the particles and the very high surface area to volume (SA/V) ratio compared to rice grain and the noodle products. The increased fluid uptake dissociated the agglomerates and dissolved the dissociated particles as they were saturated with moisture (Barkouti et al., 2014). The dissolution process during distal phase is hypothesized to be controlled by the diameter of the agglomerates and the strength of the cohesion between particles in the agglomerates, which was seen in the more rapid dissolution of rice couscous than couscous due to its smaller initial average area per particle (Figure 7.9) and generally more brittle nature. These breakdown mechanisms might explain the fast-softening behavior of couscous and rice couscous observed in Chapter 4.

In the grain structure of the cooked rice, where the starch particles are contained by cell walls (Figure 5.9), the access of α -amylase into the internal part of the rice kernels was physically limited by the protein matrix and cell walls encapsulating the starch granules (Dhital et al., 2019; Tamura et al., 2016a). Since the rice kernel had a cylindrical-like geometry, it is hypothesized that the diffusion of digestive fluids occurred in the radial direction (the shortest dimension). The diffusion was hindered by the presence of the protein matrix and cell walls, which might cause surface erosion while digestive fluids penetrate to the internal structure of the kernel at early proximal

and distal phase durations (as observed in the increasing particles $\leq 4 \text{ mm}^2$ in the digesta compared to the undigested rice grain; Figure 7.1F). However, fragmentation of the rice kernels at 30 min proximal phase (Figure 7.8), possibly suggested that the α -amylase had reached the internal structure and caused breakage in the shortest dimension of the kernels. In the distal phase, the gastric fluid uptake into the rice kernel was restrained by the cell wall and protein matrix, resulting in swelling of the matrix. When the matrix was saturated with moisture (at distal phase ≥ 120 min; Figure 7.4), the rice kernels broke in the radial direction (Figure 7.8). This might be due to the breakage and dissolution of cell walls, as previously observed during prolonged static soaking of rice kernel (Wu, Deng, et al., 2017), sweet potatoes (Mennah-Govela & Bornhorst, 2016b; Somaratne, Ye, et al., 2020), and apples (Olenskyj et al., 2020) in SGF. Despite its cylindrical-like geometry (SA/V ~ 4 times the noodle products) that resulted in physical fragmentation of the rice kernels, the hydrolyzed starch content of rice grain was similar to that of pasta and slightly lower than that of rice noodle. This suggests the microstructure of rice grain limited the breakdown and hydrolysis related to diffusion of digestive fluids, and that breakdown of the macrostructure is required to release starch from the matrix. Fragmentation that occurred due to prolonged proximal or distal phase and the slow hydrolysis of rice grain may explain its similar $t_{1/2, \text{softening}}$ in the proximal and distal *in vivo* gastric digesta, longer *in vivo* $t_{1/2, \text{softening}}$ compared to rice noodle, and shorter *in vivo* $t_{1/2, \text{softening}}$ compared to pasta (Chapter 4, Figure 4.7).




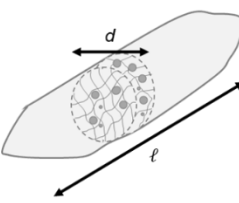
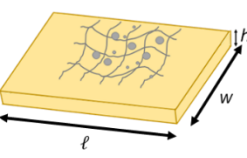
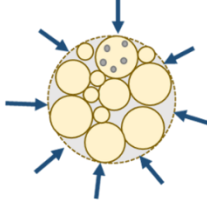
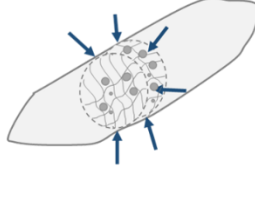
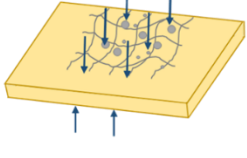
Structure	Agglomerates	Grain	Noodle
<p>Before digestion</p>  Matrix entrapping starch particles  Starch particles in the matrix	 $d = 1 - 2 \text{ mm}$	 $d = \sim 2 \text{ mm}, \ell = \sim 10 \text{ mm}$	 $w = \sim 7 \text{ mm}, \ell = \sim 15 - 18 \text{ mm}, h = 1 - 1.5 \text{ mm}$
Estimated surface area per volume (SA/V, mm^{-1})	3 – 6	2.2 – 2.3	0.5 – 0.7
Direction of digestive fluid diffusion	 Radial	 Radial	 Axial
Main breakdown mechanism due to digestive fluid diffusion	Dissolution	Surface erosion, fragmentation (at later duration)	Surface erosion
Factor limiting the release of starch particles	Agglomerate diameter, agglomerate strength	Macrostructural breakdown, matrix entrapping the starch particles	Macrostructural breakdown, matrix entrapping the starch particles

Figure 7.9 Hypothesized breakdown mechanisms of the food structures due to digestive fluids diffusion during proximal and distal phase in the current study, as affected by the geometry and direction of digestive fluid diffusion into the food matrix. The surface area per volume (SA/V) ratio was estimated from the characteristic dimension of each food. Representative starch particles and selected region showing the food matrix are shown to reflect the entrapment of starch particles in the food structure. Factor limiting the release of starch granules from the structure is also proposed based on the main breakdown mechanism.

In the noodle structure, although the thickness of the noodles was similar to the diameter of the agglomerate products (~ 1 and 1.5 mm in rice noodle and pasta, respectively), the $t_{1/2, \text{softening}}$ in both proximal and proximal-distal digestion were longer than the agglomerate products. This suggests that the microstructure of the noodles (Chapter 5) limited the diffusion of digestive fluid components. Previous microstructural observation study on the diffusion of α -amylase to intact piece of pasta reported that the diffusion occurred gradually from the outer part to the center of the pasta (Zou et al., 2015). Thus, the diffusion of α -amylase and gastric fluid components into the noodle pieces was thought to mainly take place in the direction of the thickness (the shortest dimension of the noodle). However, the small thickness relative to the

main surface of the noodles (slab geometry) may result in surface erosion on the largest surface of the particle (Figure 7.9). Starch source and microstructural differences between rice noodle (solubilized starch gel with no physical barrier encapsulating the starch; Chapter 5) and pasta (starch particles entrapped in starch-protein matrix; Chapter 5) possibly affected the rate of diffusion and surface erosion by digestive fluids, resulting in different softening kinetics between these foods in the proximal only and proximal-distal digestion (Figure 7.1A, 7.4F, 7.4H). The microstructural differences may also explain the difference in the *in vivo* $t_{1/2, \text{softening}}$ of pasta and rice noodle in the proximal and distal stomach (pasta had faster softening in the distal stomach, whereas noodle had faster softening in the proximal stomach), as well as the longer $t_{1/2, \text{softening}}$ of pasta compared to rice noodle (Chapter 4, Figure 4.7). However, it is unclear how these microstructural differences resulted in different softening profiles during the distal phase, which should be investigated in future studies.

It is worth noting that the geometrical differences between the foods that were considered to affect the direction of diffusion of digestive fluid components have similar principles to diffusion-controlled drug delivery system (Siepmann & Siepmann, 2012). The different geometries of the foods led to different SA/V ratio, where the SA/V ratio of agglomerate products > rice grain > noodle products. Higher SA/V was reported to increase the rate of drug release in a study of controlled-release tablets (Reynolds, Mitchell, & Balwinski, 2002), which agrees with the correlation between the SA/V and hydrolyzed starch content of the digesta found in the current study. This might indicate that the different mechanisms of food breakdown during the proximal and distal gastric digestion phase as affected by the food structure and geometry may be utilized for designing food structure with controlled starch release (Figure 7.9). However, microstructural observation is required to back up the hypotheses arising

from the observation. Since food structure and starch digestibility can be impacted by the preparation method, including cooking duration, storage, and the presence of non-starch meal components (Pellegrini et al., 2020; Singh et al., 2010), separate studies can be done to elucidate the effect of preparation method (beyond the standardized cooking methods used in this thesis) on food breakdown during gastric digestion. Additionally, the breakdown mechanisms may be affected by macrostructural breakdown that occurs through mastication and gastric contraction forces, which were outside the scope of the present study. Mastication and gastric contractions should be involved in future studies with similar design to elucidate the combined effect of mechanical and biochemical changes in the proximal and distal phases of gastric digestion on the physicochemical properties of digesta.

7.6 Conclusions

The proximal gastric phase, where the exposure to α -amylase is extended, is often less considered in gastric digestion studies. However, this work demonstrated that the proximal phase affected the properties of food particles during the distal phase of gastric digestion. The proximal phase contributed to the generation of small particles via starch hydrolysis. The distal phase contributed to increased gastric fluid uptake, which softened food particles. The prolonged proximal phase preceding the distal phase did not enhance the softening process during distal phase, possibly due to increasing hydrolyzed starch particles in the digestion mixture that increased the viscosity of SGF and reduced its diffusion into the intact food particles. However, the proximal phase preceding the distal phase enhanced the starch hydrolysis in agglomerated products after 180-min distal phase, suggesting that acid hydrolysis might enhance starch

hydrolysis initiated by α -amylase, but only in the absence of micro- and macrostructural barriers in the food matrix.

Results also suggested that the role of food structure and geometry (size and shape, which define its SA/V) in the current study was important to the breakdown mechanisms during proximal and distal phase, in the absence of mechanical forces. The smaller initial size, porous microstructure, and spherical shape of agglomerated products might be associated with their fast-softening behavior during gastric digestion. The larger initial size of rice grain and noodle products, combined with the presence of more barrier to enzyme diffusion in their microstructure and their shapes (cylindrical for rice grain, slab geometry for noodle products), might be associated with their slow-softening behavior during gastric digestion. Future studies should include microstructural observation to complement the current findings and elucidate the impact of proximal and distal phase on changes in the microscale. Overall, the current study demonstrates that food structure is crucial in determining the breakdown mechanisms due to digestive fluid diffusion in the proximal and distal phases of gastric digestion.

CHAPTER 8. Overall discussion, conclusions and future recommendations

8.1 Overall discussion and conclusions

This project focused on understanding the link between food structure, gastric digestion, gastric emptying, and glycemic response of starch-based foods using *in vivo* and static *in vitro* digestion approaches. This link was identified through the *in vivo* investigation of physicochemical changes during gastric digestion and the consequences of the changes on starch digestion in the small intestine and glycemic response. The contributions of the proximal and distal stomach in determining the breakdown mechanisms and the output of gastric digestion of different food structures were further investigated through static *in vitro* digestion experiments.

Rice- and wheat-based foods with varying physical structures were selected to represent high moisture, starch-based food structures with contrasting initial particle size, composition, and microstructure. In general, the diets with larger initial particle size (pasta, rice grain, and rice noodle; $d > 2$ mm) in this project had more complex physical structure than the diets with smaller initial particle size (couscous, rice couscous, and semolina; $d < 2$ mm) due to how they were processed. Semolina had the simplest structure (finely-milled native grain), couscous and rice couscous had the agglomerated structure from milled grain, rice grain had a complex structure of native grain and was the structure with the least processing compared to the other diets in this project, whereas pasta and rice noodle had a complex structure consisting of starch hydrogel (originated from the slurry/paste of finely-milled grain). In terms of their microstructure, semolina had mainly solubilized starch structure, couscous and rice couscous had porous microstructure, rice grain had a compact starch granules

arrangement encapsulated in the endosperm, and pasta and rice noodle consisted of starch particles distributed in a gel matrix (Figure 8.1).

Findings from the experimental chapters (summarized in Figure 8.1) supported a similar conclusion: food macro- and microstructure were important to determine food gastric digestion behavior, gastric emptying, and glycemic response. As shown in Chapter 4, the smaller-sized diets had shorter emptying half-times of whole stomach content and dry matter than diets with larger initial particle size. For instance, the dry matter emptying half-times ($t_{1/2,DM\ GE}$) in the smaller-sized diets were 88, 150, and 160 min in semolina, rice couscous, and couscous, respectively, which were shorter than 213, 223, and 360 min in rice noodle, rice grain, and pasta, respectively. Similarly in Chapter 5, the starch emptying half-time of the diets ($t_{1/2,starch\ GE}$) also followed similar trend to that of the $t_{1/2,DM\ GE}$. In Chapter 6, smaller-sized diets had a higher glycemic impact than larger-sized diets. The $\Delta\text{max}_{\text{overall}}$ and $\text{iAUC}_{\text{overall}}$ of diets with smaller- and larger initial size were 29.0 ± 3.2 vs. 21.7 ± 2.6 mg/dL and 5659.2 ± 727.1 vs. 2704 ± 521.3 mg/dL.min, respectively.

The different emptying half-times between the smaller- and larger-sized diets can be attributed to the combined result of gastric mixing with gastric secretions, mechanical breakdown by gastric wall contractions, and gastric sieving that only allowed particles of a certain size to be emptied. Although changes during gastric digestion and gastric emptying rate are inter-dependent, the overall consequence of the processes on the breakdown rates of the diets was reflected by the softening half-time ($t_{1/2,softening}$), which was estimated from textural kinetics measurement of the gastric digesta in Chapter 4. It was found that the $t_{1/2,DM\ GE}$ was correlated with the $t_{1/2,softening}$ of the diets in an exponential relationship. Smaller-sized diets had $t_{1/2,softening} < 6$ min, whereas the larger-

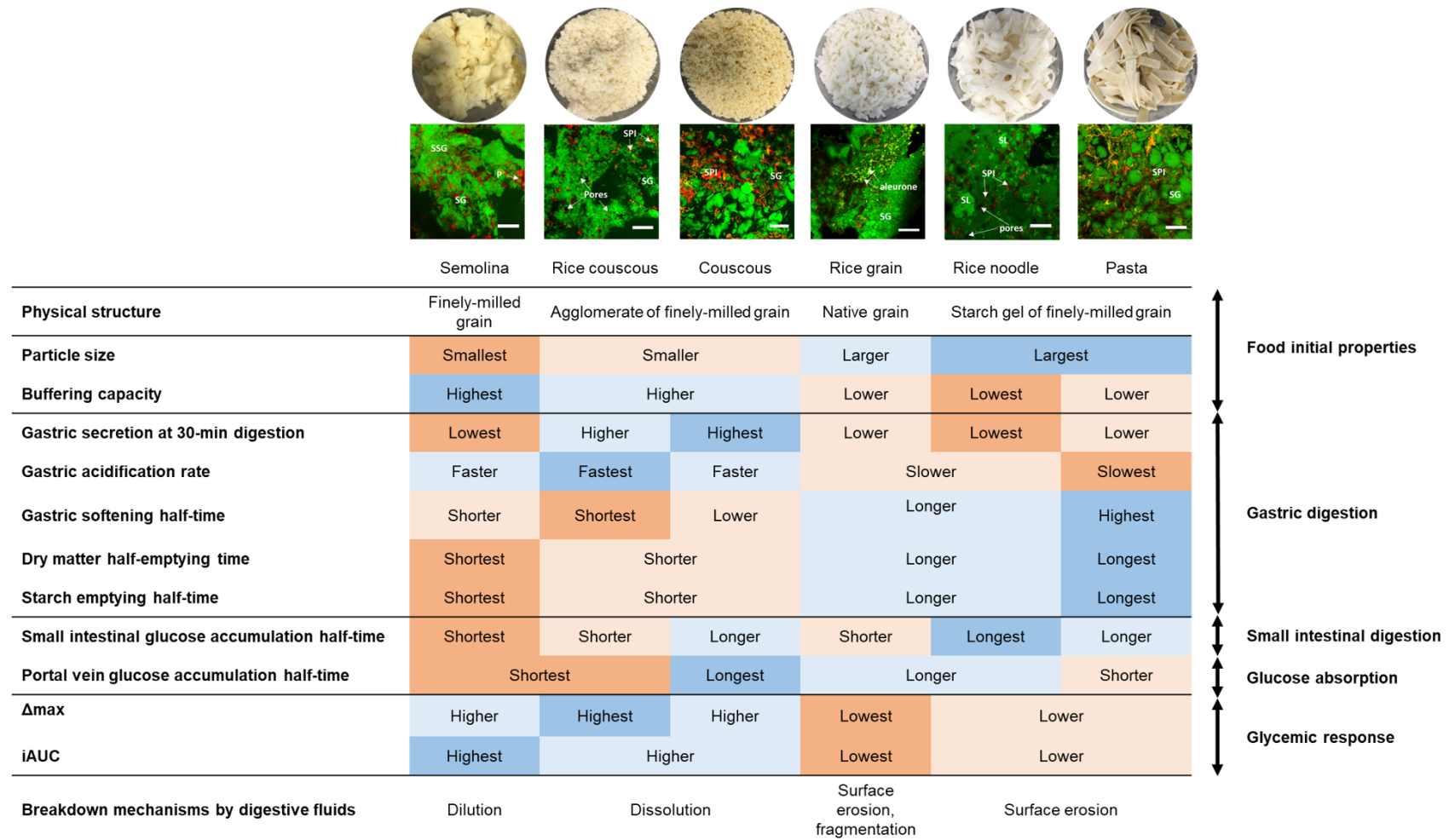


Figure 8.1 Summary of the findings from this PhD project. CLSM images of the cooked diets are presented below the diet pictures to indicate the microstructural differences of the diets (P: protein; SG: starch granules; SL: starch lumps; SSG: solubilized starch granules, SPI: starch-protein interaction). Results with low values are indicated with orange color, results with high values are indicated with blue color for ease of interpretation. The lowest and highest values for each row are indicated by darker orange and blue, respectively.

sized diets had $t_{1/2, \text{softening}}$ ranging from 17 to 152 min, which aligned with the trend where the larger-sized diets had longer $t_{1/2, \text{DM GE}}$.

An important determinant of the breakdown mechanisms and breakdown rates of the diets during gastric digestion is gastric secretion and gastric mixing between the food particles and the added secretions. In Chapter 4, it was found that estimated gastric secretion rates were high in the beginning of the digestion (9.07 g/min at 30 min, averaged across all diets), then decreased gradually to 1.89 g/min at 240 min (averaged across all diets). The initial rate of gastric secretion was related to the buffering capacity of the diets, except in semolina, which might be due to its porridge structure (liquid-like consistency) that did not require much breakdown in the stomach and quickly mixed with gastric secretions to drop the digesta pH. The buffering capacity of the smaller-sized diets was greater than the larger-sized diets and resulted in a higher rate of gastric secretion after 30 and 60 min of gastric digestion.

Different addition rates of gastric secretions between the smaller- and larger-sized diets, combined with the different physiological features of the proximal and distal stomach regions, would result in different gastric mixing in the two stomach regions. Gastric mixing affects the intragastric pH distribution, which consequently determines the local biochemical environment in the stomach for the digestive enzymes (salivary amylase, gastric lipase, or pepsin – listed in decreasing order of their optimum pH) to hydrolyze macronutrients (starch, fat, and protein, respectively) in the diets. This may impact the gastric breakdown mechanisms and rates of the diets. To understand the potential impact of varying biochemical conditions on starch digestion, the remaining salivary amylase activity in the gastric environment as affected by gastric mixing was also investigated.

Gastric mixing between the ingested diets with added gastric secretions, as reflected by intragastric pH mapping in Chapter 5, showed that the acidification kinetics of the smaller- and larger-sized diets were different. The smaller-sized diets underwent faster gastric mixing, with less variations in the proximal and distal stomach intragastric pH; by the end of 240 min digestion, all smaller-sized diet digesta had a uniform pH distribution (ranged from 1.29 ± 0.03 to 1.85 ± 0.13) in the ten pH measurement locations. Although faster gastric mixing meant less possibility of remaining salivary amylase activity to enhance starch hydrolysis, the softening rate of the smaller-sized diets was fast ($t_{1/2, \text{softening}} < 6$ min) during *in vivo* gastric digestion. This fast-softening rate might be attributed to the gastric breakdown mechanisms of the smaller-sized diets. It was proposed in Chapter 5 that the main gastric breakdown mechanism of semolina was dilution by gastric secretion due to its semi-solid (porridge) structure that did not require additional breakdown prior to gastric emptying. Meanwhile, the gastric breakdown mechanism of couscous and rice couscous was considered to be dissolution by gastric secretions. A similar trend was observed in Chapter 7, where couscous and rice couscous underwent fast softening in both the proximal and distal phases of static *in vitro* gastric digestion, indicating that their breakdown was not limited by macrostructural breakdown in the distal stomach or biochemical breakdown by remaining salivary amylase in the proximal stomach.

In contrast to the smaller-sized diets, the larger-sized diets had greater pH in the proximal stomach than in the distal stomach, which may be associated with a reduced addition of gastric secretions in these diets (Chapter 4) and less gastric motility in the proximal stomach that led to slower gastric mixing. Even after 240 min digestion, higher pH was still observed in the proximal stomach of the larger-sized diets (3.13 ± 0.26 in the proximal stomach vs. 1.58 ± 0.08 in the distal stomach, averaged across the

three diets). Due to the maintenance of pH >3 (the optimum pH for salivary amylase activity) in the proximal stomach, salivary amylase activity was maintained in the proximal stomach digesta for an extended time and increased starch hydrolysis. It was proposed in Chapter 5 that the remaining salivary amylase activity in the proximal stomach digesta of larger-sized diets would aid the breakdown of the diets through surface erosion that released starch particles, which were observed as the suspended solid fraction. The changes during proximal stomach digestion were also expected to enhance the softening process that mainly occurred in the distal stomach due to the uptake of gastric secretions.

Results from *in vitro* studies in Chapter 7 suggest that hydrolysis by α -amylase during the proximal phase caused leaching of soluble and <2-mm particles from the surface of the larger-sized diets, and caused dry matter reduction even in the absence of mechanical forces in the distal phase. The *in vitro* distal phase was also shown to generate particles <2 mm (possibly through surface erosion by acid and pepsin) and caused dry matter reduction, but the effect was very limited compared to the *in vitro* proximal phase. However, the softening rate of the larger-sized diet particles due to gastric fluid uptake during the *in vitro* distal phase digestion was not enhanced by the proximal phase, possibly suggesting that digestion by the *in vitro* proximal phase occurred mainly on the surface of the food particles. These *in vitro* findings may indicate that the extended salivary amylase activity in the proximal stomach *in vivo* contributed to the physical breakdown of the diets through surface erosion, which was observed as the suspended solid digesta fraction in Chapter 5 and 7 (Figure 8.2). Due to the gastric sieving mechanism, the suspended solid generated by the proximal phase was hypothesized to contribute in ensuring constant *in vivo* material emptying, once the digesta reached the distal stomach while the larger particles underwent slow gastric

breakdown, as shown by the constantly decreasing dry matter and starch retention over time in Chapter 4 and 5.

The faster gastric acidification rate in the smaller-sized diets, and the slower gastric acidification rate in the larger-sized diets, agreed with the trend in the $t_{1/2,DM\ GE}$ and $t_{1/2,starch\ GE}$. This suggests that the acidification rate in the proximal and distal region of the stomach contributed to the breakdown mechanisms of the diets during gastric digestion, which subsequently affected their gastric emptying rate. However, since the smaller-sized diets had $d < 2\text{ mm}$, they would be expected to have faster gastric emptying compared to the larger-sized diets as they did not require extensive breakdown to be emptied. As gastric breakdown and gastric emptying are interdependent, it is unclear if the fast gastric acidification rate and breakdown rate of the smaller-sized diets caused their fast gastric emptying rate or *vice versa*; this possible correlation is a topic for future investigation.

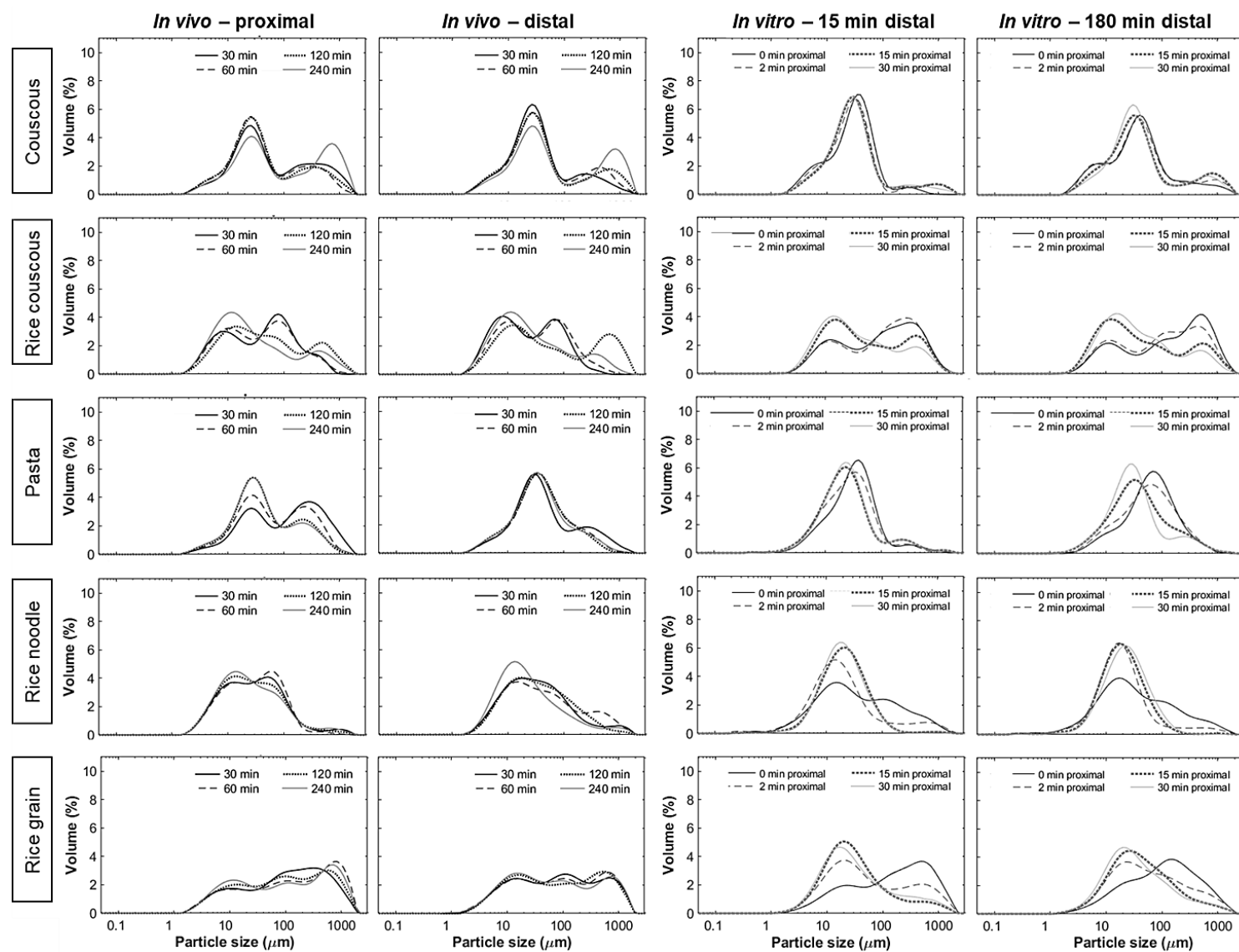


Figure 8.2 Comparison between *in vivo* and *in vitro* particle size distribution of suspended solid gastric digesta fraction. Figures within the same row correspond to one type of diet.

The differences in the physicochemical changes during *in vivo* gastric digestion between the smaller- and larger-sized diets were expected to impact the properties of the emptied materials (particularly starch and its hydrolysis products in the liquid and suspended solid fractions of digesta), small intestinal digestion, and the glycemic response. This was investigated in Chapter 7, where the hydrolyzed starch content in the liquid and suspended solid fractions of the *in vitro* digesta was measured after the proximal phase (0, 2, 15, or 30 min) followed by short (15 min) or long (180 min) distal phase digestion. For both smaller- and larger-sized diets, longer proximal phase led to increased starch hydrolysis at 15-min distal phase. Enhanced starch hydrolysis at 180-min distal phase compared to the 15-min distal phase was found only in couscous and rice couscous, after being subjected to ≥ 15 or ≥ 2 min proximal phase, respectively. This *in vitro* finding suggests that acid hydrolysis may happen during the distal phase, but only in the absence of micro- and macrostructural barriers in the food matrix. This finding of increased starch hydrolysis of the smaller-sized diets in the distal phase may also be applicable to the *in vivo* results. Although there was no direct evidence of increasing gastric starch hydrolysis in the smaller-sized diets during gastric digestion in Chapter 5, the increased starch hydrolysis may be a contributing factor to the high $iAUC_{\text{overall}}$ of the smaller-sized diets.

In Chapter 6, the impact of the output of *in vivo* gastric digestion on small intestinal digestion, portal glucose absorption, and glycemic response was examined. The results suggested that gastric emptying rate determined the amount of starch delivered to the small intestine, and subsequently affected the kinetics of starch digestion in the small intestine, glucose absorption into the portal vein, and glucose disappearance into the systemic circulation. The higher gastric emptying rate of the smaller-sized diets resulted in higher starch loading and glucose production in the small intestine, and higher

glucose accumulation in the portal vein, which was observed in their higher $\Delta\text{max}_{\text{overall}}$ and $\text{iAUC}_{\text{overall}}$. The materials emptied from the stomach were expected to consist of mainly liquid and suspended solid fractions of *in vivo* digesta, as indicated by the similarity in the particle size distribution profiles between *in vivo* and *in vitro* results (Figure 8.2). The extent of starch hydrolysis of the liquid and suspended solid fractions of gastric digesta at 30 min digestion (early digestion time) had an inverse relationship with $t_{1/2, \text{starch GE}}$ and a proportional relationship with the $\Delta\text{max}_{\text{overall}}$ and $\text{iAUC}_{\text{overall}}$ of the diets. However, such relationship was not observed at longer digestion times. This may indicate the importance of the output of gastric digestion on the physiological feedback responses at early digestion times that affected the gastric emptying and glycemic response. This aspect merits future investigation.

As the *in vivo* observation in Chapter 4 and 5 suggested different breakdown mechanisms of the solid diets, static *in vitro* digestion experiments in Chapter 7 were conducted to isolate the effect of digestive fluids diffusion on the breakdown mechanisms of couscous, rice couscous, rice grain, rice noodle and pasta. It was found that in addition to the structure, the geometry of the diets may also contribute to the breakdown mechanisms of the diets during gastric digestion. Couscous and rice couscous had a fast rate of softening in both the proximal and distal phases of digestion, as well as decreasing wet solid and dry solid retention in the distal phase even in the absence of proximal phase, which indicated that their main breakdown mechanism during gastric digestion was dissolution. The dissolution of the agglomerate structure was attributed to the ease of access of the digestive fluids into the internal structure due to their porous structure, and possibly spherical geometry ($\text{SA/V ratio} = 3 \text{ to } 6$) that enabled increased digestive fluid diffusion from all directions.

Rice grain, rice noodle, and pasta had slow rate of softening in both the proximal and distal phases ($t_{1/2, \text{softening}} > 120$ min); their dry solid retention in the distal phase decreased with longer proximal phase, but to a lesser extent compared to couscous and rice couscous. The slower breakdown rate of rice grain and noodle diets compared to the agglomerated diets may be associated to their more complex structure as a result of processing. The shortest dimension of rice grain (the radius) and the noodle diets (the thickness), which is likely to be the main direction of the diffusion of both saliva and gastric fluid, had a similar value to the radius of the agglomerate diets. However, the main breakdown mechanism of rice grain (SA/V ratio = ~ 2) and noodle (SA/V ratio < 1) was hypothesized to be surface erosion on the largest surface of the particle, possibly due to the slower diffusion as affected by their SA/V and more complex starch arrangements in the microstructures of these larger-sized diets that hindered structural dissolution by digestive enzymes (as in the case of the agglomerated diets). Additionally, rice grain also underwent fragmentation at 30 min proximal phase or 180 min distal phase, which might be attributed to its microstructure, although future studies are required to confirm this hypothesis. The different breakdown mechanisms of rice grain, noodles, and agglomerated diets may suggest that processing concurrently influences food macrostructures (through particle size reduction and re-assembling of the particles) and microstructures (through the presence of barrier to digestive enzymes within the food matrix), which subsequently determines the breakdown mechanisms of the food particles due to digestive fluid diffusion. These mechanisms are a topic of future studies for the development of advanced food structuring strategies.

This project used both *in vivo* and *in vitro* approaches, and a common question when such combined approaches are used is: how well do they correlate? This can be answered by identifying *in vitro* – *in vivo* correlation (IVIVC) between the experimental

data. The $t_{1/2, \text{softening}}$ of the *in vivo* gastric digesta correlated well with the $t_{1/2, \text{softening}}$ of the five diets used in the *in vitro* proximal digestion (Figure 8.3A), where the whole digesta mixture (digested diet + limited amount of saliva) was measured. In the proximal-distal *in vitro* digestion (selected at 0 min proximal phase, following a previously reported food breakdown measurement method (Drechsler & Bornhorst, 2018) where textural measurement was done on only the solid fraction of the digesta, the *in vivo* $t_{1/2, \text{softening}}$ also correlated well with the $t_{1/2, \text{softening}}$ of diets, except for rice noodle (Figure 8.3B).

The lack of IVIVC in the rice noodle proximal-distal *in vitro* digestion data might be due to the measurement of only the solid fraction of digesta. It was discussed in Chapter 7 that the suspended solid fraction generated due to the surface erosion of larger-sized diets might contribute to the overall rheological/textural property of the whole digesta mixture in the proximal digestion, but the separation of the solid fraction from the digestion mixture removed this suspended solid fraction. This lack of correlation possibly suggests that not all food structure will exhibit a direct IVIVC in a static proximal–distal digestion where gastric fluid is added altogether in excess and only the solid fraction is measured for the softening, hence indicating a limitation of using static digestion to develop IVIVCs. Future studies should investigate *in vitro* digestion of the diets using a dynamic system with gradual gastric fluid addition and gastric emptying, to identify if a better IVIVC may be obtained using a dynamic digestion model.

IVIVCs between the maltose content of the liquid and suspended solid fractions of *in vitro* and *in vivo* digesta, as well as between the maltose content of liquid and suspended solid fractions of *in vitro* digesta with the *in vivo* glycemic response were assessed at different *in vitro* proximal-distal duration combinations. Only the

correlations at proximal-distal duration with the highest R^2 are shown in Figure 8.3C-E. The maltose content in the liquid and suspended solid fractions of *in vitro* digesta at 2 min proximal phase and 15 min distal phase correlated well with the maltose content in the liquid and suspended solid fractions of 30-min *in vivo* gastric digesta (proximal and distal data combined together; Figure 8.3C) and the $\Delta\text{max}_{\text{overall}}$ of the glycemic response (Figure 8.3D). Maltose content in the liquid and suspended solid fractions of *in vitro* digesta at 30 min proximal phase and 15 min distal phase correlated well with $\text{iAUC}_{\text{overall}}$ of the *in vivo* glycemic response (Figure 8.3E), although the R^2 was not as high as that of the other correlations in Figure 8.3 – possibly due to various physiological responses that regulate glucose homeostasis in the *in vivo* system. These correlations suggest that the starch hydrolysis *in vivo* at early digestion times, as well as the maximum rise in glycemic response, may be well predicted with short, but sufficient contact time in the *in vitro* oral phase (2 min proximal is equivalent to 2.5 min oral phase) followed by a short distal phase. However, for predicting the overall glycemic impact of the food, the prolonged contact time with α -amylase in the proximal phase should be considered, as indicated by Figure 8.3E.

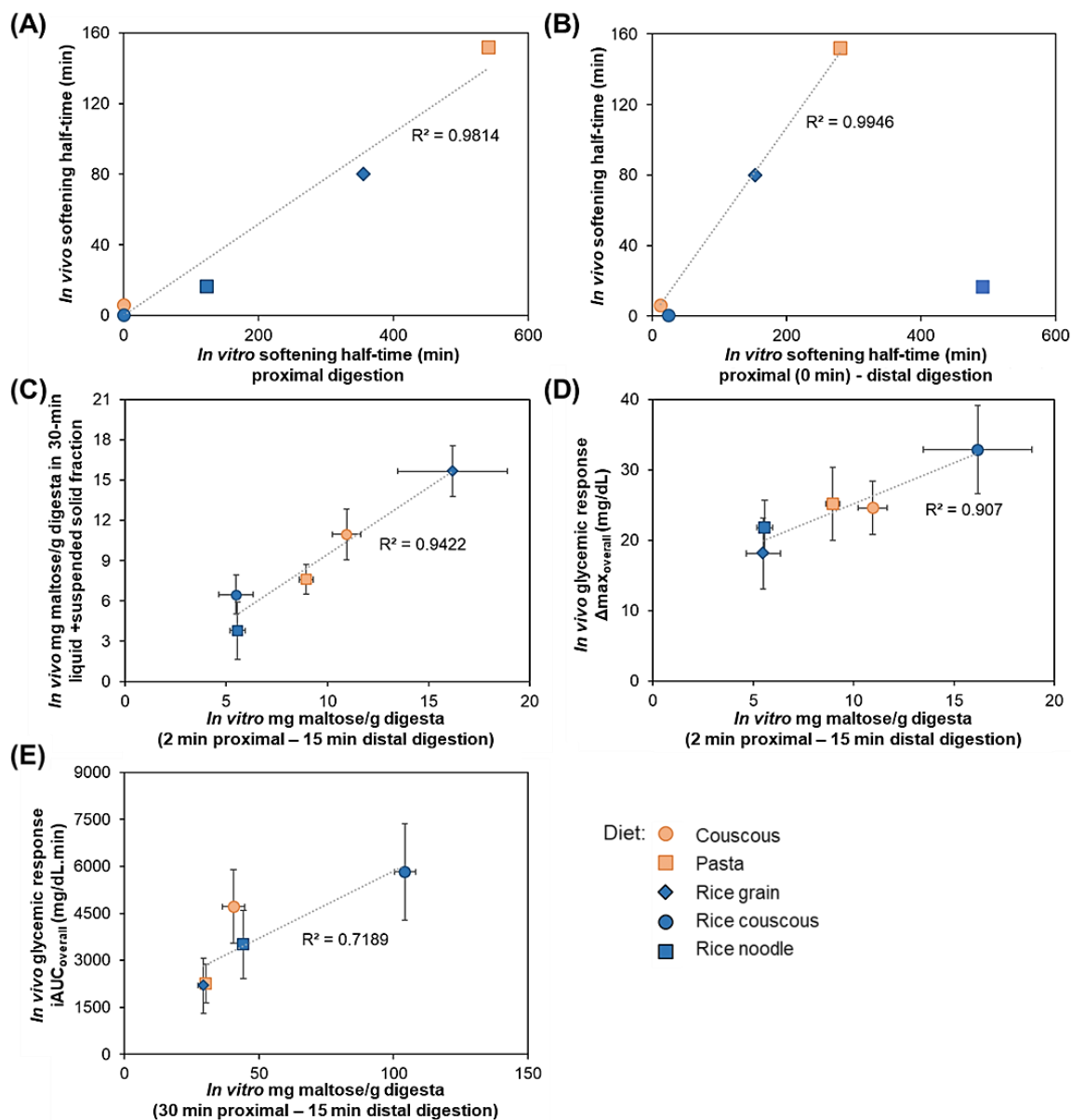


Figure 8.3 *In vitro-in vivo* correlation between the gastric softening half-time *in vivo* from Figure 4.7 and *in vitro* proximal digestion from Figure 7.1A (A) and proximal-distal digestion at 0 min proximal phase from Table 7.6 (B). *In vitro-in vivo* correlation between the maltose content in the liquid + suspended solid fractions of 30-min *in vivo* digesta (proximal and distal stomach data combined together) from Table 5.4 with 2-min proximal-15-min distal *in vitro* digesta from Figure 7.7B (C); *in vivo* glycemic response $\Delta\text{max}_{\text{overall}}$ from Table 6.1 with 2-min proximal-15-min distal *in vitro* digesta from Figure 7.7B (D); and *in vivo* glycemic response $\text{iAUC}_{\text{overall}}$ from Table 6.1 with 30-min proximal-15-min distal *in vitro* digesta from Figure 7.7B (E). Values are shown as mean \pm SE ($n = 3$ for *in vitro* data, $3 \leq n \leq 6$ for *in vivo* data).

Overall, this project has identified a link between food structure, gastric digestion, and glycemic response. Food macro- and microstructures have been shown to concurrently contribute to the gastric breakdown rate and gastric emptying rate of the food, and subsequently affect small intestinal starch loading and glucose production,

influence the portal glucose absorption, and ultimately impact the glycemic response. Based on the findings relationship between food structure, gastric digestion, and glycemic response derived from this project, the following food structuring strategies are recommended to manipulate gastric emptying rate and glycemic response to tackle health issues related to glycemic response management:

- Whenever possible, the use of finely milled raw material should be avoided and the use of whole (unmilled) structure where the structural integrity/intactness is preserved is strongly recommended.
- If finely milled raw material is to be used, an advisable form of product is gel structure, of which gel strength and microstructural compactness can be increased through ingredient formulation and processing modifications to reduce the breakdown rate in the stomach and entrap the starch granules in amylase-resistant matrices (e.g., protein matrix or amylose/lipid complexes).
- In terms of the geometry of the product, a slab-like shape is recommended to reduce the available SA/V for enzymatic or acid attack during gastric digestion.
- For the structuring of low-moisture and/or porous food structure (e.g., couscous, dry baked goods), starch source with slow digestion properties combined with additional ingredients that can increase gastric digesta viscosity (e.g., soluble fiber) to reduce gastric emptying rate should be incorporated in product formulation.

8.2 Future recommendations

For future work, the following aspects should be considered to further elucidate the link between carbohydrate-based food structures, gastric digestion, and glycemic response, and how to apply the knowledge gained here to develop better food structuring strategies:

- **Consideration of the bulk volume of the diets and the size of pigs for *in vivo* study:** Not all pigs managed to consume the entire portion of the standardized amount of meal, although they were trained to consume the meal during the acclimatization period. To minimize the amount of excluded data, a cutoff value was utilized (50% or 70% total portion given for semolina and other diets, respectively), with the justification that this cutoff value was sufficient to ensure that the minimum working volume of the stomach was achieved. However, the variations in the amount of food eaten between pigs would contribute to the variations in the results (especially in the glycemic response study, as this would affect the glycemic load), although trends still can be observed. Therefore, future *in vivo* studies using similar age/size of pigs should consider using less bulk volume of the meal. Alternatively, bigger size or older pigs can be used to tackle issues related to the amount of food eaten, to reduce external factors that can cause variations in the results.
- **Assessment of gastric digestion process using a non-invasive approach and catheterization at more vein locations to allow for continuous observation of gastric digestion and absorption processes:** The approach used to identify gastric digestion and absorption was a slaughter method, where each pig contributed to one data point (e.g., one digestion time) for each measurement parameter. Interindividual variations between the pigs contributed to the large variations and large confidence intervals in the gastric emptying and absorption model parameters. Future studies can apply non-invasive gastric emptying measurement (e.g., MRI observation) coupled with portal vein and jugular catheterization to enable continuous observation for each pig and minimize interindividual variations, which

will be useful to improve the identified food structure-gastric digestion-glycemic response relationship.

- **Incorporation of microstructural observation in the *in vitro* digestion to understand the synergistic effect of macro- and microstructural breakdown:**

The *in vitro* digestion carried out in Chapter 7 only focused on certain physicochemical properties of the digesta, while it was suggested in the results that the micro- and macrostructural (as reflected in the particle size and geometry) of food particles had a synergistic impact on their breakdown mechanisms. Microstructural observations should be conducted to further elucidate the changes during the proximal and distal phases of gastric digestion.

- **Inclusion of mastication and the dynamic aspect of gastric digestion in the *in vitro* experiments, followed by simulated small intestinal digestion:** The static *in vitro* digestion focused only on the gastric digestion part, and mechanical breakdown due to mastication and gastric wall contractions were not simulated. The mechanical breakdown aspects should be incorporated in future studies to particularly understand the breakdown rate of larger-sized diets, which was proposed to be limited by their macrostructural breakdown rate. The incorporation of the dynamics of gastric digestion (for example, using the Human Gastric Simulator) may also enable the simulation of the digesta mixture better, which was not able to be observed in Chapter 7 due to the separation of excess liquid and suspended solids from the large solids. Further, the consequences of the *in vitro* digestion on the subsequent small intestinal digestion should be explored, as it was hypothesized in Chapter 5 and 7 that the output of gastric digestion may affect the subsequent small intestinal digestion. While this gastric digestion-small intestinal digestion link was implied in the findings in Chapter 6, investigation in an *in vitro*

model would provide a better understanding on which outputs of gastric digestion contributed to the observed small intestinal digestion, glucose absorption, and glycemic response.

- **Investigation on different combinations food macrostructure and microstructure:** Diets in this project either had smaller size and less barrier to digestive enzymes (“less compact” microstructure) or larger size and more barrier to digestive enzymes (“more compact” microstructure), which resulted in different breakdown rates and gastric emptying rates of the diets. Future studies should investigate different combinations of these structures, e.g., smaller size and “more compact” microstructure such as starch gel microspheres (Hasek et al., 2020) with varying particle sizes, or larger size and “less compact” microstructure such as bread and other moist, porous bakery products (Gao et al., 2021). These future studies are needed to identify if the food structure - gastric digestion – glycemic response relationship will still be maintained or not, or if one length scale (e.g., macrostructure or microstructure) controls any of the observed phenomena in this project.
- **Extension of the study to mixed meal:** While this project focused on the consumption of single meal component, in real life a meal consists of a mixture of carbohydrate, protein, fat, and fiber components. In addition, water or a beverage is typically consumed together with a meal. The inclusion of other meal components of a mixed meal, as well as a beverage, should be considered in future studies, as these factors may affect the gastric digestion (as highlighted in the literature review), the breakdown behavior and gastric emptying of the components of the meal, and ultimately the glycemic response.

- **Further exploration of the identified IVIVC:** The correlation between *in vitro* and *in vivo* data was only briefly discussed in the general discussions (Section 8.1), and this IVIVC should be explored further. The IVIVC could be expanded to additional parts of the data set from the current study with the addition of some quantitative relationships, and complementing the correlation with *in vitro* dynamic digestion data.
- **Validation of the concept established from this project in clinical trial:** The *in vivo* studies of this project used a growing pig model to enable gut content collection and measurement, which was an important part of understanding food structure – food digestion relationships. However, the anatomy and morphology of the oral cavity, as well as the mastication behavior between pigs and humans are not identical (Herring, 1976; Štembírek et al., 2012), which may limit the translation of the findings from this thesis for human application due to difference in the characteristics of food bolus produced during mastication. With the identification of food structure –gastric digestion – glycemic response relationship from this study, the concept established should be tested in human clinical trial, which can be coupled with the measurement of hormonal responses, to extend the link to food structuring strategy for human nutrition.

REFERENCES

- Abecassis, J., Cuq, B., Boggini, G., & Namoune, H. (2012). Other traditional durum-derived products. In M. Sissons, J. Abecassis, B. Marchylo, & M. Carcea (Eds.), *Durum wheat: Chemistry and technology*. Minnesota, USA: AACC International.
- Abhilasha, A., Kaur, L., Monro, J., Hardacre, A., & Singh, J. (2021). Intact, Kibbled, and Cut Wheat Grains: Physico-Chemical, Microstructural Characteristics and Gastro-Small Intestinal Digestion In vitro. *73*(7-8), 2000267.
- Acevedo-Fani, A., & Singh, H. (2021). Biopolymer interactions during gastric digestion: implications for nutrient delivery. *Food Hydrocolloids*, 106644.
- Aguilera, J. M. (2019). The food matrix: implications in processing, nutrition and health. *Critical Reviews in Food Science and Nutrition*, *59*(22), 3612-3629.
- Ahmed, I., Qazi, I. M., Li, Z., & Ullah, J. (2016). *Rice noodles: Materials, processing and quality evaluation*. Paper presented at the Pakistan Academy of Sciences.
- Ai, Y., & Jane, J. (2018). Understanding starch structure and functionality. In M. Sjöö & L. Nilsson (Eds.), *Starch in Food (Second Edition)* (pp. 151-178): Woodhead Publishing.
- Alcázar-Alay, S. C., & Meireles, M. A. A. (2015). Physicochemical properties, modifications and applications of starches from different botanical sources. *Food Sci. Technol (Campinas)*, *35*(2), 215-236.
- Alegria, A., Garcia-Llatas, G., & Cilla, A. (2015). Static Digestion Models: General Introduction. In K. Verhoeckx, P. Cotter, I. Lopez-Exposito, C. Kleiveland, T. Lea, A. Mackie, T. Requena, D. Swiatecka, & H. Wichers (Eds.), *The Impact of Food Bioactives on Health: in vitro and ex vivo models* (pp. 3-12). Cham (CH).
- Alvarez, M. D., & Canet, W. (1999). Rheological properties of mashed potatoes made from dehydrated flakes: effect of ingredients and freezing. *European Food Research and Technology*, *209*(5), 335-342.
- Angelidis, G., Protonotariou, S., Mandala, I., & Rosell, C. M. (2016). Jet milling effect on wheat flour characteristics and starch hydrolysis. *Journal of Food Science and Technology*, *53*(1), 784-791.
- Anjana, R. M., Gayathri, R., Lakshmipriya, N., Ramya Bai, M., Shanmugam, S., Unnikrishnan, R., . . . Mohan, V. (2019). Effect of a Novel High Fiber Rice Diet on 24-Hour Glycemic Responses in Asian Indians Using Continuous Glucose Monitoring: A Randomized Clinical Trial. *Diabetes Technology & Therapeutics*, *21*(4), 177-182.
- AOAC International. (2012). *Official Methods of Analysis of AOAC International* (19th ed.). Gaithersburg, MD, USA.
- Argyri, K., Athanasatou, A., Bouga, M., & Kapsokafalou, M. (2016). The potential of an in vitro digestion method for predicting glycemic response of foods and meals. *Nutrients*, *8*(4), 209.
- Arocas, A., Sanz, T., Hernández-Carrión, M., Hernando, M. I., & Fiszman, S. M. (2010). Effect of cooking time and ingredients on the performance of different starches in white sauces. *European Food Research and Technology*, *231*(3), 395-405.
- Arvidsson-Lenner, R., Asp, N.-G., Axelsen, M., Bryngelsson, S., Haapa, E., Järvi, A., . . . Vessby, B. (2004). Glycaemic Index. *Scandinavian Journal of Nutrition*, *48*(2), 84-94.
- Atkinson, F. S., Foster-Powell, K., & Brand-Miller, J. C. (2008). International tables of glycemic index and glycemic load values: 2008. *Diabetes Care*, *31*, 2281-2283.

- Avvari, R. K. (2019). Biomechanics of the small intestinal contractions. In X. Qi & S. Koruth (Eds.), *Digestive System - Recent Advances*: IntechOpen.
- Ballance, S., Sahlstrom, S., Lea, P., Nagy, N. E., Andersen, P. V., Dessev, T., . . . Faulks, R. (2013). Evaluation of gastric processing and duodenal digestion of starch in six cereal meals on the associated glycaemic response using an adult fasted dynamic gastric model. *European Journal of Nutrition*, 52(2), 799-812.
- Barkouti, A., Delalonde, M., Rondet, E., & Ruiz, T. (2014). Structuration of wheat powder by wet agglomeration: Case of size association mechanism. *Powder Technology*, 252, 8-13.
- Barling, P. M., Shyam, S., Selvathevan, M. D., & Misra, S. (2016). Anomalous association of salivary amylase secretion with the postprandial glycaemic response to starch. *BMC Nutrition*, 2(1), 50.
- Barone, F., Laghi, L., Gianotti, A., Ventrella, D., Taneyo Saa, D. L., Bordoni, A., . . . Turrone, S. (2019). In Vivo Effects of Einkorn Wheat (*Triticum monococcum*) Bread on the Intestinal Microbiota, Metabolome, and on the Glycemic and Insulinemic Response in the Pig Model. *11*(1), 16.
- Bates, F. L., French, D., & Rundle, R. E. (1943). Amylose and Amylopectin Content of Starches Determined by their Iodine Complex Formation¹. *Journal of the American Chemical Society*, 65(2), 142-148.
- Bellmann, S., Lelieveld, J., Gorissen, T., Minekus, M., & Havenaar, R. (2016). Development of an advanced in vitro model of the stomach and its evaluation versus human gastric physiology. *Food Research International*, 88, 191-198.
- Bellmann, S., Minekus, M., Sanders, P., Bosgra, S., & Havenaar, R. (2018). Human glycemic response curves after intake of carbohydrate foods are accurately predicted by combining in vitro gastrointestinal digestion with in silico kinetic modeling. *Clinical Nutrition Experimental*, 17, 8-22.
- Benini, L., Castellani, G., Brighenti, F., Heaton, K. W., Brentegani, M. T., Casiraghi, M. C., . . . Vantini, I. (1995). Gastric emptying of a solid meal is accelerated by the removal of dietary fibre naturally present in food. *Gut*, 36, 825-830.
- Bergeim, O. (1926). Intestinal chemistry: III. Salivary digestion in the human stomach and intestines. *Archives of Internal Medicine*, 37(1), 110-117.
- Bernfeld, P. (1955). Amylases, α and β . In *Methods in Enzymology* (Vol. 1, pp. 149-158): Academic Press.
- Bertoft, E. (2017). Understanding starch structure: Recent progress. *Agronomy*, 7(3), 56.
- Bervoets, L., Mewis, A., & Massa, G. (2015). The shape of the plasma glucose curve during an oral glucose tolerance test as an indicator of Beta cell function and insulin sensitivity in end-pubertal obese girls. *Horm Metab Res*, 47(6), 445-451.
- Biliaderis, C. G. (2009). Structural transitions and related physical properties of starch. In J. N. BeMiller & R. L. Whistler (Eds.), *Starch: Chemistry and Technology* (3rd ed. ed., pp. 293-3727): Academic Press.
- Birt, D. F., Boylston, T., Hendrich, S., Jane, J.-L., Hollis, J., Li, L., . . . Whitley, E. M. (2013). Resistant starch: promise for improving human health. *Advances in Nutrition (Bethesda, Md.)*, 4(6), 587-601.
- Bizzotto, R., Natali, A., Gastaldelli, A., Muscelli, E., Krssak, M., Brehm, A., . . . Mari, A. (2016). Glucose uptake saturation explains glucose kinetics profiles measured by different tests. *311*(2), E346-E357.
- Blaak, E. E., Antoine, J. M., Benton, D., Björck, I., Bozzetto, L., Brouns, F., . . . Vinoy, S. (2012). Impact of postprandial glycaemia on health and prevention of disease.

Obesity reviews : an official journal of the International Association for the Study of Obesity, 13(10), 923-984.

- Błaszczak, W., & Lewandowicz, G. (2020). Light Microscopy as a Tool to Evaluate the Functionality of Starch in Food. *Foods*, 9(5), 670.
- Blazek, J., & Gilbert, E. P. (2011). Application of small-angle X-ray and neutron scattering techniques to the characterisation of starch structure: A review. *Carbohydrate Polymers*, 85(2), 281-293.
- Bornhorst, G. M. (2017). Gastric mixing during food digestion: Mechanisms and applications. *Annual Review of Food Science and Technology*, 8, 523-542.
- Bornhorst, G. M., Chang, L. Q., Rutherfurd, S. M., Moughan, P. J., & Singh, R. P. (2013). Gastric emptying rate and chyme characteristics for cooked brown and white rice meals in vivo. *Journal of the Science of Food and Agriculture*, 93(12), 2900-2908.
- Bornhorst, G. M., Ferrua, M. J., Rutherfurd, S. M., Heldman, D. R., & Singh, R. P. (2013). Rheological properties and textural attributes of cooked brown and white rice during gastric digestion in vivo. *Food Biophysics*, 8(2), 137-150.
- Bornhorst, G. M., Ferrua, M. J., & Singh, R. P. (2015). A proposed food breakdown classification system to predict food behavior during gastric digestion. *Journal of Food Science*, 80(5), R924-934.
- Bornhorst, G. M., Gouseti, O., Wickham, M. S., & Bakalis, S. (2016). Engineering digestion: Multiscale processes of food digestion. *Journal of Food Science*, 81(3), R534-543.
- Bornhorst, G. M., Hivert, H., & Singh, R. P. (2014). Rice bolus texture changes due to α -amylase. *LWT - Food Science and Technology*, 55(1), 27-33.
- Bornhorst, G. M., Kostlan, K., & Singh, R. P. (2013). Particle size distribution of brown and white rice during gastric digestion measured by image analysis. *Journal of Food Science*, 78(9), E1383-1391.
- Bornhorst, G. M., Roman, M. J., Dreschler, K. C., & Singh, R. P. (2014). Physical property changes in raw and roasted almonds during gastric digestion in vivo and in vitro. *Food Biophysics*, 9(1), 39-48.
- Bornhorst, G. M., Roman, M. J., Rutherfurd, S. M., Burri, B. J., Moughan, P. J., & Singh, R. P. (2013). Gastric digestion of raw and roasted almonds in vivo. *Journal of Food Science*, 78(11), H1807-1813.
- Bornhorst, G. M., Rutherfurd, S. M., Roman, M. J., Burri, B. J., Moughan, P. J., & Singh, R. P. (2014). Gastric pH distribution and mixing of soft and rigid food particles in the stomach using a dual-marker technique. *Food Biophysics*, 9(3), 292-300.
- Bornhorst, G. M., & Singh, R. P. (2012). Bolus formation and disintegration during digestion of food carbohydrates. *Comprehensive Reviews in Food Science and Food Safety*, 11(2), 101-118.
- Bornhorst, G. M., & Singh, R. P. (2013). Kinetics of *in vitro* bread bolus digestion with varying oral and gastric digestion parameters. *Food Biophysics*, 8(1), 50-59.
- Bornhorst, G. M., & Singh, R. P. (2014). Gastric digestion in vivo and in vitro: how the structural aspects of food influence the digestion process. *Annual Review of Food Science and Technology*, 5, 111-132.
- Bornhorst, G. M., Ströbinger, N., Rutherfurd, S. M., Singh, R. P., & Moughan, P. J. (2013). Properties of Gastric Chyme from Pigs Fed Cooked Brown or White Rice. *Food Biophysics*, 8(1), 12-23.
- Bourne, M. C. (2002). *Food Texture and Viscosity* (2nd Edition ed.). London: Academic Press.

- Brand-Miller, J., & Holt, S. (2004). Testing the glycaemic index of foods: in vivo, not in vitro. *European Journal of Clinical Nutrition*, 58(4), 700-701.
- Brener, W., Hendrix, T. R., & McHugh, P. R. (1983). Regulation of the gastric emptying of glucose. *Gastroenterology*, 85(1), 76-82.
- Brodkorb, A., Egger, L., Alminger, M., Alvito, P., Assuncao, R., Ballance, S., . . . Recio, I. (2019). INFOGEST static in vitro simulation of gastrointestinal food digestion. *Nature Protocols*, 14(4), 991-1014.
- Brouns, F., Bjorck, I., Frayn, K. N., Gibbs, A. L., Lang, V., Slama, G., & Wolever, T. M. S. (2005). Glycaemic index methodology. *Nutrition Research Reviews*, 18(1), 145-171.
- Brownlee, I. A., Gill, S., Wilcox, M. D., Pearson, J. P., & Chater, P. I. (2018). Starch digestion in the upper gastrointestinal tract of humans. *Starch-Stärke*, 70(9-10), 1700111.
- Bul  on, A., Colonna, P., Planchot, V., & Ball, S. (1998). Starch granules: structure and biosynthesis. *International Journal of Biological Macromolecules*, 23(2), 85-112.
- Cai, M., Dou, B., Pugh, J. E., Lett, A. M., & Frost, G. S. (2021). The impact of starchy food structure on postprandial glycemic response and appetite: a systematic review with meta-analysis of randomized crossover trials. *The American Journal of Clinical Nutrition*, 114(2), 472-487.
- Calbet, J. A., & MacLean, D. A. (1997). Role of caloric content on gastric emptying in humans. *The Journal of Physiology*, 498 (Pt 2)(Pt 2), 553-559.
- Ca  as, S., Perez-Moral, N., & Edwards, C. H. (2020). Effect of cooking, 24 h cold storage, microwave reheating, and particle size on in vitro starch digestibility of dry and fresh pasta. *Food & Function*
- Capuano, E., & Pellegrini, N. (2019). An integrated look at the effect of structure on nutrient bioavailability in plant foods. *Journal of the Science of Food and Agriculture*, 99(2), 493-498.
- Cervantes-Pahm, S. K., Liu, Y., & Stein, H. H. (2014). Comparative digestibility of energy and nutrients and fermentability of dietary fiber in eight cereal grains fed to pigs. *Journal of the Science of Food and Agriculture*, 94(5), 841-849.
- Chang, T. M., Passaro, E., Jr., Shain, L. R., & Chen, W. L. (1991). Physical properties of starch meals in vivo and in vitro and their influence on gastric emptying and oral glucose tolerance test. *Nutrition (Burbank, Los Angeles County, Calif.)*, 7(6), 410-416.
- Chen, J. (2009). Food oral processing—A review. *Food Hydrocolloids*, 23(1), 1-25.
- Chen, J., & Rosenthal, A. (2015). *Modifying Food Texture : Novel Ingredients and Processing Techniques*. Cambridge, UNITED KINGDOM: Elsevier Science & Technology.
- Chen, L., Tuo, B., & Dong, H. (2016). Regulation of intestinal glucose absorption by ion channels and transporters. *Nutrients*, 8(1), 43.
- Choy, J. Y. M., Goh, A. T., Chatonidi, G., Ponnalagu, S., Wee, S. M. M., Stieger, M., & Forde, C. G. (2021). Impact of food texture modifications on oral processing behaviour, bolus properties and postprandial glucose responses. *Current Research in Food Science*, 4, 891-899.
- Christensen, K. L., Hedemann, M. S., L  rke, H. N., J  rgensen, H., Mutt, S. J., Herzig, K.-H., & Bach Knudsen, K. E. (2013). Concentrated Arabinoxylan but Not Concentrated β -Glucan in Wheat Bread Has Similar Effects on Postprandial Insulin as Whole-Grain Rye in Porto-arterial Catheterized Pigs. *Journal of Agricultural and Food Chemistry*, 61(32), 7760-7768.

- Christian, P. E., Datz, F. L., & Moore, J. G. (1987). Technical considerations in radionuclide gastric emptying studies. *Journal of Nuclear Medicine Technology*, 15(4), 200-207.
- Church, F. C., Porter, D. H., Catignani, G. L., & Swaisgood, H. E. (1985). An o-phthalaldehyde spectrophotometric assay for proteinases. *Analytical Biochemistry*, 146(2), 343-348.
- Cisse, F., Erickson, D. P., Hayes, A. M. R., Opekun, A. R., Nichols, B. L., & Hamaker, B. R. (2018). Traditional Malian solid foods made from sorghum and millet have markedly slower gastric emptying than rice, potato, or pasta. *Nutrients*, 10, 124.
- Cisse, F., Pletsch, E. A., Erickson, D. P., Chegeni, M., Hayes, A. M. R., & Hamaker, B. R. (2017). Preload of slowly digestible carbohydrate microspheres decreases gastric emptying rate of subsequent meal in humans. *Nutrition Research*, 45, 46-51.
- Collins, P. J., Horowitz, M., Cook, D. J., Harding, P. E., & Shearman, D. J. (1983). Gastric emptying in normal subjects - A reproducible technique using a single scintillation camera and computer system. *Gut*, 24(12), 1117-1125.
- Collins, P. J., Horowitz, M., Maddox, A., Myers, J. C., & Chatterton, B. E. (1996). Effects of increasing solid component size of a mixed solid/liquid meal on solid and liquid gastric emptying. *American Journal of Physiology*, 271(4 Pt 1), G549-554.
- Conde-Petit, B. (2003). The structure and texture of starch-based foods. In B. M. McKenna (Ed.), *Texture in Food* (Vol. 1, pp. 86-108): Woodhead Publishing.
- Cordova-Fraga, T., Sosa, M., Wiechers, C., De la Roca-Chiapas, J.-M., Maldonado Moreles, A., Bernal-Alvarado, J., & Huerta-Franco, R. (2008). Effects of anatomical position on esophageal transit time: a biomagnetic diagnostic technique. *World Journal of Gastroenterology*, 14(37), 5707-5711.
- Coster, S. T., & Schwarz, W. H. (1987). Rheology and the swallow-safe bolus. *Dysphagia*, 1, 113-118.
- Coupe, A. J., Davis, S. S., Evans, D. F., & Wilding, I. R. (1991). Correlation of the gastric emptying of nondisintegrating tablets with gastrointestinal motility. *Pharmaceutical Research*, 8(10), 1281-1285.
- Dahlqvist, A., & Borgstrom, B. (1961). Digestion and absorption of disaccharides in man. *The Biochemical journal*, 81(2), 411-418.
- Dang, J. M. C., & Copeland, L. (2003). Imaging Rice Grains Using Atomic Force Microscopy. *Journal of Cereal Science*, 37(2), 165-170.
- de Almeida, P. D. V., Gregio, A. M., Machado, M. A., de Lima, A. A., & Azevedo, L. R. (2008). Saliva composition and functions: a comprehensive review. *The Journal of Contemporary Dental Practice*, 9(3), 72-80.
- de Las Casas, E. B., de Almeida, A. F., Cimini Junior, C. A., Gomes Pde, T., Cornacchia, T. P., & Saffar, J. M. (2007). Determination of tangential and normal components of oral forces. *J Appl Oral Sci*, 15(1), 70-76.
- de Zwart, I. M., Haans, J. J., Verbeek, P., Eilers, P. H., de Roos, A., & Masclee, A. A. (2007). Gastric accommodation and motility are influenced by the barostat device: Assessment with magnetic resonance imaging. *American Journal of Physiology-Gastrointestinal and Liver Physiology*, 292(1), G208-214.
- Delcour, J. A., Bruneel, C., Derde, L. J., Gomand, S. V., Pareyt, B., Putseys, J. A., . . . Lamberts, L. (2010). Fate of Starch in Food Processing: From Raw Materials to Final Food Products. *Annual Review of Food Science and Technology*, 1(1), 87-111.

- Derakhshandeh, B., Hatzikiriakos, S. G., & Bennington, C. P. J. (2010). Rheology of pulp suspensions using ultrasonic Doppler velocimetry. *Rheologica Acta*, 49(11), 1127-1140.
- Devezeaux de Lavergne, M., van de Velde, F., & Stieger, M. (2017). Bolus matters: the influence of food oral breakdown on dynamic texture perception. *Food & Function*, 8(2), 464-480.
- Dhital, S., Bhattarai, R. R., Gorham, J., & Gidley, M. J. (2016). Intactness of cell wall structure controls the in vitro digestion of starch in legumes. *Food & Function*, 7(3), 1367-1379.
- Dhital, S., Brennan, C., & Gidley, M. J. (2019). Location and interactions of starches in planta: Effects on food and nutritional functionality. *Trends in Food Science & Technology*, 93, 158-166.
- Dhital, S., Gidley, M. J., & Warren, F. J. (2015). Inhibition of α -amylase activity by cellulose: Kinetic analysis and nutritional implications. *Carbohydrate Polymers*, 123, 305-312.
- Dhital, S., Warren, F. J., Butterworth, P. J., Ellis, P. R., & Gidley, M. J. (2017). Mechanisms of starch digestion by α -amylase-Structural basis for kinetic properties. *Critical Reviews in Food Science and Nutrition*, 57(5), 875-892.
- Dona, A. C., Pages, G., Gilbert, R. G., & Kuchel, P. W. (2010). Digestion of starch: In vivo and in vitro kinetic models used to characterise oligosaccharide or glucose release. *Carbohydrate Polymers*, 80, 599-617.
- Donohoe, K. J., Maurer, A. H., Ziessman, H. A., Urbain, J. L., Royal, H. D., Martin-Comin, J., . . . Motility, S. (2009). Procedure guideline for adult solid-meal gastric-emptying study 3.0. *Journal of Nuclear Medicine Technology*, 37(3), 196-200.
- dos Santos, L. M., Tulio, L. T., Campos, L. F., Dorneles, M. R., & Krüger, C. C. H. (2015). Glycemic response to Carob (*Ceratonia siliqua* L) in healthy subjects and with the *in vitro* hydrolysis index. *Nutricion Hospitalaria (Madrid)*, 31, 482-487.
- Drechsler, K. C., & Bornhorst, G. M. (2018). Modeling the softening of carbohydrate-based foods during simulated gastric digestion. *Journal of Food Engineering*, 222, 38-48.
- Drechsler, K. C., & Ferrua, M. J. (2016). Modelling the breakdown mechanics of solid foods during gastric digestion. *Food Research International*, 88, 181-190.
- Dupont, D., Alric, M., Blanquet-Diot, S., Bornhorst, G., Cueva, C., Deglaire, A., . . . Van den Abbeele, P. (2019). Can dynamic in vitro digestion systems mimic the physiological reality? *Critical Reviews in Food Science and Nutrition*, 59(10), 1546-1562.
- Edwards, C. H., Grundy, M. M., Grassby, T., Vasilopoulou, D., Frost, G. S., Butterworth, P. J., . . . Ellis, P. R. (2015). Manipulation of starch bioaccessibility in wheat endosperm to regulate starch digestion, postprandial glycemia, insulinemia, and gut hormone responses: a randomized controlled trial in healthy ileostomy participants. *The American Journal of Clinical Nutrition*, 102(4), 791-800.
- Ehrlein, H., & Schemann, M. (2005). Gastrointestinal motility. Retrieved from <https://www.humanbiology.wzw.tum.de/motvid01/tutorial.pdf>
- Elhardallou, S. B., & Walker, A. F. (1993). The water-holding capacity of three starchy legumes in the raw, cooked and fibre-rich fraction forms. *Plant Foods for Human Nutrition*, 44(2), 171-179.

- Emami, J. (2006). In vitro - in vivo correlation: From theory to application. *Journal of Pharmacy and Pharmaceutical Sciences*, 9(2), 169-189.
- Englyst, H. N., Kingman, S. M., & Cummings, J. H. (1992). Classification and measurement of nutritionally important starch fractions. *European Journal of Clinical Nutrition*, 46, S33-S50.
- Englyst, K. N., Englyst, H. N., Hudson, G. J., Cole, T. J., & Cummings, J. H. (1999). Rapidly available glucose in foods: an in vitro measurement that reflects the glycemic response. *The American Journal of Clinical Nutrition*, 69(3), 448-454.
- Englyst, K. N., Vinoy, S., Englyst, H. N., & Lang, V. (2003). Glycaemic index of cereal products explained by their content of rapidly and slowly available glucose. *British Journal of Nutrition*, 89(3), 329-340.
- Fallingborg, J. (1999). Intraluminal pH of the human gastrointestinal tract. *Danish Medical Bulletin*, 46(3), 183-196.
- FAO. (1998). *Carbohydrates in human nutrition. Report of a Joint FAO/WHO Expert Consultation* (No. 0254-4725).
- FAO. (2020) World Food and Agriculture - Statistical Yearbook 2020. In. Rome, Italy: Food and Agriculture Organization of the United Nations.
- FDA. (1997). *Guidance for industry, Extended release dosage forms: development, evaluation and application of an in vitro/ in vivo correlation*. Washington, DC.
- Feher, J. J. (2017a). Intestinal and colonic chemoreception and motility. In *Quantitative human physiology: An introduction* (2nd ed., pp. 796-809). London, United Kingdom: Academic Press.
- Feher, J. J. (2017b). Mouth and esophagus. In *Quantitative human physiology: An introduction* (2nd ed., pp. 771-784). London, United Kingdom: Academic Press.
- Feher, J. J. (2017c). The stomach. In *Quantitative human physiology: An introduction* (2nd ed., pp. 785-795). London, United Kingdom: Academic Press.
- Feldman, M., Smith, H. J., & Simon, T. R. (1984). Gastric emptying of solid radiopaque markers: Studies in healthy subjects and diabetic patients. *Gastroenterology*, 87(4), 895-902.
- Fernandes, T., Oliveira, M. I., Castro, R., Araújo, B., Viamonte, B., & Cunha, R. (2014). Bowel wall thickening at CT: simplifying the diagnosis. *Insights into Imaging*, 5(2), 195-208.
- Ferrer-Mairal, A., Penalva-Lapuente, C., Iglesia, I., Urtasun, L., De Miguel-Etayo, P., Remon, S., . . . Moreno, L. A. (2012). In vitro and in vivo assessment of the glycemic index of bakery products: influence of the reformulation of ingredients. *European Journal of Nutrition*, 51(8), 947-954.
- Ferrua, M. J., & Singh, R. P. (2015). Human Gastric Simulator (Riddet Model). In K. Verhoeckx, P. Cotter, I. Lopez-Exposito, C. Kleiveland, T. Lea, A. Mackie, T. Requena, D. Swiatecka, & H. Wichers (Eds.), *The Impact of Food Bioactives on Health: in vitro and ex vivo models* (pp. 61-71). Cham (CH).
- Ferrua, M. J., Xue, Z., & Singh, R. P. (2014). On the kinematics and efficiency of advective mixing during gastric digestion - A numerical analysis. *Journal of Biomechanics*, 47(15), 3664-3673.
- Flynn, C. S. (2012). *The particle size distribution of solid food after human mastication*. (PhD Thesis), Massey University, Palmerston North, NZ.
- Fordtran, J. S., & Walsh, J. H. (1973). Gastric acid secretion rate and buffer content of the stomach after eating. Results in normal subjects and in patients with duodenal ulcer. *The Journal of Clinical Investigation*, 52(3), 645-657.

- Foschia, M., Peressini, D., Sensidoni, A., Brennan, M. A., & Brennan, C. S. (2014). Mastication or masceration: Does the preparation of sample affect the predictive in vitro glycemic response of pasta? , 66(11-12), 1096-1102.
- Foster-Powell, K., Holt, S. H. A., & Brand-Miller, J. C. (2002). International table of glycemic index and glycemic load values: 2002. *The American Journal of Clinical Nutrition*, 76, 5-56.
- Freitas, D., Boué, F., Benallaoua, M., Airinei, G., Benamouzig, R., & Le Feunteun, S. (2021). Lemon juice, but not tea, reduces the glycemic response to bread in healthy volunteers: a randomized crossover trial. *European Journal of Nutrition*, 60, 113-122.
- Freitas, D., & Le Feunteun, S. (2018). Acid induced reduction of the glycaemic response to starch-rich foods: the salivary α -amylase inhibition hypothesis. *Food & Function*, 9(10), 5096-5102.
- Freitas, D., & Le Feunteun, S. (2019). Oro-gastro-intestinal digestion of starch in white bread, wheat-based and gluten-free pasta: Unveiling the contribution of human salivary α -amylase. *Food Chemistry*, 274, 566-573.
- Freitas, D., Le Feunteun, S., Panouille, M., & Souchon, I. (2018). The important role of salivary alpha-amylase in the gastric digestion of wheat bread starch. *Food & Function*, 9(1), 200-208.
- Gandarillas, M., & Bas, F. (2009). The domestic pig (*Sus scrofa domestica*) as a model for evaluating nutritional and metabolic consequences of bariatric surgery practiced on morbid obese humans. *Ciencia e investigación agraria*, 36(2), 163-176.
- Gao, J., Lin, S., Jin, X., Wang, Y., Ying, J., Dong, Z., & Zhou, W. (2019). In vitro digestion of bread: How is it influenced by the bolus characteristics? *Journal of Texture Studies*, 50(3), 257-268.
- Gao, J., Tan, E. Y. N., Low, S. H. L., Wang, Y., Ying, J., Dong, Z., & Zhou, W. (2021). From bolus to digesta: How structural disintegration affects starch hydrolysis during oral-gastro-intestinal digestion of bread. *Journal of Food Engineering*, 289, 110161.
- Gardner, J. D., Sloan, S., Miner, P. B., & Robinson, M. (2003). Meal-stimulated gastric acid secretion and integrated gastric acidity in gastro-oesophageal reflux disease. *Alimentary Pharmacology & Therapeutics*, 17(7), 945-953.
- Gargouri, Y., Moreau, H., & Verger, R. (1989). Gastric lipases: biochemical and physiological studies. *Biochimica et Biophysica Acta (BBA) - Lipids and Lipid Metabolism*, 1006(3), 255-271.
- Gavião, M. B. D., Engelen, L., & van der Bilt, A. (2004). Chewing behavior and salivary secretion. *European Journal of Oral Sciences*, 112, 19-24.
- Gebauer, S. K., Novotny, J. A., Bornhorst, G. M., & Baer, D. J. (2016). Food processing and structure impact the metabolizable energy of almonds. *Food & Function*, 7(10), 4231-4238.
- Gidley, M. J., & Yakubov, G. E. (2019). Functional categorisation of dietary fibre in foods: Beyond 'soluble' vs 'insoluble'. *Trends in Food Science & Technology*, 86, 563-568.
- Giuberti, G., Gallo, A., & Masoero, F. (2012). Plasma glucose response and glycemic indices in pigs fed diets differing in in vitro hydrolysis indices. *Animal : an international journal of animal bioscience*, 6(7), 1068-1076.
- Goetze, O., Steingoetter, A., Menne, D., van der Voort, I. R., Kwiatek, M. A., Boesiger, P., . . . Schwizer, W. (2007). The effect of macronutrients on gastric volume responses and gastric emptying in humans: A magnetic resonance imaging

- study. *American Journal of Physiology-Gastrointestinal and Liver Physiology*, 292(1), G11-17.
- Goetze, O., Treier, R., Fox, M., Steingoetter, A., Fried, M., Boesiger, P., & Schwizer, W. (2009). The effect of gastric secretion on gastric physiology and emptying in the fasted and fed state assessed by magnetic resonance imaging. *Neurogastroenterology & Motility*, 21(7), 725-e742.
- Golding, M. (2019). Exploring and Exploiting the Role of Food Structure in Digestion. In O. Gouseti, G. M. Bornhorst, S. Bakalis, & A. Mackie (Eds.), *Interdisciplinary Approaches to Food Digestion* (pp. 81-128). Cham: Springer International Publishing.
- Goñi, I., Garcia-Alonso, A., & Saura-Calixto, F. (1997). A starch hydrolysis procedure to estimate glycemic index. *Nutrition Research*, 17(3), 427-437.
- Gopirajah, R., Raichurkar, K. P., Wadhwa, R., & Anandharamakrishnan, C. (2016). The glycemic response to fibre rich foods and their relationship with gastric emptying and motor functions: an MRI study. *Food & Function*, 7(9), 3964-3972.
- Goyal, M., Aydas, B., Ghazaleh, H., & Rajasekharan, S. (2019). *CarbMetSim*: A discrete-event simulator for carbohydrate metabolism in humans. 491019.
- Gray-Stuart, E. M. (2016). *Modelling food breakdown and bolus formation during mastication*. (PhD Thesis), Massey University, Palmerston North, New Zealand.
- Gray-Stuart, E. M., Jones, J. R., & Bronlund, J. E. (2017). Defining the end-point of mastication: A conceptual model. *Journal of Texture Studies*, 48(5), 345-356.
- Gray, J. A., & Bemiller, J. N. (2003). Bread Staling: Molecular Basis and Control. *Comprehensive Reviews in Food Science and Food Safety*, 2(1), 1-21.
- Guerin, S., Ramonet, Y., LeCloarec, J., Meunier-Salaün, M. C., Bourguet, P., & Malbert, C. H. (2001). Changes in intragastric meal distribution are better predictors of gastric emptying rate in conscious pigs than are meal viscosity or dietary fibre concentration. *British Journal of Nutrition*, 85(03), 343-350.
- Guerrieri, N., & Cavaletto, M. (2018). Cereals proteins. In R. Y. Yada (Ed.), *Proteins in Food Processing*, 2nd Ed. (2 ed., pp. 223-244). Cambridge, UK: Woodhead Publishing.
- Guo, Q., Ye, A., Lad, M., Ferrua, M., Dalglish, D., & Singh, H. (2015). Disintegration kinetics of food gels during gastric digestion and its role on gastric emptying: an in vitro analysis. *Food & Function*, 6(3), 756-764.
- Guo, Q., Ye, A., Singh, H., & Rousseau, D. (2020). Deconstructing and restructuring of foods during gastric digestion. *Comprehensive Reviews in Food Science and Food Safety*, 19(4), 1658-1679.
- Haldar, S., Egli, L., De Castro, C. A., Tay, S. L., Koh, M. X. N., Darimont, C., . . . Henry, C. J. (2020). High or low glycemic index (GI) meals at dinner results in greater postprandial glycemia compared with breakfast: a randomized controlled trial. 8(1), e001099.
- Harmsen, K. (2000). A modified mitscherlich equation for rainfed crop production in semi-arid areas: 1. Theory. *NJAS - Wageningen Journal of Life Sciences*, 48(3), 237-250.
- Hasek, L. Y., Phillips, R. J., Hayes, A. M. R., Kinzig, K., Zhang, G., Powley, T. L., & Hamaker, B. R. (2020). Carbohydrates designed with different digestion rates modulate gastric emptying response in rats. *International Journal of Food Sciences and Nutrition*, 71(7), 839-844.

- Hasjim, J., Lavau, G. C., Gidley, M. J., & Gilbert, R. G. (2010). In vivo and in vitro starch digestion: Are current in vitro techniques adequate? *Biomacromolecules*, *11*, 3600-3608.
- Hasler, W. L. (2009). The physiology of gastric motility and gastric emptying. In T. Yamada, D. H. Alpers, A. N. Kalloo, N. Kaplowitz, C. Owyang, & D. W. Powell (Eds.), *Textbook of Gastroenterology, Fifth Edition*: Blackwell Publishing Ltd.
- Haub, M. D., Hubach, K. L., Al-Tamimi, E. K., Ornelas, S., & Seib, P. A. (2010). Different types of resistant starch elicit different glucose responses in humans. *J Nutr Metab*, *2010*
- Hayes, A. M. R., Swackhamer, C., Mennah-Govela, Y. A., Martinez, M. M., Diatta, A., Bornhorst, G. M., & Hamaker, B. R. (2020). Pearl millet (*Pennisetum glaucum*) couscous breaks down faster than wheat couscous in the Human Gastric Simulator, though has slower starch hydrolysis. *Food & Function*, *11*(1), 111-122.
- Hefni, M. E., Thomsson, A., & Witthöft, C. M. (2020). Bread making with sourdough and intact cereal and legume grains – effect on glycaemic index and glycaemic load. *International Journal of Food Sciences and Nutrition*, 1-9.
- Hellström, P. M., Grybäck, P., & Jacobsson, H. (2006). The physiology of gastric emptying. *Best Practice & Research Clinical Anaesthesiology*, *20*(3), 397-407.
- Helm, J. F., Dodds, W. J., Hogan, W. J., Soergel, K. H., Egide, M. S., & Wood, C. M. (1982). Acid Neutralizing Capacity of Human Saliva. *Gastroenterology*, *83*(1, Part 1), 69-74.
- Herring, S. W. (1976). The dynamics of mastication in pigs. *Archives of Oral Biology*, *21*(8), 473-480.
- Hiilema, K. M., & Palmer, J. B. (1999). Food transport and bolus formation during complete feeding sequences on foods of different initial consistency. *Dysphagia*, *14*(1), 31-42.
- Hlebowicz, J., Darwiche, G., Bjorgell, O., & Almer, L. O. (2007). Effect of cinnamon on postprandial blood glucose, gastric emptying, and satiety in healthy subjects. *The American Journal of Clinical Nutrition*, *85*(6), 1552-1556.
- Hlebowicz, J., Jönsson, J. M., Lindstedt, S., Björgell, O., Darwich, G., & Almér, L.-O. (2009). Effect of commercial rye whole-meal bread on postprandial blood glucose and gastric emptying in healthy subjects. *Nutrition Journal*, *8*(26)
- Hlebowicz, J., Wickenberg, J., Fahlstrom, R., Bjorgell, O., Almer, L. O., & Darwiche, G. (2007). Effect of commercial breakfast fibre cereals compared with corn flakes on postprandial blood glucose, gastric emptying and satiety in healthy subjects: a randomized blinded crossover trial. *Nutrition Journal*, *6*, 22.
- Hoad, C. L., Parker, H., Hudders, N., Costigan, C., Cox, E. F., Perkins, A. C., . . . Gowland, P. A. (2015). Measurement of gastric meal and secretion volumes using magnetic resonance imaging. *Physics in Medicine and Biology*, *60*, 1367.
- Hoebler, C., Devaux, M. F., Karinthi, A., Belleville, C., & Barry, J. L. (2000). Particle size of solid food after human mastication and in vitro simulation of oral breakdown. *International Journal of Food Sciences and Nutrition*, *51*(5), 353-366.
- Hoebler, C., Karinthi, A., Devaux, M. F., Guillon, F., Gallant, D. J., Bouchet, B., . . . Barry, J. L. (1998). Physical and chemical transformations of cereal food during oral digestion in human subjects. *British Journal of Nutrition*, *80*(5), 429-436.
- Hoebler, C., Lecannu, G., Belleville, C., Devaux, M. F., Popineau, Y., & Barry, J. L. (2002). Development of an in vitro system simulating bucco-gastric digestion to

- assess the physical and chemical changes of food. *International Journal of Food Sciences and Nutrition*, 53(5), 389-402.
- Holmes, R. (1971). Carbohydrate digestion and absorption. *Journal of Clinical Pathology. Supplement (Royal College of Pathologists)*, 5, 10-13.
- Holst, J. J., Gribble, F., Horowitz, M., & Rayner, C. K. (2016). Roles of the Gut in Glucose Homeostasis. *Diabetes Care*, 39(6), 884-892.
- Horowitz, M., Edelbroek, M. A. L., Wishart, J., & Straathof, J. W. (1993). Relationship between oral glucose tolerance and gastric emptying in healthy subjects. *Diabetologia*, 36, 857-862.
- Huckabee, M.-L., McIntosh, T., Fuller, L., Curry, M., Thomas, P., Walshe, M., . . . Sella-Weiss, O. (2018). The Test of Masticating and Swallowing Solids (TOMASS): reliability, validity and international normative data. *International Journal of Language & Communication Disorders*, 53(1), 144-156.
- Hunt, J. N., Smith, J. L., & Jiang, C. L. (1985). Effect of meal volume and energy density on the gastric emptying of carbohydrates. *Gastroenterology*, 89(6), 1326-1330.
- Hutchings, J. B., & Lillford, P. J. (1988). The perception of food texture - The philosophy of the breakdown path. *Journal of Texture Studies*, 19, 103-115.
- Hutchings, S. C., Foster, K. D., Bronlund, J. E., Lentle, R. G., Jones, J. R., & Morgenstern, M. P. (2011). Mastication of heterogeneous foods: Peanuts inside two different food matrices. *Food Quality and Preference*, 22(4), 332-339.
- Iida, Y., Katsumata, A., & Fujishita, M. (2011). Videofluorographic evaluation of mastication and swallowing of Japanese udon noodles and white rice. *Dysphagia*, 26(3), 246-249.
- International Standards Organization. (2010). Food products—Determination of the glycaemic index (GI) and recommendation for food classification. In. Geneva, Switzerland.
- Itoh, T., Higuchi, T., Gardner, C. R., & Caldwell, L. (1986). Effect of particle size and food on gastric residence time of non-disintegrating solids in beagle dogs. *Journal of Pharmacy and Pharmacology*, 38(11), 801-806.
- Jacobsen, N., Melvaer, K. L., & Hensten-Pettersen, A. (1972). Some Properties of Salivary Amylase: A Survey of the Literature and Some Observations. *Journal of Dental Research*, 51(2), 381-388.
- Jain, N. K., Boivin, M., Zinsmeister, A. R., Brown, M. L., Malagelada, J. R., & DiMagno, E. P. (1989). Effect of ileal perfusion of carbohydrates and amylase inhibitor on gastrointestinal hormones and emptying. *Gastroenterology*, 96(2 Pt 1), 377-387.
- Jeltema, M., Beckley, J., & Vahalik, J. (2015). Model for understanding consumer textural food choice. *Food Science & Nutrition*, 3(3), 202-212.
- Jenkins, D. J., Kendall, C. W. C., Augustin, L. S. A., Franseschi, S., Hamaidi, M., Marcihe, A., . . . Taylor, R. H. (1981). Glycemic index of foods: A physiological basis for carbohydrate exchange. *American Journal of Clinical Nutrition*, 34, 362-366.
- Jenkins, D. J., Wolever, T. M., Taylor, R. H., Griffiths, C., Krzeminska, K., Lawrie, J. A., . . . Bloom, S. R. (1982). Slow release dietary carbohydrate improves second meal tolerance. *The American Journal of Clinical Nutrition*, 35(6), 1339-1346.
- Jenkins, D. J., Wolever, T. M., Thorne, M. J., Jenkins, A. L., Wong, G. S., Josse, R. G., & Csimas, A. (1984). The relationship between glycemic response, digestibility, and factors influencing the dietary habits of diabetics. *The American Journal of Clinical Nutrition*, 40(6), 1175-1191.

- Jin, Z., Bai, F., Chen, Y., & Bai, B. (2019). Interactions between protein, lipid and starch in foxtail millet flour affect the in vitro digestion of starch. *CyTA - Journal of Food*, 17(1), 640-647.
- Johansen, H. N., Knudsen, K. E., Sandström, B., & Skjøth, F. (1996). Effects of varying content of soluble dietary fibre from wheat flour and oat milling fractions on gastric emptying in pigs. *British Journal of Nutrition*, 75(3), 339-351.
- Jolliffe, D. M. (2009). Practical gastric physiology. *Continuing Education in Anaesthesia Critical Care & Pain*, 9(6), 173-177.
- Jones, K. L., Horowitz, M., Carney, B. I., Wishart, J. M., Guha, S., & Green, L. (1996). Gastric emptying in early noninsulin-dependent diabetes mellitus. *The Journal of Nuclear Medicine*, 37(10), 1643-1648.
- Joyner, H. S. (2018). Explaining food texture through rheology. *Current Opinion in Food Science*, 21, 7-14.
- Kararli, T. T. (1995). Comparison of the gastrointestinal anatomy, physiology, and biochemistry of humans and commonly used laboratory animals. *Biopharmaceutics and Drug Disposition*, 16, 351-380.
- Katoh, E., Murata, K., & Fujita, N. (2020). ¹³C CP/MAS NMR Can Discriminate Genetic Backgrounds of Rice Starch. *ACS Omega*, 5(38), 24592-24600.
- Kearney, J. (2010). Food consumption trends and drivers. *Philosophical Transactions of the Royal Society B: Biological Sciences*, 365(1554), 2793-2807.
- Kelly, K. A. (1980). Gastric emptying of liquids and solids: roles of proximal and distal stomach. *American Journal of Physiology*, 239, G71-76.
- Keppler, S., O'Meara, S., Bakalis, S., Fryer, P. J., & Bornhorst, G. M. (2020). Characterization of individual particle movement during in vitro gastric digestion in the Human Gastric Simulator (HGS). *Journal of Food Engineering*, 264, 106974.
- Khatoon, S., Sreerama, Y. N., Raghavendra, D., Bhattacharya, S., & Bhat, K. K. (2009). Properties of enzyme modified corn, rice and tapioca starches. *Food Research International*, 42(10), 1426-1433.
- Kienzle, E., Schrag, I., Butterwick, R., & Opitz, B. (2002). Calculation of Gross Energy in Pet Foods: Do We Have the Right Values for Heat of Combustion? *The Journal of Nutrition*, 132(6), 1799S-1800S.
- Kim, I.-Y., Park, S., Kim, Y., Chang, Y., Choi, C. S., Suh, S.-H., & Wolfe, R. R. (2020). In Vivo and In Vitro Quantification of Glucose Kinetics: From Bedside to Bench. *Endocrinol Metab*, 35(4), 733-749.
- Kittler, J., & Illingworth, J. (1986). Minimum error thresholding. *Pattern Recognition*, 19(1), 41-47.
- Kong, F., Oztop, M. H., Singh, R. P., & McCarthy, M. J. (2011). Physical changes in white and brown rice during simulated gastric digestion. *Journal of Food Science*, 76(6), E450-457.
- Kong, F., & Singh, R. P. (2008). Disintegration of solid foods in human stomach. *Journal of Food Science*, 73(5), R67-80.
- Kong, F., & Singh, R. P. (2009a). Digestion of raw and roasted almonds in simulated gastric environment. *Food Biophysics*, 4(4), 365-377.
- Kong, F., & Singh, R. P. (2009b). Modes of disintegration of solid foods in simulated gastric environment. *Food Biophysics*, 4(3), 180-190.
- Kong, F., & Singh, R. P. (2010). A human gastric simulator (HGS) to study food digestion in human stomach. *Journal of Food Science*, 75(9), E627-635.
- Kong, F., & Singh, R. P. (2011). Solid loss of carrots during simulated gastric digestion. *Food Biophysics*, 6(1), 84-93.

- Korompokis, K., Verbeke, K., & Delcour, J. A. (2021). Structural factors governing starch digestion and glycemic responses and how they can be modified by enzymatic approaches: A review and a guide. *n/a(n/a)*
- Koziolek, M., Schneider, F., Grimm, M., Modebeta, C., Seekamp, A., Roustom, T., . . . Weitschies, W. (2015). Intragastric pH and pressure profiles after intake of the high-caloric, high-fat meal as used for food effect studies. *Journal of Controlled Release*, 220(Pt A), 71-78.
- Kozu, H., Nakata, Y., Nakajima, M., Neves, M. A., Uemura, K., Sato, S., . . . Ichikawa, S. (2015). Analysis of disintegration of agar gel particles with different textures using gastric digestion simulator. *Japan Journal of Food Engineering*, 16(2), 161-166.
- Lærke, H. N., & Hedemann, M. S. (2012). The digestive system of the pig. In K. E. Bach Knudsen, N. J. Kjeldsen, H. D. Poulsen, & B. B. Jensen (Eds.), *Nutritional physiology of pigs - Online publication*. Foulum: Videncenter for Svineproduktion.
- Lamy, E., Santos, V., Barrambana, S., Simões, C., Carreira, L., Infante, P., & Capela e Silva, F. (2021). Saliva Protein Composition Relates with Interindividual Variations in Bread Sensory Ratings. *Starch - Stärke*, 73(1-2), 2000052.
- Lapis, T. J., Penner, M. H., Balto, A. S., & Lim, J. (2017). Oral Digestion and Perception of Starch: Effects of Cooking, Tasting Time, and Salivary α -Amylase Activity. *Chemical Senses*, 42(8), 635-645.
- Ledezma, C. C. Q. (2018). Starch interactions with native and added food components. In L. N. Malin Sjöö (Ed.), *Starch in Food* (2nd Ed. ed., pp. 769-801): Woodhead Publishing.
- Lentle, R. G., & Janssen, P. W. M. (2011). Physical aspects of the digestion of carbohydrate particles. In P. W. M. J. Roger G. Lentle (Ed.), *The physical processes of digestion*. Berlin: Springer.
- Li, C., Cao, P., Wu, P., Yu, W., Gilbert, R. G., & Li, E. (2021). Effects of endogenous proteins on rice digestion during small intestine (in vitro) digestion. *Food Chemistry*, 344, 128687.
- Li, C., Gong, B., Hu, Y., Liu, X., Guan, X., & Zhang, B. (2020). Combined crystalline, lamellar and granular structural insights into in vitro digestion rate of native starches. *Food Hydrocolloids*, 105, 105823.
- Li, H., Zhu, Y., Jiao, A., Zhao, J., Chen, X., Wei, B., . . . Tian, Y. (2013). Impact of α -amylase combined with hydrochloric acid hydrolysis on structure and digestion of waxy rice starch. *International Journal of Biological Macromolecules*, 55, 276-281.
- Li, M., Dhital, S., & Wei, Y. (2017). Multilevel Structure of Wheat Starch and Its Relationship to Noodle Eating Qualities. *Comprehensive Reviews in Food Science and Food Safety*, 16(5), 1042-1055.
- Li, M., Zhu, K.-X., Guo, X.-N., Brijs, K., & Zhou, H.-M. (2014). Natural Additives in Wheat-Based Pasta and Noodle Products: Opportunities for Enhanced Nutritional and Functional Properties. *Comprehensive Reviews in Food Science and Food Safety*, 13(4), 347-357.
- Li, W., Wu, G., Luo, Q., Jiang, H., Zheng, J., Ouyang, S., & Zhang, G. (2016). Effects of removal of surface proteins on physicochemical and structural properties of A- and B-starch isolated from normal and waxy wheat. *Journal of Food Science and Technology*, 53(6), 2673-2685.

- Li, Z., Kong, X., Zhou, X., Zhong, K., Zhou, S., & Liu, X. (2016). Characterization of multi-scale structure and thermal properties of Indica rice starch with different amylose contents. *RSC Advances*, 6(109), 107491-107497.
- Lin, H. C., Kim, B. H., Elashoff, J. D., Doty, J. E., Gu, Y. G., & Meyer, J. H. (1992). Gastric emptying of solid food is most potently inhibited by carbohydrate in the canine distal ileum. *Gastroenterology*, 102(3), 793-801.
- Lu, R. (2013). Principles of solid food texture analysis. In D. Kilcast (Ed.), *Instrumental Assessment of Food Sensory Quality* (pp. 103-128): Woodhead Publishing.
- Ma, J., Pilichiewicz, A. N., Feinle-Bisset, C., Wishart, J. M., Jones, K. L., Horowitz, M., & Rayner, C. K. (2012). Effects of variations in duodenal glucose load on glycaemic, insulin, and incretin responses in type 2 diabetes. *Diabetic Medicine*, 29(5), 604-608.
- Ma, J., Stevens, J. E., Cukier, K., Maddox, A. F., Wishart, J. M., Jones, K. L., . . . Rayner, C. K. (2009). Effects of a Protein Preload on Gastric Emptying, Glycemia, and Gut Hormones After a Carbohydrate Meal in Diet-Controlled Type 2 Diabetes. *Diabetes Care*, 32(9), 1600-1602.
- Mackie, A. R. (2019). The Digestive Tract: A Complex System. In O. Gouseti, G. M. Bornhorst, S. Bakalis, & A. Mackie (Eds.), *Interdisciplinary Approaches to Food Digestion* (pp. 11-27). Cham: Springer International Publishing.
- Mackie, A. R., Bajka, B. H., Rigby, N. M., Wilde, P. J., Alves-Pereira, F., Mosleth, E. F., . . . Salt, L. J. (2017). Oatmeal particle size alters glycemic index but not as a function of gastric emptying rate. *American Journal of Physiology-Gastrointestinal and Liver Physiology*, 313(3), G239-G246.
- Maeda, R., Takei, E., Ito, K., Magara, J., Tsujimura, T., & Inoue, M. (2020). Inter-individual variation of bolus properties in triggering swallowing during chewing in healthy humans. *Journal of Oral Rehabilitation*, 47(9), 1161-1170.
- Maegdenbergh, V. D., Urbain, J. L., Siegel, J. A., Mortelmans, L., & Roo, M. D. (1990). Effect of solids, caloric content on dual-phase gastric emptying. *Journal of Nuclear Medicine Technology*, 18(1), 31-33.
- Magallanes-Cruz, P. A., Flores-Silva, P. C., & Bello-Perez, L. A. (2017). Starch Structure Influences Its Digestibility: A Review. *Journal of Food Science*, 82(9), 2016-2023.
- Mahasukhonthachat, K., Sopade, P. A., & Gidley, M. J. (2010). Kinetics of starch digestion in sorghum as affected by particle size. *Journal of Food Engineering*, 96(1), 18-28.
- Malagelada, J.-R., Go, V. L. W., & Summerskill, W. H. J. (1979). Different gastric, pancreatic, and biliary responses to solid-liquid or homogenized meals. *Digestive Diseases and Sciences*, 24(2), 101-110.
- Malagelada, J.-R., Longstreth, G. F., Summerskill, W. H. J., & Go, V. L. W. (1976). Measurement of Gastric Functions During Digestion of Ordinary Solid Meals in Man. *Gastroenterology*, 70(2), 203-210.
- Mandalari, G., Merali, Z., Ryden, P., Chessa, S., Bisignano, C., Barreca, D., . . . Waldron, K. W. (2018). *Durum* wheat particle size affects starch and protein digestion in vitro. *European Journal of Nutrition*, 57, 319-325.
- Mandel, A. L., & Breslin, P. A. S. (2012). High endogenous salivary amylase activity is associated with improved glycemic homeostasis following starch ingestion in adults. *The Journal of Nutrition*, 142(5), 853-858.
- Manell, E., Hedenqvist, P., Svensson, A., & Jensen-Waern, M. (2016). Establishment of a Refined Oral Glucose Tolerance Test in Pigs, and Assessment of Insulin, Glucagon and Glucagon-Like Peptide-1 Responses. *PLoS One*, 11(2), e0148896.

- Manell, E., Jensen-Waern, M., & Hedenqvist, P. (2017). Anaesthesia and changes in parameters that reflect glucose metabolism in pigs – a pilot study. *51*(5), 509-517.
- Marathe, C. S., Horowitz, M., Trahair, L. G., Wishart, J. M., Bound, M., Lange, K., . . . Jones, K. L. (2015). Relationships of Early And Late Glycemic Responses With Gastric Emptying During An Oral Glucose Tolerance Test. *The Journal of Clinical Endocrinology & Metabolism*, *100*(9), 3565-3571.
- Marciani, L., Gowland, P. A., Fillery-Travis, A., Manoj, P., Wright, J., Smith, A., . . . Spiller, R. C. (2001). Assessment of antral grinding of a model solid meal with echo-planar imaging. *American Journal of Physiology-Gastrointestinal and Liver Physiology*, *280*(5), G844-849.
- Marciani, L., Gowland, P. A., Spiller, R. C., Manoj, P., Moore, R. J., Young, P., . . . Fillery-Travis, A. J. (2000). Gastric response to increased meal viscosity assessed by echo-planar magnetic resonance imaging in humans. *The Journal of Nutrition*, *130*(1), 122-127.
- Marciani, L., Gowland, P. A., Spiller, R. C., Manoj, P., Moore, R. J., Young, P., & Fillery-Travis, A. (2001). Effect of meal viscosity and nutrients on satiety, intragastric dilution and emptying assessed by MRI. *American Journal of Physiology-Gastrointestinal and Liver Physiology*, *280*, G1227-1233.
- Marciani, L., Hall, N., Pritchard, S. E., Cox, E. F., Totman, J. J., Lad, M., . . . Spiller, R. C. (2012). Preventing Gastric Sieving by Blending a Solid/Water Meal Enhances Satiation in Healthy Humans. *The Journal of Nutrition*, *142*(7), 1253-1258.
- Marciani, L., Pritchard, S. E., Hellier-Woods, C., Costigan, C., Hoad, C. L., Gowland, P. A., & Spiller, R. C. (2013). Delayed gastric emptying and reduced postprandial small bowel water content of equicaloric whole meal bread versus rice meals in healthy subjects: novel MRI insights. *European Journal of Clinical Nutrition*, *67*(7), 754-758.
- Martens, B. M. J., Bruininx, E. M. A. M., Gerrits, W. J. J., & Schols, H. A. (2020). The importance of amylase action in the porcine stomach to starch digestion kinetics. *Animal Feed Science and Technology*, *267*, 114546.
- Martens, B. M. J., Flécher, T., de Vries, S., Schols, H. A., Bruininx, E. M. A. M., & Gerrits, W. J. J. (2019). Starch digestion kinetics and mechanisms of hydrolysing enzymes in growing pigs fed processed and native cereal-based diets. *British Journal of Nutrition*, *121*(10), 1124-1136.
- Martens, B. M. J., Noorloos, M., de Vries, S., Schols, H. A., Bruininx, E., & Gerrits, W. J. J. (2019). Whole digesta properties as influenced by feed processing explain variation in gastrointestinal transit times in pigs. *British Journal of Nutrition*, *122*(11), 1242-1254.
- McGhee, M. L., & Stein, H. H. (2018). Apparent and standardized ileal digestibility of AA and starch in hybrid rye, barley, wheat, and corn fed to growing pigs¹. *Journal of Animal Science*, *96*(8), 3319-3329.
- McLauchlan, G., Fullarton, G. M., Crean, G. P., & McColl, K. E. (1989). Comparison of gastric body and antral pH: a 24 hour ambulatory study in healthy volunteers. *Gut*, *30*(5), 573-578.
- Meng, H., Matthan, N. R., Ausman, L. M., & Lichtenstein, A. H. (2017). Effect of prior meal macronutrient composition on postprandial glycemic responses and glycemic index and glycemic load value determinations. *The American Journal of Clinical Nutrition*, *106*(5), 1246-1256.

- Mennah-Govela, Y. A., & Bornhorst, G. M. (2016a). Acid and moisture uptake in steamed and boiled sweet potatoes and associated structural changes during in vitro gastric digestion. *Food Research International*, 88, 247-255.
- Mennah-Govela, Y. A., & Bornhorst, G. M. (2016b). Mass transport processes in orange-fleshed sweet potatoes leading to structural changes during in vitro gastric digestion. *Journal of Food Engineering*, 191, 48-57.
- Mennah-Govela, Y. A., & Bornhorst, G. M. (2021). Food buffering capacity: quantification methods and its importance in digestion and health. *Food & Function*, 12, 543-563.
- Mennah-Govela, Y. A., Bornhorst, G. M., & Singh, R. P. (2015). Acid diffusion into rice boluses is influenced by rice type, variety, and presence of alpha-amylase. *Journal of Food Science*, 80(2), E316-325.
- Mennah-Govela, Y. A., Cai, H., Chu, J., Kim, K., Maborang, M.-K., Sun, W., & Bornhorst, G. M. (2020). Buffering capacity of commercially available foods is influenced by composition and initial properties in the context of gastric digestion. *Food & Function*, 11(3), 2255-2267.
- Mennah-Govela, Y. A., Singh, R. P., & Bornhorst, G. M. (2019). Buffering capacity of protein-based model food systems in the context of gastric digestion. *Food & Function*, 10(9), 6074-6087.
- Meyer, J. H. (1980). Gastric emptying of ordinary food: effect of antrum on particle size. *American Journal of Physiology*, 239(3), G133-135.
- Meyer, J. H., Elashoff, J., Porter-Fink, V., Dressman, J., & Amidon, G. L. (1988). Human postprandial gastric emptying of 1-3-millimeter spheres. *Gastroenterology*, 94(6), 1315-1325.
- Mihai, B. M., Michai, C., Cijevschi-Prelicean, C., Grigorescu, E.-D., Dranga, M., Drug, V., . . . Lăcătușu, C. M. (2018). Bidirectional relationship between gastric emptying and plasma glucose control in normoglycemic individuals and diabetic patients. *Journal of Diabetes Research*, 2018, 9.
- Mikolajczyk, A. E., Watson, S., Surma, B. L., & Rubin, D. T. (2015). Assessment of Tandem Measurements of pH and Total Gut Transit Time in Healthy Volunteers. *Clinical and translational gastroenterology*, 6(7), e100-e100.
- Miller, G. L. (1959). Use of Dinitrosalicylic Acid Reagent for Determination of Reducing Sugar. *Analytical Chemistry*, 31(3), 426-428.
- Minekus, M., Alminger, M., Alvito, P., Ballance, S., Bohn, T., Bourlieu, C., . . . Brodkorb, A. (2014). A standardised static in vitro digestion method suitable for food - an international consensus. *Food & Function*, 5(6), 1113-1124.
- Mishra, S., Monro, J., & Hardacre, A. (2011). Food structure and carbohydrate digestibility. In C.-F. Chang (Ed.), *Carbohydrates*: InTechOpen.
- Monro, J., Mishra, S., Blandford, E., Anderson, J., & Genet, R. (2009). Potato genotype differences in nutritionally distinct starch fractions after cooking, and cooking plus storing cool. *Journal of Food Composition and Analysis*, 22(6), 539-545.
- Monro, J. A., Mishra, S., & Venn, B. (2010). Baselines representing blood glucose clearance improve in vitro prediction of the glycaemic impact of customarily consumed food quantities. *British Journal of Nutrition*, 103(2), 295-305.
- Montoya, C. A., Rutherford, S. M., Olson, T. D., Purba, A. S., Drummond, L. N., Boland, M. J., & Moughan, P. J. (2014). Actinidin from kiwifruit (*Actinidia deliciosa* cv. Hayward) increases the digestion and rate of gastric emptying of meat proteins in the growing pig. *British Journal of Nutrition*, 111, 957-967.

- Moongngarm, A., Bronlund, J., Grigg, N., & Sriwai, N. (2012). Chewing behavior and bolus properties as affected by different rice types. *International Journal of Medical and Biological Sciences*, 6, 51-56.
- Motoi, L., Morgenstern, M. P., Hedderley, D. I., Wilson, A. J., & Balita, S. (2013). Bolus moisture content of solid foods during mastication. *Journal of Texture Studies*, 44(468-479)
- Mourot, J., Thouvenot, P., Couet, C., Antoine, J. M., Krobicka, A., & Debry, G. (1988). Relationship between the rate of gastric emptying and glucose and insulin responses to starchy foods in young healthy adults. *The American Journal of Clinical Nutrition*, 48(4), 1035-1040.
- Muangchan, N., Khiewvan, B., Chatree, S., Pongwattanapakin, K., Kunlaket, N., Dokmai, T., & Chaikomin, R. (2021). Riceberry rice (*Oryza sativa* L.) slows gastric emptying and improves the postprandial glycaemic response. *British Journal of Nutrition*, 1-9.
- Mulet-Cabero, A.-I., Egger, L., Portmann, R., Ménard, O., Marze, S., Minekus, M., . . . Mackie, A. R. (2020). A standardised semi-dynamic in vitro digestion method suitable for food – an international consensus. *Food & Function*, 11(2), 1702-1720.
- Muttakin, S., Moxon, T. E., & Gouseti, O. (2019). In vivo, In vitro, and In silico Studies of the GI Tract. In O. Gouseti, G. M. Bornhorst, S. Bakalis, & A. Mackie (Eds.), *Interdisciplinary Approaches to Food Digestion* (pp. 29-67). Cham: Springer International Publishing.
- National Research Council. (2012). *Nutrient Requirements of Swine: Eleventh Revised Edition*. Washington, DC: The National Academies Press.
- Nau, F., Nyemb-Diop, K., Lechevalier, V., Floury, J., Serrière, C., Stroebinger, N., . . . Rutherford, S. M. (2019). Spatial-temporal changes in pH, structure and rheology of the gastric chyme in pigs as influenced by egg white gel properties. *Food Chemistry*, 280, 210-220.
- Nawaz, M. A., Gaiani, C., Fukai, S., & Bhandari, B. (2016). X-ray photoelectron spectroscopic analysis of rice kernels and flours: Measurement of surface chemical composition. *Food Chemistry*, 212, 349-357.
- Nguyen, T. C., Fillaudeau, L., Anne-Archard, D., Chu-Ky, S., Luong, H. N., Vu, T. T., . . . Nguyen, V. H. (2021). Impact of Particle Size on the Rheological Properties and Amylolysis Kinetics of Ungelatinized Cassava Flour Suspensions. 9(6), 989.
- Nichols, B. L., Avery, S., Sen, P., Swallow, D. M., Hahn, D., & Sterchi, E. (2003). The maltase-glucoamylase gene: common ancestry to sucrase-isomaltase with complementary starch digestion activities. *Proceedings of the National Academy of Sciences of the United States of America*, 100(3), 1432-1437.
- Nielsen, K. L., Hartvigsen, M. L., Hedemann, M. S., Lærke, H. N., Hermansen, K., & Bach Knudsen, K. E. (2014). Similar metabolic responses in pigs and humans to breads with different contents and compositions of dietary fibers: a metabolomics study. *The American Journal of Clinical Nutrition*, 99(4), 941-949.
- Nordlund, E., Katina, K., Mykkanen, H., & Poutanen, K. (2016). Distinct Characteristics of Rye and Wheat Breads Impact on Their in Vitro Gastric Disintegration and in Vivo Glucose and Insulin Responses. *Foods*, 5(2)
- Norton, J. E., Wallis, G. A., Spyropoulos, F., Lillford, P. J., & Norton, I. T. (2014). Designing food structures for nutrition and health benefits. *Annual Review of Food Science and Technology*, 5, 177-195.

- Nusynowitz, M. L., & Benedetto, A. R. (1994). The lag phase of gastric emptying: clinical, mathematical and in vitro studies. *The Journal of Nuclear Medicine*, 35(6), 1023-1027.
- Nyachoti, C. M., de Lange, C. F. M., & Schulze, H. (1997). Estimating endogenous amino acid flows at the terminal ileum and true ileal amino acid digestibilities in feedstuffs for growing pigs using the homoarginine method. *Journal of Animal Science*, 75(12), 3206-3213.
- O'Grady, G., Du, P., Cheng, L. K., Egbuji, J. U., Lammers, W. J. E. P., Windsor, J. A., & Pullan, A. J. (2010). Origin and propagation of human gastric slow-wave activity defined by high-resolution mapping. *American Journal of Physiology-Gastrointestinal and Liver Physiology*, 299(3), 585-592.
- Okwudili, U. C., Chinedu, E. A., & Anayo, O. J. (2014). Biochemical Effects of Xylazine, Propofol, and Ketamine in West African Dwarf Goats. *Journal of Veterinary Medicine*, 2014, 758581.
- Olenskyj, A. G., Donis-González, I. R., & Bornhorst, G. M. (2020). Nondestructive characterization of structural changes during in vitro gastric digestion of apples using 3D time-series micro-computed tomography. *Journal of Food Engineering*, 267, 109692.
- Pallares Pallares, A., Loosveldt, B., Karimi, S. N., Hendrickx, M., & Grauwet, T. (2019). Effect of process-induced common bean hardness on structural properties of in vivo generated boluses and consequences for in vitro starch digestion kinetics. *British Journal of Nutrition*, 122(4), 388-399.
- Parada, J., & Aguilera, J. M. (2011). Review: Starch matrices and the glycemic response. *Food Science and Technology International*, 17(3), 187-204.
- Parker, R., & Ring, S. G. (2001). Aspects of the Physical Chemistry of Starch. *Journal of Cereal Science*, 34(1), 1-17.
- Patarin, J., Blésès, D., Magnin, A., Guérin, S., & Malbert, C.-H. (2015). Rheological Characterization of Gastric Juices from Bread with Different Amylose/Amylopectin Ratios. *Food Digestion: Research and Current Opinion*, 6(1), 2-9.
- Pellegrini, N., Vittadini, E., & Fogliano, V. (2020). Designing food structure to slow down digestion in starch-rich products. *Current Opinion in Food Science*, 32, 50-57.
- Pera, P., Bucca, C., Borro, P., Bernocco, C., De, L. A., & Carossa, S. (2002). Influence of mastication on gastric emptying. *Journal of Dental Research*, 81(3), 179-181.
- Pereira, L. J. (2012). Oral Cavity. In J. Chen & L. Engelen (Eds.), *Food Oral Processing*.
- Pérez, S., & Bertoft, E. (2010). The molecular structures of starch components and their contribution to the architecture of starch granules: A comprehensive review. *Starch-Stärke*, 62(8), 389-420.
- Pfister, B., & Zeeman, S. C. (2016). Formation of starch in plant cells. *Cellular and molecular life sciences : CMLS*, 73(14), 2781-2807.
- Pickhardt, P. J., & Asher, D. B. (2003). Wall thickening of the gastric antrum as a normal finding: Multidetector CT with cadaveric comparison. *American Journal of Roentgenology*, 181(4), 973-979.
- Pilichiewicz, A. N., Chaikomin, R., Brennan, I. M., Wishart, J. M., Rayner, C. K., Jones, K. L., . . . Feinle-Bisset, C. (2007). Load-dependent effects of duodenal glucose on glycemia, gastrointestinal hormones, antropyloroduodenal motility, and energy intake in healthy men. *American Journal of Physiology-Endocrinology and Metabolism*, 293(3), E743-E753.

- Pletsch, E. A. (2018). *Investigating the purported slow transit and starch digestion of whole grain foods*. (PhD Dissertation), Purdue University, West Lafayette, Indiana.
- Pletsch, E. A., & Hamaker, B. R. (2018). Brown rice compared to white rice slows gastric emptying in humans. *European Journal of Clinical Nutrition*, 72(3), 367-373.
- Pluschke, A. M., Williams, B. A., Zhang, D., Anderson, S. T., Roura, E., & Gidley, M. J. (2018). Male grower pigs fed cereal soluble dietary fibres display biphasic glucose response and delayed glycaemic response after an oral glucose tolerance test. *PLoS One*, 13(3), e0193137.
- Prinz, J. F., & Lucas, P. W. (1995). Swallow thresholds in human mastication. *Archives of Oral Biology*, 40(5), 401-403.
- Prodan, A., Brand, H. S., Ligtenberg, A. J. M., Imangaliyev, S., Tsivtsivadze, E., van der Weijden, F., . . . Veerman, E. C. I. (2015). Interindividual variation, correlations, and sex-related differences in the salivary biochemistry of young healthy adults. *European Journal of Oral Sciences*, 123(3), 149-157.
- Ramadoss, B. R., Gangola, M. P., Agasimani, S., Jaiswal, S., Venkatesan, T., Sundaram, G. R., & Chibbar, R. N. (2019). Starch granule size and amylopectin chain length influence starch in vitro enzymatic digestibility in selected rice mutants with similar amylose concentration. *Journal of Food Science and Technology*, 56(1), 391-400.
- Ramdath, D. D., Wolever, T. M. S., Siow, Y. C., Ryland, D., Hawke, A., Taylor, C., . . . Aliani, M. (2018). Effect of Processing on Postprandial Glycemic Response and Consumer Acceptability of Lentil-Containing Food Items. 7(5), 76.
- Ranawana, V., Clegg, M. E., Shafat, A., & Henry, C. J. (2011). Postmastication digestion factors influence glycemic variability in humans. *Nutrition Research*, 31(6), 452-459.
- Ranawana, V., Henry, C. J. K., & Pratt, M. (2010). Degree of habitual mastication seems to contribute to interindividual variations in the glycemic response to rice but not to spaghetti. *Nutrition Research*, 30, 382-391.
- Ranawana, V., Leow, M. K. S., & Henry, C. J. K. (2014). Mastication effects on the glycaemic index: impact on variability and practical implications. *European Journal of Clinical Nutrition*, 68(1), 137-139.
- Ranawana, V., Monroe, J. A., Mishra, S., & Henry, C. J. (2010). Degree of particle size breakdown during mastication may be a possible cause of interindividual glycemic variability. *Nutrition Research*, 30(4), 246-254.
- Read, N. W., Welch, I. M., Austen, C. J., Barnish, C., Bartlett, C. E., Baxter, A. J., . . . Worlding, J. (1986). Swallowing food without chewing; a simple way to reduce postprandial glycaemia. *British Journal of Nutrition*, 55, 43-47.
- Reinke, D. A., Rosenbaum, A. H., & Bennett, D. R. (1967). Patterns of dog gastrointestinal contractile activity monitored in vivo with extraluminal force transducers. *The American Journal of Digestive Diseases*, 12(2), 113-141.
- Ren, X., Chen, J., Molla, M. M., Wang, C., Diao, X., & Shen, Q. (2016). In vitro starch digestibility and in vivo glycemic response of foxtail millet and its products. *Food & Function*, 7(1), 372-379.
- Reynaud, Y., Buffière, C., David, J., Cohade, B., Vauris, M., Lopez, M., . . . Rémond, D. (2020). Temporal changes in postprandial intragastric pH: Comparing measurement methods, food structure effects, and kinetic modelling. *Food Research International*, 128, 108784.

- Reynolds, T. D., Mitchell, S. A., & Balwinski, K. M. (2002). Investigation of the Effect of Tablet Surface Area/Volume on Drug Release from Hydroxypropylmethylcellulose Controlled-Release Matrix Tablets. *Drug Development and Industrial Pharmacy*, 28(4), 457-466.
- Richardson, C. T., Walsh, J. H., Hicks, M. I., & Fordtran, J. S. (1976). Studies on the mechanisms of food-stimulated gastric acid secretion in normal human subjects. *Journal of Clinical Investigation*, 58, 623-631.
- Roberts, P. J., & Whelan, W. J. (1960). The mechanism of carbohydrase action. 5. Action of human salivary alpha-amylase on amylopectin and glycogen. *The Biochemical journal*, 76(2), 246-253.
- Robin, F., & Palzer, S. (2015). Texture of breakfast cereals and extruded products. In J. Chen & A. Rosenthal (Eds.), *Modifying Food Texture : Novel Ingredients and Processing Techniques* (pp. 203-235). Cambridge, UNITED KINGDOM: Elsevier Science & Technology.
- Rodrigues, S. A., Young, A. K., James, B. J., & Morgenstern, M. P. (2014). Structural Changes Within a Biscuit Bolus During Mastication. 45(2), 89-96.
- Rodríguez Varón, A., & Zuleta, J. (2010). From the physiology of gastric emptying to the understanding of gastroparesis. *Revista Colombiana de Gastroenterologia*, 25(2), 219-225.
- Rojas-Bonzi, P., Vangsøe, C. T., Nielsen, K. L., Lærke, H. N., Hedemann, M. S., & Knudsen, K. E. B. (2020). The Relationship between In Vitro and In Vivo Starch Digestion Kinetics of Breads Varying in Dietary Fibre. 9(9), 1337.
- Rongkaumpan, G., Amsbury, S., Andablo-Reyes, E., Linford, H., Connell, S., Knox, J. P., . . . Orfila, C. (2019). Cell Wall Polymer Composition and Spatial Distribution in Ripe Banana and Mango Fruit: Implications for Cell Adhesion and Texture Perception. 10(858)
- Rosenbaum, A. H., Reinke, D. A., & Bennett, D. R. (1967). In-vivo force, frequency, and velocity of dog gastrointestinal contractile activity. *The American Journal of Digestive Diseases*, 12(2), 142-153.
- Rosenblum, J. L., Irwin, C. L., & Alpers, D. H. (1988). Starch and glucose oligosaccharides protect salivary-type amylase activity at acid pH. *American Journal of Physiology*, 254(5 Pt 1), G775-780.
- Ross, S. W., Brand, J. C., Thorburn, A. W., & Truswell, A. S. (1987). Glycemic index of processed wheat products. *The American Journal of Clinical Nutrition*, 46(4), 631-635.
- Sadler, M. (2011). *Food, glycaemic response and health*. Belgium: ILSI Europe.
- Saha, J. K., Xia, J., Grondin, J. M., Engle, S. K., & Jakubowski, J. A. (2005). Acute Hyperglycemia Induced by Ketamine/Xylazine Anesthesia in Rats: Mechanisms and Implications for Preclinical Models. 230(10), 777-784.
- Salmerón, J., Ascherio, A., Rimm, E. B., Colditz, G. A., Spiegelman, D., Jenkins, D. J., . . . Willett, W. C. (1997). Dietary Fiber, Glycemic Load, and Risk of NIDDM in Men. *Diabetes Care*, 20(4), 545-550.
- Sangpring, Y., Fukuoka, M., & Ratanasumawong, S. (2015). The effect of sodium chloride on microstructure, water migration, and texture of rice noodle. *LWT - Food Science and Technology*, 64(2), 1107-1113.
- Schop, M., Jansman, A. J. M., de Vries, S., & Gerrits, W. J. J. (2020). Increased diet viscosity by oat β -glucans decreases the passage rate of liquids in the stomach and affects digesta physicochemical properties in growing pigs. *Animal : an international journal of animal bioscience*, 14(2), 269-276.

- Schulze, K. (2006). Imaging and modelling of digestion in the stomach and the duodenum. *Neurogastroenterology & Motility*, 18(3), 172-183.
- Sensoy, I. (2014). A review on the relationship between food structure, processing, and bioavailability. *Critical Reviews in Food Science and Nutrition*, 54(7), 902-909.
- Seung, D. (2020). Amylose in starch: towards an understanding of biosynthesis, structure and function. *New Phytologist*, 228(5), 1490-1504.
- Shafik, A., Sibai, O. E., Shafik, A. A., & Shafik, I. A. (2007). Mechanism of gastric emptying through the pyloric sphincter: A human study. *Medical Science Monitor*, 13(1), 24-29.
- Shani-Levi, C., Alvito, P., Andrés, A., Assunção, R., Barberá, R., Blanquet-Diot, S., . . . Lesmes, U. (2017). Extending in vitro digestion models to specific human populations: Perspectives, practical tools and bio-relevant information. *Trends in Food Science & Technology*, 60, 52-63.
- Sharif, S. I., Abouazra, H. A. J. A. J. o. P., & Toxicology. (2009). Effect of Intravenous Ketamine Administration on Blood Glucose Levels in Conscious Rabbits. 4, 38-45.
- Shelat, K. J., Nicholson, T., Flanagan, B. M., Zhang, D., Williams, B. A., & Gidley, M. J. (2015). Rheology and microstructure characterisation of small intestinal digesta from pigs fed a red meat-containing Western-style diet. *Food Hydrocolloids*, 44, 300-308.
- Shewry, P. R. (2008). Improving the nutritional quality of cereals by conventional and novel approaches. In B. R. Hamaker (Ed.), *Technology of Functional Cereal Products* (pp. 159-183): Woodhead Publishing.
- Short, F. J., Gorton, P., Wiseman, J., & Boorman, K. N. (1996). Determination of titanium dioxide added as an inert marker in chicken digestibility studies. *Animal Feed Science and Technology*, 59(4), 215-221.
- Siegel, J. A., Urbain, J. L., Adler, L. P., Charkes, N. D., Maurer, A. H., Krevsky, B., . . . Malmud, L. S. (1988). Biphasic nature of gastric emptying. *Gut*, 29(1), 85-89.
- Siepmann, J., & Siepmann, F. (2012). Modeling of diffusion controlled drug delivery. *Journal of Controlled Release*, 161(2), 351-362.
- Simonian, H. P., Maurer, A. H., Knight, L. C., Kantor, S., Kontos, D., Megalooikonomou, V., . . . Parkman, H. P. (2004). Simultaneous assessment of gastric accommodation and emptying: studies with liquid and solid meals. *The Journal of Nuclear Medicine*, 45(7), 1155-1160.
- Simonian, H. P., Vo, L., Doma, S., Fisher, R. S., & Parkman, H. P. (2005). Regional postprandial differences in pH within the stomach and gastroesophageal junction. *Digestive Diseases and Sciences*, 50(12), 2276-2285.
- Singh, H., Ye, A., & Ferrua, M. J. (2015). Aspects of food structures in the digestive tract. *Current Opinion in Food Science*, 3, 85-93.
- Singh, J., Dartois, A., & Kaur, L. (2010). Starch digestibility in food matrix: a review. *Trends in Food Science & Technology*, 21, 168-180.
- Singh, V., & Ali, S. Z. (2006). In vitro hydrolysis of starches by α -amylase in comparison to that by acid. *American Journal of Food Technology*, 1(1), 43-51.
- Smith, M. E., & Morton, D. G. (2010a). Basic functions of the stomach. In M. M. Smith & D. G. Morton (Eds.), *The Digestive System* (2 ed., pp. 39-50). Edinburgh: Elsevier.
- Smith, M. E., & Morton, D. G. (2010b). Overview of the digestive system. In *The Digestive System* (2 ed., pp. 1-18). Edinburgh: Elsevier.

- Smith, M. E., & Morton, D. G. (2010c). The Small Intestine. In M. E. Smith & D. G. Morton (Eds.), *The Digestive System (Second Edition)* (pp. 107-127): Churchill Livingstone.
- Smith, M. M., & Morton, D. G. (2010d). *The Digestive System* (2 ed.). Edinburgh: Elsevier.
- Somaratne, G., Ferrua, M. J., Ye, A., Nau, F., Floury, J., Dupont, D., & Singh, J. (2020). Food material properties as determining factors in nutrient release during human gastric digestion: a review. *Critical Reviews in Food Science and Nutrition*, 1-17.
- Somaratne, G., Reis, M. M., Ferrua, M. J., Ye, A., Nau, F., Floury, J., . . . Singh, J. (2019). Mapping the Spatiotemporal Distribution of Acid and Moisture in Food Structures during Gastric Juice Diffusion Using Hyperspectral Imaging. *Journal of Agricultural and Food Chemistry*, 67(33), 9399-9410.
- Somaratne, G., Ye, A., Nau, F., Ferrua, M. J., Dupont, D., Paul Singh, R., & Singh, J. (2020). Role of biochemical and mechanical disintegration on β -carotene release from steamed and fried sweet potatoes during in vitro gastric digestion. *Food Research International*, 136, 109481.
- Sotomayor, R. O., & Schalkwijk, L. (2020). *Possible unexpected peaks from oil drop size measurements in milk*. (MSc Thesis), Lund University, Lund, Sweden. Retrieved from <https://lup.lub.lu.se/student-papers/search/publication/9016663>
- Soybel, D. I. (2005). Anatomy and the physiology of the stomach. *Surgical Clinics of North America*, 875-894.
- Spiller, R., & Marciani, L. (2019). Intraluminal impact of food: New insights from MRI. *Nutrients*, 11(5), 1147.
- Steffe, J. F. (1996). *Rheological methods in food process engineering* (2nd ed. ed.). East Lansing, USA: Freeman Press.
- Štembírek, J., Kyllar, M., Putnová, I., Stehlík, L., & Buchtová, M. (2012). The pig as an experimental model for clinical craniofacial research. *Laboratory Animals*, 46(4), 269-279.
- Sun, L., Ranawana, D. V., Tan, W. J. K., Quek, Y. C. R., & Henry, C. J. (2015). The impact of eating methods on eating rate and glycemic response in healthy adults. *Physiology & Behavior*, 139, 505-510.
- Swackhamer, C., Doan, R., & Bornhorst, G. M. (2022). Development and characterization of standardized model, solid foods with varying breakdown rates during gastric digestion. *Journal of Food Engineering*, 316, 110827.
- Swackhamer, C., Zhang, Z., Taha, A. Y., & Bornhorst, G. M. (2019). Fatty acid bioaccessibility and structural breakdown from in vitro digestion of almond particles. *Food & Function*, 10(8), 5174-5187.
- Szczesniak, A. S. (1963). Classification of Textural Characteristics. *Journal of Food Science*, 28(4), 385-389.
- Takeda, Y., Shibahara, S., & Hanashiro, I. (2003). Examination of the structure of amylopectin molecules by fluorescent labeling. *Carbohydrate Research*, 338(5), 471-475.
- Tamura, M., Okazaki, Y., Kumagai, C., & Ogawa, Y. (2017). The importance of an oral digestion step in evaluating simulated in vitro digestibility of starch from cooked rice grain. *Food Research International*, 94, 6-12.
- Tamura, M., Singh, J., Kaur, L., & Ogawa, Y. (2016a). Impact of structural characteristics on starch digestibility of cooked rice. *Food Chemistry*, 191, 91-97.

- Tamura, M., Singh, J., Kaur, L., & Ogawa, Y. (2016b). Impact of the degree of cooking on starch digestibility of rice – An in vitro study. *Food Chemistry*, 191, 98-104.
- Tamura, M., Singh, J., Kaur, L., & Ogawa, Y. (2019). Effect of post-cooking storage on texture and in vitro starch digestion of Japonica rice. *Journal of Food Process Engineering*, 42(2), e12985.
- Tan, J., Martini, S., Wang, Y., Kong, F., Hartel, R., Barbosa-Cánovas, G., . . . Joyner, H. (2019). Interlaboratory measurement of rheological properties of tomato salad dressing. *Journal of Food Science*, 84(11), 3204-3212.
- Thuenemann, E. C. (2015). Dynamic digestion models: General introduction. In K. Verhoeckx, P. Cotter, I. López-Expósito, C. Kleiveland, T. Lea, A. Mackie, T. Requena, D. Swiatecka, & H. Wichers (Eds.), *The impact of food bioactives on health: in vitro and ex vivo models* (pp. 33-36). Cham: Springer International Publishing.
- Tjørve, K. M. C., & Tjørve, E. (2017). The use of Gompertz models in growth analyses, and new Gompertz-model approach: An addition to the Unified-Richards family. *PLoS One*, 12(6), e0178691.
- Torsdottir, I., Alpsten, M., Andersson, H., Schweizer, T. F., Tölle, J., & Wüsch, P. (1989). Gastric emptying and glycemic response after ingestion of mashed bean or potato flakes in composite meals. *The American Journal of Clinical Nutrition*, 50(6), 1415-1419.
- Torsdottir, I., & Andersson, H. (1989). Effect on the postprandial glycaemic level of the addition of water to a meal ingested by healthy subjects and type 2 (non-insulin-dependent) diabetic patients. *Diabetologia*, 32(4), 231-235.
- Tschritter, O., Fritsche, A., Shirkavand, F., Machicao, F., Häring, H., & Stumvoll, M. (2003). Assessing the Shape of the Glucose Curve During an Oral Glucose Tolerance Test. 26(4), 1026-1033.
- Tuaño, A. P. P., Barcellano, E. C. G., & Rodriguez, M. S. (2021). Resistant starch levels and in vitro starch digestibility of selected cooked Philippine brown and milled rices varying in apparent amylose content and glycemic index. *Food Chemistry: Molecular Sciences*, 2, 100010.
- Urbain, J. L., Siegel, J. A., Charkes, N. D., Maurer, A. H., Malmud, L. S., & Fisher, R. S. (1989). The two-component stomach: effects of meal particle size on fundal and antral emptying. *European Journal of Nuclear Medicine*, 15, 254-259.
- USDA-ARS. (2014). A simplified chemical method for determining classes of rice amylose content which control cooked rice texture. Retrieved from https://www.ars.usda.gov/ARSUserFiles/60280500/OUTREACH/Amylose%20Protocol%20_final%202014.pdf
- van de Velde, F., van Riel, J., & Tromp, R. H. (2002). Visualisation of starch granule morphologies using confocal scanning laser microscopy (CSLM). *Journal of the Science of Food and Agriculture*, 82(13), 1528-1536.
- van der Sman, R. G. M., & van der Goot, A. J. (2009). The science of food structuring. *Soft Matter*, 5, 501-510.
- van Eck, A., Hardeman, N., Karatza, N., Fogliano, V., Scholten, E., & Stieger, M. (2019). Oral processing behavior and dynamic sensory perception of composite foods: Toppings assist saliva in bolus formation. *Food Quality and Preference*, 71, 497-509.
- van Kempen, T. A., Regmi, P. R., Matte, J. J., & Zijlstra, R. T. (2010). In vitro starch digestion kinetics, corrected for estimated gastric emptying, predict portal glucose appearance in pigs. *The Journal of Nutrition*, 140(7), 1227-1233.

- Vardakou, M., Mercuri, A., Barker, S. A., Craig, D. Q. M., Faulks, R. M., & Wickham, M. J. S. (2011). Achieving antral grinding forces in biorelevant in vitro models: Comparing the USP dissolution apparatus II and the dynamic gastric model with human in vivo data. *AAPS Pharm Sci Tech*, 12(2), 620-626.
- Velchik, M. G., Reynolds, J. C., & Alavi, A. (1989). The effect of meal energy content on gastric emptying. *The Journal of Nuclear Medicine*, 30, 1106-1110.
- Venn, B. J., & Green, T. (2007). Glycemic index and glycemic load: Measurement issues and their effect on diet-disease relationships. *European Journal of Clinical Nutrition*, 61, S122-131.
- Venn, B. J., Wallace, A. J., Monro, J. A., Perry, T., Brown, R., Frampton, C., & Green, T. J. (2006). The Glycemic Load Estimated from the Glycemic Index Does Not Differ Greatly from That Measured Using a Standard Curve in Healthy Volunteers. *The Journal of Nutrition*, 136(5), 1377-1381.
- Versantvoort, C. H., van de Kamp, E., & Rempelberg, C. J. M. (2004). *Development and applicability of an in vitro digestion model in assessing the bioaccessibility of contaminants from food* (No. RIVM report 320102002/2004). Bilthoven, The Netherlands: National Institute for Public Health and the Environment.
- Vicente, B., Valencia, D. G., Serrano, M. P., Lázaro, R., & Mateos, G. G. (2009). Effects of feeding rice and the degree of starch gelatinisation of rice on nutrient digestibility and ileal morphology of young pigs. *British Journal of Nutrition*, 101(9), 1278-1281.
- Villemejeane, C., Wahl, R., Aymard, P., Denis, S., & Michon, C. (2015). In vitro digestion of short-dough biscuits enriched in proteins and/or fibres using a multi-compartmental and dynamic system (1): Viscosity measurement and prediction. *Food Chemistry*, 182, 55-63.
- Virtanen, P., Gommers, R., Oliphant, T. E., Haberland, M., Reddy, T., Cournapeau, D., . . . SciPy, C. (2020). SciPy 1.0: fundamental algorithms for scientific computing in Python. *Nature Methods*, 17(3), 261-272.
- Waldum, H. L., Hauso, O., & Fossmark, R. (2014). The regulation of gastric acid secretion - clinical perspectives. *Acta Physiologica*, 210(2), 239-256.
- Walsh, J. H., Richardson, C. T., & Fordtran, J. S. (1975). pH dependence of acid secretion and gastrin release in normal and ulcer subjects. *The Journal of Clinical Investigation*, 55(3), 462-468.
- Wang, H., Liu, Y., Chen, L., Li, X., Wang, J., & Xie, F. (2018). Insights into the multi-scale structure and digestibility of heat-moisture treated rice starch. *Food Chemistry*, 242, 323-329.
- Wang, S., Blazek, J., Gilbert, E., & Copeland, L. (2012). New insights on the mechanism of acid degradation of pea starch. *Carbohydrate Polymers*, 87(3), 1941-1949.
- Wang, S., & Copeland, L. (2013). Molecular disassembly of starch granules during gelatinization and its effect on starch digestibility: a review. *Food & Function*, 4, 1564-1580.
- Wang, S., Li, C., Copeland, L., Niu, Q., & Wang, S. (2015). Starch retrogradation: A comprehensive review. *Comprehensive Reviews in Food Science and Food Safety*, 14, 569-585.
- Wang, S., Luo, H., Zhang, J., Zhang, Y., He, Z., & Wang, S. (2014). Alkali-Induced Changes in Functional Properties and in Vitro Digestibility of Wheat Starch: The Role of Surface Proteins and Lipids. *Journal of Agricultural and Food Chemistry*, 62(16), 3636-3643.

- Wang, Z., Ichikawa, S., Kozu, H., Neves, M. A., Nakajima, M., Uemura, K., & Kobayashi, I. (2015). Direct observation and evaluation of cooked white and brown rice digestion by gastric digestion simulator provided with peristaltic function. *Food Research International*, 71, 16-22.
- Wang, Z., Kozu, H., Uemura, K., Kobayashi, I., & Ichikawa, S. (2021). Effect of hydrogel particle mechanical properties on their disintegration behavior using a gastric digestion simulator. *Food Hydrocolloids*, 110, 106166.
- Warren, F. J., Zhang, B., Waltzer, G., Gidley, M. J., & Dhital, S. (2015). The interplay of α -amylase and amyloglucosidase activities on the digestion of starch in in vitro enzymic systems. *Carbohydrate Polymers*, 117, 192-200.
- Weinstein, D. H., deRijke, S., Chow, C. C., Foruraghi, L., Zhao, X., Wright, E. C., . . . Wank, S. A. (2013). A new method for determining gastric acid output using a wireless pH-sensing capsule. *Alimentary Pharmacology & Therapeutics*, 37(12), 1198-1209.
- Weurding, R. E., Veldman, A., Veen, W. A. G., van der Aar, P. J., & Verstegen, M. W. A. (2001). Starch digestion rate in the small intestine of broiler chickens differs among feedstuffs. *The Journal of Nutrition*, 131(9), 2329-2335.
- Whelan, W. J., & Roberts, P. J. P. (1953). 261. The mechanism of carbohydrase action. Part II. α -Amylolysis of linear substrates. *Journal of the Chemical Society (Resumed)*(0), 1298-1304.
- Woerle, H. J., Meyer, C., Dostou, J. M., Gosmanov, N. R., Islam, N., Popa, E., . . . Gerich, J. E. (2003). Pathways for glucose disposal after meal ingestion in humans. 284(4), E716-E725.
- Wolever, T. M., Jenkins, D. J., Ocana, A. M., Rao, V. A., & Collier, G. R. (1988). Second-meal effect: low-glycemic-index foods eaten at dinner improve subsequent breakfast glycemic response. *The American Journal of Clinical Nutrition*, 48(4), 1041-1047.
- Wolever, T. M., Tosh, S. M., Spruill, S. E., Jenkins, A. L., Ezatagha, A., Duss, R., . . . Steinert, R. E. (2019). Increasing oat β -glucan viscosity in a breakfast meal slows gastric emptying and reduces glycemic and insulinemic responses but has no effect on appetite, food intake, or plasma ghrelin and PYY responses in healthy humans: a randomized, placebo-controlled, crossover trial. *The American Journal of Clinical Nutrition*, 111(2), 319-328.
- Woolnough, J. W., Bird, A. R., Monro, J. A., & Brennan, C. S. (2010). The effect of a brief salivary α -amylase exposure during chewing on subsequent in vitro starch digestion curve profiles. *International Journal of Molecular Sciences*, 11(8), 2780-2790.
- Woolnough, J. W., Monro, J. A., Brennan, C. S., & Bird, A. R. (2008). Simulating human carbohydrate digestion in vitro: a review of methods and the need for standardisation. *International Journal of Food Science & Technology*, 43(12), 2245-2256.
- Wu, P., Bhattarai, R. R., Dhital, S., Deng, R., Chen, X. D., & Gidley, M. J. (2017). In vitro digestion of pectin- and mango-enriched diets using a dynamic rat stomach-duodenum model. *Journal of Food Engineering*, 202, 65-78.
- Wu, P., Deng, R., Wu, X., Wang, Y., Dong, Z., Dhital, S., & Chen, X. D. (2017). In vitro gastric digestion of cooked white and brown rice using a dynamic rat stomach model. *Food Chemistry*, 237, 1065-1072.
- Wu, P., Dhital, S., Williams, B. A., Chen, X. D., & Gidley, M. J. (2016). Rheological and microstructural properties of porcine gastric digesta and diets containing pectin or mango powder. *Carbohydrate Polymers*, 148, 216-226.

- Zhang, X., Young, R. L., Bound, M., Hu, S., Jones, K. L., Horowitz, M., . . . Wu, T. (2019). Comparative Effects of Proximal and Distal Small Intestinal Glucose Exposure on Glycemia, Incretin Hormone Secretion, and the Incretin Effect in Health and Type 2 Diabetes. *42*(4), 520-528.
- Zheng, Z., Stanley, R., Gidley, M. J., & Dhital, S. (2016). Structural properties and digestion of green banana flour as a functional ingredient in pasta. *Food & Function*, *7*, 771.
- Zhu, Y., Hsu, W. H., & Hollis, J. H. (2013). The impact of food viscosity on eating rate, subjective appetite, glycemic response and gastric emptying rate. *PLoS One*, *8*(6), e67482.
- Zhu, Y., Hsu, W. H., & Hollis, J. H. (2014). Increased number of chews during a fixed-amount meal suppresses postprandial appetite and modulates glycemic response in older males. *Physiology & Behavior*, *133*, 136-140.
- Ziegler, A., Gonzalez, L., & Blikslager, A. (2016). Large Animal Models: The Key to Translational Discovery in Digestive Disease Research. *Cellular and Molecular Gastroenterology and Hepatology*, *2*(6), 716-724.
- Zobel, H. F. (1988). Molecules to Granules: A Comprehensive Starch Review. *Starch-Stärke*, *40*(2), 44-50.
- Zou, W., Sissons, M., Gidley, M. J., Gilbert, R. G., & Warren, F. J. (2015). Combined techniques for characterising pasta structure reveals how the gluten network slows enzymic digestion rate. *Food Chemistry*, *188*, 559-568.
- Zou, W., Sissons, M., Warren, F. J., Gidley, M. J., & Gilbert, R. G. (2016). Compact structure and proteins of pasta retard *in vitro* digestive evolution of branched starch molecular structure. *Carbohydrate Polymers*, *152*, 441-449.
- Zurbau, A., Jenkins, A. L., Jovanovski, E., Au-Yeung, F., Bateman, E. A., Brissette, C., . . . Vuksan, V. (2019). Acute effect of equicaloric meals varying in glycemic index and glycemic load on arterial stiffness and glycemia in healthy adults: a randomized crossover trial. *European Journal of Clinical Nutrition*, *73*(1), 79-85.

APPENDIX A

RICE COUSCOUS MANUFACTURING PROTOCOL

Rice couscous manufacturing protocol was developed from the wheat couscous production process (Table A.1). The key aspect of the process is to achieve the range of water addition that is sufficient to form wet agglomerates (Barkouti et al., 2014). Based on preliminary trials, water content range that is suitable for agglomerating rice flour was identified and this range was used to scale up the production process. The production of rice couscous was conducted at the FoodPilot (Massey University's food pilot plant), and in the end the total amount produced was around 160 kg.

Table A.1 Typical steps in couscous production in the industry and their functions (summarized from Abecassis et al. (2012))

Step	Function
Mixing	Hydrate the starch grains, making it can be gelatinized sufficiently in the steam cooking stage Form raw couscous grains by agglomerating the raw material
Rolling and sieving	Strengthen the wet agglomerates, producing stable couscous grains Classify them based on their size
Steam cooking	Gelatinize the wheat starch Solidify the couscous grains Induce formation of amylose-lipid complexes Insolubilize the wheat proteins → decrease the sticky behavior of cooked couscous
Lump breaking	Break the lump of cooked couscous to separate grains
Drying and cooling	Stabilize the water content, extending shelf life

The protocol developed is summarized in Figure A.1. Batches of 1 kg dry materials (rice flour and maximum 10% product rework) were mixed and pre-conditioned for agglomeration in a high-speed food processor (Robot Coupe, Burgundy, France) at 800 rpm for 2 min. Water (55 to 61% of the total dry material weight) was introduced at 2.67 mL/s, under constant stirring at 800 rpm. Once the required amount of water was added, the material was agitated at 1,500 rpm for 2 min. The agglomerates were sieved in a vibratory shaker (Grain Engineering Ltd., Auckland, NZ) with a sieve size of 0.5

mm. Particles larger than 0.5 mm were used for steaming and any smaller particles were reworked into the mixing process. After 12 to 15 batches, the sieved agglomerates were spread on perforated trays lined with baking paper, and were steamed in a retort (Mauri Engineering, Palmerston North, NZ) for 20 min at 100 °C. Any lumps in the steamed agglomerates were broken by mixing (Thunderbird Food Machinery, USA) at the lowest speed setting for 30 s, followed by drying in a convection oven (INOXTREND, Italy) at 70 to 80 °C for 18 to 20 h. The dried products were sieved to remove particles with desired size range (final product, $0.5 \text{ mm} < d \leq 2 \text{ mm}$), smaller particles ($d \leq 0.5 \text{ mm}$) to be reworked to the first stage, and larger particles ($d > 2 \text{ mm}$) for additional grinding step in a hammer mill (Siemens-Schuckert, Germany). The ground particles were sieved again, and only particles within the desired size range were collected and combined with the other final product fraction.

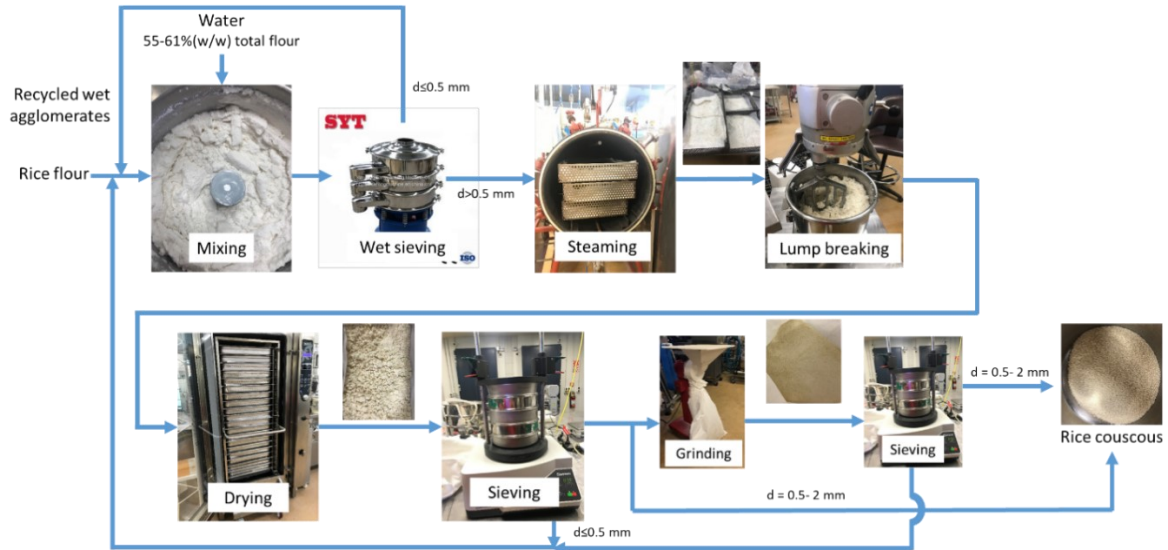


Figure A.1 Diagram of rice couscous production process.

APPENDIX B

***IN VIVO* DIGESTA PICTURES**

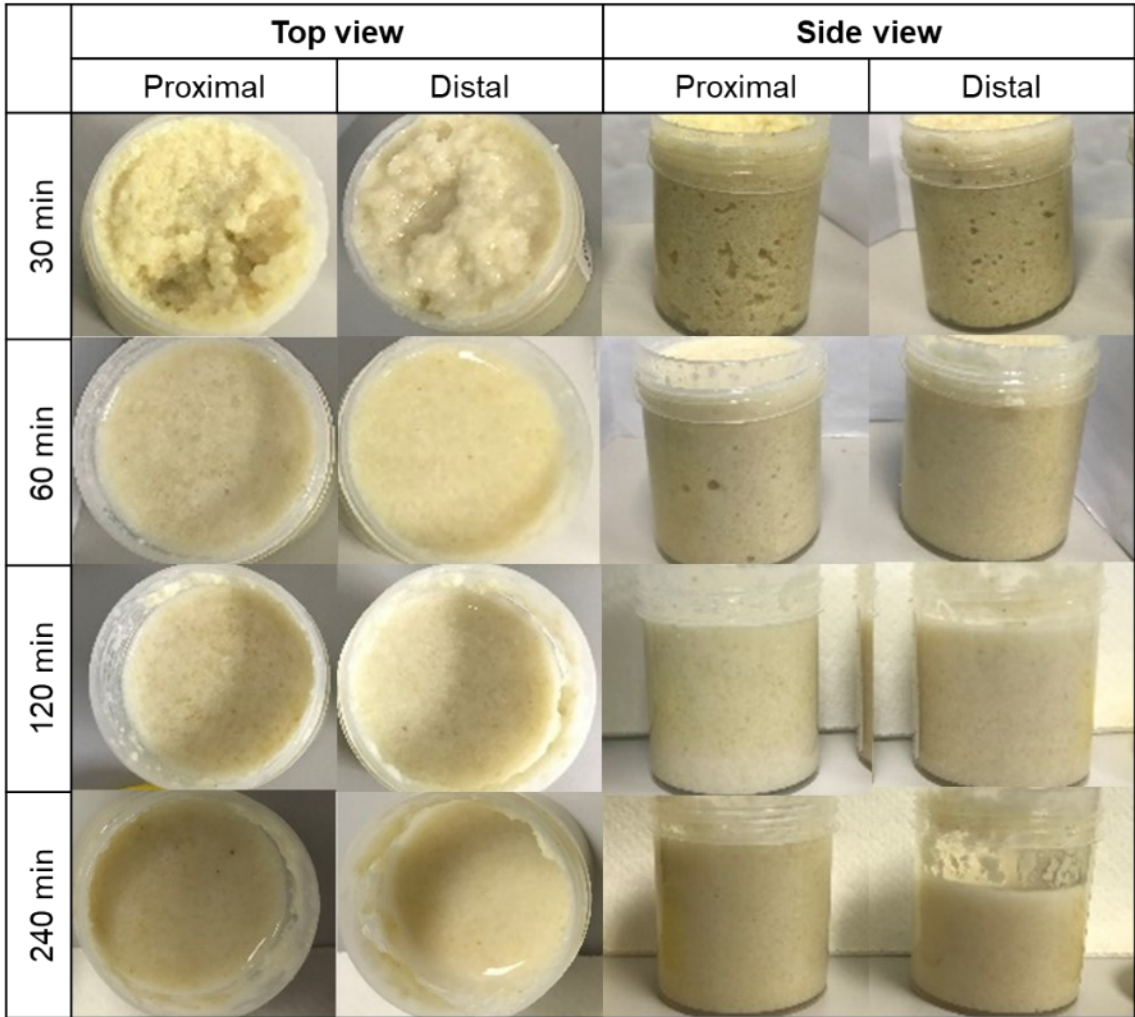


Figure B.1 Example photographs of proximal and distal gastric digesta of pigs fed with couscous after 30, 60, 120, and 240 min digestion time.

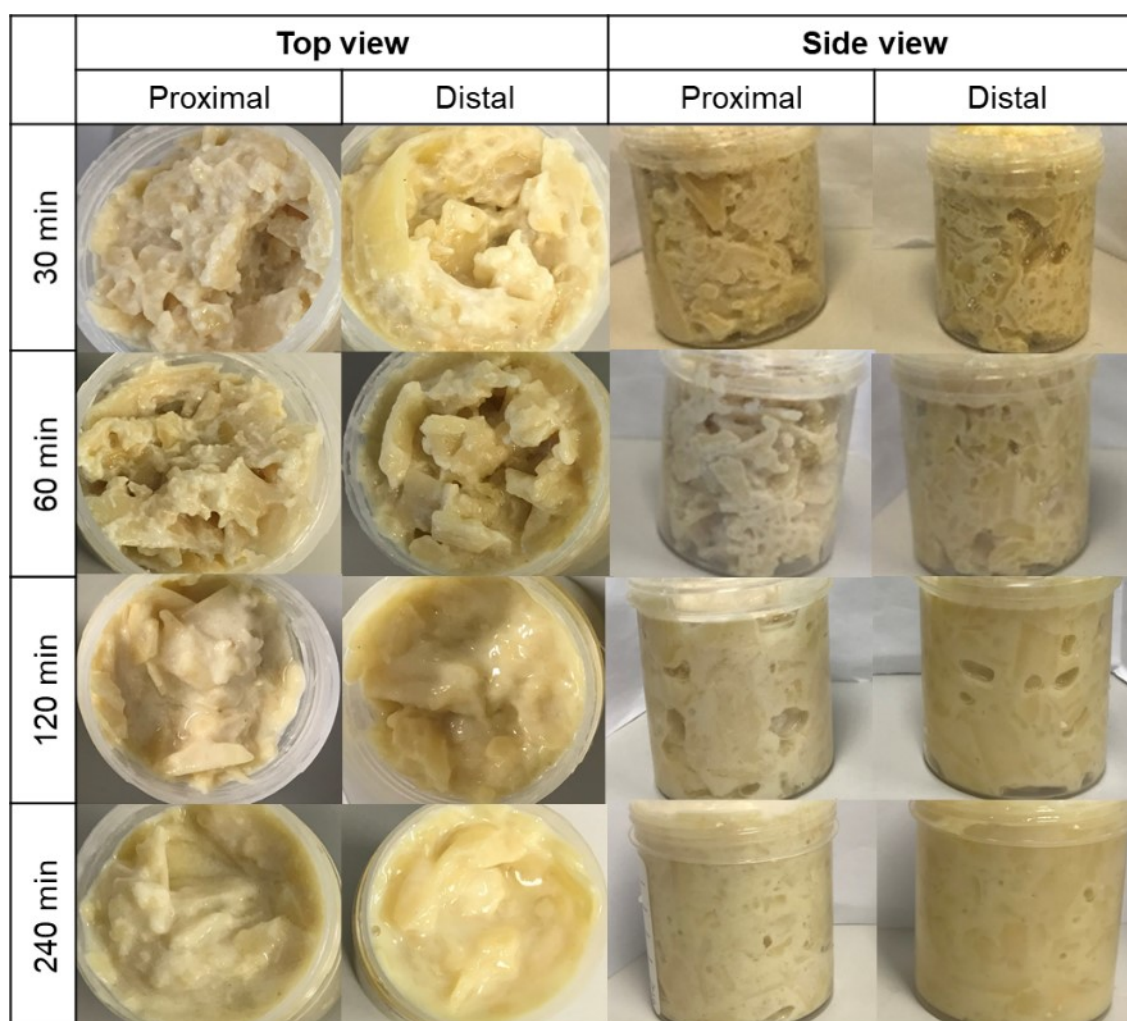


Figure B.2 Example photographs of proximal and distal gastric digesta of pigs fed with pasta after 30, 60, 120, and 240 min digestion time.

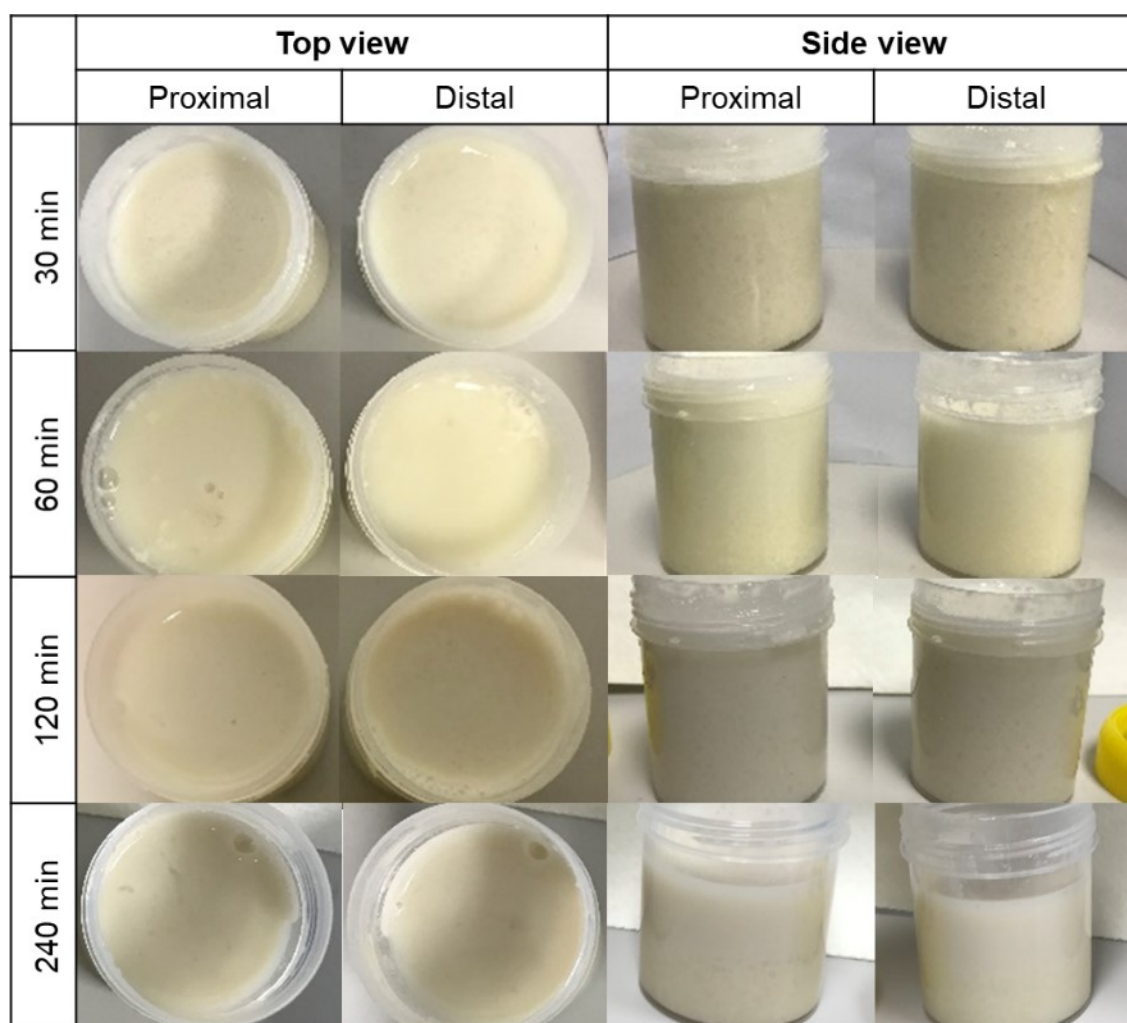


Figure B.3 Example photographs of proximal and distal gastric digesta of pigs fed with rice couscous after 30, 60, 120, and 240 min digestion time.

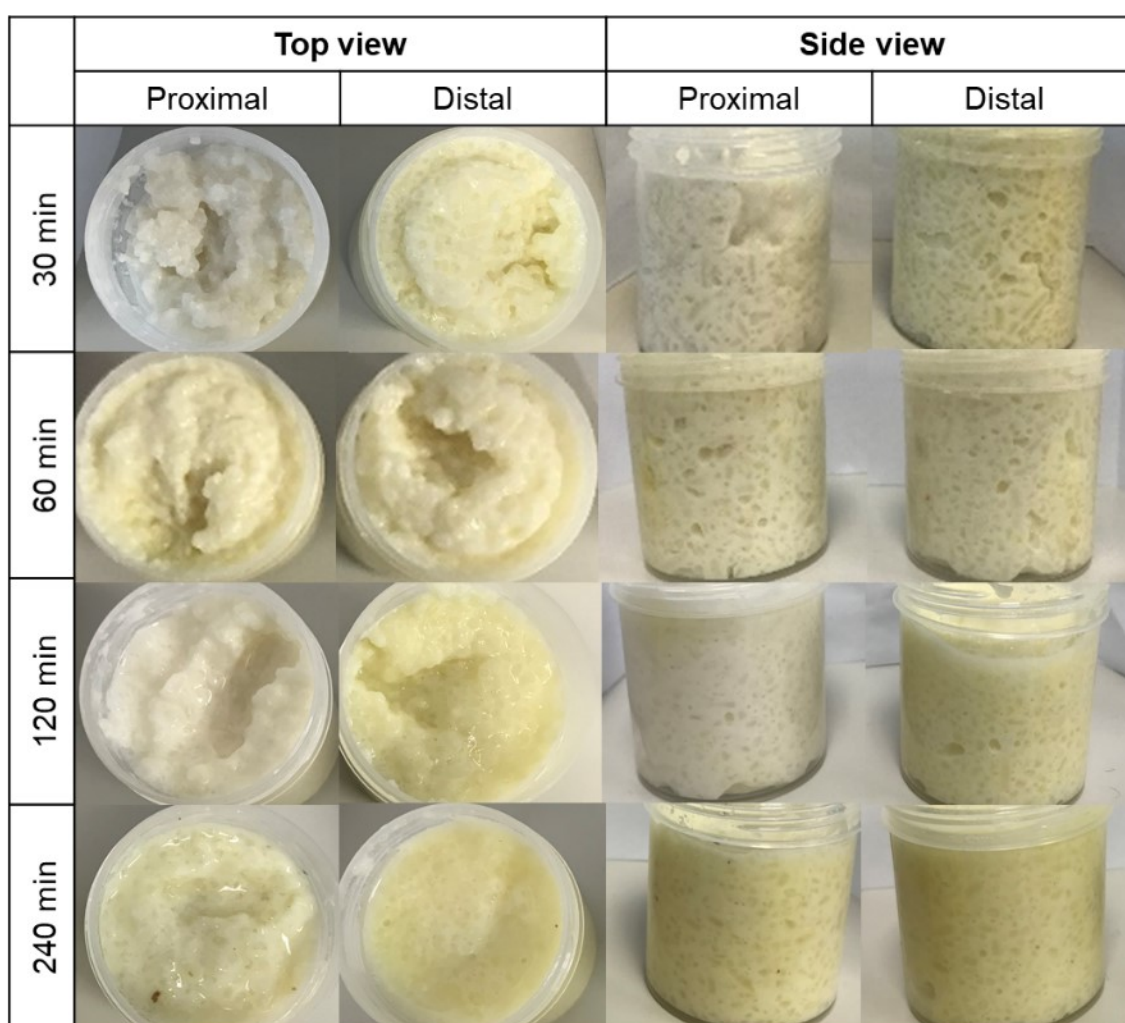


Figure B.4 Example photographs of proximal and distal gastric digesta of pigs fed with rice grain after 30, 60, 120, and 240 min digestion time.

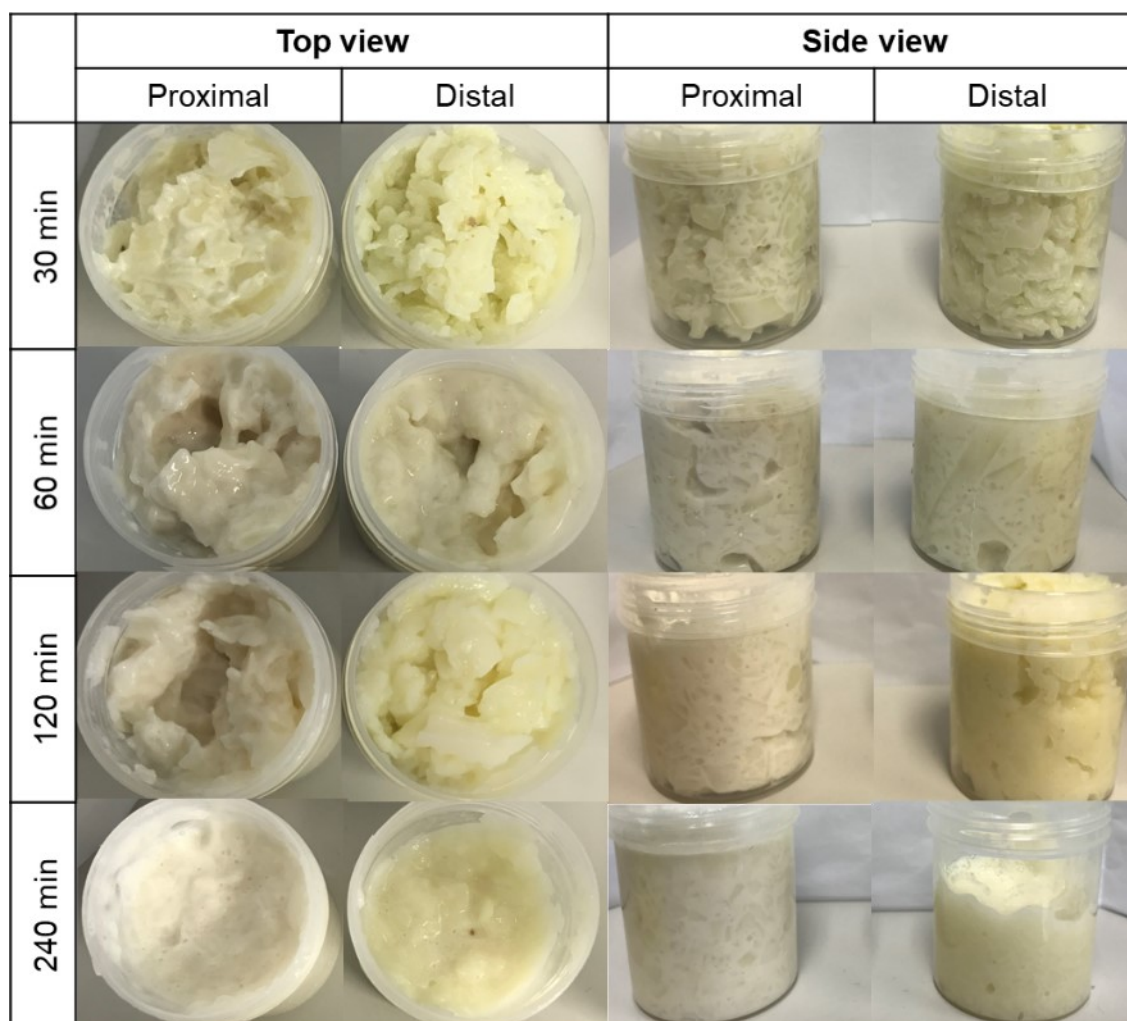


Figure B.5 Example photographs of proximal and distal gastric digesta of pigs fed with rice noodle after 30, 60, 120, and 240 min digestion time.

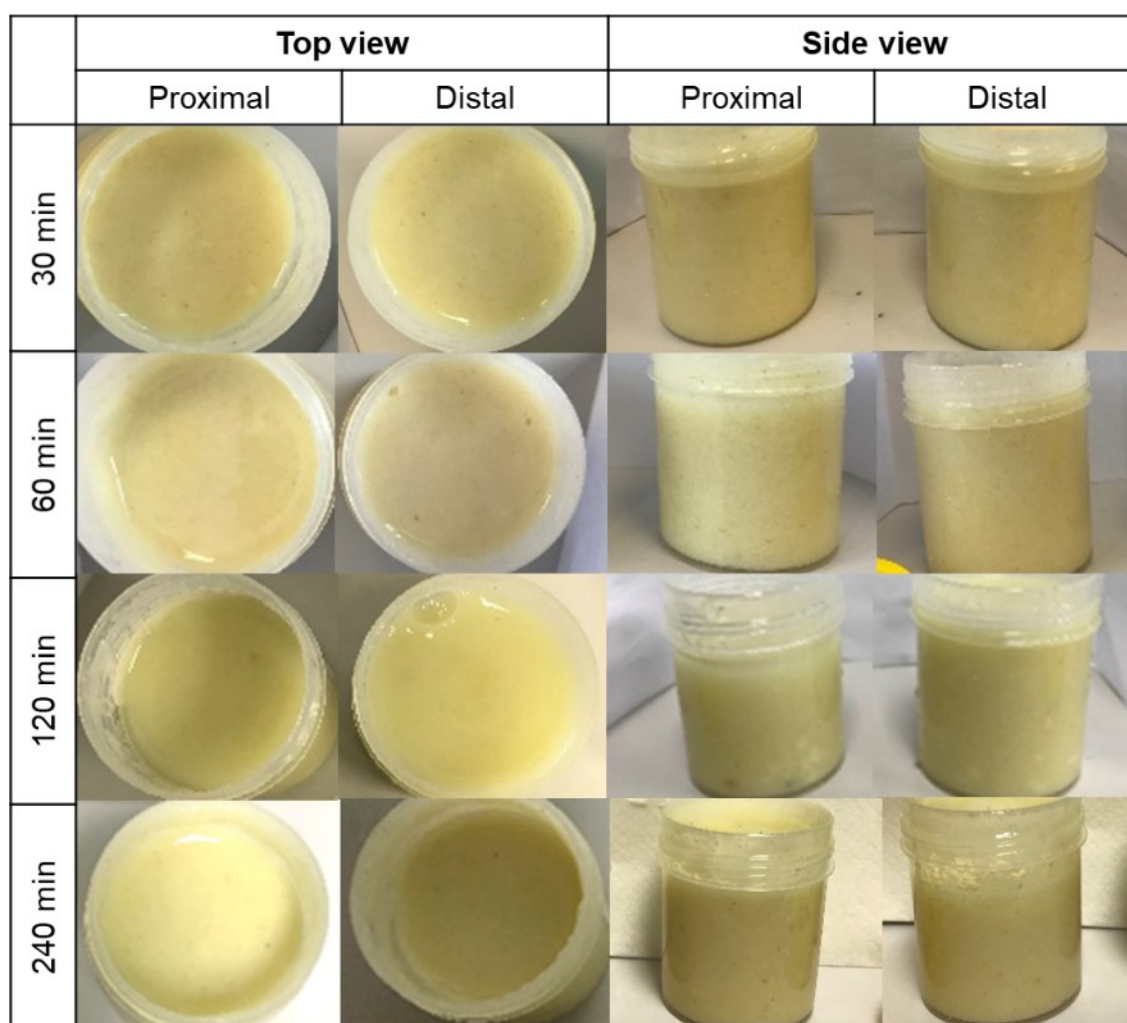


Figure B.6 Example photographs of proximal and distal gastric digesta of pigs fed with semolina after 30, 60, 120, and 240 min digestion time.

APPENDIX C

SUPPLEMENTARY MATERIALS TO CHAPTER 4

C.1 Supplementary Tables

Table C.1 Moisture content values of digesta from proximal and distal stomach regions over 240 min digestion (mean values \pm SE, $2 \leq n \leq 5$). Significantly different values within the same row (diet \times stomach region) are represented with superscripts zyx ($p < 0.05$); significantly different values within the same column (diet \times digestion time) are represented with superscripts abcd ($p < 0.05$).

Diet	Stomach region	Digestion time (min)			
		30	60	120	240
Semolina	Proximal	5.39 \pm 0.14 ^{a,x}	5.80 \pm 0.15 ^{a,yx}	9.10 \pm 2.08 ^{a,zy}	8.70 \pm 1.09 ^{a,z}
	Distal	5.81 \pm 0.12 ^{a,y}	6.10 \pm 0.15 ^{a,y}	7.28 \pm 1.10 ^{a,zy}	9.61 \pm 1.52 ^{a,z}
Couscous	Proximal	3.07 \pm 0.16 ^b	3.55 \pm 0.28 ^b	3.76 \pm 0.28 ^{bc}	4.76 \pm 0.51 ^b
	Distal	3.36 \pm 0.16 ^b	3.86 \pm 0.17 ^b	4.12 \pm 0.26 ^{bc}	4.99 \pm 0.41 ^b
Pasta	Proximal	2.54 \pm 0.09 ^b	2.72 \pm 0.06 ^b	3.07 \pm 0.10 ^{bc}	3.51 \pm 0.31 ^b
	Distal	2.77 \pm 0.09 ^b	3.12 \pm 0.07 ^b	3.44 \pm 0.16 ^{bc}	3.83 \pm 0.37 ^b
Rice grain	Proximal	2.50 \pm 0.10 ^b	2.52 \pm 0.07 ^b	2.84 \pm 0.18 ^{bc}	3.23 \pm 0.29 ^b
	Distal	2.98 \pm 0.16 ^b	3.01 \pm 0.10 ^b	3.40 \pm 0.15 ^{bc}	3.82 \pm 0.20 ^b
Rice couscous	Proximal	2.91 \pm 0.15 ^b	3.41 \pm 0.31 ^b	3.54 \pm 0.10 ^{bc}	4.19 \pm 0.32 ^b
	Distal	2.93 \pm 0.11 ^{b,y}	3.32 \pm 0.33 ^{b,zy}	3.82 \pm 0.18 ^{bc,zy}	4.80 \pm 0.61 ^{b,z}
Rice noodle	Proximal	2.40 \pm 0.11 ^b	2.69 \pm 0.11 ^b	2.80 \pm 0.06 ^c	3.27 \pm 0.23 ^b
	Distal	2.80 \pm 0.18 ^b	3.23 \pm 0.16 ^b	3.64 \pm 0.09 ^b	3.97 \pm 0.24 ^b

Table C.2 Correction factor calculation for correcting the effect of lubrication on H_0 . Data at 33 and 67% bulk compression strain were obtained from (Drechsler & Bornhorst, 2018).

Compression strain (%)	Lubricating agent	Hardness with lubrication: hardness without lubrication ratio				
		Brown Rice	Couscous	Orzo	Quinoa	White Rice
33	Water	2.00	2.61	4.18	1.53	1.50
	NES [§]	2.26	2.19	2.87	1.26	1.87
67	Water	1.75	2.01	3.71	2.27	0.97
	NES [§]	1.73	1.67	3.45	1.93	1.10
Approximated correction factor at 50% strain						
50	Water	1.88	2.31	3.94	1.90	1.24
	NES [§]	1.99	1.93	3.16	1.60	1.49
Average correction factor (Water and NES lubricated)		1.94	2.12	3.55	1.75	1.36
Averaged overall correction factor		2.14				

[§]NES: simulated saliva that contained mucins, without salivary enzymes.

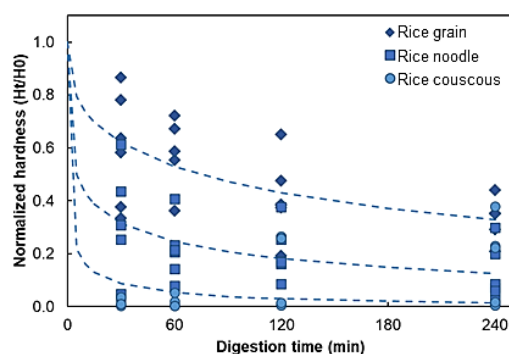
Table C.3 Hardness and normalized hardness values of undigested cooked diets and gastric digesta from proximal and distal stomach regions over 240 min digestion (mean values \pm SE, $4 \leq n \leq 6$) used for Weibull model fitting. For the digesta data (30 to 240 min), significantly different values within the same row (diet \times digestion time) are represented with superscripts abcd; significantly different values of within the same column (diet \times stomach region) are represented with superscripts zyx ($p < 0.05$).

Hardness (N)												
Diet	Semolina		Couscous		Pasta		Rice grain		Rice couscous		Rice noodle	
Time (min)	Proximal	Distal	Proximal	Distal	Proximal	Distal	Proximal	Distal	Proximal	Distal	Proximal	Distal
0*	5.51 \pm 1.47		52.09 \pm 7.10		29.40 \pm 5.13		66.71 \pm 6.40		67.24 \pm 7.82		38.80 \pm 1.30	
30	0.76 \pm 0.20 ^c	0.70 \pm 0.16 ^c	14.56 \pm 2.50 ^{bc,z}	7.80 \pm 0.76 ^{cde}	22.62 \pm 2.93 ^b	21.28 \pm 1.96 ^{bc}	39.63 \pm 5.57 ^{a,z}	42.87 \pm 1.89 ^{a,z}	1.17 \pm 0.40 ^{de}	1.22 \pm 0.36 ^{de}	12.88 \pm 3.64 ^{bcd}	23.66 \pm 4.02 ^b
60	0.45 \pm 0.06 ^d	0.30 \pm 0.04 ^d	9.99 \pm 2.55 ^{cd,zy}	3.01 \pm 0.25 ^d	20.42 \pm 1.08 ^{bc}	18.76 \pm 3.22 ^{bc}	38.68 \pm 4.14 ^{a,zy}	30.88 \pm 1.26 ^{ab,zy}	1.16 \pm 0.63 ^d	0.53 \pm 0.11 ^d	8.29 \pm 1.75 ^{cd}	11.35 \pm 1.52 ^{cd}
120	0.27 \pm 0.07 ^f	0.25 \pm 0.06 ^f	9.39 \pm 2.20 ^{cdef,zy}	2.47 \pm 0.30 ^{ef}	14.94 \pm 2.65 ^{bc}	14.90 \pm 1.67 ^{bc}	24.19 \pm 3.08 ^{b,y}	35.21 \pm 3.01 ^{a,zy}	6.32 \pm 3.60 ^{cdef}	2.56 \pm 1.44 ^{df}	7.87 \pm 1.58 ^{cdef}	14.17 \pm 1.43 ^{bce}
240	0.19 \pm 0.04 ^c	0.16 \pm 0.02 ^c	1.19 \pm 0.57 ^{c,y}	1.77 \pm 0.85 ^c	11.14 \pm 1.49 ^{bc}	9.04 \pm 1.85 ^{bc}	21.93 \pm 2.54 ^{ab,y}	26.38 \pm 3.05 ^{a,y}	6.45 \pm 3.57 ^c	3.78 \pm 1.87 ^c	4.78 \pm 1.66 ^c	9.65 \pm 2.73 ^c
Normalized hardness, H _t /H ₀												
Diet	Semolina		Couscous		Pasta		Rice grain		Rice couscous		Rice noodle	
Time (min)	Proximal	Distal	Proximal	Distal	Proximal	Distal	Proximal	Distal	Proximal	Distal	Proximal	Distal
0	1.00		1.00		1.00		1.00		1.00		1.00	
30	0.14 \pm 0.04 ^{de}	0.13 \pm 0.03 ^{de}	0.28 \pm 0.05 ^{cde}	0.15 \pm 0.01 ^{de}	0.68 \pm 0.04 ^{a,zy}	0.72 \pm 0.07 ^{a,z}	0.6 \pm 0.09 ^{ab}	0.58 \pm 0.07 ^{ab}	0.33 \pm 0.01 ^c	0.02 \pm 0.01 ^c	0.33 \pm 0.09 ^{bcd}	0.50 \pm 0.14 ^{abc}
60	0.09 \pm 0.01 ^d	0.05 \pm 0.01 ^d	0.19 \pm 0.05 ^{cd}	0.06 \pm 0.005 ^d	0.69 \pm 0.04 ^{a,z}	0.53 \pm 0.04 ^{ab,zy}	0.58 \pm 0.06 ^a	0.46 \pm 0.02 ^{abc}	0.21 \pm 0.01 ^d	0.01 \pm 0.001 ^d	0.21 \pm 0.05 ^{cd}	0.29 \pm 0.04 ^{bcd}
120	0.05 \pm 0.01 ^c	0.04 \pm 0.01 ^c	0.18 \pm 0.04 ^{bc}	0.05 \pm 0.01 ^c	0.58 \pm 0.06 ^{a,zy}	0.51 \pm 0.06 ^{a,zy}	0.41 \pm 0.06 ^{ab}	0.53 \pm 0.05 ^a	0.20 \pm 0.05 ^c	0.04 \pm 0.02 ^c	0.20 \pm 0.04 ^{bc}	0.39 \pm 0.04 ^{ab}
240	0.03 \pm 0.01 ^{bc}	0.03 \pm 0.004 ^{bc}	0.02 \pm 0.01 ^c	0.03 \pm 0.02 ^{bc}	0.38 \pm 0.05 ^{a,y}	0.31 \pm 0.06 ^{abc,y}	0.33 \pm 0.04 ^{ab}	0.40 \pm 0.05 ^a	0.12 \pm 0.06 ^{abc}	0.06 \pm 0.03 ^{bc}	0.12 \pm 0.04 ^{abc}	0.25 \pm 0.07 ^{abc}

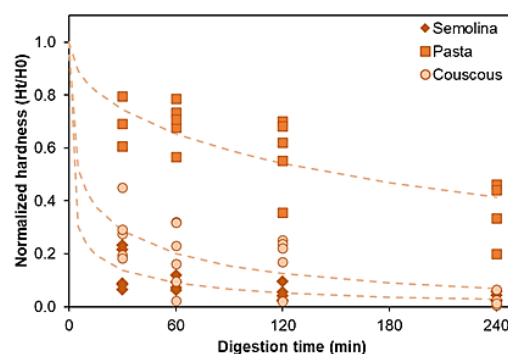
*Initial hardness of the diet multiplied with the correction factor of 2.14 (see Table C.2).

C.2 Supplementary Figures

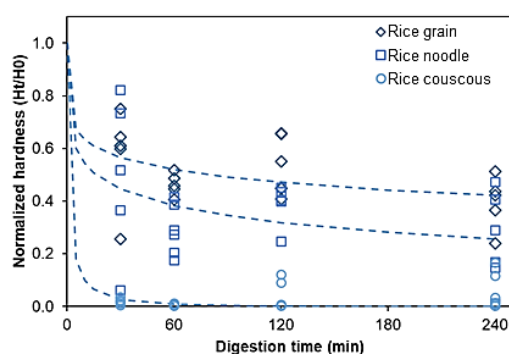
(A) Rice-based diets, proximal stomach



(B) Wheat-based diets, proximal stomach



(C) Rice-based diets, distal stomach



(D) Wheat-based diets, distal stomach

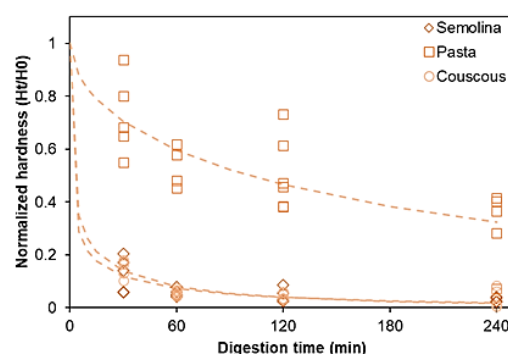


Figure C.1 Data spread of normalized hardness values of gastric digesta from (A-B) proximal and (C-D) distal stomach regions during 240 min digestion (total 252 data points). The predicted softening curves from average Weibull model parameters are represented as dashed lines. Rice- and wheat-based diets are represented as dark blue- and orange-colored data points and lines, respectively.

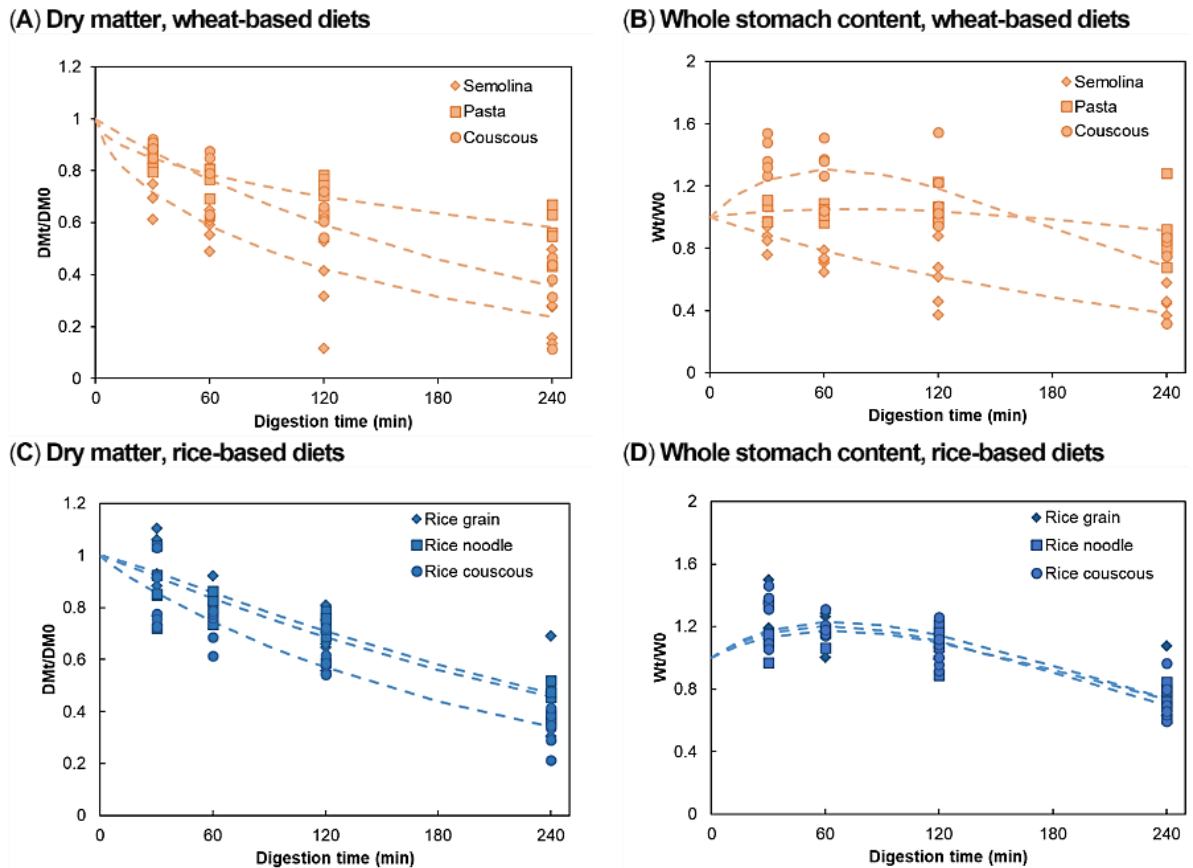


Figure C.2 Data spread of dry matter retention (A,C) and whole stomach content retention (B,D) during 240 min digestion (total 128 and 127 data points for dry matter retention and whole stomach content retention, respectively). The predicted softening curves from gastric emptying model parameters are represented by the dashed lines. Rice- and wheat-based diets are represented as blue- and orange-colored data points and lines, respectively.

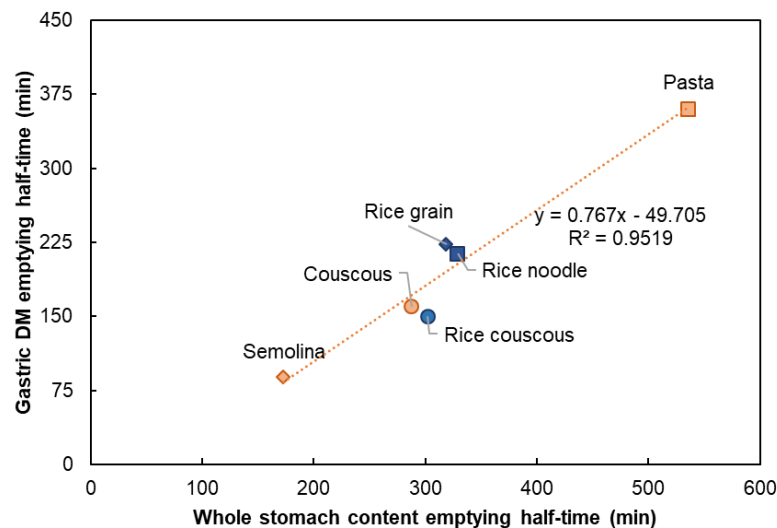


Figure C.3 Relationship between gastric dry matter emptying half- time ($t_{1/2,DM\ GE}$) and whole stomach content emptying half- time ($t_{1/2,whole\ GE}$).

APPENDIX D

SUPPLEMENTARY MATERIALS TO CHAPTER 5

D.1 Supplementary Tables

Table D.1 Averaged pH values of digesta from different diets at different measurement locations and digestion times (to establish pH colormaps in Figure 5.4A). Values are presented as mean \pm SE ($4 \leq n \leq 6$ for each diet \times digestion time \times measurement location).

		Diet					
	Time (min)	Semolina	Couscous	Pasta	Rice grain	Rice couscous	Rice noodle
Location 1	30	4.20 \pm 0.44	3.54 \pm 0.72	3.55 \pm 0.74	3.79 \pm 0.33	5.00 \pm 0.21	4.38 \pm 0.93
	60	2.98 \pm 0.41	2.80 \pm 0.51	2.25 \pm 0.47	2.54 \pm 0.52	3.84 \pm 0.47	2.85 \pm 0.71
	120	2.28 \pm 0.44	1.72 \pm 0.19	1.74 \pm 0.25	1.62 \pm 0.11	2.21 \pm 0.14	1.47 \pm 0.11
	240	1.82 \pm 0.34	1.93 \pm 0.45	1.82 \pm 0.39	1.88 \pm 0.32	1.41 \pm 0.10	1.61 \pm 0.13
Location 2	30	4.40 \pm 0.41	4.22 \pm 0.9	4.24 \pm 0.84	4.97 \pm 0.57	4.79 \pm 0.19	5.25 \pm 0.81
	60	3.59 \pm 0.57	2.92 \pm 0.67	2.33 \pm 0.51	2.11 \pm 0.27	3.80 \pm 0.62	3.47 \pm 0.73
	120	2.97 \pm 0.75	2.59 \pm 0.46	1.74 \pm 0.23	2.21 \pm 0.42	2.14 \pm 0.12	1.40 \pm 0.14
	240	1.81 \pm 0.35	1.85 \pm 0.45	1.79 \pm 0.21	1.89 \pm 0.37	1.33 \pm 0.12	1.60 \pm 0.14
Location 3	30	4.35 \pm 0.96	2.58 \pm 0.32	2.91 \pm 0.67	2.11 \pm 0.48	5.91 \pm 0.38	2.64 \pm 0.94
	60	4.82 \pm 0.58	2.17 \pm 0.40	1.71 \pm 0.40	1.51 \pm 0.24	5.43 \pm 0.61	1.37 \pm 0.12
	120	4.39 \pm 1.24	1.53 \pm 0.21	1.37 \pm 0.11	1.31 \pm 0.12	2.18 \pm 0.19	0.93 \pm 0.07
	240	1.74 \pm 0.33	1.74 \pm 0.43	1.41 \pm 0.13	1.29 \pm 0.07	1.28 \pm 0.10	1.40 \pm 0.12
Location 4	30	6.39 \pm 0.20	4.99 \pm 0.78	5.26 \pm 0.52	4.78 \pm 0.95	6.05 \pm 0.22	4.26 \pm 0.90
	60	5.88 \pm 0.39	3.41 \pm 0.72	3.96 \pm 1.14	4.28 \pm 0.69	4.65 \pm 0.84	1.58 \pm 0.20
	120	3.60 \pm 1.13	2.25 \pm 0.67	2.11 \pm 0.34	2.47 \pm 0.55	2.13 \pm 0.21	1.33 \pm 0.37
	240	1.78 \pm 0.38	1.7 \pm 0.43	1.69 \pm 0.37	1.29 \pm 0.06	1.27 \pm 0.11	1.51 \pm 0.18
Location 5	30	5.28 \pm 0.85	1.74 \pm 0.27	2.84 \pm 0.87	3.60 \pm 0.81	5.49 \pm 0.49	3.23 \pm 0.96
	60	3.94 \pm 0.42	1.86 \pm 0.38	1.45 \pm 0.21	1.58 \pm 0.19	4.45 \pm 0.56	1.59 \pm 0.27
	120	2.33 \pm 0.50	1.63 \pm 0.32	1.37 \pm 0.14	1.33 \pm 0.14	2.19 \pm 0.16	0.83 \pm 0.05
	240	1.76 \pm 0.38	1.82 \pm 0.46	1.31 \pm 0.12	1.13 \pm 0.04	1.26 \pm 0.11	1.36 \pm 0.13
Location 6	30	6.56 \pm 0.14	6.44 \pm 0.34	6.13 \pm 0.5	6.22 \pm 0.38	4.97 \pm 0.58	6.48 \pm 0.21
	60	5.78 \pm 0.37	4.38 \pm 0.46	4.62 \pm 0.86	5.08 \pm 0.75	4.95 \pm 0.66	6.50 \pm 0.14
	120	2.97 \pm 0.86	3.02 \pm 0.62	3.93 \pm 0.84	4.83 \pm 1.09	2.22 \pm 0.28	2.27 \pm 0.63
	240	1.91 \pm 0.52	1.88 \pm 0.46	2.18 \pm 0.41	2.23 \pm 0.61	1.28 \pm 0.12	2.75 \pm 0.51
Location 7	30	6.26 \pm 0.43	6.59 \pm 0.23	6.72 \pm 0.1	6.96 \pm 0.06	5.51 \pm 0.89	6.87 \pm 0.10
	60	5.88 \pm 0.25	6.71 \pm 0.07	6.00 \pm 0.61	6.72 \pm 0.13	4.65 \pm 0.66	6.70 \pm 0.09
	120	3.44 \pm 1.02	5.36 \pm 0.67	5.97 \pm 0.32	6.23 \pm 0.32	2.29 \pm 0.13	5.20 \pm 0.67
	240	1.97 \pm 0.57	1.87 \pm 0.45	4.45 \pm 0.64	3.42 \pm 0.52	1.26 \pm 0.11	3.8 \pm 0.35
Location 8	30	6.69 \pm 0.09	6.38 \pm 0.27	6.65 \pm 0.15	6.71 \pm 0.21	5.45 \pm 0.69	6.94 \pm 0.07
	60	5.66 \pm 0.54	6.68 \pm 0.11	6.78 \pm 0.06	6.26 \pm 0.26	3.87 \pm 0.69	6.79 \pm 0.05
	120	3.30 \pm 1.00	5.23 \pm 0.92	5.88 \pm 0.28	6.08 \pm 0.29	2.27 \pm 0.08	6.32 \pm 0.25
	240	1.89 \pm 0.48	1.94 \pm 0.47	4.89 \pm 0.77	4.04 \pm 0.61	1.28 \pm 0.12	4.58 \pm 0.50
Location 9	30	5.65 \pm 0.66	6.50 \pm 0.17	6.78 \pm 0.07	6.99 \pm 0.02	5.33 \pm 0.30	7.03 \pm 0.06
	60	5.51 \pm 0.28	5.87 \pm 0.36	6.72 \pm 0.05	6.58 \pm 0.35	5.05 \pm 0.57	6.57 \pm 0.15
	120	4.33 \pm 1.21	4.97 \pm 0.8	5.07 \pm 0.57	5.66 \pm 0.28	2.19 \pm 0.18	5.88 \pm 0.57
	240	1.85 \pm 0.45	1.89 \pm 0.48	4.21 \pm 0.91	3.58 \pm 0.54	1.26 \pm 0.12	3.50 \pm 0.75

(continued)

		Diet					
	Time (min)	Semolina	Couscous	Pasta	Rice grain	Rice couscous	Rice noodle
Location 10	30	6.57 ± 0.15	6.62 ± 0.19	6.66 ± 0.12	7.04 ± 0.04	5.61 ± 0.61	6.90 ± 0.04
	60	5.78 ± 0.30	6.50 ± 0.08	6.71 ± 0.03	6.61 ± 0.27	5.09 ± 0.56	6.62 ± 0.11
	120	3.33 ± 1.01	4.58 ± 0.76	5.27 ± 0.30	6.09 ± 0.30	2.12 ± 0.10	5.79 ± 0.31
	240	1.98 ± 0.58	1.83 ± 0.48	3.90 ± 0.67	3.08 ± 0.58	1.26 ± 0.11	3.24 ± 0.72

Table D.2 Additional particle size distribution parameters (mean \pm SE, $4 \leq n \leq 6$) of *in vivo* gastric digesta from the proximal or distal region. For each particle size parameter, values that are significantly different within the same row (diet \times digestion time) are noted by superscripts abcd ($p < 0.05$). No significant difference was found between values across digestion times (i.e., data within the same column (diet \times stomach region)).

	Semolina		Couscous		Pasta		Rice grain		Rice couscous		Rice noodle	
Time (min)	Proximal	Distal	Proximal	Distal	Proximal	Distal	Proximal	Distal	Proximal	Distal	Proximal	Distal
d₁₀ (μm)												
30	19.3 \pm 1.44 ^a	16.9 \pm 1.38 ^a	10.5 \pm 0.68 ^{abc}	8.23 \pm 1.88 ^{bcd}	14.4 \pm 1.02 ^{ab}	10.3 \pm 0.58 ^{abc}	8.00 \pm 0.57 ^{cde}	8.01 \pm 1.48 ^{cd}	5.59 \pm 0.30 ^{ef}	5.00 \pm 0.30 ^f	6.40 \pm 0.56 ^{def}	6.94 \pm 0.46 ^{cde}
60	15.3 \pm 0.47 ^a	14.3 \pm 0.87 ^{ab}	8.95 \pm 0.54 ^{abcd}	8.31 \pm 1.55 ^{bcd}	12.2 \pm 0.93 ^{ab}	10.4 \pm 0.52 ^{abc}	7.39 \pm 0.74 ^{cdef}	7.77 \pm 0.64 ^{cdef}	6.04 \pm 0.36 ^{ef}	5.90 \pm 0.40 ^f	6.26 \pm 0.14 ^{def}	6.96 \pm 0.46 ^{def}
120	15.8 \pm 0.45 ^a	15.6 \pm 0.77 ^a	8.94 \pm 0.51 ^{abc}	7.96 \pm 0.44 ^{bcd}	11.2 \pm 0.85 ^{ab}	9.38 \pm 0.41 ^{abc}	7.51 \pm 0.58 ^{cde}	7.65 \pm 0.33 ^{bcd}	6.37 \pm 0.47 ^{de}	5.88 \pm 0.24 ^e	6.06 \pm 0.24 ^{de}	8.12 \pm 0.98 ^{bcd}
240	14.2 \pm 0.77 ^a	13.8 \pm 0.60 ^a	15.6 \pm 6.08 ^{ab}	9.9 \pm 0.9 ^{ab}	10.8 \pm 1.19 ^{ab}	9.28 \pm 0.29 ^{ab}	6.52 \pm 0.35 ^{cd}	7.52 \pm 0.23 ^{bc}	5.40 \pm 0.21 ^d	5.17 \pm 0.96 ^d	5.99 \pm 0.10 ^{cd}	6.14 \pm 0.29 ^{cd}
d₅₀ (μm)												
30	169.6 \pm 42.3 ^{ac}	92.6 \pm 13.1 ^{acd}	57.8 \pm 19.4 ^{abc}	30.8 \pm 6.98 ^{bc}	132.2 \pm 25.8 ^{ac}	43.9 \pm 6.72 ^{bc}	129.8 \pm 18.3 ^c	88.6 \pm 16.8 ^c	47.2 \pm 2.86 ^{abcde}	24.6 \pm 4.74 ^e	31.9 \pm 5.57 ^{bde}	32.5 \pm 4.69 ^{bc}
60	51.0 \pm 3.44 ^{abd}	45.8 \pm 3.87 ^{abd}	36.0 \pm 2.26 ^{abd}	34.1 \pm 6.49 ^{bd}	76.7 \pm 23.8 ^{abd}	42.9 \pm 3.83 ^{abd}	130.1 \pm 30.2 ^a	79.2 \pm 4.58 ^{ac}	45.3 \pm 7.61 ^{abd}	35.6 \pm 6.55 ^{bd}	31.2 \pm 1.95 ^{bcd}	30.8 \pm 4.04 ^d
120	70.7 \pm 18.9 ^{abc}	58.8 \pm 6.92 ^{abc}	41.6 \pm 6.73 ^{abc}	34.1 \pm 3.59 ^c	51.7 \pm 10.7 ^{abc}	40.3 \pm 2.30 ^{bc}	114.4 \pm 20.6 ^a	75.9 \pm 5.77 ^{ab}	31.6 \pm 2.95 ^{bc}	31.0 \pm 3.71 ^c	27.3 \pm 3.12 ^c	36.1 \pm 6.67 ^c
240	57.8 \pm 5.50 ^{ab}	55.4 \pm 5.11 ^a	118.1 \pm 53.4 ^a	68.8 \pm 28.0 ^a	54.2 \pm 18.4 ^{ab}	39.2 \pm 2.05 ^{ab}	82.0 \pm 18.4 ^a	61.9 \pm 3.46 ^a	27.0 \pm 7.24 ^{ab}	21.7 \pm 4.42 ^b	24.7 \pm 2.26 ^{ab}	22.3 \pm 2.98 ^b
d₉₀ (μm)												
30	788.3 \pm 90.8 ^{ab}	736.9 \pm 62.3 ^{ab}	651.0 \pm 122.7 ^{ab}	288.4 \pm 85.9 ^{bc,y}	682.2 \pm 94.3 ^{ab}	381.4 \pm 89.6 ^{bc}	729.2 \pm 79 ^{ab}	849 \pm 157.1 ^a	256.8 \pm 39.9 ^{bc}	128.8 \pm 14.6 ^c	248.4 \pm 134.2 ^c	356.5 \pm 186.6 ^{bc}
60	552.4 \pm 61.0 ^{abd}	450.7 \pm 110.6 ^{abde}	438.9 \pm 47.9 ^{abd}	472.8 \pm 101.6 ^{abd,zy}	442.1 \pm 69.7 ^{abd}	230.7 \pm 31.0 ^{bcd}	749.4 \pm 129.4 ^{ac}	790.4 \pm 69.9 ^a	261.1 \pm 46.1 ^{bcd}	188.9 \pm 32.9 ^{de}	121.8 \pm 7.83 ^c	274.3 \pm 89.5 ^{bde}
120	602.1 \pm 55.0 ^{abc}	613.1 \pm 51.1 ^{abc}	506.6 \pm 143.9 ^{abc}	581.5 \pm 132.7 ^{abc,zy}	319.3 \pm 65.4 ^{bcd}	190.6 \pm 19.4 ^{cd}	730.4 \pm 98.3 ^{ab}	852.7 \pm 13.4 ^a	513.2 \pm 112.2 ^{abc}	583.9 \pm 151.2 ^{abc}	138.6 \pm 15.3 ^d	220.8 \pm 31.4 ^{cd}
240	622.3 \pm 28.4 ^{abdf}	623.7 \pm 36.8 ^{abdf}	933.8 \pm 118.4 ^a	908.1 \pm 149.1 ^{ac,z}	328 \pm 80.1 ^{bcddeg}	230.4 \pm 32.8 ^{efg}	770.9 \pm 81.7 ^{abdf}	852.2 \pm 58.2 ^{abd}	411.7 \pm 139.3 ^{bdeg}	321.5 \pm 98.3 ^{deg}	224.1 \pm 78.6 ^g	235.1 \pm 117.7 ^{eg}

Table D.3 Location, % volume, and particle distribution spread of each peak in the averaged particle size distribution curves of *in vivo* gastric digesta (Figure 5.12-5.13) from the proximal (Prox) or distal (Dist). The parameters were determined through fitting to a lognormal function on DistFit software (DistFit™, Chimera Technologies Inc., USA).

Diet	Time (min)	Region	Mode 1			Mode 2			Mode 3			Mode 4		
			%volume	Peak location (μm)	Spread	%volume	Peak location (μm)	Spread	%volume	Peak location (μm)	Spread	%volume	Peak location (μm)	Spread
Semolina	30	Prox	3.80	6.8	1.65	49.0	44.4	2.15	47.6	509.5	1.80	-	-	-
		Dist	9.07	9.4	1.82	49.2	42.1	1.77	41.9	510.2	1.73	-	-	-
	60	Prox	13.9	8.9	1.85	58.7	40.3	1.77	27.5	436.0	1.83	-	-	-
		Dist	11.7	8.8	1.9	66.8	38.8	1.73	21.5	393.7	1.77	-	-	-
	120	Prox	8.88	8.9	1.83	58.2	40.8	1.76	33.1	466.2	1.74	-	-	-
		Dist	9.21	8.0	1.78	58.2	40.9	1.80	33.0	507.9	1.89	-	-	-
	240	Prox	8.45	7.9	1.77	56.6	38.1	1.85	35.1	456.0	1.72	-	-	-
		Dist	9.56	8.3	1.82	57.5	38.3	1.82	33.1	471.6	1.75	-	-	-
Couscous	30	Prox	8.01	5.5	1.74	52.3	26.2	1.81	28	245.9	2.06	11.9	834.4	1.60
		Dist	16.1	7.1	1.87	63.6	29.0	1.75	20.5	291.9	2.21	-	-	-
	60	Prox	10.2	5.6	1.71	58.9	26.6	1.81	31	303.3	2.20	-	-	-
		Dist	12.4	6.1	1.72	64.1	29.3	1.85	23.7	410.8	1.99	-	-	-
	120	Prox	12.3	6.3	1.79	56.8	28.0	1.78	31.4	355.6	2.36	-	-	-
		Dist	16.1	6.8	1.82	60.1	29.2	1.79	13.4	333.7	1.88	10.8	867.9	1.55
	240	Prox	9.34	6.1	1.77	44.3	28.0	1.82	20.3	267.7	2.13	26.7	837.4	1.58
		Dist	10.8	6.8	1.74	52.9	28.7	1.84	14.7	355.7	2.05	22.2	918.6	1.54
Pasta	30	Prox	4.80	5.1	1.74	35.6	27.0	1.87	60.3	304.3	2.4	-	-	-
		Dist	11.0	6.8	1.88	62	32.2	1.86	27.2	297.1	2.25	-	-	-
	60	Prox	4.82	4.6	1.65	51.1	28.3	1.98	44.2	258.0	2.03	-	-	-
		Dist	9.91	6.6	1.76	70.6	37.2	2.01	19.6	226.8	1.98	-	-	-
	120	Prox	7.45	5.4	1.76	61.6	29.8	1.88	31.1	246.8	2.00	-	-	-
		Dist	12.9	7.0	1.84	68.9	37.1	1.99	18.4	196.3	1.96	-	-	-
	240	Prox	9.66	6.2	1.90	59.7	29.9	1.86	30.8	243.3	2.18	-	-	-
		Dist	12.1	6.6	1.81	67.8	35.1	1.95	20.3	219.5	2.16	-	-	-

(continued)

Diet	Time (min)	Region	Mode 1			Mode 2			Mode 3			Mode 4		
			%volume	Peak location (μm)	Spread	%volume	Peak location (μm)	Spread	%volume	Peak location (μm)	Spread	%volume	Peak location (μm)	Spread
Rice grain	30	Prox	23.6	8.9	2.18	56.9	132.5	2.9	20.3	613.0	1.82	-	-	-
		Dist	33.5	12.4	2.26	49.5	132.9	2.75	17.7	847.0	1.6	-	-	-
	60	Prox	5.95	4.4	1.58	17.6	11.9	2.08	51.4	140.6	3.32	26.3	866.8	1.61
		Dist	36.9	13.3	2.45	40.1	131.9	2.6	23.4	762.6	1.66	-	-	-
	120	Prox	25.8	9.7	2.23	52.1	117.3	3.04	23	720.1	1.7	-	-	-
		Dist	40.8	14.6	2.38	36.9	152.8	2.74	23	689.2	1.73	-	-	-
	240	Prox	32.4	10.6	2.22	42.2	138.8	2.98	26.3	794.3	1.64	-	-	-
		Dist	43.8	14.5	2.47	36	137.0	2.59	20.7	839.1	1.61	-	-	-
Rice couscous	30	Prox	9.38	4.7	1.56	31.4	11.3	1.89	51.5	85.7	1.97	7.75	429.0	1.44
		Dist	41.3	7.7	1.87	43.8	46.9	2.79	15.2	85.3	1.58	-	-	-
	60	Prox	8.05	4.9	1.58	37.4	12.5	1.96	45.7	86.7	1.97	8.94	425.5	1.64
		Dist	42.2	9.5	1.98	48.8	75.5	2.78	9.31	88.8	1.5	-	-	-
	120	Prox	43.6	12.1	2.16	34.4	70.3	2.21	22.1	548.3	1.77	-	-	-
		Dist	39.8	10.9	2.1	33.2	60.0	2.98	27.8	723.1	1.72	-	-	-
	240	Prox	50.1	10.1	2.08	33.4	46.4	2.66	16.8	506.3	1.83	-	-	-
		Dist	51	9.9	2.1	38.3	51.9	2.93	11	450.4	1.71	-	-	-
Rice noodle	30	Prox	43.4	10.3	2.02	53	58.4	2.11	3.98	862.1	1.74	-	-	-
		Dist	27.5	10.2	1.99	67.3	46.1	2.85	5.44	916.6	1.66	-	-	-
	60	Prox	53.9	12.8	2.24	44.7	70.7	1.82	1.58	583.8	1.58	-	-	-
		Dist	38.0	11.7	2.01	46.5	59.6	2.51	15.8	525.5	1.82	-	-	-
	120	Prox	51.7	11.4	2.11	44.8	61.4	2.11	3.76	605.7	1.88	-	-	-
		Dist	30.2	12.3	2.01	70.1	58.3	3.43	-	-	-	-	-	-
	240	Prox	58.7	12.4	2.15	37.2	66.9	2.14	4.43	749.7	1.65	-	-	-
		Dist	56.2	12.4	2.07	40.8	52.0	3.12	3.46	959.6	1.53	-	-	-

Table D.4 Starch content of the proximal and distal gastric digesta, quantified in freeze-dried samples (mean \pm SE, $4 \leq n \leq 6$). Values that are significantly different within the same column (digestion time) are noted by superscripts abcde ($p < 0.05$). Values that are significantly different within the same row (diet \times stomach region) are noted by superscripts zyxw ($p < 0.05$).

Diet	Region	Starch content (g/100 g DM)			
		30 min	60 min	120 min	240 min
Semolina	Proximal	59.42 \pm 1.87 ^d	62.97 \pm 0.99 ^{cde}	57.17 \pm 1.6 ^d	57.96 \pm 2.57 ^d
	Distal	57.73 \pm 0.92 ^d	58.66 \pm 0.79 ^e	59.00 \pm 0.35 ^{cd}	56.88 \pm 0.59 ^d
Couscous	Proximal	63.15 \pm 2.09 ^{cd}	60.49 \pm 1.02 ^e	64.3 \pm 1.03 ^{cd}	63.36 \pm 1.56 ^{bcd}
	Distal	63.10 \pm 1.02 ^{cd}	62.88 \pm 1.23 ^{de}	61.96 \pm 1.2 ^{cd}	62.31 \pm 1.32 ^{cd}
Pasta	Proximal	64.55 \pm 1.05 ^{bcd}	66.62 \pm 1.61 ^{bcde}	65.32 \pm 1.03 ^{bc}	64.06 \pm 1.77 ^{bcd}
	Distal	62.53 \pm 1.36 ^{cd}	63.97 \pm 2.04 ^{cde}	63.80 \pm 1.01 ^{cd}	64.3 \pm 1.09 ^{abcd}
Rice grain	Proximal	70.25 \pm 2.60 ^{abc,zy}	71.75 \pm 2.42 ^{abc,zy}	75.52 \pm 1.69 ^{a,z}	67.62 \pm 3.95 ^{abc,y}
	Distal	69.56 \pm 1.81 ^{abc,y}	75.21 \pm 2.12 ^{ab,zy}	77.11 \pm 1.39 ^{a,z}	69.06 \pm 3.06 ^{abc,y}
Rice couscous	Proximal	75.75 \pm 1.23 ^a	74.39 \pm 1.57 ^{ab}	72.39 \pm 2.13 ^{ab}	72.85 \pm 1.53 ^a
	Distal	74.57 \pm 1.62 ^a	69.62 \pm 1.74 ^{abcd}	72.23 \pm 1.68 ^{ab}	69.22 \pm 3.13 ^{abc}
Rice noodle	Proximal	73.86 \pm 1.69 ^{ab,zy}	74.50 \pm 0.96 ^{ab,zy}	77.28 \pm 1.11 ^{a,z}	69.06 \pm 2.33 ^{abc,y}
	Distal	73.75 \pm 1.46 ^{ab,zy}	75.25 \pm 1.45 ^{a,zy}	77.67 \pm 0.67 ^{a,z}	70.40 \pm 1.03 ^{ab,y}

D.2 Supplementary Figures

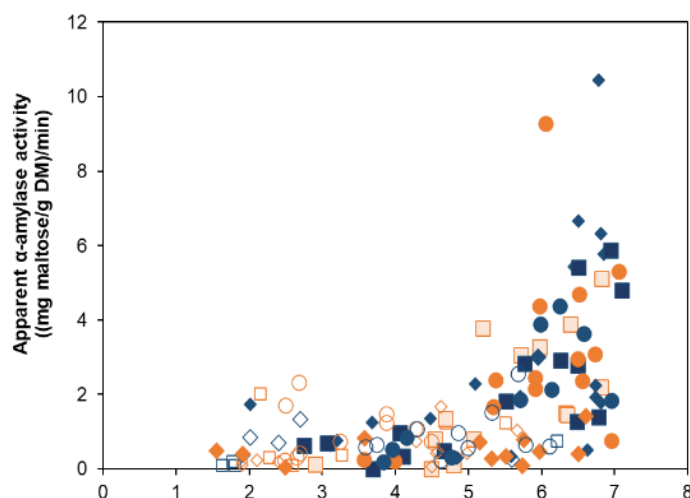


Figure D.1 Apparent salivary amylase activity in the gastric digesta of pigs fed with pasta or rice noodle (■□), semolina or rice grain (▲△), and couscous or rice couscous (●○). Rice- and wheat-based diets are indicated by blue and orange-colored data points, respectively. Filled (■▲●) and void (□△○) symbols represented data points from the proximal and distal stomach, respectively. Each data point represents one pig which is one diet \times time combination ($n = 215$ data points)

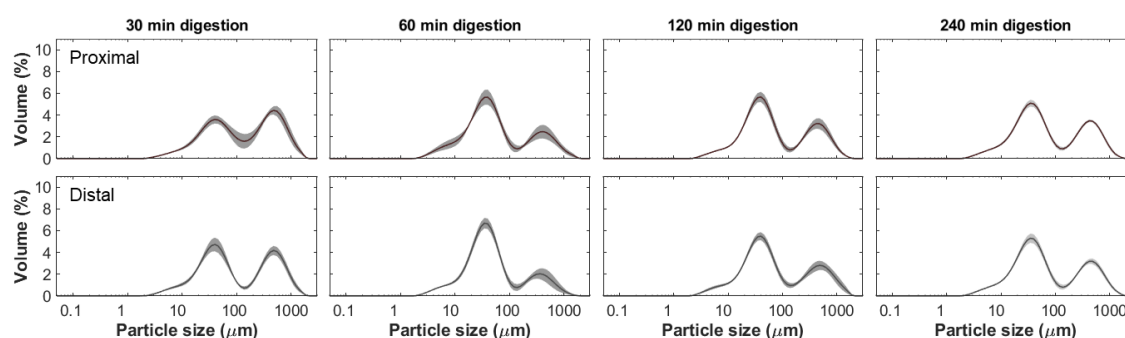


Figure D.2 Individual plots for particle size distribution of semolina digesta in the proximal (first row) and distal stomach (second row) at different digestion times. Figures within the same column correspond to the same digestion time, as indicated on the top of the first-row figures. The standard error of each curve is indicated by error shades around the line.

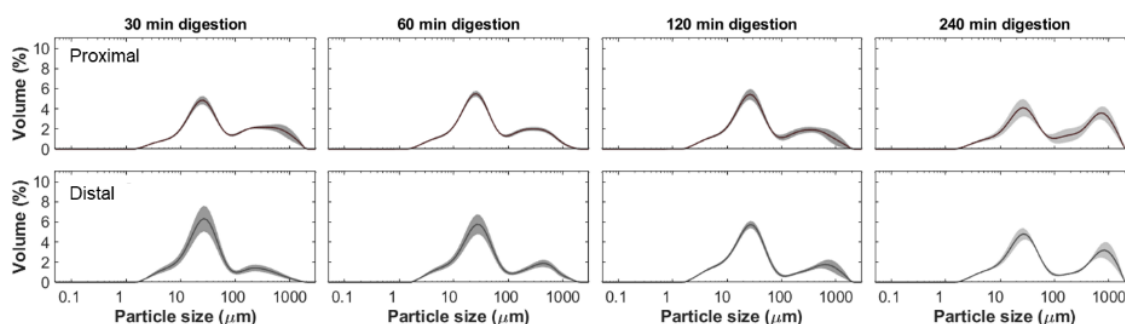


Figure D.3 Individual plots for particle size distribution of couscous digesta in the proximal (first row) and distal stomach (second row) at different digestion times. Figures within the same column correspond to the same digestion time, as indicated on the top of the first-row figures. The standard error of each curve is indicated by error shades around the line.

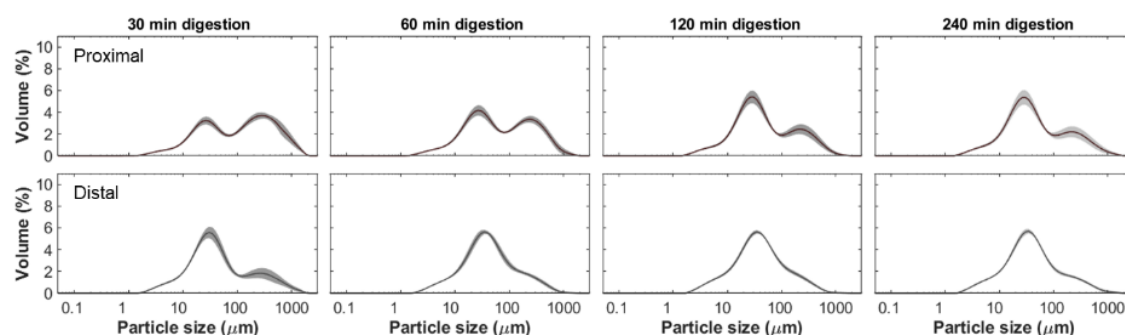


Figure D.4 Individual plots for particle size distribution of pasta digesta in the proximal (first row) and distal stomach (second row) at different digestion times. Figures within the same column correspond to the same digestion time, as indicated on the top of the first-row figures. The standard error of each curve is indicated by error shades around the line.

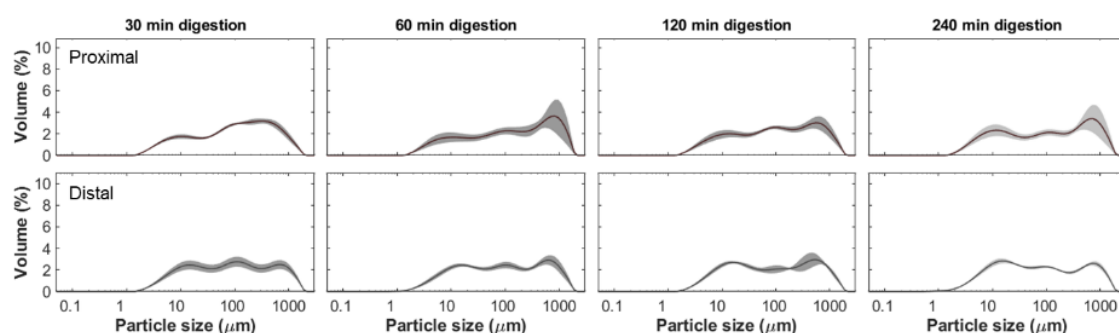


Figure D.5 Individual plots for particle size distribution of rice grain digesta in the proximal (first row) and distal stomach (second row) at different digestion times. Figures within the same column correspond to the same digestion time, as indicated on the top of the first-row figures. The standard error of each curve is indicated by error shades around the line.

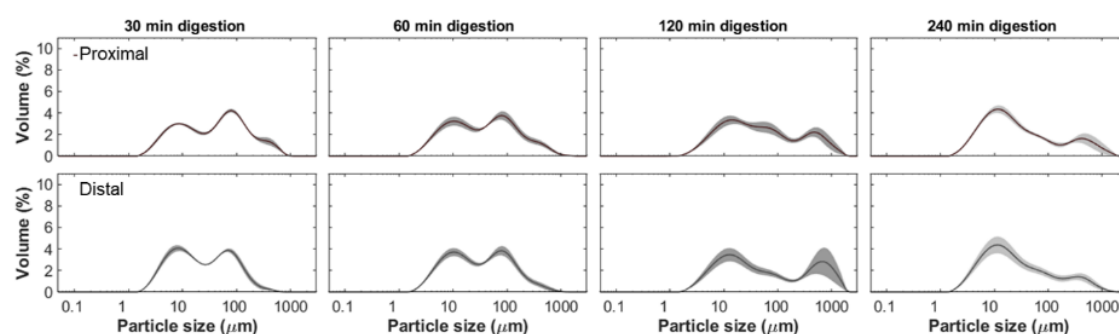


Figure D.6 Individual plots for particle size distribution of rice couscous digesta in the proximal (first row) and distal stomach (second row) at different digestion times. Figures within the same column correspond to the same digestion time, as indicated on the top of the first-row figures. The standard error of each curve is indicated by error shades around the line.

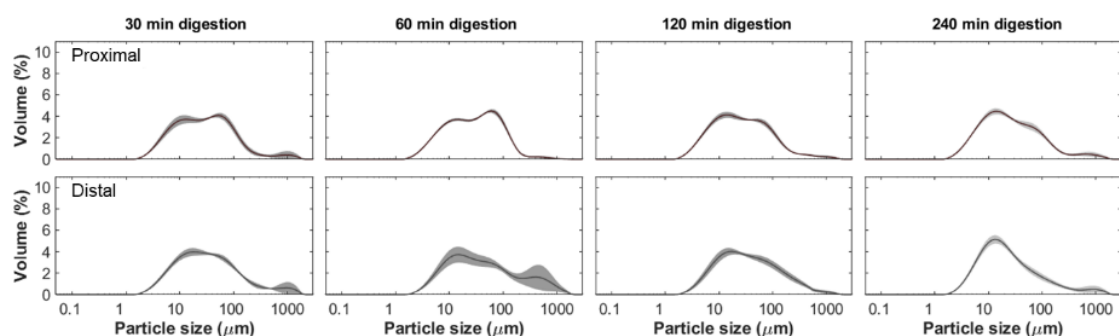


Figure D.7 Individual plots for particle size distribution of rice noodle digesta in the proximal (first row) and distal stomach (second row) at different digestion times. Figures within the same column correspond to the same digestion time, as indicated on the top of the first-row figures. The standard error of each curve is indicated by error shades around the line.

APPENDIX E

SUPPLEMENTARY MATERIALS TO CHAPTER 6

E.1 Supplementary Tables

Table E.1 Particle size distribution parameters of the intestinal digesta retrieved from the duodenum and terminal ileum (mean \pm SE, $n \leq 6$). Missing values (indicated with “-”) were due to obscuration $<2\%$, which would generate unreliable data for analysis (Sotomayor & Schalkwijk, 2020). Data from a single replicate are marked with “*”.

Region	Time (min)	Diet					
		Semolina	Couscous	Pasta	Rice grain	Rice couscous	Rice noodle
D[4,3] (μm)							
Duodenum	30	384.5 ± 24.5	*695.4	*177.4	385.5 ± 54.1	309.7 ± 51.7	275.1 ± 48.4
	60	316.1 ± 28.3	494.7 ± 53.4	*185.0	*428.8	287.6 ± 46.4	*58.8
	120	335.4 ± 45.0	*727	*74.0	454.3 ± 63.5	119.2 ± 16.0	*214.1
	240	*360.8	621.6 ± 63.0	*377.0	-	-	-
Terminal ileum	30	-	*723.5	134.4 ± 14.1	586.1 ± 50.4	*48.3	95.5 ± 49.0
	60	-	407.4 ± 256.3	137.2 ± 11.5	626.5 ± 54.9	71.4 ± 19.1	65.8 ± 26.1
	120	387.8 ± 14.2	674.4 ± 24.1	151.4 ± 11.6	614.0 ± 66.4	85.5 ± 25.9	77.1 ± 39.2
	240	402.2 ± 15.2	669 ± 31.2	214.7 ± 92.1	384.6 ± 147.9	100.1 ± 37.8	47.6 ± 4.32
D[3,2] (μm)							
Duodenum	30	54.9 ± 9.66	*66.1	*46.9	58.3 ± 5.56	23.6 ± 2.93	35.1 ± 10.2
	60	46.3 ± 12.1	48.9 ± 14.4	*23.9	*32.1	21.5 ± 2.83	*13.6
	120	41.2 ± 0.03	*84.7	*17.8	34.9 ± 7.96	15.0 ± 0.89	*39.2
	240	*40.0	65.9 ± 11.0	*50.8	-	-	-
Terminal ileum	30	-	*78.2	21.8 ± 0.89	40.8 ± 6.26	*7.35	13.3 ± 2.44
	60	-	138.3 ± 118.7	22.7 ± 0.80	42.7 ± 4.99	7.7 ± 2.5	8.94 ± 2.46
	120	74.6 ± 15.9	79.3 ± 8.90	20.7 ± 2.68	52.3 ± 14.1	10.9 ± 1.7	8.16 ± 1.95
	240	100.7 ± 5.37	104.5 ± 13.0	25.7 ± 10.6	33.3 ± 7.01	10.6 ± 1.7	9.26 ± 1.08
Specific surface area, SSA (×10 ² m ² /kg)							
Duodenum	30	10.4 ± 2.40	*7.74	*12.8	7.51 ± 0.92	24.2 ± 3.43	14.3 ± 2.92
	60	14.8 ± 2.91	14.4 ± 3.80	*13.3	*15.2	27.6 ± 3.38	*44.3
	120	13.9 ± 0.15	*6.44	*33.8	16.0 ± 1.90	36.5 ± 2.27	*8.08
	240	*13.1	8.81 ± 1.78	*11.8	-	-	-
Terminal ileum	30	-	*3.37	27.2 ± 0.82	15.9 ± 2.06	*73.8	47.2 ± 7.10
	60	-	13.7 ± 11.4	23.8 ± 0.47	13.7 ± 1.09	64.6 ± 9.78	57.0 ± 16.8
	120	7.94 ± 2.11	7.82 ± 0.75	28.2 ± 3.98	14.9 ± 3.58	52.9 ± 5.33	83.5 ± 23.5
	240	5.75 ± 0.25	5.68 ± 0.86	32.2 ± 12.3	20.7 ± 4.90	54.0 ± 11.36	56.7 ± 5.35
d ₁₀ (μm)							
Duodenum	30	19.8 ± 4.47	*24.42	*18.70	29.7 ± 4.28	8.03 ± 0.95	18.4 ± 7.54
	60	18.9 ± 6.62	18.5 ± 6.28	*9.97	*11.4	7.62 ± 1.11	*5.39
	120	15.4 ± 2.67	*37.7	*8.58	15.8 ± 5.92	5.61 ± 0.29	*20.03
	240	*13.0	24.5 ± 5.58	*17.51	-	-	-
Terminal ileum	30	-	*125.3	7.92 ± 0.07	15.4 ± 2.67	*2.72	5.18 ± 0.95
	60	-	64.3 ± 54.4	8.50 ± 0.65	17.9 ± 1.77	3.42 ± 1.22	3.35 ± 0.90

(continued)

Region	Time (min)	Diet					
		Semolina	Couscous	Pasta	Rice grain	Rice couscous	Rice noodle
	120	43.7 ± 15.3	55.4 ± 12.7	7.99 ± 1.06	24.7 ± 7.34	4.58 ± 1.02	3.47 ± 0.58
	240	57.4 ± 12.1	63.9 ± 11.8	11.0 ± 4.56	15.2 ± 3.58	4.17 ± 1.07	4.10 ± 0.47
d₅₀ (μm)							
Duodenum	30	338.7 ± 23.9	*705.9	*112.9	257.4 ± 48.7	147.6 ± 51.2	136.3 ± 43.4
	60	236.1 ± 62.7	351.4 ± 106.8	*49.2	*263.3	103.2 ± 42.9	*31.63
	120	210.3 ± 129.3	*725.0	*26.6	312.3 ± 88.2	35.0 ± 5.18	*125.1
	240	*319.0	581.8 ± 86.1	*293.7	-	-	-
Terminal ileum	30	-	*690.8	73.1 ± 18.0	513.1 ± 85.7	*17.9	35.6 ± 9.89
	60	-	323.5 ± 297.9	65.1 ± 9.41	582.8 ± 81.1	17.5 ± 2.23	27.3 ± 7.03
	120	351.2 ± 15.1	634.7 ± 25.9	72.4 ± 8.30	554.5 ± 92.8	36.4 ± 10.1	28.0 ± 7.33
	240	371.9 ± 13.5	629.3 ± 36.4	94.8 ± 44.9	299.5 ± 156.5	35.2 ± 6.77	24.5 ± 0.99
d₉₀ (μm)							
Duodenum	30	820.9 ± 42.7	*1420.5	*112.9	937.8 ± 129.1	877.0 ± 104.0	770.6 ± 166.2
	60	733.4 ± 15.2	1246.2 ± 46.2	*49.2	*1094.1	851.5 ± 104.1	*149.0
	120	823.3 ± 1.04	*1422.5	*26.6	1132.1 ± 99.6	378.1 ± 63.4	*528.0
	240	*801.3	1321.8 ± 67.0	*293.7	-	-	-
Terminal ileum	30	-	*1292.9	357 ± 25.5	1323.1 ± 45.4	*146.2	302.7 ± 197.4
	60	-	921.7 ± 332.9	374.1 ± 25.3	1367.6 ± 37.8	153.8 ± 38.3	171.9 ± 81.2
	120	767.0 ± 20.2	1313.0 ± 21.9	396.1 ± 23.5	1307.8 ± 62.5	217.7 ± 79.7	235.8 ± 150.8
	240	759.3 ± 16.7	1307.2 ± 28.1	596.5 ± 252.2	889 ± 324.7	281.0 ± 141.0	94.4 ± 6.22

Table E.2 Particle size distribution parameters (d_{10} , d_{50} , and d_{90}) of the intestinal digesta retrieved from the proximal jejunum, distal jejunum, and ileum sections (mean \pm SE, $4 \leq n \leq 6$). For each parameter, significantly different values within one column for each parameter (difference across times and small intestinal regions, within the same diet) are indicated with superscript abcd ($p < 0.05$). Significantly different values within one row (difference between diets at one digestion time, within the same small intestinal region) are indicated by superscript zyxw ($p < 0.05$).

Region	Time (min)	Diet					
		Semolina	Couscous	Pasta	Rice grain	Rice couscous	Rice noodle
d₁₀ (μm)							
Proximal jejunum	30	47.0 ± 9.25 ^{ab,z}	35.7 ± 11.0 ^{cde,z}	12.8 ± 0.71 ^y	18.0 ± 2.18 ^y	6.32 ± 0.91 ^{a,x}	12.6 ± 2.57 ^{a,y}
	60	44.7 ± 7.78 ^{b,z}	23.9 ± 3.73 ^{e,y}	10.9 ± 0.52 ^{xw}	17.8 ± 2.44 ^{yx}	4.04 ± 0.07 ^{abc,v}	9.37 ± 2.86 ^{ab,w}
	120	45.2 ± 5.01 ^{ab,z}	26.0 ± 0.29 ^{de,zy}	11.8 ± 0.55 ^x	15.1 ± 1.64 ^{yx}	5.02 ± 0.27 ^{ab,w}	5.39 ± 0.72 ^{bcd,w}
	240	32.7 ± 2.34 ^{b,z}	47.3 ± 18.5 ^{abcde,z}	11.9 ± 0.56 ^y	11.5 ± 2.20 ^y	4.11 ± 0.29 ^{abc,x}	7.27 ± 0.98 ^{abc,yx}
Distal jejunum	30	58.3 ± 10.7 ^{ab,z}	38.8 ± 8.11 ^{abcde,z}	13.9 ± 1.18 ^y	14.3 ± 1.28 ^y	3.98 ± 0.40 ^{abc,x}	4.17 ± 0.44 ^{cde,x}
	60	54.2 ± 2.98 ^{ab,z}	33.5 ± 4.41 ^{de,z}	11.1 ± 0.71 ^y	11.9 ± 1.72 ^y	3.57 ± 0.10 ^{abc,x}	4.34 ± 0.51 ^{cde,x}
	120	53.1 ± 6.92 ^{ab,z}	44.1 ± 9.68 ^{abcd,z}	10.8 ± 0.34 ^y	11.9 ± 1.10 ^y	3.46 ± 0.23 ^{bc,x}	4.02 ± 0.44 ^{cd,x}
	240	38.9 ± 8.94 ^{b,z}	36.8 ± 6.87 ^{bcd,z}	10.9 ± 0.31 ^y	10.9 ± 0.89 ^y	3.24 ± 0.15 ^{bc,x}	4.95 ± 1.28 ^{cde,x}
Ileum	30	57.2 ± 5.75 ^{ab,z}	67.6 ± 19.7 ^{abc,z}	9.47 ± 0.4 ^y	14.9 ± 2.32 ^y	2.97 ± 0.11 ^{bc,x}	3.50 ± 0.23 ^{cde,x}
	60	75.8 ± 11.5 ^{a,z}	70.0 ± 10.4 ^{a,z}	9.00 ± 0.38 ^x	16.5 ± 1.88 ^y	3.01 ± 0.21 ^{bc,w}	2.94 ± 0.28 ^{de,w}
	120	54.3 ± 2.69 ^{ab,z}	63.1 ± 7.95 ^{ab,z}	10.3 ± 0.48 ^y	12.3 ± 0.34 ^y	2.77 ± 0.20 ^{c,x}	2.59 ± 0.25 ^{e,x}
	240	58.7 ± 10.2 ^{ab,z}	59.3 ± 6.11 ^{abc,z}	10.3 ± 0.54 ^y	13.8 ± 0.81 ^y	2.63 ± 0.06 ^{c,x}	3.21 ± 0.25 ^{de,x}
d₅₀ (μm)							
Proximal jejunum	30	345.7 ± 19.6 ^z	405.3 ± 101.4 ^{ab,z}	78.8 ± 5.63 ^{ab,yx}	241.6 ± 31.5 ^{d,z}	59.0 ± 12.4 ^{a,x}	99.4 ± 13.9 ^{a,y}
	60	361.6 ± 14.8 ^z	412.9 ± 74.7 ^{a,zy}	57.3 ± 6.12 ^{ab,x}	282.1 ± 71.3 ^{cd,y}	26.0 ± 3.35 ^{bcd,w}	78.0 ± 17.3 ^{ab,x}
	120	292.1 ± 30.9 ^z	519.9 ± 65.9 ^{ab,z}	67.0 ± 11.1 ^{ab,y}	303.5 ± 46.6 ^{bcd,z}	38.1 ± 5.45 ^{abc,x}	46.3 ± 6.30 ^{bc,y}
	240	319.7 ± 21.5 ^y	583.5 ± 61.2 ^{ab,z}	70.1 ± 5.79 ^{ab,x}	254.6 ± 52.3 ^{cd,y}	41.0 ± 5.41 ^{ab,w}	89.7 ± 21.8 ^{ab,xw}
Distal jejunum	30	349.1 ± 22.0 ^{zy}	552.2 ± 63.3 ^{ab,z}	74.4 ± 8.65 ^{ab,x}	309 ± 49.2 ^{bcd,y}	32.1 ± 4.17 ^{bcd,w}	35.5 ± 4.13 ^{cd,x}
	60	350.7 ± 5.87 ^z	511.7 ± 51.9 ^{ab,z}	56 ± 8.08 ^{ab,x}	212.7 ± 35.1 ^{d,y}	21.6 ± 0.44 ^{d,w}	34.9 ± 5.95 ^{cde,w}
	120	339.2 ± 15.3 ^y	610.7 ± 19.4 ^{ab,z}	71.1 ± 7.16 ^{ab,x}	324.5 ± 56.5 ^{bcd,y}	26.6 ± 1.94 ^{bcd,w}	25.4 ± 2.75 ^{def,w}
	240	306.1 ± 48.4 ^y	607.5 ± 42.0 ^{ab,z}	65.9 ± 10.6 ^{ab,x}	456 ± 31.7 ^{ab,zy}	25.5 ± 2.65 ^{bcd,w}	18.0 ± 1.28 ^{f,w}

(continued)

(continued)

Region	Time (min)	Diet					
		Semolina	Couscous	Pasta	Rice grain	Rice couscous	Rice noodle
Ileum	30	367.3 ± 12.2 ^y	661.2 ± 25.1 ^{ab,z}	73.2 ± 8.48 ^{ab,x}	504.1 ± 83.1 ^{ab,zy}	24.6 ± 2.69 ^{bcd,w}	24.9 ± 2.79 ^{def,w}
	60	373.7 ± 7.66 ^y	666.2 ± 20.4 ^{a,z}	52.6 ± 4.34 ^{b,x}	610 ± 29.2 ^{a,zy}	25.0 ± 2.08 ^{bcd,w}	21.5 ± 0.44 ^{def,w}
	120	370.3 ± 4.51 ^y	669 ± 15.8 ^{a,z}	64.5 ± 3.02 ^{ab,x}	405 ± 22.2 ^{abc,y}	22.1 ± 1.60 ^{cd,w}	18.3 ± 1.11 ^{f,w}
	240	372.3 ± 8.36 ^y	663.1 ± 15.0 ^{a,z}	98.8 ± 20.8 ^{a,x}	465.7 ± 29.3 ^{ab,zy}	22.1 ± 0.78 ^{cd,w}	19.9 ± 1.09 ^{ef,w}
d₉₀ (µm)							
Proximal jejunum	30	758.2 ± 19.8 ^y	1213.2 ± 61.7 ^z	382.2 ± 10.9 ^x	1062.7 ± 58.1 ^{bc,z}	386.4 ± 80.6 ^{bc,x}	640.8 ± 114.5 ^{a,y}
	60	777.1 ± 25.1 ^y	1186.6 ± 66.3 ^z	376.8 ± 18.1 ^x	1151.5 ± 72.3 ^{abc,z}	178.9 ± 60.6 ^{cd,x}	596.6 ± 143.0 ^{a,y}
	120	710.0 ± 33.1 ^y	1223.4 ± 100.2 ^z	417.7 ± 70.0 ^x	1149.0 ± 47.7 ^{abc,z}	434.6 ± 110.1 ^{ab,x}	505.3 ± 65.8 ^{ab,yx}
	240	706.1 ± 25.3 ^y	1310.2 ± 38.7 ^z	480.6 ± 40.8 ^y	1100.0 ± 12.8 ^{abc,z}	671.7 ± 55.1 ^{a,y}	582.0 ± 62.7 ^{a,y}
Distal jejunum	30	721.3 ± 21.6 ^y	1294.0 ± 35.4 ^z	352.3 ± 31.2 ^x	1110.7 ± 52.1 ^{abc,z}	302.1 ± 101.7 ^{bcd,x}	280.2 ± 77.5 ^{bc,x}
	60	720.6 ± 7.63 ^x	1260.7 ± 34.3 ^z	338.0 ± 25.6 ^w	1011.8 ± 37.4 ^{c,y}	100.4 ± 5.89 ^{d,x}	250.9 ± 59.0 ^{c,wx}
	120	715.0 ± 18.2 ^y	1326.7 ± 10.6 ^z	436.9 ± 79.1 ^x	1156.7 ± 67.3 ^{abc,z}	292.1 ± 72.5 ^{bcd,x}	230.4 ± 55.8 ^{e,x}
	240	691.0 ± 67.2 ^y	1317.1 ± 32.0 ^z	451.2 ± 86.3 ^x	1270.8 ± 22.3 ^{abc,z}	224.9 ± 85.5 ^{bcd,xw}	175.4 ± 68.8 ^{c,w}
Ileum	30	749.6 ± 25.2 ^y	1337.5 ± 23.0 ^z	357.1 ± 5.92 ^x	1305.7 ± 53.5 ^{ab,z}	115.3 ± 15.6 ^{d,w}	148.3 ± 25.5 ^{c,xw}
	60	744.0 ± 12.3 ^y	1350.9 ± 10.7 ^z	352.8 ± 18.9 ^x	1368.1 ± 22.1 ^{a,z}	141.3 ± 27.4 ^{d,w}	114.2 ± 6.83 ^{c,w}
	120	746.8 ± 6.25 ^y	1347.1 ± 8.74 ^z	343.1 ± 8.52 ^x	1249.3 ± 19.2 ^{abc,z}	92.3 ± 9.51 ^{d,w}	99.2 ± 10.7 ^{c,w}
	240	740.1 ± 16.9 ^y	1340.7 ± 8.56 ^z	390.5 ± 10.7 ^x	1265.8 ± 18.2 ^{abc,z}	81.5 ± 1.93 ^{d,w}	85.1 ± 2.71 ^{c,w}

Table E.3 Maltose and glucose concentration in different sections of small intestinal digesta after feeding with different diets and digestion time mean \pm SE, $4 \leq n \leq 6$). For each parameter, significantly different values between one row (difference between small intestinal sections for one type of diet, within the same digestion time) are indicated with superscript abcd ($p < 0.05$). Significantly different values between digestion times for one type of diet and small intestinal region are indicated by superscript zyxw ($p < 0.05$).

Diet	Time (min)	Small intestinal section				
		Duodenum	Proximal jejunum	Distal jejunum	Ileum	Terminal ileum
Maltose concentration (mg maltose/g DM digesta)						
Semolina	30	309.4 ± 57.4 ^a	510.6 ± 31.3 ^a	345.9 ± 86.1 ^a	355.1 ± 57.3 ^{a,z}	81.7 ± 73.3 ^{b,y}
	60	448 ± 125.3	537.7 ± 50.3	411.0 ± 37.8	257.2 ± 32.9 ^{zy}	303.0 ± 105.6 ^z
	120	424.9 ± 108.8 ^a	359.8 ± 91.4 ^a	267.7 ± 54.6 ^{ab}	181.2 ± 51.8 ^{ab,zy}	76.4 ± 25.4 ^{b,y}
	240	257.3 ± 70.0 ^{a,b}	337.9 ± 118.7 ^a	299.7 ± 82.6 ^a	87.9 ± 20.9 ^{ab,y}	58.5 ± 14.1 ^{b,y}
Couscous	30	403.9 ± 108.3 ^a	432.8 ± 39.1 ^a	378.7 ± 79.9 ^a	345.8 ± 34.9 ^a	87.4 ± 25.9 ^b
	60	335.5 ± 47.4 ^{ab}	447.5 ± 84.4 ^a	444.9 ± 11.9 ^a	130.9 ± 30.1 ^{bc}	81.2 ± 34.5 ^c
	120	476.3 ± 148.6 ^a	456.6 ± 23.1 ^a	456.1 ± 41.7 ^a	206.8 ± 52.0 ^{ab}	156.4 ± 46.1 ^b
	240	285.9 ± 82.7 ^a	497.4 ± 51.4 ^a	347.1 ± 79.6 ^a	205.1 ± 20.2 ^a	25.6 ± 11.1 ^b
Pasta	30	238.6 ± 65.0 ^{ab}	402.1 ± 44.6 ^a	421.9 ± 60.3 ^a	217.5 ± 61.6 ^{ab}	126.7 ± 65.8 ^b
	60	258.4 ± 25.9 ^a	448.1 ± 57.3 ^a	384.3 ± 67.1 ^a	198.9 ± 60.9 ^{ab}	80.9 ± 53.4 ^b
	120	256.9 ± 62.5 ^{ab}	406.8 ± 50.3 ^a	321.8 ± 62.3 ^{ab}	159.8 ± 30.1 ^{bc}	41.8 ± 20.8 ^c
	240	208.7 ± 51.8 ^{ab}	458.1 ± 129.2 ^a	393.3 ± 59 ^a	117.5 ± 19.6 ^{bc}	121.2 ± 83.8 ^b
Rice grain	30	269.1 ± 43.6 ^a	558.7 ± 82.4 ^a	484.8 ± 76.4 ^a	273.6 ± 55.8 ^a	73.3 ± 30.1 ^{b,y}
	60	182.1 ± 77.5 ^b	621.4 ± 102.3 ^a	510.2 ± 74.7 ^a	337.3 ± 51.2 ^{ab}	389.2 ± 174.5 ^{ab,z}
	120	421.5 ± 145.6 ^a	588.6 ± 81.5 ^a	541.3 ± 45.8 ^a	292 ± 39.4 ^{ab}	112.6 ± 29.6 ^{b,zy}
	240	378.7 ± 114.1 ^{ab}	474.1 ± 121.7 ^a	498.2 ± 109.4 ^a	191.7 ± 35.2 ^{ab}	152.0 ± 65.8 ^{b,zy}
Rice couscous	30	548.2 ± 68.0 ^a	598.1 ± 32.6 ^a	548.1 ± 44.8 ^a	332.7 ± 101.3 ^{a,zy}	45.4 ± 14.4 ^b
	60	460.7 ± 108.6 ^a	675.7 ± 54.6 ^a	608.0 ± 27.7 ^a	568.0 ± 42.3 ^{a,z}	64.4 ± 63.4 ^b
	120	422.3 ± 66.2 ^{ab}	667.2 ± 57.6 ^a	586.2 ± 34.1 ^a	281.2 ± 63.5 ^{b,y}	84.6 ± 37.4 ^c
	240	429.7 ± 155.3 ^a	421.8 ± 96.6 ^a	434.9 ± 57.1 ^a	230.7 ± 56.4 ^{a,y}	42.9 ± 30.4 ^b
Rice noodle	30	264.9 ± 65.3 ^{ab}	556.7 ± 58.4 ^a	491.7 ± 98.1 ^a	158.2 ± 45.2 ^b	110.0 ± 54.1 ^b
	60	359.3 ± 126.7 ^a	431.9 ± 28.4 ^a	478.8 ± 69.5 ^a	334.0 ± 45.9 ^a	107.5 ± 55.0 ^b
	120	242.9 ± 74.7 ^c	539.2 ± 122 ^{ab}	584.8 ± 80.4 ^a	280.1 ± 55.1 ^{bc}	154.2 ± 54.9 ^c
	240	258.7 ± 61.1 ^{abc}	393.5 ± 54.1 ^{ab}	465.9 ± 99.6 ^a	158.8 ± 35.5 ^{bc}	111.1 ± 56.8 ^c
Glucose concentration (mg glucose/g DM digesta)						
Semolina	30	84.7 ± 36.7 ^b	187.2 ± 32.7 ^a	255.8 ± 31.4 ^a	161.3 ± 21.5 ^{ab,z}	1.99 ± 1.32 ^c
	60	57.4 ± 17.0 ^c	247.3 ± 26.5 ^a	235.6 ± 16.6 ^{ab}	121.3 ± 9.74 ^{bc,zy}	2.90 ± 2.25 ^d
	120	114.1 ± 44.0 ^b	242.4 ± 19.5 ^a	143.4 ± 31.3 ^{ab}	73.1 ± 21.1 ^{b,yx}	6.06 ± 2.11 ^c
	240	119.3 ± 29.3 ^b	251.8 ± 35.7 ^a	180.6 ± 12.4 ^{ab}	37.7 ± 7.99 ^{c,x}	18.7 ± 8.18 ^c
Couscous	30	93.8 ± 11.1 ^b	211.4 ± 14.8 ^a	199.8 ± 33.9 ^{ab}	156.2 ± 23.2 ^{ab}	1.42 ± 0.96 ^c
	60	120.2 ± 14.9 ^{bc}	240.9 ± 16.2 ^a	216.7 ± 21.5 ^{ab}	80.6 ± 13.1 ^c	1.68 ± 1.07 ^d
	120	162.4 ± 47.7 ^{ab}	238.2 ± 12.9 ^a	212.2 ± 36.1 ^a	73.0 ± 16.0 ^b	7.31 ± 2.13 ^c
	240	124.9 ± 28.3 ^{bc}	256.9 ± 19.2 ^a	208.4 ± 14.1 ^{ab}	77.0 ± 6.82 ^c	10.2 ± 2.61 ^d
Pasta	30	119.4 ± 28.3 ^{ab}	213.5 ± 18.6 ^a	201.0 ± 22.5 ^a	75.3 ± 17.8 ^b	8.66 ± 3.86 ^c
	60	141.5 ± 13.5 ^{ab}	229.0 ± 24.8 ^a	185.0 ± 29.2 ^a	82.5 ± 28.9 ^b	15.6 ± 6.43 ^c
	120	116.2 ± 13.4 ^b	232.5 ± 35.2 ^a	179.6 ± 33.2 ^{ab}	46.4 ± 10.4 ^c	10.2 ± 4.44 ^d
	240	98.8 ± 8.23 ^{bc}	266.1 ± 41.1 ^a	175.8 ± 20.2 ^{ab}	39.4 ± 13.1 ^{cd}	24.1 ± 15.2 ^d
Rice grain	30	107.1 ± 11.6 ^{c,zy}	320.6 ± 59.8 ^a	226.8 ± 48.2 ^{ab}	139 ± 17.0 ^{bc}	21.7 ± 11.3 ^d
	60	72.8 ± 21.5 ^{c,y}	323.5 ± 38.1 ^a	231.0 ± 35.5 ^{ab}	133.6 ± 18.3 ^{bc}	19.5 ± 8.75 ^d

(continued)

Diet	Time (min)	Small intestinal section				
		Duodenum	Proximal jejunum	Distal jejunum	Ileum	Terminal ileum
Rice couscous	120	111.7 ± 32.5 ^{b,zy}	323.5 ± 41.1 ^a	216.5 ± 23.1 ^a	111.7 ± 15.5 ^b	21.5 ± 9.52 ^c
	240	164.7 ± 20.2 ^{a,z}	253 ± 49.4 ^a	233.6 ± 39.4 ^a	70.4 ± 14.2 ^b	8.63 ± 5.30 ^c
	30	77.9 ± 23.9 ^{c,zy}	294.2 ± 6.54 ^a	234.5 ± 32.1 ^{ab}	120.5 ± 21.1 ^{bc}	1.23 ± 1.23 ^{d,y}
	60	102.7 ± 36.9 ^{b,zy}	215.5 ± 24.1 ^a	162.1 ± 19.5 ^{ab}	143.7 ± 8.86 ^{ab}	5.78 ± 2.61 ^{c,zy}
	120	80.9 ± 27.4 ^{b,y}	310.6 ± 23.7 ^a	267.4 ± 31.4 ^a	106.5 ± 10.1 ^b	7.98 ± 5.43 ^{c,y}
	240	156.9 ± 32.1 ^{ab,z}	276.6 ± 61.7 ^a	242 ± 38.9 ^a	69.7 ± 13.2 ^{bc}	25.8 ± 8.69 ^{c,z}
Rice noodle	30	136.9 ± 34.3 ^{bc}	319 ± 37.2 ^a	252.7 ± 43.4 ^{ab}	66.7 ± 23.9 ^c	18.2 ± 10.0 ^d
	60	160.3 ± 43.7 ^{ab}	237.9 ± 28.5 ^a	267.4 ± 29.6 ^a	126.2 ± 15.8 ^b	9.74 ± 6.68 ^c
	120	116.2 ± 20.5 ^b	204.1 ± 31.9 ^{ab}	295.5 ± 37.6 ^a	124.7 ± 12.7 ^b	20.6 ± 9.48 ^c
	240	125.7 ± 32.8 ^{bc}	239.9 ± 24.7 ^a	204.0 ± 33.1 ^{ab}	73.6 ± 10.6 ^{cd}	28.9 ± 7.83 ^d

Table E.4 Plasma glucose concentration of samples collected from different vein locations of the pig under anesthesia (mean \pm SE, $4 \leq n \leq 6$). Statistical comparison was conducted only on portal vein glucose data. Significantly different values between diets within the same digestion time are indicated with superscript abcd ($p < 0.05$). Significantly different values between digestion times within one type of diet are indicated by superscript zyxw ($p < 0.05$).

Diet	Time (min)	Venous plasma glucose concentration (mg/dL)				
		Portal	Hepatic	Vena cava	Left ventricle	Jugular
Semolina	30	148.2 \pm 14.0	203.6 \pm 45.5	124.7 \pm 11.2	151.0 \pm 18.5	117.3 \pm 14.3
	60	193.7 \pm 20.6 ^{ab}	152.1 \pm 9.92	118.0 \pm 17.4	141.9 \pm 10.2	102.8 \pm 14.5
	120	155.2 \pm 23.4	159.8 \pm 29.7	121.0 \pm 13.7	146.4 \pm 23.6	113.9 \pm 11.3
	240	134.7 \pm 6.54	137.0 \pm 7.80	111.1 \pm 4.20	118.6 \pm 3.24	96.7 \pm 2.73
Couscous	30	161.4 \pm 25.9	142.3 \pm 12.7	118.0 \pm 12.0	138.4 \pm 14.6	104.4 \pm 8.98
	60	170.5 \pm 11.9 ^b	119.2 \pm 13.8	107.9 \pm 5.81	131.4 \pm 8.08	103.2 \pm 3.75
	120	183.8 \pm 20.2	161.7 \pm 16.6	131.2 \pm 16.9	154.9 \pm 15.0	115.4 \pm 9.14
	240	155.3 \pm 29.7	155.2 \pm 22.5	99.0 \pm 13.4	116.2 \pm 13.7	87.1 \pm 7.78
Pasta	30	174.7 \pm 22.2	154.1 \pm 15.7	131.8 \pm 15.8	137.3 \pm 10.5	106.8 \pm 14.1
	60	160.6 \pm 11.0 ^b	164.5 \pm 10.7	123.1 \pm 8.43	142.4 \pm 7.56	109.8 \pm 5.04
	120	151.3 \pm 9.26	161.0 \pm 9.55	118.4 \pm 6.52	138.2 \pm 8.86	101.7 \pm 3.62
	240	136.0 \pm 12.0	156.7 \pm 20.8	119.2 \pm 7.19	129.6 \pm 12.1	106.0 \pm 7.11
Rice grain	30	157.0 \pm 8.88	146.3 \pm 10.1	115.3 \pm 6.76	129 \pm 6.07	106.8 \pm 7.96
	60	182.3 \pm 18.3 ^{ab}	174.8 \pm 17.3	115.3 \pm 18.2	150.8 \pm 14.3	119.8 \pm 9.46
	120	190.3 \pm 14.6	150.9 \pm 10.1	126.7 \pm 7.39	141.9 \pm 6.99	110.4 \pm 4.15
	240	140.4 \pm 12.1	152.5 \pm 11.5	120.3 \pm 6.59	135.1 \pm 10.3	92.5 \pm 8.22
Rice couscous	30	199.3 \pm 16.6 ^{zy}	182.8 \pm 16.7	134.8 \pm 12.3	161.9 \pm 18.5	120.0 \pm 13.8
	60	257.7 \pm 9.9 ^{a,z}	203.3 \pm 28.6	126.5 \pm 10.4	149.3 \pm 10.1	104.1 \pm 5.37
	120	183.9 \pm 15.4 ^y	160.1 \pm 11.4	134.9 \pm 9.43	150.3 \pm 10.2	122.4 \pm 8.36
	240	159.6 \pm 31.4 ^y	132.8 \pm 15.1	107.0 \pm 6.35	113.6 \pm 8.7	100.6 \pm 4.29
Rice noodle	30	140.5 \pm 11.1	148.7 \pm 14.6	103.0 \pm 11.2	124.5 \pm 10.0	89.9 \pm 5.74
	60	184.1 \pm 24.2 ^a	145.5 \pm 8.49	115.9 \pm 7.32	135 \pm 8.50	101.6 \pm 7.82
	120	174.0 \pm 15.1	134.7 \pm 6.42	113.0 \pm 5.66	119.9 \pm 5.01	112.6 \pm 3.43
	240	135.8 \pm 15.0	138.2 \pm 15.1	122.0 \pm 14.1	122.0 \pm 12.3	105.9 \pm 12.3

E.2 Supplementary Figures

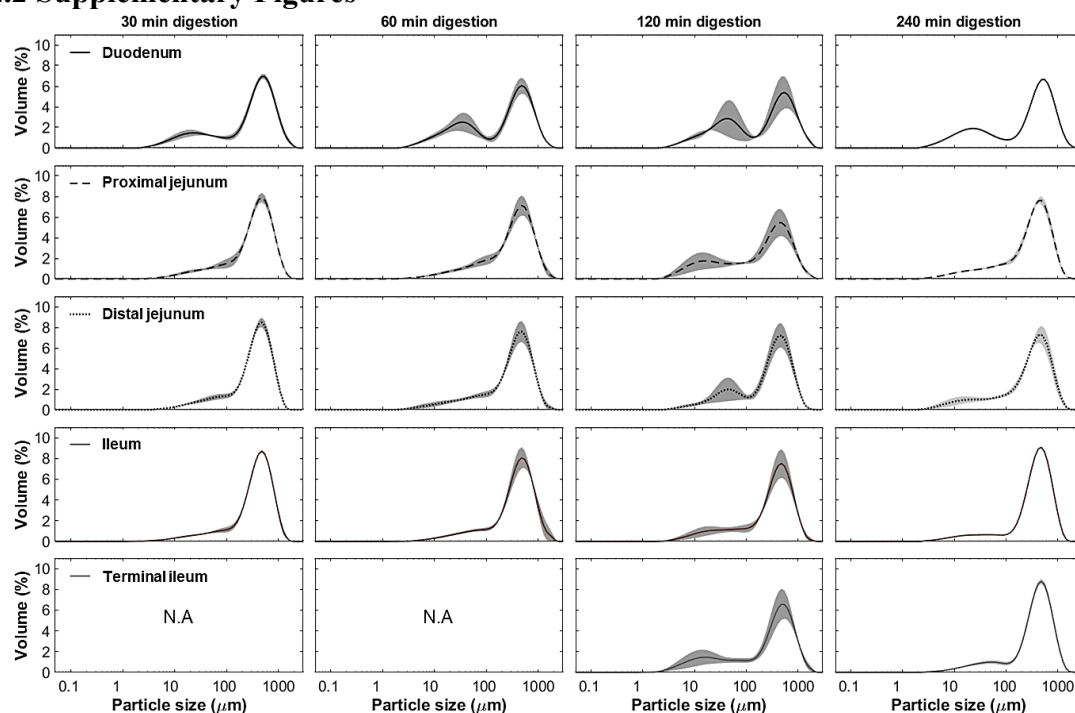


Figure E.1 Individual plots for particle size distribution of semolina intestinal digesta in different small intestinal sections at different digestion times. The standard error of each curve is indicated by error shades around the line. Curves established from a single data set do not have error shades, and certain digestion time \times small intestinal region combinations denoted by N.A. do not have any data due to removal of data points with low obscuration ($<2\%$).

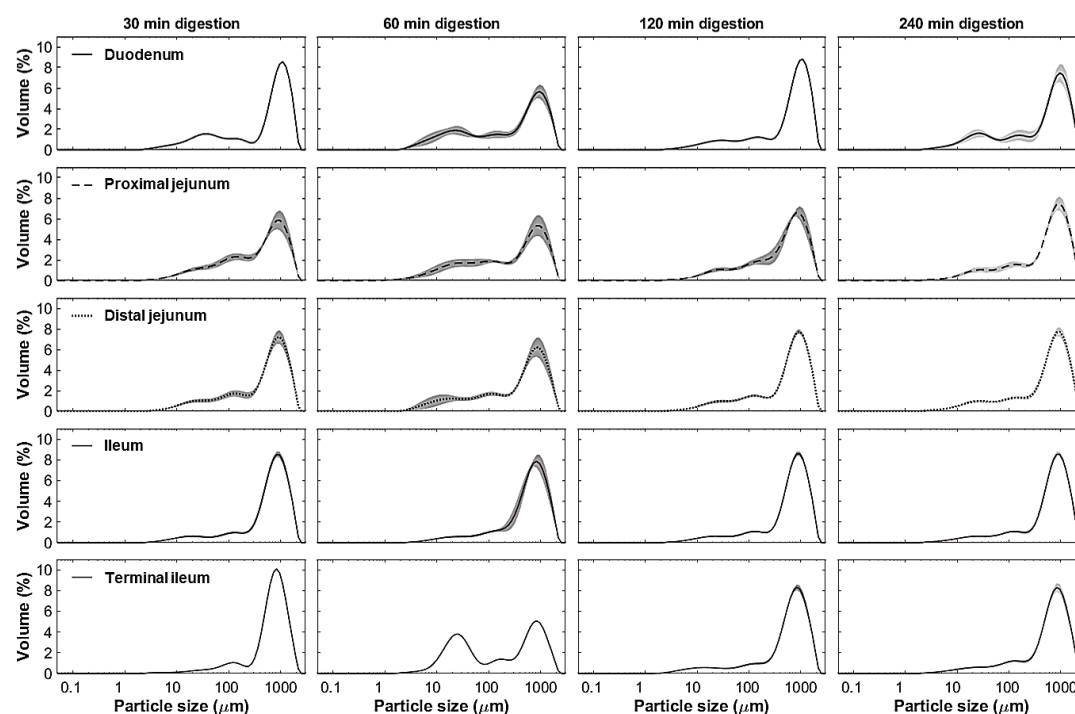


Figure E.2 Individual plots for particle size distribution of couscous intestinal digesta in different small intestinal sections at different digestion times. The standard error of each curve is indicated by error shades around the line. Curves established from a single data set do not have error shades.

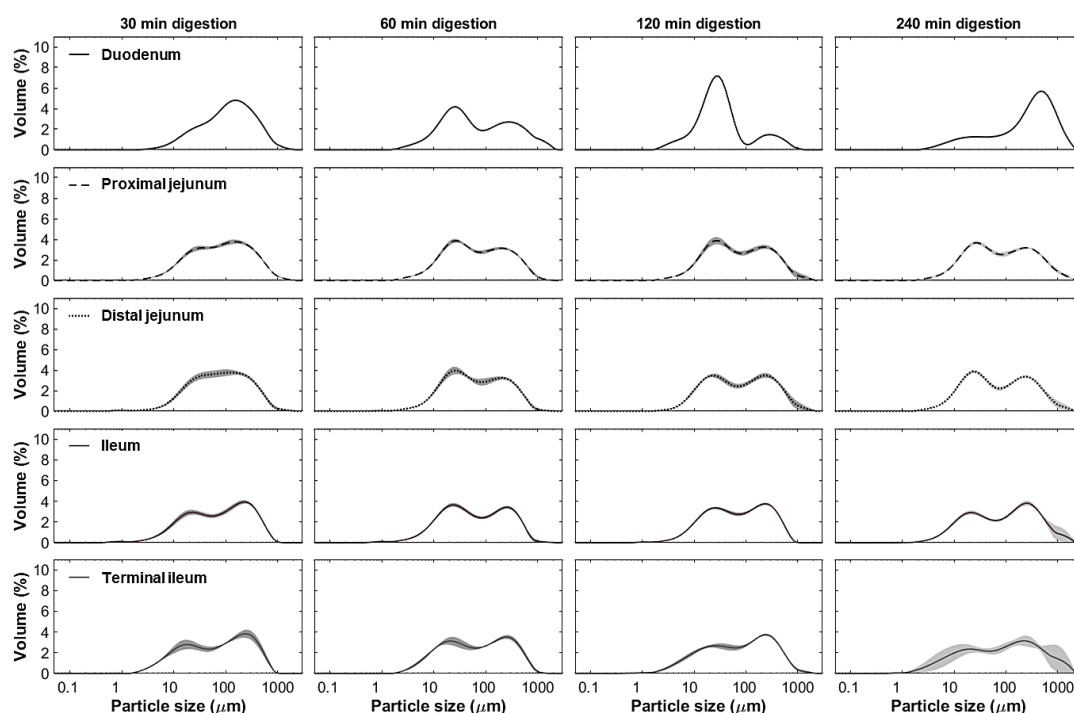


Figure E.3 Individual plots for particle size distribution of pasta intestinal digesta in different small intestinal sections at different digestion times. The standard error of each curve is indicated by error shades around the line. Curves established from a single data set do not have error shades.

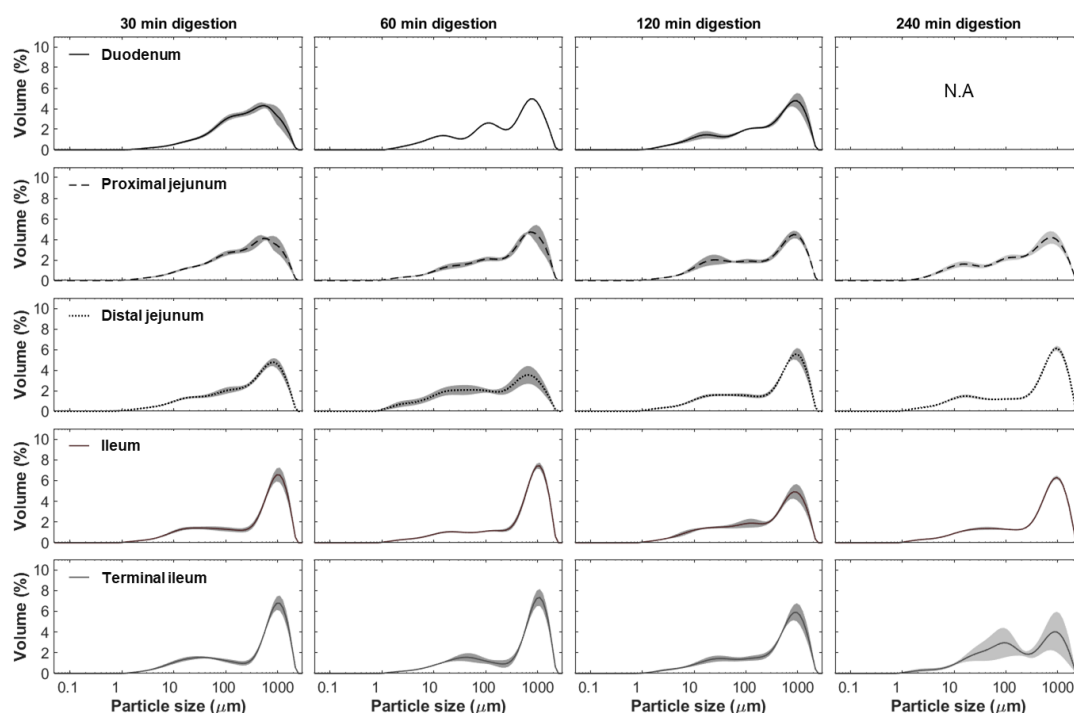


Figure E.4 Individual plots for particle size distribution of rice grain intestinal digesta in different small intestinal sections at different digestion times. The standard error of each curve is indicated by error shades around the line. Curves established from a single data set do not have error shades, and certain digestion time \times small intestinal region combinations denoted by N.A do not have any data due to removal of data points with low obscuration ($<2\%$).

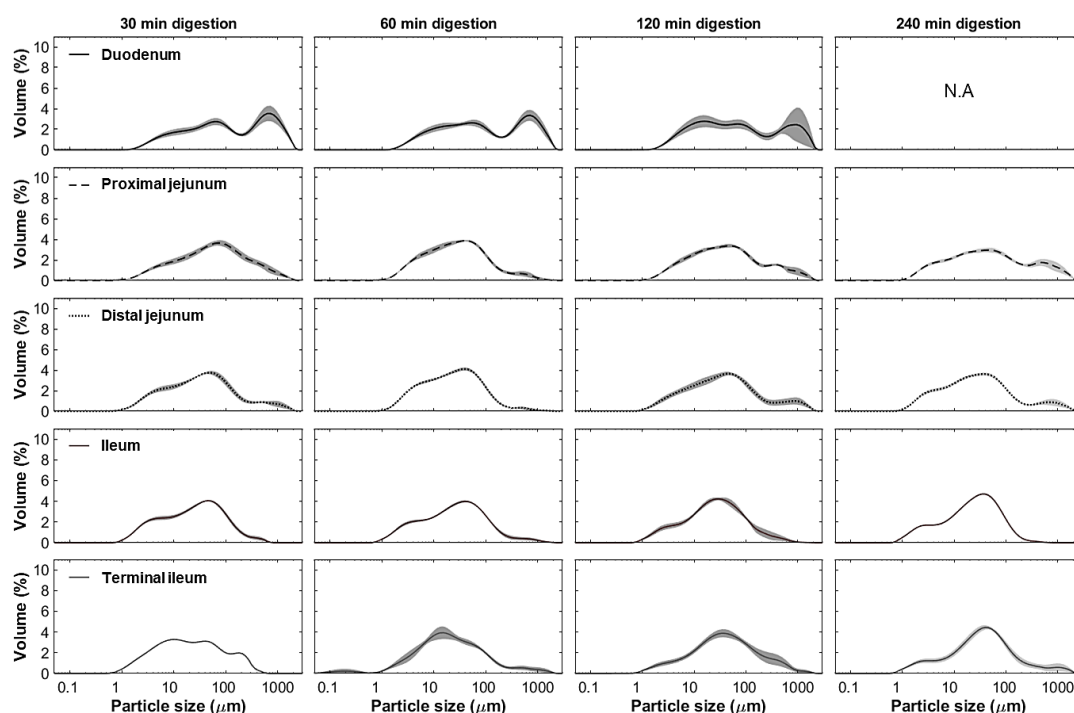


Figure E.5 Individual plots for particle size distribution of rice couscous intestinal digesta in different small intestinal sections at different digestion times. The standard error of each curve is indicated by error shades around the line. Curves established from a single data set do not have error shades, and certain digestion time \times small intestinal region combinations denoted by N.A do not have any data due to removal of data points with low obscuration ($<2\%$).

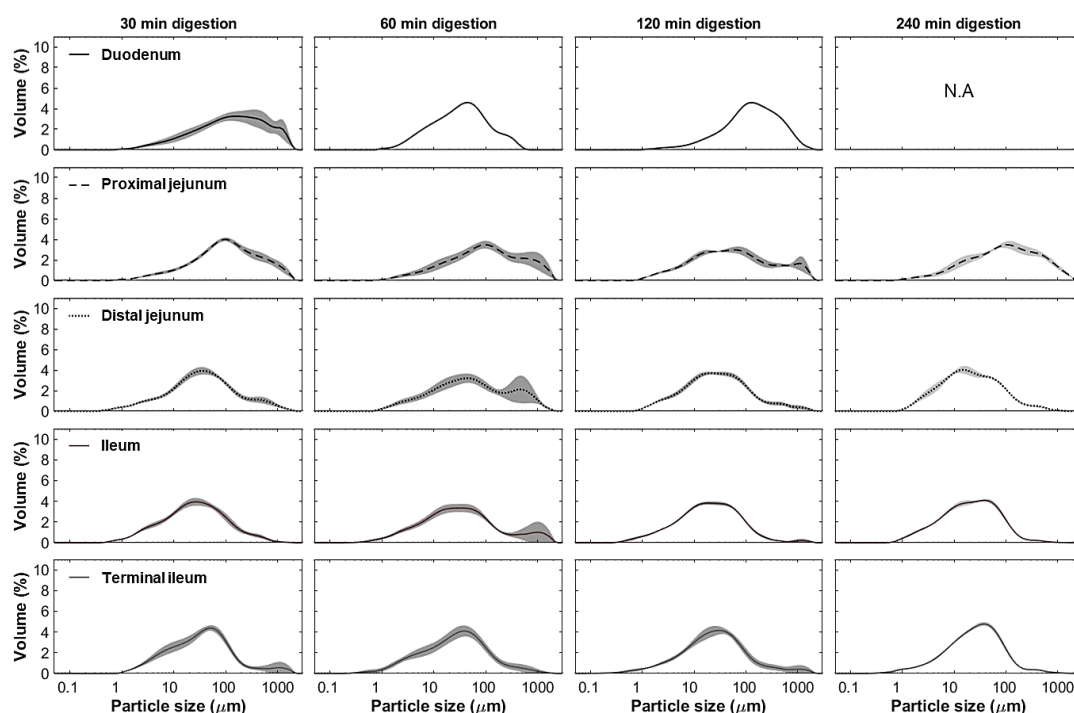


Figure E.6 Individual plots for particle size distribution of rice noodle intestinal digesta in different small intestinal sections at different digestion times. The standard error of each curve is indicated by error shades around the line. Curves established from a single data set do not have error shades, and certain digestion time \times small intestinal region combinations denoted by N.A do not have any data due to removal of data points with low obscuration ($<2\%$).

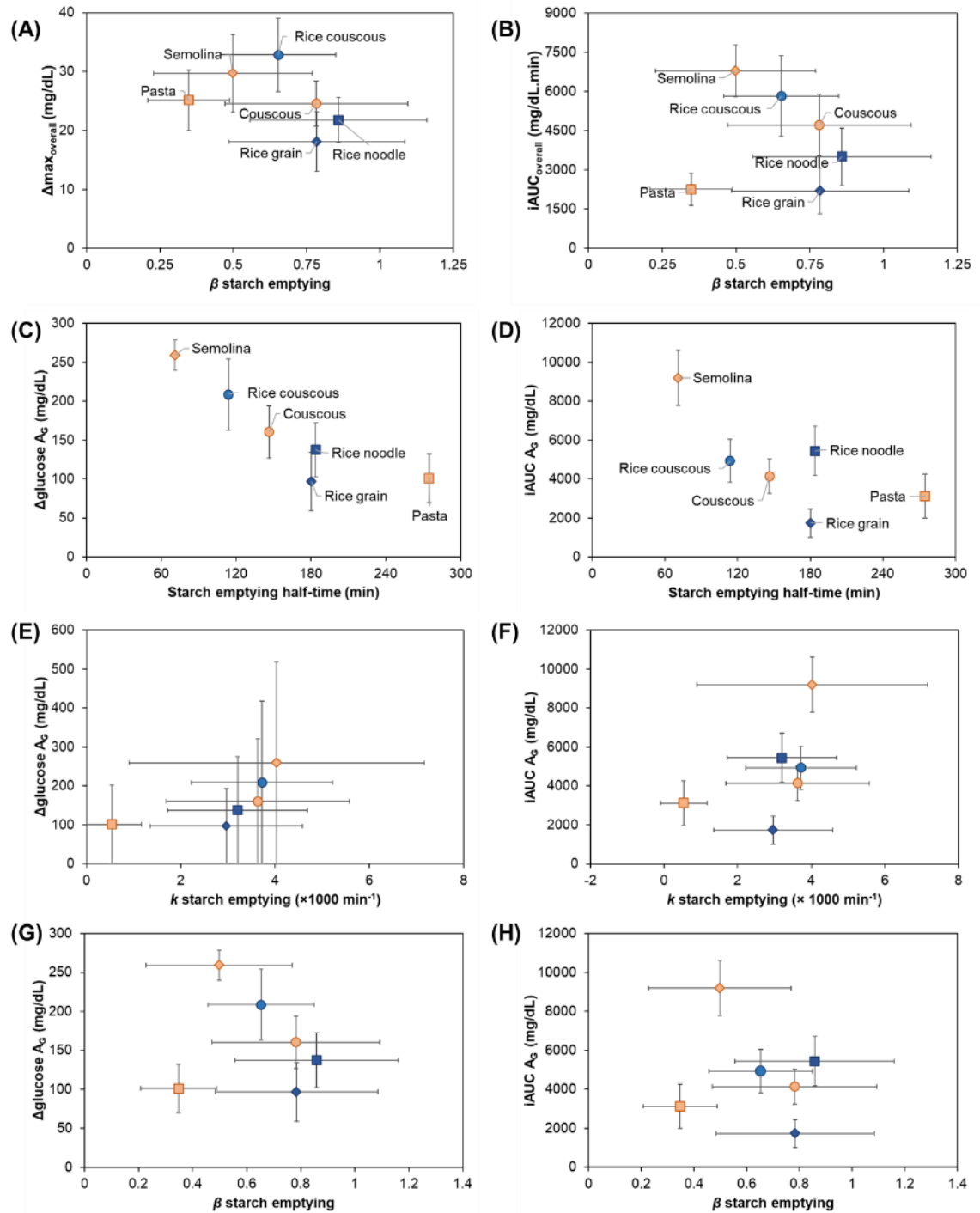


Figure E.7 Relationship between glycemic response parameters with lag phase parameter of starch emptying (β) (A-B) and between the asymptote (A_G) of $\Delta\text{glucose}$ and iAUC growth curve with: the starch emptying half-time (C-D), starch emptying rate (k) (E-F), and lag phase parameter of starch emptying (β) (G-H). Each symbol in subfigure E-H corresponds to one diet: semolina (♦), couscous (●), pasta (■), rice grain (◆), rice couscous (●), rice noodle (■). Starch emptying parameters (k and β) were obtained from **Figure 5.12G** and are shown as fitted parameter \pm 95% confidence interval. Starch emptying half-time was calculated from the starch emptying parameters.

APPENDIX F

SUPPLEMENTARY MATERIALS TO CHAPTER 7

F.1 Supplementary Tables

Table F.1 Hardness values of the whole digesta mixture from proximal digestion (mean \pm SD; $n = 3$ for all parameters for each food \times proximal phase \times distal phase combination, except values indicated with asterisk (*), $n=2$ due to outlier removal). Significantly different values between proximal phase durations for one type of food are indicated with abcd superscript; significantly different values between food types within the same proximal phase duration are indicated with zyxw superscript ($p < 0.05$).

Food	Proximal phase (min)			
	0	2	15	30
Couscous	21.82 \pm 1.22 ^{a,y}	23.20 \pm 1.77 ^{a,x}	12.50 \pm 2.01 ^{b,x}	7.18 \pm 1.87 ^{b,x}
Rice couscous	*3.51 \pm 2.00 ^x	8.63 \pm 5.58 ^w	3.20 \pm 2.96 ^x	3.36 \pm 4.33 ^x
Pasta	44.2 \pm 9.13 ^{a,z}	45.28 \pm 8.01 ^{a,y}	39.95 \pm 3.54 ^{ab,y}	34.47 \pm 6.82 ^{b,y}
Rice noodle	33.07 \pm 7.36 ^{zy}	32.96 \pm 5.43 ^{yx}	30.41 \pm 4.41 ^y	25.69 \pm 6.18 ^y
Rice grain	75.94 \pm 10.45 ^{b,z}	73.3 \pm 7.17 ^{b,z}	*91.93 \pm 5.40 ^{a,z}	62.78 \pm 1.79 ^{c,z}

Table F.2 Hardness values of the solid digesta fraction from proximal-distal digestion (mean \pm SD; $n = 3$ for all parameters for each food \times proximal phase \times distal phase combination, except values indicated with asterisk (*), $n=2$ due to outlier removal). For one type of food, significantly different values between distal phase durations within the same proximal phase are indicated with abcd superscript; significantly different values between proximal phase durations within the same distal phase duration are indicated with zyxw superscript ($p < 0.05$).

Food	Distal phase (min)	Proximal phase (min)			
		0	2	15	30
Couscous	15	37.76 \pm 2.74 ^a	34.76 \pm 4.94 ^a	38.4 \pm 11.79 ^a	34.05 \pm 10.22 ^a
	30	24.78 \pm 0.85 ^a	24.33 \pm 5.43 ^{ab}	25.45 \pm 7.91 ^{ab}	22.15 \pm 8.24 ^{ab}
	60	10.23 \pm 1.47 ^b	15.78 \pm 2.81 ^{bc}	16.4 \pm 9.23 ^{bc}	14.18 \pm 5.28 ^{bc}
	120	6.24 \pm 1.07 ^b	7.26 \pm 1.29 ^c	8.16 \pm 4.79 ^c	7.49 \pm 3.00 ^c
	180	4.60 \pm 0.60 ^b	5.04 \pm 0.32 ^c	4.84 \pm 1.66 ^c	4.30 \pm 1.61 ^c
Rice couscous	15	22.20 \pm 12.73 ^y	34.35 \pm 12.81 ^{a,y}	30.06 \pm 14.07 ^y	55.20 \pm 3.85 ^{a,z}
	30	17.95 \pm 14.03 ^x	28.82 \pm 9.28 ^{ab,yx}	33.99 \pm 12.67 ^y	55.72 \pm 1.28 ^{a,z}
	60	18.18 \pm 11.90 ^y	23.45 \pm 4.94 ^{ab,y}	23.78 \pm 12.17 ^y	43.94 \pm 6.84 ^{ab,z}
	120	14.54 \pm 9.97	17.52 \pm 5.04 ^b	22.93 \pm 9.58	31.83 \pm 5.98 ^{bc}
	180	14.54 \pm 8.82	15.7 \pm 5.73 ^b	24.87 \pm 14.76	26.59 \pm 11.03 ^c
Pasta	15	52.08 \pm 14.6 ^{a,zy}	48.86 \pm 3.05 ^{a,y}	56.63 \pm 7.02 ^{ab,zy}	63.69 \pm 12.59 ^{a,z}
	30	60.73 \pm 3.07 ^{ab}	56.39 \pm 3.65 ^{ab}	63.03 \pm 7.22 ^a	50.17 \pm 8.82 ^b
	60	43.32 \pm 7.90 ^{bc}	50.37 \pm 8.65 ^{ab}	46.02 \pm 9.66 ^{bc}	47.23 \pm 14.46 ^b
	120	39.03 \pm 7.23 ^{bc}	41.47 \pm 6.31 ^b	45.01 \pm 0.98 ^c	49.11 \pm 5.94 ^b
	180	35.99 \pm 5.10 ^c	44.05 \pm 2.51 ^{ab}	40.55 \pm 6.82 ^{bc}	41.65 \pm 3.84 ^b
Rice noodle	15	32.6 \pm 7.21	37.92 \pm 10.42	43.92 \pm 3.94	37.50 \pm 10.64
	30	36.66 \pm 3.48	37.50 \pm 6.71	40.98 \pm 9.43	41.82 \pm 14.27

(continued)

Food	Distal phase (min)	Proximal phase (min)			
		0	2	15	30
Rice grain	60	33.95 ± 5.77	35.48 ± 5.26	41.51 ± 3.45	41.25 ± 12.65
	120	26.27 ± 7.26	32.26 ± 2.87	39.86 ± 4.18	33.35 ± 8.55
	180	26.75 ± 1.33	31.96 ± 3.29	35.78 ± 1.10	33.53 ± 5.23
	15	102.06 ± 17.26 ^{ab,y}	*119.81 ± 2.22 ^{a,z}	100.04 ± 6.16 ^{a,y}	94.26 ± 5.43 ^{a,y}
	30	109.45 ± 7.95 ^{a,z}	92.85 ± 15.83 ^{b,y}	95.53 ± 8.30 ^{a,y}	92.94 ± 11.26 ^{a,y}
	60	95.4 ± 9.62 ^b	91.42 ± 6.32 ^b	94.19 ± 4.42 ^a	86.13 ± 4.94 ^a
	120	66.79 ± 4.14 ^c	74.05 ± 1.11 ^c	70.96 ± 1.58 ^b	71.64 ± 5.73 ^b
	180	52.13 ± 3.76 ^{d,y}	57.32 ± 5.14 ^{d,y}	65.48 ± 2.33 ^{b,y}	69.64 ± 8.55 ^{b,z}

Table F.3 Percentage of total area of particles within defined range of area used to establish Figure 7.1B-F. Values are obtained by pooling the particle area data from three replicates of each proximal condition or selected proximal-distal condition. For each food × proximal × distal combination, “-” in the distal phase time corresponds to proximal digestion. “Initial” indicates the data for undigested cooked diet.

Food	Proximal phase (min)	Distal phase (min)	Percent of particle area (%)						
			≤0.1 mm ²	0.1<mm ² ≤4	4<mm ² ≤10	10<mm ² ≤100	100<mm ² ≤200	mm ² >200	
Couscous	Initial		0.09	34.11	48.48	17.32	0.00	0	
		0	-	0.27	53.94	35.81	9.98	0.00	0
		30	0.26	75.86	23.21	0.67	0.00	0	
		180	0.34	76.72	20.53	2.41	0.00	0	
	2	-	0.27	57.18	32.86	9.69	0.00	0	
		30	0.24	55.75	34.16	9.86	0.00	0	
		180	0.32	65.81	28.20	5.67	0.00	0	
	15	-	0.21	44.58	31.74	23.48	0.00	0	
		30	0.24	60.56	32.12	7.08	0.00	0	
		180	0.37	79.93	17.84	1.87	0.00	0	
	30	-	0.32	69.53	26.77	3.37	0.00	0	
		30	0.32	75.11	20.49	4.08	0.00	0	
180		0.33	83.45	14.12	2.10	0.00	0		
Rice couscous	Initial		0.47	50.02	30.75	18.76	0.00	0	
		0	-	0.91	61.08	29.72	8.28	0.00	0
		30	0.67	60.08	29.82	9.44	0.00	0	
		180	0.60	61.85	30.67	6.88	0.00	0	
	2	-	1.12	58.48	27.96	12.44	0.00	0	
		30	0.77	62.12	28.74	8.37	0.00	0	
		180	0.64	63.07	30.01	6.28	0.00	0	
	15	-	0.89	69.59	24.49	5.02	0.00	0	
		30	0.64	68.78	26.57	4.01	0.00	0	
		180	0.51	60.91	37.57	1.02	0.00	0	
	30	-	0.99	63.69	26.81	8.50	0.00	0	
		30	0.73	58.98	28.70	11.60	0.00	0	
180		0.50	68.08	28.09	3.34	0.00	0		
Pasta	Initial		0.03	0.30	0.13	0.90	24.24	74.40	

(continued)

Food	Proximal phase (min)	Distal phase (min)	Percent of particle area (%)					
			$\leq 0.1 \text{ mm}^2$	$0.1 < \text{mm}^2 \leq 4$	$4 < \text{mm}^2 \leq 10$	$10 < \text{mm}^2 \leq 100$	$100 < \text{mm}^2 \leq 200$	$\text{mm}^2 > 200$
	0	-	0.09	1.71	0.54	1.58	10.82	85.26
		30	0.04	0.85	0.12	0.55	15.39	83.05
		180	0.07	1.70	0.38	0.77	32.26	64.83
	2	-	0.06	1.10	0.34	2.54	30.68	65.27
		30	0.01	0.37	0.16	0.26	10.78	88.41
		180	0.09	2.13	1.07	0.20	20.07	76.45
	15	-	0.13	1.63	0.25	2.98	18.36	76.66
		30	0.02	0.35	0.08	0.00	18.23	81.32
		180	0.06	1.78	0.14	1.99	31.65	64.38
	30	-	0.10	1.02	0.10	0.76	28.90	69.12
		30	0.03	0.80	0.76	0.14	28.16	70.11
		180	0.05	1.02	0.32	5.20	19.94	73.46
Rice noodle	Initial		0.05	0.27	0.14	4.23	34.80	60.52
		0						
		-	0.03	0.50	0.26	2.27	25.39	71.56
		30	0.01	0.19	0.38	2.26	37.20	59.95
	0	180	0.02	0.70	0.55	4.15	22.97	71.61
		-	0.03	1.22	0.75	2.91	30.09	65.00
		30	0.02	0.36	0.48	2.52	29.54	67.08
	2	180	0.03	0.82	0.77	1.60	29.06	67.72
		-	0.05	1.33	1.05	8.50	43.81	45.25
		30	0.02	0.21	0.37	2.48	36.33	60.59
	15	180	0.03	0.66	0.41	2.76	28.90	67.24
		-	0.03	0.90	0.41	12.66	29.69	56.31
		30	0.02	0.37	0.55	3.69	19.77	75.59
	30	180	0.03	0.62	0.61	5.93	22.26	70.55
Rice grain	Initial		0.15	2.21	2.66	94.41	0.57	0
		0						
		-	0.25	2.69	2.21	94.84	0.00	0
		30	0.24	3.88	2.21	93.08	0.58	0
	0	180	0.25	9.85	8.69	81.20	0.00	0
		-	0.34	4.21	3.55	89.20	2.69	0
		30	0.28	3.20	2.62	89.16	4.74	0
	2	180	0.24	7.98	10.18	81.60	0.00	0
		-	0.39	6.26	8.56	83.61	1.17	0
		30	0.22	3.54	6.91	89.33	0.00	0
	15	180	0.16	7.51	13.26	78.53	0.54	0
		-	0.42	11.31	10.40	73.74	4.13	0
		30	0.29	4.72	8.74	86.24	0.00	0
	30	180	0.13	7.89	19.65	71.61	0.72	0

Table F.4 Particle size parameters (d_{10} , d_{50} , and d_{90}) of the liquid and suspended solid digesta fractions measured using Mastersizer. Values are shown as mean \pm SD ($n = 3$ for all parameters, except values indicated with asterisk (*), $n=2$ due to outlier removal). For each food, significantly different values between distal phase durations within the same proximal phase durations are indicated with abcd superscript; significantly different values between proximal phase durations within the same distal phase duration are indicated with zyxw superscript ($p < 0.05$).

Food	Proximal phase (min)	Distal phase (min)				
		15	30	60	120	180
d ₁₀ (μm)						
Couscous	0	6.91 ± 1.77	7.00 ± 1.66	7.97 ± 1.43 ^{zy}	7.76 ± 0.66	7.23 ± 1.17
	2	7.06 ± 1.66	6.93 ± 1.48	7.25 ± 0.99 ^y	7.61 ± 0.86	7.63 ± 1.2
	15	7.90 ± 1.66	8.22 ± 1.78	8.34 ± 1.38 ^{zy}	8.86 ± 1.57	8.09 ± 1.27
	30	7.90 ± 1.56	8.42 ± 2.14	9.01 ± 1.41 ^z	8.57 ± 1.50	8.52 ± 1.36
Rice couscous	0	7.91 ± 0.71 ^z	7.89 ± 0.22	7.97 ± 0.51	7.93 ± 0.89 ^{zy}	8.37 ± 0.77 ^z
	2	8.08 ± 0.62 ^z	7.81 ± 0.47	7.59 ± 1.01	8.47 ± 0.81 ^z	8.31 ± 1.92 ^z
	15	7.02 ± 0.81 ^{zy}	6.78 ± 0.95	6.54 ± 0.92	6.68 ± 1.18 ^y	6.19 ± 1.37 ^y
	30	6.05 ± 1.03 ^y	6.67 ± 1.56	6.92 ± 1.69	6.77 ± 1.14 ^y	6.99 ± 1.58 ^{zy}
Pasta	0	7.34 ± 1.03 ^d	8.38 ± 0.71 ^{cd,z}	9.68 ± 0.44 ^{bc,zy}	10.98 ± 1.03 ^{ab,z}	12.69 ± 0.65 ^{a,z}
	2	6.11 ± 0.85 ^c	7.56 ± 0.24 ^{bc,zy}	8.51 ± 0.91 ^{ab,zy}	9.73 ± 0.54 ^{a,z}	9.96 ± 0.47 ^{a,y}
	15	6.04 ± 0.79 ^b	6.40 ± 0.69 ^{ab,y}	6.72 ± 0.67 ^{ab,x}	7.40 ± 0.73 ^{ab,y}	8.05 ± 0.56 ^{a,yx}
	30	6.54 ± 0.85	6.98 ± 0.96 ^y	7.48 ± 1.06 ^{yx}	7.82 ± 1.09 ^y	7.92 ± 1.1 ^x
Rice noodle	0	4.78 ± 1.71 ^z	5.66 ± 2.81 ^z	5.91 ± 2.51 ^{zy}	5.95 ± 2.37 ^z	5.80 ± 2.85 ^{yx}
	2	4.36 ± 2.14 ^{b,y}	4.51 ± 2.21 ^{ab,y}	5.34 ± 3.17 ^{ab,y}	4.72 ± 2.24 ^{ab,y}	5.32 ± 1.42 ^{a,x}
	15	6.58 ± 2.75 ^z	5.84 ± 1.85 ^z	6.80 ± 3.08 ^z	6.78 ± 3.04 ^z	6.56 ± 2.6 ^{zy}
	30	6.31 ± 1.89 ^z	6.39 ± 1.92 ^z	7.23 ± 3.35 ^z	7.18 ± 3.3 ^z	7.34 ± 2.61 ^z
Rice grain	0	12.31 ± 3.36 ^z	11.56 ± 2.53 ^z	10.44 ± 2.06 ^z	11.24 ± 2.3 ^z	13.17 ± 4.21 ^z
	2	6.89 ± 1.52 ^{c,y}	7.26 ± 1.09 ^{bc,y}	8.52 ± 1.52 ^{abc,z}	9.2 ± 1.03 ^{a,z}	9.11 ± 2.11 ^{ab,y}
	15	6.86 ± 0.83 ^y	6.72 ± 0.58 ^y	7.06 ± 1.40 ^y	7.45 ± 1.08 ^y	8.28 ± 0.33 ^y
	30	6.35 ± 0.84 ^y	6.71 ± 1.15 ^y	6.55 ± 0.91 ^y	6.09 ± 0.45 ^y	7.29 ± 0.64 ^y
d ₅₀ (μm)						
Couscous	0	27.56 ± 6.07	29.26 ± 4.57	34.49 ± 5.28	36.46 ± 1.62	34.09 ± 6.02
	2	26.07 ± 4.45	26.33 ± 5.30	31.33 ± 3.56	34.40 ± 3.36	36.73 ± 5.67
	15	26.24 ± 5.02	26.73 ± 4.31	28.11 ± 1.95	32.31 ± 3.99	32.30 ± 3.35
	30	24.90 ± 3.79	26.71 ± 4.51	28.10 ± 2.55	29.05 ± 3.34	30.50 ± 2.51
Rice couscous	0	113.41 ± 51.83 ^{b,z}	111.42 ± 45.45 ^{b,z}	121.4 ± 47.62 ^{ab,z}	*115.43 ± 39.8 ^{ab,z}	162.61 ± 58.81 ^{a,z}
	2	116.16 ± 21.14 ^{b,z}	111.58 ± 24.92 ^{b,z}	120.89 ± 57.17 ^{b,z}	*196.4 ± 23.78 ^{a,z}	135.57 ± 84.02 ^{b,z}
	15	*44.64 ± 2.68 ^{a,y}	42.58 ± 18.46 ^{a,y}	34.15 ± 9.05 ^{ab,y}	34.84 ± 11.49 ^{ab,y}	*23.56 ± 1.08 ^{b,y}
	30	26.84 ± 7.3 ^x	*42.89 ± 11.17 ^y	32.18 ± 13.05 ^y	27.48 ± 7.17 ^y	32.06 ± 15.65 ^y
Pasta	0	30.52 ± 2.62 ^{c,z}	36.13 ± 2.38 ^{bc,z}	45.28 ± 4.1 ^{ab,z}	54.57 ± 8.38 ^{a,z}	62.31 ± 3.92 ^{a,z}
	2	24.81 ± 0.07 ^{c,zy}	34.25 ± 3.18 ^{bc,zy}	43.13 ± 4.69 ^{ab,z}	51.78 ± 2.74 ^{a,z}	54.47 ± 1.20 ^{a,z}
	15	20.82 ± 0.9 ^{c,y}	22.88 ± 0.37 ^{bc,yx}	26.07 ± 0.46 ^{abc,y}	30.47 ± 1.23 ^{ab,y}	33.83 ± 2.63 ^{a,y}
	30	21.38 ± 1.10 ^{zy}	22.62 ± 0.80 ^x	24.54 ± 1.30 ^y	26.60 ± 1.54 ^y	27.22 ± 1.65 ^y
Rice noodle	0	29.24 ± 11.30 ^z	32.69 ± 15.37 ^z	34.08 ± 13.96 ^z	31.39 ± 10.3 ^z	30.46 ± 16.67 ^z
	2	15.99 ± 5.89 ^y	15.66 ± 4.43 ^y	19.07 ± 10.15 ^y	15.84 ± 5.05 ^y	16.55 ± 1.70 ^y
	15	19.95 ± 8.14 ^{zy}	16.97 ± 4.78 ^y	19.87 ± 9.03 ^y	19.83 ± 8.55 ^y	18.53 ± 6.76 ^{zy}
	30	18.34 ± 4.96 ^z	18.60 ± 5.56 ^y	21.79 ± 10.20 ^y	20.62 ± 9.65 ^y	21.88 ± 7.35 ^{zy}
Rice grain	0	173.00 ± 70.59 ^{a,z}	134.48 ± 37.83 ^{ab,z}	101.6 ± 2.34 ^{b,z}	97.24 ± 25.17 ^{b,z}	108.1 ± 42.71 ^{b,z}

(continued)

Food	Proximal phase (min)	Distal phase (min)				
		15	30	60	120	180
	2	34.75 ± 16.95 ^{b,y}	40.82 ± 14.92 ^{ab,y}	44.92 ± 13.5 ^{ab,y}	49.25 ± 2.87 ^{a,y}	46.64 ± 11.8 ^{ab,y}
	15	25.83 ± 7.20 ^{ab,y}	24.37 ± 3.82 ^{b,x}	29.32 ± 10.79 ^{ab,x}	30.28 ± 7.5 ^{ab,x}	35.45 ± 3.18 ^{a,yx}
	30	24.91 ± 5.15 ^y	26.03 ± 7.72 ^x	25.94 ± 7.06 ^x	20.93 ± 3.23 ^x	28.43 ± 1.64 ^x
d₉₀ (µm)						
Couscous	0	73.52 ± 20.15 ^{b,y}	86.85 ± 11.19 ^{b,y}	148.13 ± 63.81 ^{ab}	238.44 ± 144.35 ^a	287.59 ± 127.81 ^{a,y}
	2	*70.56 ± 2.57 ^{b,y}	127.23 ± 72.11 ^{b,y}	174.39 ± 77.14 ^{ab}	303.66 ± 196.50 ^a	417.95 ± 277.31 ^{a,zy}
	15	275.41 ± 235.82 ^{b,z}	229.04 ± 209.55 ^{b,z}	213.76 ± 193.11 ^b	421.37 ± 294.54 ^{ab}	540.82 ± 217.62 ^{a,z}
	30	164.87 ± 93.02 ^{b,z}	201.59 ± 118.3 ^{b,z}	330.92 ± 368.31 ^{ab}	408.21 ± 223.64 ^a	440.85 ± 131.25 ^{a,zy}
Rice couscous	0	524.05 ± 173.08	571.33 ± 164.1	523.28 ± 63.81	563.15 ± 86.76	749.24 ± 55.34
	2	510.55 ± 120.22	566.33 ± 144.23	565.65 ± 78.72	578.54 ± 157.87	630.00 ± 231.9
	15	461.13 ± 60.25	568.37 ± 210.65	440.48 ± 98.05	485.93 ± 82.24	535.56 ± 172.23
	30	399.22 ± 209.8	389.67 ± 205.07	338.82 ± 61.32	372.8 ± 147.31	406.89 ± 84.50
Pasta	0	97.23 ± 23.97 ^b	109.34 ± 22.87 ^{ab}	163.26 ± 56.24 ^{ab}	184.5 ± 44.49 ^{ab}	226.26 ± 67.54 ^a
	2	83.62 ± 7.74 ^b	128.06 ± 14.99 ^{ab}	174.16 ± 43.33 ^{ab}	203.55 ± 49.87 ^a	226.38 ± 29.04 ^a
	15	125.38 ± 34.81 ^b	95.78 ± 13.84 ^{ab}	137.93 ± 19.28 ^{ab}	191.45 ± 2.56 ^{ab}	208.11 ± 18.48 ^a
	30	115.72 ± 38.34	108.66 ± 43.73	133.87 ± 19.81	155.03 ± 30	181.96 ± 44.03
Rice noodle	0	334.19 ± 97.19 ^z	278.06 ± 116.29 ^z	291.07 ± 117.49 ^z	342.15 ± 111.16 ^z	328.22 ± 192.90 ^z
	2	198.06 ± 61.54 ^{a,z}	178.84 ± 123.27 ^{ab,zy}	197.87 ± 175.62 ^{ab,zy}	275.92 ± 214.53 ^{a,z}	83.05 ± 17.86 ^{b,y}
	15	59.04 ± 22.08 ^y	50.63 ± 16.37 ^y	59.24 ± 25.51 ^x	58.55 ± 24.04 ^y	55.92 ± 21.46 ^y
	30	56.09 ± 17.82 ^y	57.34 ± 19.51 ^y	66.48 ± 30.85 ^{yx}	62.20 ± 28.5 ^y	65.77 ± 23.43 ^y
Rice grain	0	795.82 ± 173.84 ^z	764.35 ± 39.12 ^z	622.16 ± 37.84	586.64 ± 72.56 ^z	552.6 ± 187.18
	2	434.53 ± 65.13 ^{zy}	570.93 ± 189.78 ^z	481.75 ± 91.77	481.50 ± 106.54 ^z	482.94 ± 114.79
	15	271.36 ± 193.11 ^y	250.19 ± 153.57 ^y	396.58 ± 214.54	410.60 ± 232.60 ^z	276.36 ± 126.85
	30	336.82 ± 162.72 ^{abc,zy}	408.89 ± 178.15 ^{ab,zy}	522.70 ± 174.02 ^a	173.48 ± 14.47 ^{c,y}	252.73 ± 69.44 ^{bc}

F.2 Supplementary Figures

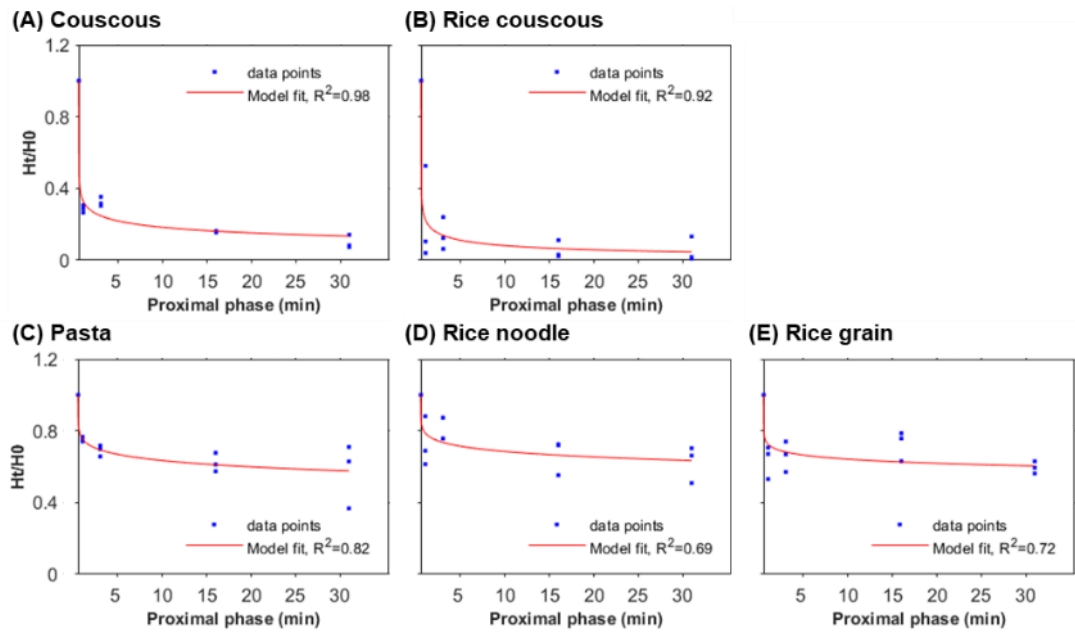


Figure F.1 Weibull model (Eqn. 7.2) fitting to all data points for each diet in the proximal digestion. Data points are indicated with blue dots and the curve of the model fit is indicated with the red line.

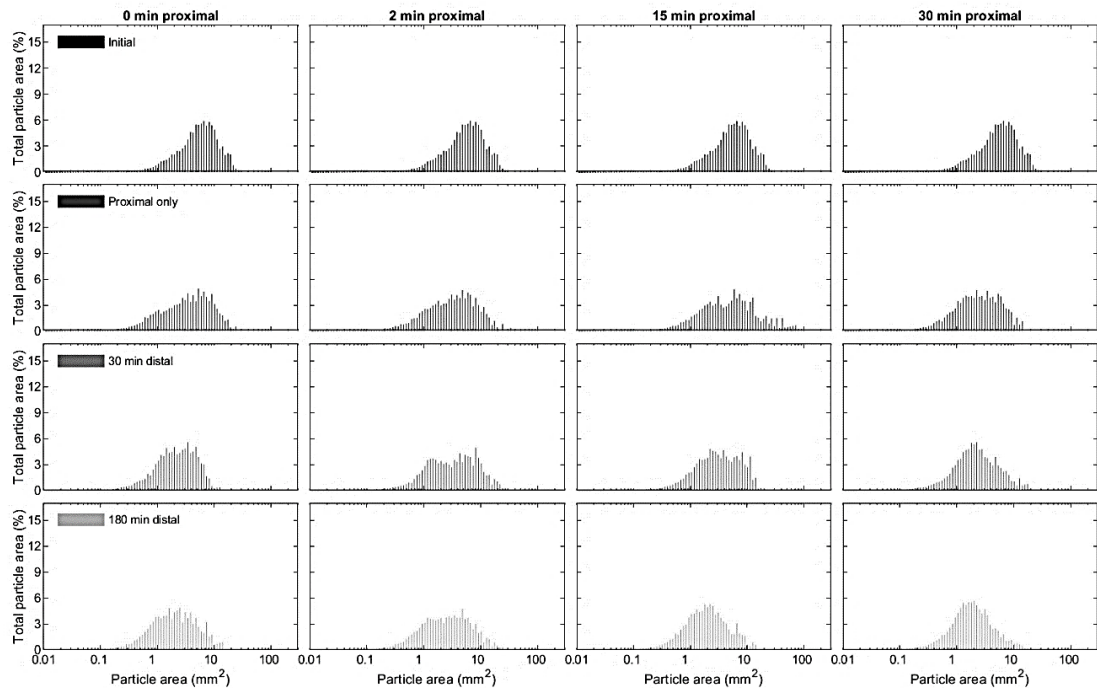


Figure F.2 Particle area distribution of solid fractions in couscous digesta at different proximal phase (indicated on the leftmost figure) durations either after proximal digestion (“Proximal only”) or selected distal phase during proximal-distal digestion (indicated on the top of each column). Distribution for each plot was established by combining the data from three experimental replicates. Note that the x-axis is presented in logarithmic scale to cover several magnitudes of area. For ease of comparison, the distribution of undigested food (“Initial”) is given for each proximal phase duration.

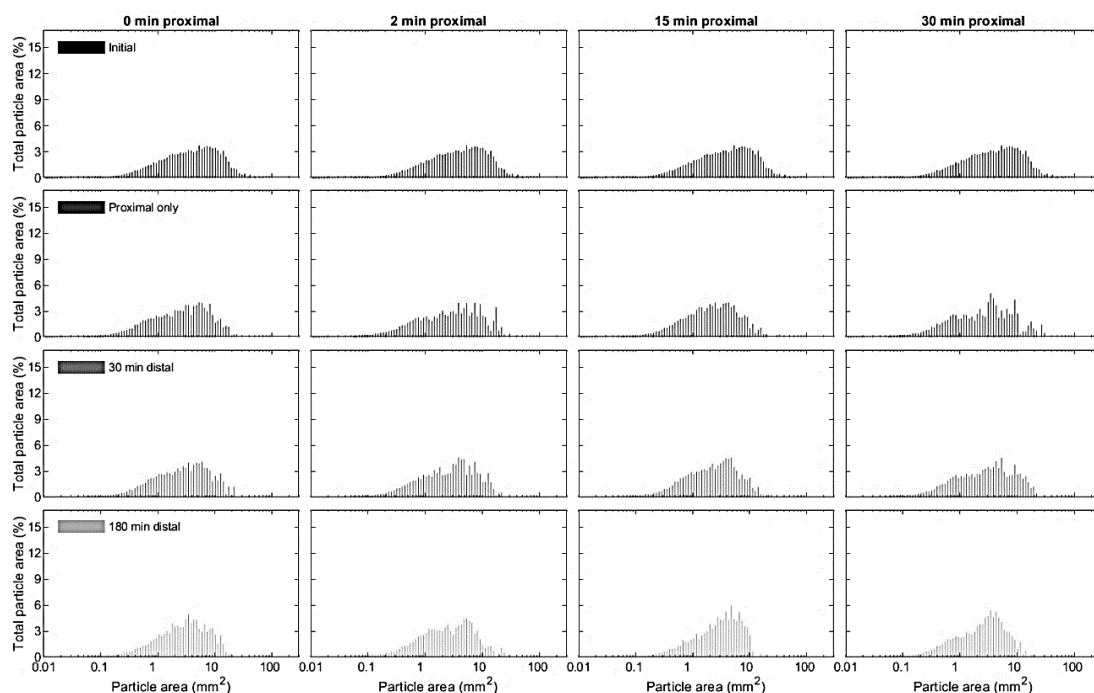


Figure F.3 Particle area distribution of solid fractions in rice couscous digesta at different proximal phase (indicated on the leftmost figure) durations either after proximal digestion (“Proximal only”) or selected distal phase during proximal-distal digestion (indicated on the top of each column). Distribution for each plot was established by combining the data from three experimental replicates. Note that the x-axis is presented in logarithmic scale to cover several magnitudes of area. For ease of comparison, the distribution of undigested food (“Initial”) is given for each proximal phase duration.

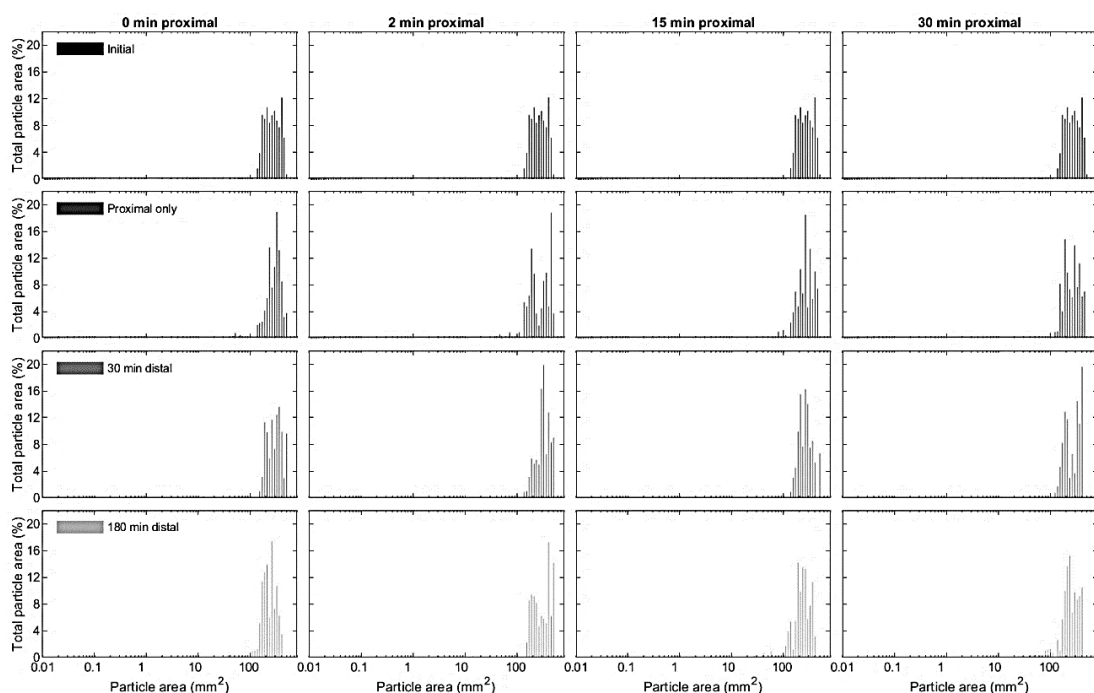


Figure F.4 Particle area distribution of solid fractions in pasta digesta at different proximal phase (indicated on the leftmost figure) durations either after proximal digestion (“Proximal only”) or selected distal phase during proximal-distal digestion (indicated on the top of each column). Distribution for each plot was established by combining the data from three experimental replicates. Note that the x-axis is presented in logarithmic scale to cover several magnitudes of area. For ease of comparison, the distribution of undigested food (“Initial”) is given for each proximal phase duration.

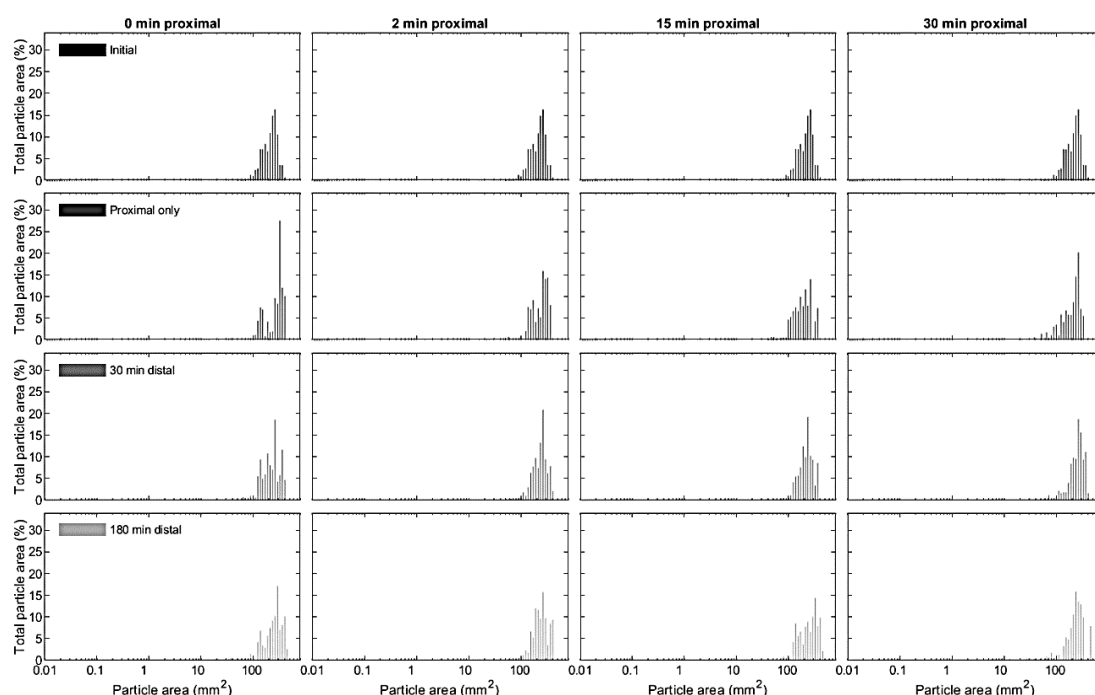


Figure F.5 Particle area distribution of solid fractions in rice noodle digesta at different proximal phase (indicated on the leftmost figure) durations either after proximal digestion (“Proximal only”) or selected distal phase during proximal-distal digestion (indicated on the top of each column). Distribution for each plot was established by combining the data from three experimental replicates. Note that the x-axis is presented in logarithmic scale to cover several magnitudes of area. For ease of comparison, the distribution of undigested food (“Initial”) is given for each proximal phase duration.

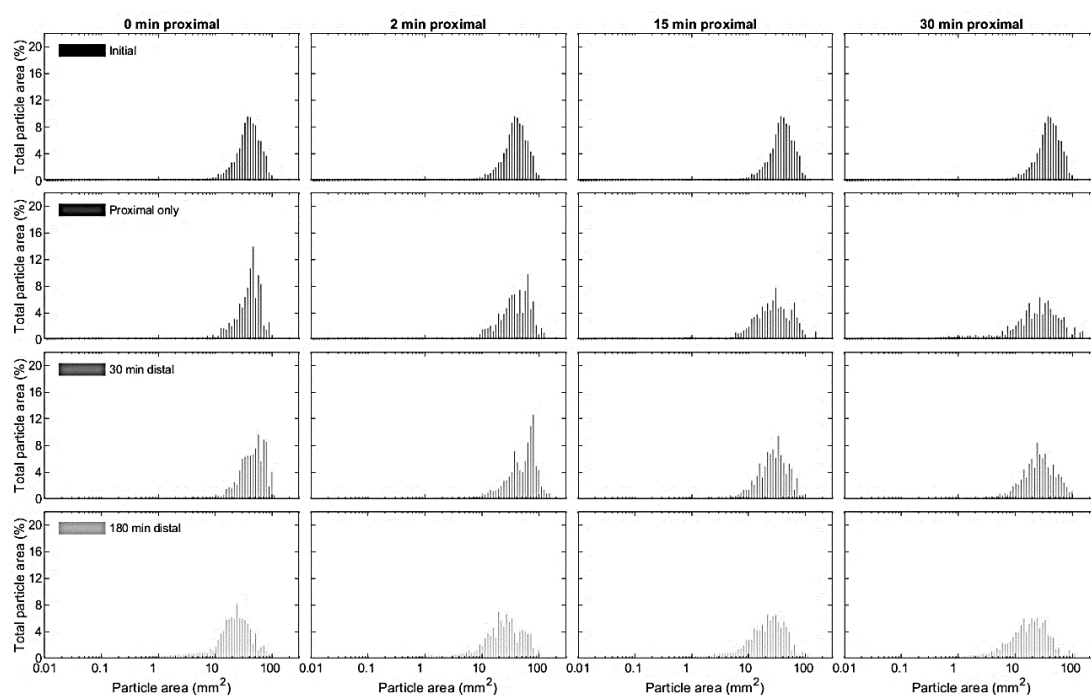


Figure F.6 Particle area distribution of solid fractions in rice grain digesta at different proximal phase (indicated on the leftmost figure) durations either after proximal digestion (“Proximal only”) or selected distal phase during proximal-distal digestion (indicated on the top of each column). Distribution for each plot was established by combining the data from three experimental replicates. Note that the x-axis is presented in logarithmic scale to cover several magnitudes of area. For ease of comparison, the distribution of undigested food (“Initial”) is given for each proximal phase duration.

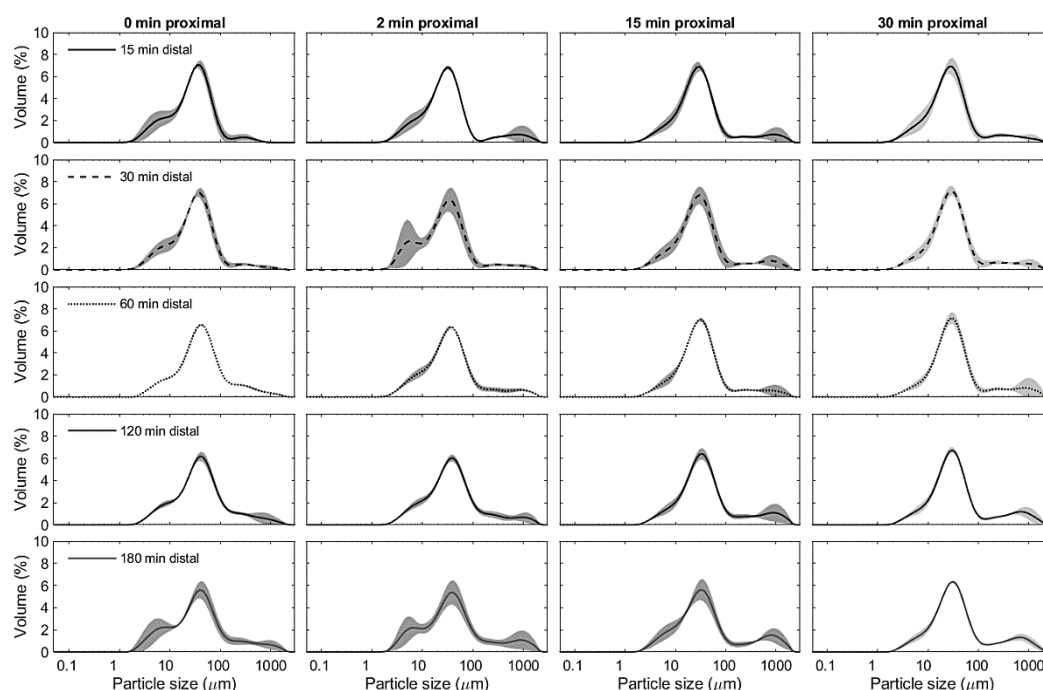


Figure F.7 Individual plots of particle size distribution of liquid and suspended solid fractions in couscous digesta at different proximal phase (indicated on the top of each column), over different distal phase (indicated on the leftmost figure). The standard deviation of each proximal \times distal combination is indicated with error shades around the line.

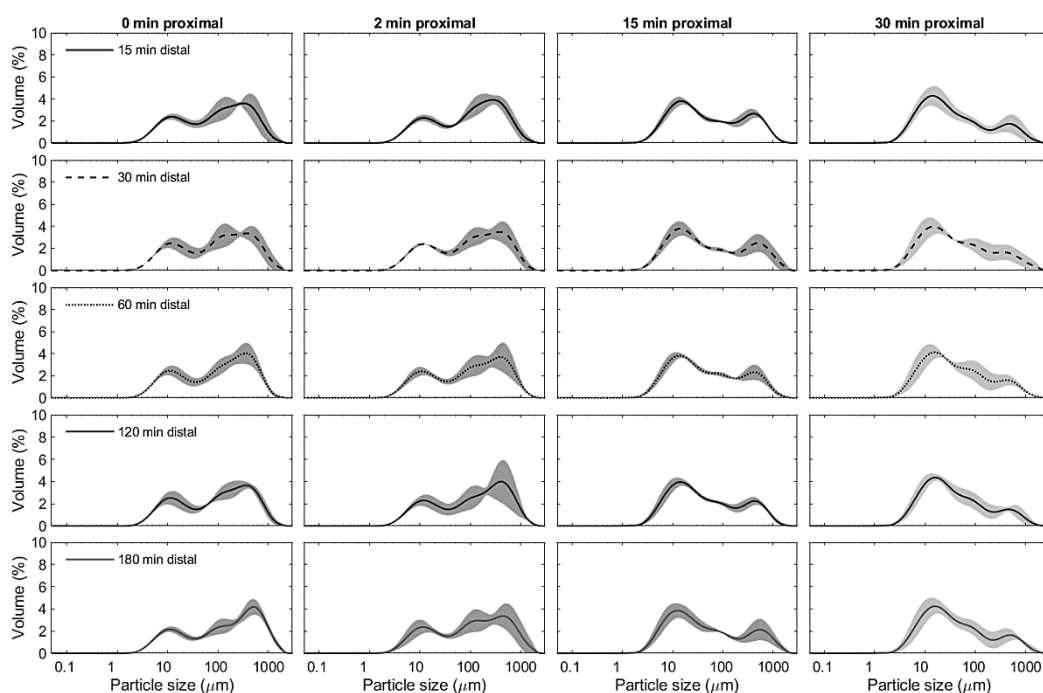


Figure F.8 Individual plots of particle size distribution of liquid and suspended solid fractions in rice couscous digesta at different proximal phase (indicated on the top of each column), over different distal phase (indicated on the leftmost figure). The standard deviation of each proximal \times distal combination is indicated with error shades around the line.

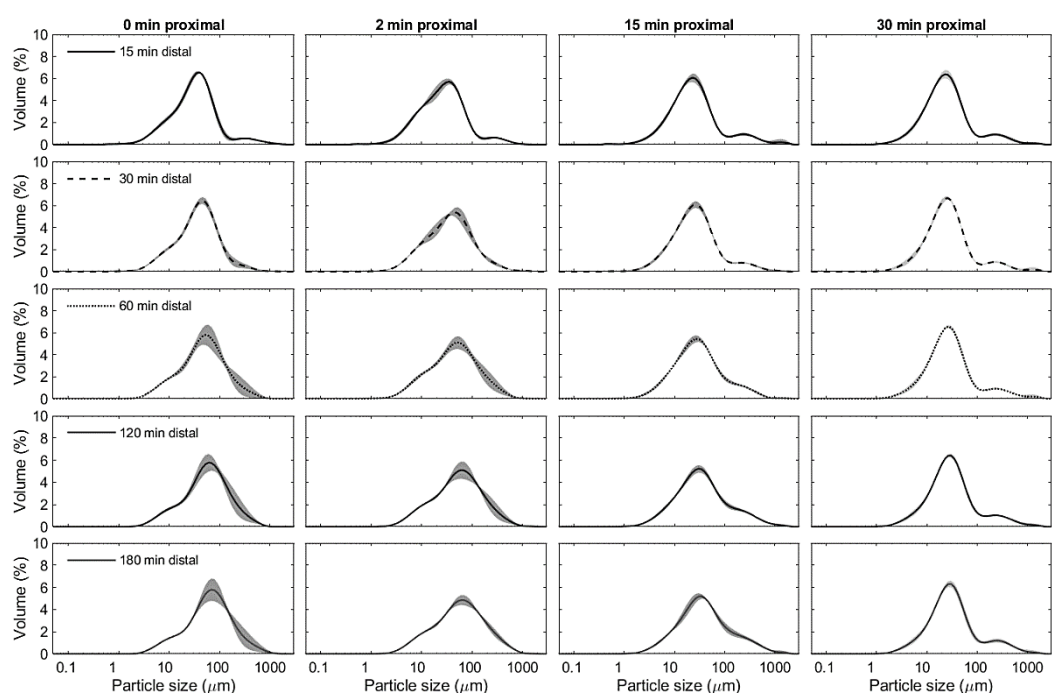


Figure F.9 Individual plots of particle size distribution of liquid and suspended solid fractions in pasta digesta at different proximal phase (indicated on the top of each column), over different distal phase (indicated on the leftmost figure). The standard deviation of each proximal \times distal combination is indicated with error shades around the line.

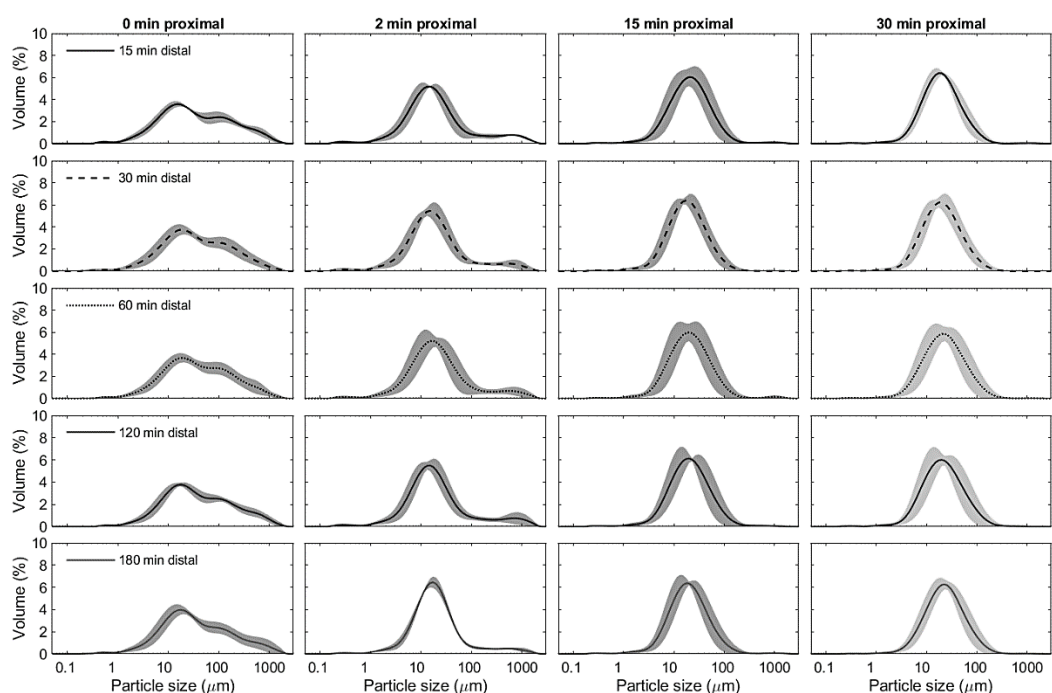


Figure F.10 Individual plots of particle size distribution of liquid and suspended solid fractions in rice noodle digesta at different proximal phase (indicated on the top of each column), over different distal phase (indicated on the leftmost figure). The standard deviation of each proximal \times distal combination is indicated with error shades around the line.

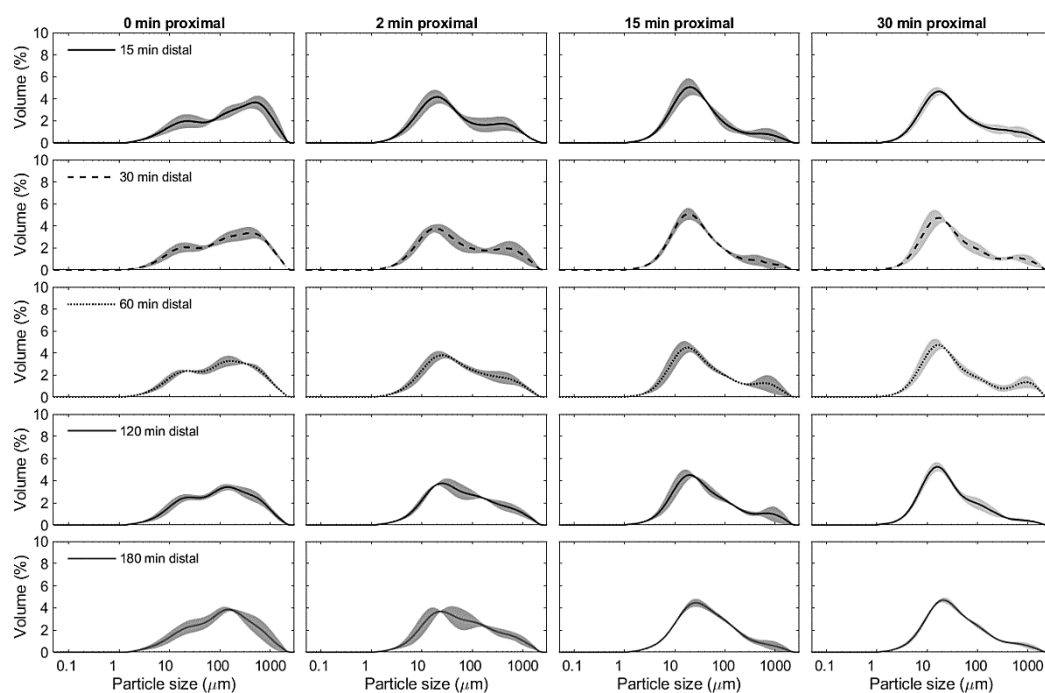



Figure F.11 Individual plots of particle size distribution of liquid and suspended solid fractions in rice grain digesta at different proximal phase (indicated on the top of each column), over different distal phase (indicated on the leftmost figure). The standard deviation of each proximal \times distal combination is indicated with error shades around the line.

APPENDIX G

DRC 16 FORMS AND COPYRIGHT PERMISSION

G.1 DRC 16 forms

DRC 16


MASSEY
 UNIVERSITY
TE KUNINGA KI PŪWHIRIO
 UNIVERSITY OF NEW ZEALAND

GRADUATE
 RESEARCH
 SCHOOL

STATEMENT OF CONTRIBUTION DOCTORATE WITH PUBLICATIONS/MANUSCRIPTS

We, the candidate and the candidate's Primary Supervisor, certify that all co-authors have consented to their work being included in the thesis and they have accepted the candidate's contribution as indicated below in the *Statement of Originality*.

Name of candidate:	Joanna Nadia
Name/title of Primary Supervisor:	Dist. Prof. Harjinder Singh
In which chapter is the manuscript /published work:	Chapter 2

Please select one of the following three options:

☒ The manuscript/published work is published or in press

- Please provide the full reference of the Research Output:
 Nadia, J., Bronlund, J., Singh, R.P., Singh, H., and Bornhorst, G.M. (2021). Structural breakdown of starch-based foods during gastric digestion and its link to glycemic response: In vivo and in vitro considerations. *Comprehensive Review in Food Science and Food Safety*, 2021, 20:1–39.

☐ The manuscript is currently under review for publication – please indicate:

- The name of the journal:
- The percentage of the manuscript/published work that was contributed by the candidate: 85.00
- Describe the contribution that the candidate has made to the manuscript/published work:
 The candidate conceived the idea of the manuscript, collected relevant literature, drafted and edited the manuscript for submission. The candidate also drafted the responses to reviewers' comments in the review process.

☐ It is intended that the manuscript will be published, but it has not yet been submitted to a journal

Candidate's Signature:	Joanna Nadia <small>Digitally signed by Joanna Nadia Date: 2021.12.13 10:25:13 +1300</small>
Date:	13-Dec-2021
Primary Supervisor's Signature:	Harjinder Singh <small>Digitally signed by Harjinder Singh Date: 2021.12.16 13:50:44 +1300</small>
Date:	16-Dec-2021

This form should appear at the end of each thesis chapter/section/appendix submitted as a manuscript/ publication or collected as an appendix at the end of the thesis.

GRS Version 5 – 13 December 2019
DRC 19/09/10

STATEMENT OF CONTRIBUTION DOCTORATE WITH PUBLICATIONS/MANUSCRIPTS

We, the candidate and the candidate's Primary Supervisor, certify that all co-authors have consented to their work being included in the thesis and they have accepted the candidate's contribution as indicated below in the *Statement of Originality*.

Name of candidate:	Joanna Nadia
Name/title of Primary Supervisor:	Dist. Prof. Harjinder Singh
In which chapter is the manuscript /published work:	3.1-3.2, 4
Please select one of the following three options:	
<input checked="" type="radio"/> The manuscript/published work is published or in press <ul style="list-style-type: none"> • Please provide the full reference of the Research Output: Nadia, J., Olenskyj, A.G., Stroebinger, N., Hodgkinson, S.M., Estevez, T.G., Subramanian, P., Singh, H., Singh, R.P., and Bornhorst, G.M. (2021). Tracking physical breakdown of rice- and wheat-based foods with varying structures during gastric digestion and its influence on gastric emptying in a growing pig model. <i>Food Funct.</i> 2021. 12: 4349-4372 	
<input type="radio"/> The manuscript is currently under review for publication – please indicate: <ul style="list-style-type: none"> • The name of the journal: <div style="background-color: #e0e0ff; height: 20px; width: 100%;"></div> • The percentage of the manuscript/published work that was contributed by the candidate: <div style="background-color: #e0e0ff; width: 100px; text-align: center;">50.00</div> • Describe the contribution that the candidate has made to the manuscript/published work: The candidate was involved in the planning of the animal trial, logistical preparation and execution of the animal trial, measurements of gastric emptying and digesta properties (pH, texture, moisture content), and measurement of diet initial properties. Data analysis and draft preparation of the manuscript was conducted by the candidate in a shared main authorship with A.G. Olenskyj. The candidate also drafted the responses to reviewers' comments during the peer-review process. 	
<input type="radio"/> It is intended that the manuscript will be published, but it has not yet been submitted to a journal	
Candidate's Signature:	Joanna Nadia <small>Digitally signed by Joanna Nadia Date: 2021.12.13 13:24:15 +1300</small>
Date:	13-Dec-2021
Primary Supervisor's Signature:	Harjinder Singh <small>Digitally signed by Harjinder Singh Date: 2021.12.16 12:30:15 +1300</small>
Date:	16-Dec-2021

This form should appear at the end of each thesis chapter/section/appendix submitted as a manuscript/publication or collected as an appendix at the end of the thesis.

STATEMENT OF CONTRIBUTION DOCTORATE WITH PUBLICATIONS/MANUSCRIPTS

We, the candidate and the candidate's Primary Supervisor, certify that all co-authors have consented to their work being included in the thesis and they have accepted the candidate's contribution as indicated below in the *Statement of Originality*.

Name of candidate:	Joanna Nadia
Name/title of Primary Supervisor:	Dist. Prof. Harjinder Singh
In which chapter is the manuscript /published work:	3.1-3.2, 5
<p>Please select one of the following three options:</p> <p><input type="radio"/> The manuscript/published work is published or in press</p> <ul style="list-style-type: none"> Please provide the full reference of the Research Output: 	
<p><input checked="" type="radio"/> The manuscript is currently under review for publication – please indicate:</p> <ul style="list-style-type: none"> The name of the journal: Nadia, J., Olenskyj, A.G., Subramanian, P., Hodgkinson, S.M., Stroebling, N., Estevez, T.G., Singh, R.P., Singh, H., and Bornhorst, G.M. Influence of food macrostructure on the kinetics of acidification in the pig stomach: implications for starch hydrolysis and starch emptying rate The percentage of the manuscript/published work that was contributed by the candidate: 70.00 Describe the contribution that the candidate has made to the manuscript/published work: The candidate was involved in the planning of the animal trial, logistical preparation and execution of the animal trial, measurements of gastric emptying and digesta properties (pH, reducing sugar, free amino groups, apparent amylase activity), and measurement of diet initial properties. The candidate also conducted the data analysis, data visualization, and preparation of the manuscript for submission. 	
<p><input type="radio"/> It is intended that the manuscript will be published, but it has not yet been submitted to a journal</p>	
Candidate's Signature:	Joanna Nadia <small>Digitally signed by Joanna Nadia Date: 2021.12.13 18:36:22 +1300'</small>
Date:	13-Dec-2021
Primary Supervisor's Signature:	Harjinder Singh <small>Digitally signed by Harjinder Singh Date: 2021.12.16 13:54:45 +1300'</small>
Date:	16-Dec-2021

This form should appear at the end of each thesis chapter/section/appendix submitted as a manuscript/ publication or collected as an appendix at the end of the thesis.



GRADUATE
RESEARCH
SCHOOL

STATEMENT OF CONTRIBUTION DOCTORATE WITH PUBLICATIONS/MANUSCRIPTS

We, the candidate and the candidate's Primary Supervisor, certify that all co-authors have consented to their work being included in the thesis and they have accepted the candidate's contribution as indicated below in the *Statement of Originality*.

Name of candidate:	Joanna Nadia
Name/title of Primary Supervisor:	Dist. Prof. Harjinder Singh
In which chapter is the manuscript /published work:	3.1-3.2, 6
<p>Please select one of the following three options:</p> <p><input type="radio"/> The manuscript/published work is published or in press</p> <ul style="list-style-type: none"> Please provide the full reference of the Research Output: <p><input type="radio"/> The manuscript is currently under review for publication – please indicate:</p> <ul style="list-style-type: none"> The name of the journal: The percentage of the manuscript/published work that was contributed by the candidate: 70.00 Describe the contribution that the candidate has made to the manuscript/published work: The candidate was involved in the planning of the animal trial, logistical preparation and execution of the animal trial, gastric digesta collection, glycemic response measurement, measurements of gastric emptying and small intestinal digesta properties. The candidate also conducted the data analysis, data visualization, and writing of the draft of the manuscript. <p><input checked="" type="radio"/> It is intended that the manuscript will be published, but it has not yet been submitted to a journal</p>	
Candidate's Signature:	Joanna Nadia <small>Digitally signed by Joanna Nadia Date: 2021.12.13 10:42:27 +1300</small>
Date:	13-Dec-2021
Primary Supervisor's Signature:	Harjinder Singh <small>Digitally signed by Harjinder Singh Date: 2021.12.16 13:55:23 +1300</small>
Date:	16-Dec-2021

This form should appear at the end of each thesis chapter/section/appendix submitted as a manuscript/publication or collected as an appendix at the end of the thesis.

GRS Version 5 – 13 December 2019
DRC 19/09/10



GRADUATE
RESEARCH
SCHOOL

STATEMENT OF CONTRIBUTION DOCTORATE WITH PUBLICATIONS/MANUSCRIPTS

We, the candidate and the candidate's Primary Supervisor, certify that all co-authors have consented to their work being included in the thesis and they have accepted the candidate's contribution as indicated below in the *Statement of Originality*.

Name of candidate:	Joanna Nadia
Name/title of Primary Supervisor:	Dist. Prof. Harjinder Singh
In which chapter is the manuscript /published work:	3.1, 3.3, 7
<p>Please select one of the following three options:</p> <p><input type="radio"/> The manuscript/published work is published or in press</p> <ul style="list-style-type: none"> Please provide the full reference of the Research Output: <p><input type="radio"/> The manuscript is currently under review for publication – please indicate:</p> <ul style="list-style-type: none"> The name of the journal: The percentage of the manuscript/published work that was contributed by the candidate: 85.00 Describe the contribution that the candidate has made to the manuscript/published work: The candidate planned the experiments, conducted the digestion experiments, and measured the digesta properties except the particle size measurement using Mastersizer that was mostly (70%) conducted by Dr. Parthasarathi Subramanian. The candidate conducted the data analysis, data visualization, and writing of the draft of the manuscript. <p><input checked="" type="radio"/> It is intended that the manuscript will be published, but it has not yet been submitted to a journal</p>	
Candidate's Signature:	Joanna Nadia <small>Digitally signed by Joanna Nadia Date: 2021.12.13 10:54:16 +1300</small>
Date:	13-Dec-2021
Primary Supervisor's Signature:	Harjinder Singh <small>Digitally signed by Harjinder Singh Date: 2021.12.16 13:55:57 +1300</small>
Date:	16-Dec-2021

This form should appear at the end of each thesis chapter/section/appendix submitted as a manuscript/publication or collected as an appendix at the end of the thesis.

GRS Version 5 – 13 December 2019
DRC 19/09/10

G.2 Copyright permission

Dear Ms. Joanna Nadia,

Royal Society of Chemistry has approved your recent request. Before you can use this content, you must accept the license fee and terms set by the publisher.

Use this [link](#) to accept (or decline) the publisher's fee and terms for this order.

Request Summary:

Submit date: 03-Dec-2021

Request ID: 600062405

Publication: Food & function

Title: Tracking physical breakdown of rice- and wheat-based foods with varying structures during gastric digestion and its influence on gastric emptying in a growing pig model

Type of Use: Republish in a thesis/dissertation

Please do not reply to this message.



Thank you for your order!

Dear Ms. Joanna Nadia,

Thank you for placing your order through Copyright Clearance Center's RightsLink® service.

Order Summary

Licensee: Riddet Institute

Order Date: Dec 3, 2021

Order Number: 5201560533498

Publication: Comprehensive Reviews in Food Science and Food Safety
Structural breakdown of starch-based foods during gastric

Title: digestion and its link to glycemic response: In vivo and in vitro
considerations

Type of Use: Dissertation/Thesis

Order Total: 0.00 USD